CONSTRUCTION MATERIALS CONSULTANTS, INC.

Laboratory Investigation of Early 19th Century Calcined Clay-Lime Setting and Dolomitic Lime Pointing Mortars From the Perimeter Walls of the Historic Eastern State Penitentiary in Philadelphia, PA

Eastern State Penitentiary Perimeter Walls
2027 Fairmount Avenue
Philadelphia, PA 19130

August 22, 2022
CMC 0722152

TABLE OF CONTENTS

LABORATORY INVESTIGATION OF EARLY 19TH CENTURY MASONRY MORTARS FROM EASTERN STATE PENITENTIARY PERIMETER WALLS, PHILADELPHIA, PA

EXECUTIVE SUMMARY

The Eastern State Penitentiary is a former American prison in Philadelphia, Pennsylvania. Constructed in 1822, the prison was operational from 1829 until 1971. At its completion, the building was the largest and most expensive public structure ever erected in the United States, and quickly became a model for more than 300 prisons worldwide. The prison is currently registered as a U.S. National Historic Landmark.

As part of the renovation process, three reddish-brown colored moderately hard to moderately soft fragments of reported original setting mortars were provided from interiors of the east (SET-3), west (SWM-2), and south (SSB-3) walls of the penitentiary after removing the exterior stone masonry units, along with a medium gray colored moderately hard pointing mortar (CB6-Link) reportedly also from the original construction.

The purposes of this investigation are comprehensive laboratory studies of setting and pointing mortars to determine: (a) the compositions of sands and binders used, (b) conditions of the mortars, (c) comprehensive microstructural examinations to diagnose evidence of alterations of mortars during the last 200 years of service history, and (d) eventually, an assessment of suitable repointing mortars to be for restoration.

Field photos of three walls of the penitentiary showed stone masonry walls where the exterior head and bed joints of stone masonry units were repointed with relatively dense, hard, medium gray pointing mortars, whereas the setting mortars provided for examinations are noticeably softer, reddish-brown, and situated inside the exterior pointing mortars as the original mortars of construction. The pointing mortar sample provided for examination appeared visually similar in appearance to the exterior pointing mortars seen in the field photos of three walls.

The samples were examined by the procedures of ASTM C 1324, "Standard Test Method for Examination and Analysis of Hardened Masonry Mortar," and European (the RILEM) Test Methods. Laboratory testing protocol includes an exhaustive investigation consisting of: (1) detailed optical microscopical examinations of as-received, lapped, and thin sectioned pieces of mortars with stereo-zoom microscopes, and petrographic microscope to determine the types, conditions, and compositions of sand, binder, and overall mortars used; (2) scanning electron microscopy and energy-dispersive X-ray microanalyses (SEM-EDS) of interstitial paste fractions of mortars to ascertain the binder compositions determined from optical microscopy; (3) extraction of acid-insoluble (e.g., siliceous and argillaceous) components of sand by HCl digestion, followed by sieve analyses of extracted sand to determine grain-size distribution of original sands; (4) chemical (gravimetric) analyses to determine the soluble silica contents from cold-acid digestion of mortars followed by hot-alkali digestion of the residues; (5) siliceous sand contents from hydrochloric-acid insoluble residue contents, (6) free and combined water and carbonate contents from loss on ignition at 110°C, 550°C, and 950°C respectively, (7) X-ray fluorescence spectroscopy (XRF) to determine bulk chemical (oxide) compositions of mortars, (8) X-ray diffraction (XRD) to determine the mineralogical compositions, (9) thermal analysis to determine the hydrous, sulfate, and carbonate phases in the mortars as well as the binder compositions, and (10) ion chromatography of water-soluble anions in the filtrates after digesting the mortars in deionized water to determine potentially deleterious soluble salts (e.g., of chloride, sulfate, etc.) in the mortars. Based on all these comprehensive analyses, the overall conditions, extents of

deterioration, and compositions of the mortars can be assessed, from which a suitable replacement mortar for the examined one can be evaluated.

Three setting mortars showed some noticeable difference in properties of sands from the pointing mortar. Setting mortars have two grain size fractions of sand, which are well-graded with continuous variations in sand sizes: (a) a coarser fraction (maximum 4 mm size) of subangular to rounded grains, similar to river sand consisting of major amounts of siliceous sand (dominantly quartz and quartzite and subordinate amount of quartz siltstone and sandstone) and minor to subordinate amounts of argillaceous (shale, argillaceous siltstone) and ferruginous (ferruginous shale and siltstone) grains, and (b) a finer fraction (< 1 mm) of mostly crushed (angular) sand. By contrast, pointing mortar has only one sand size class, which is noticeably finer than the coarser size fraction in setting mortars but more similar to the finer size fraction of setting mortar, well-sorted (dominance of a few size fractions as opposed to well graded sand in setting mortar) and characteristically angular for use of a crushed sand.

Fineness modulus of sands extracted from the mortars after acid digestion were calculated from the sum of cumulative percentages retained on Sieves 4, 8, 16, 30, 50, and 100 divided by 100. Results showed values consistent with fine sand, e.g., 2.53 for east wall setting mortar SET-3, 1.88 for west wall setting mortar SWM-2, 2.07 for south wall setting mortar SSB-3, and a noticeably lower 0.75 value for sand in the pointing mortar. Fineness modulus typically ranges from 2.2 to 2.6 for fine sand, 2.6 to 2.9 for medium sand, and 2.9 to 3.2 for coarse sand. Grain size distribution of sand used in three setting mortars are all finer than size distribution of modern ASTM C 144 sand, hence cannot be substituted with an ASTM C 144 sand. This is especially true for the sand in the pointing mortar, which shows noticeably finer size distribution for all sieve fractions compared to sand in the setting mortars, or the modern-day ASTM C 144 masonry sand. Therefore, based on compositions and grain size distributions of extracted sand, the pointing mortar is judged to be consistent with its 'original' vintage where a fine crushed sand was mixed with river sand in production of the main setting mortars, whereas only a clean washed and finer size crushed silica-based sand was used in pointing mortar.

Image analyses were done on mosaics of multiple thin section micrographs of sand taken with a transmitted-light stereo-zoom microscope to determine the volumetric proportions of sand in each mortar. Results showed 28.1%, 19.2%, 22.9% and 34.4% sand volumes in samples SET-3, SWM-2, SSB-3, and CB6-Link, respectively, which, assuming a sand specific gravity of 2.65, respectively correspond to 74.4%, 50.9%, 60.7%, and 91.1% sand, by mass. Pointing mortar showed a noticeably higher proportion of sand (along with its finer grain size and angularity) compared to sand volumes in three setting mortars.

An illustrated atlas of hundreds of photomicrographs of lapped sections and thin sections of mortars collected using a reflected-light stereomicroscope, transmitted-light high-power stereo-zoom microscope, and petrographic microscope are provided in the report, which showed the dominantly siliceous components of sand, both in the coarser size fractions in setting mortars as well as in the finer size fractions in both setting and pointing mortars.

An interesting feature observed in coarse and fine sand fractions in all three setting mortars but not in the angular finer sands in the pointing mortar is the presence of thin, discontinuous reddish-brown coatings on the sand grains, formed in many grains irrespective of angular, subangular to rounded grains in the setting mortars. These reddish-brown coatings could represent: (a) clay coats or weathering rims formed in the sand stockpile from associated reddish-brown ferruginous shale-siltstone particles prior to the incorporation in the mortar, or, more plausibly, (b) from their formation in the mortar *per se*, during 200 years of water migration, leaching and dissolution where iron

oxide components were derived not just from the ferruginous component of sand but more commonly from the residual calcined clay (brick dust) particles determined to be intentionally added as a pozzolan to the dominant lime binder component. These calcined clay (brick dust) pozzolans have reacted with lime and contributed the iron oxide components to the matrix eventually imparting the reddish-brown color tone of paste and mortar. Leaching and dissolution of iron oxide from lime-pozzolan reaction products in paste (and some may also from the ferruginous matrix in sand) have contributed to the formation of reddish-brown coats on the sand grains. Subsequent SEM-EDS studies of coats showed enriched Si-Al-Mg in these coats from pozzolanic reactions followed by leaching of lime in these coats. Formation of these coats specifically on angular fractions of sand grains questions the possibility of their prior presence as weathering rims (clay coatings), and rather indicate their in-situ formation from pozzolanic reactions of calcined clay (brick dust) with lime.

The basic difference in the color tones of pastes and the entire reddish-brown setting versus medium gray pointing mortars are determined to be due to the inherent difference in their binder components. Extensive SEM-EDS studies have determined the paste fractions in the setting mortar, after reverse engineering from the present leached and altered states, to be a two-component mixture of a dominant dolomitic lime component and a subordinate calcined clay (brick dust) component, where the latter component has imparted the characteristic reddish-brown color tones in setting mortars. Iron oxide impurities in the original clay component of calcined clay binder have imparted the reddish-brown color in all three setting mortars. Paste color is judged not necessarily from reddish-brown ferruginous grains in sand as such grains are present only in minor amounts and in both setting and pointing mortars. However, leaching actions on setting mortars may have dissolved some iron oxide components from reddish-brown ferruginous matrix in sand grains and may have contributed to the overall color tone of paste and mortar but it is indeed the calcined clay component added with lime, which has provided the characteristic reddish-brown color tone of setting mortars collected from the interiors of east, west, and south walls.

Paste in setting mortars showed variably dense to porous, severely carbonated as well as leached appearances. There is no evidence of any residual hydraulic lime phase (e.g., belite) found in the paste indicating use of a non-hydraulic to feebly hydraulic dolomitic lime binder, which was produced from calcination of a relatively pure dolomitic limestone. This feebly hydraulic dolomitic lime binder component in setting mortar is found to be similar to the feebly hydraulic dolomitic lime binder used entirely in the pointing mortar without any calcined clay component to impart the characteristic medium gray color in pointing mortar.

Evidence of extensive lime leaching of paste in all three setting mortars are seen where leached areas show optically isotropic nature due to the presence of essentially an amorphous or gelatinous precipitate after leaching of lime, which from subsequent SEM-EDS studies is determined to be noticeably enriched in Mg, Si, and Al as opposed to Ca-rich carbonated areas. A viscous gelatinous film was formed in the filtrates during acid digestion of setting mortars, which was not present in the acid-digested filtrate of the pointing mortar.

The most startling microstructural feature found in all three setting mortars but not in the pointing mortar is scattered, very fine reddish-brown residual calcined clay (brick dust) particles, varying in sizes from 600 to less than 45 microns, which are separate from reddish-brown ferruginous matrix in some ferruginous shale and siltstone grains in sand but are indicative of intentional addition of a calcined clay component as brick dust at a subordinate proportion to the dominant dolomitic lime binder. The purpose of addition of these fine-grained, dominantly amorphous aluminosilicate calcined clay particles in the lime binder is to encourage pozzolanic reactions of amorphous aluminosilicate components of calcined clay particles with the lime to form calcium-silicate hydrate

and calcium-aluminum-silicate hydrate components, which would densify the paste compared to a carbonated lime paste. Use of such calcined clay was common in many early 19th century masonry structures mostly across Europe and America.

A close examination of many residual calcined clay particles showed dominantly amorphous nature with verry little quartz or other mineral grains, where the original clay component used during calcination process was very rich in the plastic component of clay (optically isotropic, e.g., amorphous clay matrix) with very little non-plastic component (which are optically birefringent, e.g., fine-grained quartz). A few calcined clay particles showed formation of cristobalite, indicating a calcination temperature as high as 1470ºC.

Many residual calcined clay particles showed a dense rim of paste around, which are stained reddish-brown from leaching of iron oxide during lime-calcined clay pozzolanic reaction, and subsequently carbonated. Densification of paste immediately around such calcined clay particles from lime-pozzolana reactions have prevented the densified paste rims from leaching even when the dominant paste matrix away from those particles showed extensive leaching. This indicates the importance of using such calcined clay pozzolans in historic lime mortars to overall densify the paste microstructure, and mortar to make them more durable than the straight lime mortars. Romans have mastered this technique to create many durable lime-pozzolana masonry structures, where aluminosilicate glass in volcanic ash was used as the pozzolanic source.

Based on the proportions of leftover remains of scattered calcined clay pozzolans in all three setting mortars, samples SET-3 and SSB-3 from east and south walls, respectively, showed an overall higher abundance of calcined clay component in the original binder compared to the amount in SWM-2 from the west wall mortar. Pointing mortar, as mentioned, showed no evidence of intentional addition of calcined clay in the binder, which is the reason for its medium gray color tone as opposed to reddish-brown color of setting mortars.

Fine-grained, porous, variably and severely carbonated paste, patches of optically isotropic leached paste areas, occasional lime lumps, and most importantly fine, discontinuous carbonation shrinkage microcracks – these four telltale microstructural features of an altered historic lime mortar are all present in the setting bed mortars. Rings of carbonation products around leached areas of paste are seen, indicating carbonation of re-precipitated lime after dissolution from the leached areas. Bright golden yellow interference colors of such re-precipitated secondary calcium carbonate rings around dark optically isotropic leached paste areas and sand grains are appeared as ‘rings of fire’ while observing the features in a petrographic microscope at cross polarized light mode.

By contrast, paste in the pointing mortar showed an overall homogeneous appearance, which is very similar to a carbonated lime paste in a historic lime mortar. As mentioned, there is no evidence of any residual hydraulic phase (e.g., residual belite and interstitial dark brown ferrite skeletons) found in the paste, which are common in many historic hydraulic lime mortars, which indicates use of a rather non-hydraulic to feebly hydraulic dolomitic lime binder. The feebly hydraulic nature and dolomitic nature of lime were determined from SEM-EDS studies of paste where the presence of some silica and noticeable magnesia contents confirmed their potential light hydraulicity and dolomitic nature, respectively. Subsequent thermal analysis has confirmed the use of dolomitic lime from brucite, and its carbonation product (magnesite) which are common hydration and subsequent carbonation products of a dolomitic lime binder.

An interesting microstructure found in the carbonated lime paste in the pointing mortar are denser globules of 0.05 to 0.1 mm size, which from SEM-EDS studies are found to have an essentially similar composition as the rest of the

paste except in having a slightly higher silica and alumina (hydraulicity?) contents than the rest of the overwhelming dolomitic lime paste. Perhaps the original silica-alumina-based impurities in otherwise relatively pure dolomitic limestone feed has formed such isolated nucleation sites of a denser paste in the globules than elsewhere even though no trace of any residual hydraulic phase was found within the globules.

Both setting and pointing mortars are non-air-entrained, which is not unusual for their reported early 19th century derivations.

Besides the ubiquitous calcium carbonate 'secondary' deposits in the leached and carbonated areas of paste in setting mortars which were re-precipitated after dissolution of original calcium carbonate products of carbonated lime binder, some other carbonated products are detected at minor to trace amounts in some void spaces e.g., short prismatic to lath-shaped deposits of trona, and fibrous highly birefringent deposits of thaumasite, and gypsum. Subsequent SEM-EDS studies, thermal analysis, FTIR, and XRD studies, however, could not detect their identity for their overall low abundance.

Extensive SEM-EDS analyses were done on the paste fractions of mortars along with residual calcined clay and other reddish-brown grains, and coatings on sands. Results were eventually plotted in various oxide variation diagrams to depict their compositional differences. In the CaO vs. MgO plot, paste from the pointing mortar showed a distinct compositional space in having the highest MgO (50-60%) amongst all phases analyzed and intermediate CaO (between 20 and 40%) indicating use of an original dolomitic lime binder, which had a characteristically higher CaO than MgO but during service a portion of lime has been leached out thus reducing the overall CaO content lower at the expense of MgO (CaO/MgO <1). Restricted composition of pointing mortar paste indicates its overall compositional homogeneity compared to variably leached paste in three setting mortars. By contrast, paste from all three setting mortars showed negligible lime in the severely leached areas in having high MgO contents (CaO/MgO <<1) as opposed to a range of CaO contents in partially leached and variably carbonated paste areas (carbonated paste areas include both the original carbonated paste as well as carbonates formed from secondary precipitation after leaching of lime). Lime lump showed overall compositional similarity to the original carbonated paste.

In the SiO_2 vs. Al_2O_3 plot, paste from the pointing mortar again showed a distinct compositional space in having the lowest SiO_2 amongst all phases analyzed but a detectable amount ranging from <10 to 20%, indicating use of a feebly hydraulic dolomitic lime binder produced from calcination of a relatively pure dolomitic limestone feed. Paste from three setting mortars showed a large range of silica and alumina contents where the leached areas of paste showed consistently higher silica and alumina than the carbonated areas, which indicate (a) use of an original calcined clay binder, which was the main source for Si and Al in the paste as opposed to Ca and Mg from the dolomitic lime source, as well as (b) leaching of lime from the paste thus enriching the Si-Al-Mg contents in leached areas relative to lime. Lesser albeit noticeable silica and alumina in the partially leached to carbonated areas of paste approached the original Si-Al contents in the mixed subordinate calcined clay and dominant dolomitic lime binder components, where the former provided the silica and alumina and the latter provided lime and magnesia.

In the CaO vs. SiO_2 plot, paste from the pointing mortar again showed a distinct compositional space in having the lowest silica (<10-20%) at 20-40% lime, again indicating use of a feebly hydraulic dolomitic lime binder produced from calcination of a relatively pure dolomitic limestone feed. Paste from three setting mortars showed negligible

lime at appreciable silica contents for the leached areas as opposed to variable and noticeable lime in the partially leached and carbonated areas.

In all these oxide variation diagrams reddish-brown coats showed overall compositional similarity to reddish-brown calcined clay grains and ferruginous matrixes of sand grains but have more heterogeneity in coats (higher Mg) due to leaching and interactions with adjacent paste during service. Reddish brown coats showed consistently higher silica and alumina (along with iron, not shown in the plots) from calcined clay components, along with lowest virtually non-detectable lime, which is compositionally similar to the overwhelming occurrences of leached paste (in the latter, silica and alumina contents were derived not from the coatings on sand or sand per se, but from the original calcined clay binder, now left as optically isotropic gelatinous aluminosilicate mass).

As opposed to single oxide plots, when oxides were combined, e.g., CaO+MgO (i.e., total contribution from dolomitic lime binder components) vs. $(CaO+MgO)/(SiO_2+Al_2O_3)$ i.e., relative proportions of contributions from dolomitic lime and calcined clay binder components, an excellent trend was found amongst all variants of paste from setting and pointing mortars, where leached paste in setting mortar and non-leached carbonated paste in pointing mortar defined the two extreme end members. Pointing mortar paste showed the highest CaO+MgO with some variations from some leaching of lime, as well as the ratio of lime-magnesia over silica-alumina from use of only dolomitic lime binder without any calcined clay, whereas leached paste showed the lowest lime-magnesia (mostly magnesia left after lime leaching) and lowest lime-magnesia over silica-alumina ratio from leaching of lime, enriching leached areas in silica and alumina originally contributed from the calcined clay binder. Carbonated and partially leached paste in setting mortars unoccupied the intermediate positions in the curvilinear trend. Similarly, in the $SiO_2+Al_2O_3$ (i.e., total contribution from calcined clay binder) vs. $(CaO+MgO)/(SiO_2+Al_2O_3)$ i.e., relative proportions of contributions from dolomitic lime and calcined clay binder components), a reciprocal trend was obtained, as expected, from highest silica-alumina in the leached paste of setting mortar to lowest silica-alumina and highest lime-magnesia in the feebly hydraulic dolomitic lime binder in pointing mortar.

A perfectly linear trend was found amongst all measured components of paste when plotted in lime + magnesia vs. silica + alumina, where leached paste from setting mortar and carbonated paste from pointing mortar occupied the extreme ends. Carbonated paste in setting mortar showed a large range from the pointing mortar paste end depending on various degrees of lime leaching. A very similar trend was found when lime was plotted against magnesia + silica + alumina where paste in pointing mortar occupied an intermediate space between carbonated and leached paste areas in setting mortar. Due to very high silica + alumina content in the leached paste, total magnesia +silica + alumina content in leached paste was higher than the values in the paste in pointing mortar.

In the silica + alumina vs. magnesia plot, carbonated paste and lime lump in setting mortar deviated from a linear tread established by the leached paste and pointing mortar paste due to relatively lower silica + alumina content in carbonated paste than leached areas.

When lime, silica, and alumina contents were plotted against the cementation indices (CIs) of paste, which is a measure of relative hydraulicities of various binders originally used by Eckel (1922) for historic binders, and calculated as [(2.8×silica)+(1.1×alumina)+(0.7×iron)/(lime+1.4×magnesia)] all binder components showed < 5 CI, whereas reddish brown coats, reddish brown grains, and shale particles in sand showed CIs between 5 and 10. Although CI cannot be used for non-binder components, such plots indeed effectively separated all non-binder components in having very high CIs than the binder ones. Amongst the binder components, paste from pointing

mortar showed the lowest paste-CI of all binders examined, and leached areas of paste in setting mortars showed the highest CIs from highest silica and alumina contents.

In summary, SEM-EDS compositional analysis of paste from three setting mortars and one pointing mortar showed: (a) a lime-leached component of paste in setting mortars characterized by negligible lime and high silica, magnesia, and alumina (Si>Mg>Al), and, as a result, an average paste CI of 3.26, (b) variably carbonated and partially leached paste areas in setting mortars having average paste-CI of 1.66, and (c) carbonated areas of paste in setting mortars having Ca>>Mg>Si>Al and paste CIs <1 (average 0.85). Lime lump showed high Ca and Mg (Ca>>Mg, Si>Al) from mixed calcined clay and lime binders. Lime lumps are the best candidates to determine the original compositions of binders, which is judged to be a two-component mix having a higher proportion of dolomitic lime (source for Ca and Mg) and a subordinate proportion of calcined clay (source for Si and Al).

Reddish-brown aluminosilicate coats on sand grains are essentially similar in compositions to isolated occurrences of fine reddish-brown aluminosilicate calcined clay and other grains as well as reddish-brown matrix in ferruginous shale-siltstone sand particles, except some noted differences. Reddish-brown coats on sand grains showed an overall lower silica, and higher magnesia contents than reddish-brown residual calcined clay grains, which is due to chemical interactions of coats with the adjacent paste during service. Consistently higher magnesia contents in almost all reddish-brown coats analyzed compared to the residual calcined clay grains are the best chemical signatures of formation or at least chemical evolution of these coats from chemical interactions with magnesia-rich dolomitic lime paste with calcined clay binder component during service. Chemical interactions in coats have reduced the overall chemical variability seen in the isolated reddish-brown grains. Therefore, reddish-brown coats seen on sand grains could not have formed on sand prior to their incorporation in mortars (besides their occurrence on crushed angular fine quartz sand grains does not necessarily support the notion of their formation as clay coats on sand in the stockpile).

SEM-EDS analyses of a few shale grains in sand showed the characteristically high Si, Al, Mg, and K contents, all of which are determined (from subsequent XRD studies) to be from illitic clay in shale.

The high silica and alumina contents in leached areas of paste from the clay component of binder showed overall homogeneous compositions. Such compositional homogeneity of silica and alumina despite leaching, along with ultrafine size of clay components indicate the source of silica and alumina in paste could be either or a combination of separate addition of calcined clay (an amorphous aluminosilicate mass, which has been ground to fine size) and/or brick dust where the former option is more plausible than the latter since brick dust component should have been easily identified in paste per se in optical microscopy of thin sections of paste from fine, angular, reddish-brown brick fragments, which are not found (the reddish-brown grains in paste are sand-sized and contained subrounded to rounded grains most plausibly derived from the ferruginous components of sand).

X-ray diffraction patterns of both setting mortar and pointing mortar showed the presence of illitic clay from the argillaceous components of sand, dominance of quartz from the dominant siliceous component of sand, and minor calcite from leached and carbonated paste. Minor muscovite and albite feldspar are detected from sand, hematite from reddish-brown iron oxide in sand, and brucite from use of dolomitic lime component in the binder. Calcination of an illitic clay component can produce Mg-Si-Al based calcined clay pozzolan to be used with lime where Si and Al occupy the tetrahedral sites and Mg, Al, Fe occupy the octahedral sites in illite crystal structure.

Major element oxide compositions of mortars were determined from pressed pellets of pulverized (< 45-micron size) bulk mortars in XRF. Dominance of silica (53-58% in setting mortar and 46.3% in pointing mortar) reflect corresponding dominance of siliceous components in sand particles, as also seen in optical microscopy and XRD analysis of the mortars. Lower lime contents (7%) in setting mortars compared to the pointing mortar (11%) is consistent with: (a) leaching of lime in setting mortars, and (b) addition of lime with a clay component in the setting mortar binder where clay also increased the bulk alumina (5-6% as opposed to 2.7% in pointing mortar) and iron contents (2.5-3% as opposed to 2% in pointing mortar). Magnesia content is higher in the pointing mortar (8.2% as opposed to 6-6.5% in setting mortar) for dolomitic lime only binder in pointing mortar. Alumina, iron, and alkalis are contributed from both sand and paste. Sulfate is from cement paste, which is negligible (<0.01%) in setting mortars but 0.4 percent in pointing mortar. Soluble silica contents are from the silica-rich amorphous leached areas of paste in setting mortar, and not from any hydraulic phase.

Chemical (gravimetric) analysis showed acid-insoluble residue contents of 55-70% in setting mortars but 57.5% in pointing mortar. Due to the presence of only siliceous and argillaceous/ferruginous components and no calcareous components in sands (as determined from petrography), the determined acid-insoluble residue contents are considered representative of the overall sand contents of the mortars.

Losses on ignition of separate aliquots of pulverized mortars to 110ºC, 550ºC, and 950ºC correspond to free water, combined (hydrate) water, and degree of carbonation, respectively. The losses on ignition at 550ºC correspond to the water contents from dehydration and dehydroxylation of clay and hydrous and some carbonate phases. The loss on ignition at 950ºC corresponds to degree of carbonation of carbonated paste. Results from losses on ignition were similar to the ones determined from thermal analyses.

Amongst the three setting mortars, samples from east and south walls are very similar to each other in terms of major oxide compositions, acid-insoluble residue contents, and losses on ignition results but slightly different from the setting mortar from the west wall.

Thermal analyses of all three setting mortars showed very consistent and similar thermal decompositions indicating their overall compositional similarities in terms of the phases being decomposed. Mass loss at <100ºC corresponds to loss of free water, whereas loss at 210 to 250ºC range correspond to dehydroxylation of hydrous phases, including the amorphous gelatinous leached paste in setting mortars. Pointing mortar showed overall similarities in thermal behaviors with the setting mortars up to a temperature of 300ºC after which it showed no appearance of an endothermic peak, which is common for dehydroxylation of brucite in dolomitic lime mortars occurring at temperatures between 300 and 350ºC. Despite the detection of high magnesia and lime in the paste from the use of a dolomitic lime binder, this lack of appearance of a brucite dehydroxylation peak suggests severe carbonation of brucite to other carbonate-hydrate phases of magnesia, such as magnesite or hydromagnesite, where latter usually decomposes over a temperature range of 220 to 550ºC. Loss of mass of pointing mortar at 400 to 415ºC range is twice the corresponding mass loss of setting mortar indicating a higher proportion of portlandite (slaked lime) component of the original slaked dolomitic lime putty that has remained in the pointing mortar. Almost 10 times higher loss of mass of pointing mortar at 490 to 520ºC range (4.8%) compared to the corresponding loss of setting mortar (0.5%) confirmed a higher abundance of magnesite component formed from carbonation of the original brucite (the slaked hydration product from original slaking of dolomitic lime putty) in the pointing mortar than the dolomitic lime plus calcined clay mixed binder in the setting mortars. Finally, degree of decarbonation of calcite

in all four mortars are similar at 750 to 775ºC range corresponding to 5 to 7% mass loss. Corresponding calcite contents are determined to be 7 to 12%, which are consistent with calcite contents found from XRD studies.

Concentration of water-soluble salts in the setting and pointing mortars were determined by ion chromatography after digesting about a gram of pulverized mortar in deionized water for 30 minutes at a temperature below boiling, followed by continued digestion in water at the ambient laboratory condition for 24 hours. The filtrates were analyzed by ion chromatography for water-soluble chloride and sulfate salts that are potentially deleterious to long-term performance of mortars. Filtrates shows the presence of negligible but detectable chloride (250 ppm, 350 ppm, and 540 ppm) and sulfate (120 ppm, 140 ppm and 160 ppm) ions in SET-3, SWM-2, and SSB-3, respectively, indicating the absence of any major chloride and/or sulfate salt source in the setting mortars. Pointing mortar showed the opposite result i.e., lower (150 ppm) chloride and higher (320 ppm) sulfate due to the presence of higher sulfate in the original dolomitic limestone feed.

In summary, the early 19th century setting and pointing mortars examined here are determined to be representative of many common historic lime or calcined clay-lime mortars, which do not contain any Portland or masonry cement binders, hence are not representative of any modern-day e.g., ASTM C 270 mortars. The lime binder component is found in all mortar types examined, which in setting mortars showed variably degrees of leaching of lime from the original lime-magnesia-silica-alumina based binders leaving amorphous or gelatinous residues of silica-alumina-magnesia rich patches of leached areas of little or no cementitious properties as a skeleton of the original paste where lime mostly found as secondary precipitates after leaching. Lime and magnesia components in the binder were contributed from the use of a magnesian or dolomitic lime binder, which, in turn, was produced from calcination of a relatively pure magnesian or dolomitic lime with very little impurities (silica, alumina, iron) i.e., to not produce a calcium silica-aluminate-based hydraulic phase typically found as residual hydraulic phases in many historic hydraulic lime binders, which are produced from calcination of an impure dolomitic limestone. Overall paste on the setting mortars are porous, fine-grained, skeletal microstructures of leached lime patches with secondary carbonate precipitates, carbonation shrinkage microcracks in lime-rich less-leached areas, residual lumps of unmixed lime, and other common microstructural features of historic lime mortars.

A separate calcined clay (brick dust) component was added in subordinate amount to lime in setting mortars, which was very fine-grained and intimately mixed with lime to create a relatively homogenous mix of lime-magnesia-silica-alumina based original binder from which after lime leaching a relatively homogeneous gelatinous mass of magnesia-silica-alumina-based leached areas were left across the microstructures of setting mortars. All three setting mortars from east, west, and south interior walls showed evidence of lime leaching and enrichment of silica-alumina-magnesia-based leached amorphous areas in the microstructures.

The reddish-brown color tones of interstitial paste and the overall setting mortars are found to be contributed from the iron impurities in clay in the original calcined clay binder, along with leaching of reddish-brown ferruginous components of sand particles. Many angular to subangular to rounded sand particles in both coarser and finer fractions of sand showed reddish-brown clay coats which are determined to be magnesia-silica-alumina-iron-based compositions where silica, alumina, and iron components came from the clay binder and reddish-brown ferruginous components of sand whereas the magnesia component came from prolonged interactions with the paste during leaching, which became the storehouse for magnesia. Hence, the reddish-brown coats on sand particles are not necessarily incorporated as clay coats or contaminants from sand but more probably from its evolution during prolonged chemical interactions (e.g., leaching) with paste.

Absence of a clay component, and use of a non-hydraulic or feebly hydraulic dolomitic/magnesian lime binder mixed with colorless to light gray very fine crushed dominantly silica-based sand in the pointing mortar has produced the typical light gray color tone of paste and overall mortar seen in many historic dolomitic lime mortars. Pointing mortar is relatively denser and harder due to lesser amount of leaching of lime than setting mortars. Some lime leaching has still occurred reducing the overall lime/magnesia ratio in paste from >1 in original binder to <1.

Due to extensive leaching of lime in setting mortars, along with use of a calcined clay binder component with lime, traditional methods of calculations of mix components in masonry mortars as described in ASTM C 1324 are not possible. Procedures of mix calculations from petrography and chemical analysis as described in ASTM C 1324 are applicable to modern-day cement-lime or masonry/mortar cement mortars prepared according to the procedures of ASTM C 270 where modern-day cement and lime binder components have far restricted chemical compositions for their productions under far stricter quality controls than their historic analogues. For example, modern Portland cements have a very restricted silica contents of 20-22%, and lime contents of 63-65% than their historic natural cement analogues, which showed a large range of compositions for use of argillaceous dolomitic limestones of different clay-silica impurities in raw feeds. Modern hydrated limes are produced by high-temperature slaking of quicklimes than the traditional historic lime production in putty form where original limestones being calcined contained various impurities to produce lime with a range of hydraulicities. Therefore, no single chemical parameter for a binder can be used for historic mortars to calculate proportion of that binder.

The petrography-plus-chemical based combined approach, however, can still be extended to historic lime mortars to a certain extent with some reasonable assumptions of the properties historic binders as long as the mortar is not extensively altered to decompose the original binder compositions, and historic records of the original binders show more or less restricted chemical compositions to be used for mix calculations, e.g., to determine the hydraulic binder content from soluble silica content in the mortar assuming no additional source of soluble silica besides the historic binder. Limitation of this approach of historic cement content calculation from soluble silica content of mortar, as mentioned, lies in having a large range of soluble silica contents of historic cements for use of raw feeds of large range of impurities to produce large range of hydraulic phases, which would contribute to the soluble silica budget from subsequent hydration. This limits use of an 'assumed' silica content, e.g., use of 20-22% silica for calculation of Portland cement content in modern cement-lime mortars from soluble silica content in modern mortars. Presence of siliceous sand and no acid-soluble (calcareous) components in sand helps to determine the sand content directly from the acid-insoluble residue after digestion, from which binder content can be estimated from the rest (acid-soluble component) with the help of information obtained from petrography. Other alternative approaches such as determination of dolomitic lime content from the determined non-carbonated brucite content from thermal analysis, hydraulic lime or cement content from soluble silica from gravimetry and modal silica content in paste from SEM-EDS analysis, non-hydraulic calcitic lime content from degree of carbonation at loss on ignition at 950ºC, etc. are sometimes used for determination of historic binder contents, which, again is dependent on the degree of alterations and decompositions of historic mortars during service.

Compared to the estimation of binder contents, however, sand contents are relatively straightforward especially when sand is dominantly siliceous in composition, as mentioned, where acid-insoluble residue contents roughly correspond to the sand contents of mortars, as in the present case for all mortars examined.

In the absence of a reliable method of determination of mix proportions of historic mortar, especially after a century-long period of alternations is to examine the microstructures from petrography and SEM-EDS analysis, determine

the original binders and sand used, qualitatively assess the extent of alterations, and from SEM-EDS based determination of paste compositions from least altered areas or samples estimate relative proportions consistent with the historical record of binder proportions used.

Taking into considerations of all the information obtained from petrography, chemical and other techniques, the best 'estimation' of relation proportions of mortar ingredients used during mixing of setting mortars are 1-part dolomitic lime to less than ¼-part calcined clay to 2 to 2½-part the total sum of calcined clay and lime components of binder. This recipe is very similar to the ones used during calcined clay-lime based historic mortars from the early 9th century across eastern US and the microstructure produced from such proportions, after century-long carbonation, leaching, and alterations would not different noticeably from the setting mortars seen in the present case. For the pointing mortar, a recipe of 1-part feebly hydraulic dolomitic lime or an NHL of NHL 2 to NHL 3.5 to 2-part sand would produce a similar mix. The best mix for both mortar types should be tested with multiple trials with mock-up batches over small test areas. Due to interior locations of setting mortars protected by a separate pointing mortar at the exterior, however, an exact match to the existing setting mortars are not crucial.

Mixing of lime with clay at various proportions changes the overall color tones of mortars in various shades of reddish-brown tones and variable hardness. So, to match with the existing interior clay-lime mortars similar to the examined three setting mortars, an appropriate clay-lime or pigmented (iron oxide or fine brick dust based) lime mockup mortars can be tried over a small test area. The mortar, however, can be protected with an exterior feebly hydraulic dolomitic lime mortar as the one seen in the pointing mortar. A natural hydraulic lime (e.g., NHL 2 or 3.5) can be tried for the exterior pointing mortar as an alternate to dolomitic lime. Binder-to-sand volumetric ratio should be restricted to 1-part total binder to maximum 3-part sand, which will be consistent with most historic mortars' proportions used during the 19th century.

Overall appearance of the final mortar, however, would depend on a match on sand, which constitutes the dominant proportion of the mortar. Sand to be used should be (a) siliceous in composition (silica sand based), which should rather not contain any argillaceous or ferruginous components to produce reddish-brown stains if the mortar mixes contain a reddish-brown iron oxide or brick dust-based pigment; (b) match in color to the color of sand in the examined mortar; (c) preferably be from similar sources; (d) be free of any debris, unsound, or any potentially deleterious constituents such as mica flakes; (e) conform be relatively finer than the size requirements of ASTM C 144 for masonry sand since sand in both setting and pointing mortars are finer than the modern ASTM C 144 sand; (f) not exceed maximum 3 times the sum of separate volumes of binder components; and (g) be durable.

An iron oxide or brick dust-based pigment can be added to substitute the reddish-brown setting mortars as long as dosage rate can be determined from trial batches for a good match. For its interior location inside the exterior pointing mortar, however, a perfect match may not be necessary. Use of Portland cement or Portland cement-based blended cement or slag cement should be avoided.

Initial rate of absorption (suction), and compressive strength of host stone masonry units are also important to determine the suitable mortar type, e.g., water retention properties (controlled by lime content) of mortar should be matched with the suction properties of masonry units.

Due to atmospheric weathering and alterations, an exact match in color to the existing setting or pointing mortars may not be possible, which, even if possible, could alter in future due to continued atmospheric weathering in the presence of oxygen, moisture, and other elements.

INTRODUCTION

This report provides results of detailed laboratory examinations of three setting mortars and one pointing mortar sample from the Eastern State Penitentiary in Philadelphia, Pennsylvania.

BACKGROUND INFORMATION

The Eastern State Penitentiary is a former American prison in Philadelphia, Pennsylvania. Constructed in 1822, the prison was operational from 1829 until 1971. At its completion, the building was the largest and most expensive public structure ever erected in the United States, and quickly became a model for more than 300 prisons worldwide. The prison is currently a U.S. National Historic Landmark. Figure 1 shows an exterior wall of the prison, and associated documentation, which are retrieved from the Wikipedia.

FIELD PHOTOS

Figure 2 shows key plan of the Eastern State Penitentiary with the location of the test areas highlighted in red. Figures 3 through 22 show field photos of conditions of mortar and adjacent stone masonry units on three walls of the penitentiary from where mortar samples were retrieved. A total of four samples provided for detailed laboratory examinations. Three setting mortar samples identified as SET-3, SWM-2, and SSB-3 were retrieved from the East, West, and South walls, respectively.

Figures 3 through 8 show setting mortar sample locations from the top, middle and bottom elevations of the east interior wall where mortars to be examined were exposed after removing the outer masonry units. Mortars from all three elevations show overall similarity in appearance in having soft to moderately soft to moderately hard reddish-brown mortars, which from the characteristic reddish brown color tones are similar to many pigmented lime, or, historic clay-lime mortars.

Figures 9 through 13 show setting mortar sample locations from the top, middle and bottom elevations of the west interior wall where mortars to be examined were exposed after removing the outer masonry units. Mortars from all three elevations show overall similarity in appearance to each other as well as to setting mortars from east interior wall in having soft to moderately soft to moderately hard reddish-brown mortars, which from the characteristic reddish brown color tones are similar to many pigmented lime, or, historic clay-lime mortars.

Figures 14 through 20 show setting mortar sample locations from the top, middle and bottom elevations of the south interior wall. Mortars from all three elevations show overall similarity in appearance to each other as well as to setting mortars from east and west interior walls in having soft to moderately soft to moderately hard reddish-brown mortars, similar to many pigmented lime, or, historic clay-lime mortars.

Figure 21 shows all three walls and locations of setting mortar samples from a total of nine elevations.

Figure 22 shows the central tower wall at link to cell block 5. A reportedly original pointing mortar sample CB6-Link was obtained from the grade at similar location in the cell block 6 link space.

The Exterior of Eastern State Penitentiary
(from: https://en.wikipedia.org/wiki/Eastern_State_Penitentiary)

The Eastern State Penitentiary, also known as ESP, is a former American prison in Philadelphia, Pennsylvania. It is located at 2027 Fairmount Avenue between Corinthian Avenue and North 22nd Street in the Fairmount section of the city. It was operational from 1829 until 1971. The penitentiary refined the revolutionary system of separate incarceration first pioneered at the Walnut Street Jail, which emphasized principles of reform rather than punishment. At its completion, the building was the largest and most expensive public structure ever erected in the United States, and quickly became a model for more than 300 prisons worldwide. The prison is currently a U.S. National Historic Landmark.

Figure 1: Internet photo and associated background information of the Eastern State Penitentiary from Wikipedia.

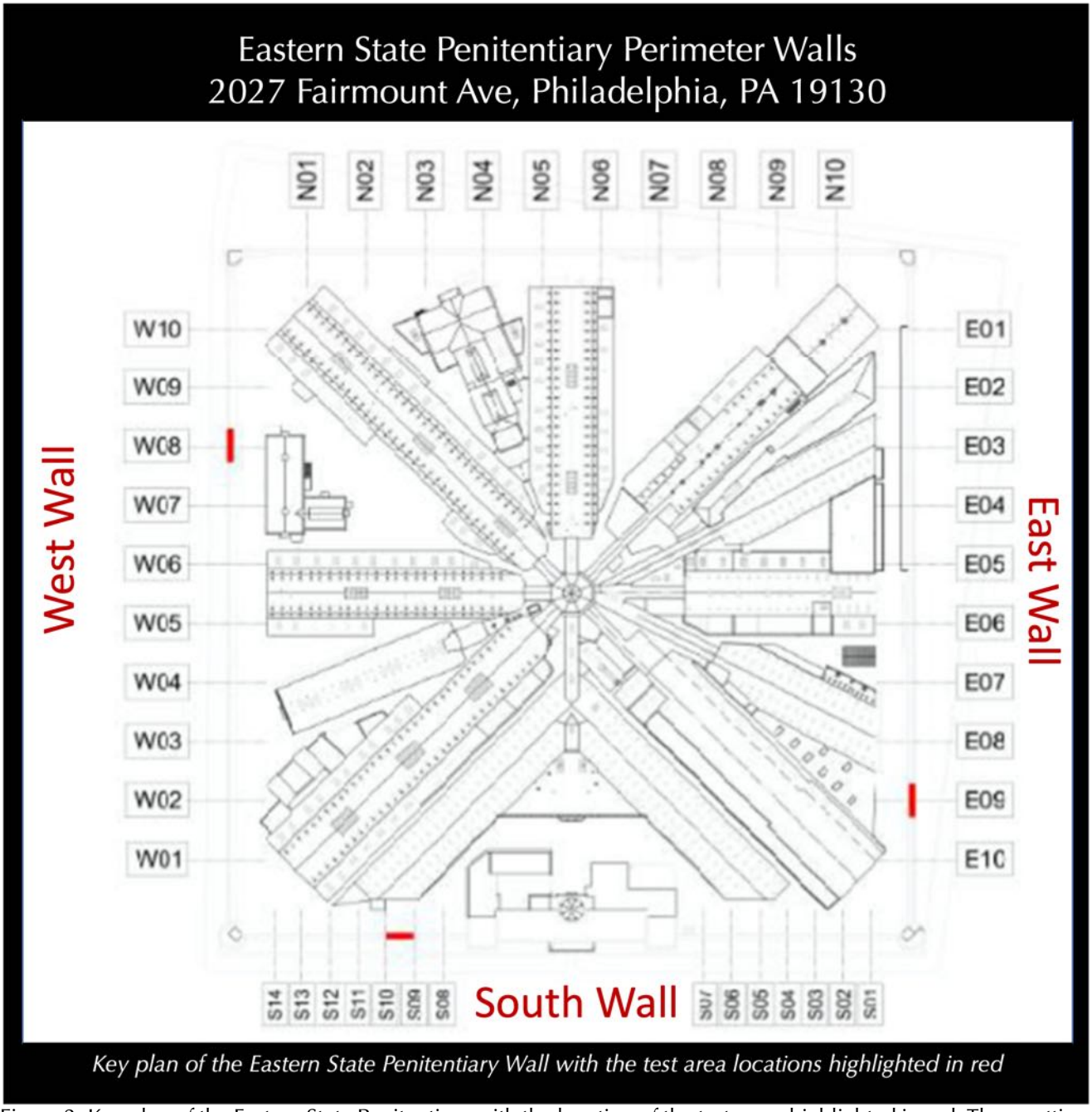

Figure 2: Key plan of the Eastern State Penitentiary with the location of the test areas highlighted in red. Three setting mortar samples identified as SET-3, SWM-2, and SSB-3 were retrieved from the East, West, and South walls, respectively. A fourth sample is received, which is believed to be an original pointing mortar, identified as CB6-Link, from the link between cell block 6 and the original center tower; this area was enclosed early in the construction of the penitentiary, and the tower pointing mortar is believed to be original.

Figure 3: Field photo of the east interior wall showing overall view of three probe locations (circled). Setting mortar sample SET-3 was retrived from the top probe. Next Figures 4 through 8 show details of individual probe locations.

Figure 4: Overall view of the bottom probe at east interior wall where interior reddish-brown mortar is seen.

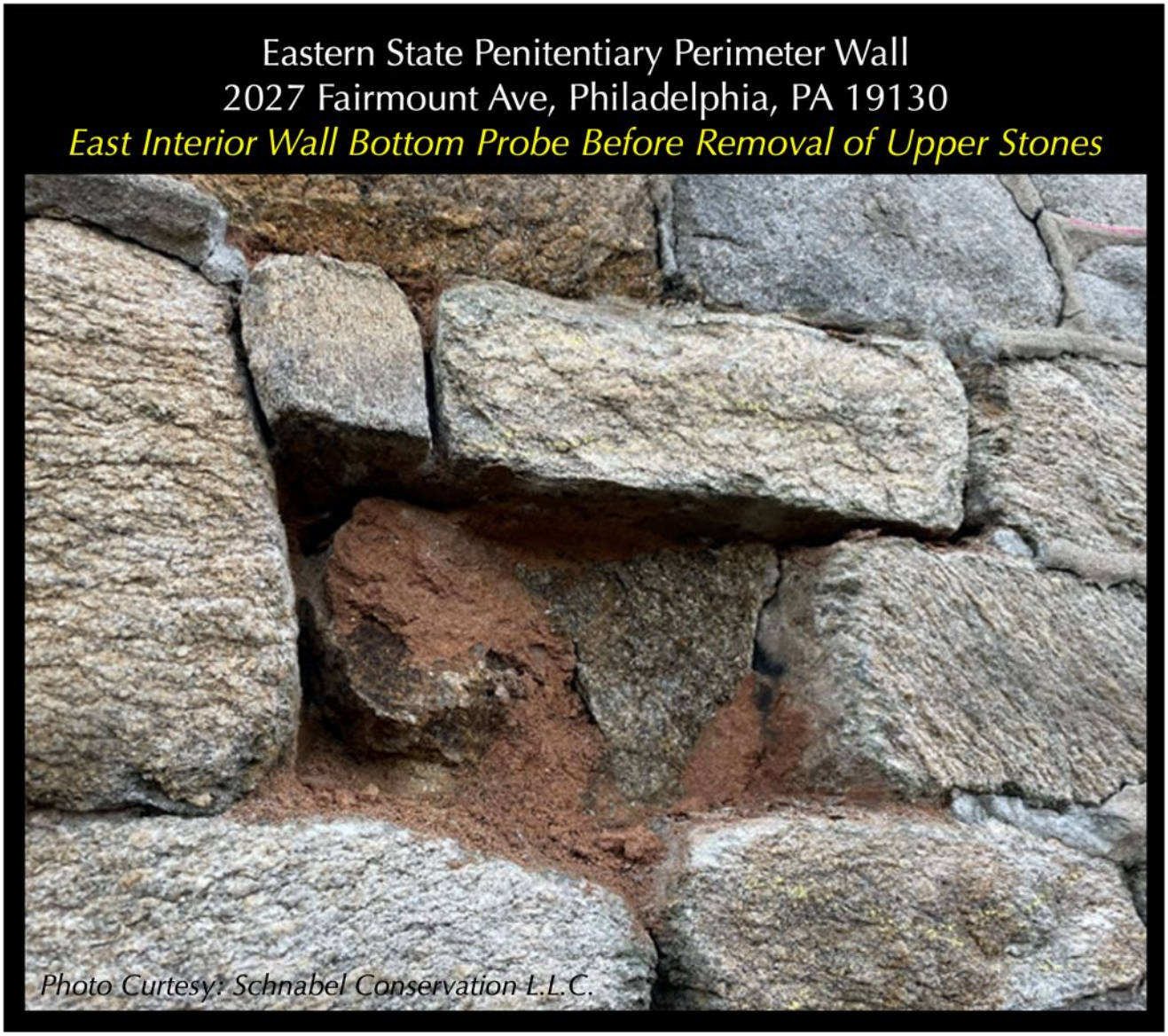

Figure 5: Overall view of the bottom probe at east interior wall before removal of upper stones where interior reddish-brown mortar is seen.

Figure 6: Overall view of the middle probe at east interior wall where interior reddish-brown mortar is seen, which shows similar appearance to the mortar seen in the bottom probe. Boxed area in the top photo is enlarged at bottom photo.

Figure 7: Overall view of the middle probe at east interior wall where interior reddish-brown mortar is seen.

Figure 8: Overall view of the top probe at east interior wall where interior reddish-brown mortar is seen, which shows similar appearance to the mortars seen in the bottom and middle probes.

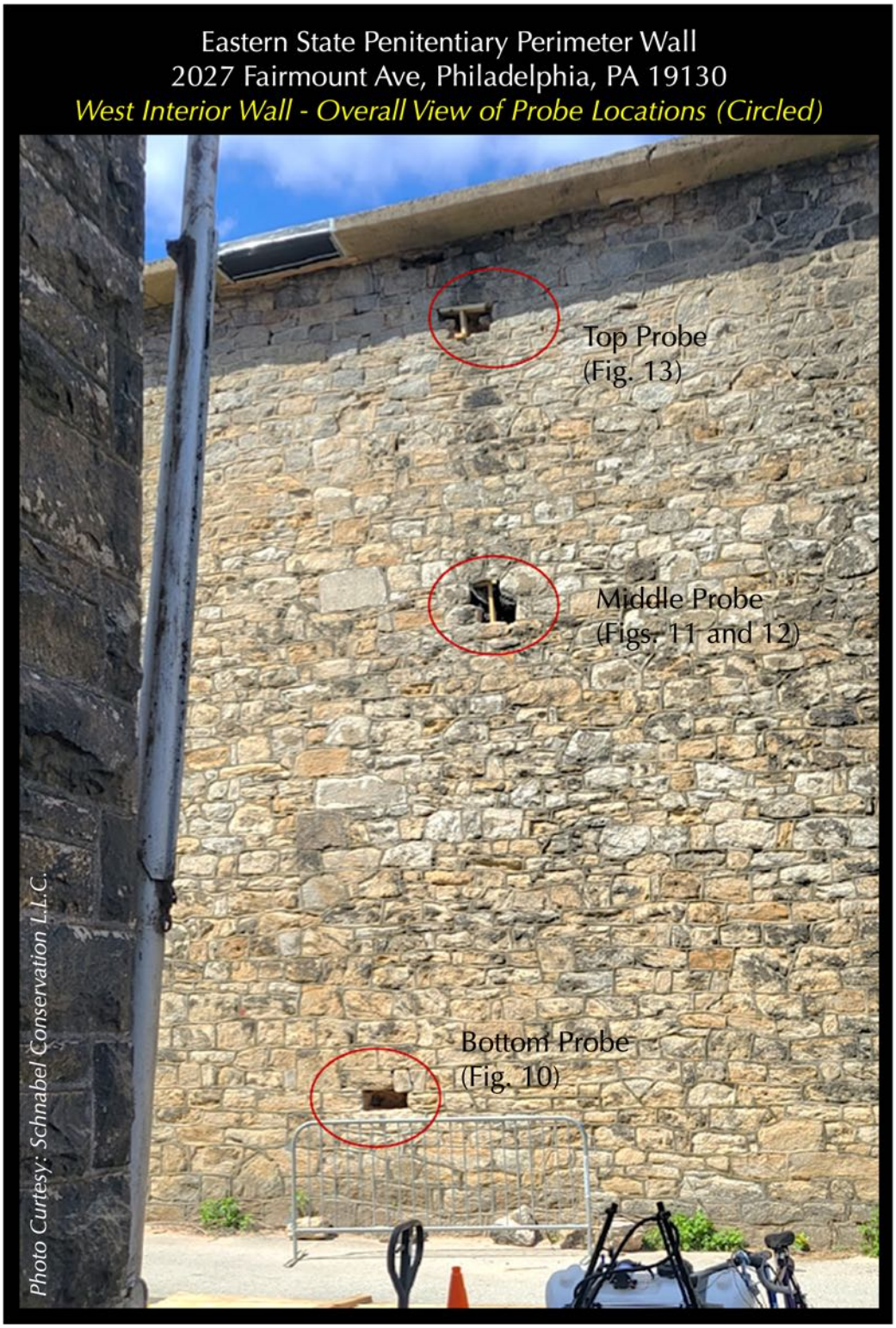

Figure 9: Field photo of the west interior wall showing overall view of three probe locations (circled). Setting mortar sample SWM-2 was retrived from the middle probe. Next Figures 10 through 13 show details of individual probe locations.

Figure 10: Overall (top) and right side (bottom) views of the bottom probe at west interior wall where interior reddish-brown mortar is seen, which shows overall similarity in appearance to the mortars seen in the east wall probes.

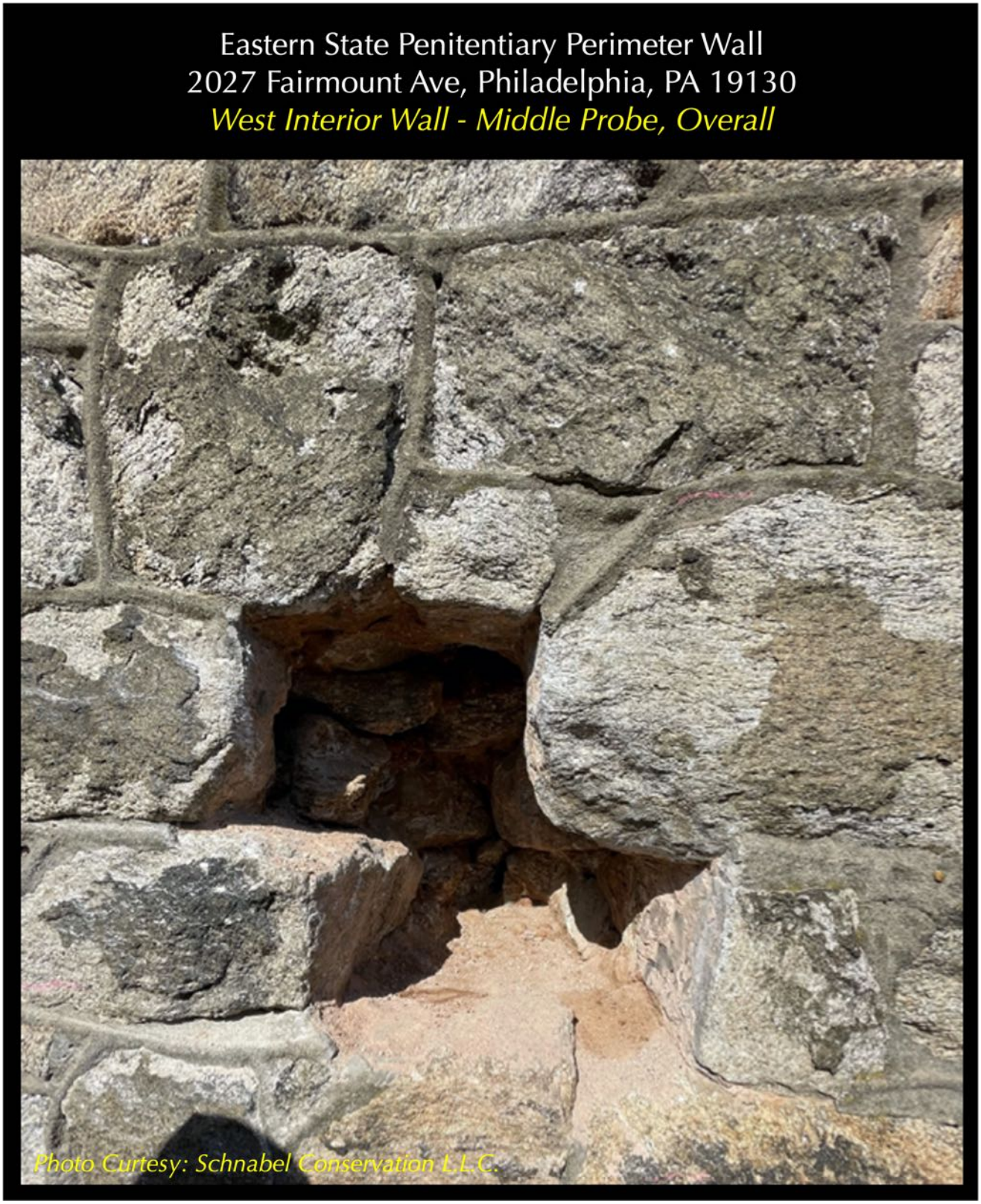

Figure 11: Overall view of the middle probe at west interior wall where interior reddish-brown mortar is seen. Sample SWM-2 was provided from this probe, which shows similar appearance as the mortar from the east wall probes, as well as the one from the bottom probe of west wall.

Figure 12: Close-up view of the middle probe of west interior wall from where Sample SWM-2 was provided. Notice similar appearance of the reddish-brown mortar as seen in the probes from the east wall as well as from the bottom probe of west wall.

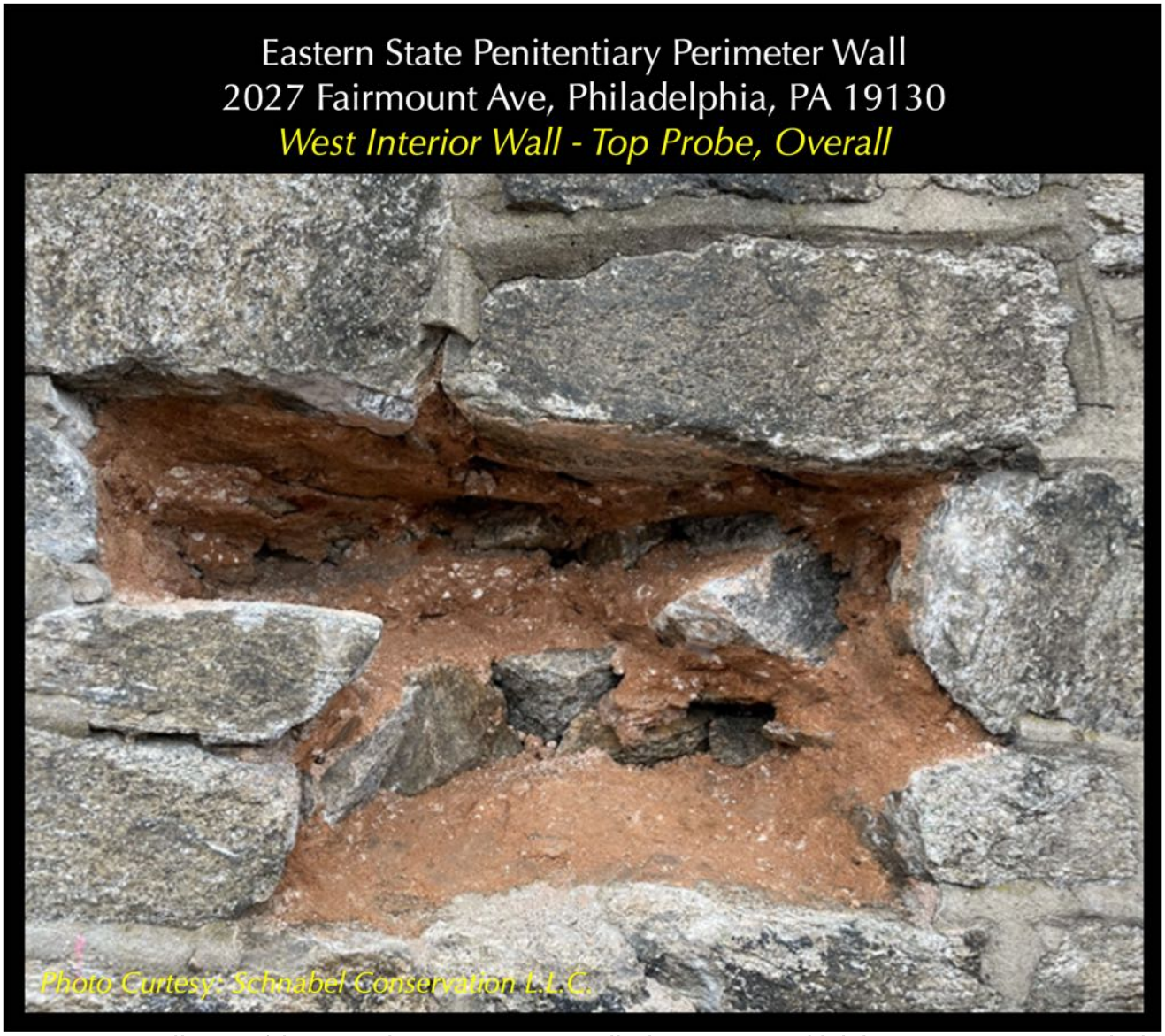

Figure 13: Overall view of the top probe at west interior wall where interior reddish-brown mortar is seen, which, again shows overall similarity in appearance as the mortars from east wall probes as well as the ones from the bottom and middle probes of this west wall.

Figure 14: Field photo of the south interior wall showing overall view of three probe locations (circled). Setting mortar sample SSB-3 was retrived from the bottom probe. Next Figures 15 through 20 show details of individual probe locations.

Figure 15: Overall view of the bottom probe of south interior wall where interior reddish-brown mortar is seen, which shows overall similarity in appearance to the mortars seen in the east and west walls. Sample SSB-3 was retrieved from this probe.

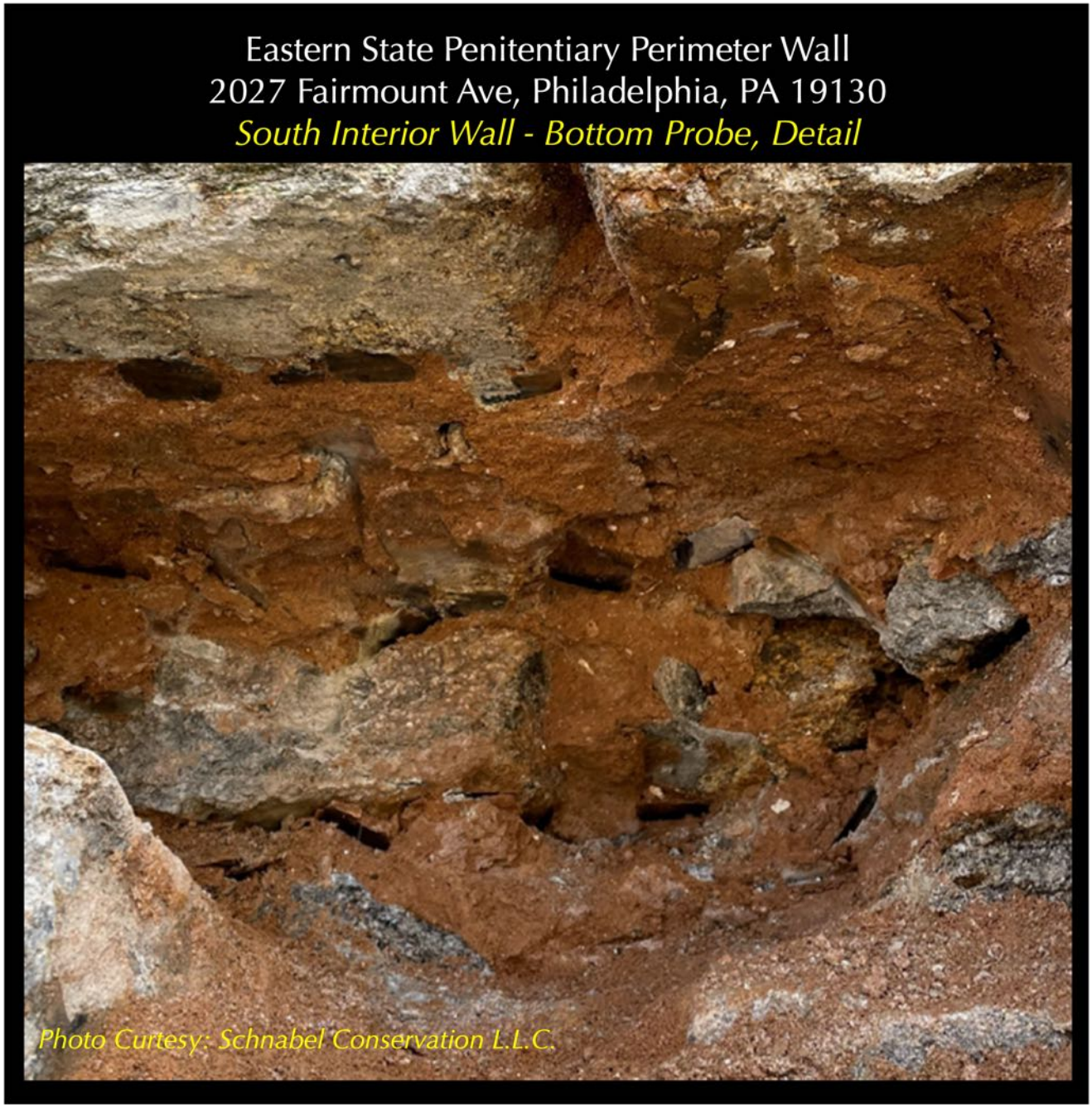

Figure 16: Close-up view of the bottom probe of south interior wall where interior reddish-brown mortar is seen, which shows overall similarity in appearance to the mortars seen in the east and west walls. Sample SSB-3 was retrieved from this probe.

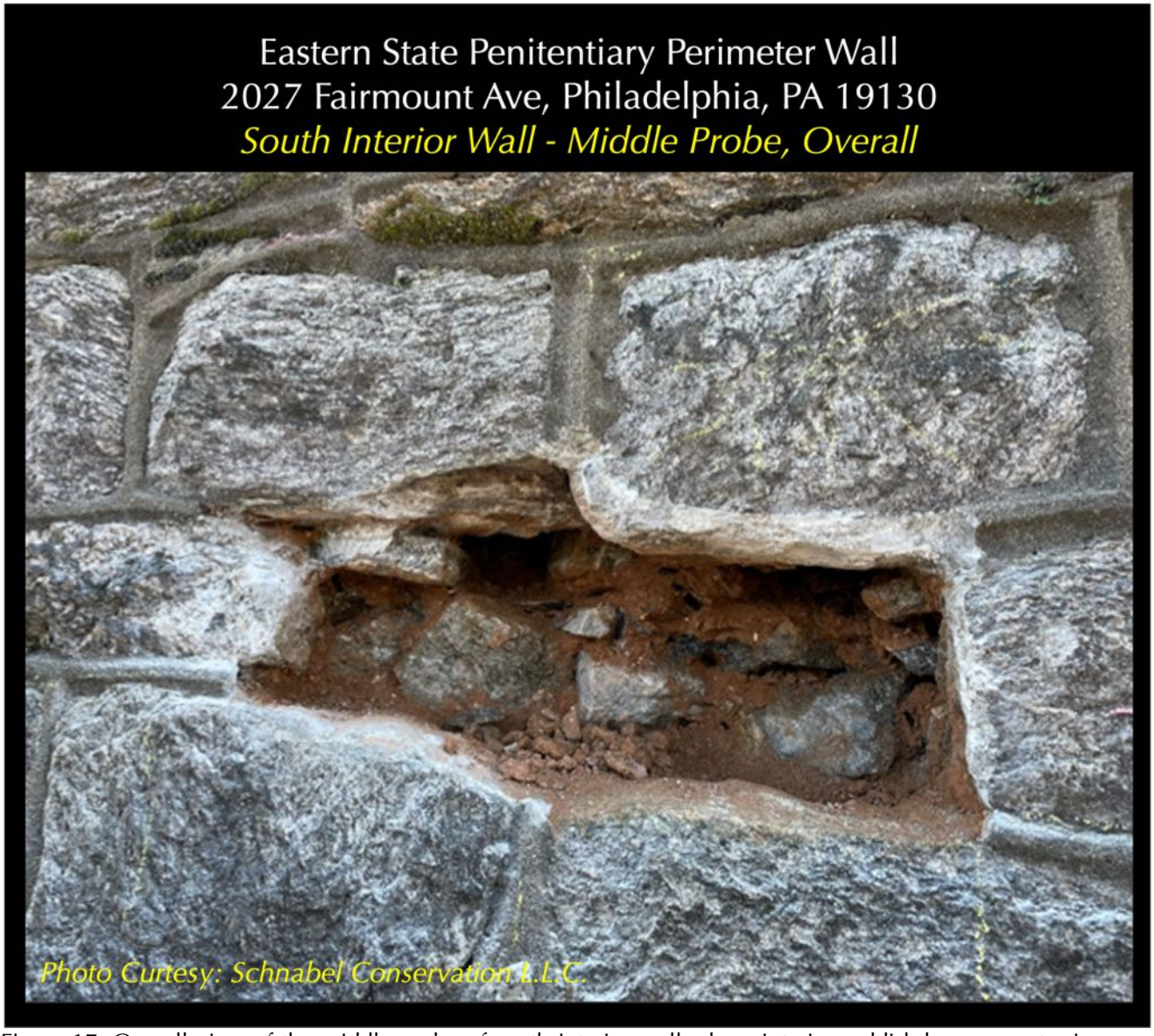

Figure 17: Overall view of the middle probe of south interior wall where interior reddish-brown mortar is seen, which shows overall similarity in appearance to the mortars seen in the east and west walls as well as the mortar from the bottom probe of this wall.

Figure 18: Right (top) and left (bottom) side of the middle probe at south interior wall showing reddish brown mortars in similar appearance to the mortars seen from the east and west walls as well as from the bottom probe of this wall.

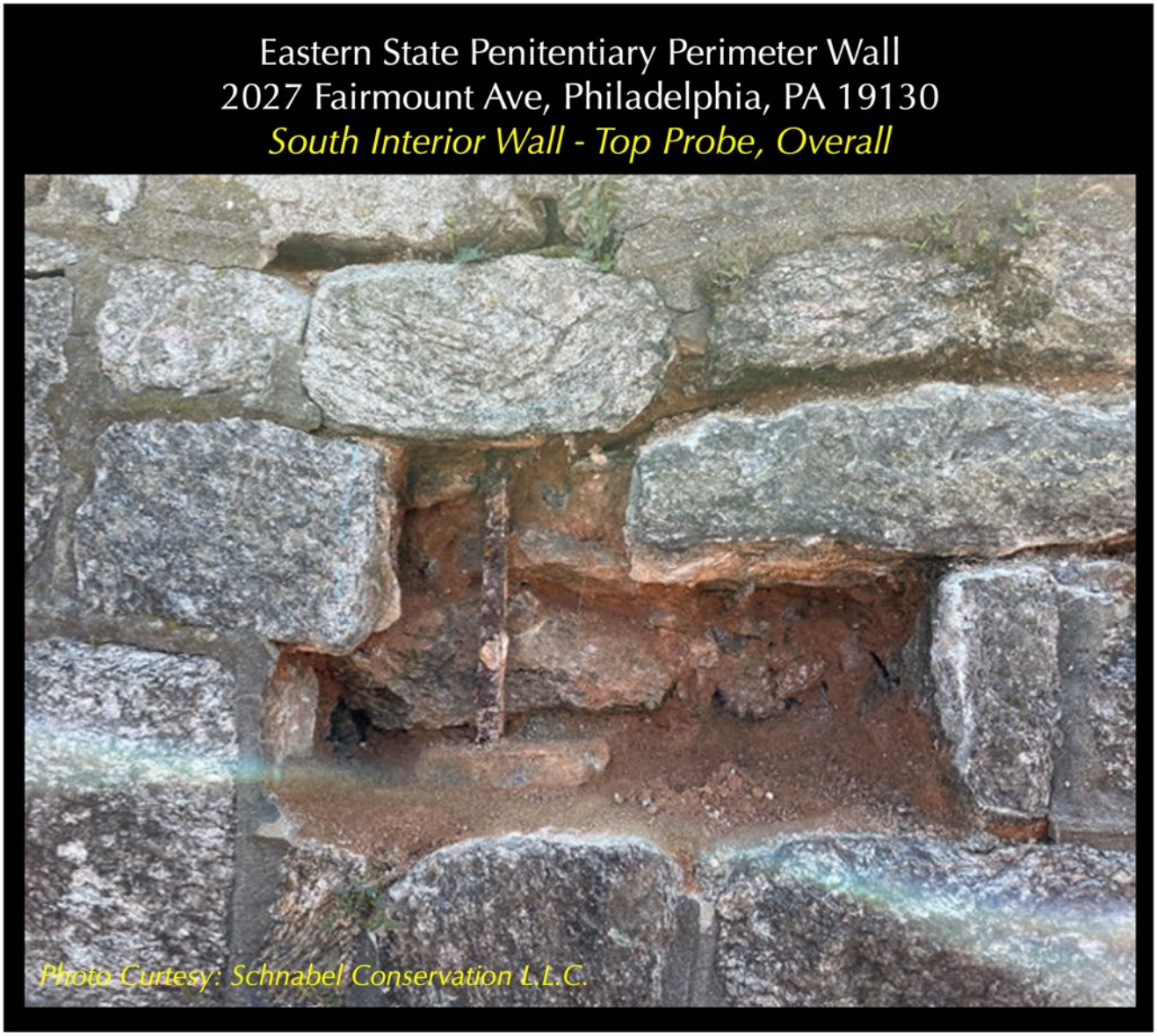

Figure 19: Overall view of the top probe of south interior wall where interior reddish-brown mortar is seen, which shows overall similarity in appearance to the mortars seen in the east and west walls as well as the mortars from the bottom and middle probes of this wall.

Figure 20: Right (top) and left (bottom) side of the top probe at south interior wall showing reddish brown mortars in similar appearance to the mortars seen from the east and west walls as well as from the bottom and middle probes of this wall.

Figure 21: Overall views of east (left), west (middle), and south (right) interior walls from where three setting mortar samples were provided, all showing similar reddish-brown appearance, and identified as SET-3, SWM-2, and SSB-3, respectively. Samples came from the top probe in east wall, middle probe in west wall, and bottom probe in south wall.

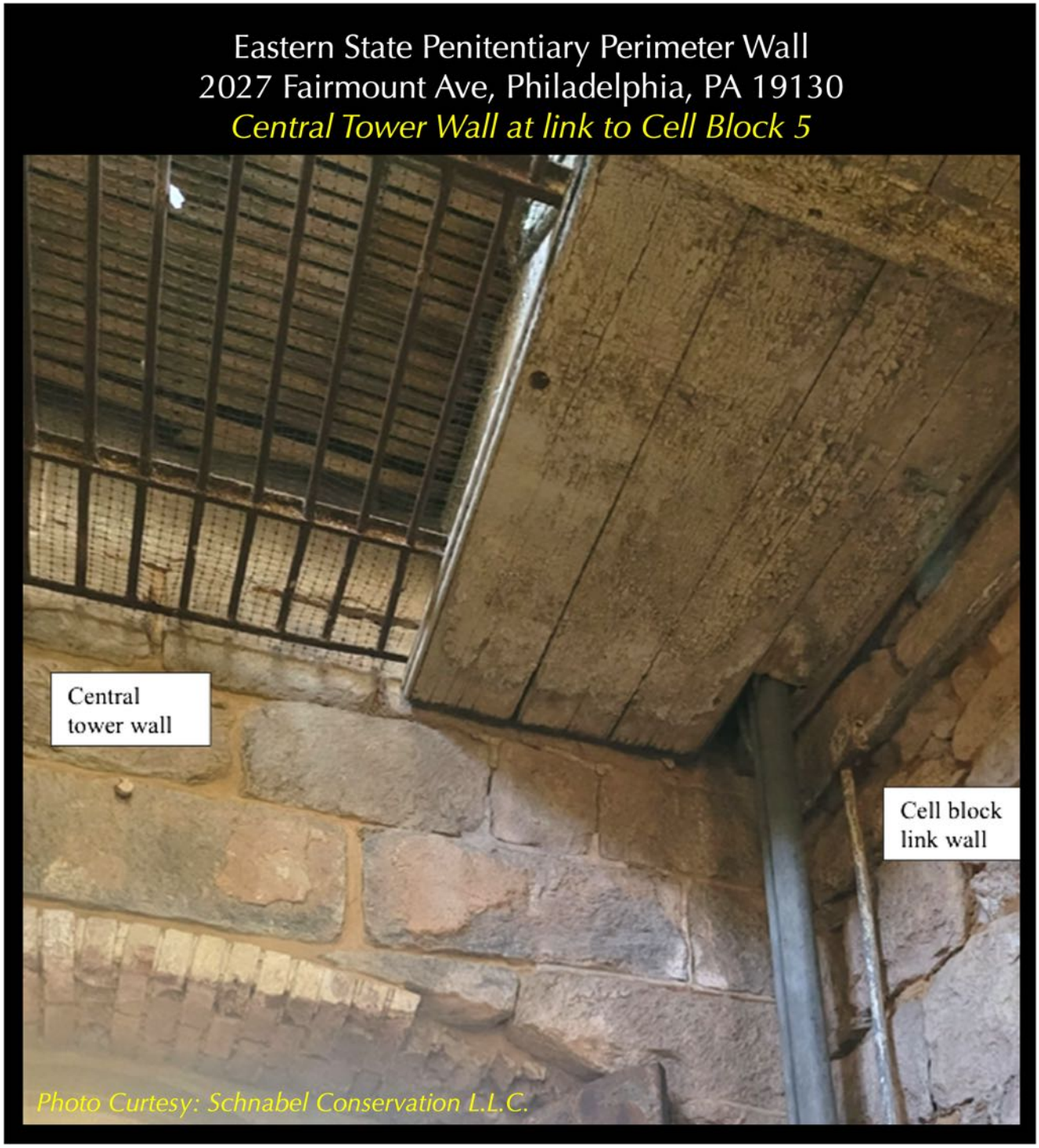

Figure 22: Central tower wall at link to cell block 5. Sample CB6-Link was obtained from the grade at similar location in the cell block 6 link space.

SAMPLES

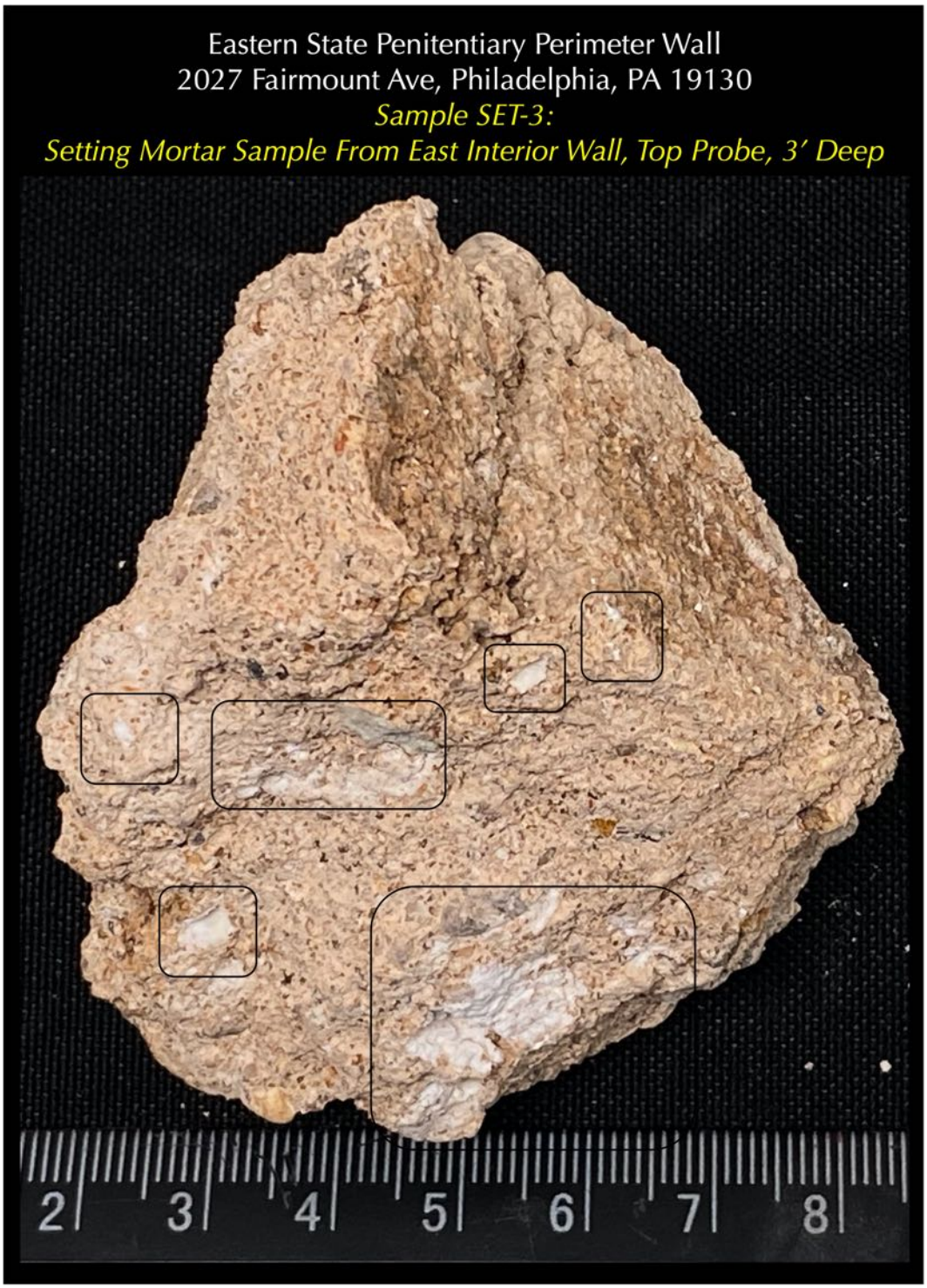

Figure 23: Sample SET-3 from the top probe of east interior wall, as received. Boxed areas show isolated occurrences of white stains as efflorescence deposits, from less than 5 mm to approximately 20 mm in areas. Total weight of the sample received is 149 grams and measures 65 × 64 × 57 mm.

Figure 24: Two sides of the Sample SET-3 from the top probe of east interior wall, as received. Boxed areas show isolated occurrences of white stains as efflorescence deposits, from less than 5 mm to approximately 20 mm in areas. Total weight of the sample received is 149 grams and measures 65 × 64 × 57 mm.

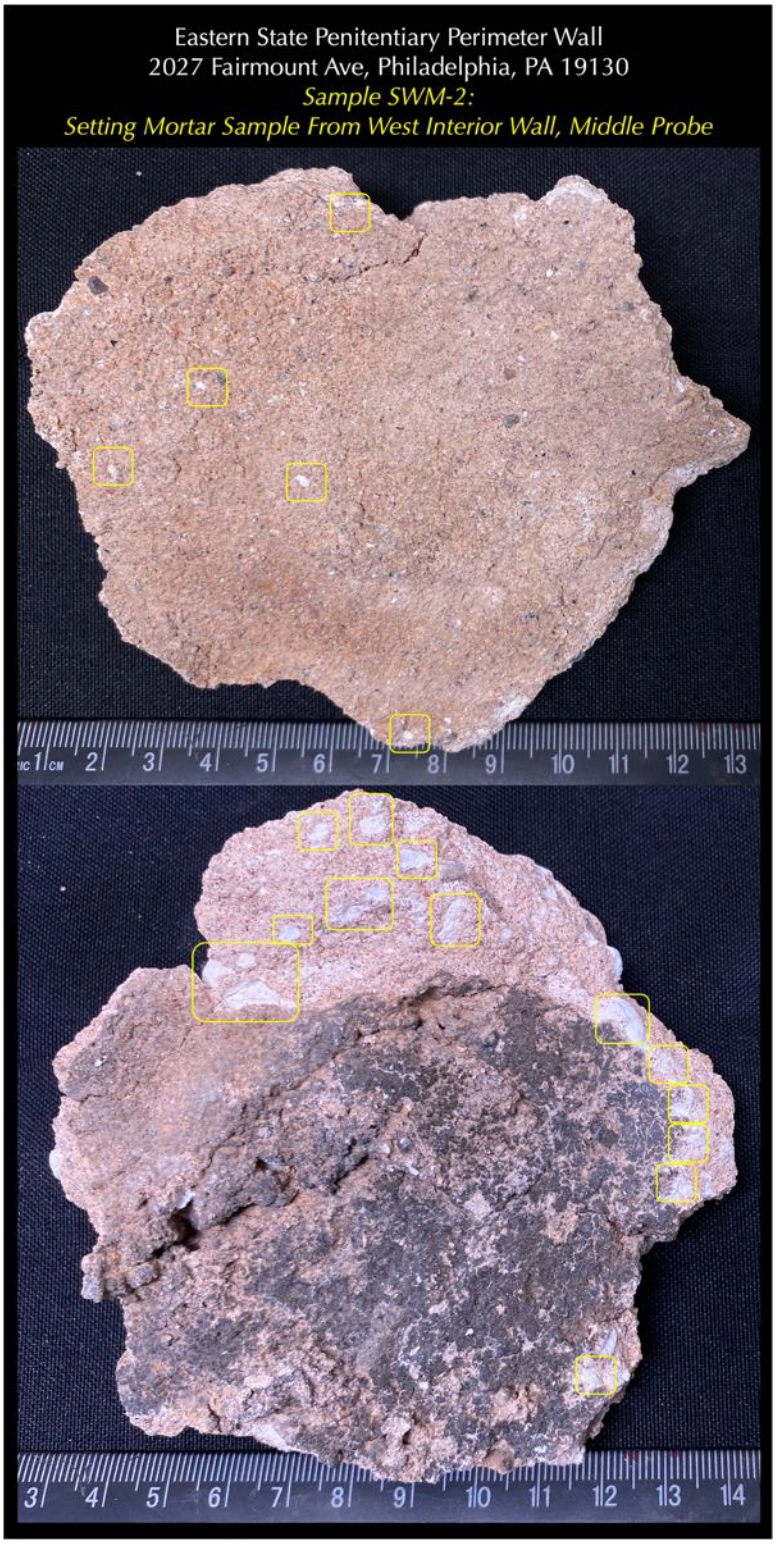

Figure 25: Sample SWM-2 from the middle probe of west interior wall, as received. Boxed areas show isolated occurrences of white grains (similar in appearance to lime lumps), from less than 5 mm to approximately 10 mm in areas. Total weight of the sample received is 225 grams and measures 108 × 95 × 32 mm.

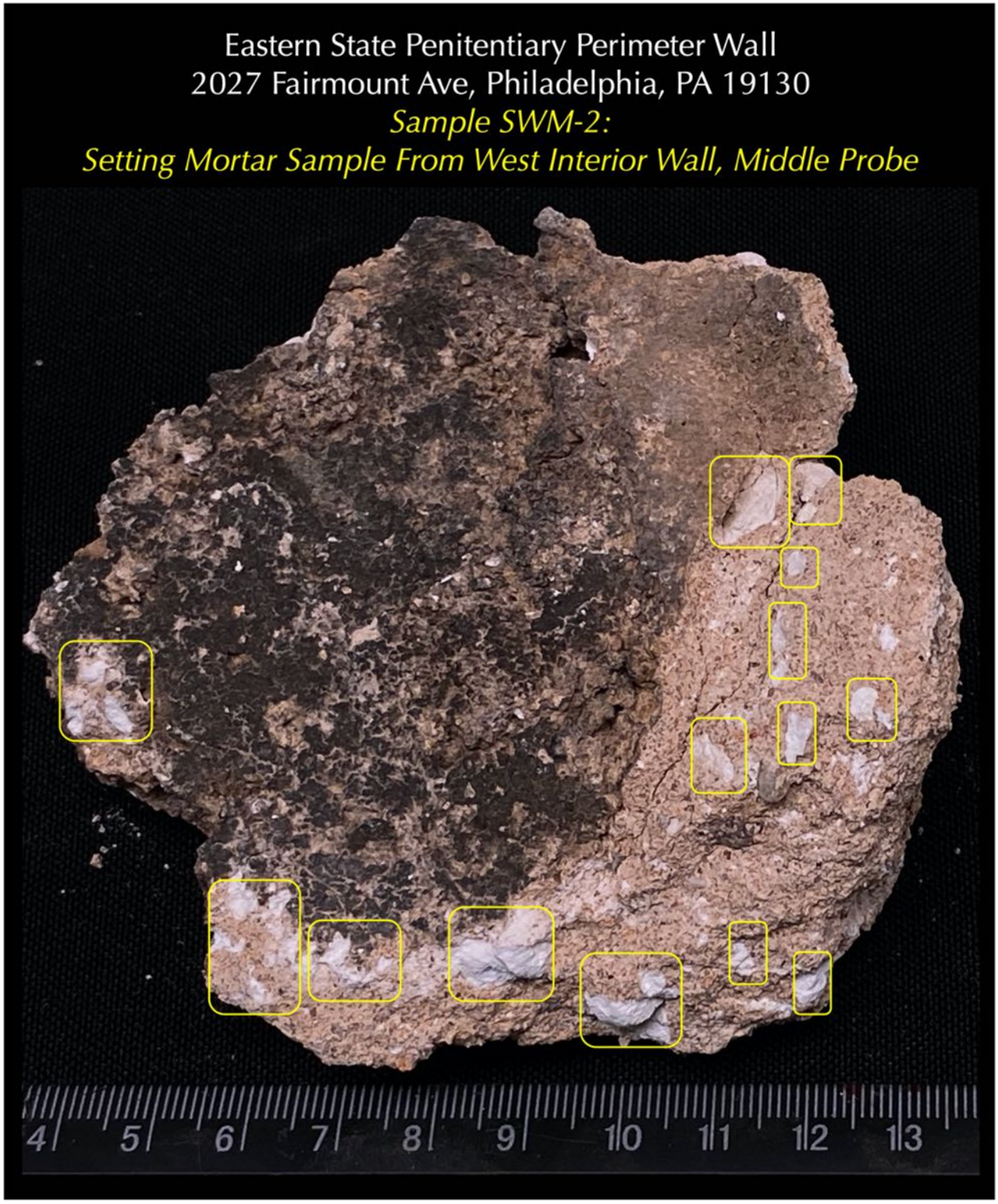

Figure 26: Dark weathered surface of Sample SWM-2 from the middle probe of west interior wall, as received. Boxed areas show isolated occurrences of white grains (similar in appearance to lime lumps), from less than 5 mm to approximately 10 mm in areas. Total weight of the sample received is 225 grams and measures 108 × 95 × 32 mm.

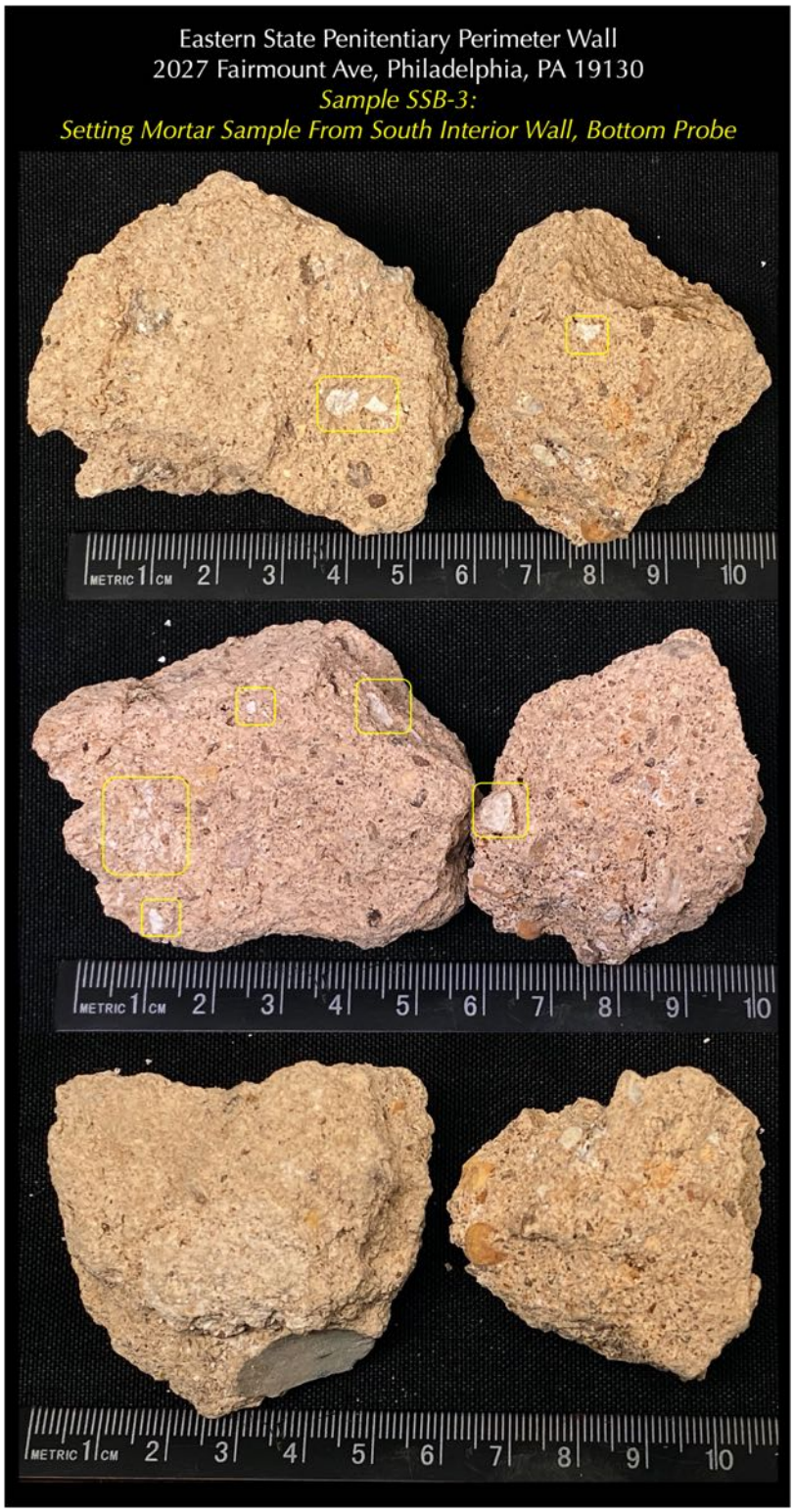

Figure 27: Sample SSB-3 from the bottom probe of south interior wall, as received. Boxed areas show isolated occurrences of white grains (similar in appearance to lime lumps), from less than 5 mm to approximately 8 mm in areas. Total weight of the sample received is 140 grams and measures 60 × 45 × 44 mm.

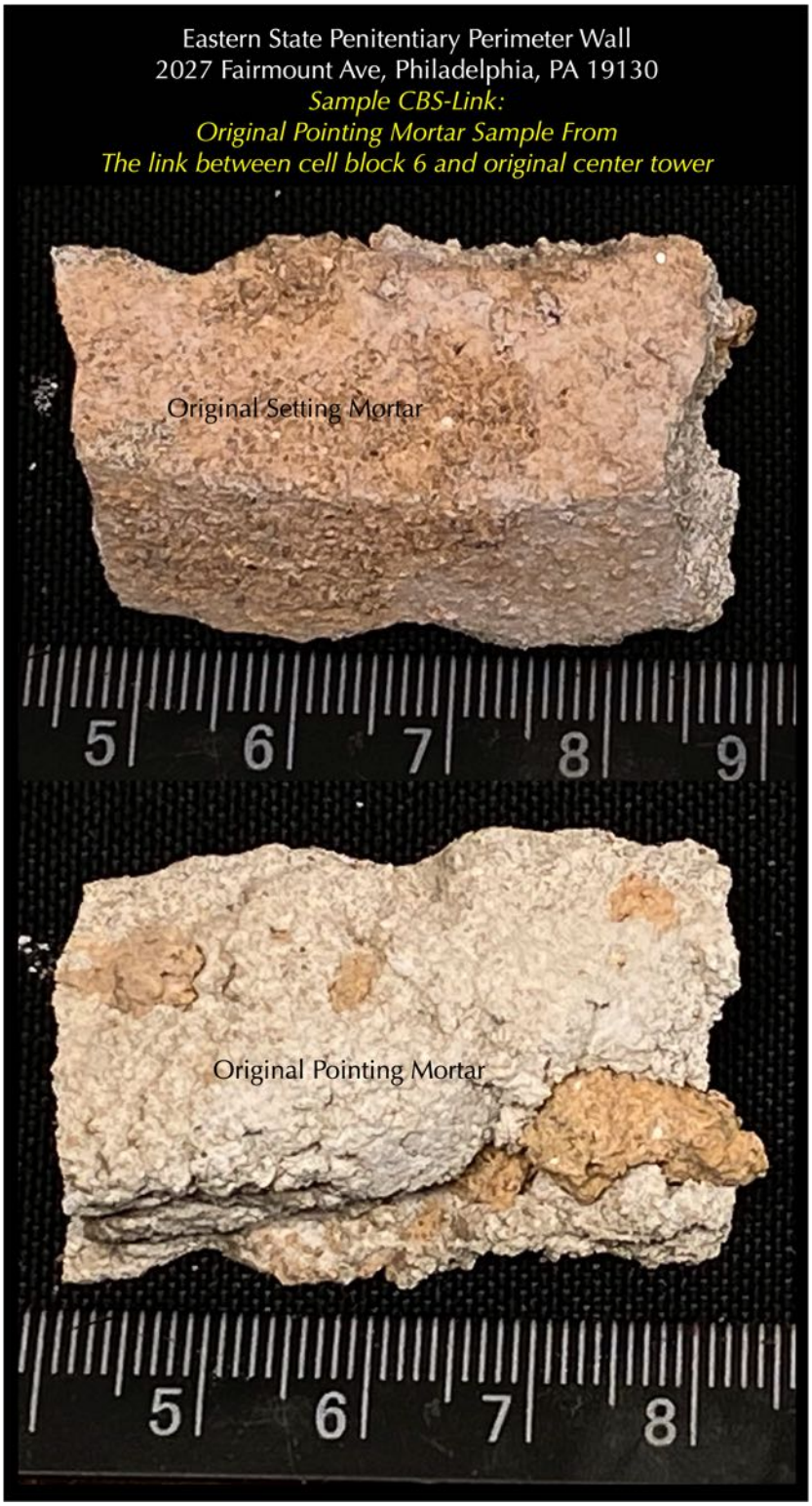

Figure 28: Pointing mortar sample CB6-Link as received showing remains of reddish-brown to beige-toned setting mortar on exposed surface and gray-toned pointing mortar inside, where the gray mortar was examined.

RESULTS

Grain-size Distribution & Micrographs of Sand Extracted from Mortars

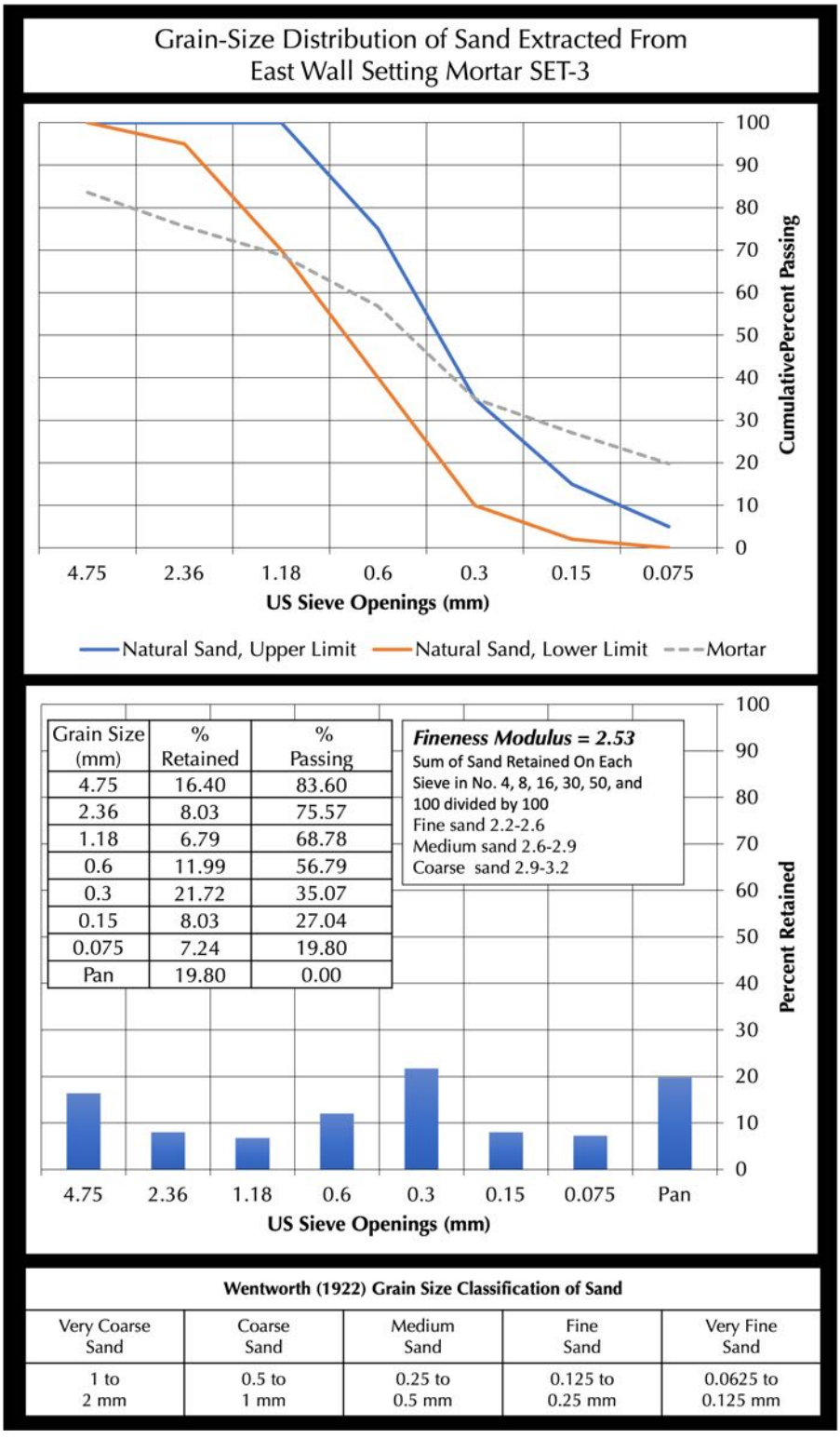

Grain Size (mm)	% Retained	% Passing
4.75	16.40	83.60
2.36	8.03	75.57
1.18	6.79	68.78
0.6	11.99	56.79
0.3	21.72	35.07
0.15	8.03	27.04
0.075	7.24	19.80
Pan	19.80	0.00

Fineness Modulus = 2.53
Sum of Sand Retained On Each Sieve in No. 4, 8, 16, 30, 50, and 100 divided by 100
Fine sand 2.2-2.6
Medium sand 2.6-2.9
Coarse sand 2.9-3.2

Wentworth (1922) Grain Size Classification of Sand

Very Coarse Sand	Coarse Sand	Medium Sand	Fine Sand	Very Fine Sand
1 to 2 mm	0.5 to 1 mm	0.25 to 0.5 mm	0.125 to 0.25 mm	0.0625 to 0.125 mm

Figure 29: Grain-size distribution of sand extracted from the setting mortar SET-3 after hydrochloric acid digestion.

In the top plot, grain size distribution of sand is compared with the upper and lower limits of natural sand in ASTM C 144 (blue and red lines, respectively) showing overall finer grain size distribution of sand compared to the modern ASTM C 144 masonry sand.

The bottom plot shows a histogram of size distribution of sand, which shows no dominance of a particular size fraction in sand.

Inset Table shows the percent retained, and cumulative percent passing through each sieve.

Fineness modulus of sand is calculated to be 2.53 from the sum of cumulative percent retained on Sieves 4, 8, 16, 30, 50, and 100 divided by 100 where fine sand size is again depicted from low fineness modulus.

Next Figures 30 through 33 show micrographs of size fractions of sand particles retained on Nos. 8, 16, 30, 50, 100 and 200 sieves.

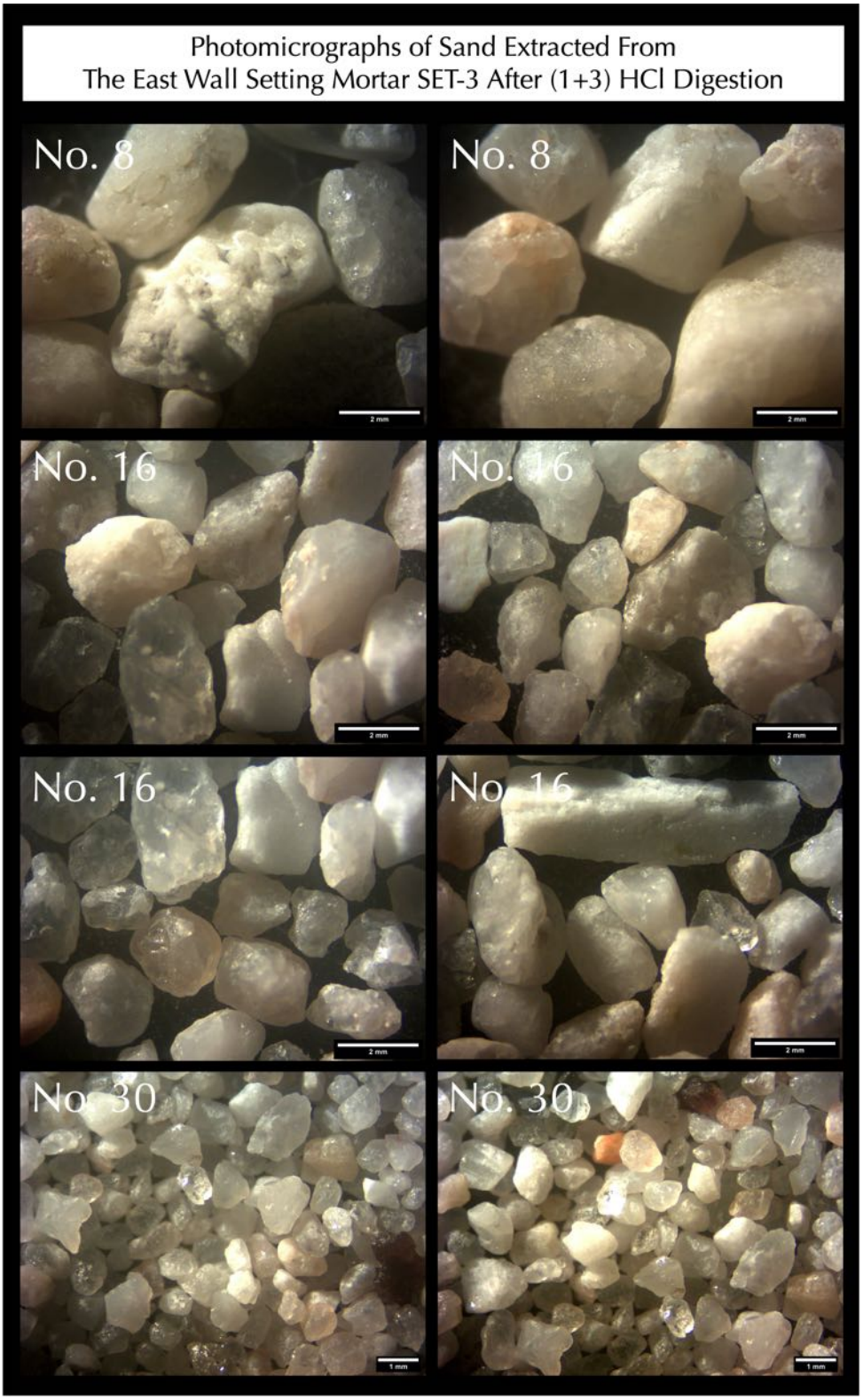

Figure 30: Micrographs of sand particles extracted from the setting mortar SET-3 after acid digestion, which are retained on Sieves 8, 16, and 30. Sand particles are mostly transparent to translucent clear quartz sand, with a few off-white and light gray particles. Sand particles are mixtures of a coarser subrounded to well-rounded to subangular grains, and a finer fraction of mostly angular to subangular grains, all of which are equidimensional/equant in shape.

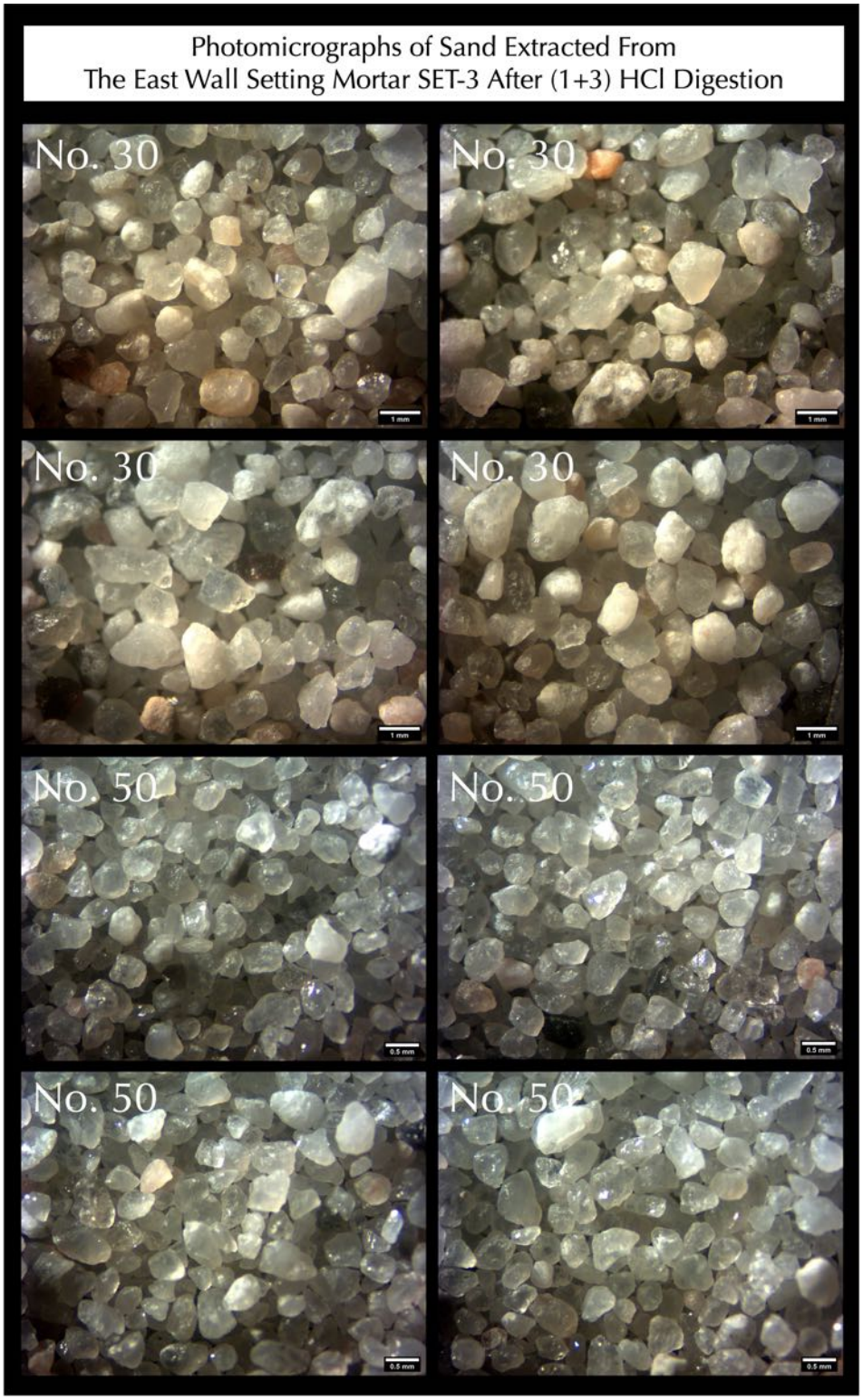

Figure 31: Micrographs of sand particles extracted from the setting mortar SET-3 after acid digestion, which are retained on Sieves 30 and 50. Sand particles are mostly transparent to translucent clear quartz sand, with a few off-white and light gray particles. Sand particles are mixtures of a coarser subrounded to well-rounded to subangular grains, and a finer fraction of mostly angular to subangular grains, all of which are equidimensional/equant in shape.

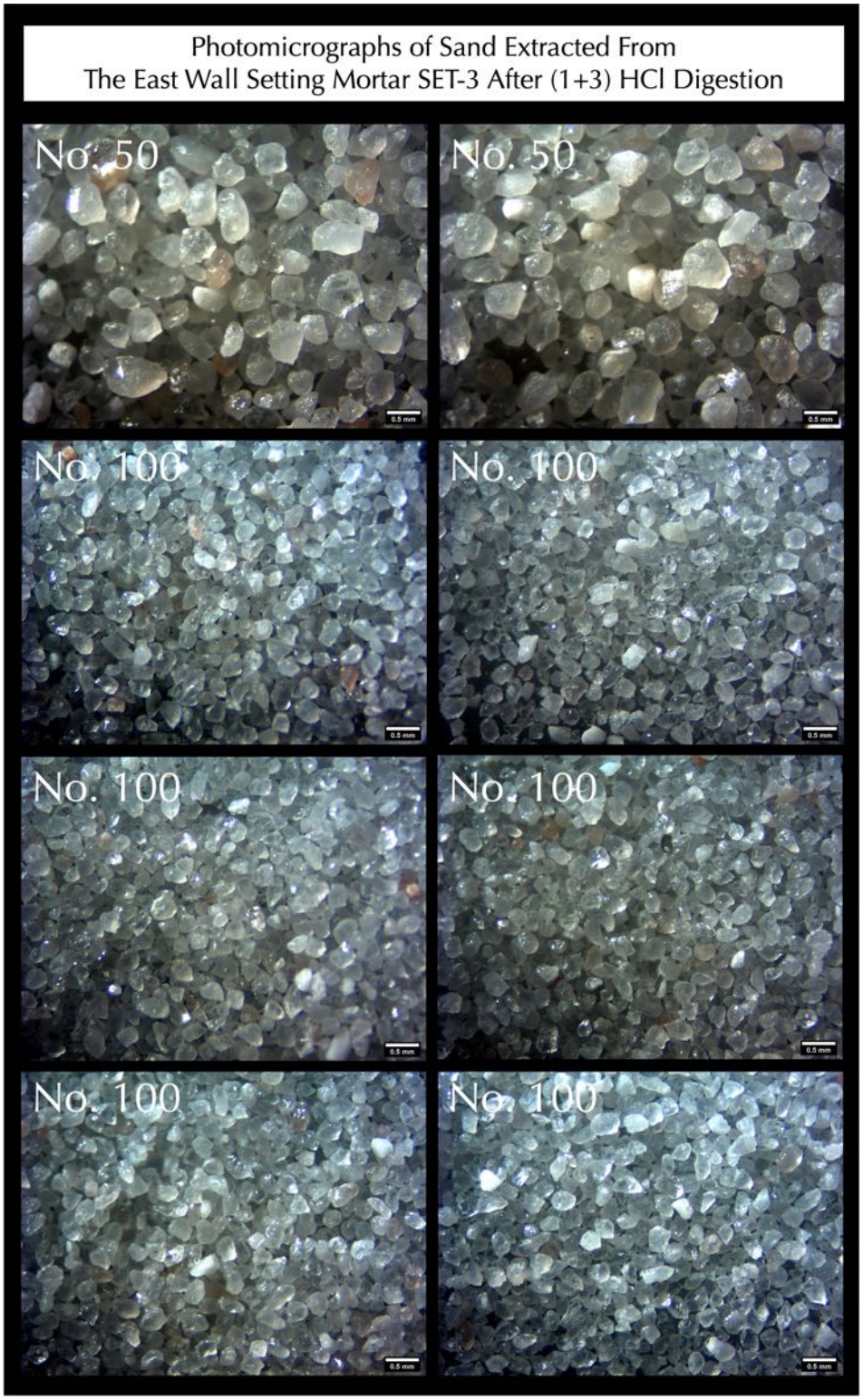

Figure 32: Micrographs of sand particles extracted from the setting mortar SET-3 after acid digestion, which are retained on Sieves 50 and 100. Sand particles are mostly transparent to translucent clear quartz sand, with a few off-white and light gray particles. Sand particles are mixtures of a coarser subrounded to well-rounded to subangular grains, and a finer fraction of mostly angular to subangular grains, all of which are equidimensional/equant in shape.

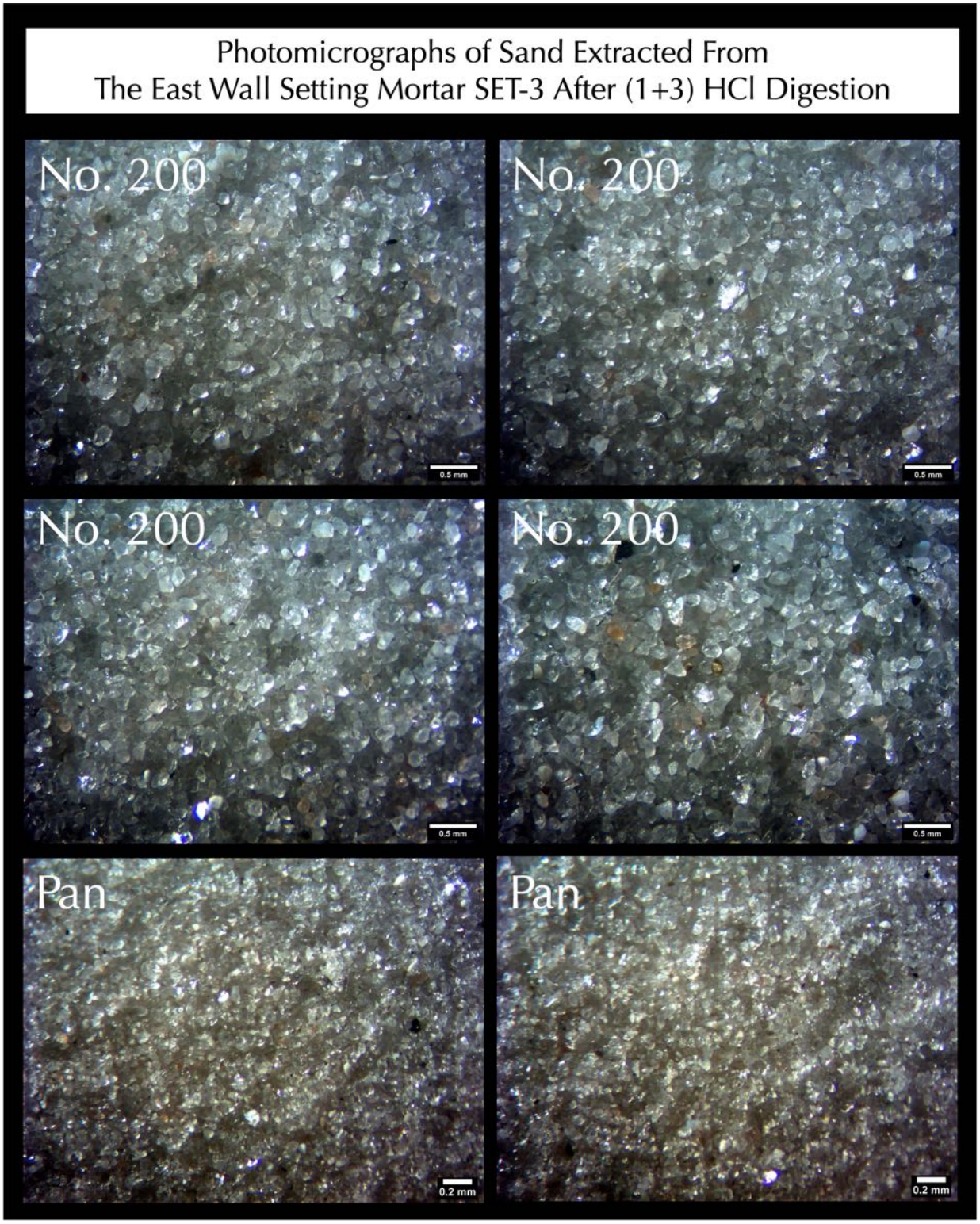

Figure 33: Micrographs of sand particles extracted from the setting mortar SET-3 after acid digestion, which are retained on Sieves 100, 200, and pan. Sand particles are mostly transparent to translucent clear quartz sand, with a few off-white and light gray particles. Sand particles are mostly the finer fraction of bulk sand, which are mostly angular to subangular grains, all of which are equidimensional/equant in shape.

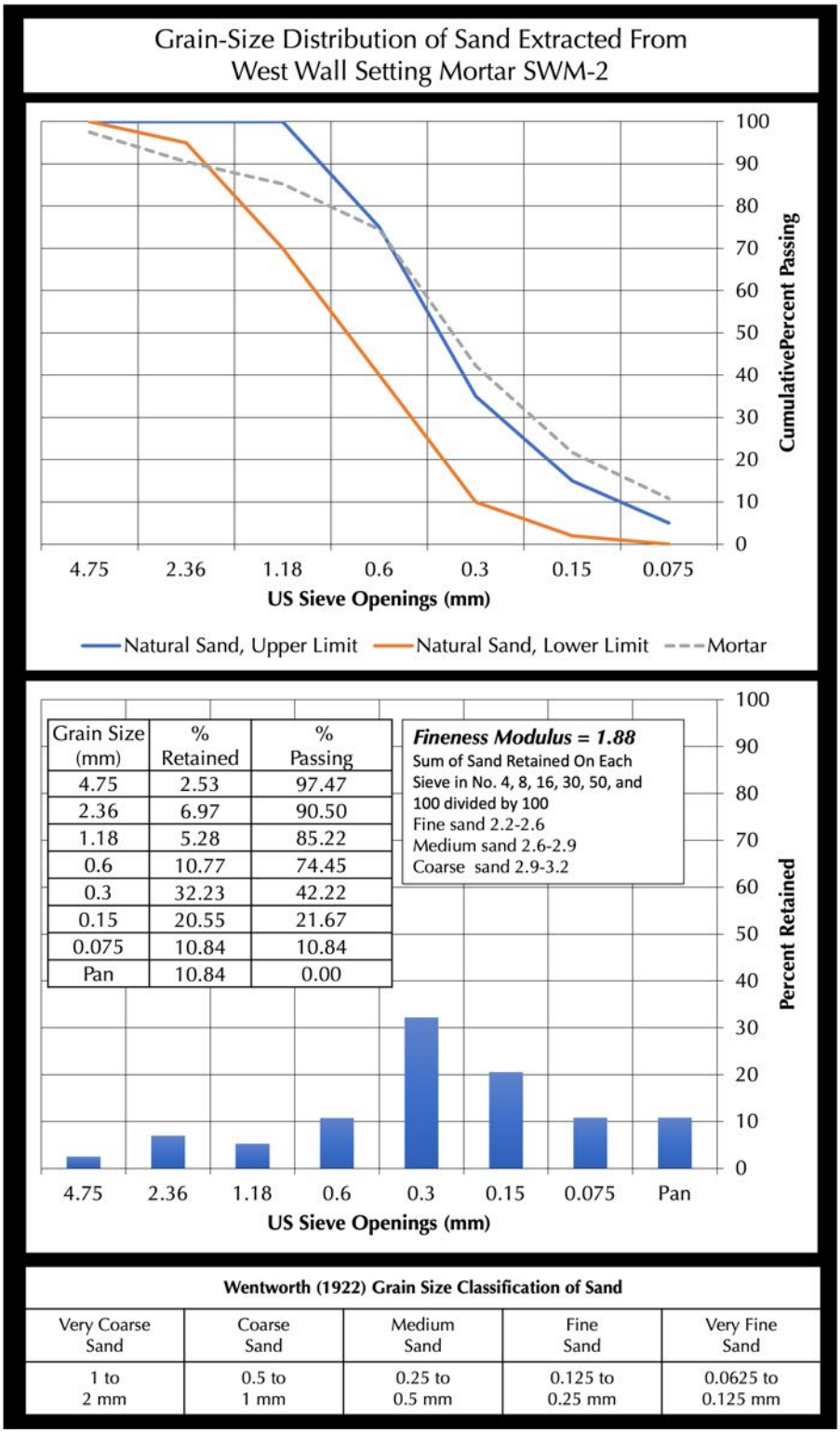

Figure 34: Grain-size distribution of sand extracted from the setting mortar SWM-2 after hydrochloric acid digestion.

In the top plot, grain size distribution of sand is compared with the upper and lower limits of natural sand in ASTM C 144 (blue and red lines, respectively) showing overall finer grain size distribution of sand compared to the modern ASTM C 144 masonry sand.

The bottom plot shows a histogram of size distribution of sand, which again shows the dominance of fine size fractions in sand.

Inset Table shows the percent retained, and cumulative percent passing through each sieve.

Fineness modulus of sand is calculated to be 1.88 from the sum of cumulative percent retained on Sieves 4, 8, 16, 30, 50, and 100 divided by 100 where very fine sand size is again depicted from very low fineness modulus.

Next Figures 35 through 38 show micrographs of size fractions of sand particles retained on Nos. 8, 16, 30, 50, 100 and 200 sieves.

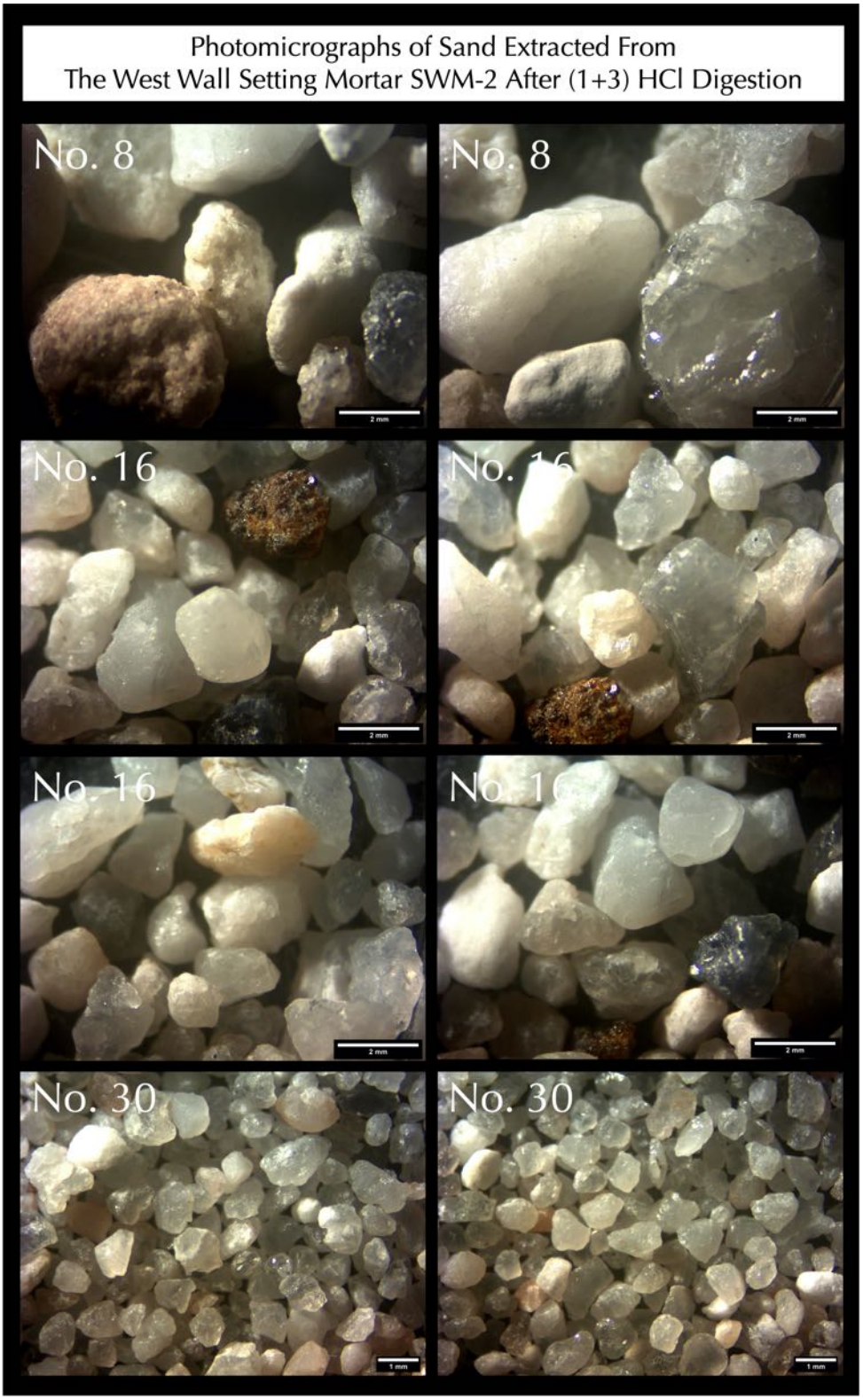

Figure 35: Micrographs of sand particles extracted from the setting mortar SWM-2 after acid digestion, which are retained on Sieves 8, 16, and 30. Sand particles are mostly transparent to translucent clear quartz sand, with a few off-white and light gray particles. Sand particles are mixtures of a coarser subrounded to well-rounded to subangular grains, and a finer fraction of mostly angular to subangular grains, all of which are equidimensional/equant in shape.

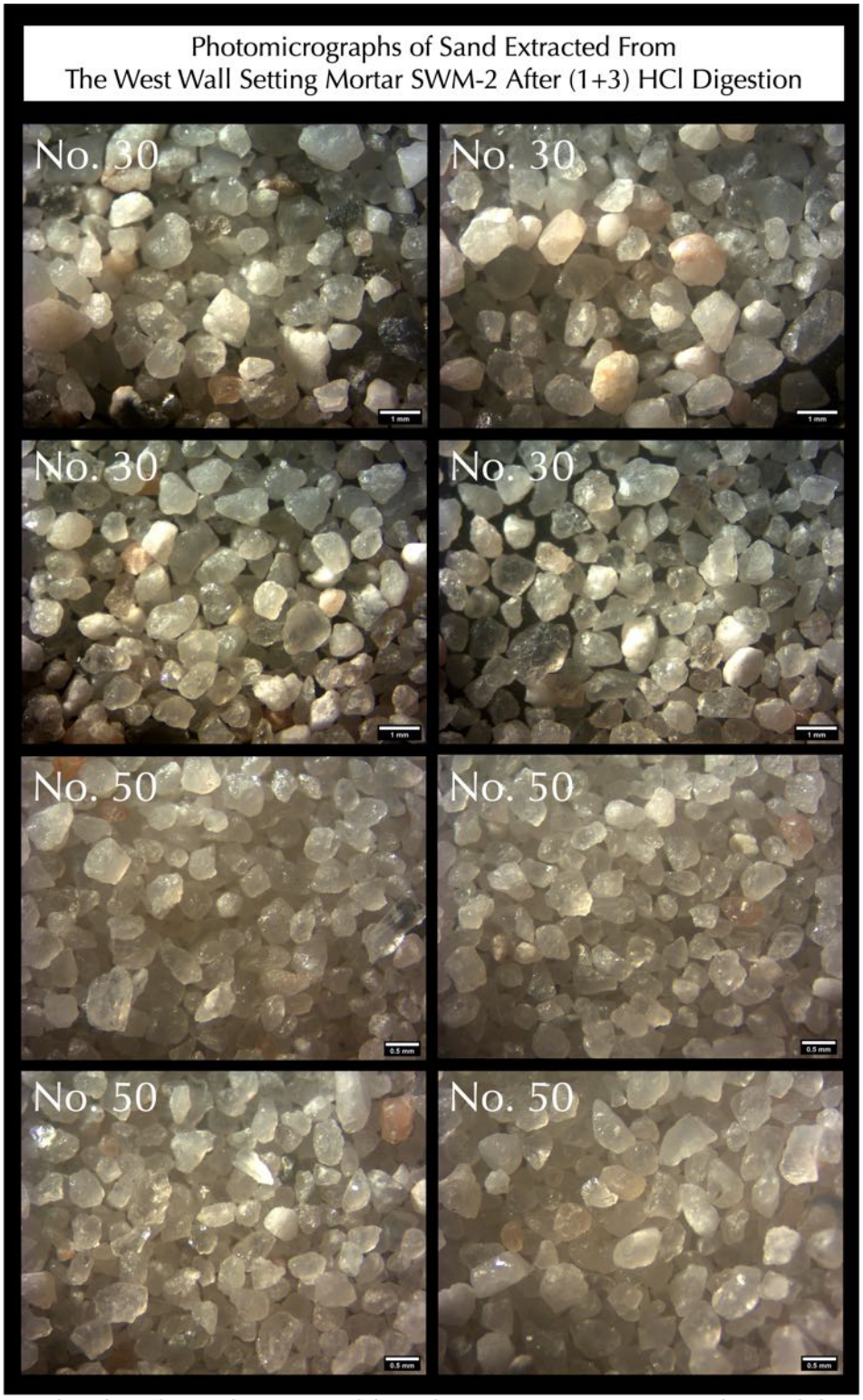

Figure 36: Micrographs of sand particles extracted from the setting mortar SWM-2 after acid digestion, which are retained on Sieves 30 and 50. Sand particles are mostly transparent to translucent clear quartz sand, with a few off-white and light gray particles. Sand particles are mixtures of a coarser subrounded to well-rounded to subangular grains, and a finer fraction of mostly angular to subangular grains, all of which are equidimensional/equant in shape.

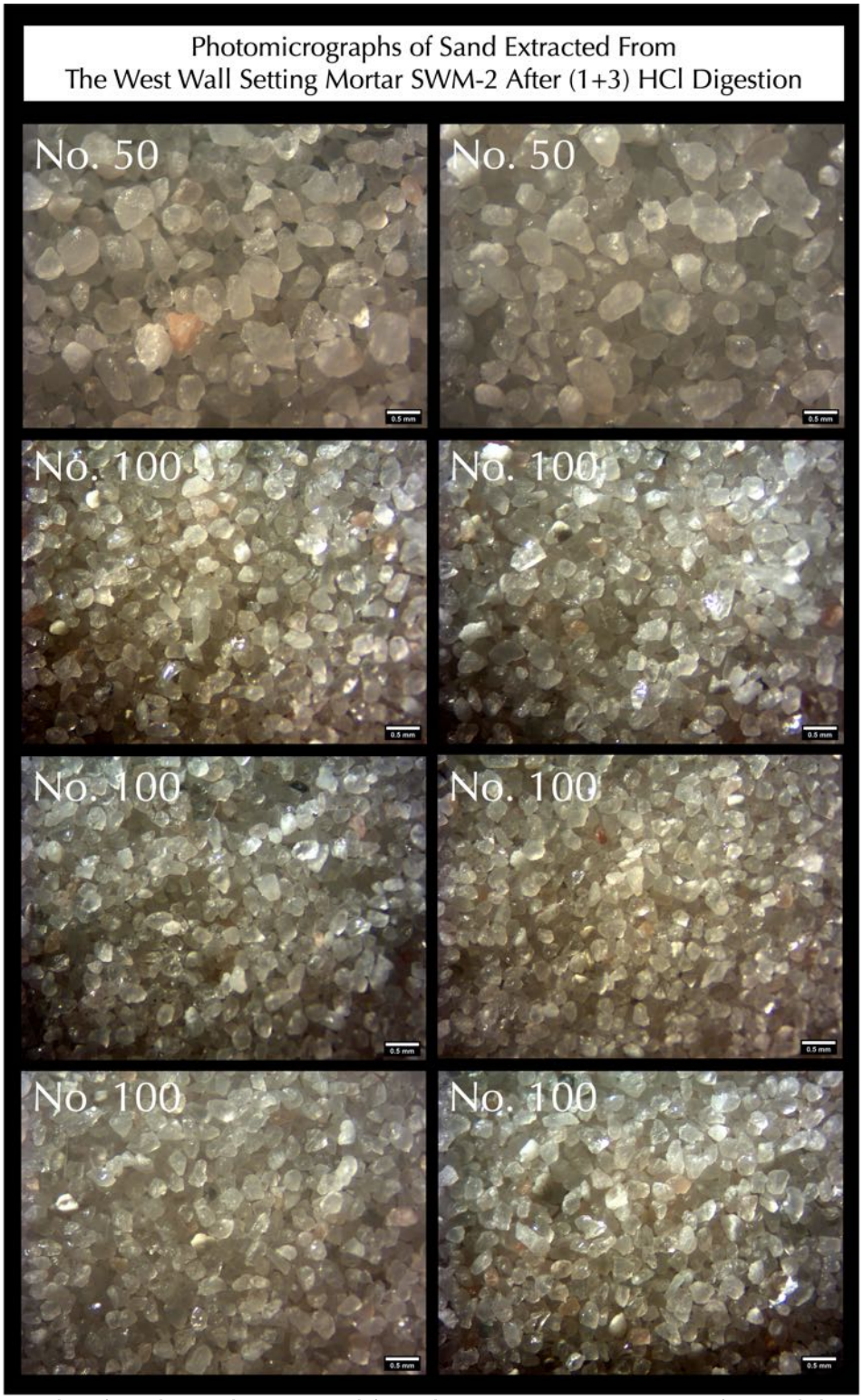

Figure 37: Micrographs of sand particles extracted from the setting mortar SWM-2 after acid digestion, which are retained on Sieves 50 and 100. Sand particles are mostly transparent to translucent clear quartz sand, with a few off-white and light gray particles. Sand particles are mixtures of a coarser subrounded to well-rounded to subangular grains, and a finer fraction of mostly angular to subangular grains, all of which are equidimensional/equant in shape.

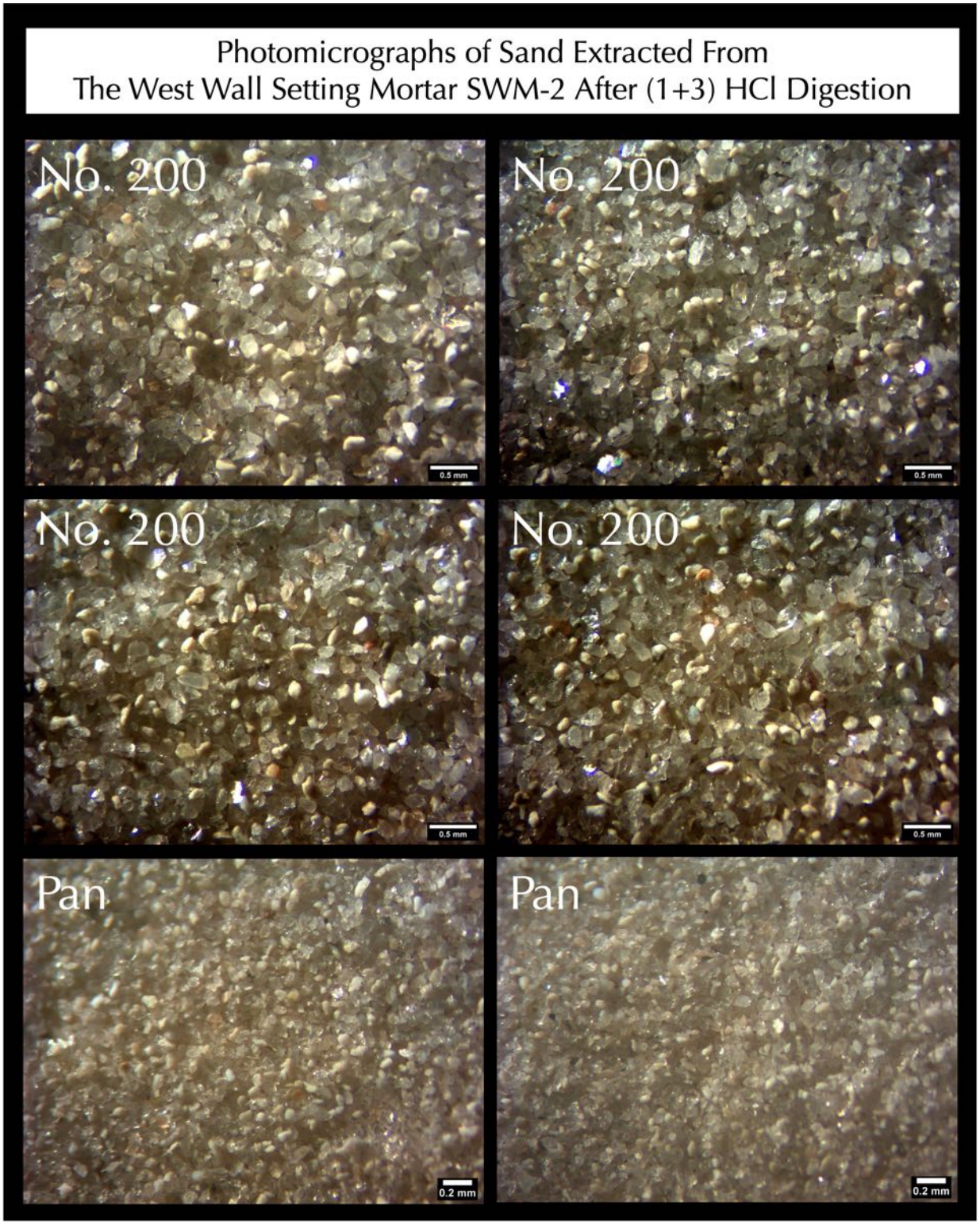

Figure 38: Micrographs of sand particles extracted from the setting mortar SWM-2 after acid digestion, which are retained on Sieves 200, and pan. Sand particles are mostly transparent to translucent clear quartz sand, with a few off-white and light gray particles. Sand particles are mostly the finer fraction of bulk sand, which are mostly angular to subangular grains, all of which are equidimensional/equant in shape.

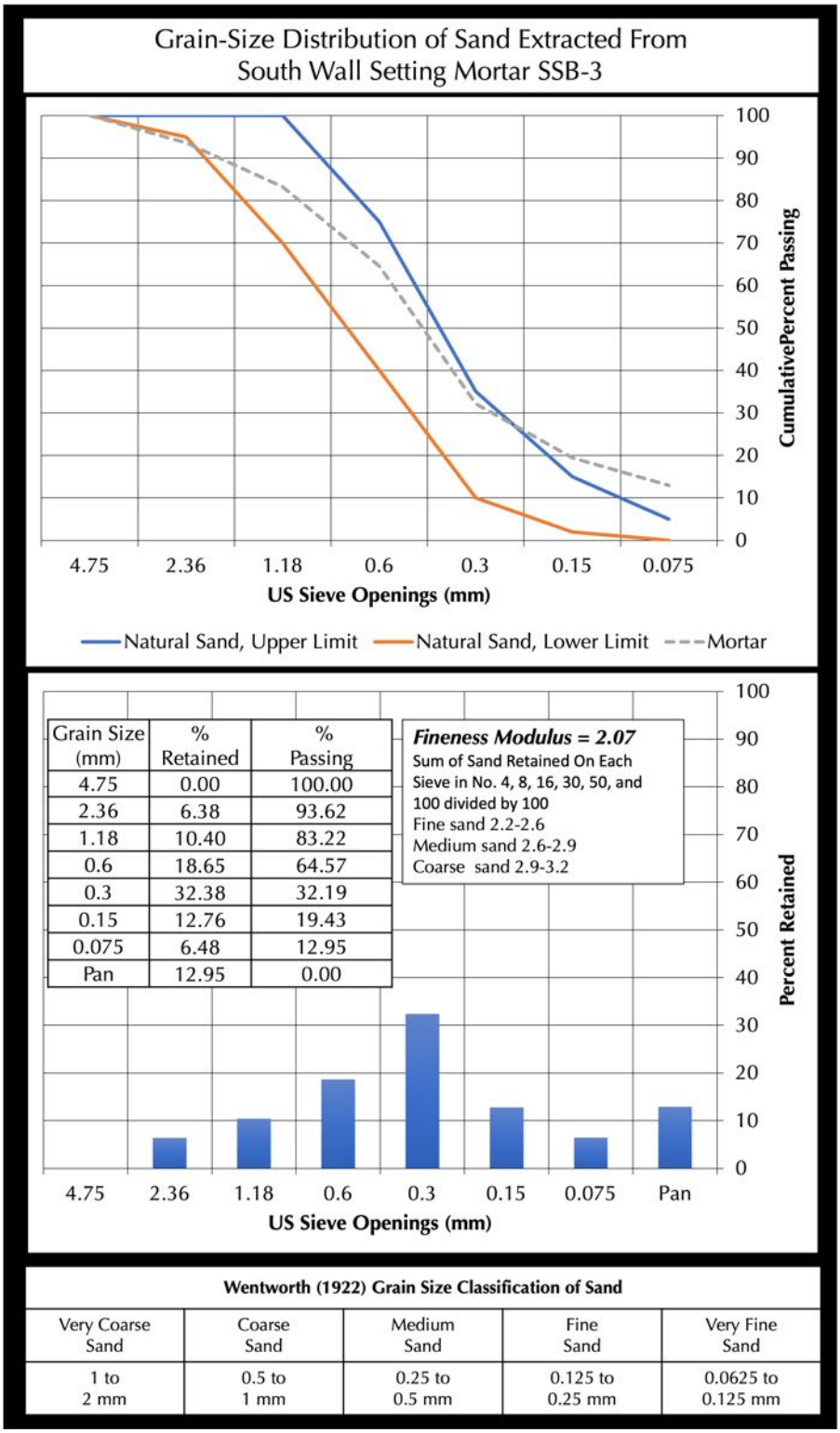

Grain Size (mm)	% Retained	% Passing
4.75	0.00	100.00
2.36	6.38	93.62
1.18	10.40	83.22
0.6	18.65	64.57
0.3	32.38	32.19
0.15	12.76	19.43
0.075	6.48	12.95
Pan	12.95	0.00

Figure 39: Grain-size distribution of sand extracted from the setting mortar SSB-3 after hydrochloric acid digestion.

In the top plot, grain size distribution of sand is compared with the upper and lower limits of natural sand in ASTM C 144 (blue and red lines, respectively) showing overall finer grain size distribution of sand compared to the modern ASTM C 144 masonry sand.

The bottom plot shows a histogram of size distribution of sand, which again shows the dominance of fine size fractions in sand.

Inset Table shows the percent retained, and cumulative percent passing through each sieve.

Fineness modulus of sand is calculated to be 2.07 from the sum of cumulative percent retained on Sieves 4, 8, 16, 30, 50, and 100 divided by 100 where very fine sand size is again depicted from very low fineness modulus.

Next Figures 40 through 43 show micrographs of size fractions of sand particles retained on Nos. 8, 16, 30, 50, 100 and 200 sieves.

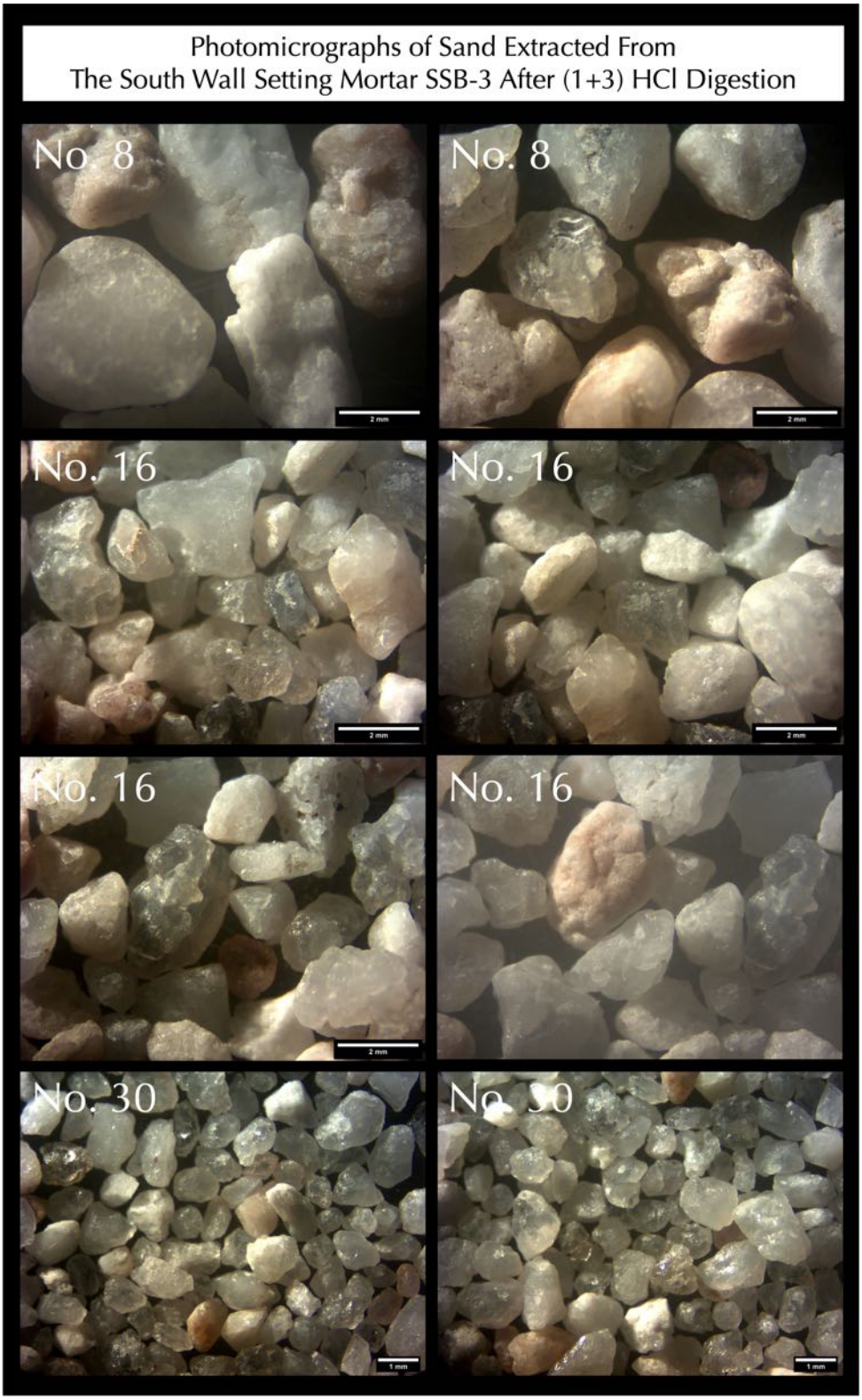

Figure 40: Micrographs of sand particles extracted from the setting mortar SSB-3 after acid digestion, which are retained on Sieves 8, 16, and 30. Sand particles are mostly transparent to translucent clear quartz sand, with a few off-white and light gray particles. Sand particles are mixtures of a coarser subrounded to well-rounded to subangular grains, and a finer fraction of mostly angular to subangular grains, all of which are equidimensional/equant in shape.

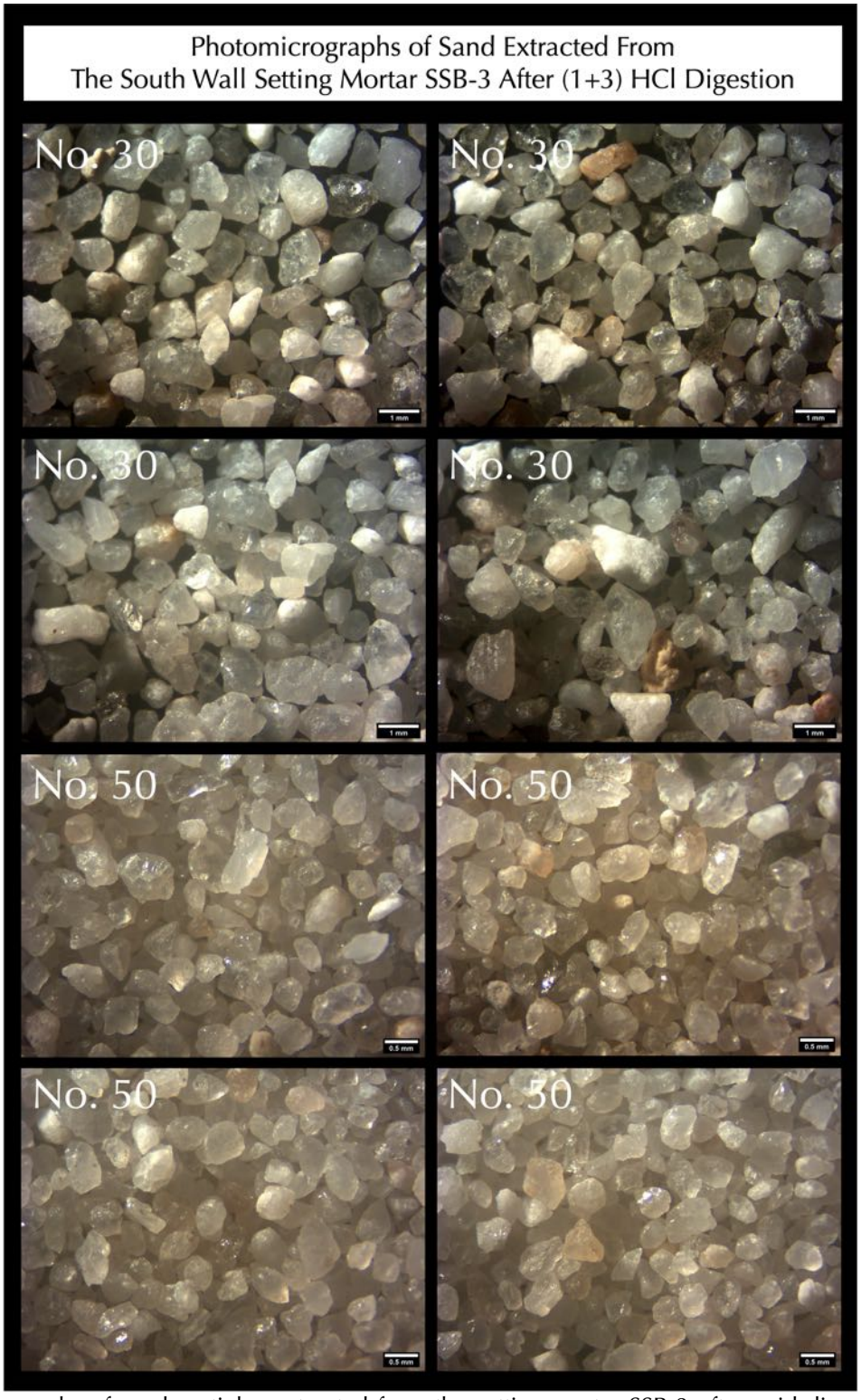

Figure 41: Micrographs of sand particles extracted from the setting mortar SSB-3 after acid digestion, which are retained on Sieves 30 and 50. Sand particles are mostly transparent to translucent clear quartz sand, with a few off-white and light gray particles. Sand particles are mixtures of a coarser subrounded to well-rounded to subangular grains, and a finer fraction of mostly angular to subangular grains, all of which are equidimensional/equant in shape.

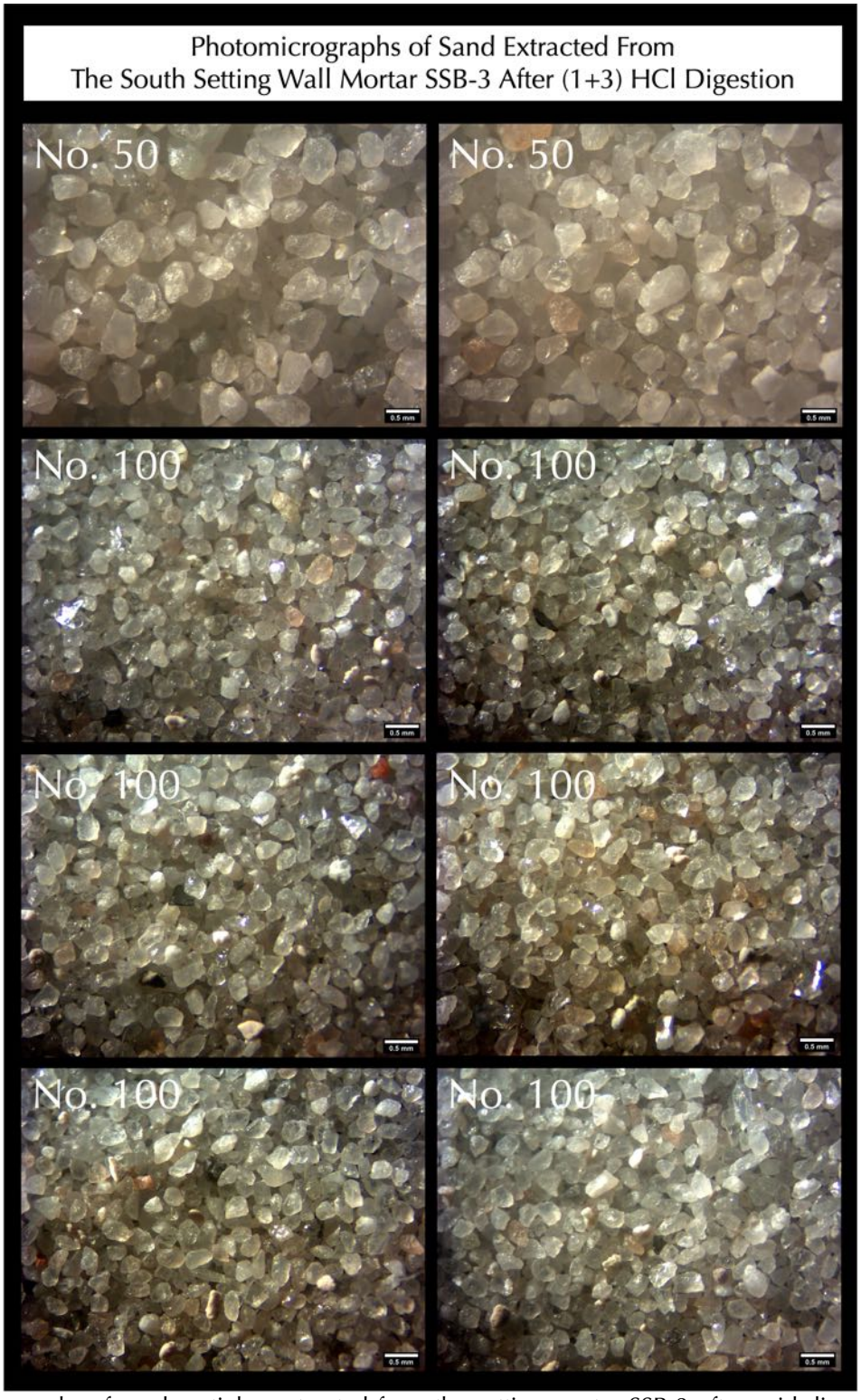

Figure 42: Micrographs of sand particles extracted from the setting mortar SSB-3 after acid digestion, which are retained on Sieves 50 and 100. Sand particles are mostly transparent to translucent clear quartz sand, with a few off-white and light gray particles. Sand particles are mixtures of a coarser subrounded to well-rounded to subangular grains, and a finer fraction of mostly angular to subangular grains, all of which are equidimensional/equant in shape.

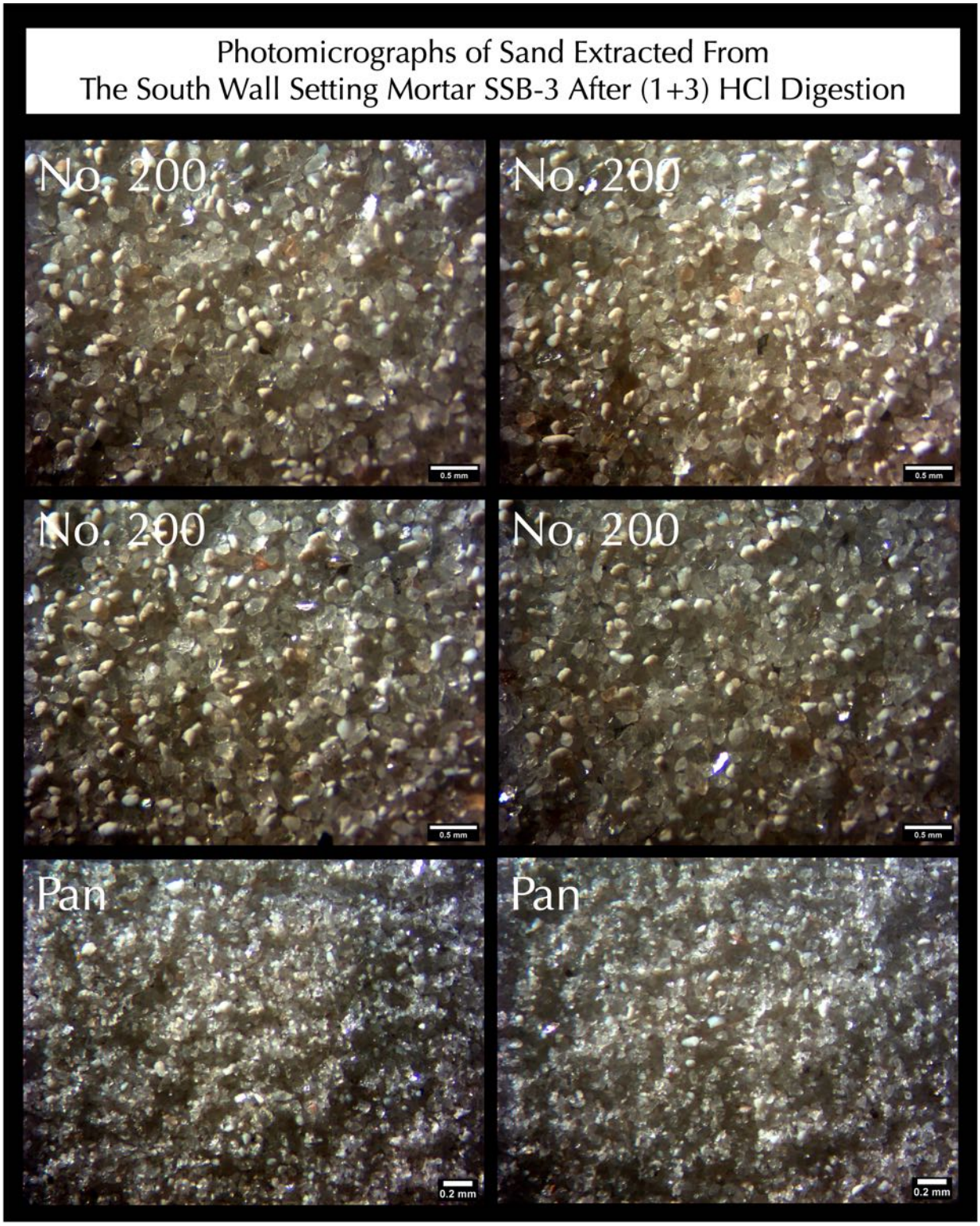

Figure 43: Micrographs of sand particles extracted from the setting mortar SSB-3 after acid digestion, which are retained on Sieves 200, and pan. Sand particles are mostly transparent to translucent clear quartz sand, with a few off-white and light gray particles. Sand particles are mostly the finer fraction of bulk sand, which are mostly angular to subangular grains, all of which are equidimensional/equant in shape.

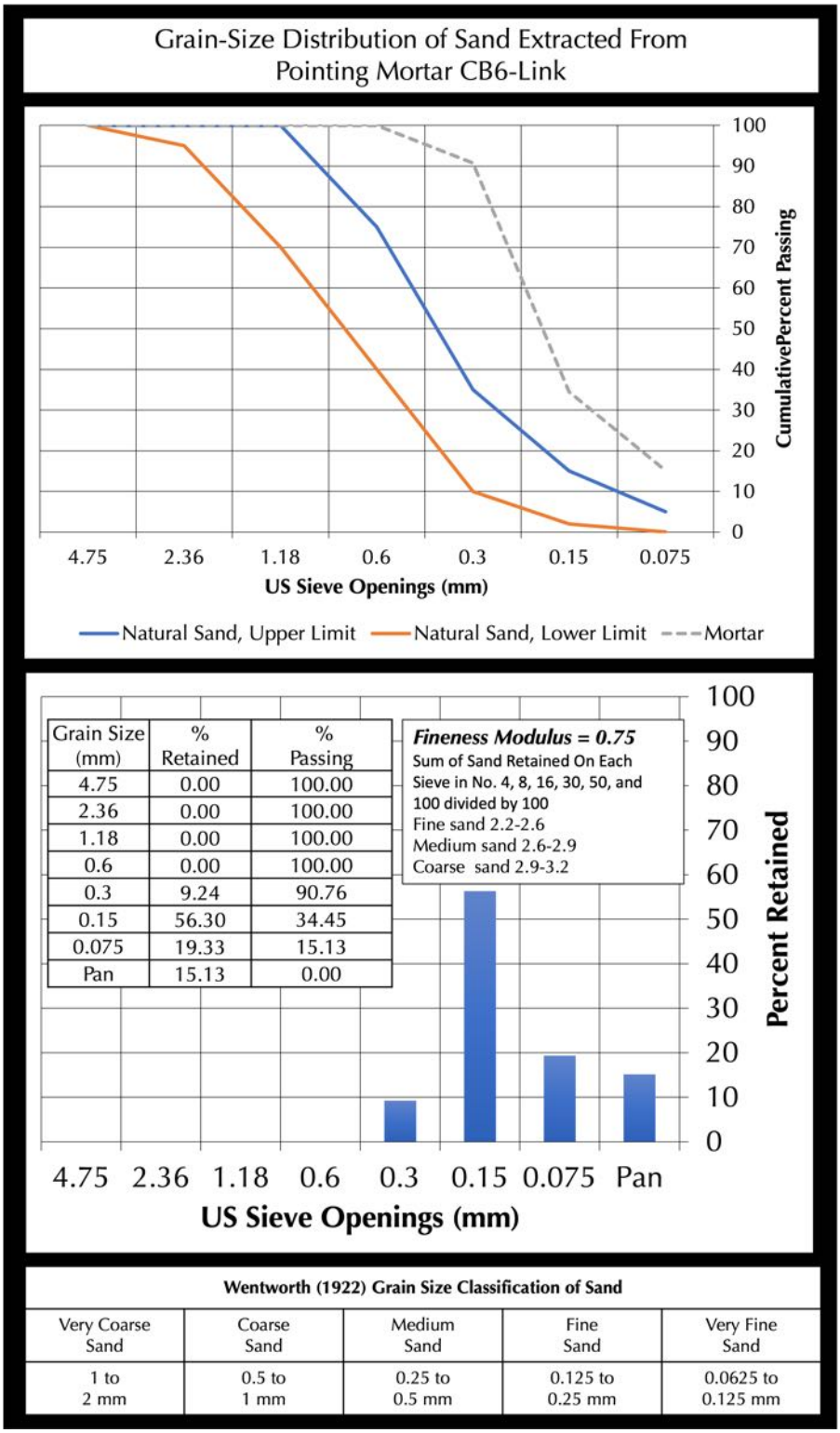

Figure 44: Grain-size distribution of sand extracted from the pointing mortar CB6-Link after hydrochloric acid digestion.

In the top plot, grain size distribution of sand is compared with the upper and lower limits of natural sand in ASTM C 144 (blue and red lines, respectively) showing overall noticeably finer grain size distribution of sand compared to the modern ASTM C 144 masonry sand.

The bottom plot shows a histogram of size distribution of sand, which again shows the dominance of fine size fractions in sand.

Inset Table shows the percent retained, and cumulative percent passing through each sieve.

Fineness modulus of sand is calculated to be 0.75 from the sum of cumulative percent retained on Sieves 4, 8, 16, 30, 50, and 100 divided by 100 where very fine sand size is again depicted from very low fineness modulus.

Notice this sand in the pointing mortar is noticeably finer than the sand from three setting mortars.

Next Figures 45 and 46 show micrographs of size fractions of sand particles retained on Nos. 50, 100 and 200 sieves.

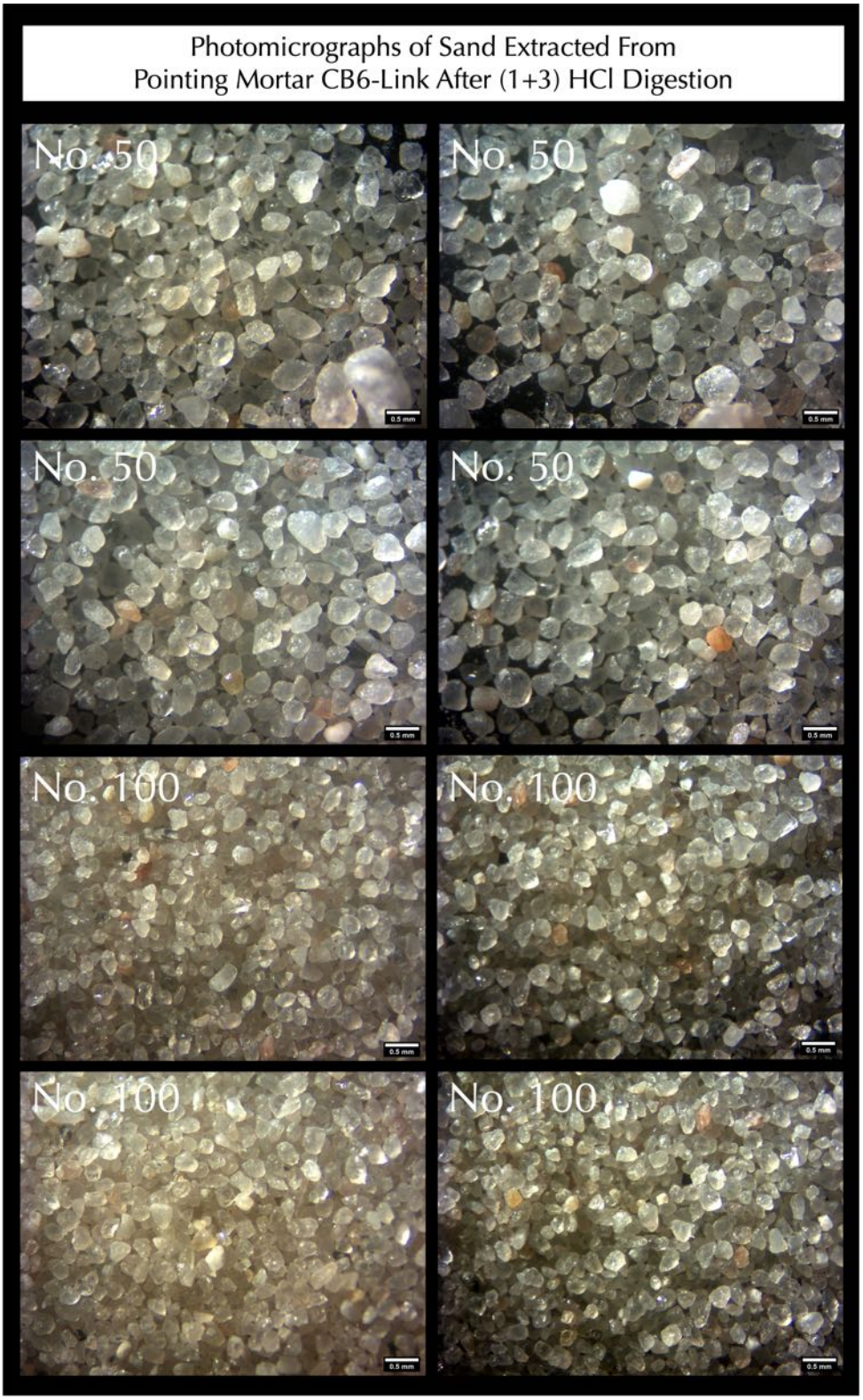

Figure 45: Micrographs of sand particles extracted from the pointing mortar CB6-Link after acid digestion, which are retained on Sieves 50 and 100. Sand particles are mostly transparent to translucent clear quartz sand, with a few off-white and light gray particles. Sand particles are mostly angular to subangular grains, all of which are equidimensional/equant in shape.

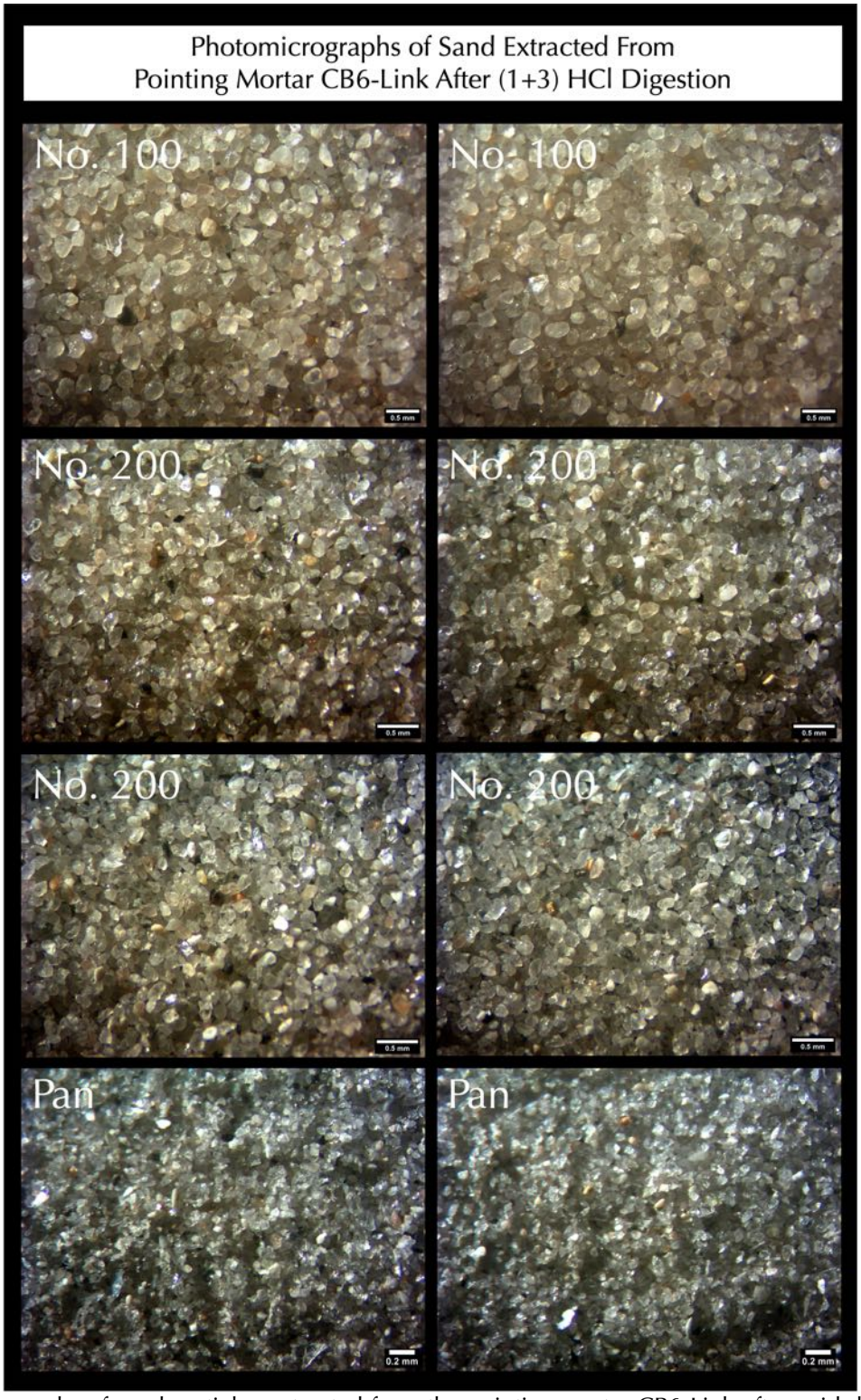

Figure 46: Micrographs of sand particles extracted from the pointing mortar CB6-Link after acid digestion, which are retained on Sieves 100, 200, and pan. Sand particles are mostly transparent to translucent clear quartz sand, with a few off-white and light gray particles. Sand particles are mostly angular to subangular grains, all of which are equidimensional/equant in shape.

a. To extract the acid-insoluble components of mortar for the study of grain-size distribution of sand, all four mortar samples were subjected to acid digestion in 1+1 hydrochloric acid. To retain the original grain sizes, representative fragments of mortars, as received, were selected from each sample and immersed in a beaker of 1+1 hydrochloric acid without any breakdown to minimize any further reduction in grain size during sampling. Repeated washings of acid, tap water, and re-immersion in fresh acid solution were done for multiple times over a period of a week followed by stereo-microscopical examinations of acid-washed residues to make sure no residues of acid-soluble component is present in the sand. At the end of repeated acid washings, only the acid-insoluble components of sand were remained for oven drying and use for sieve analysis.

b. Sand extracted from each of the three setting bed mortars show overall compositional similarities in having dominantly siliceous components consisting of major amounts of clear, transparent to translucent clear, off-white, to light gray quartz sand, and minor amounts of argillaceous and ferruginous components.

c. Sand extracted from the pointing mortar is noticeably finer than the sand from three setting bed mortars. Moreover, sand in pointing mortar is mostly angular to subangular indicating use of a fine crushed sand component in the mortar. Sand in the pointing mortar is well-sorted in having a dominant fine size fraction, as opposed to sand in setting mortars, which are well-graded in having multiple size fractions.

d. Sand in three setting mortars consists of two components: (a) a coarser size fraction consisting of major amounts of quartz, quartzite, and subordinate amounts of various argillaceous and ferruginous components where grains are well-graded in having uniform distribution of grain sizes, subangular to subrounded to well-rounded (similar to river sand) having a nominal maximum size of 4 mm, and (b) a finer fraction of mostly finely crushed angular quartz sand and a minor fraction of argillaceous components. The latter (finer) sand size fraction appeared to be similar to the sand used in the pointing mortar.

e. Fineness modulus of extracted sands calculated from the sum of cumulative percent retained on Sieves 4, 8, 16, 30, 50, and 100 divided by 100 showed values consistent with fine sand, e.g., 2.53 for east wall setting mortar SET-3, 1.88 for west wall setting mortar SWM-2, 2.07 for south wall setting mortar SSB-3, and a noticeably lower 0.75 for sand in the pointing mortar. Fineness modulus is typically from 2.2 to 2.6 for fine sand, 2.6 to 2.9 for medium sand, and 2.9 to 3.2 for coarse sand.

f. Grain size distribution of sand used in three setting mortars are all finer than size distribution of modern ASTM C 144 sand, hence cannot be substituted with an ASTM C 144 sand. This is especially true for the sand in the pointing mortar, which shows noticeably finer size distribution for all sieve fractions compared to modern-day ASTM C 144 masonry sand.

g. Therefore, based on compositions and grain size distributions of extracted sand, the pointing mortar is judged to be consistent with its 'original' vintage where a fine crushed sand was mixed with river sand in production of the main setting mortars whereas only a clean washed and finer size crushed silica-based sand was used in pointing mortar.

Lapped Sections

Figure 47: Clear epoxy-impregnated lapped cross section of the setting mortar SET-3 showing: (a) the size, shape, angularity, gradation, and distribution of sand particles, showing the presence of a coarser rounded to subangular size fraction of nominal 4 mm size and a finer, mostly angular size fraction of maximum 1 mm size; (b) reddish-brown colored interstitial paste fraction, and (c) overall non-air-entrained nature of the mortar, consistent with its reported early 19th century derivation.

Figure 48: Clear epoxy-impregnated lapped cross section of the setting mortar SWM-2 showing: (a) the size, shape, angularity, gradation, and distribution of sand particles, showing the presence of a coarser rounded to subangular size fraction of nominal 4 mm size and a finer, mostly angular size fraction of maximum 1 mm size, (b) reddish-brown colored interstitial paste fraction, and (c) overall non-air-entrained nature of the mortar, consistent with its reported early 19th century derivation.

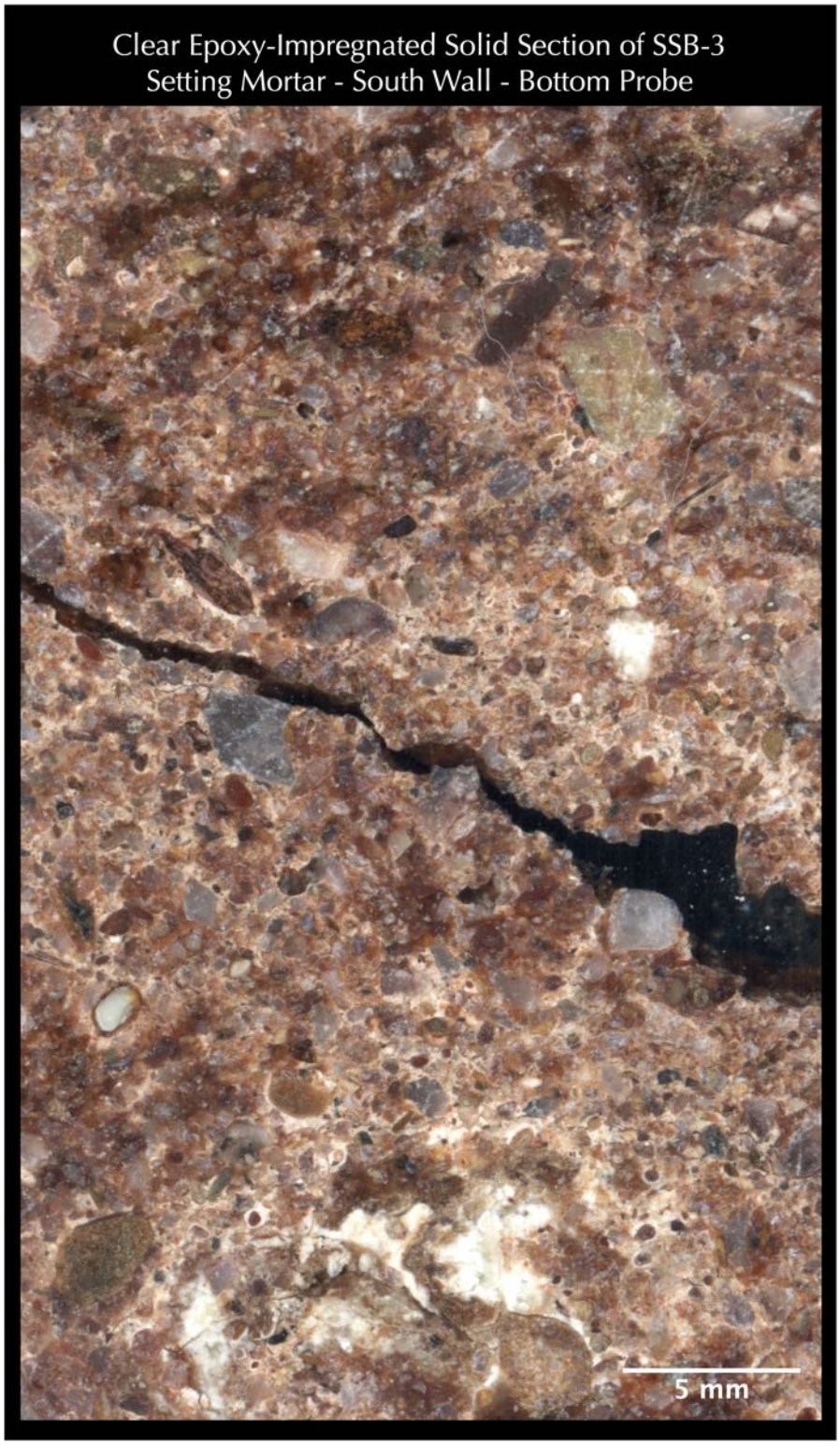

Figure 49: Clear epoxy-impregnated lapped cross section of the setting mortar SSB-3 showing: (a) the size, shape, angularity, gradation, and distribution of sand particles, showing the presence of a coarser rounded to subangular size fraction of nominal 4 mm size and a finer, mostly angular size fraction of maximum 1 mm size, (b) reddish-brown colored interstitial paste fraction, and (c) overall non-air-entrained nature of the mortar, consistent with its reported early 19th century derivation.

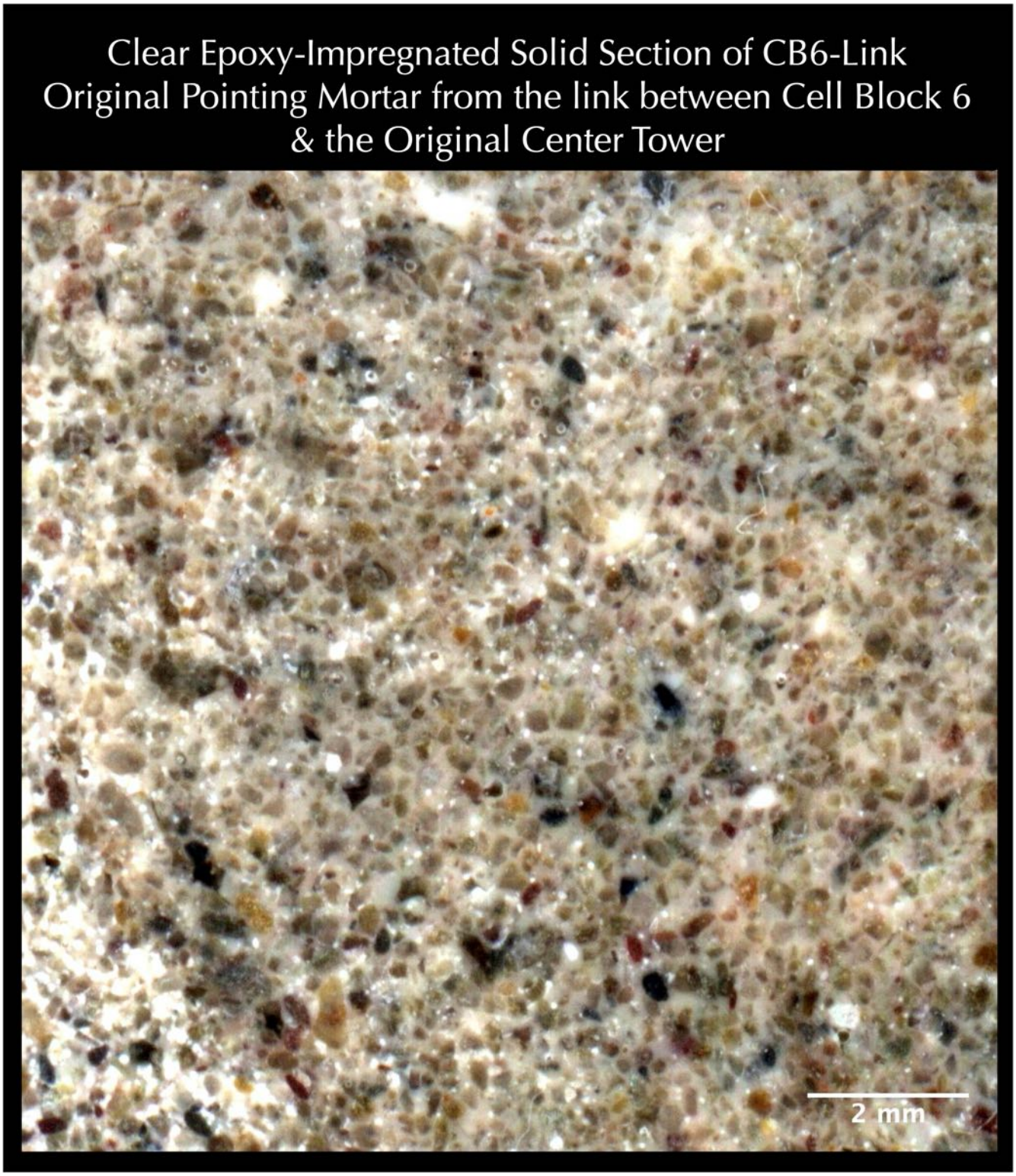

Figure 50: Clear epoxy-impregnated lapped cross section of the pointing mortar CB6-Link showing: (a) the size, shape, angularity, gradation, and distribution of sand particles, showing the presence of very fine, mostly angular sand fragments of less than 0.5 mm in size; (b) light gray colored interstitial paste fraction, and (c) overall non-air-entrained nature of the mortar. Notice: (a) significantly finer size, and consistent (well-sorted) grain size of sand particles as opposed to overall coarser and well-graded sand in the three setting mortars; and (b) light gray as opposed to reddish-brown color tone of paste due to the use of different binder components between setting and pointing mortars.

Micrographs of Lapped Sections

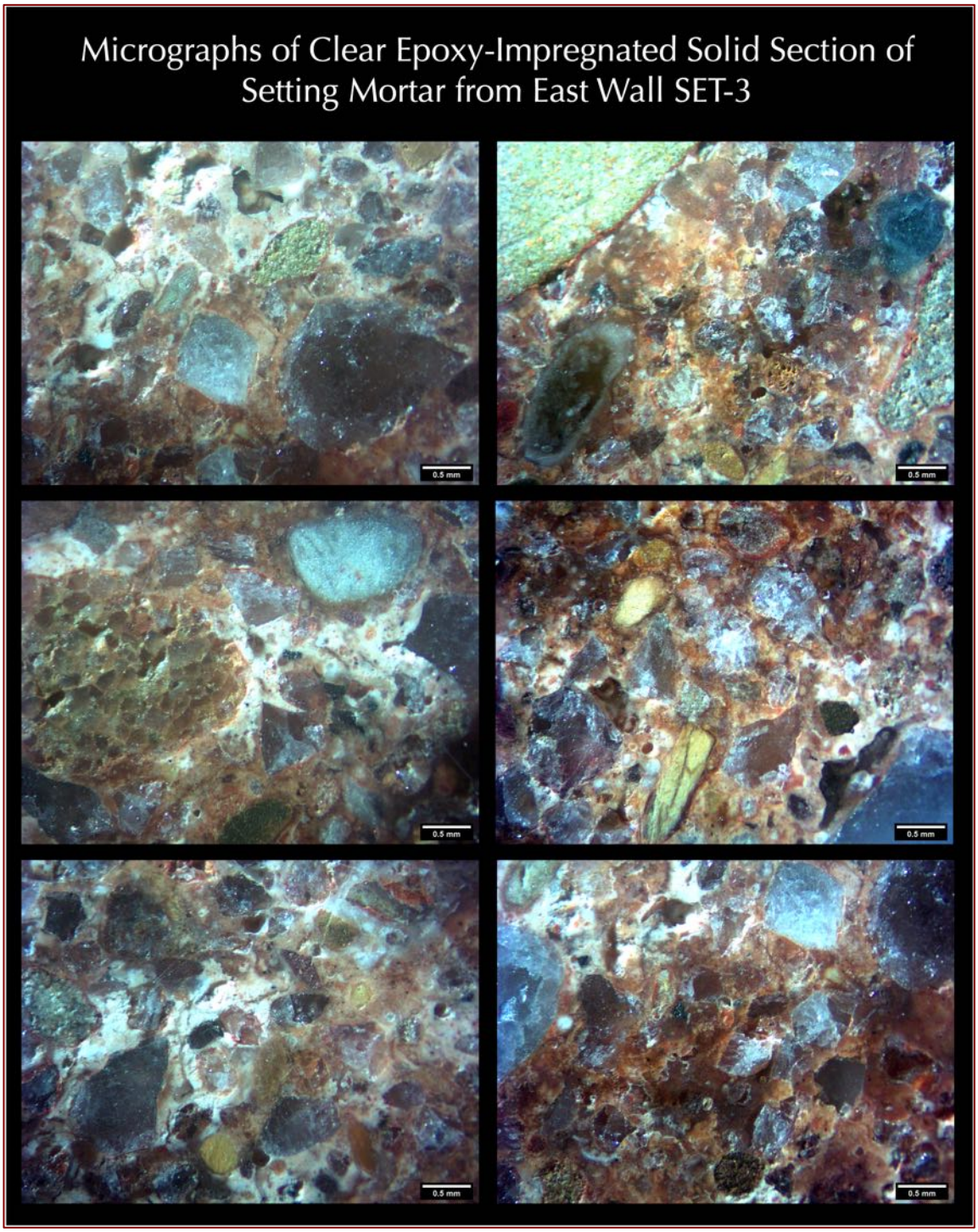

Figure 51: Micrographs of clear epoxy-impregnated cross section of the setting mortar SET-3 showing: (a) the size, shape, angularity, gradation, and distribution of sand particles, (b) reddish brown colored interstitial paste fraction, and (c) overall non-air-entrained nature of the mortar, consistent with its reported early 19th century derivation.

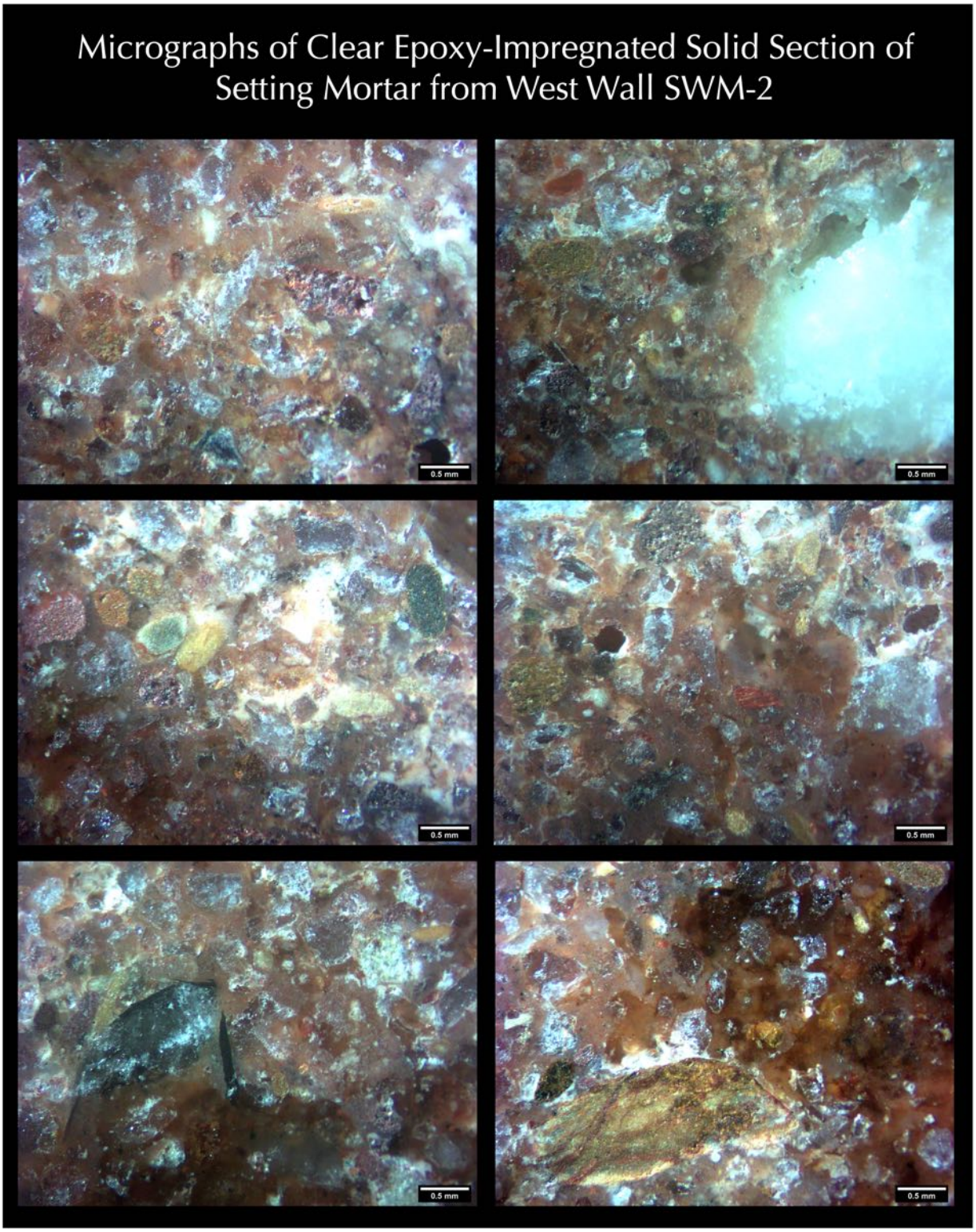

Figure 52: Micrographs of clear epoxy-impregnated cross section of the setting mortar SWM-2 showing: (a) the size, shape, angularity, gradation, and distribution of sand particles, (b) reddish brown colored interstitial paste fraction, and (c) overall non-air-entrained nature of the mortar, consistent with its reported early 19th century derivation.

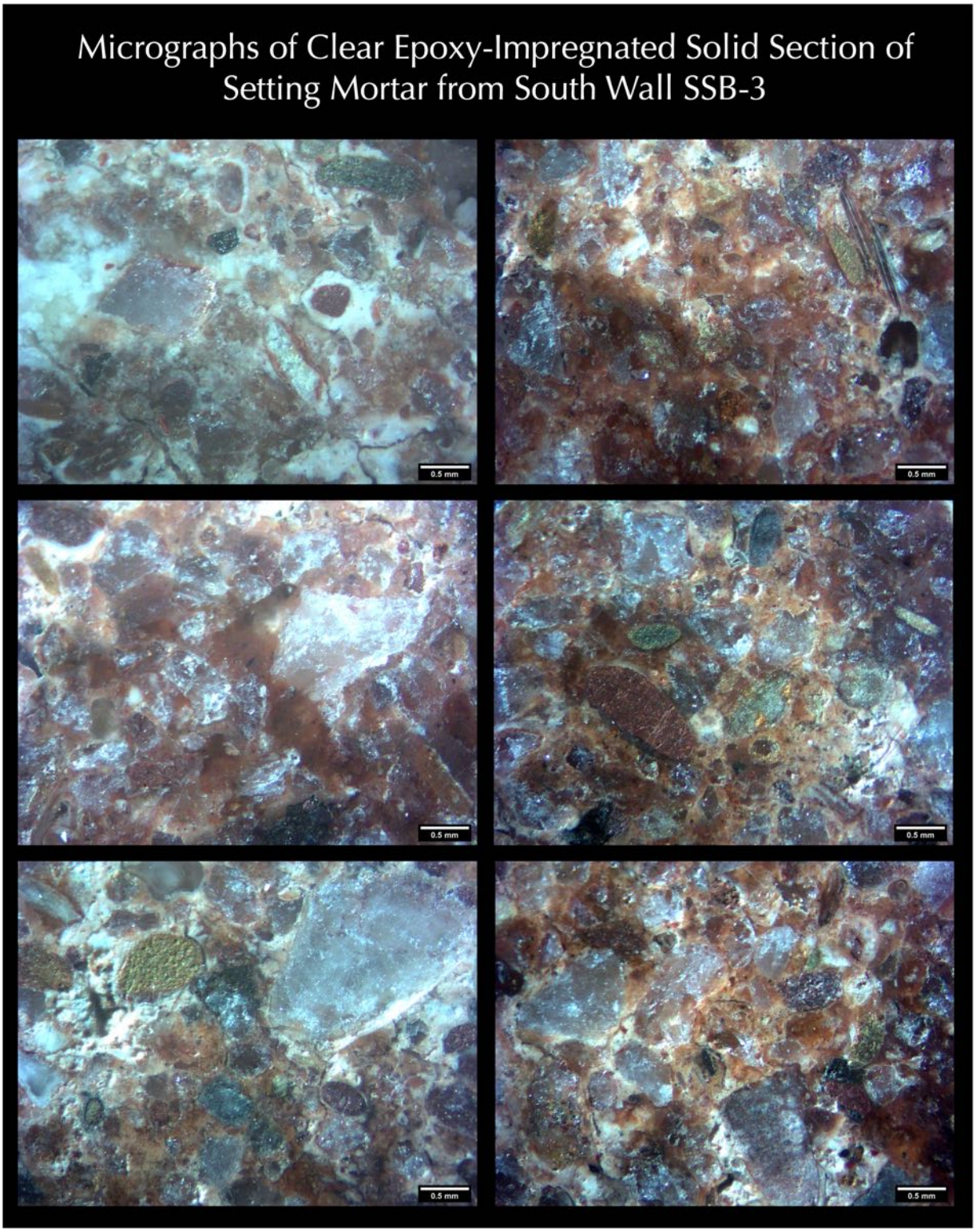

Figure 53: Micrographs of clear epoxy-impregnated cross section of the setting mortar SSB-3 showing: (a) the size, shape, angularity, gradation, and distribution of sand particles, (b) reddish brown colored interstitial paste fraction, and (c) overall non-air-entrained nature of the mortar, consistent with its reported early 19th century derivation.

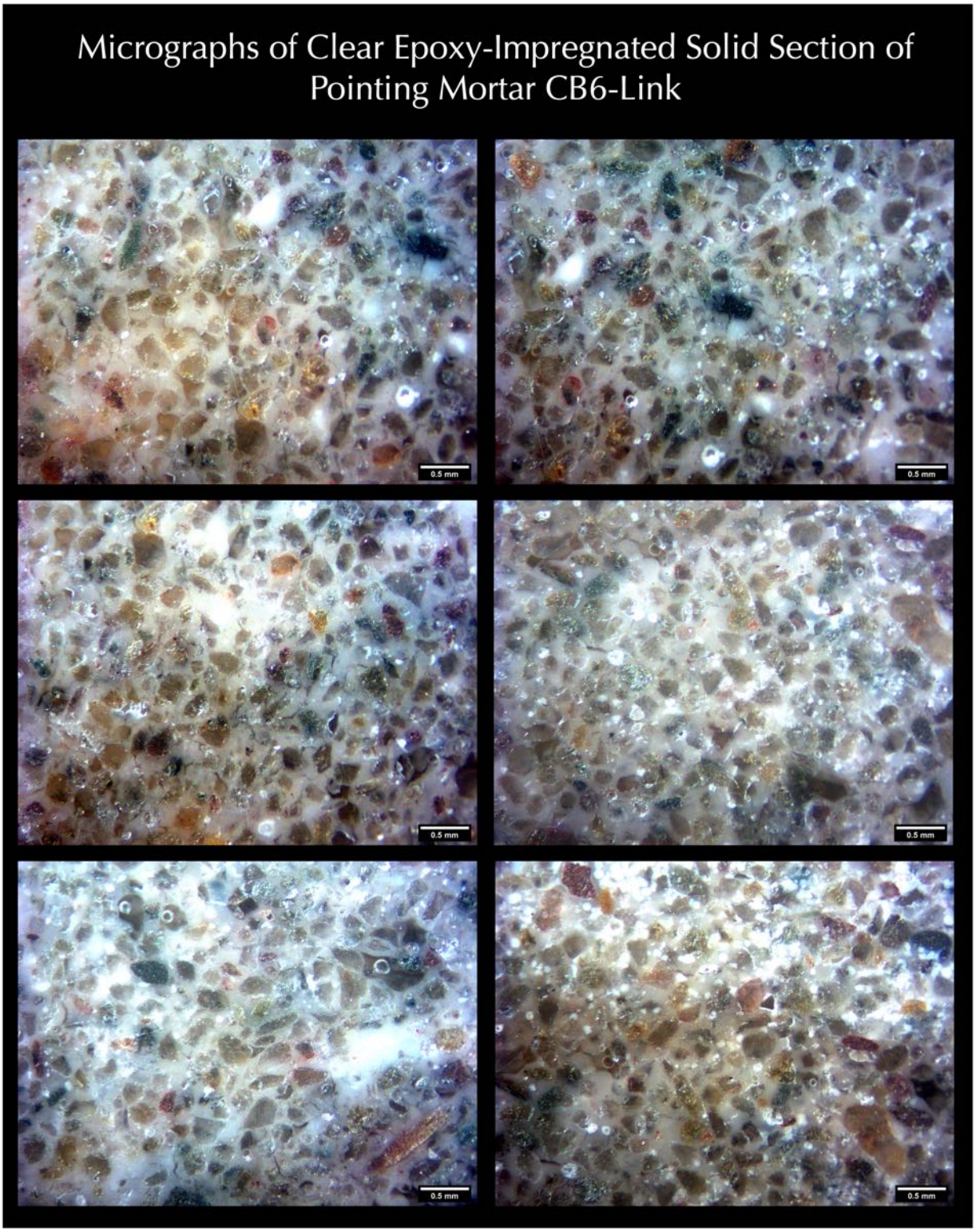

Figure 54: Micrographs of clear epoxy-impregnated lapped cross section of the pointing mortar CB6-Link showing: (a) the size, shape, angularity, gradation, and distribution of sand particles, (b) light gray colored interstitial paste fraction, and (c) overall non-air-entrained nature of the mortar. Notice: (a) significantly finer size, and consistent (well-sorted) grain size of sand particles as opposed to overall coarser and well-graded sand in the three setting mortars; and (b) light gray as opposed to reddish brown color tone of paste due to the use of different binder components between setting and pointing mortars, which are described later.

Thin Sections

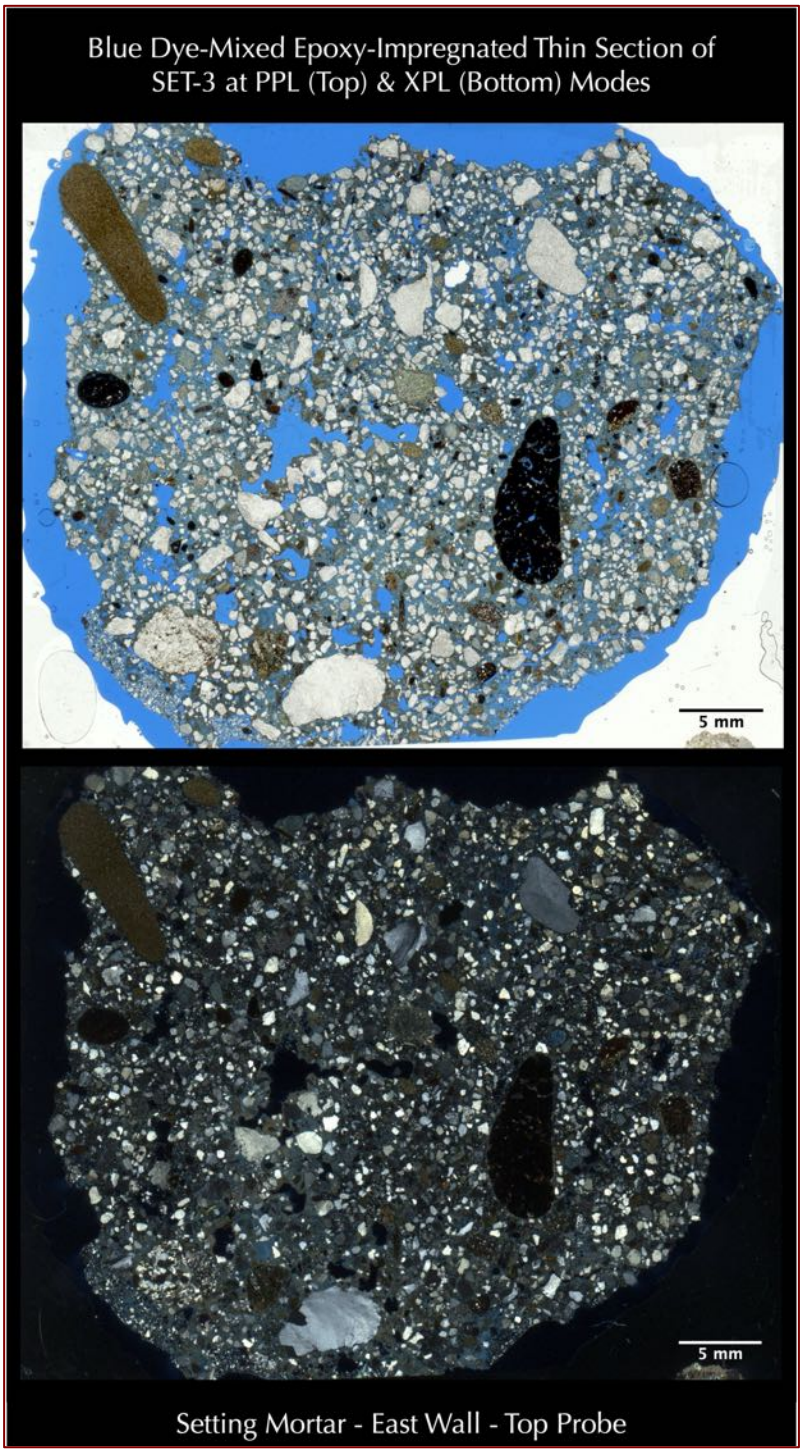

Figure 55: Blue dye-mixed epoxy impregnated thin section of the setting mortar SET-3 scanned from a flatbed film scanner, where thin section was scanned first with a polarizing filter to generate the plane polarized light view of mortar (top photo), which shows sand grain size, shape, angularity, and distribution, and interstitial pore and void spaces in mortar highlighted from blue epoxy, and then with two perpendicular polarizing filters to generate cross polarized light view (bottom photo), which shows siliceous sand components and overall near-isotropic appearance of interstitial matrix, which is very different from a typical historic lime mortar.

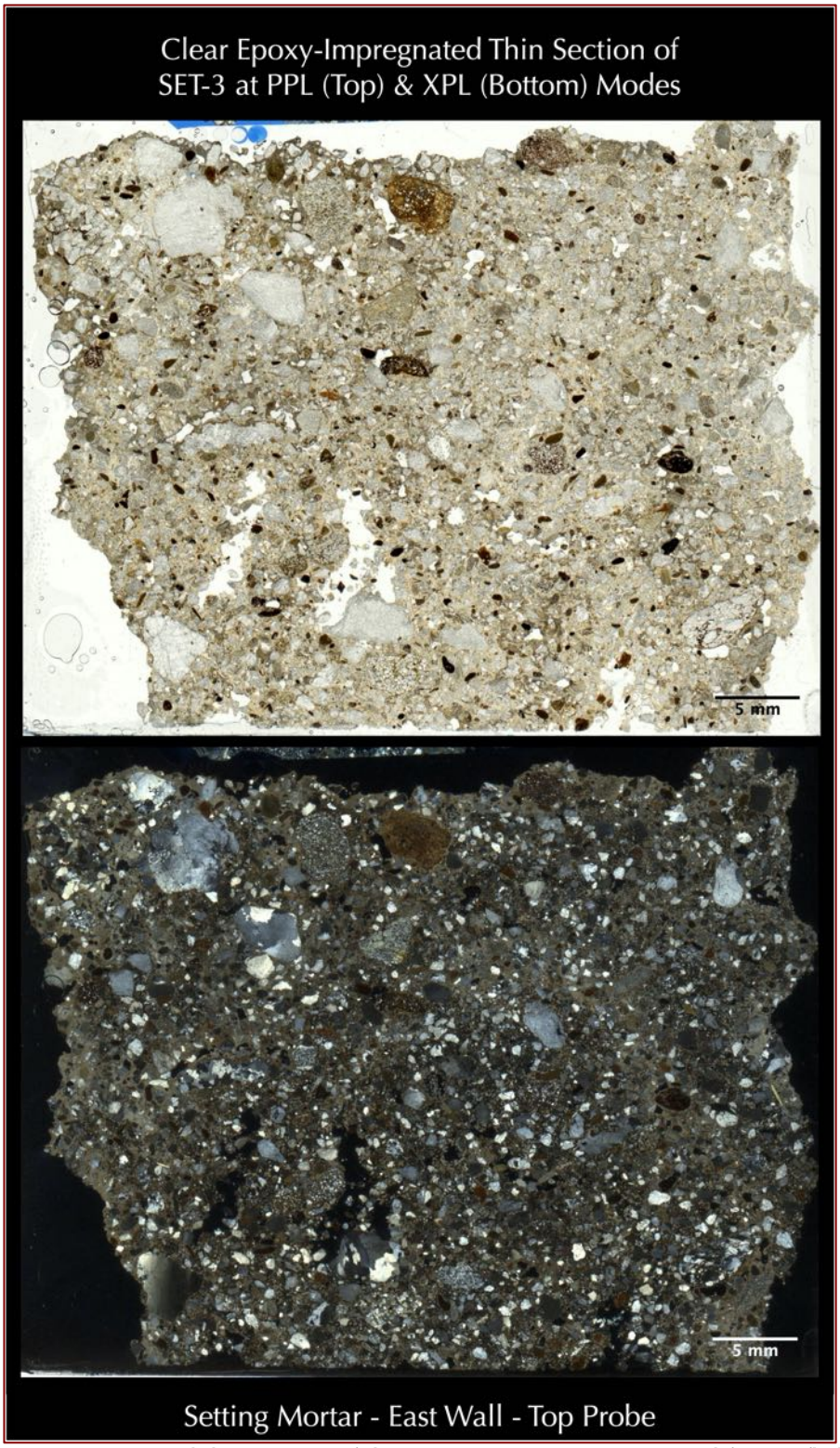

Figure 56: Clear epoxy impregnated thin section of the setting mortar SET-3 scanned from a flatbed film scanner, where thin section was scanned first with a polarizing filter to generate the plane polarized light view of mortar (top photo), which shows sand grain size, shape, angularity, and distribution, and then with two perpendicular polarizing filters to generate cross polarized light view (bottom photo), which shows siliceous composition of sand.

Figure 57: Residue of blue dye-mixed epoxy encapsulated (top) and clear epoxy encapsulated (bottom) block of setting mortar SET-3 showing distribution of sand particles and interstitial paste fraction.

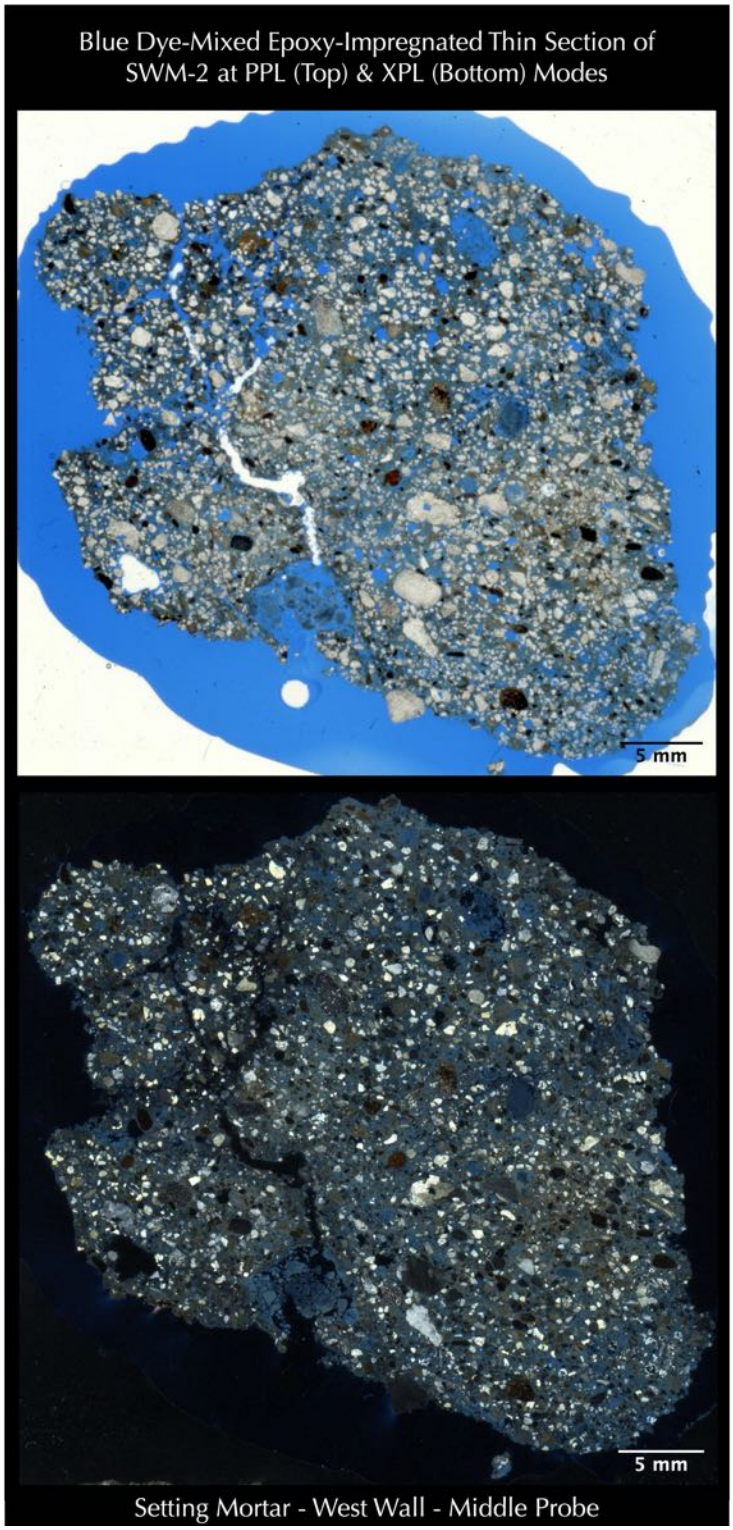

Figure 58: Blue dye-mixed epoxy impregnated thin section of the setting mortar SWM-2 scanned from a flatbed film scanner, where thin section was scanned first with a polarizing filter to generate the plane polarized light view of mortar (top photo), which shows sand grain size, shape, angularity, and distribution, and interstitial pore and void spaces in mortar highlighted from blue epoxy, and then with two perpendicular polarizing filters to generate cross polarized light view (bottom photo), which shows siliceous sand components and overall near-isotropic appearance of interstitial matrix, which is very different from a typical historic lime mortar.

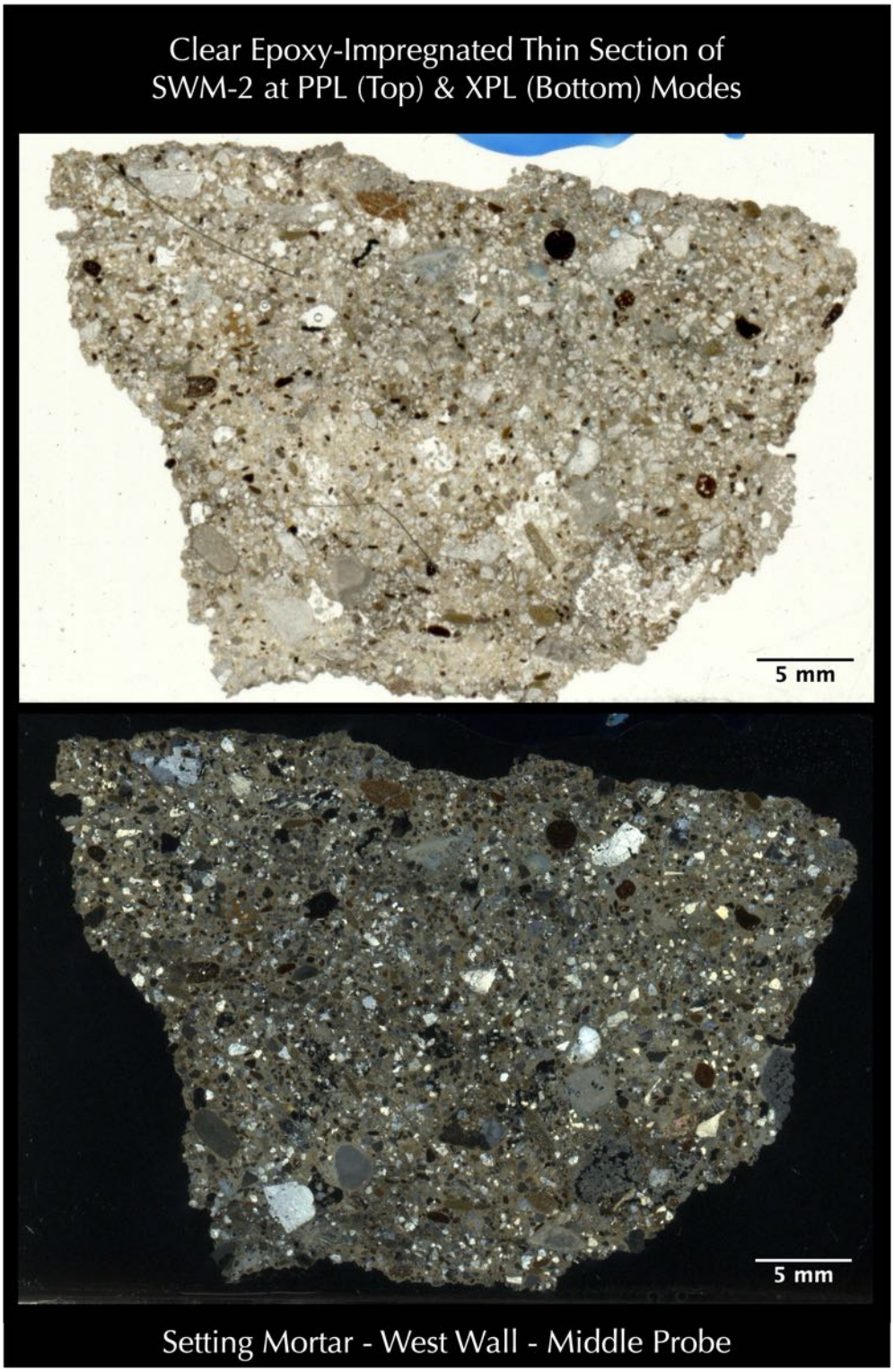

Figure 59: Clear epoxy impregnated thin section of the setting mortar SWM-2 scanned from a flatbed film scanner, where thin section was first scanned with a polarizing filter to generate the plane polarized light view of mortar (top photo), which shows sand grain size, shape, angularity, and distribution, and then re-scanned with two perpendicular polarizing filters to generate cross polarized light view (bottom photo), which shows the dominantly siliceous composition of sand.

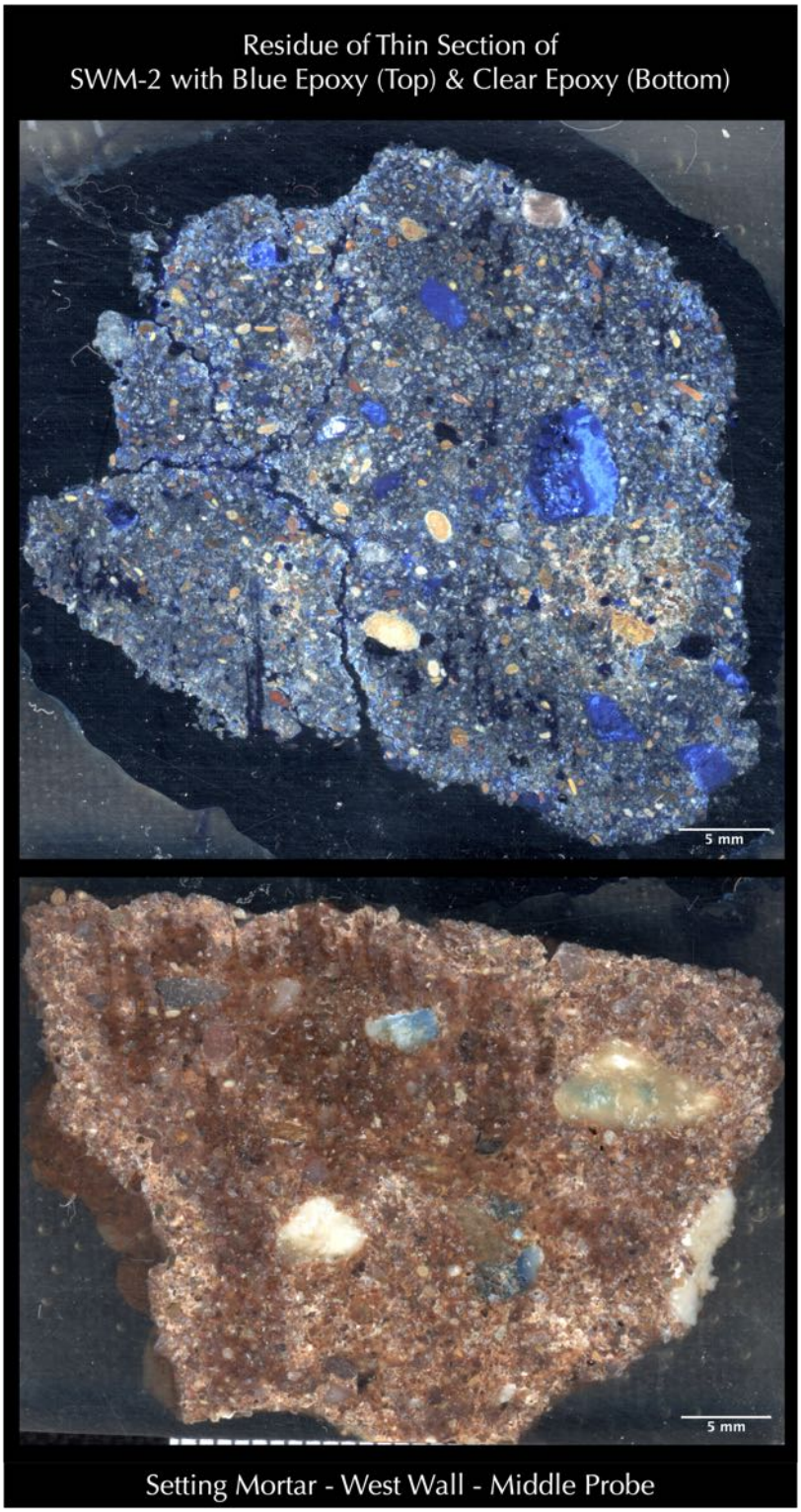

Figure 60: Residue of blue dye-mixed epoxy encapsulated (top) and clear epoxy encapsulated (bottom) block of setting mortar SWM-2 showing distribution of sand particles and interstitial paste fraction.

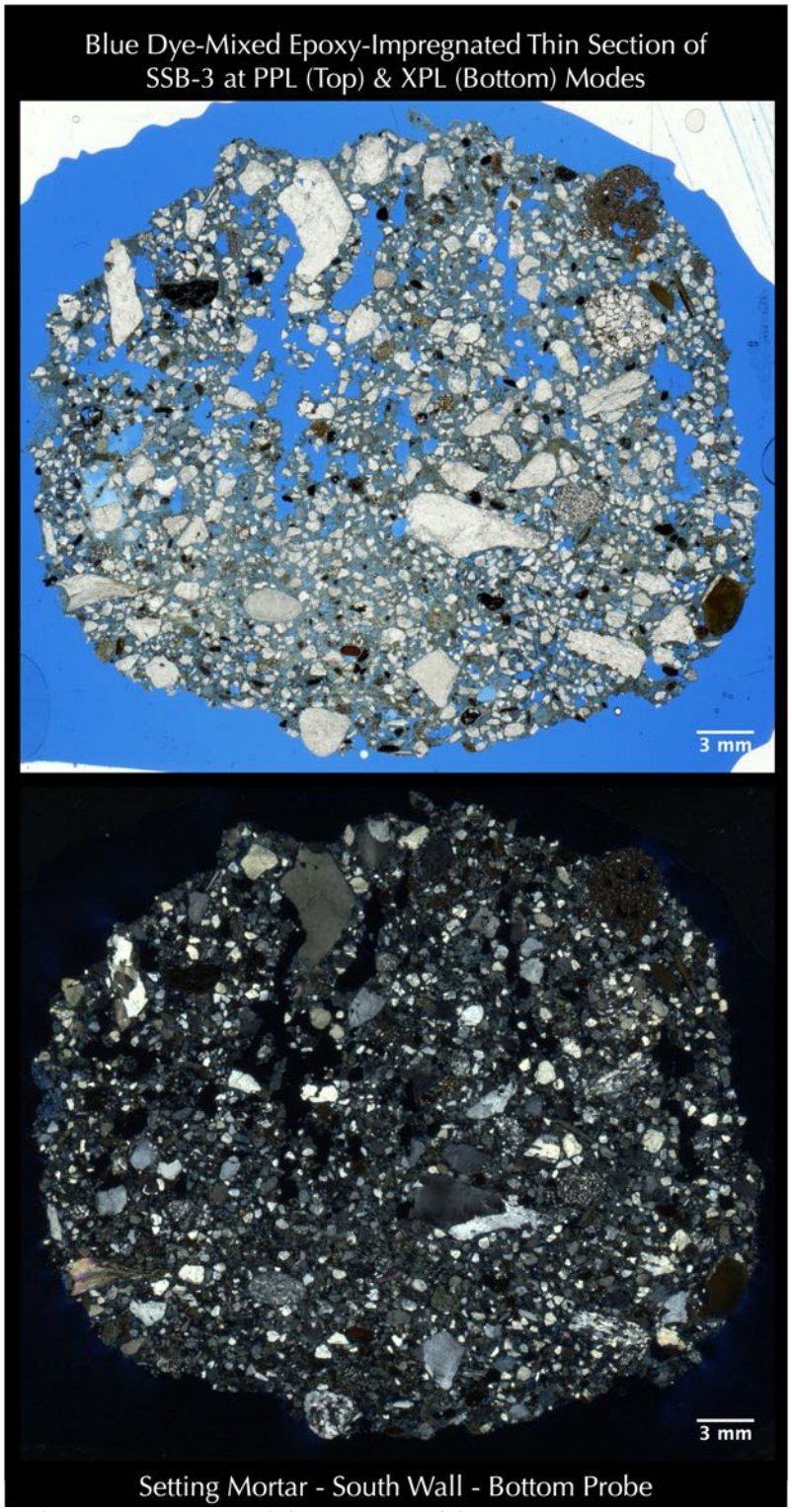

Figure 61: Blue dye-mixed epoxy impregnated thin section of the setting mortar SSB-3 scanned from a flatbed film scanner, where thin section was scanned first with a polarizing filter to generate the plane polarized light view of mortar (top photo), which shows sand grain size, shape, angularity, and distribution, and interstitial pore and void spaces in mortar highlighted from blue epoxy, and then with two perpendicular polarizing filters to generate cross polarized light view (bottom photo), which shows siliceous sand components and overall near-isotropic appearance of interstitial matrix, which is very different from a typical historic lime mortar.

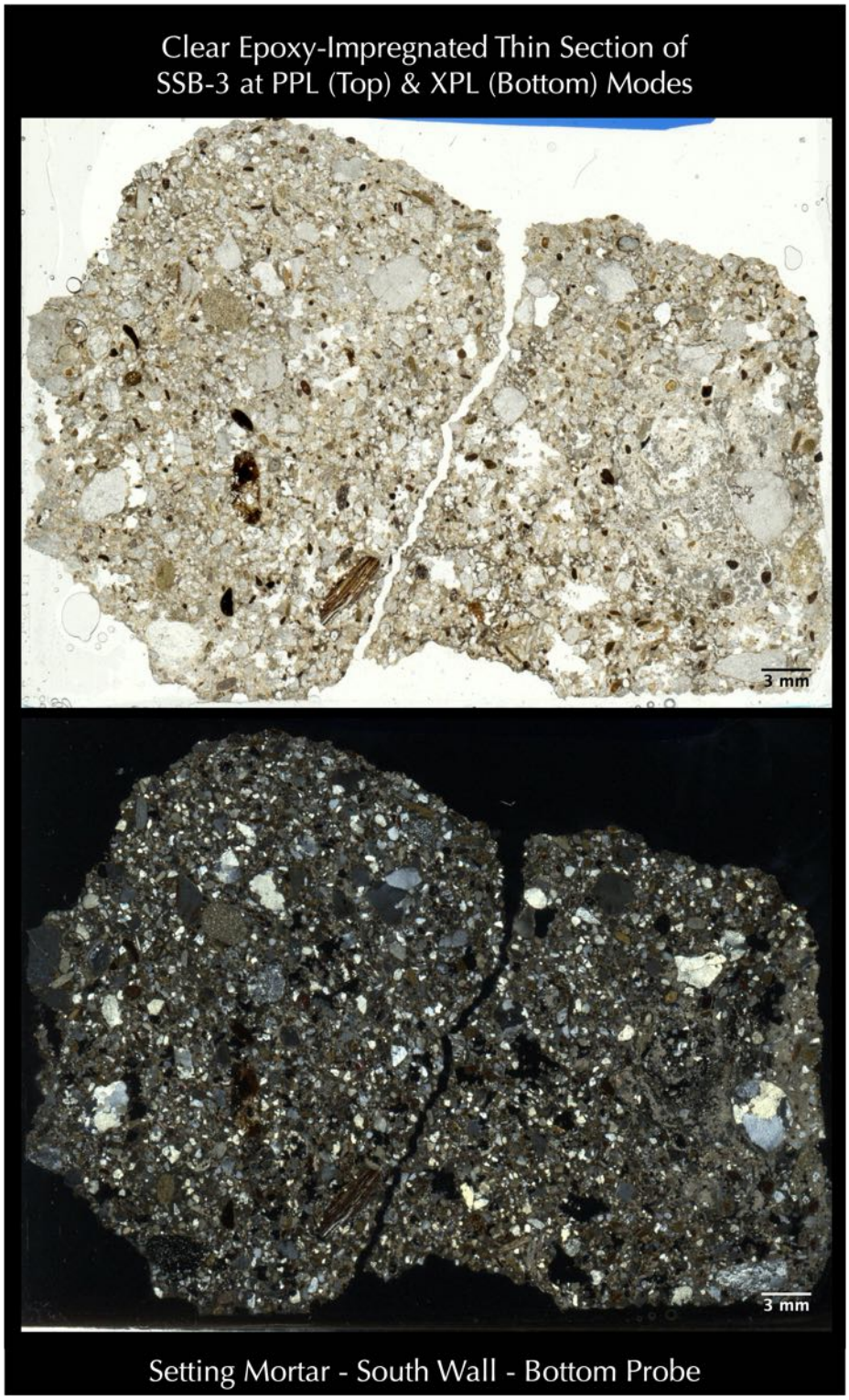

Figure 62: Clear epoxy impregnated thin section of the setting mortar SSB-3 scanned from a flatbed film scanner, where thin section was scanned first with a polarizing filter to generate the plane polarized light view of mortar (top photo), which shows sand grain size, shape, angularity, and distribution, and then with two perpendicular polarizing filters to generate cross polarized light view (bottom photo), which shows siliceous composition of sand.

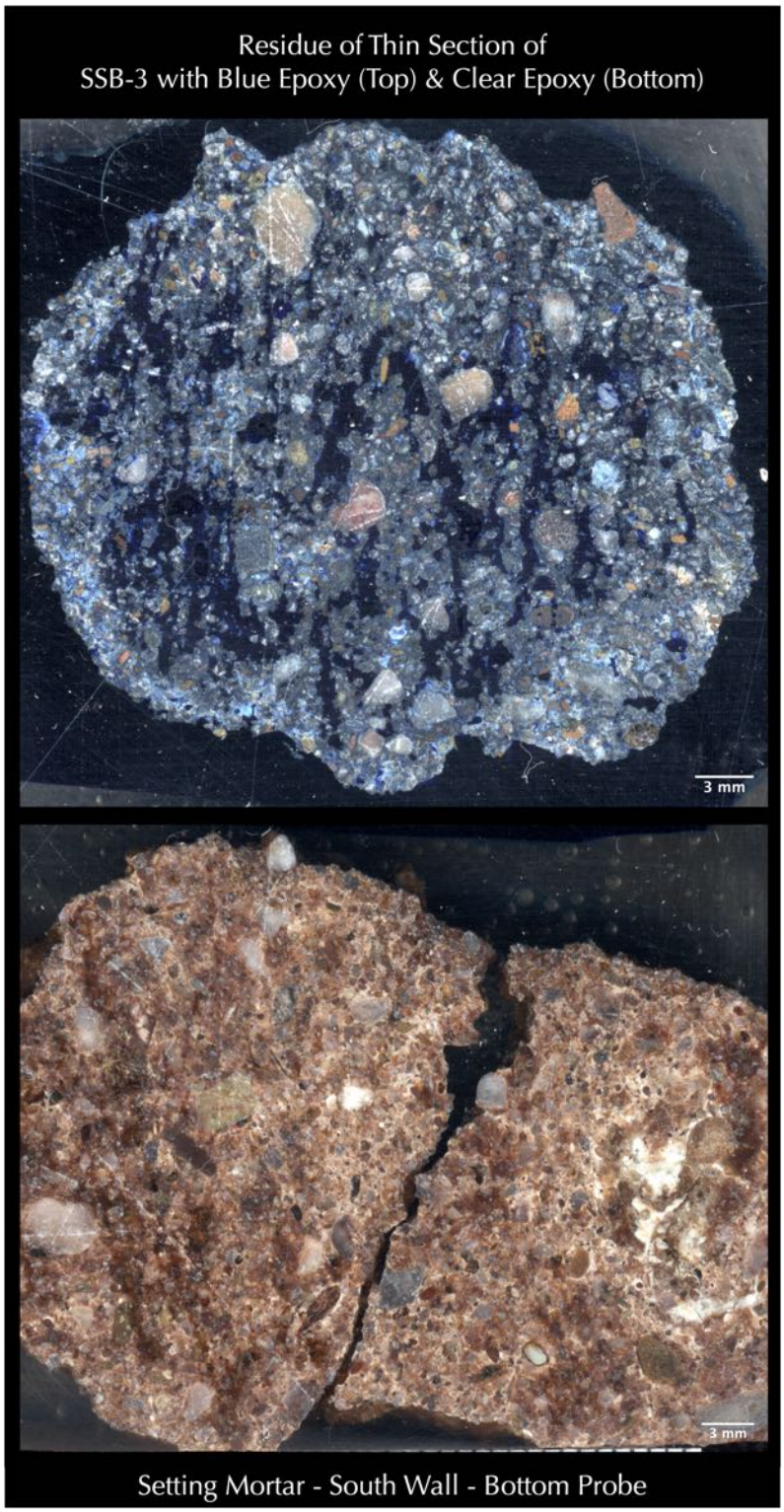

Figure 63: Residue of blue dye-mixed epoxy encapsulated (top) and clear epoxy encapsulated (bottom) block of setting mortar SSB-3 showing distribution of sand particles and interstitial paste fraction.

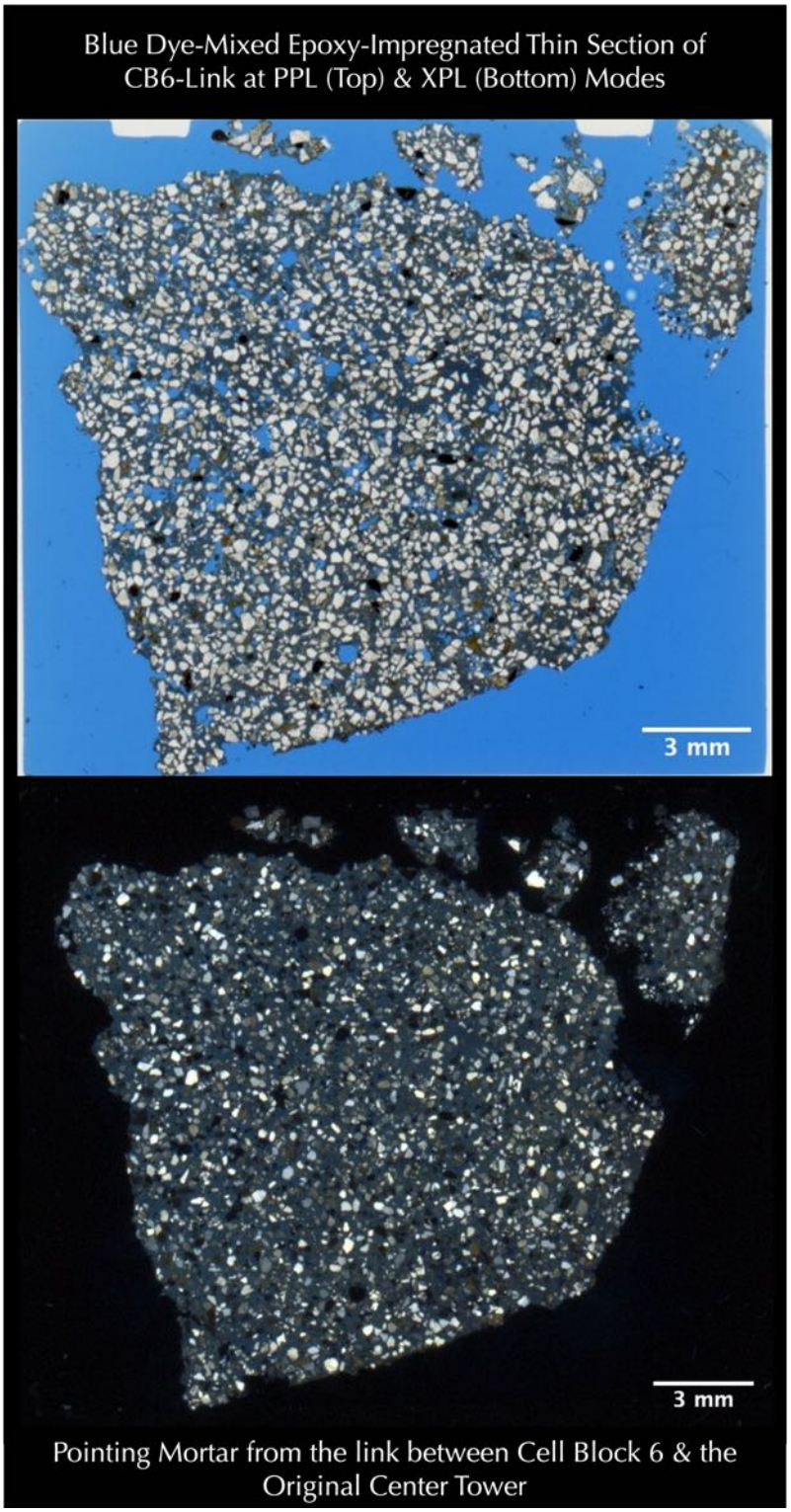

Figure 64: Blue dye-mixed epoxy impregnated thin section of the pointing mortar CB6-Link scanned from a flatbed film scanner, where thin section was scanned first with a polarizing filter to generate the plane polarized light view of mortar (top photo), which shows sand grain size, shape, angularity, and distribution, and interstitial pore and void spaces in mortar highlighted from blue epoxy, and then with two perpendicular polarizing filters to generate cross polarized light view (bottom photo), which shows siliceous composition of sand.

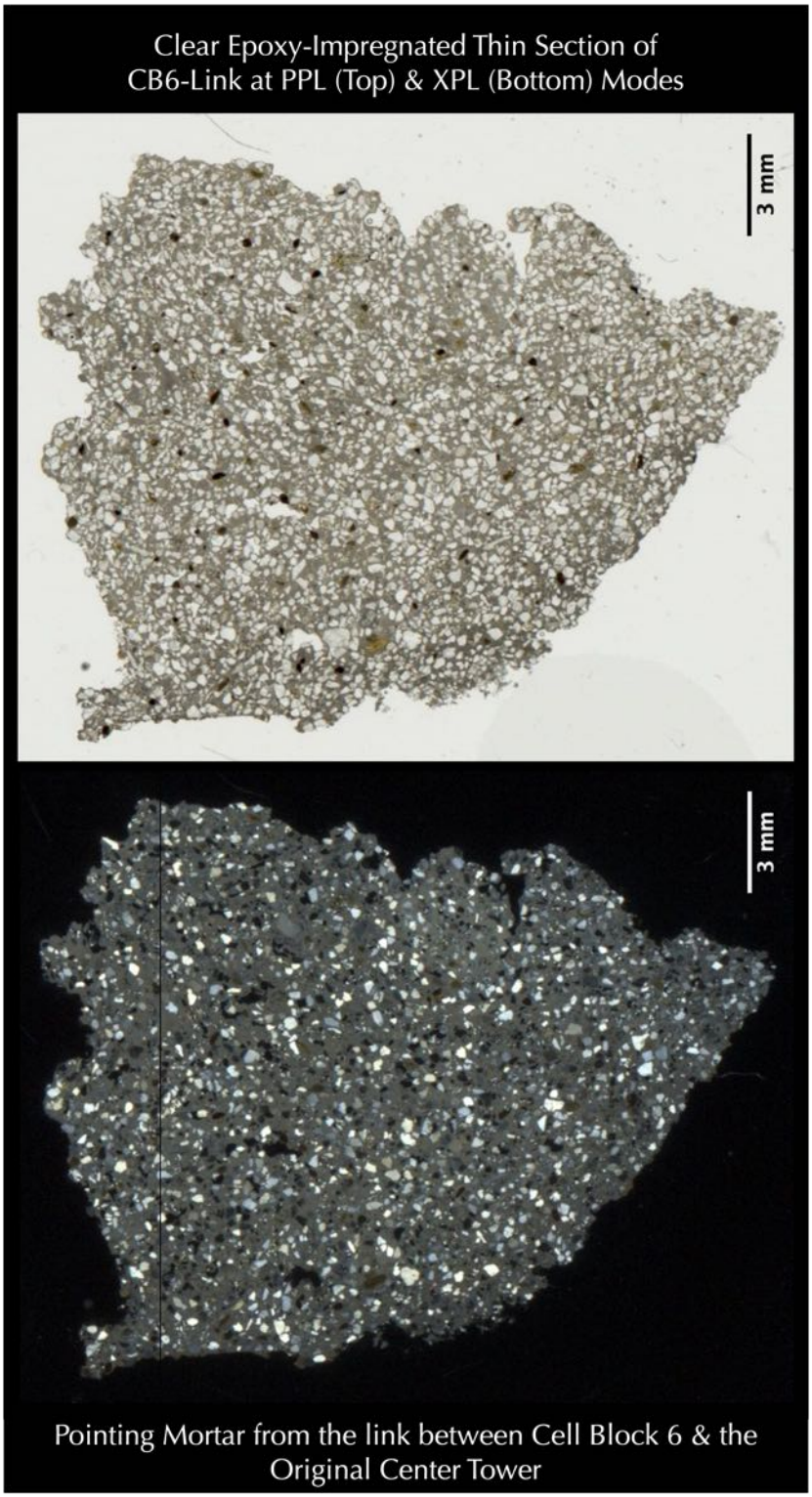

Figure 65: Clear epoxy impregnated thin section of the pointing mortar CB6-Link scanned from a flatbed film scanner, where thin section was scanned first with a polarizing filter to generate the plane polarized light view of mortar (top photo), which shows sand grain size, shape, angularity, and distribution, and then with two perpendicular polarizing filters to generate cross polarized light view (bottom photo), which shows siliceous composition of sand.

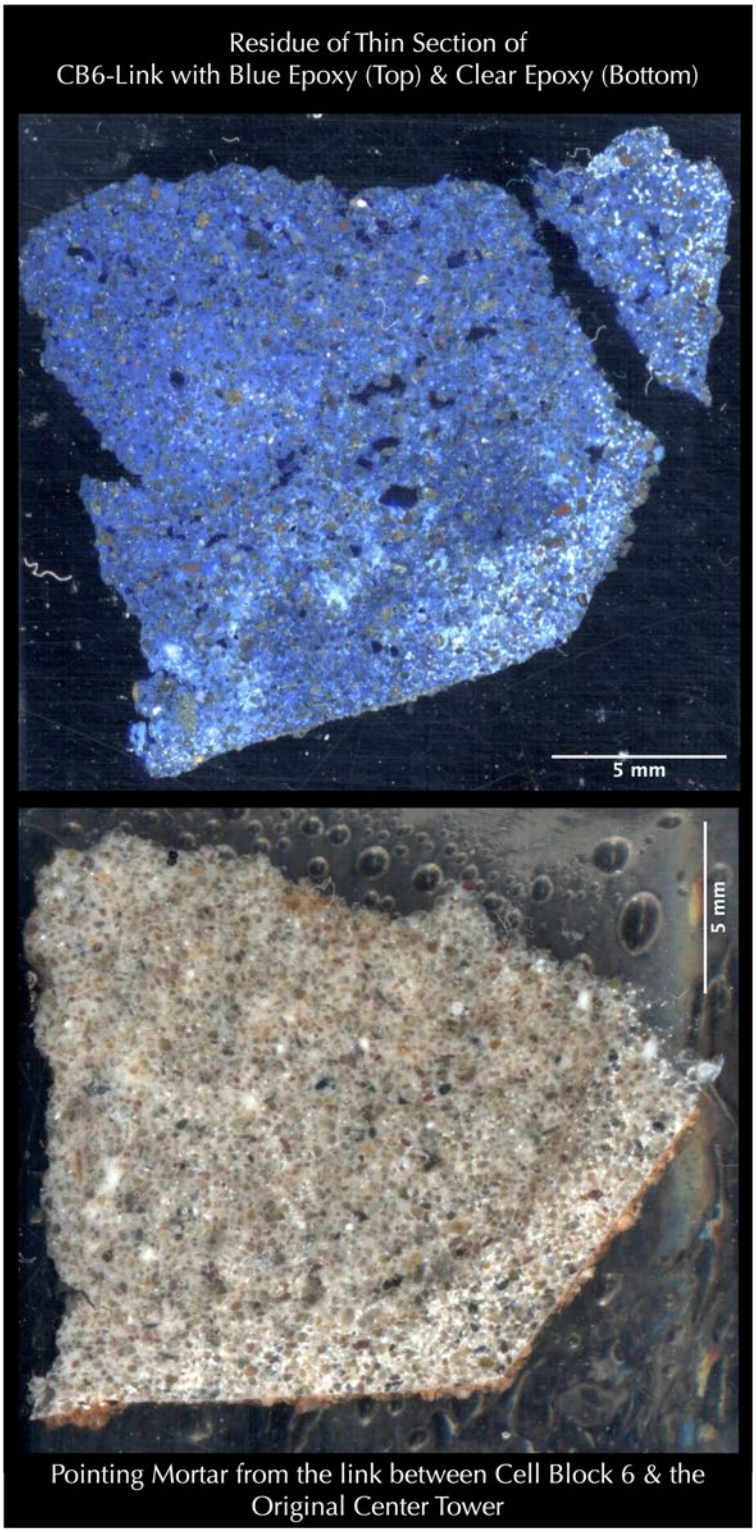

Figure 66: Residue of blue dye-mixed epoxy encapsulated (top) and clear epoxy encapsulated (bottom) block of pointing mortar CB6-Link showing distribution of sand particles and interstitial paste fraction.

Micrographs of Thin Sections

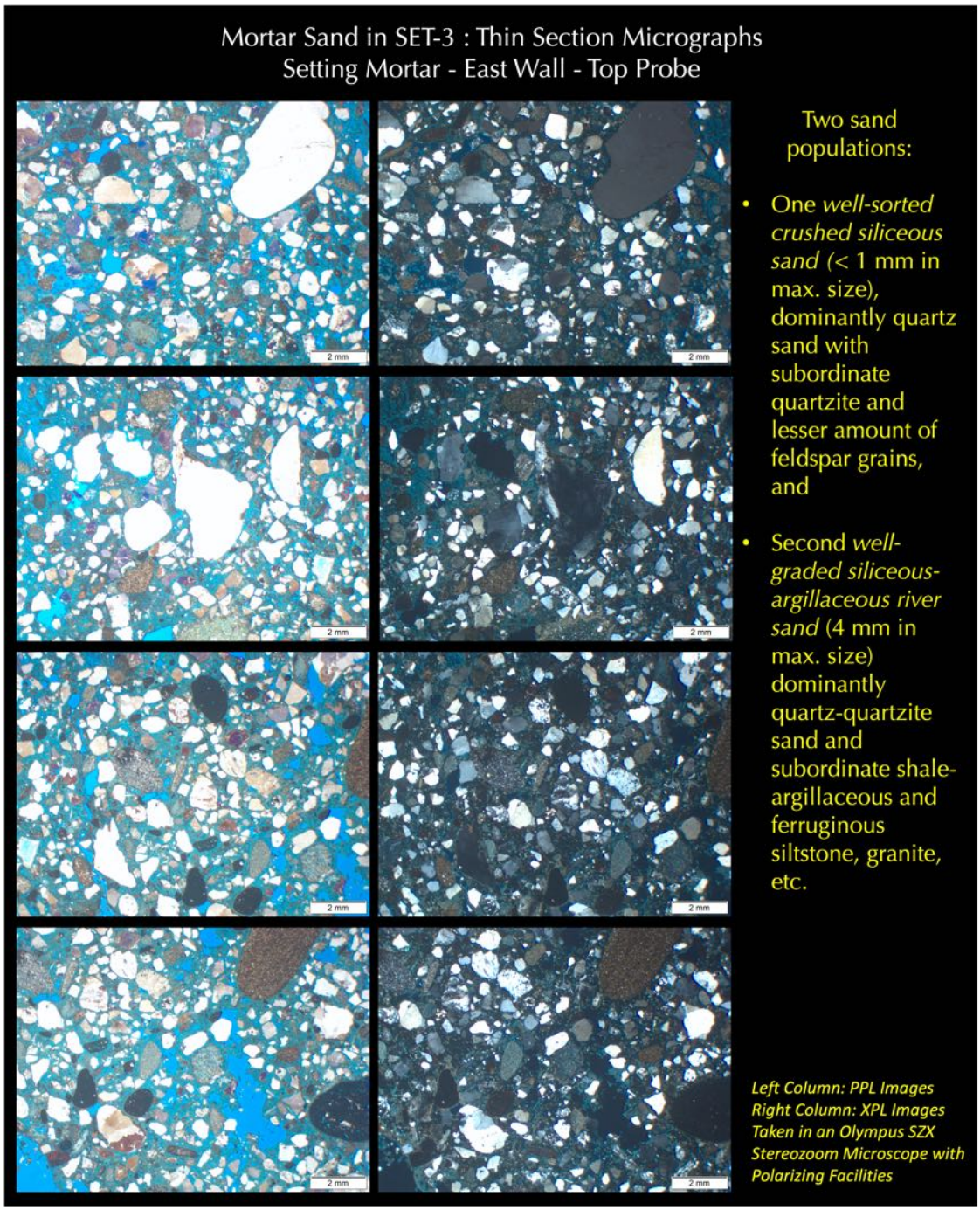

Figure 67: Micrographs of thin section of setting mortar SET-3 showing two components of sand: (1) a coarser component of maximum 4 mm size, consisting of rounded to subrounded to subangular grains of major amounts of quartz and quartzite, subordinate amounts of chert, shale, and reddish brown ferruginous shale and siltstone, and (2) a relatively finer size fraction of maximum 1 mm size, consisting of major amounts of mostly angular to subangular quartz, subordinate amounts of quartzite, feldspar, and minor amounts of shale, reddish brown shale-siltstone. Coarse fraction grains are well-graded, i.e., showing a uniform size distribution of grains, whereas finer fraction is well-sorted, i.e., showing one dominant size fraction over others. Interstitial matrix shows a near-isotropic nature and appeared dark in cross polarized light images in the right column.

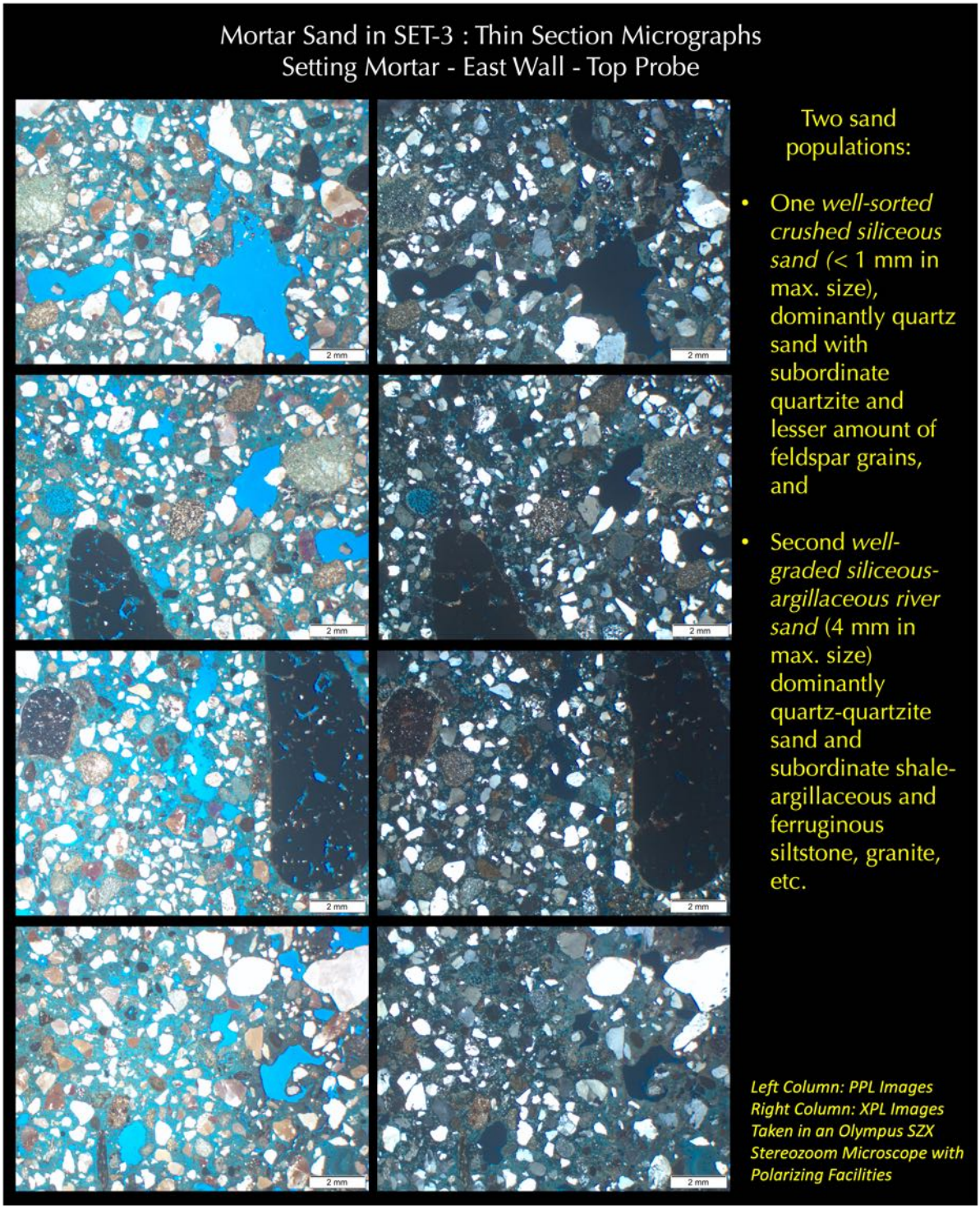

Figure 68: Micrographs of thin section of setting mortar SET-3 showing two components of sand: (1) a coarser component of maximum 4 mm size, consisting of rounded to subrounded to subangular grains of major amounts of quartz and quartzite, subordinate amounts of chert, shale, and reddish brown ferruginous shale and siltstone, and (2) a relatively finer size fraction of maximum 1 mm size, consisting of major amounts of mostly angular to subangular quartz, subordinate amounts of quartzite, feldspar, and minor amounts of shale, reddish brown shale-siltstone. Coarse fraction grains are well-graded, i.e., showing a uniform size distribution of grains, whereas finer fraction is well-sorted, i.e., showing one dominant size fraction over others. Interstitial matrix shows a near-isotropic nature and appeared dark in cross polarized light images in the right column.

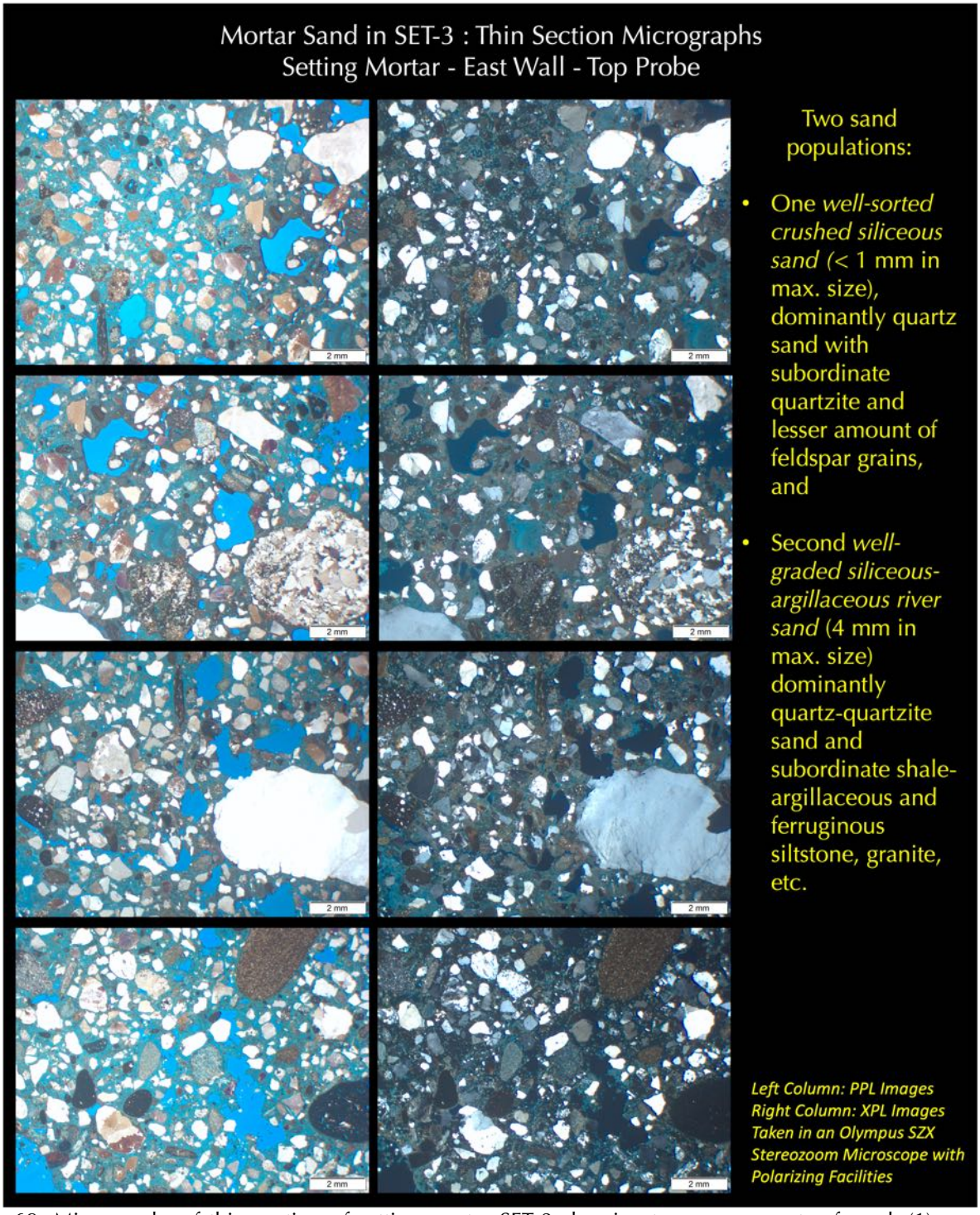

Figure 69: Micrographs of thin section of setting mortar SET-3 showing two components of sand: (1) a coarser component of maximum 4 mm size, consisting of rounded to subrounded to subangular grains of major amounts of quartz and quartzite, subordinate amounts of chert, shale, and reddish brown ferruginous shale and siltstone, and (2) a relatively finer size fraction of maximum 1 mm size, consisting of major amounts of mostly angular to subangular quartz, subordinate amounts of quartzite, feldspar, and minor amounts of shale, reddish brown shale-siltstone. Coarse fraction grains are well-graded, i.e., showing a uniform size distribution of grains, whereas finer fraction is well-sorted, i.e., showing one dominant size fraction over others. Interstitial matrix shows a near-isotropic nature and appeared dark in cross polarized light images in the right column.

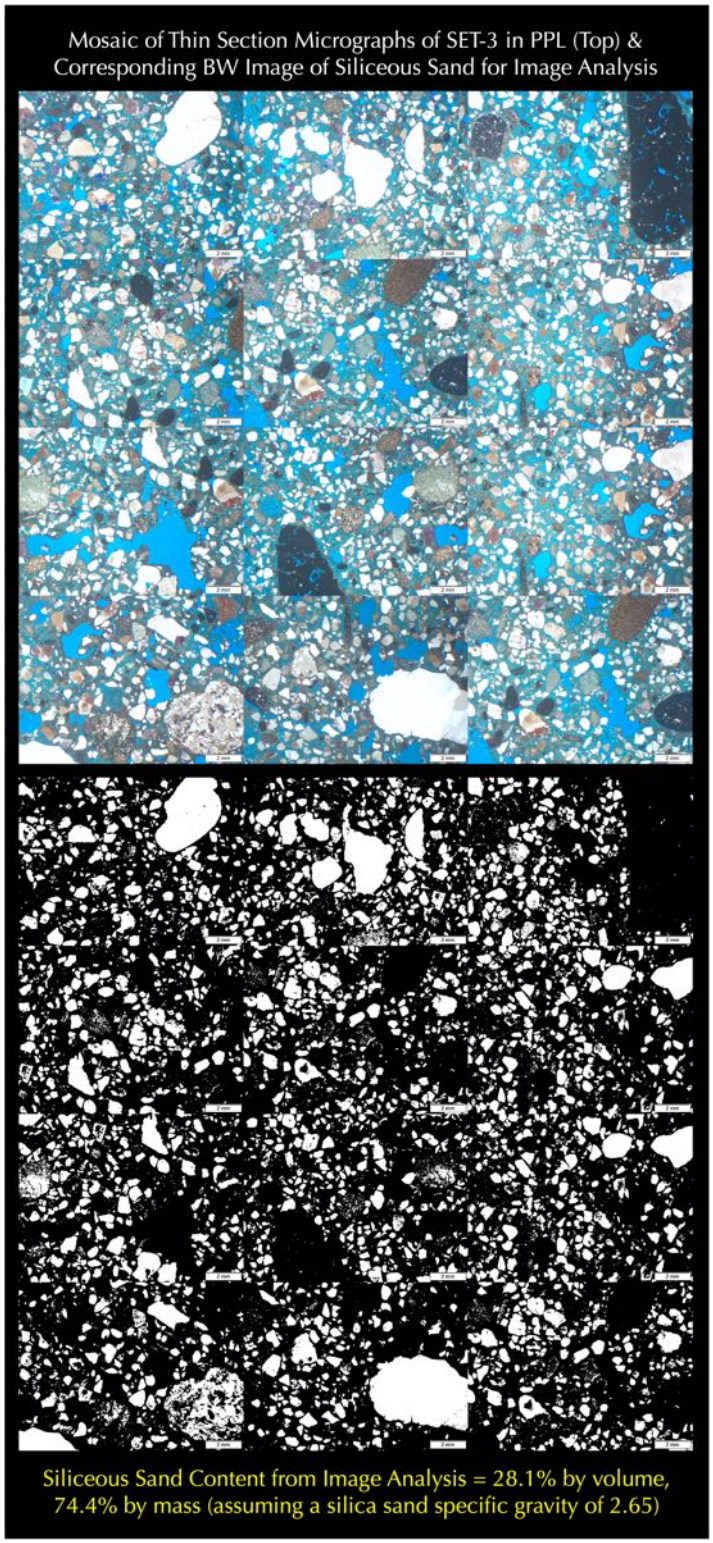

Figure 70: Image analysis of a mosaic of 12 thin section micrographs of setting mortar SET-3 in PPL (top photo) converted to a black and white contrast enhanced image at the bottom to highlight only the siliceous sand components in white against everything else in black. Image analysis (by ImageJ) showed 28% by volume of siliceous sand, which assuming a sand specific gravity of 2.65 corresponds to 74.4% siliceous sand by mass.

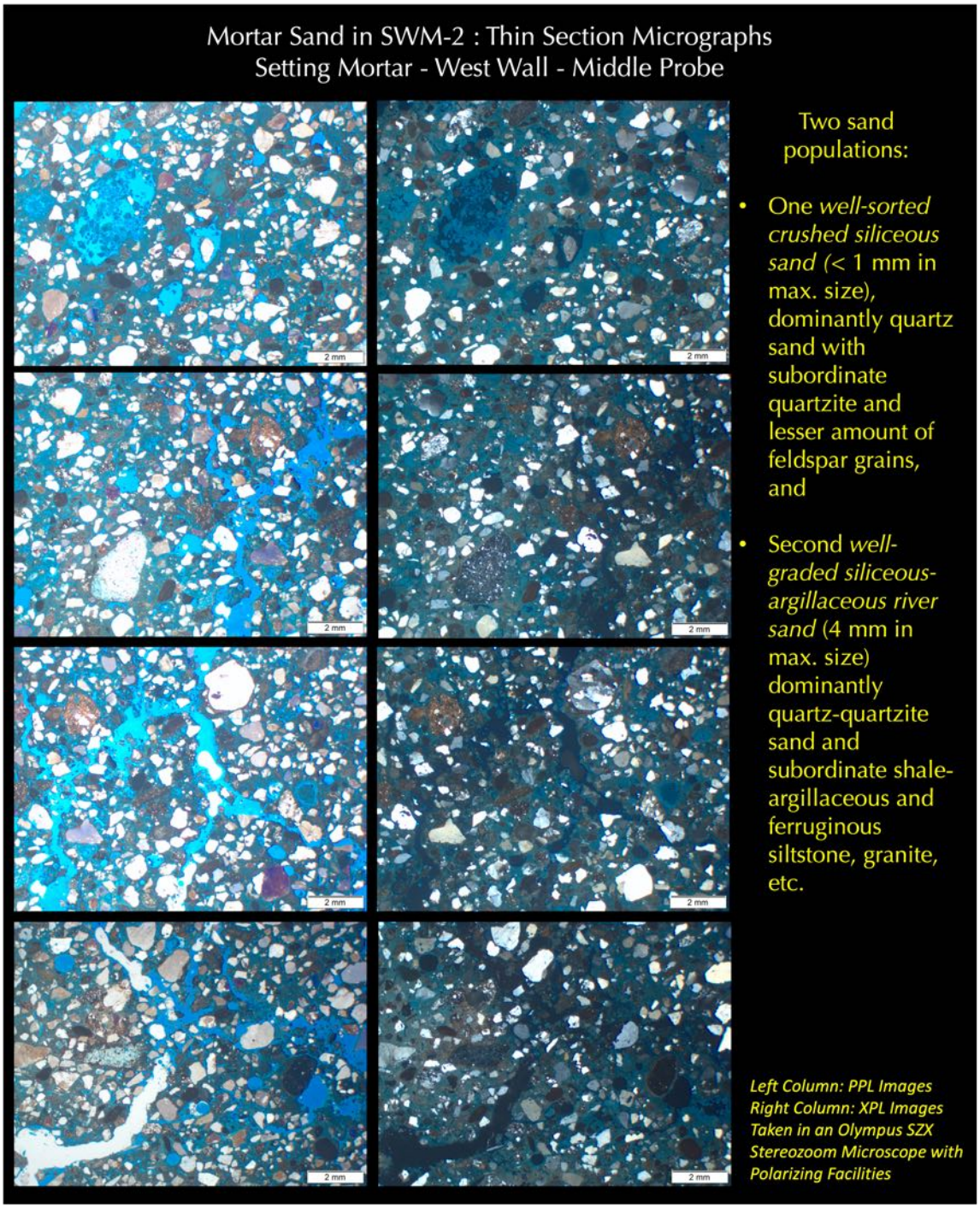

Figure 71: Micrographs of thin section of setting mortar SWM-2 showing two components of sand: (1) a coarser component of maximum 4 mm size, consisting of rounded to subrounded to subangular grains of major amounts of quartz and quartzite, subordinate amounts of chert, shale, and reddish brown ferruginous shale and siltstone, and (2) a relatively finer size fraction of maximum 1 mm size, consisting of major amounts of mostly angular to subangular quartz, subordinate amounts of quartzite, feldspar, and minor amounts of shale, reddish brown shale-siltstone. Coarse fraction grains are well-graded, i.e., showing a uniform size distribution of grains, whereas finer fraction is well-sorted, i.e., showing one dominant size fraction over others. Interstitial matrix shows a near-isotropic nature, and appeared dark in cross polarized light images in the right column.

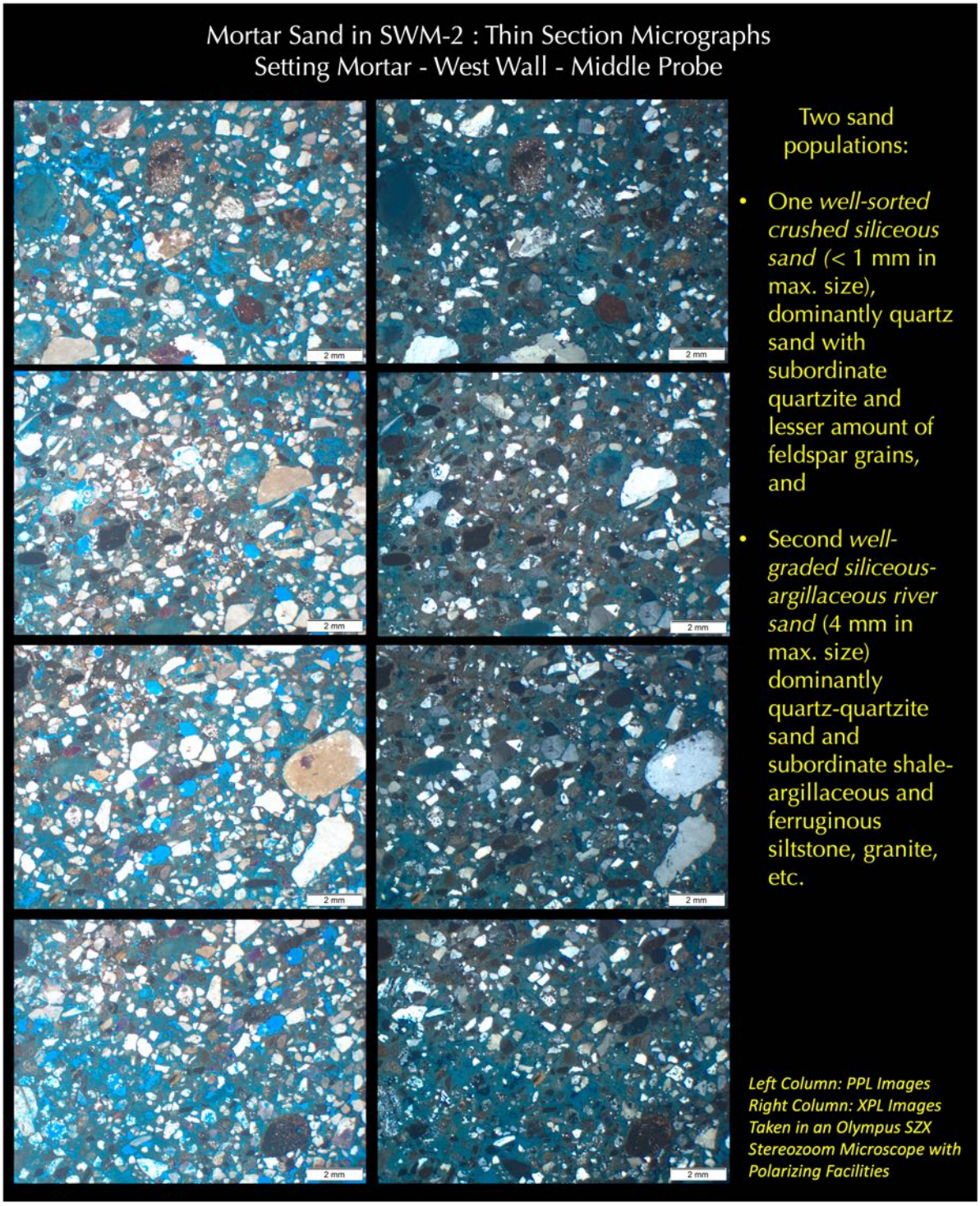

Figure 72: Micrographs of thin section of setting mortar SWM-2 showing two components of sand: (1) a coarser component of maximum 4 mm size, consisting of rounded to subrounded to subangular grains of major amounts of quartz and quartzite, subordinate amounts of chert, shale, and reddish brown ferruginous shale and siltstone, and (2) a relatively finer size fraction of maximum 1 mm size, consisting of major amounts of mostly angular to subangular quartz, subordinate amounts of quartzite, feldspar, and minor amounts of shale, reddish brown shale-siltstone. Coarse fraction grains are well-graded, i.e., showing a uniform size distribution of grains, whereas finer fraction is well-sorted, i.e., showing one dominant size fraction over others. Interstitial matrix shows a near-isotropic nature, and appeared dark in cross polarized light images in the right column.

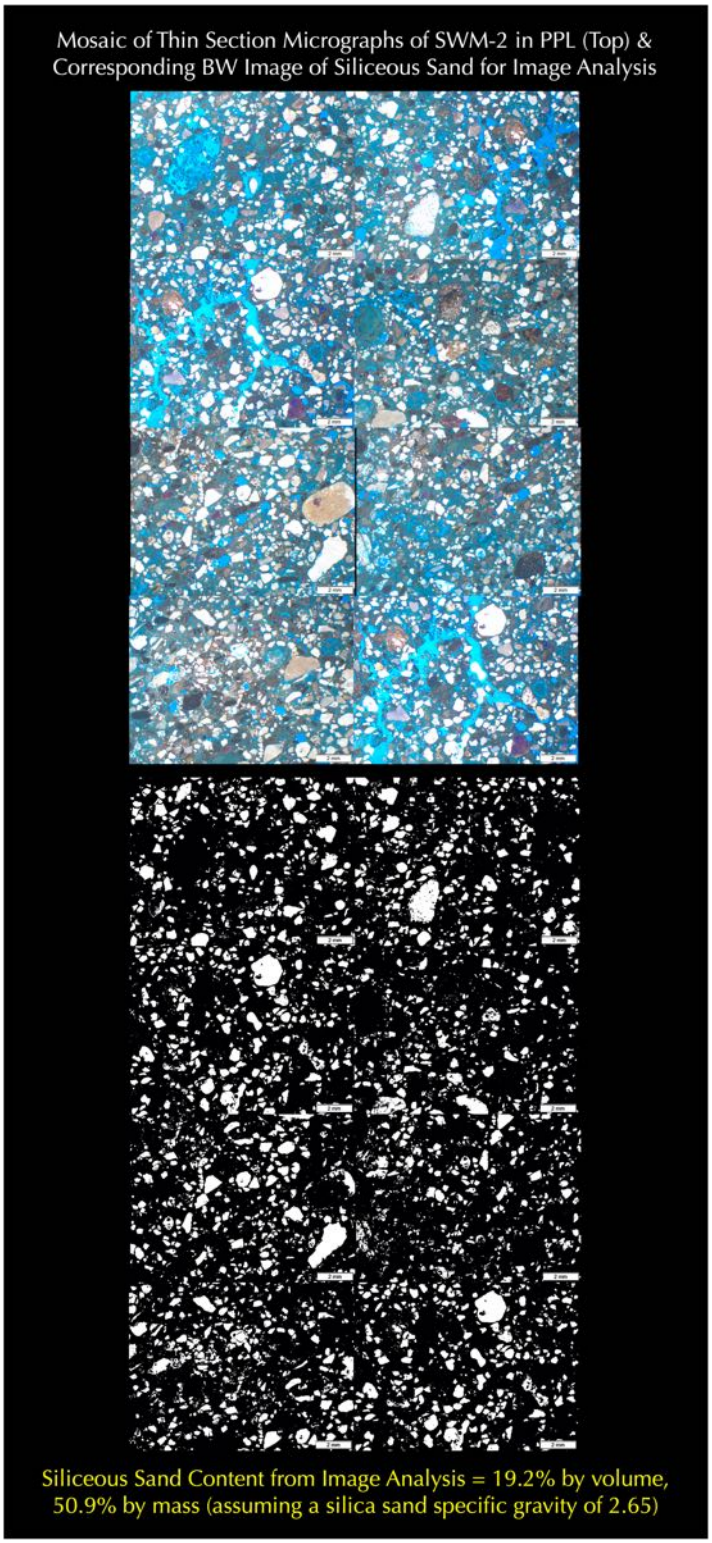

Figure 73: Image analysis of a mosaic of 8 thin section micrographs of setting mortar SWM-2 in PPL (top photo) converted to a black and white contrast enhanced image at the bottom to highlight only the siliceous sand components in white against everything else in black. Image analysis (by ImageJ) showed 19.2% by volume of siliceous sand, which assuming a sand specific gravity of 2.65 corresponds to 50.9% siliceous sand by mass.

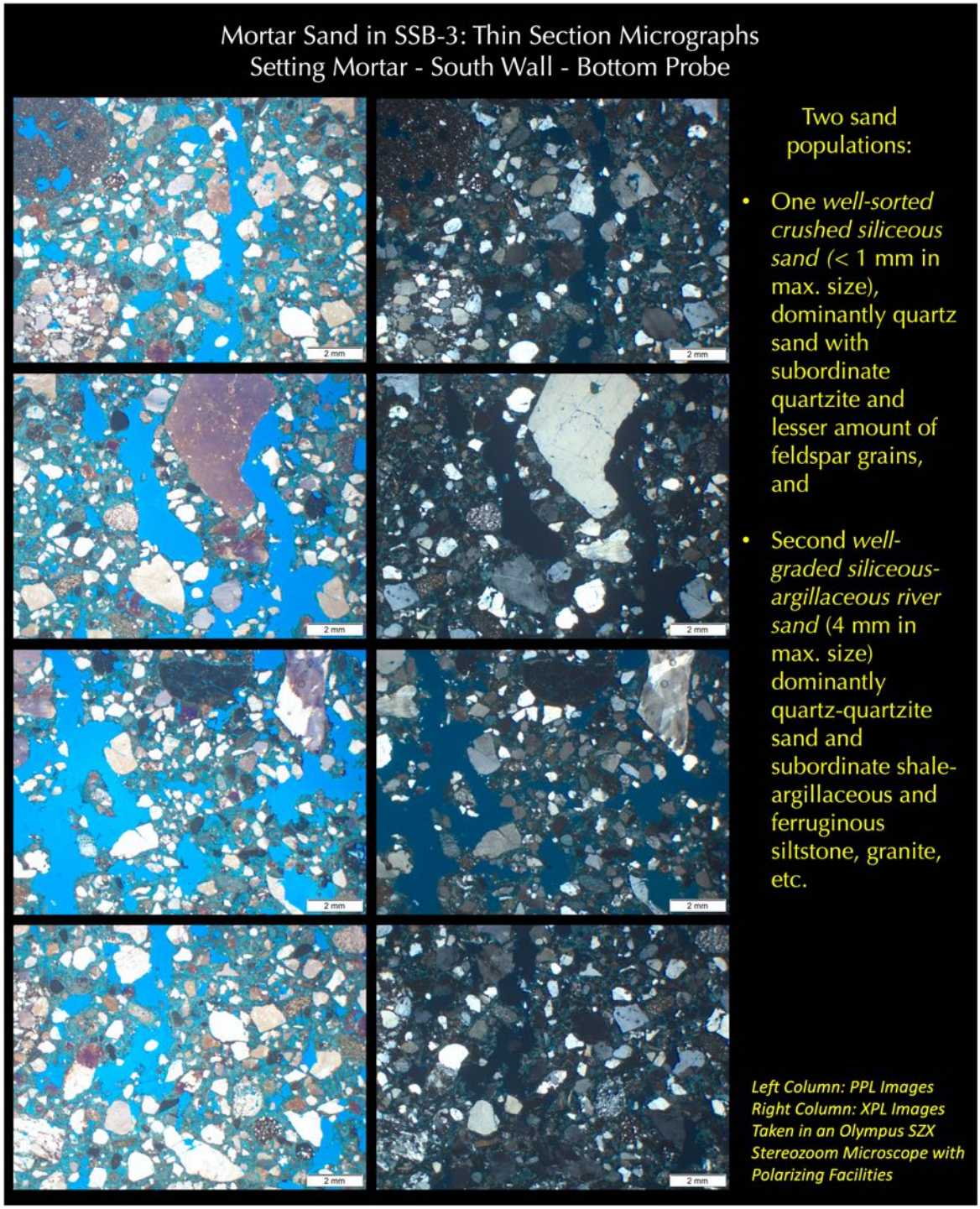

Figure 74: Micrographs of thin section of setting mortar SSB-3 showing two components of sand: (1) a coarser component of maximum 4 mm size, consisting of rounded to subrounded to subangular grains of major amounts of quartz and quartzite, subordinate amounts of chert, shale, and reddish brown ferruginous shale and siltstone, and (2) a relatively finer size fraction of maximum 1 mm size, consisting of major amounts of mostly angular to subangular quartz, subordinate amounts of quartzite, feldspar, and minor amounts of shale, reddish brown shale-siltstone. Coarse fraction grains are well-graded, i.e., showing a uniform size distribution of grains, whereas finer fraction is well-sorted, i.e., showing one dominant size fraction over others. Interstitial matrix shows a near-isotropic nature, and appeared dark in cross polarized light images in the right column.

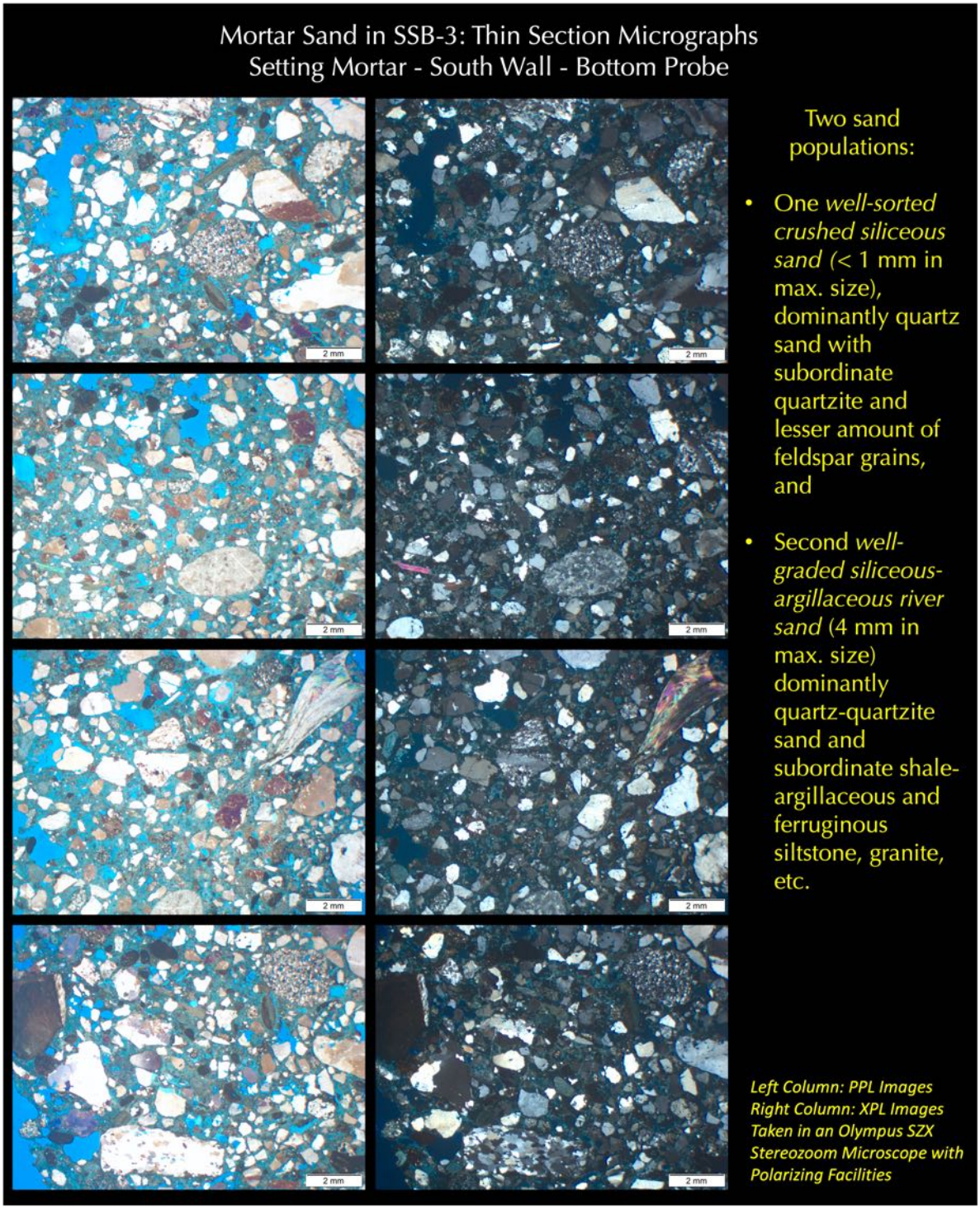

Figure 75: Micrographs of thin section of setting mortar SSB-3 showing two components of sand: (1) a coarser component of maximum 4 mm size, consisting of rounded to subrounded to subangular grains of major amounts of quartz and quartzite, subordinate amounts of chert, shale, and reddish brown ferruginous shale and siltstone, and (2) a relatively finer size fraction of maximum 1 mm size, consisting of major amounts of mostly angular to subangular quartz, subordinate amounts of quartzite, feldspar, and minor amounts of shale, reddish brown shale-siltstone. Coarse fraction grains are well-graded, i.e., showing a uniform size distribution of grains, whereas finer fraction is well-sorted, i.e., showing one dominant size fraction over others. Interstitial matrix shows a near-isotropic nature, and appeared dark in cross polarized light images in the right column.

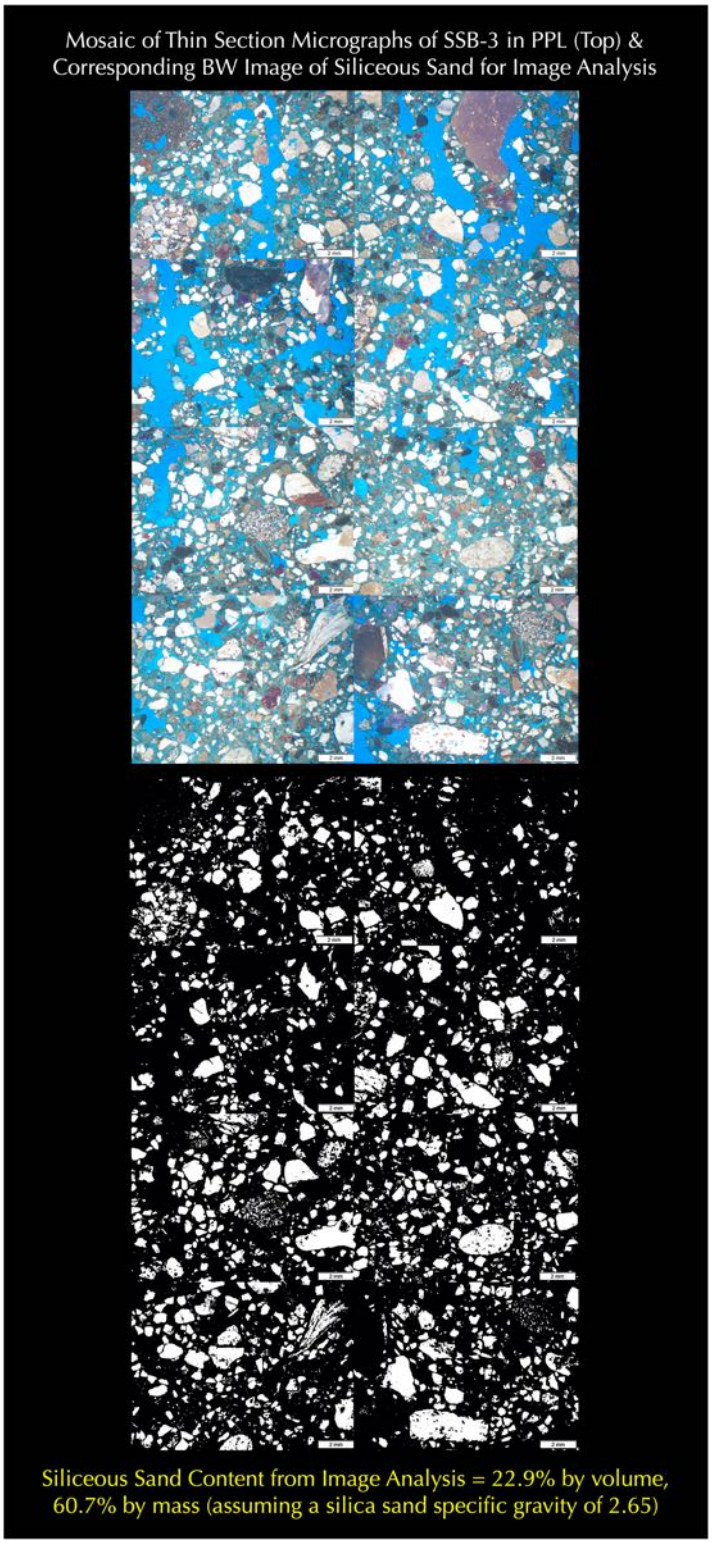

Figure 76: Image analysis of a mosaic of 8 thin section micrographs of setting mortar SSB-3 in PPL (top photo) converted to a black and white contrast enhanced image at the bottom to highlight only the siliceous sand components in white against everything else in black. Image analysis (by ImageJ) showed 22.9% by volume of siliceous sand, which assuming a sand specific gravity of 2.65 corresponds to 60.7% siliceous sand by mass.

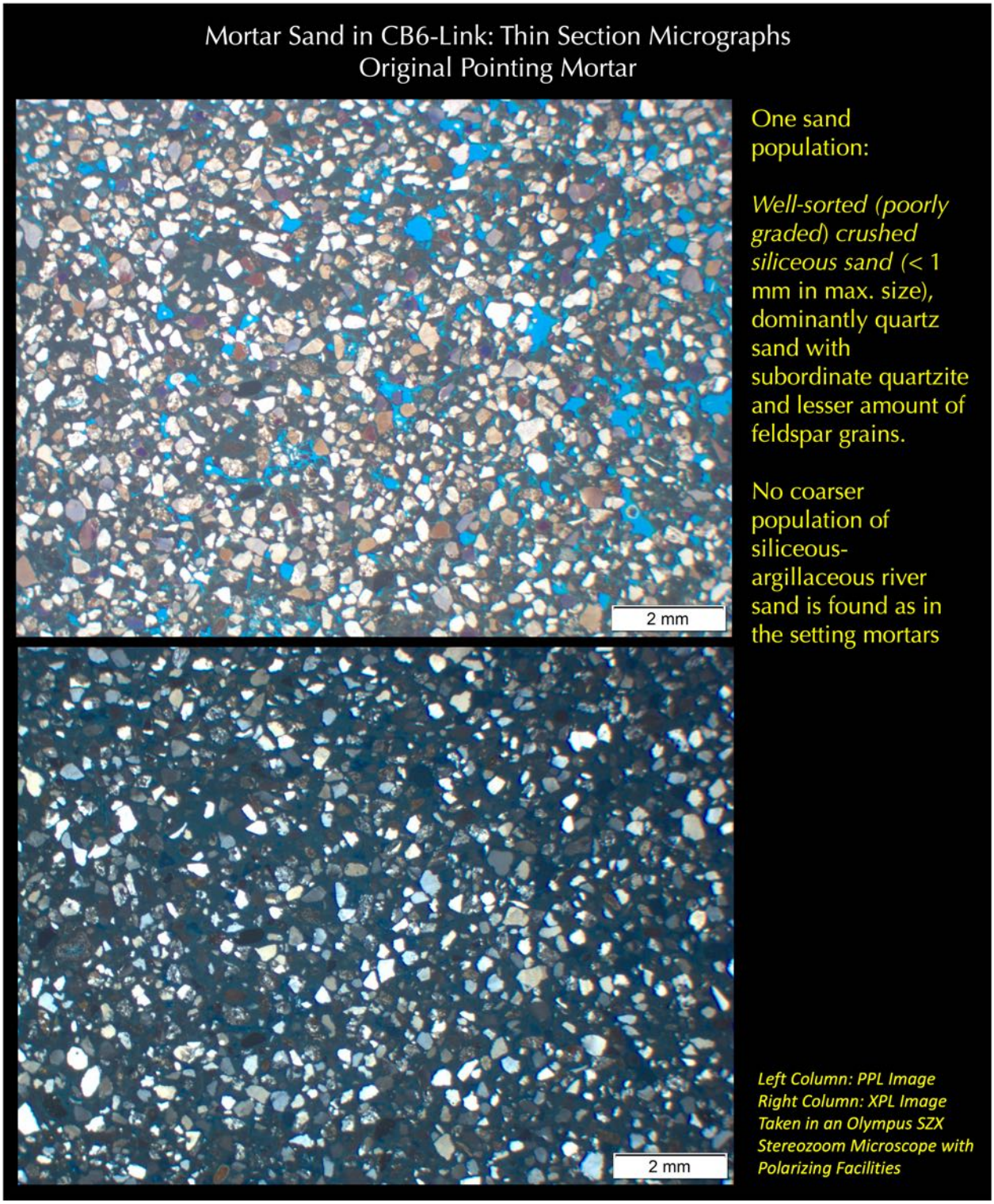

Figure 77: Micrographs of thin section of pointing mortar CB6-Link showing one size component of sand having a maximum 1 mm size, consisting of major amounts of mostly angular to subangular quartz, subordinate amounts of quartzite, feldspar, and minor amounts of shale, reddish brown shale-siltstone. Grains are well-sorted, i.e., showing one dominant size fraction over others. Sand shows very different size, and size distribution than the sand in setting mortars.

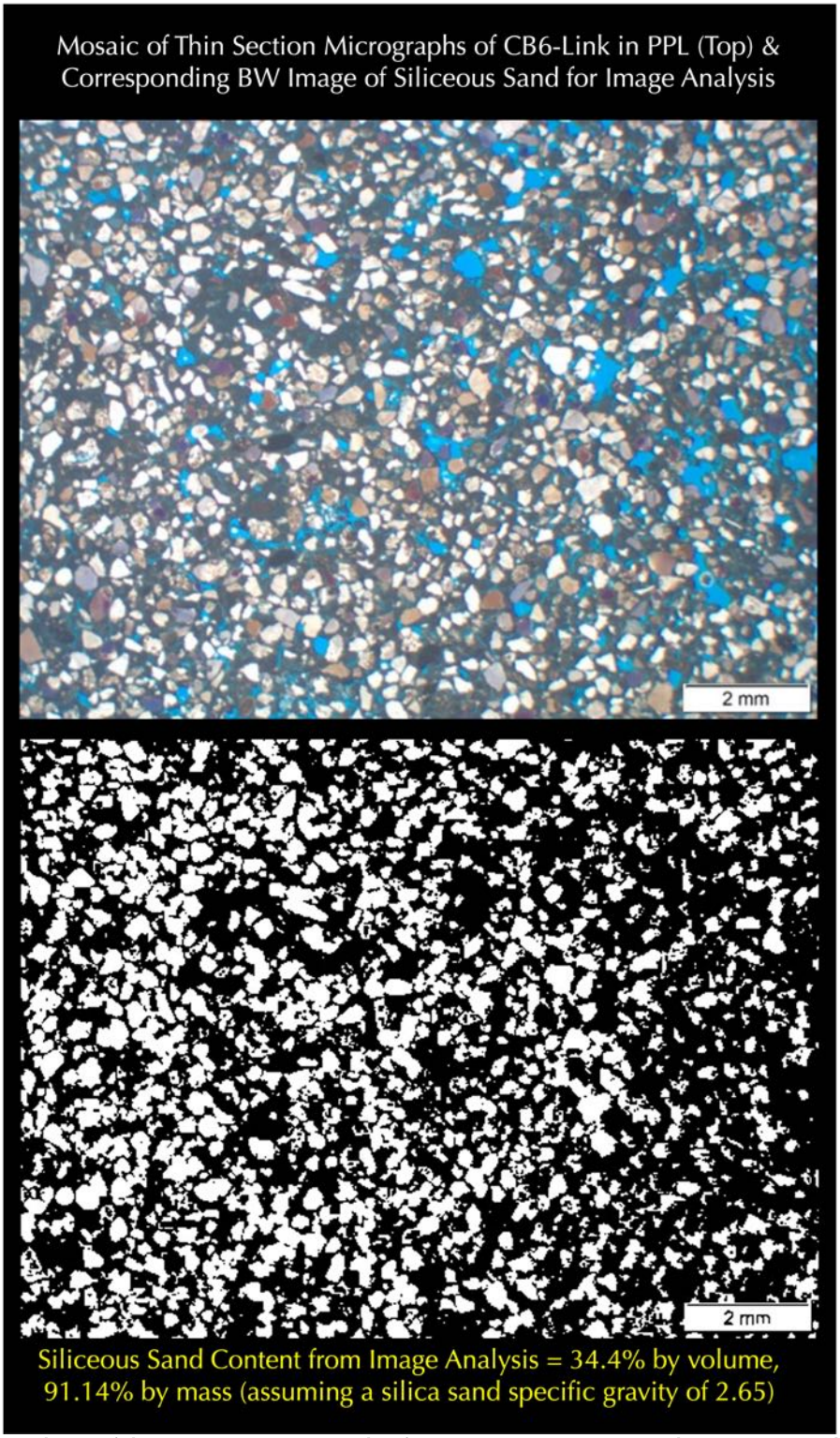

Figure 78: : Image analysis of thin section micrograph of pointing mortar CB6-Link in PPL (top photo) converted to a black and white contrast enhanced image at the bottom to highlight only the siliceous sand components in white against everything else in black. Image analysis (by ImageJ) showed 34.4% by volume of siliceous sand, which assuming a sand specific gravity of 2.65 corresponds to 91.1% siliceous sand by mass.

Microstructure of Mortars from Optical Microscopy

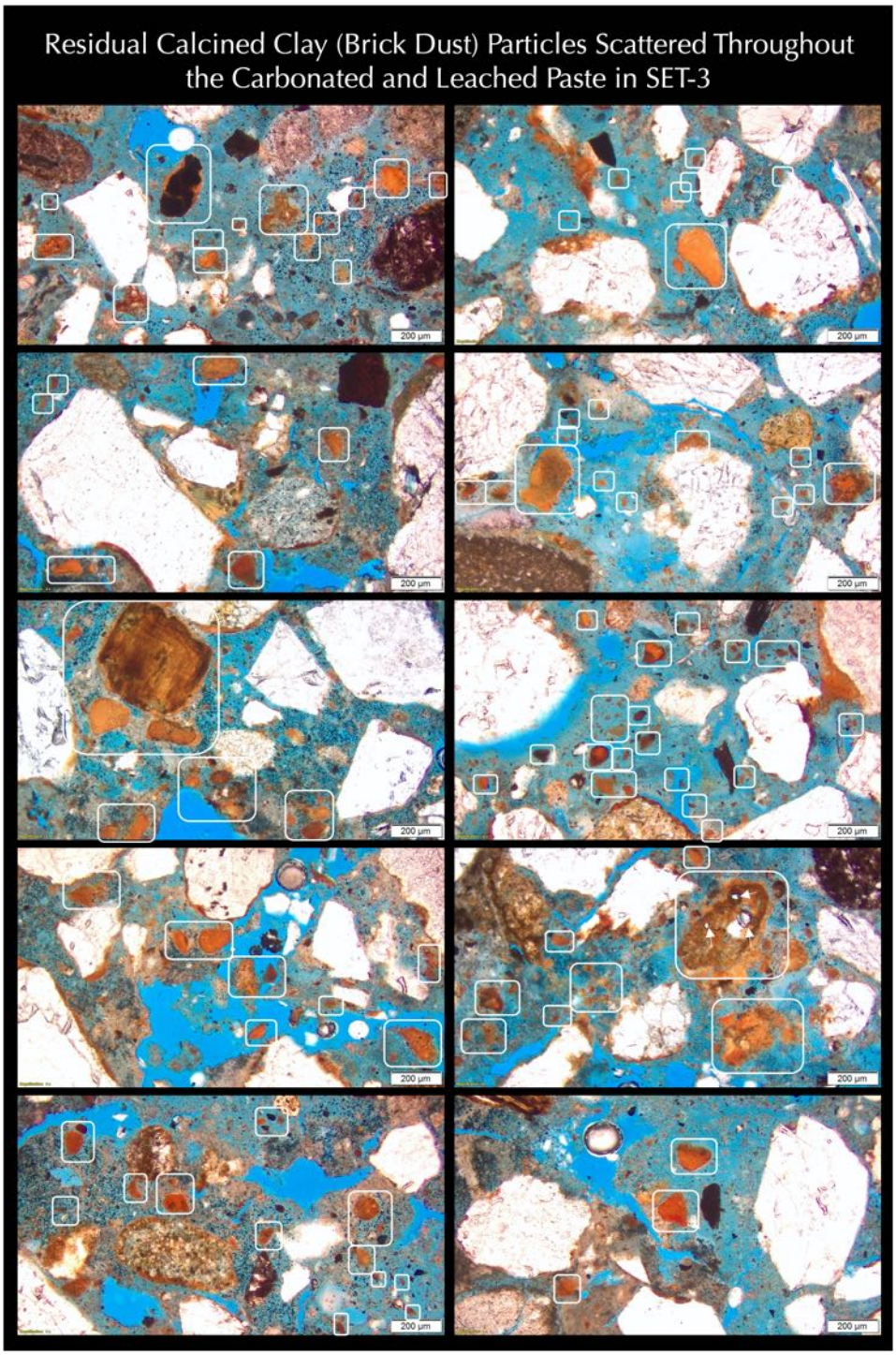

Figure 79: Micrographs of thin section of setting mortar SET-3 showing residual calcined clay (brick dust) particles (boxed) scattered throughout the leached and carbonated paste, which are characterized by reddish-brown color and dominantly amorphous nature of the plastic component of original calcined clay with very little non-plastic (optically birefringent fillers, e.g., quartz) left from pozzolanic reactions with the dominant dolomitic lime component of binder. Micrographs were taken at plane polarized light mode in a petrographic microscope.

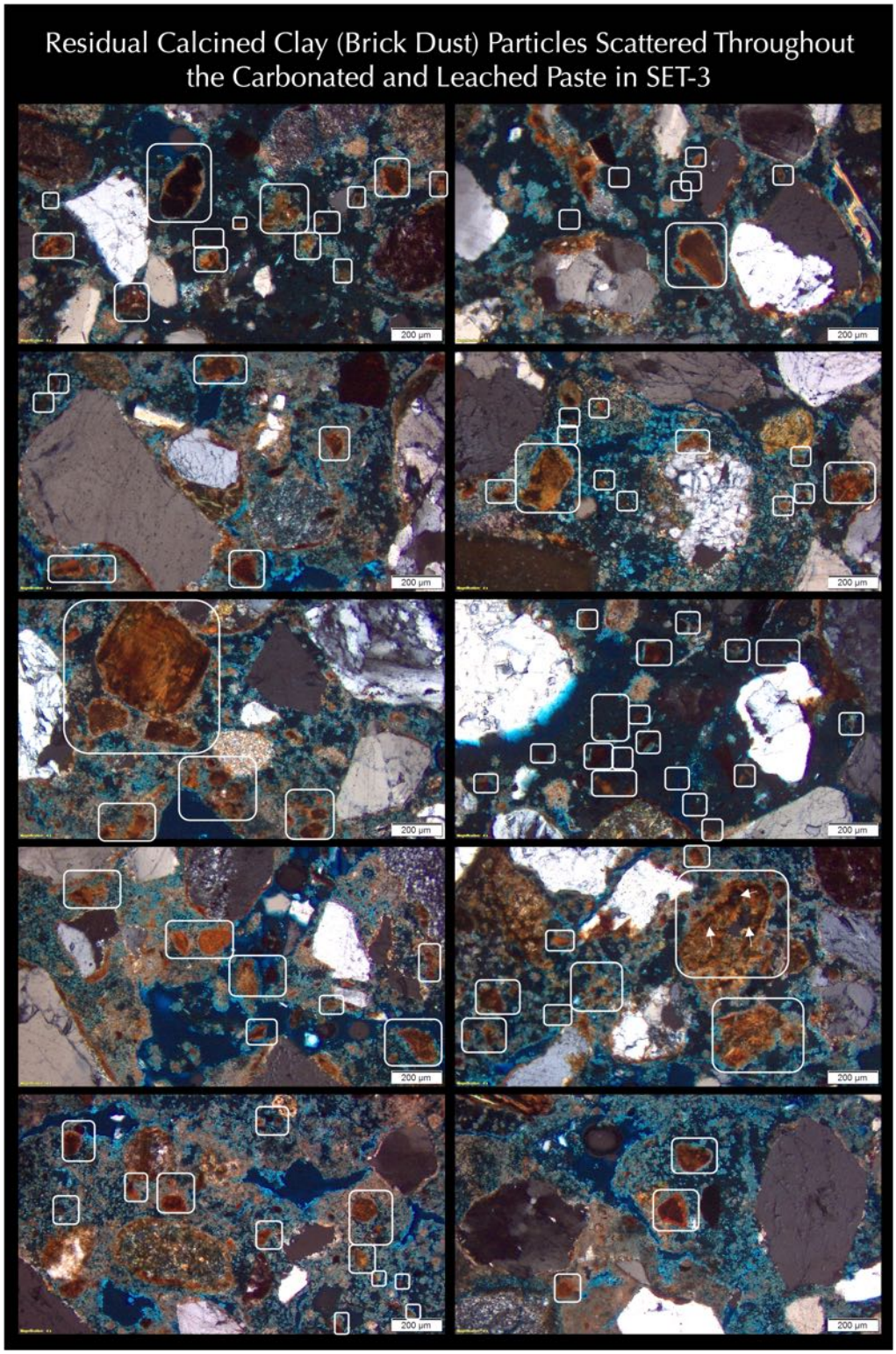

Figure 80: Micrographs of thin section of setting mortar SET-3 showing residual calcined clay (brick dust) particles (boxed) scattered throughout the leached and carbonated paste, which are characterized by reddish-brown color and dominantly amorphous nature of the plastic component of original calcined clay with very little non-plastic (optically birefringent fillers, e.g., quartz) left from pozzolanic reactions with the dominant dolomitic lime component of binder. Micrographs were taken at cross polarized light mode in a petrographic microscope.

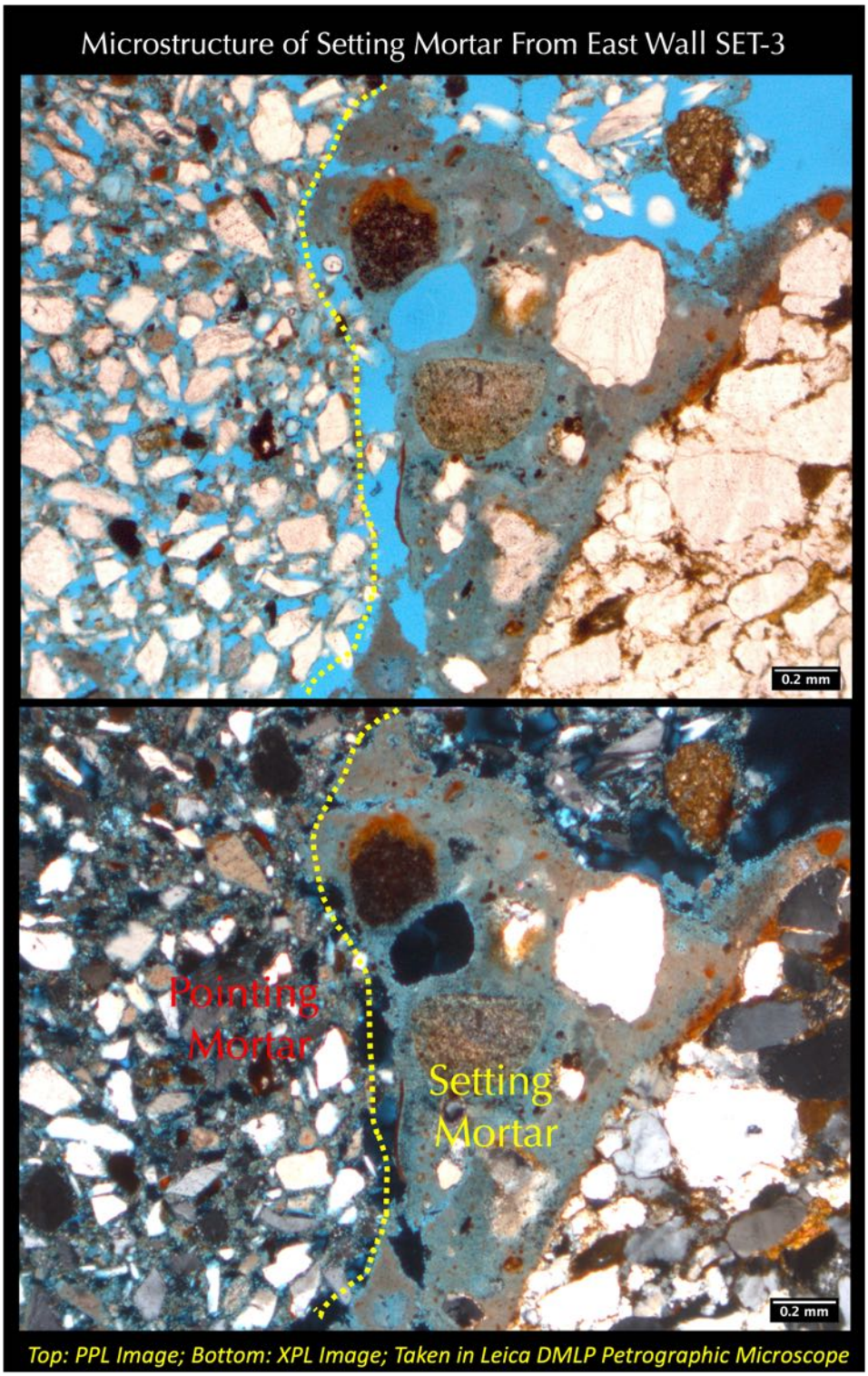

Figure 81: Micrographs of thin section of setting mortar SET-3 showing: (a) remains of a pointing mortar at left well-bonded to the setting mortar at right; (b) contrasting grain size and angularity of sands between noticeably finer and mostly angular sand in the pointing mortar at left versus angular to rounded and noticeably coarser sand in the setting mortar at right; (b) severely carbonated interstitial paste fraction in the setting mortar adjacent to the interface to pointing mortar. Coarsest sand grain in the setting mortar at the bottom right corner is a quartz sandstone.

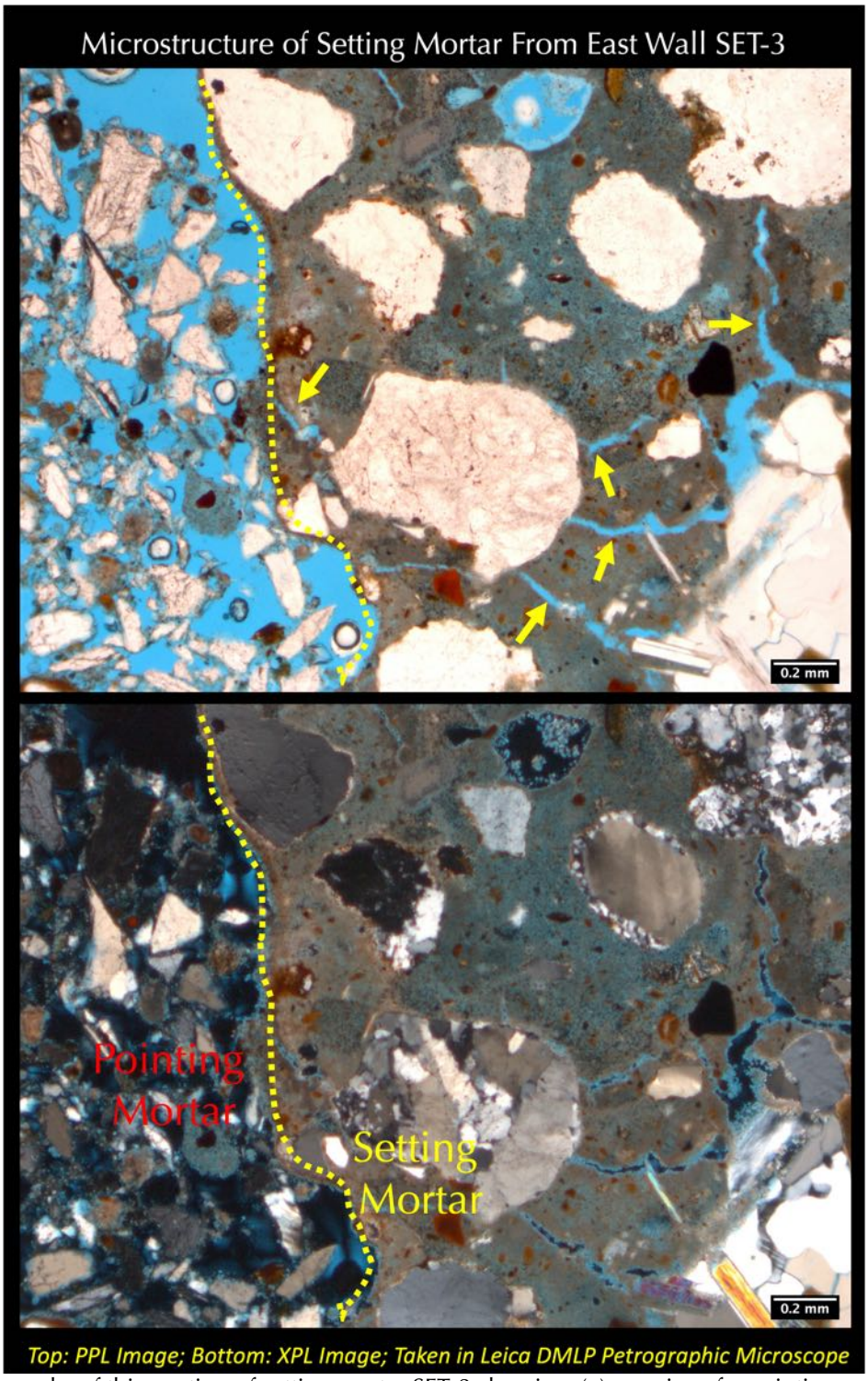

Figure 82: Micrographs of thin section of setting mortar SET-3 showing: (a) remains of a pointing mortar at left well-bonded to the setting mortar at right; (b) contrasting grain size and angularity of sands between noticeably finer and mostly angular sand in the pointing mortar at left versus angular to rounded and noticeably coarser sand in the setting mortar at right; and (b) severely carbonated interstitial paste fraction in the setting mortar with fine, discontinuous carbonation shrinkage microcracks (some are marked with yellow arrows). Many rounded to subrounded strained quartzite sand grains are seen in the setting mortar, as opposed to finer angular quartz sand in the pointing mortar.

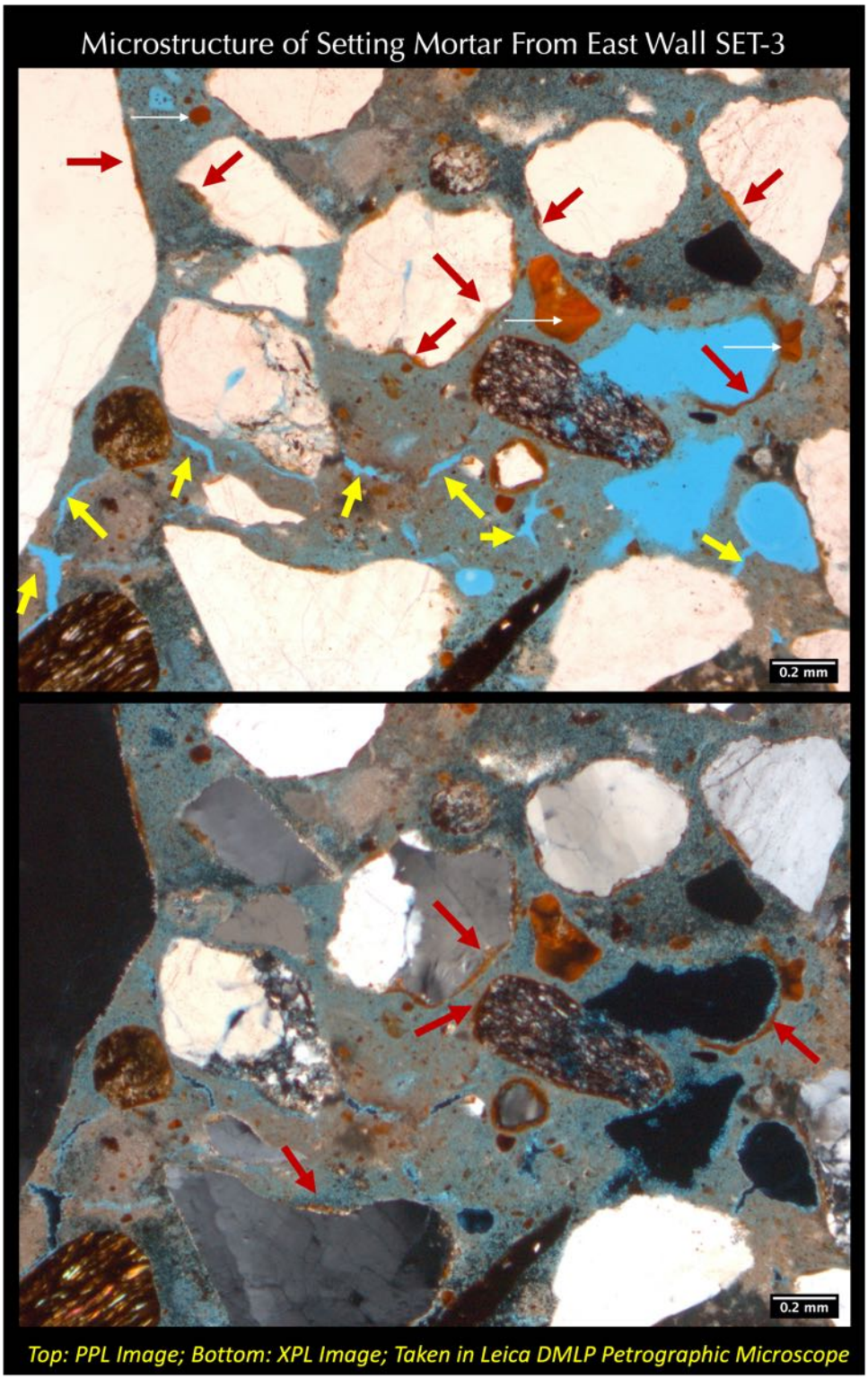

Figure 83: Micrographs of thin section of setting mortar SET-3 showing severely carbonated interstitial paste fraction in the setting mortar with fine, discontinuous carbonation shrinkage microcracks (some are marked with yellow arrows). Many rounded to subrounded strained quartz and quartzite sand grains are seen in the setting mortar, along with some reddish-brown ferruginous shale particles. Reddish-brown arrows show reddish-brown coats on sand particles. Thin white arrows show a few isolated reddish-brown particles of residual calcined clay (brick dust).

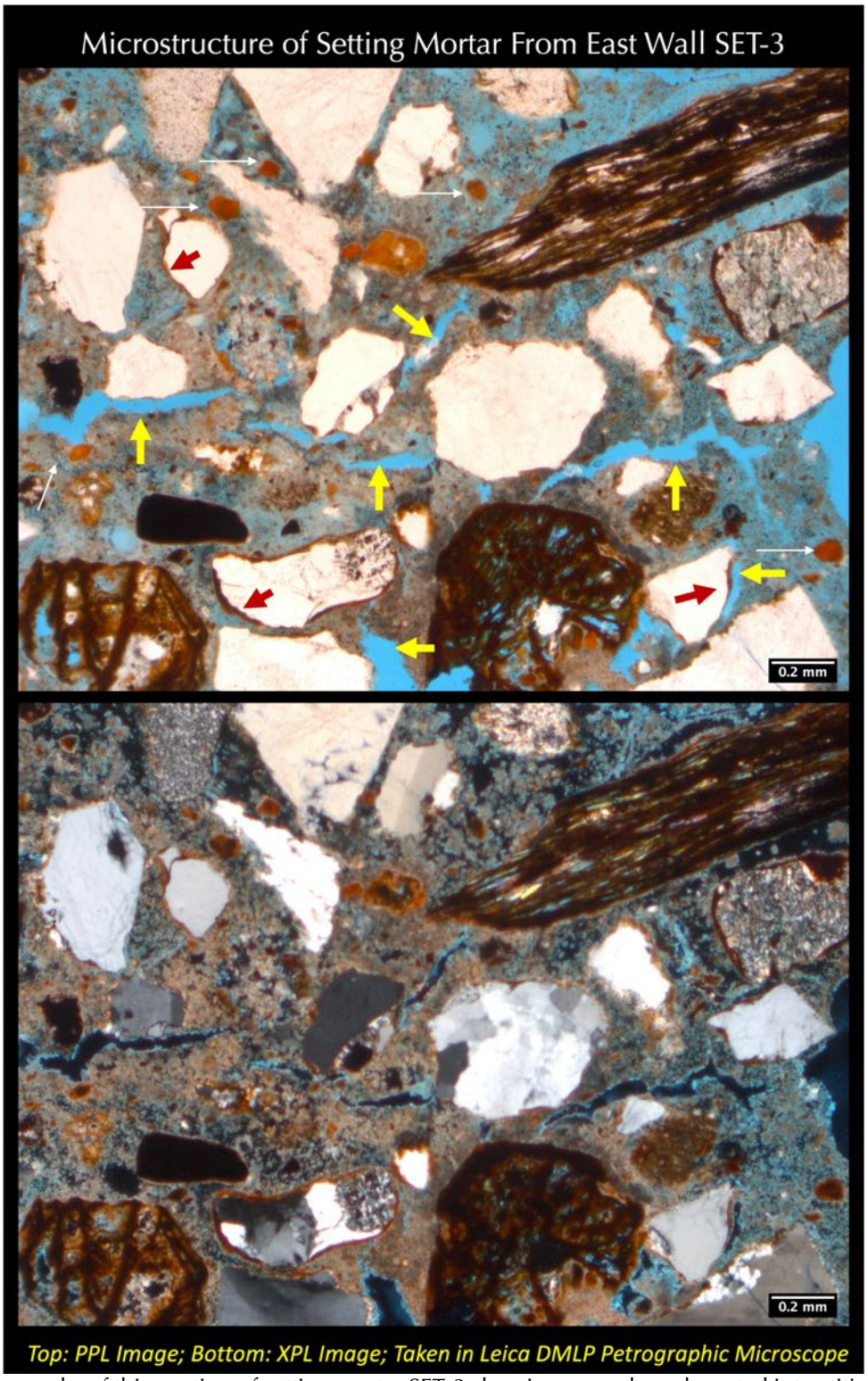

Figure 84: Micrographs of thin section of setting mortar SET-3 showing severely carbonated interstitial paste fraction in the setting mortar with fine, discontinuous carbonation shrinkage microcracks (some are marked with yellow arrows). Many rounded to subrounded strained quartz and quartzite sand grains are seen in the setting mortar, along with some reddish-brown ferruginous shale and siltstone particles. Reddish-brown arrows show reddish-brown coats on sand particles. Thin white arrows show a few isolated reddish-brown particles of residual calcined clay (brick dust).

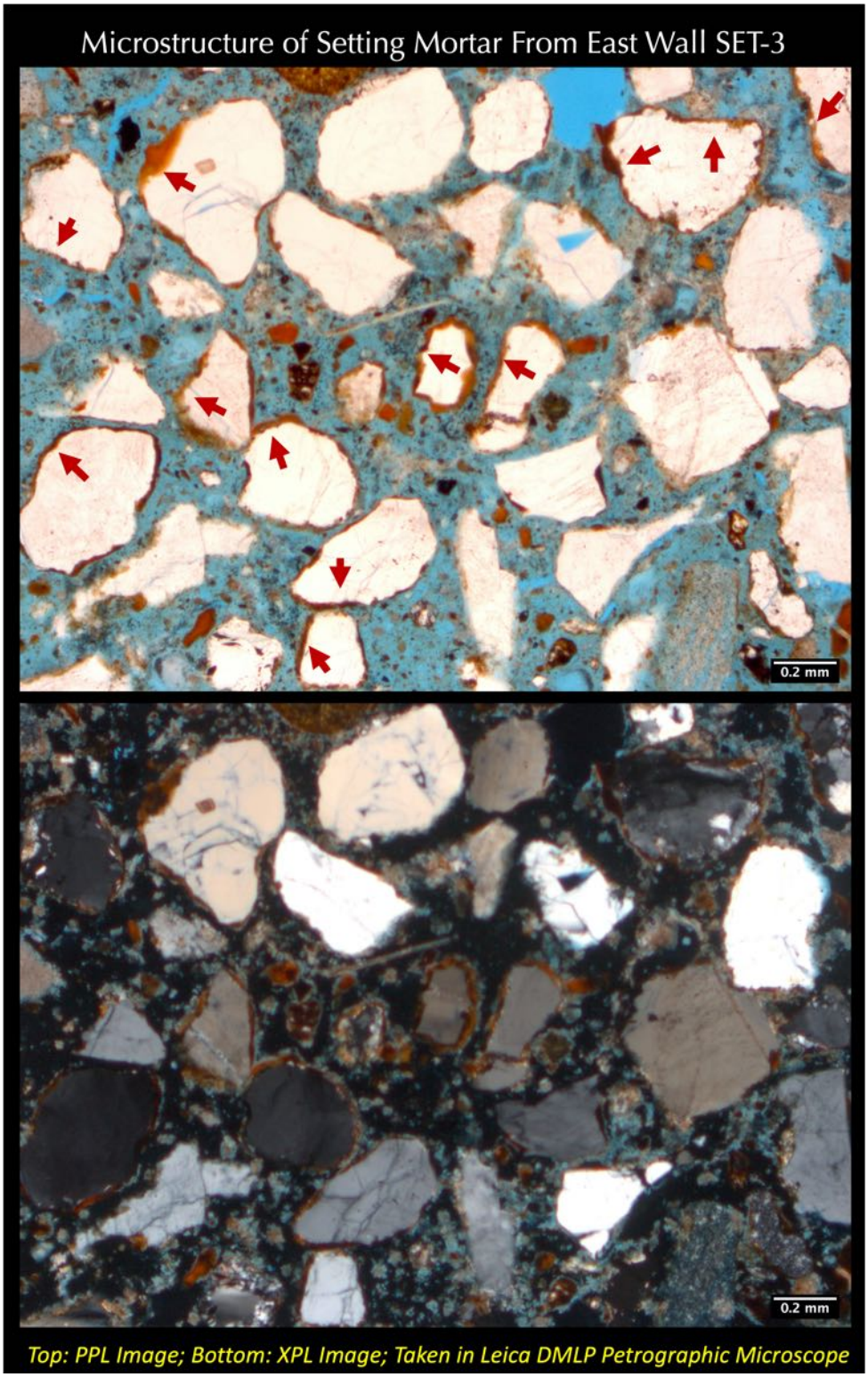

Figure 85: Micrographs of thin section of setting mortar SET-3 showing the lime-leached interstitial paste fraction in the setting mortar. Many rounded to subrounded strained quartz and quartzite sand grains are seen in the setting mortar, along with some reddish-brown ferruginous shale and siltstone particles. Reddish-brown arrows show reddish-brown coats on sand particles.

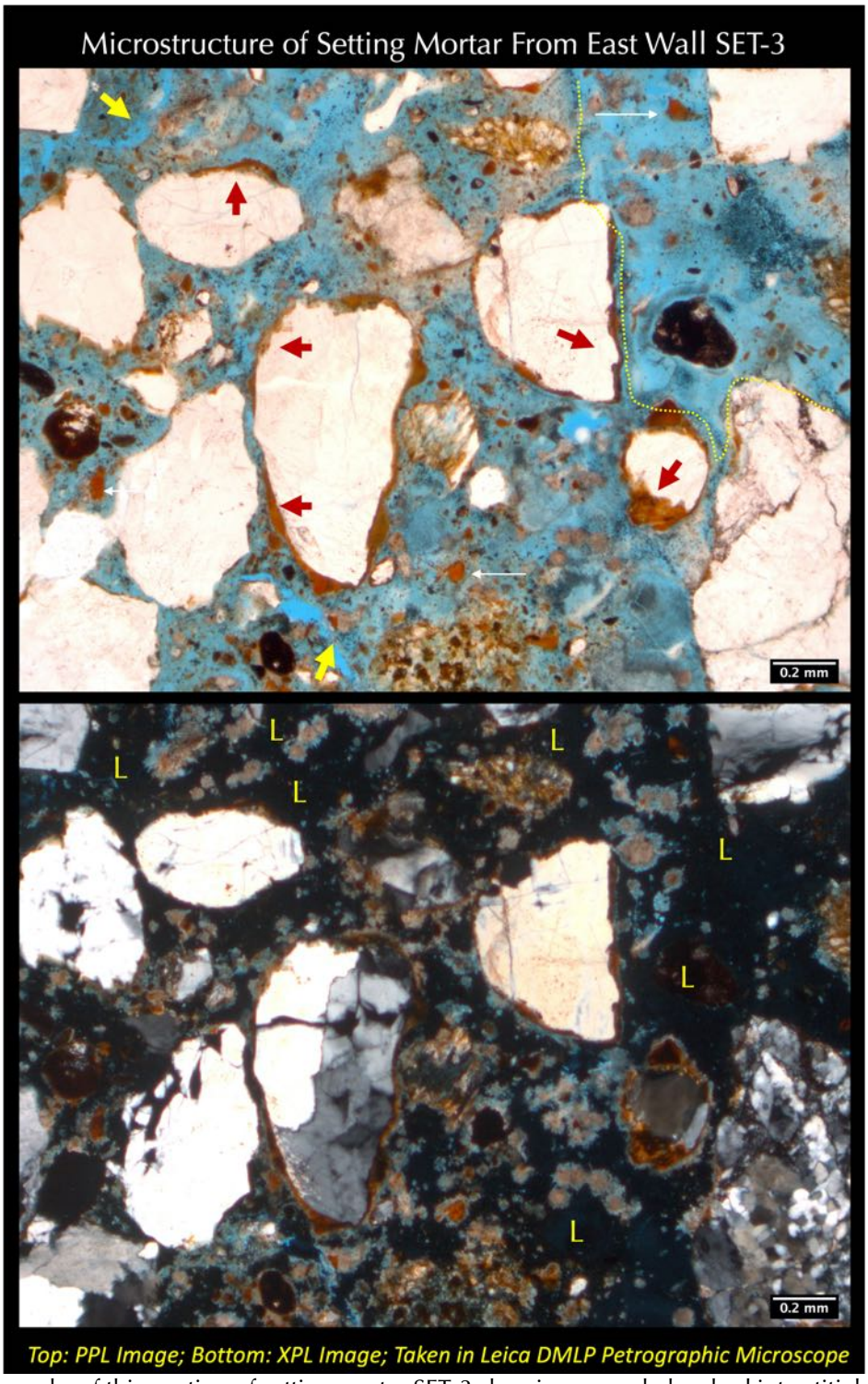

Figure 86: Micrographs of thin section of setting mortar SET-3 showing severely leached interstitial paste fraction in the setting mortar with fine, discontinuous carbonation shrinkage microcracks (some are marked with yellow arrows). Many rounded to subrounded strained quartz and quartzite sand grains are seen in the setting mortar, along with some reddish-brown ferruginous shale and siltstone particles. Reddish-brown arrows show reddish-brown coats on sand particles. Thin white arrows show a few isolated reddish-brown particles of residual calcined clay (brick dust). Letter 'L' marks the lime-leached patchy areas of paste, which appear optically isotropic in XPL image due to inherent gelatinous or amorphous nature (determined in subsequent SEM-EDS studies to be enriched in Mg, Si, and Al).

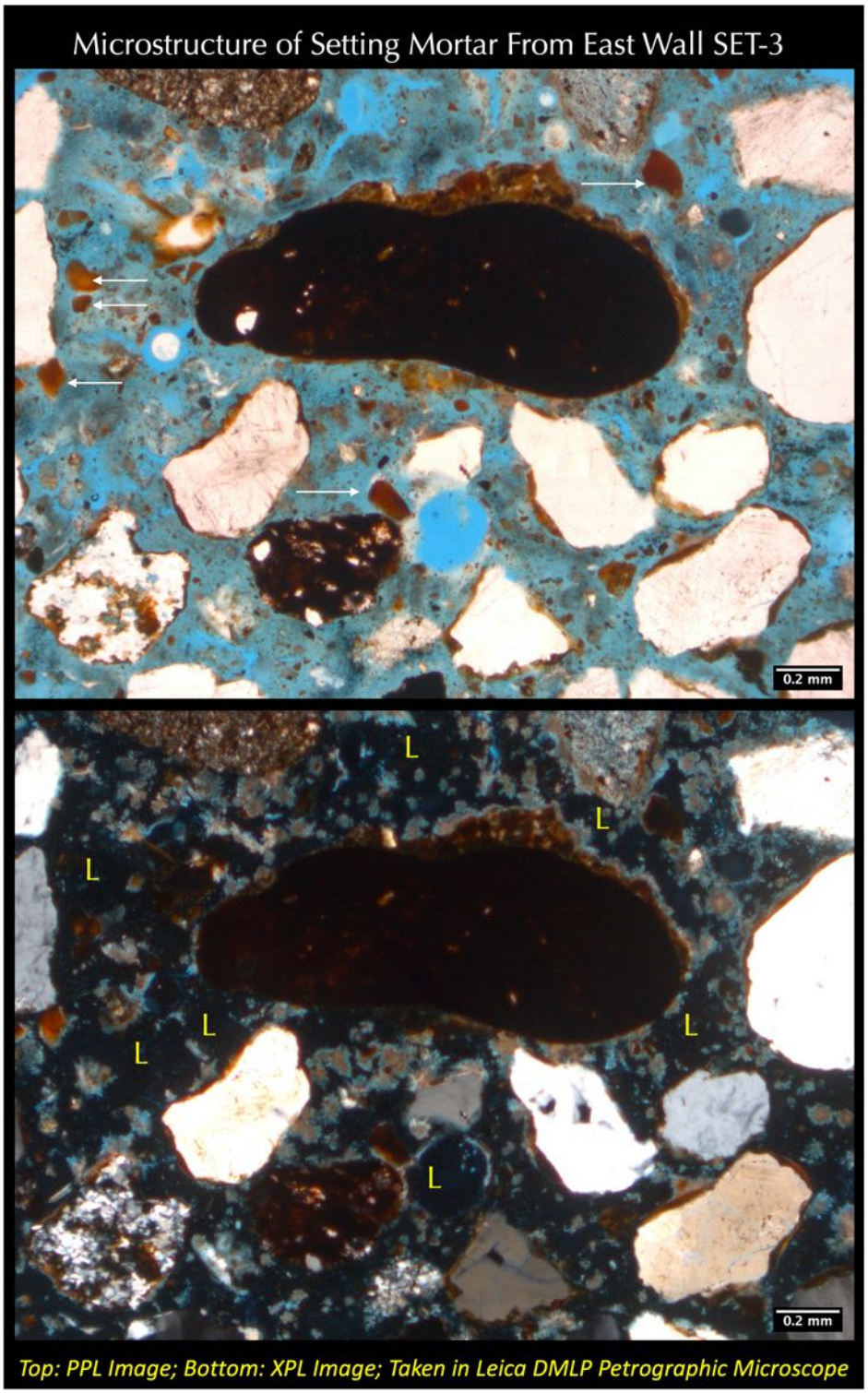

Figure 87: Micrographs of thin section of setting mortar SET-3 showing severely leached interstitial paste fraction in the setting mortar with fine, discontinuous carbonation shrinkage microcracks. Many rounded to subrounded strained quartz and quartzite sand grains are seen in the setting mortar, along with some reddish-brown ferruginous shale and siltstone particles. Thin white arrows show a few isolated reddish-brown particles of residual calcined clay (brick dust). Letter 'L' marks the lime-leached patchy areas of paste, which appear optically isotropic in XPL image due to inherent gelatinous or amorphous nature (determined in subsequent SEM-EDS studies to be enriched in Mg, Si, and Al).

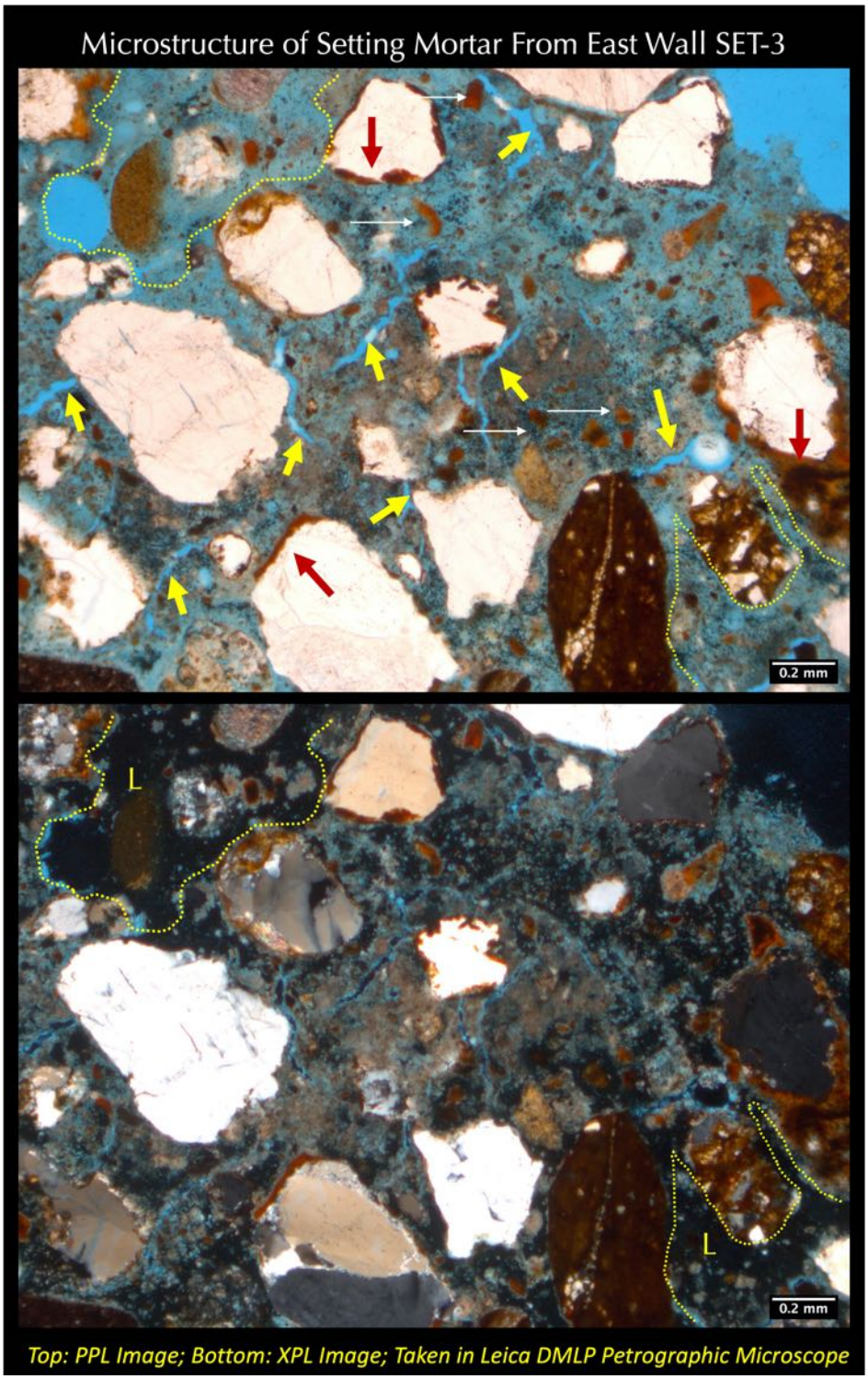

Figure 88: Micrographs of thin section of setting mortar SET-3 showing severely leached interstitial paste fraction in the setting mortar with fine, discontinuous carbonation shrinkage microcracks (some are marked with yellow arrows). Many rounded to subrounded strained quartz and quartzite sand grains are seen in the setting mortar, along with some reddish-brown ferruginous shale and siltstone particles. Reddish-brown arrows show reddish-brown coats on sand particles. Thin white arrows show a few isolated reddish-brown particles of residual calcined clay (brick dust). Letter 'L' marks the lime-leached patchy areas of paste, which appear optically isotropic in XPL image due to inherent gelatinous or amorphous nature (determined in subsequent SEM-EDS studies to be enriched in Mg, Si, and Al).

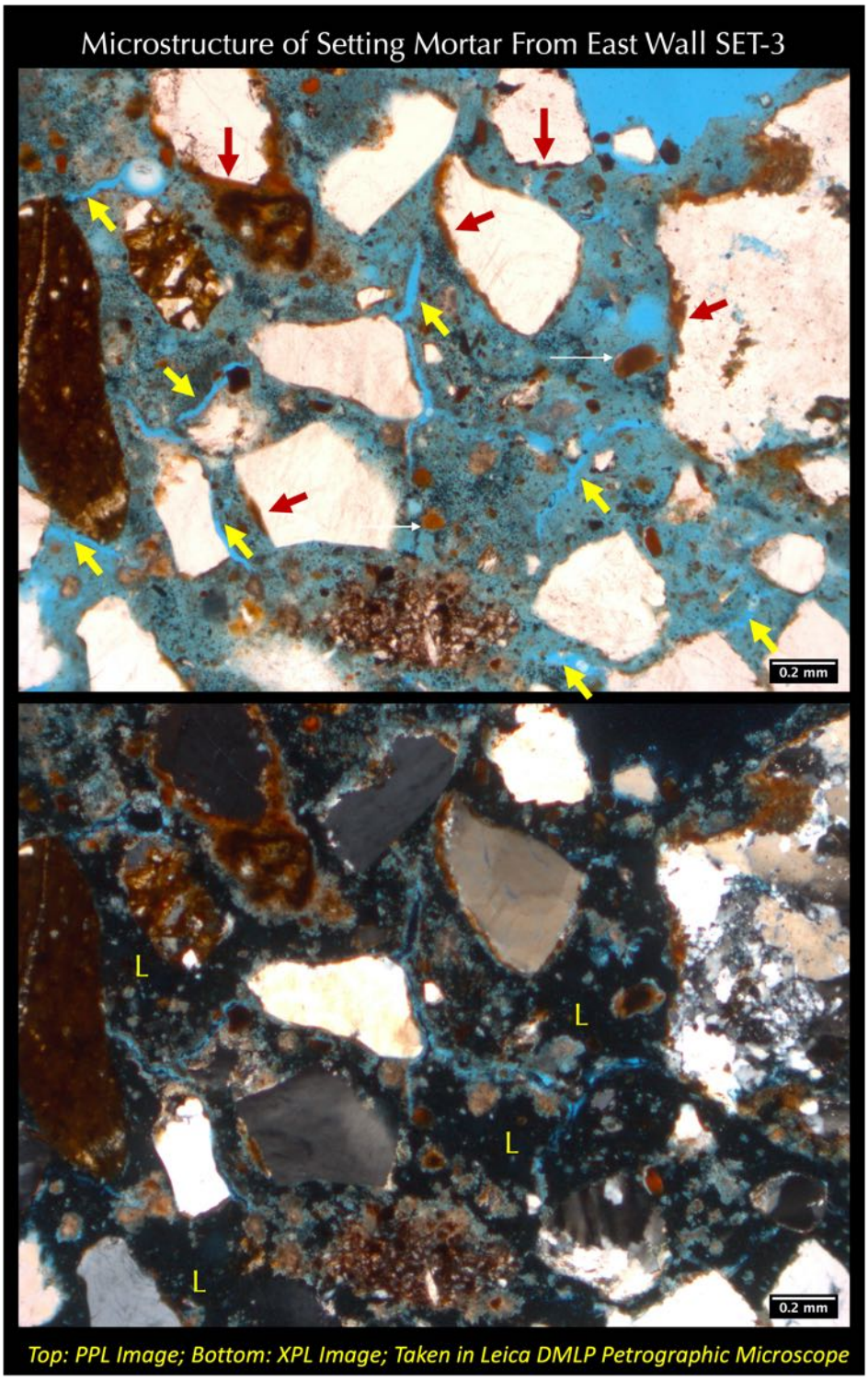

Figure 89: Micrographs of thin section of setting mortar SET-3 showing severely leached interstitial paste fraction in the setting mortar with fine, discontinuous carbonation shrinkage microcracks (some are marked with yellow arrows). Many rounded to subrounded strained quartz and quartzite sand grains are seen in the setting mortar, along with some reddish-brown ferruginous shale and siltstone particles. Reddish-brown arrows show reddish-brown coats on sand particles. Thin white arrows show a few isolated reddish-brown particles of residual calcined clay (brick dust). Letter 'L' marks the lime-leached patchy areas of paste, which appear optically isotropic in XPL image due to inherent gelatinous or amorphous nature (determined in subsequent SEM-EDS studies to be enriched in Mg, Si, and Al).

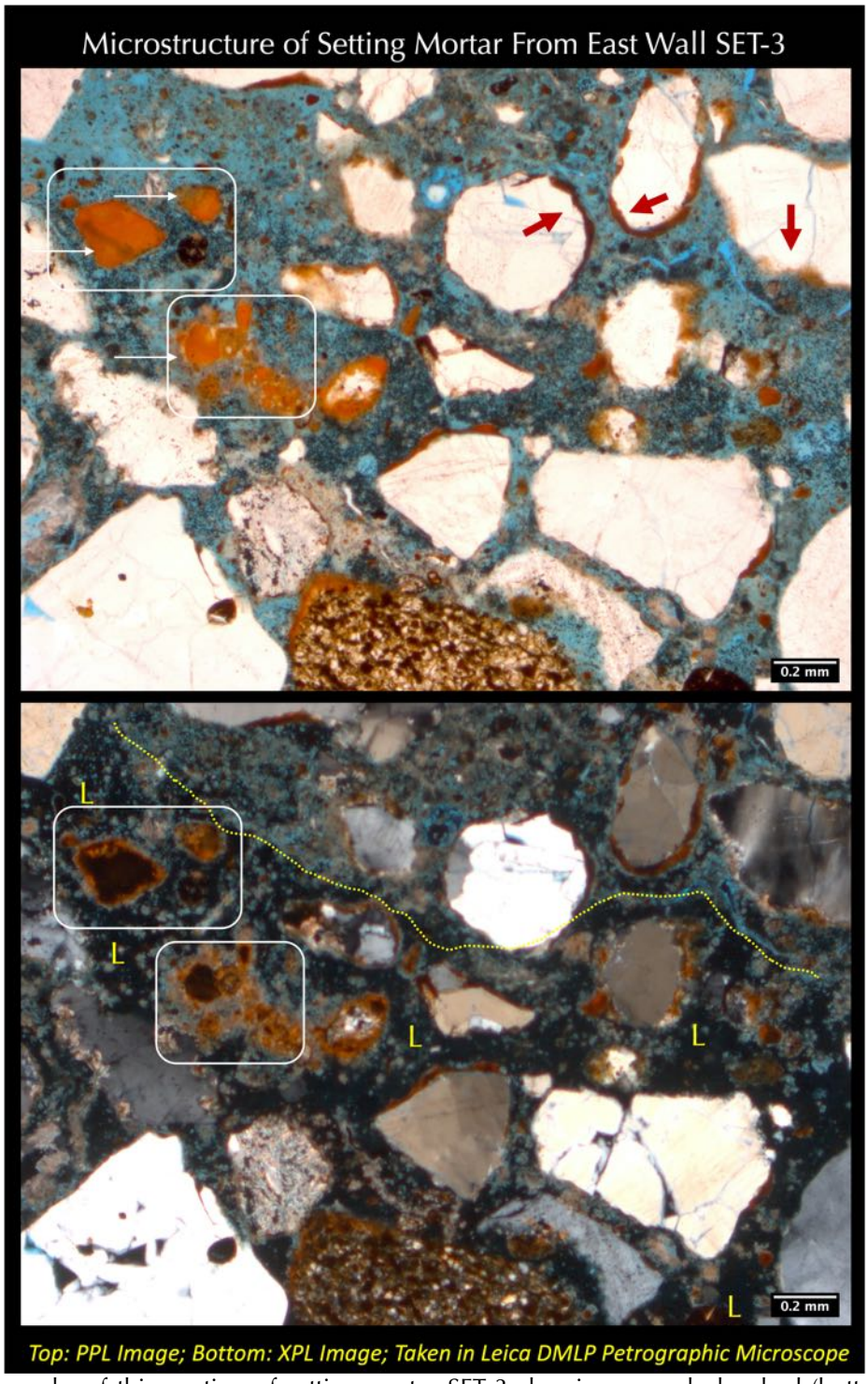

Figure 90: Micrographs of thin section of setting mortar SET-3 showing severely leached (bottom left) and less leached (top right) interstitial paste fraction in the setting mortar. Many rounded to subrounded strained quartz and quartzite sand grains are seen in the setting mortar, along with some reddish-brown ferruginous shale and siltstone particles. Reddish-brown arrows show reddish-brown coats on sand particles. Thin white arrows show a few isolated reddish-brown particles of residual calcined clay (brick dust, (some are boxed). Letter 'L' marks the lime-leached patchy areas of paste, which appear optically isotropic in XPL image due to inherent gelatinous or amorphous nature (determined in subsequent SEM-EDS studies to be enriched in Mg, Si, and Al).

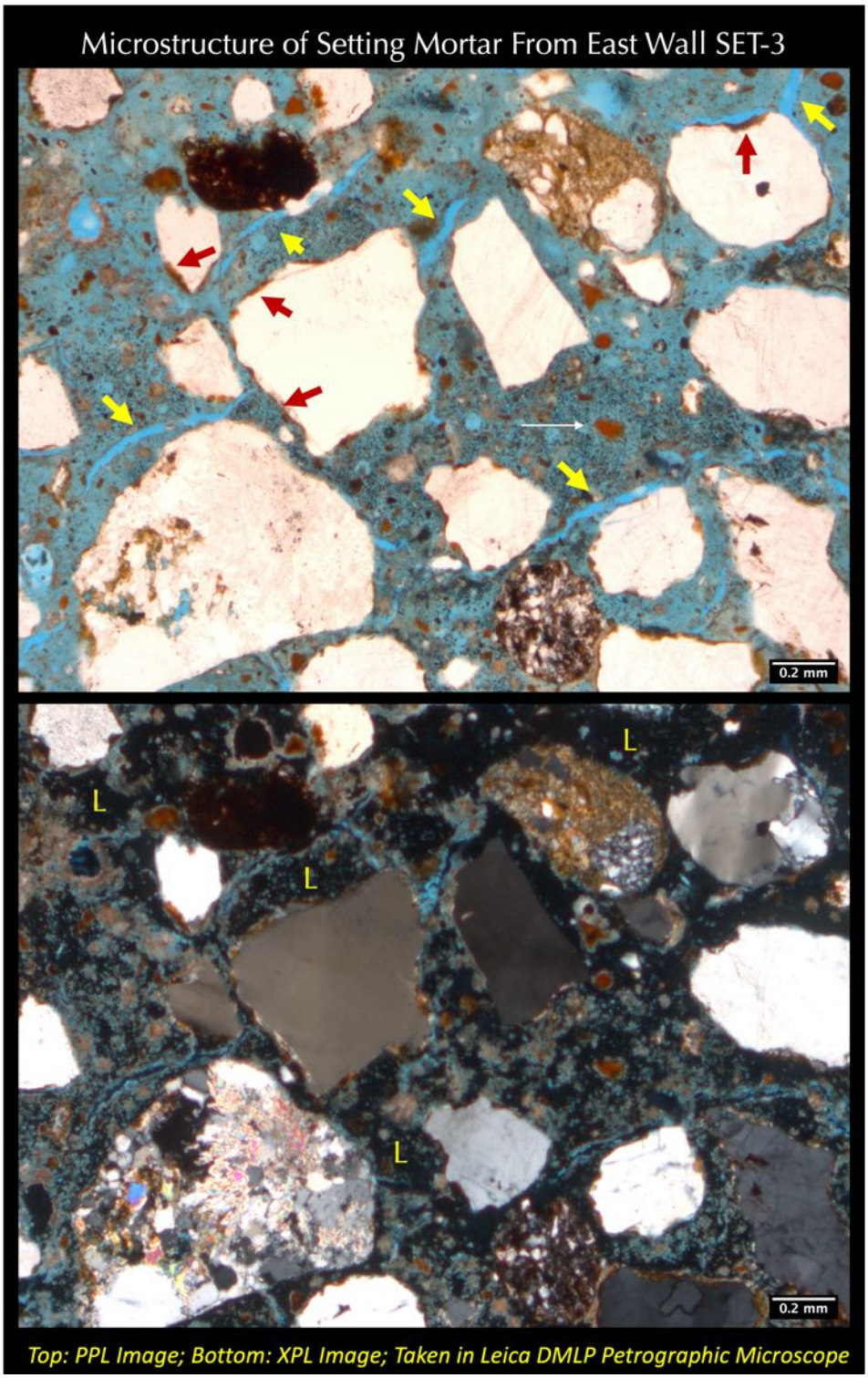

Figure 91: Micrographs of thin section of setting mortar SET-3 showing severely leached interstitial paste fraction in the setting mortar with fine, discontinuous carbonation shrinkage microcracks (some are marked with yellow arrows). Many rounded to subrounded strained quartz and quartzite sand grains are seen in the setting mortar, along with some reddish-brown ferruginous shale and siltstone particles. Reddish-brown arrows show reddish-brown coats on sand particles. Thin white arrows show a few isolated reddish-brown particles of residual calcined clay (brick dust). Letter 'L' marks the lime-leached patchy areas of paste, which appear optically isotropic in XPL image due to inherent gelatinous or amorphous nature (determined in subsequent SEM-EDS studies to be enriched in Mg, Si, and Al).

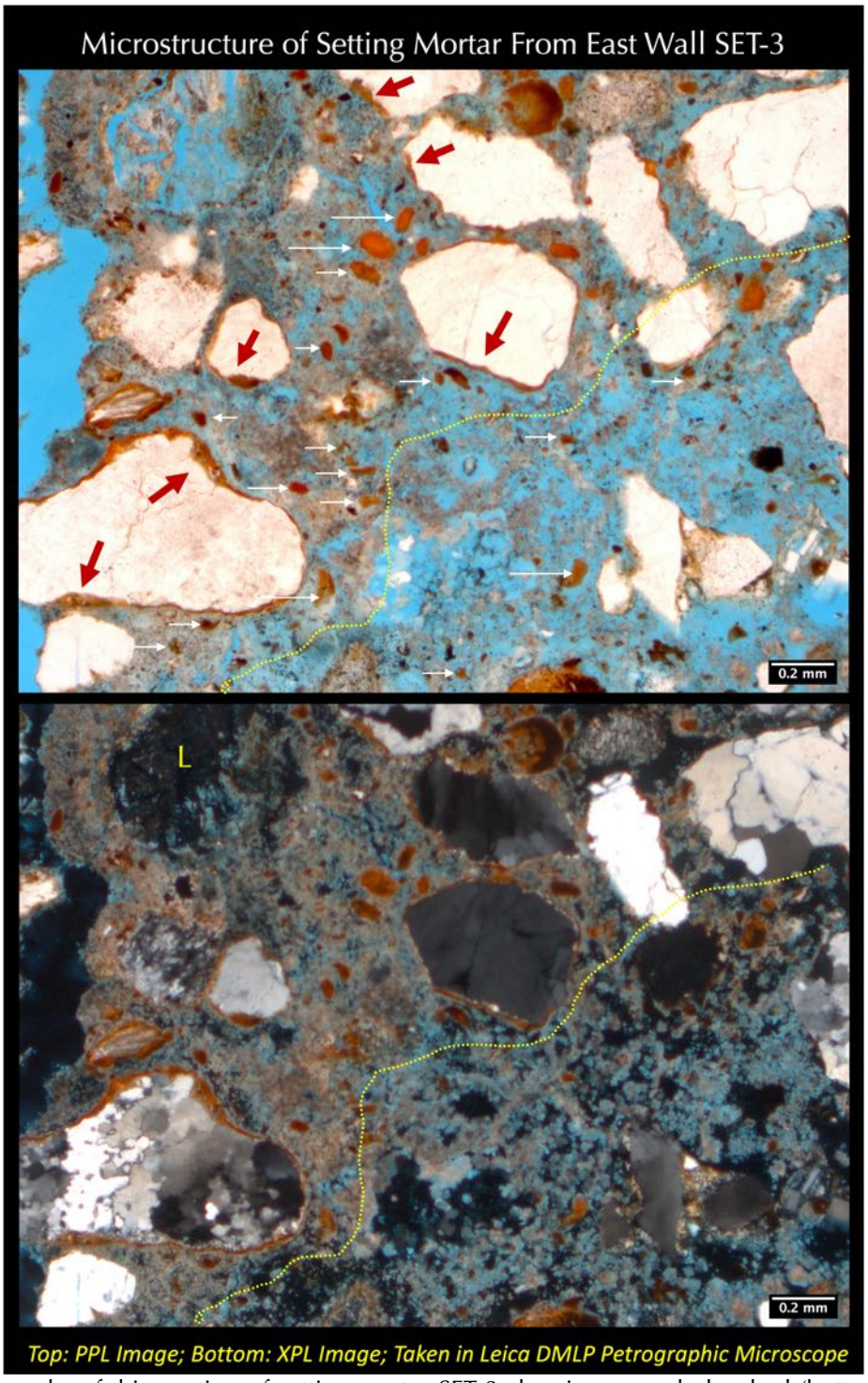

Figure 92: Micrographs of thin section of setting mortar SET-3 showing severely leached (bottom right) and less leached (top left) interstitial paste fraction in the setting mortar. Many rounded to subrounded strained quartz and quartzite sand grains are seen in the setting mortar, along with some reddish-brown ferruginous shale and siltstone particles. Reddish-brown arrows show reddish-brown coats on sand particles. Thin white arrows show a few isolated reddish-brown particles of residual calcined clay (brick dust). Letter 'L' marks the lime-leached patchy areas of paste, which appear optically isotropic in XPL image due to inherent gelatinous or amorphous nature (determined in subsequent SEM-EDS studies to be enriched in Mg, Si, and Al). Dotted line separates paste fractions of different degrees of lime leaching.

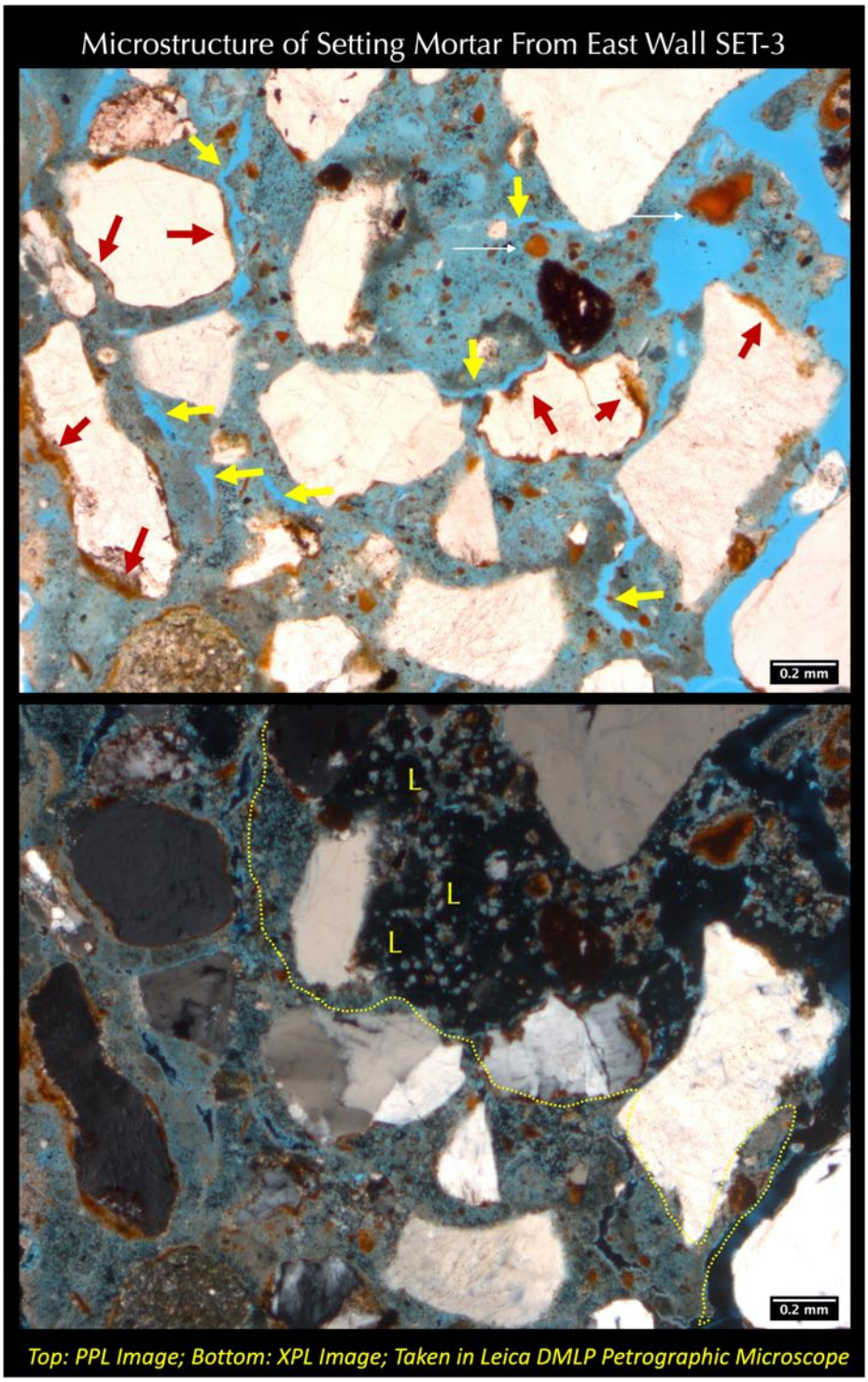

Figure 93: Micrographs of thin section of setting mortar SET-3 showing severely leached (top right) and less leached (bottom left) interstitial paste fraction in the setting mortar with fine, discontinuous carbonation shrinkage microcracks (some are marked with yellow arrows). Many rounded to subrounded strained quartz and quartzite sand grains are seen in the setting mortar, along with some reddish-brown ferruginous shale and siltstone particles. Reddish-brown arrows show reddish-brown coats on sand particles. Thin white arrows show a few isolated reddish-brown particles of residual calcined clay (brick dust). Letter 'L' marks the lime-leached patchy areas of paste, which appear optically isotropic in XPL image due to inherent gelatinous or amorphous nature (determined in subsequent SEM-EDS studies to be enriched in Mg, Si, and Al). Dotted line separates paste fractions of different degrees of lime leaching.

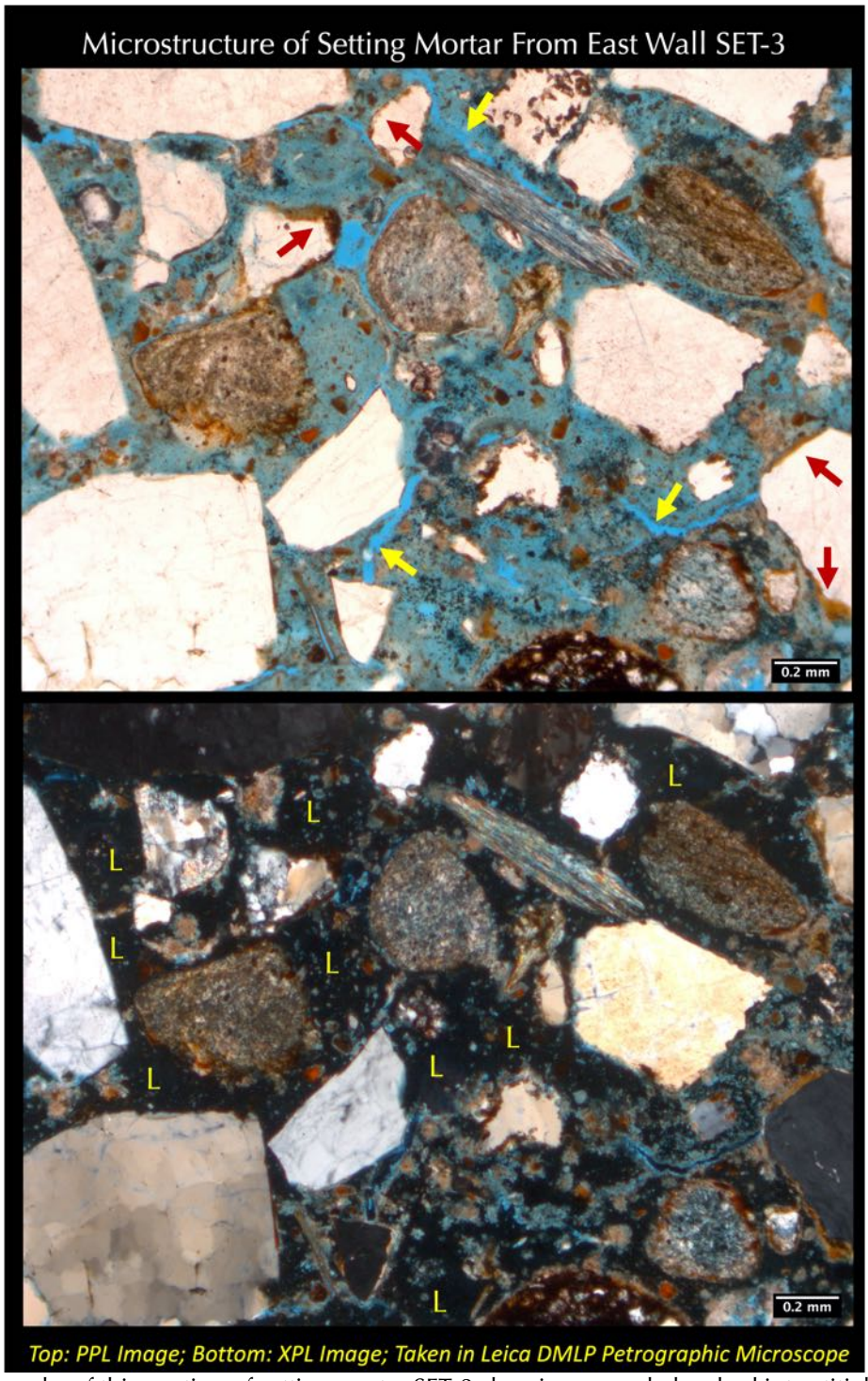

Figure 94: Micrographs of thin section of setting mortar SET-3 showing severely leached interstitial paste fraction in the setting mortar with fine, discontinuous carbonation shrinkage microcracks (some are marked with yellow arrows). Many rounded to subrounded strained quartz and quartzite sand grains are seen in the setting mortar, along with some reddish-brown ferruginous shale and siltstone particles. Reddish-brown arrows show reddish-brown coats on sand particles. Thin white arrows show a few isolated reddish-brown particles of residual calcined clay (brick dust). Letter 'L' marks the lime-leached patchy areas of paste, which appear optically isotropic in XPL image due to inherent gelatinous or amorphous nature (determined in subsequent SEM-EDS studies to be enriched in Mg, Si, and Al).

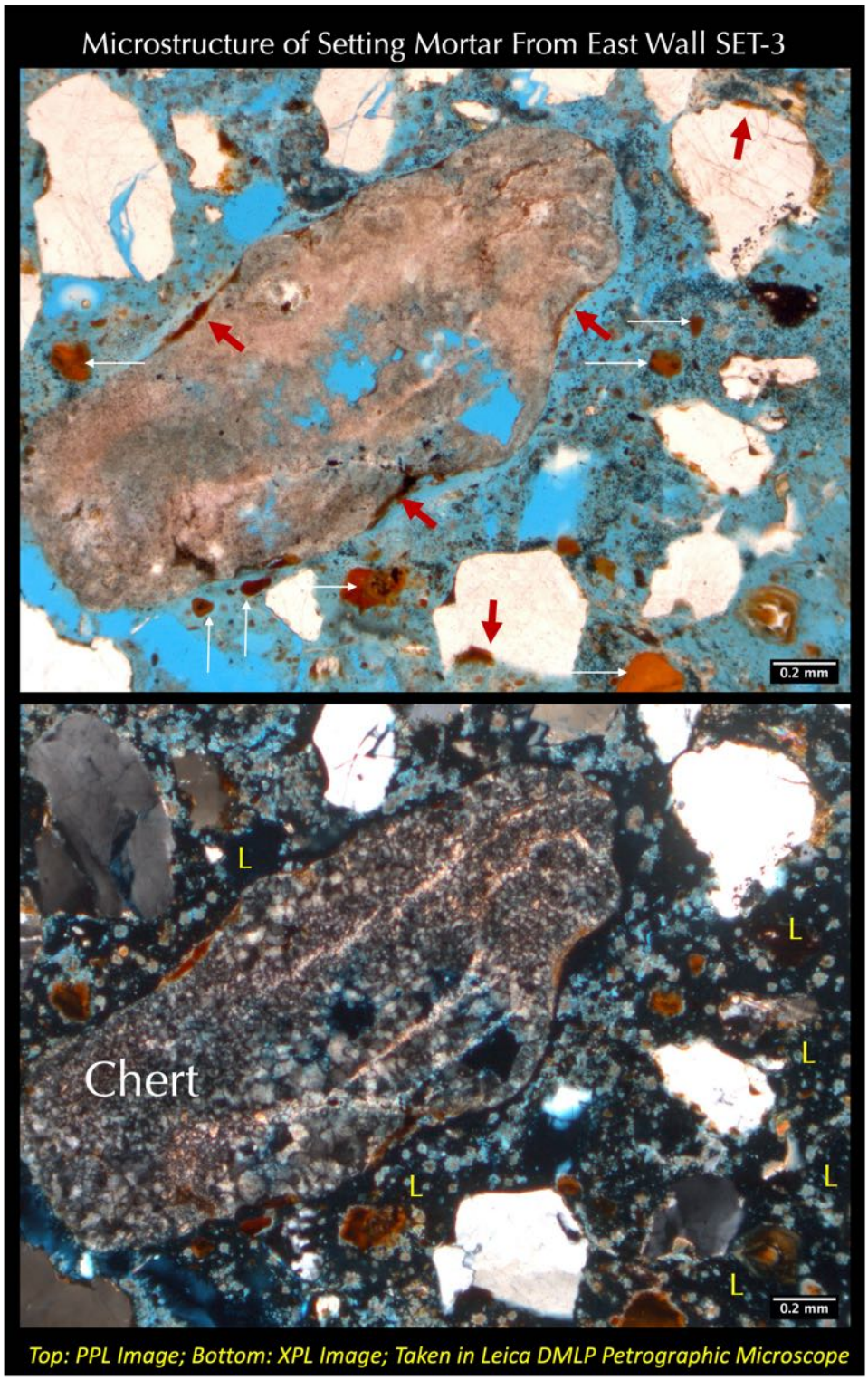

Figure 95: Micrographs of thin section of setting mortar SET-3 showing severely leached interstitial paste fraction in the setting mortar. Many rounded to subrounded chert, strained quartz and quartzite sand grains are seen in the setting mortar. Reddish-brown arrows show reddish-brown coats on sand particles. Thin white arrows show a few isolated reddish-brown particles of residual calcined clay (brick dust). Letter 'L' marks the lime-leached patchy areas of paste, which appear optically isotropic in XPL image due to inherent gelatinous or amorphous nature (determined in subsequent SEM-EDS studies to be enriched in Mg, Si, and Al).

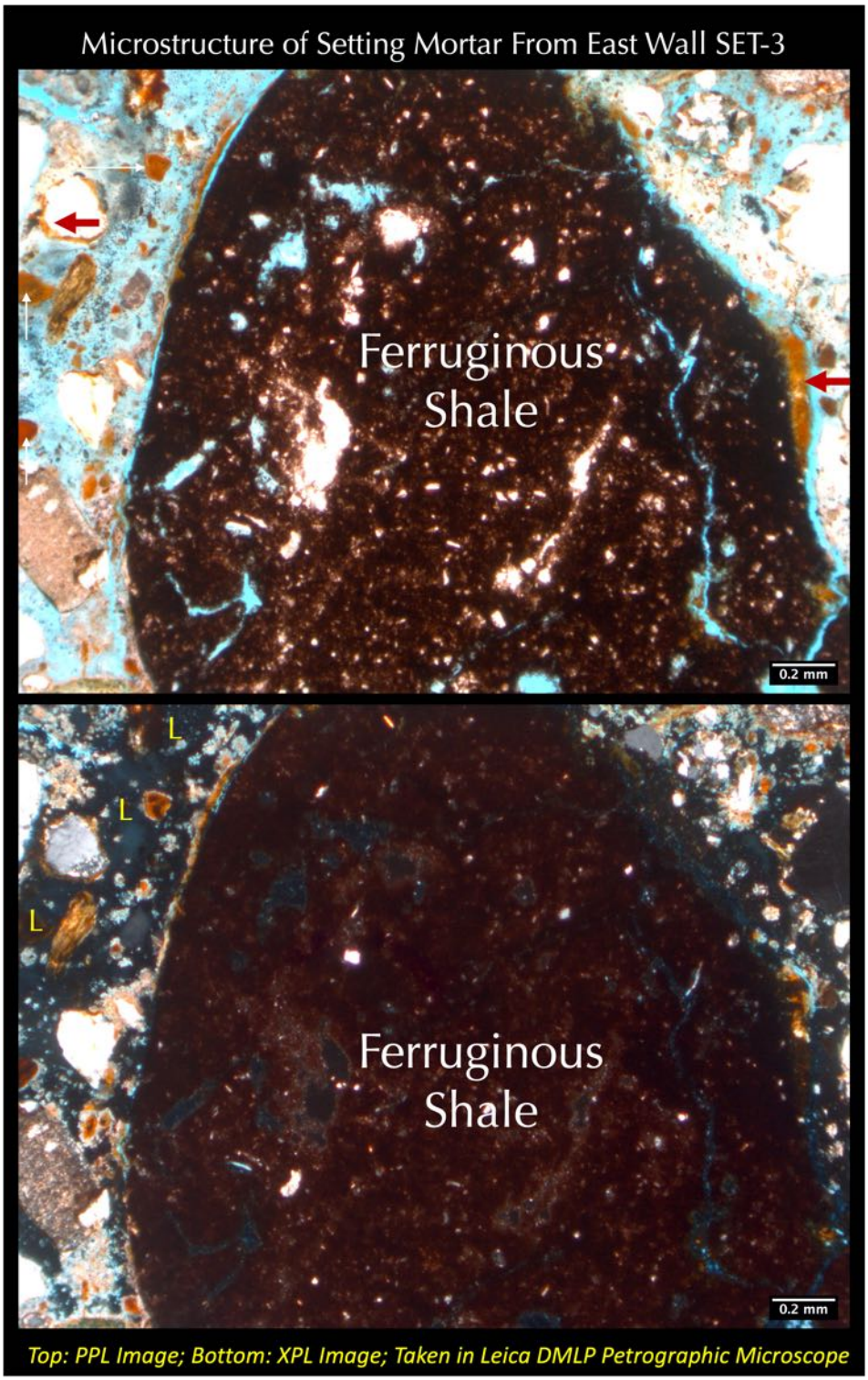

Figure 96: Micrographs of thin section of setting mortar SET-3 showing a reddish-brown rounded ferruginous shale particle in sand (resembling calcined clay) in the middle of a severely leached interstitial paste fraction. Reddish-brown arrows show reddish-brown coats on sand particles. Thin white arrows show a few isolated reddish-brown particles of residual calcined clay (brick dust). Letter 'L' marks the lime-leached patchy areas of paste, which appear optically isotropic in XPL image due to inherent gelatinous or amorphous nature (determined in subsequent SEM-EDS studies to be enriched in Mg, Si, and Al).

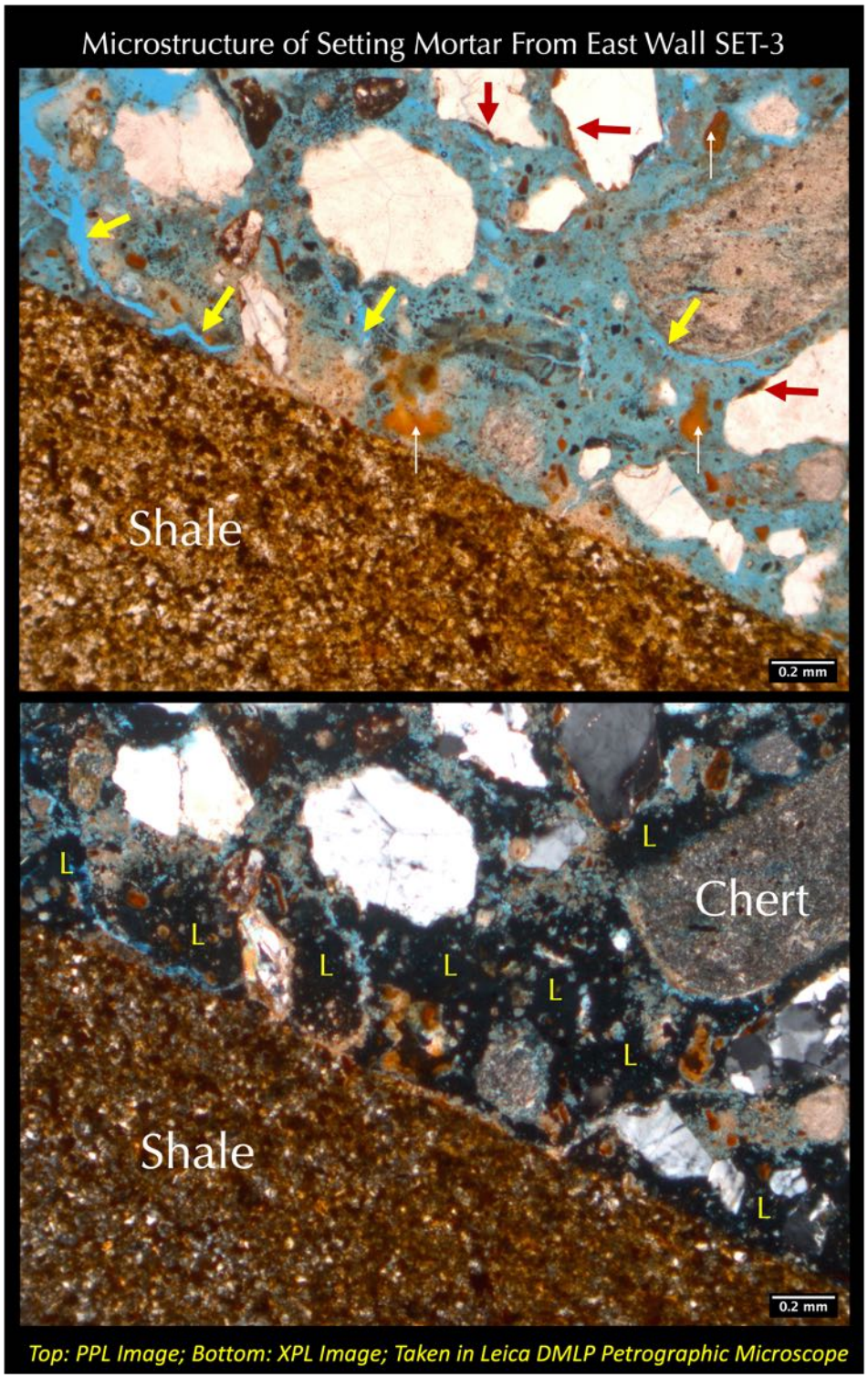

Figure 97: Micrographs of thin section of setting mortar SET-3 showing a reddish-brown ferruginous shale particle in sand in the middle of a severely leached interstitial paste fraction. Yellow arrows show carbonation shrinkage microcracks in paste. Reddish-brown arrows show reddish-brown coats on sand particles. Thin white arrows show a few isolated reddish-brown particles of residual calcined clay (brick dust). Letter 'L' marks the lime-leached patchy areas of paste, which appear optically isotropic in XPL image due to inherent gelatinous or amorphous nature (determined in subsequent SEM-EDS studies to be enriched in Mg, Si, and Al).

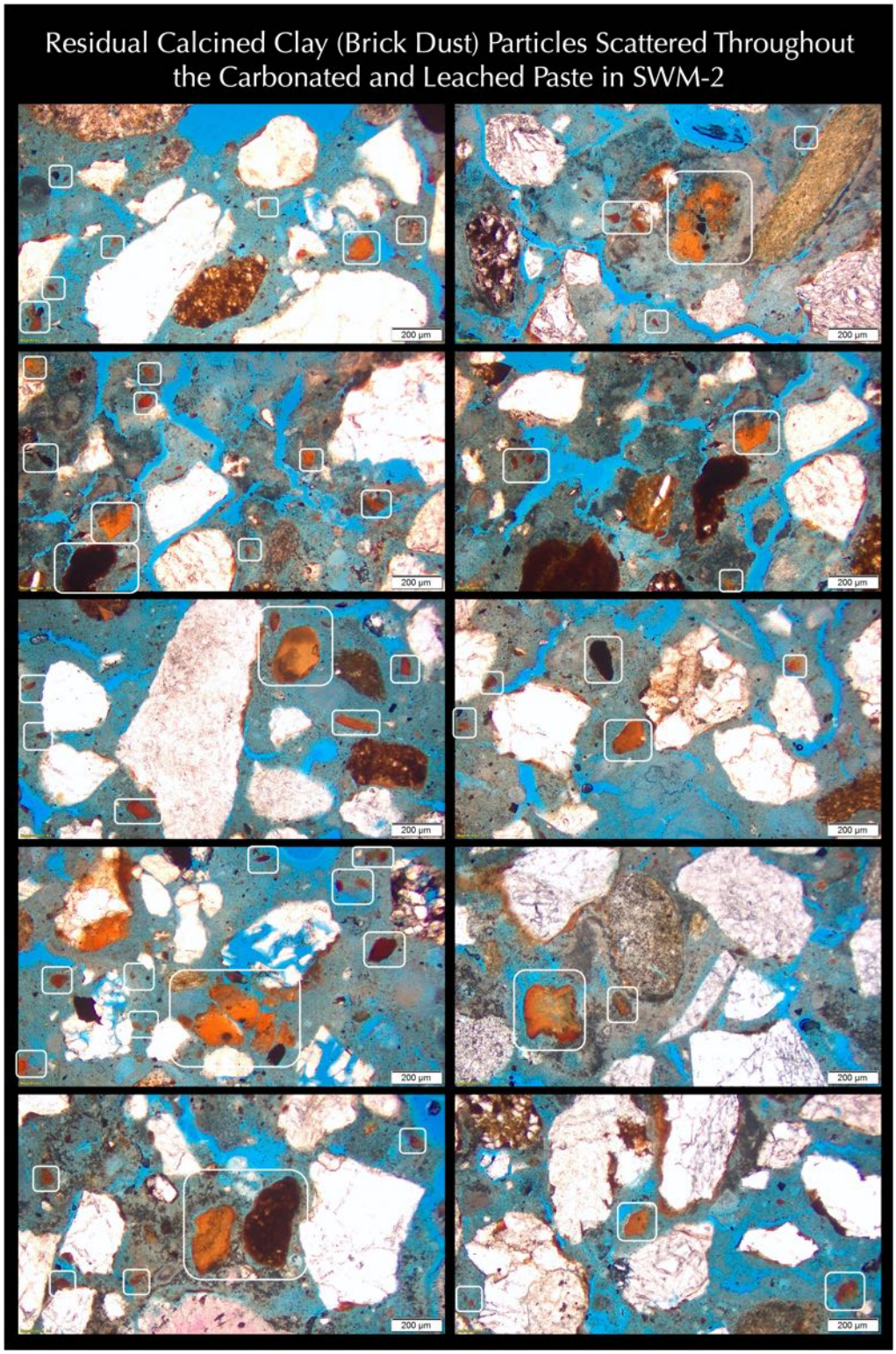

Figure 98: Micrographs of thin section of setting mortar SWM-2 showing residual calcined clay (brick dust) particles (boxed) scattered throughout the leached and carbonated paste, which are characterized by reddish-brown color and dominantly amorphous nature of the plastic component of original calcined clay with very little non-plastic (optically birefringent fillers, e.g., quartz) left from pozzolanic reactions with the dominant dolomitic lime component of binder. Micrographs were taken at plane polarized light mode in a petrographic microscope.

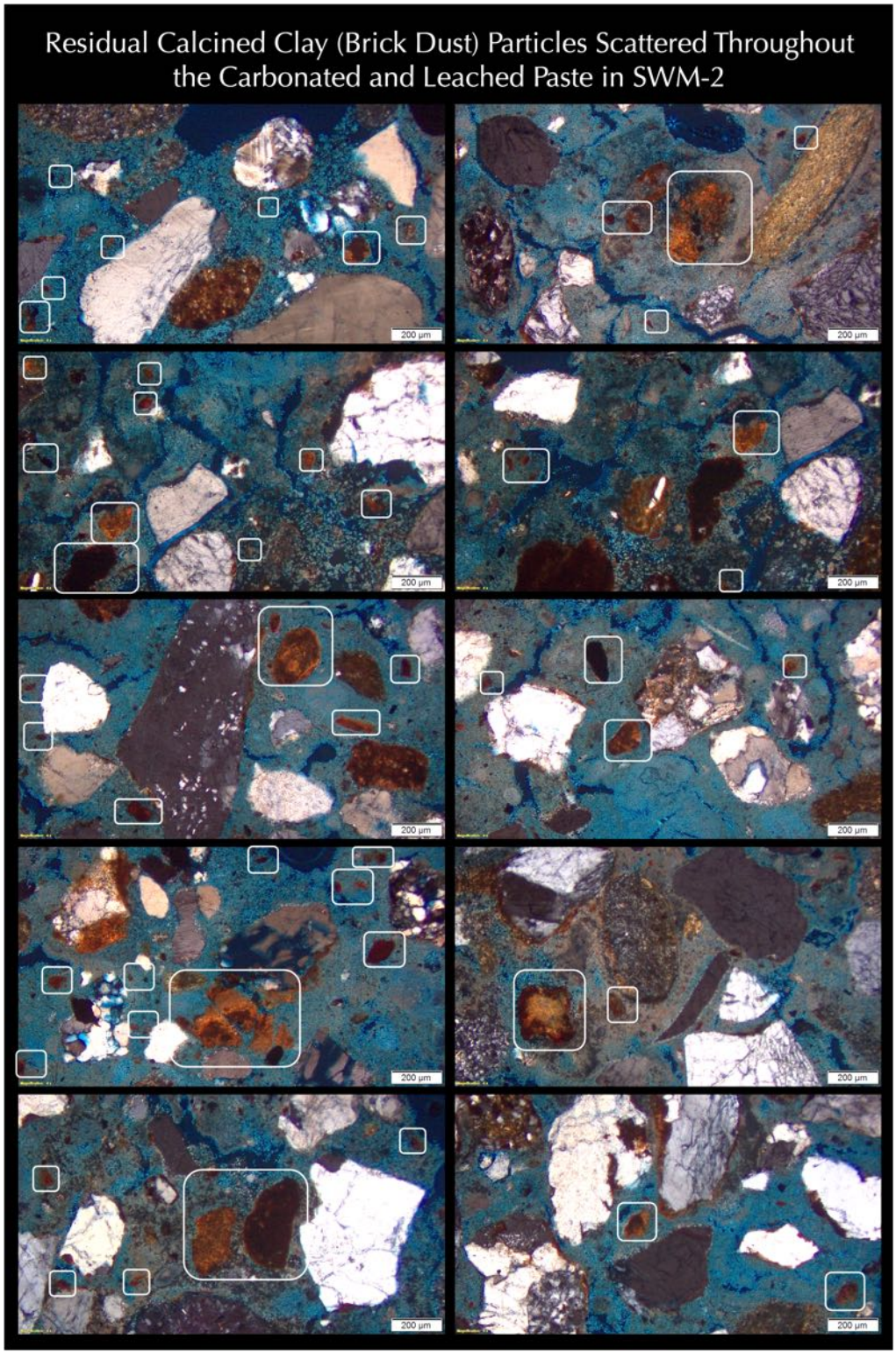

Figure 99: Micrographs of thin section of setting mortar SWM-2 showing residual calcined clay (brick dust) particles (boxed) scattered throughout the leached and carbonated paste, which are characterized by reddish-brown color and dominantly amorphous nature of the plastic component of original calcined clay with very little non-plastic (optically birefringent fillers, e.g., quartz) left from pozzolanic reactions with the dominant dolomitic lime component of binder. Micrographs were taken at cross polarized light mode in a petrographic microscope.

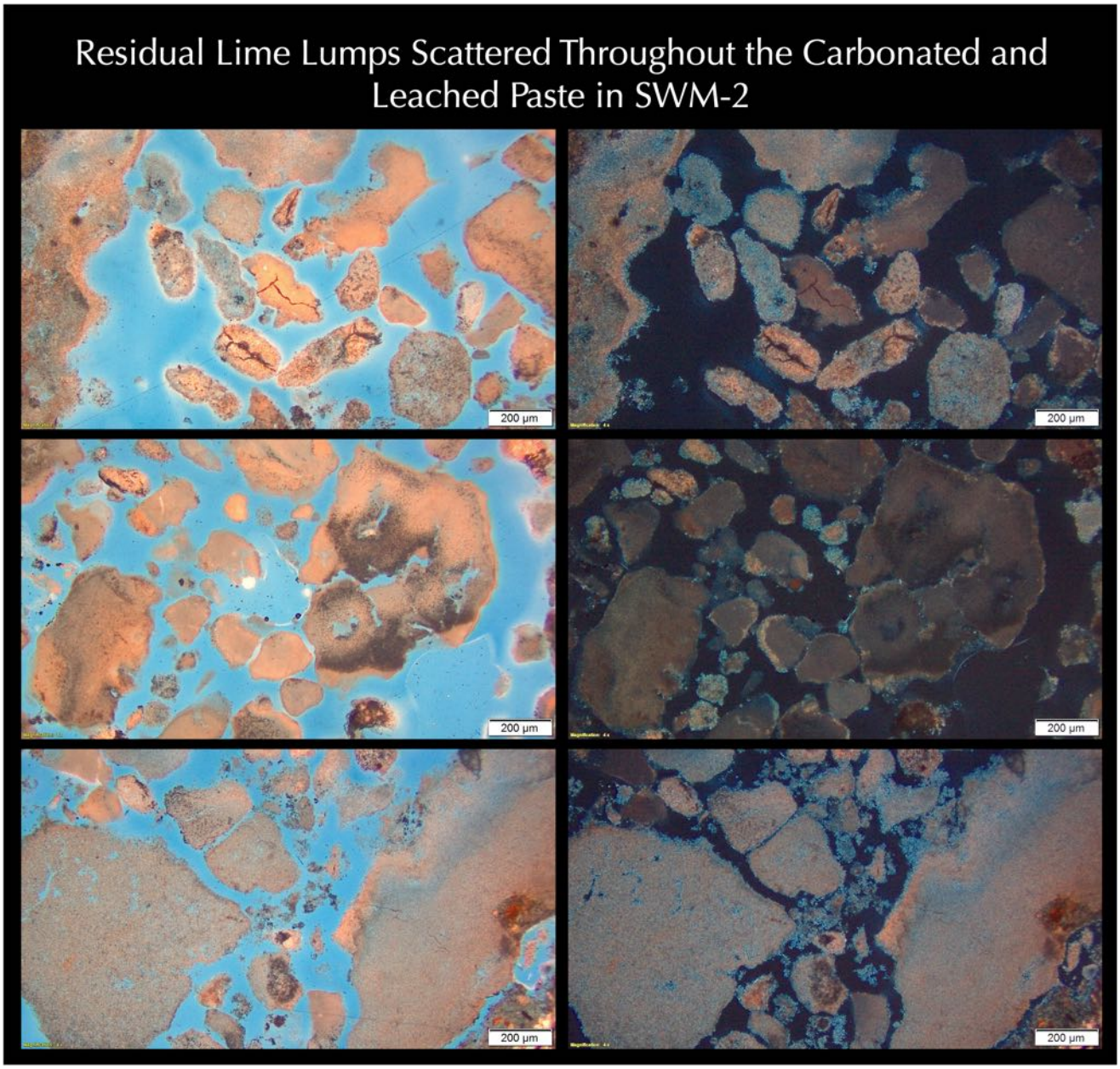

Figure 100: Micrographs of thin section of setting mortar SWM-2 showing residual lumps of unmixed lime of the original dominant dolomitic lime binder that are characterized by very fine-grained, porous, and severely carbonated nature. Micrographs were taken at plane (left column) and corresponding cross polarized light mode (right column) in a petrographic microscope.

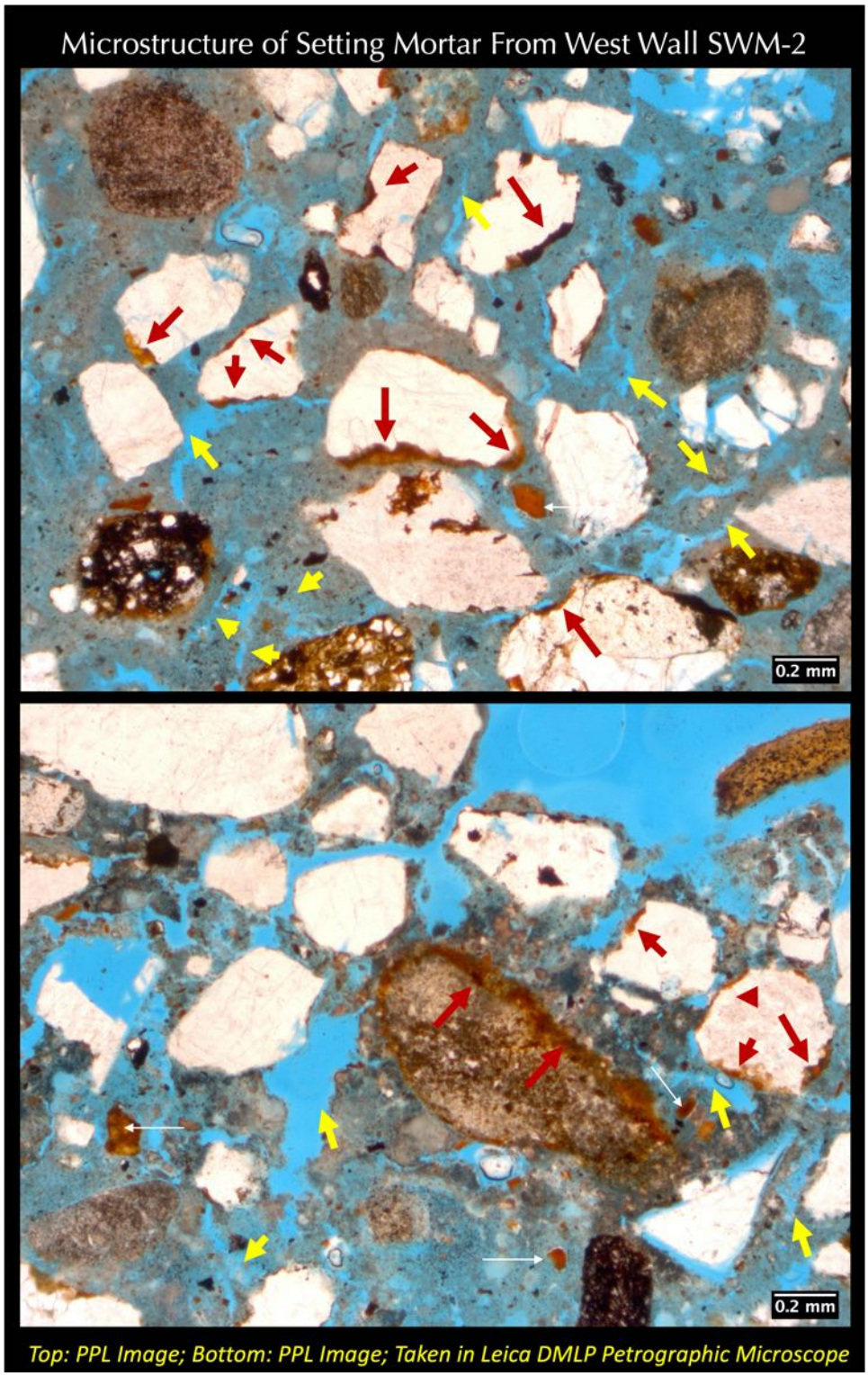

Figure 101: Micrographs of thin section of setting mortar SWM-2 showing interstitial paste fraction in the setting mortar with fine, discontinuous carbonation shrinkage microcracks (some are marked with yellow arrows). Many rounded to subrounded strained quartz and quartzite sand grains are seen in the setting mortar, along with some reddish-brown ferruginous shale and siltstone particles. Reddish-brown arrows show reddish-brown coats on sand particles. Thin white arrows show a few isolated reddish-brown particles of residual calcined clay (brick dust).

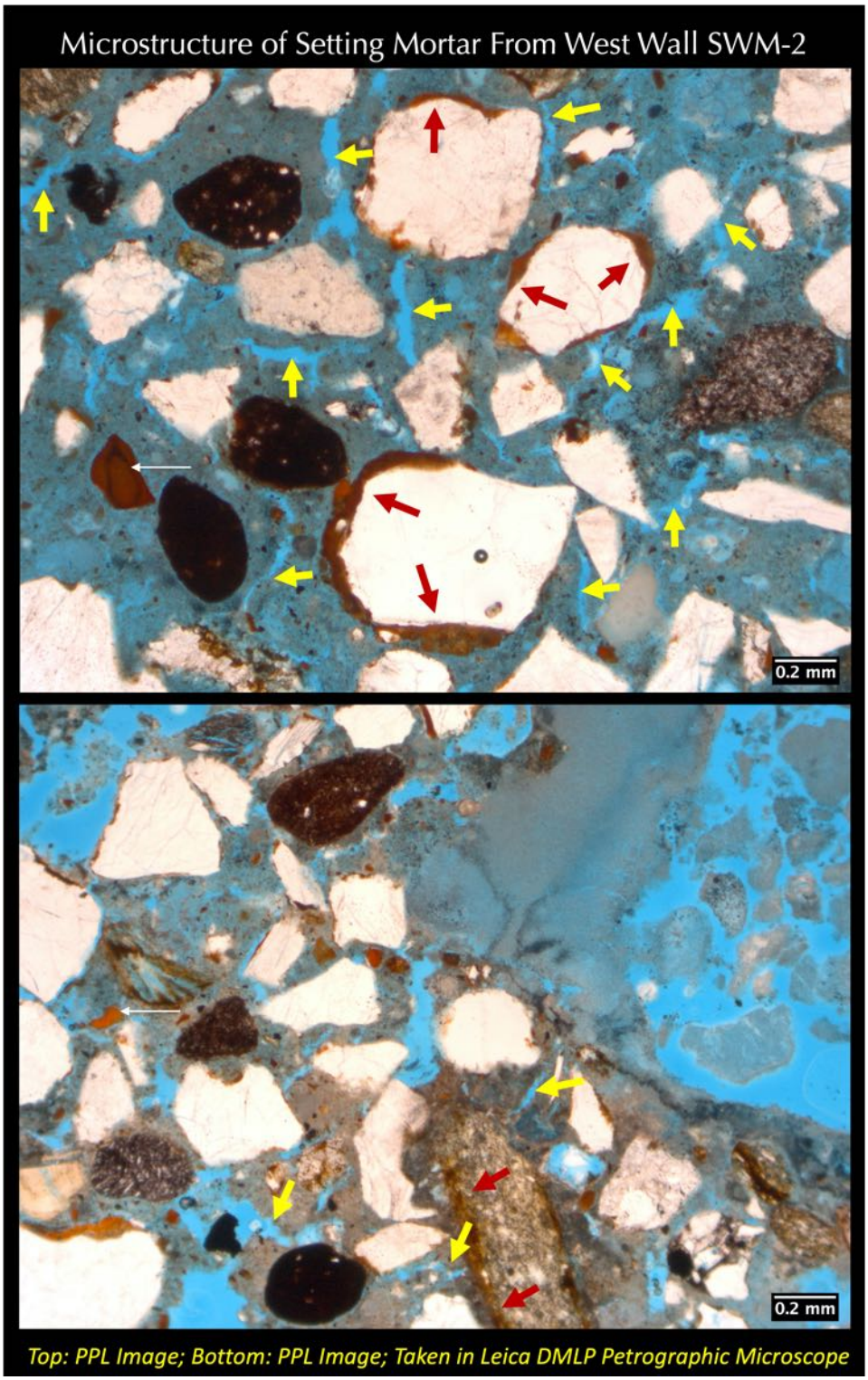

Figure 102: Micrographs of thin section of setting mortar SWM-2 interstitial paste fraction in the setting mortar with fine, discontinuous carbonation shrinkage microcracks (some are marked with yellow arrows). Many rounded to subrounded strained quartz and quartzite sand grains are seen in the setting mortar, along with some reddish-brown ferruginous shale and siltstone particles. Reddish-brown arrows show reddish-brown coats on sand particles. Thin white arrows show a few isolated reddish-brown particles of residual calcined clay (brick dust). Bottom photo shows an unmixed lump from lime putty at the right side.

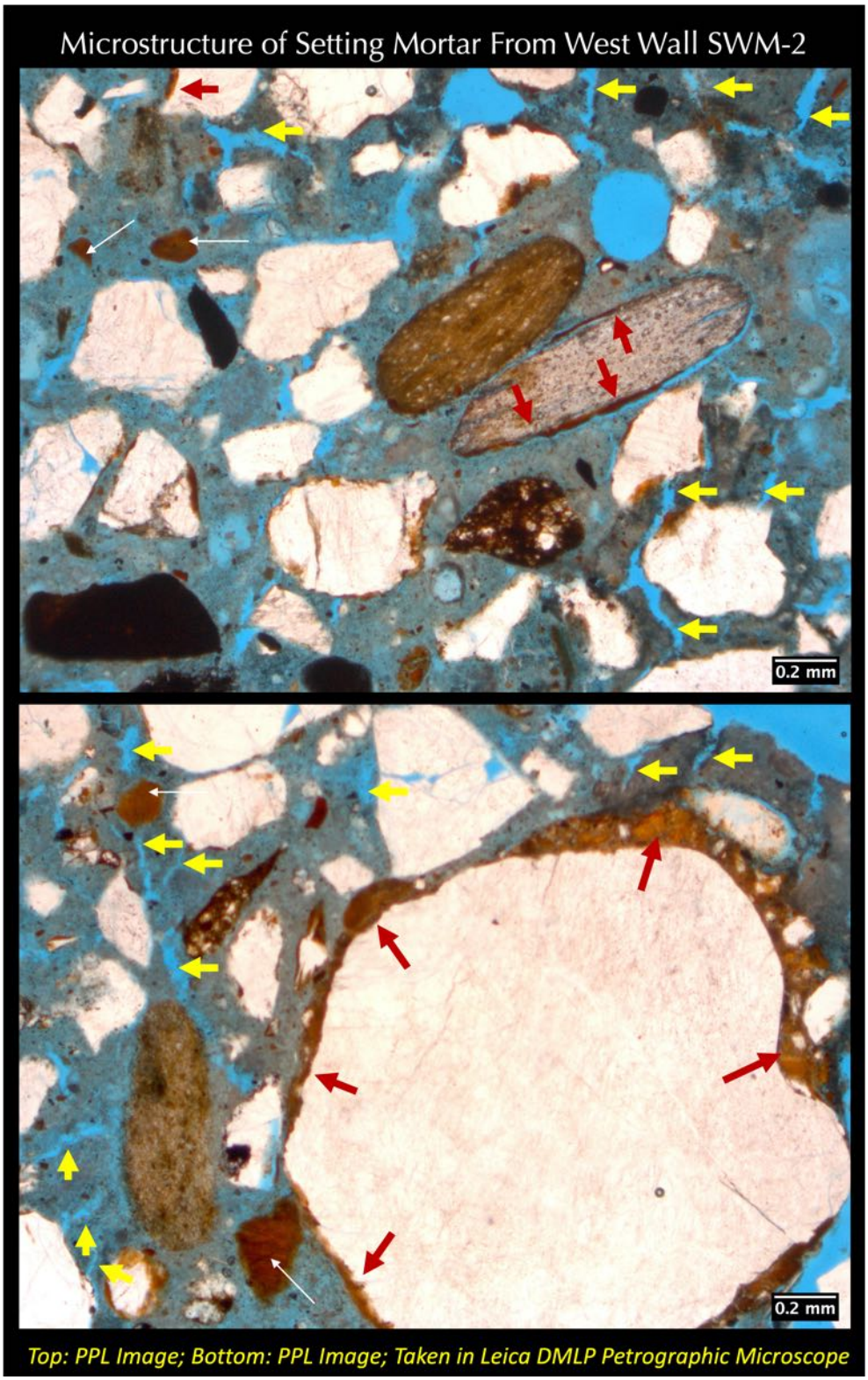

Figure 103: Micrographs of thin section of setting mortar SWM-2 showing interstitial paste fraction in the setting mortar with fine, discontinuous carbonation shrinkage microcracks (some are marked with yellow arrows). Many rounded to subrounded strained quartz and quartzite sand grains are seen in the setting mortar, along with some reddish-brown ferruginous shale and siltstone particles. Reddish-brown arrows show reddish-brown coats on sand particles. Thin white arrows show a few isolated reddish-brown particles of residual calcined clay (brick dust).

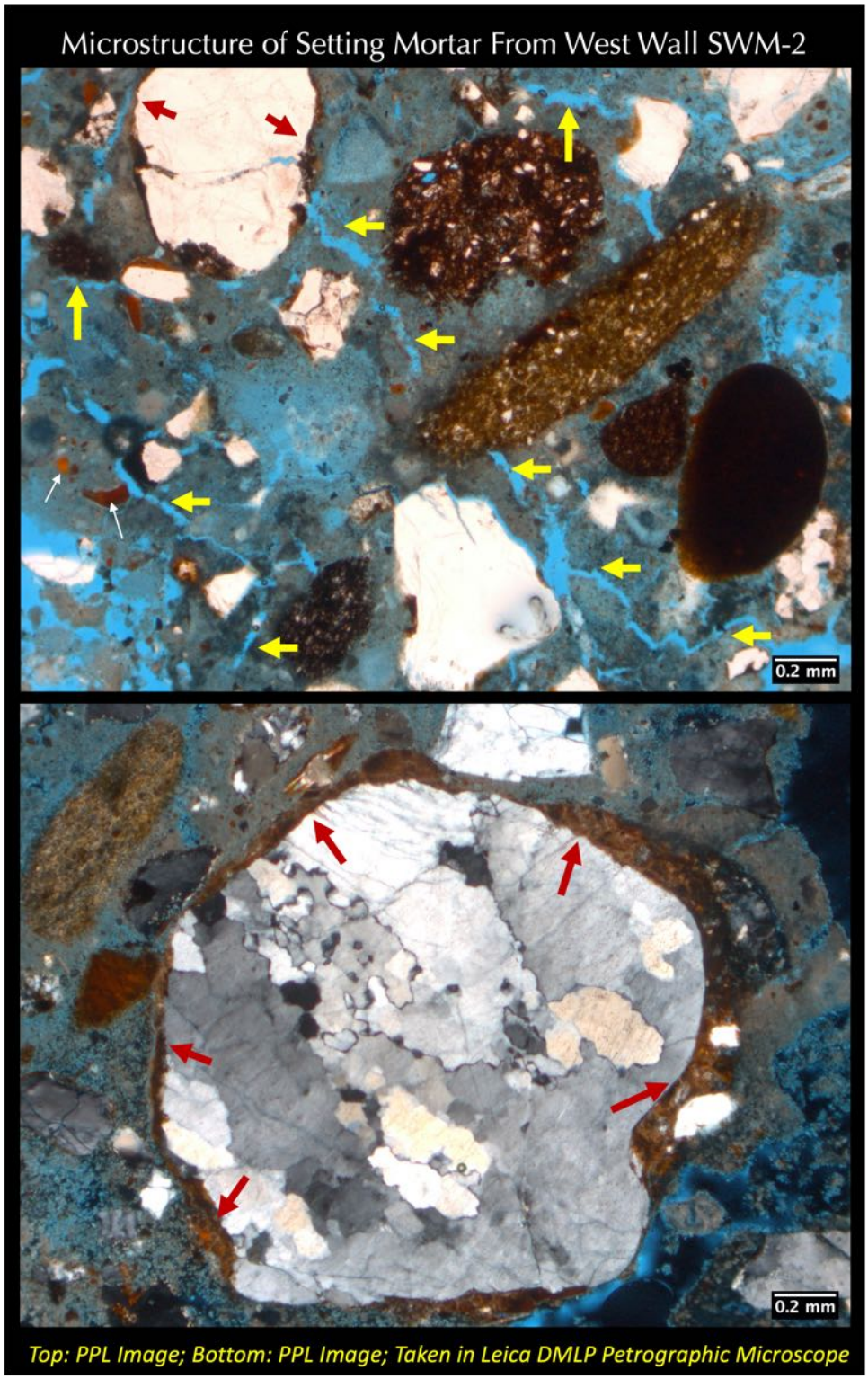

Figure 104: Micrographs of thin section of setting mortar SWM-2 showing interstitial paste fraction in the setting mortar with fine, discontinuous carbonation shrinkage microcracks (some are marked with yellow arrows). Many rounded to subrounded strained quartz and quartzite sand grains are seen in the setting mortar, along with some reddish-brown ferruginous shale and siltstone particles. Reddish-brown arrows show reddish-brown coats on sand particles. Thin white arrows show a few isolated reddish-brown particles of residual calcined clay (brick dust).

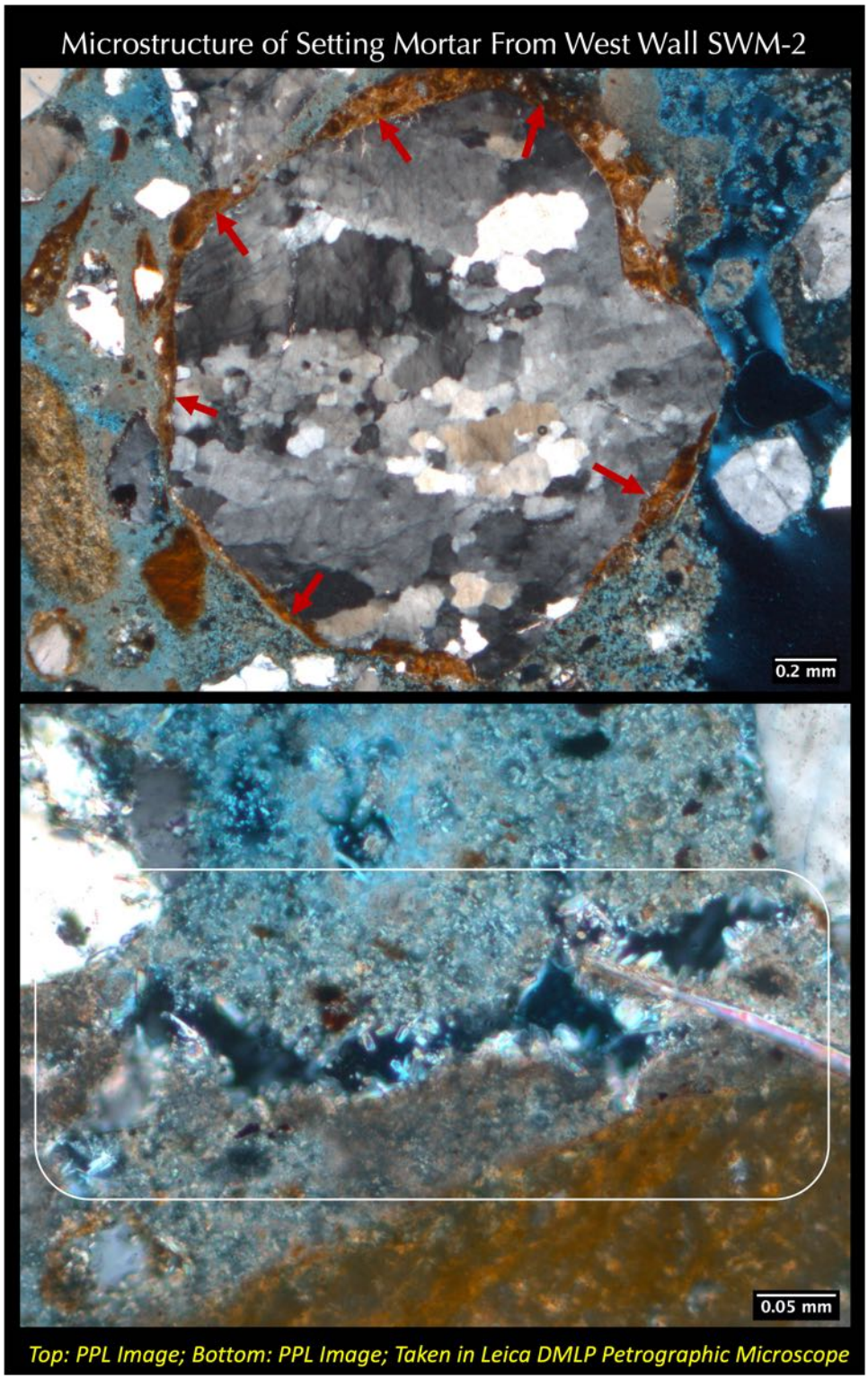

Figure 105: Micrographs of thin section of setting mortar SWM-2 showing interstitial paste fraction in the setting mortar. Many rounded to subrounded strained quartz and quartzite sand grains are seen in the setting mortar, along with some reddish-brown ferruginous shale and siltstone particles. Reddish-brown arrows show reddish-brown coats on sand particles. Boxed area in the bottom photo shows some fine, lath-shaped secondary carbonate precipitates in a void space.

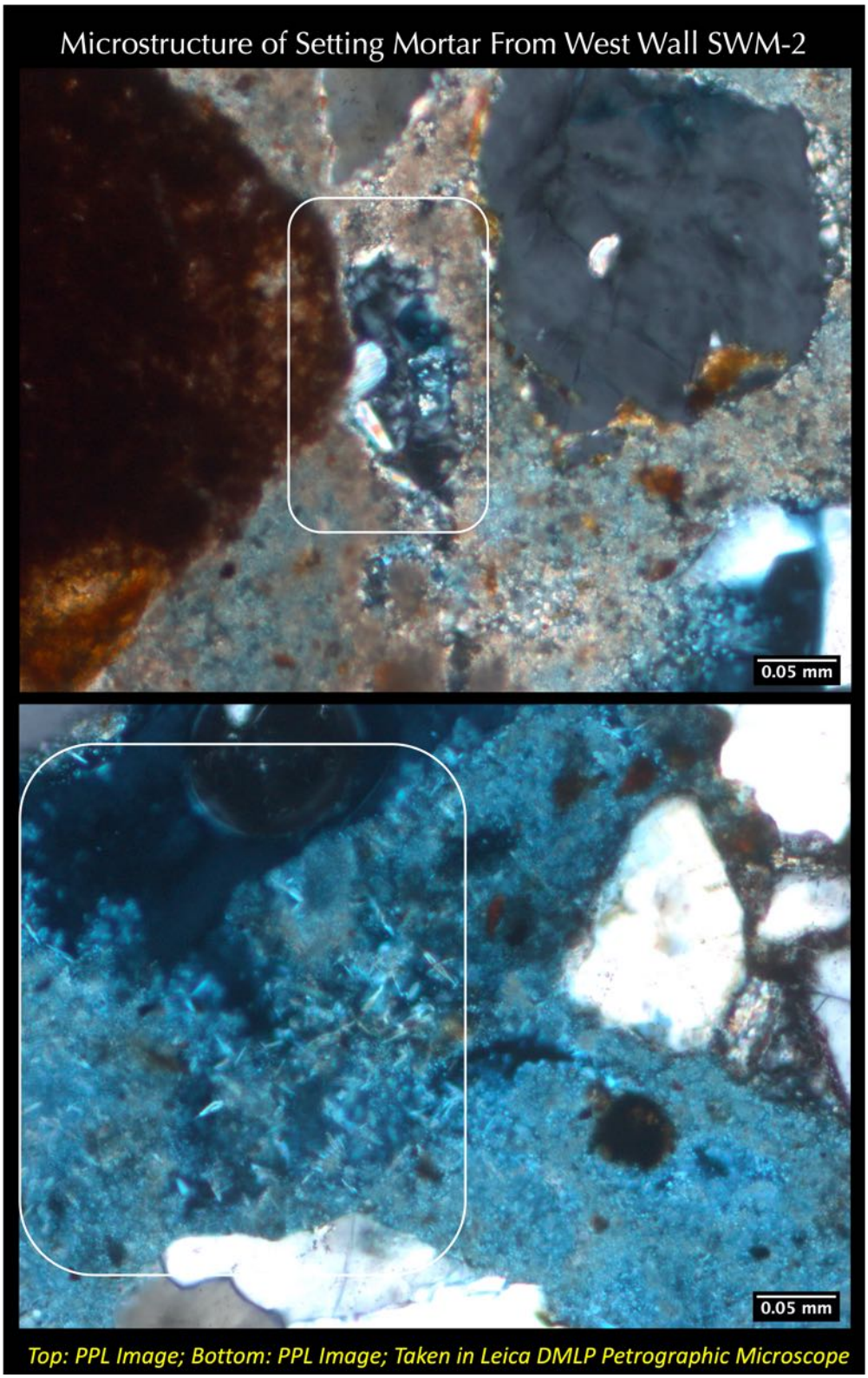

Figure 106: Micrographs of thin section of setting mortar SWM-2 showing fine, lath-shaped secondary carbonate precipitates in void spaces (boxed).

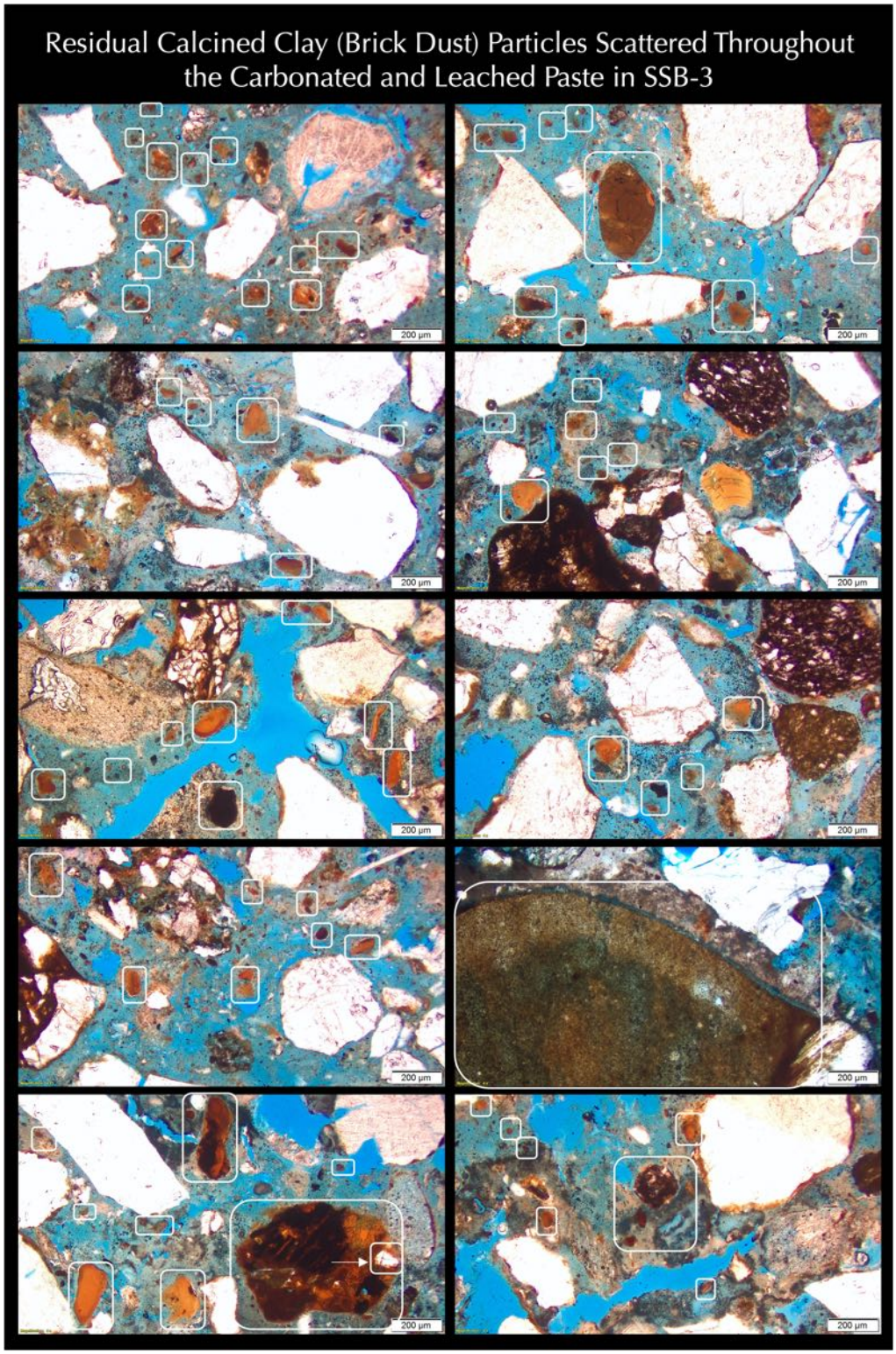

Figure 107: Micrographs of thin section of setting mortar SSB-3 showing residual calcined clay (brick dust) particles (boxed) scattered throughout the leached and carbonated paste, which are characterized by reddish-brown color and dominantly amorphous nature of the plastic component of original calcined clay with very little non-plastic (optically birefringent fillers, e.g., quartz) left from pozzolanic reactions with the dominant dolomitic lime component of binder. Micrographs were taken at plane polarized light mode in a petrographic microscope.

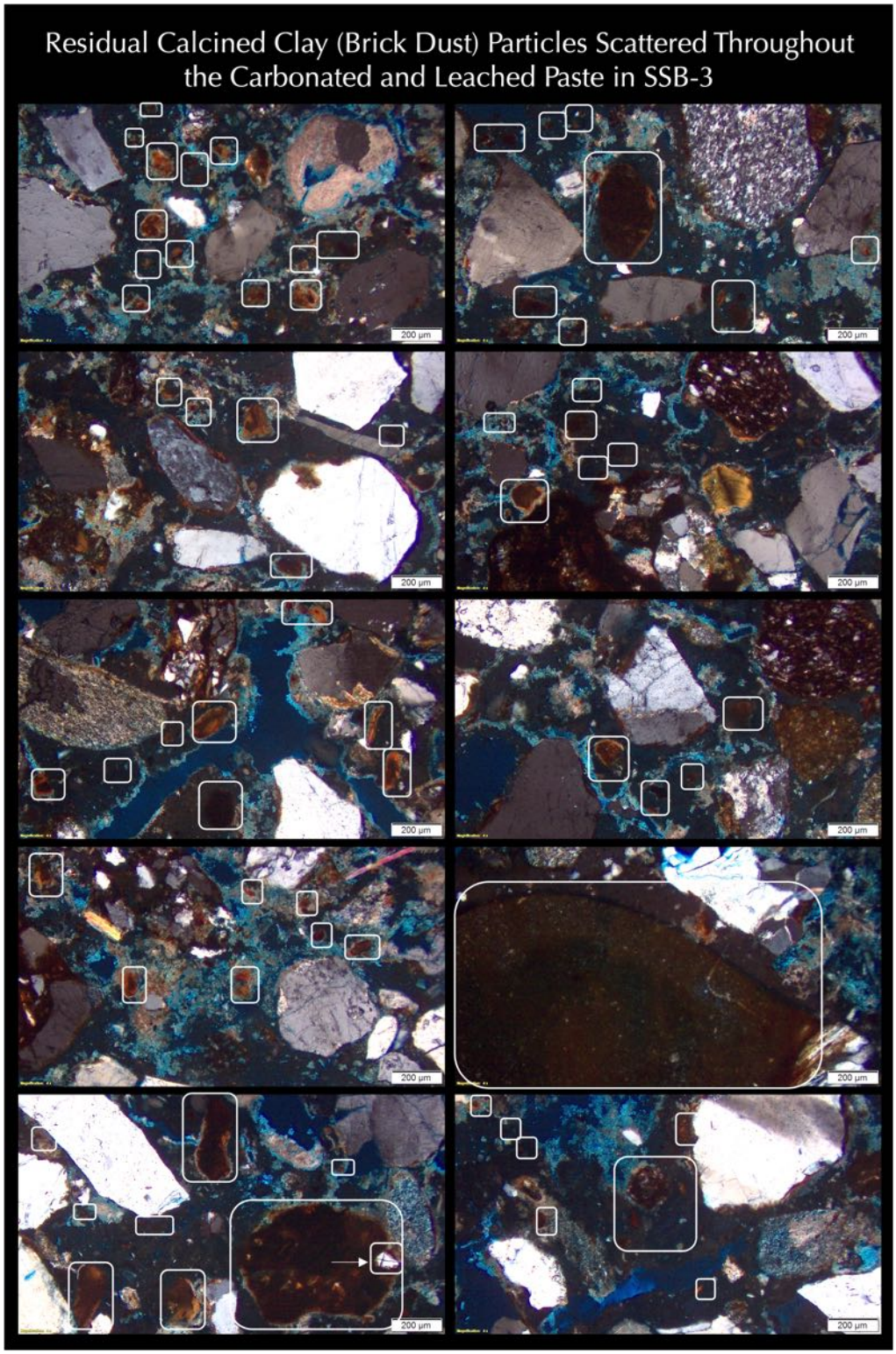

Figure 108: Micrographs of thin section of setting mortar SSB-3 showing residual calcined clay (brick dust) particles (boxed) scattered throughout the leached and carbonated paste, which are characterized by reddish-brown color and dominantly amorphous nature of the plastic component of original calcined clay with very little non-plastic (optically birefringent fillers, e.g., quartz) left from pozzolanic reactions with the dominant dolomitic lime component of binder. Micrographs were taken at cross polarized light mode in a petrographic microscope.

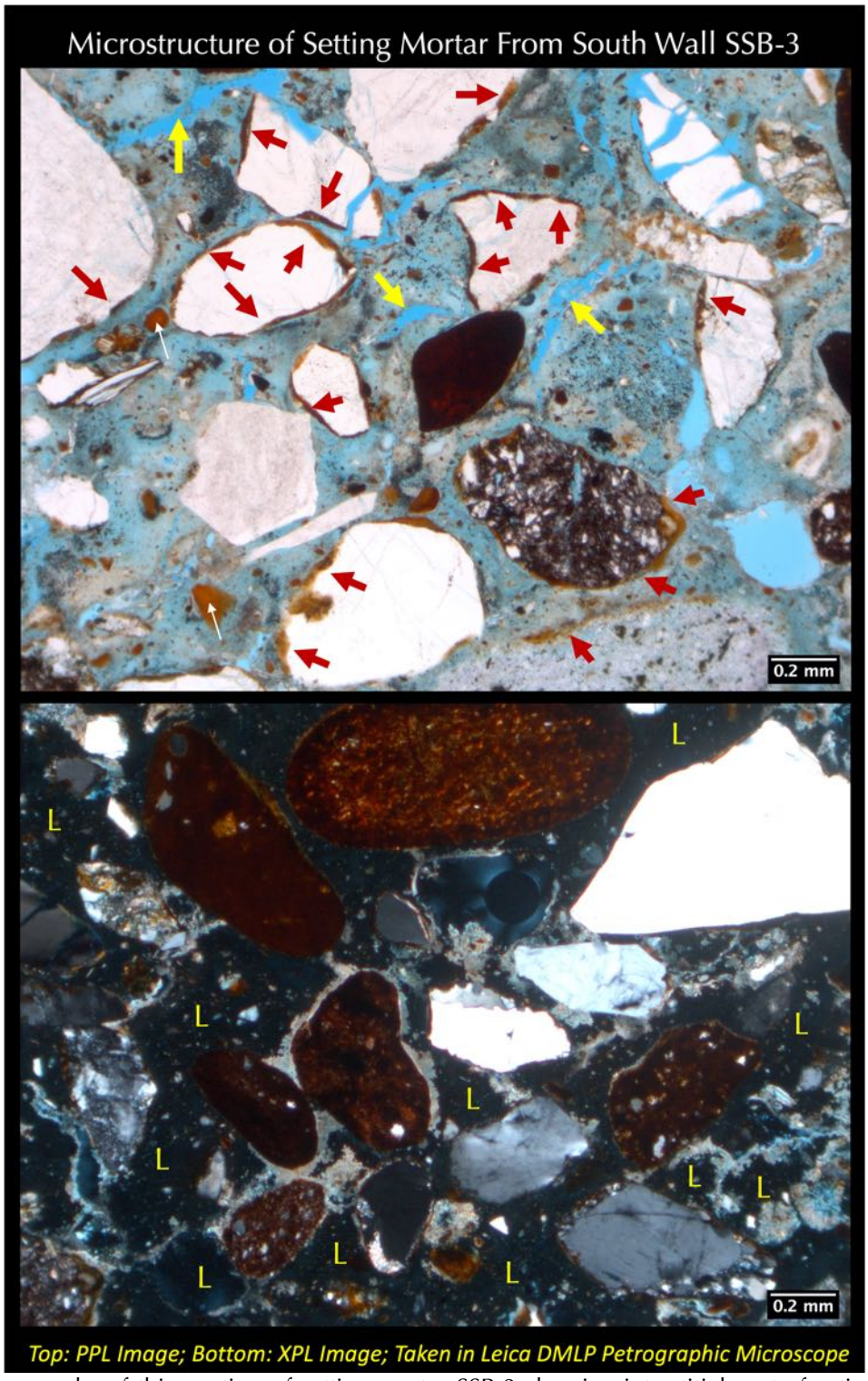

Figure 109: Micrographs of thin section of setting mortar SSB-3 showing interstitial paste fraction in the setting mortar with fine, discontinuous carbonation shrinkage microcracks (some are marked with yellow arrows). Many rounded to subrounded strained quartz and quartzite sand grains are seen in the setting mortar, along with some reddish-brown ferruginous shale and siltstone particles. Reddish-brown arrows show reddish-brown coats on sand particles. Thin white arrows show a few isolated reddish-brown particles of residual calcined clay (brick dust). Letter 'L' marks the lime-leached patchy areas of paste, which appear optically isotropic in XPL image due to inherent gelatinous or amorphous nature (determined in subsequent SEM-EDS studies to be enriched in Mg, Si, and Al).

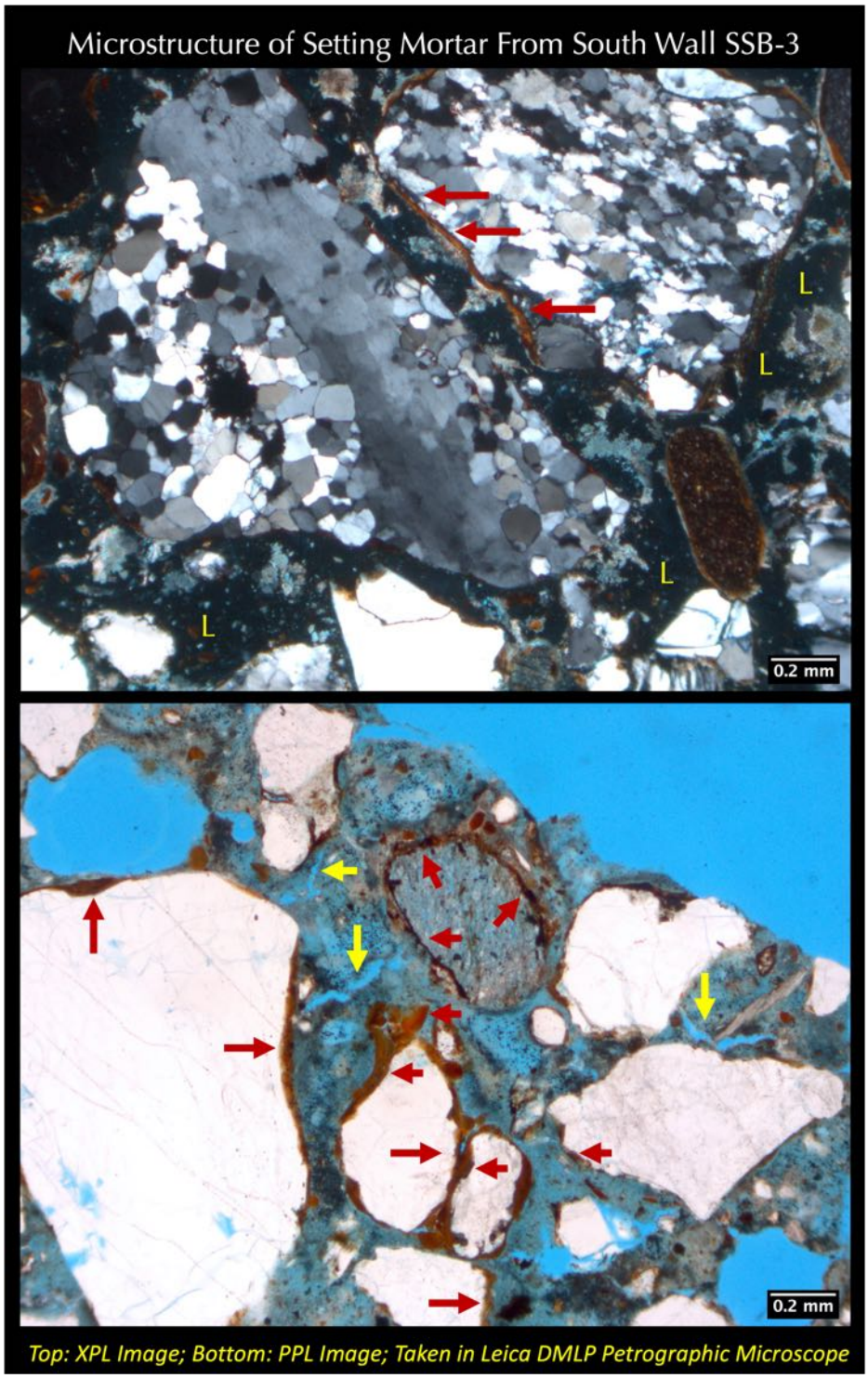

Figure 110: Micrographs of thin section of setting mortar SSB-3 showing interstitial paste fraction in the setting mortar with fine, discontinuous carbonation shrinkage microcracks (some are marked with yellow arrows). Many rounded to subrounded strained quartz and quartzite sand grains are seen in the setting mortar, along with some reddish-brown ferruginous shale and siltstone particles. Reddish-brown arrows show reddish-brown coats on sand particles. Letter 'L' marks the lime-leached patchy areas of paste, which appear optically isotropic in XPL image due to inherent gelatinous or amorphous nature (determined in subsequent SEM-EDS studies to be enriched in Mg, Si, and Al).

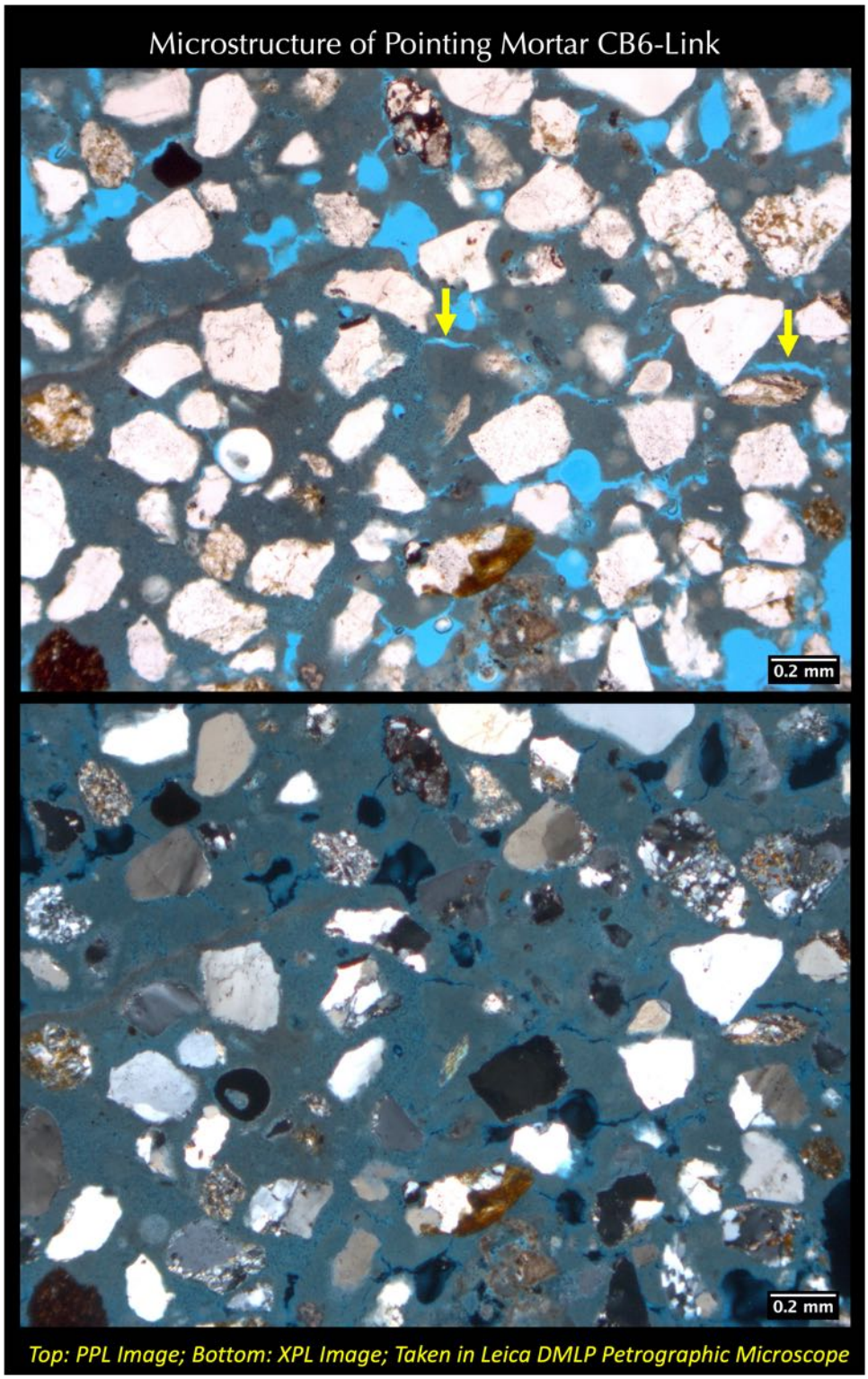

Figure 111: Micrographs of thin section of pointing mortar CB6-Link showing fine (< 1 mm size), angular, well-sorted siliceous sand consisting of major amount of quartz and subordinate amounts of quartzite, shale, and siltstone; and interstitial severely carbonated paste having many fine, discontinuous carbonation shrinkage microcracks (some are marked with yellow arrows). Notice very different i.e., finer grain-size of sand as well as of dense, carbonated interstitial paste compared to coarse sand and leached paste, respectively seen in the three setting mortars. Notice the absence of any residual calcined clay particles (brick dust) in pointing mortar.

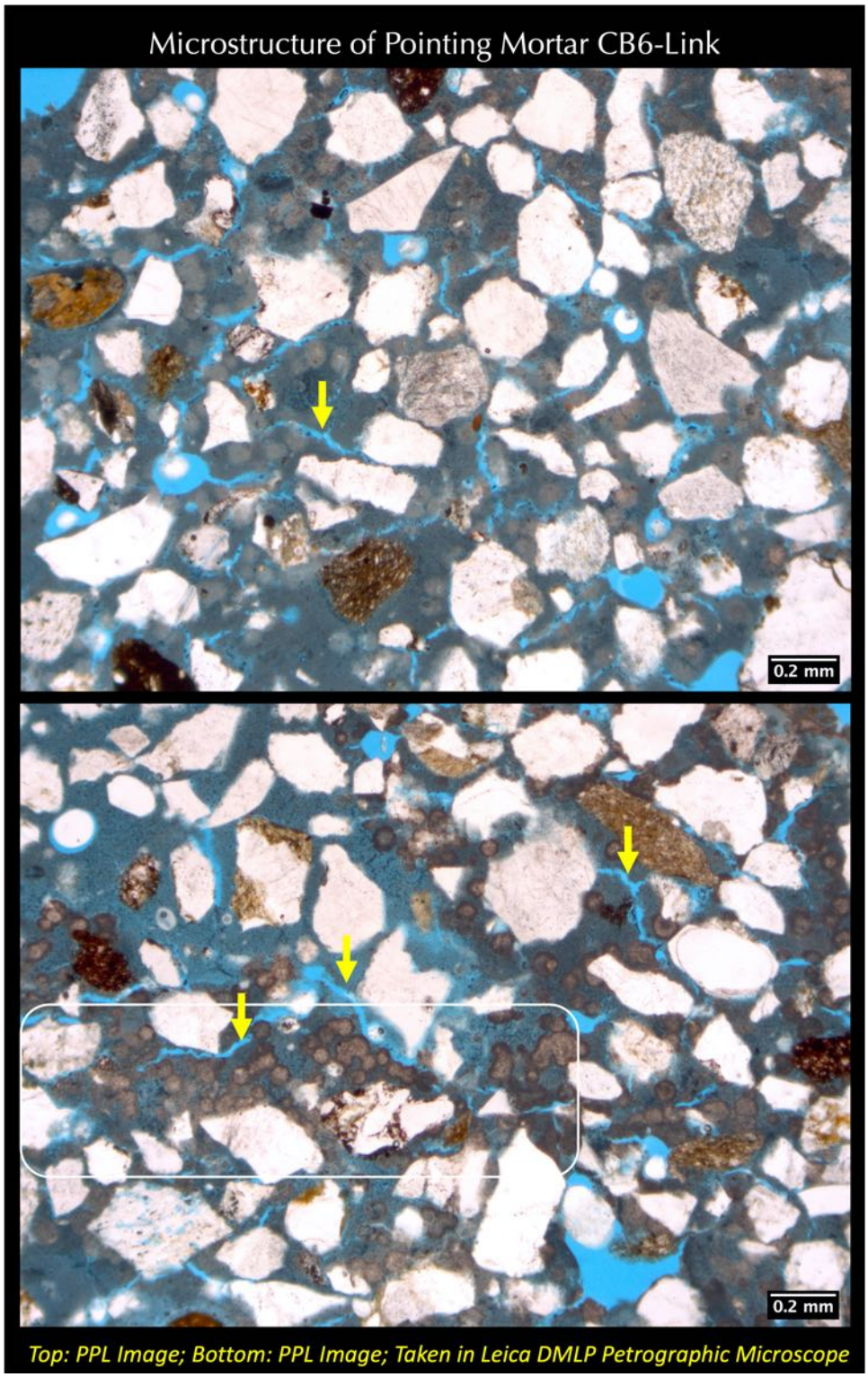

Figure 112: Micrographs of thin section of pointing mortar CB6-Link showing fine (< 1 mm size), angular, well-sorted siliceous sand consisting of major amount of quartz and subordinate amounts of quartzite, shale, and siltstone; and interstitial severely carbonated paste having many fine, discontinuous carbonation shrinkage microcracks (some are marked with yellow arrows). Notice very different i.e., finer grain-size of sand as well as of dense, carbonated interstitial paste compared to coarse sand and leached paste, respectively seen in the three setting mortars. Notice the absence of any residual calcined clay particles (brick dust) in pointing mortar.

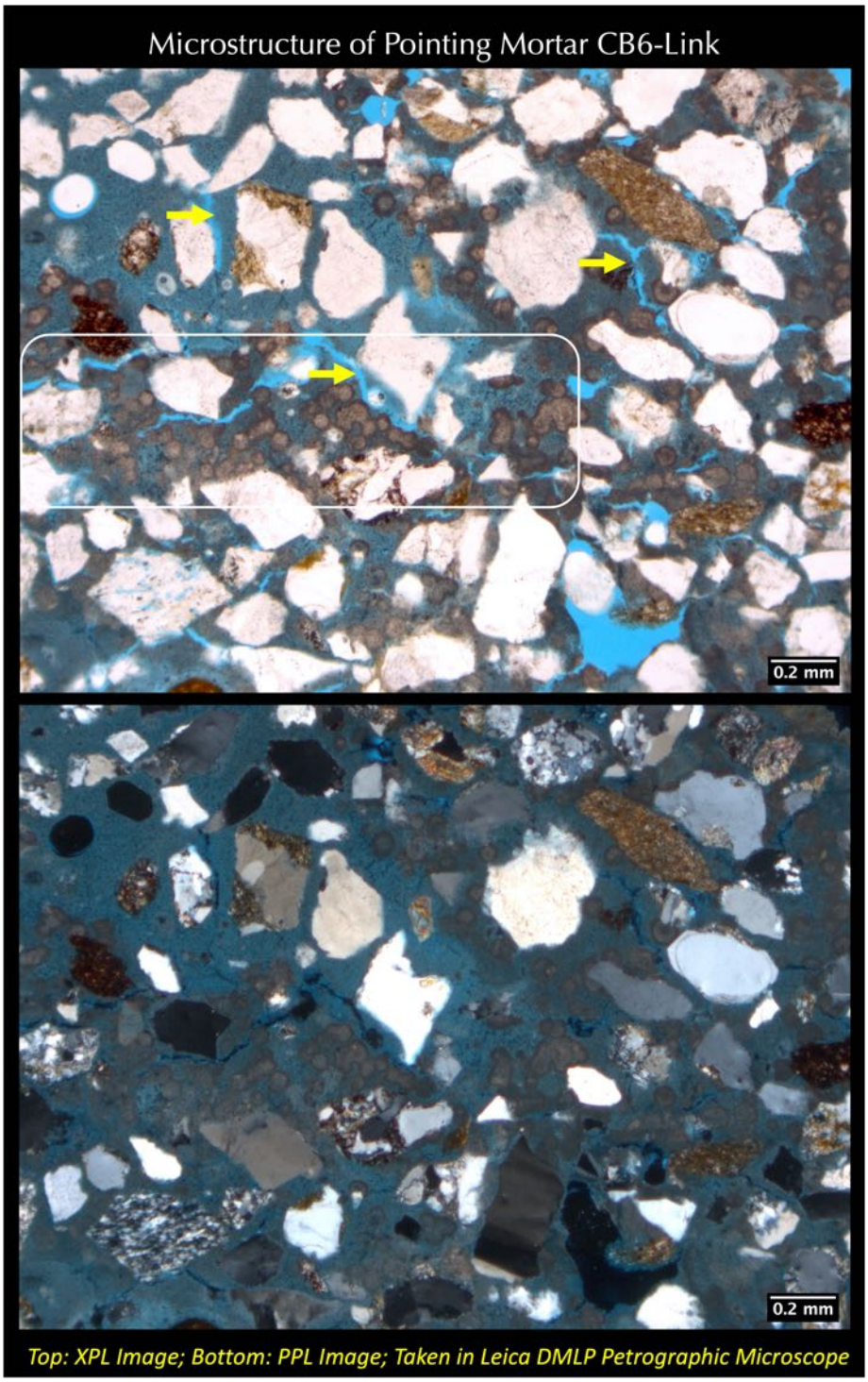

Figure 113: Micrographs of thin section of pointing mortar CB6-Link showing fine (< 1 mm size), angular, well-sorted siliceous sand consisting of major amount of quartz and subordinate amounts of quartzite, shale, and siltstone; and interstitial severely carbonated paste having many fine, discontinuous carbonation shrinkage microcracks (some are marked with yellow arrows). Notice very different i.e., finer grain-size of sand as well as of dense, carbonated interstitial paste compared to coarse sand and leached paste, respectively seen in the three setting mortars. Boxed area shows some small lime globules, which are determined in SEM-EDS studies to be essentially similar in composition to the rest of the paste except in having a slightly higher silica (hydraulicity) than the rest.

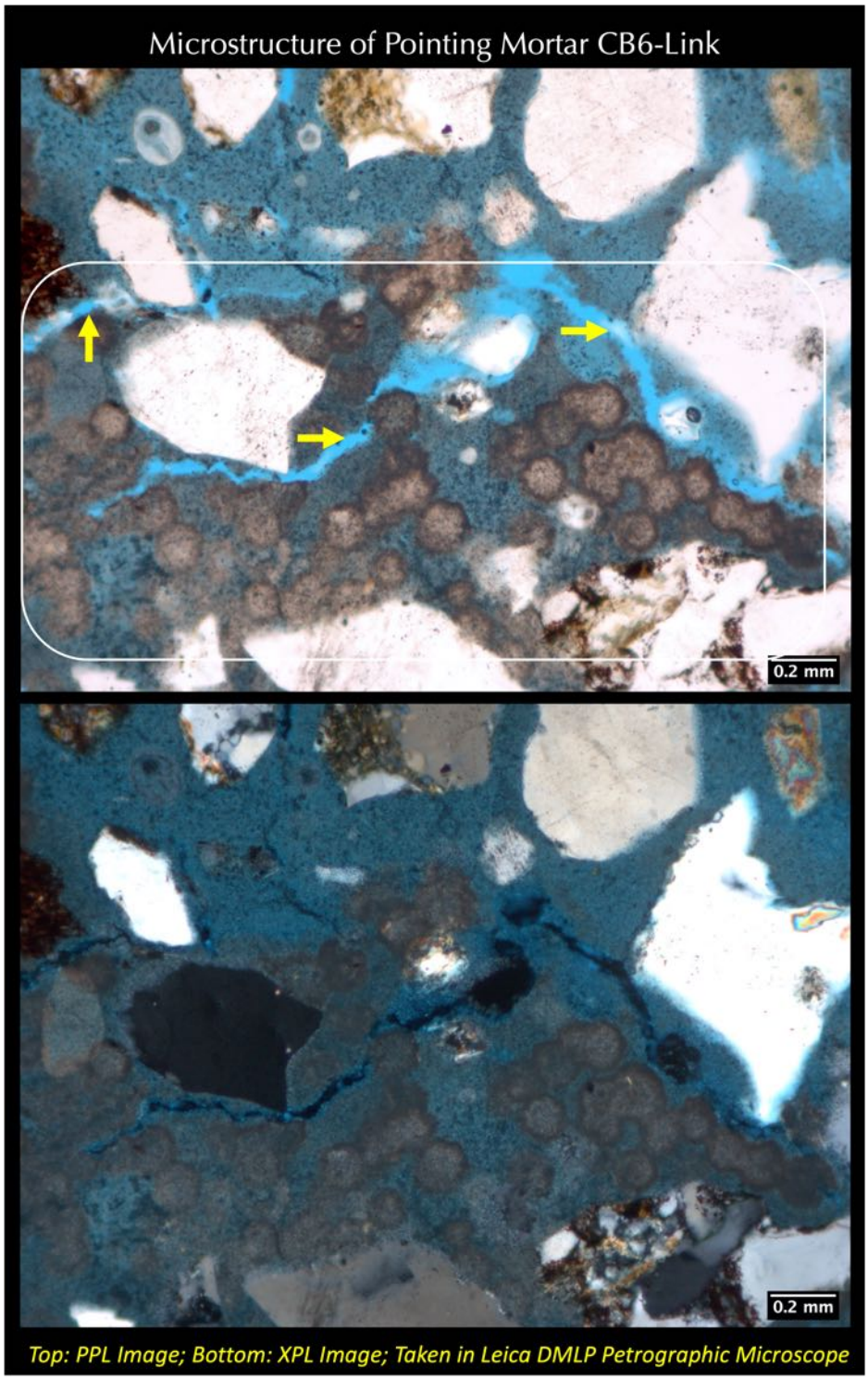

Figure 114: Micrographs of thin section of pointing mortar CB6-Link showing fine (< 1 mm size), angular, well-sorted siliceous sand consisting of major amount of quartz and subordinate amounts of quartzite, shale, and siltstone; and interstitial severely carbonated paste having many fine, discontinuous carbonation shrinkage microcracks (some are marked with yellow arrows). Notice very different i.e., finer grain-size of sand as well as of dense, carbonated interstitial paste compared to coarse sand and leached paste, respectively seen in the three setting mortars. Boxed area shows some small lime globules, which are determined in SEM-EDS studies to be essentially similar in composition to the rest of the paste except in having a slightly higher silica (hydraulicity) than the rest.

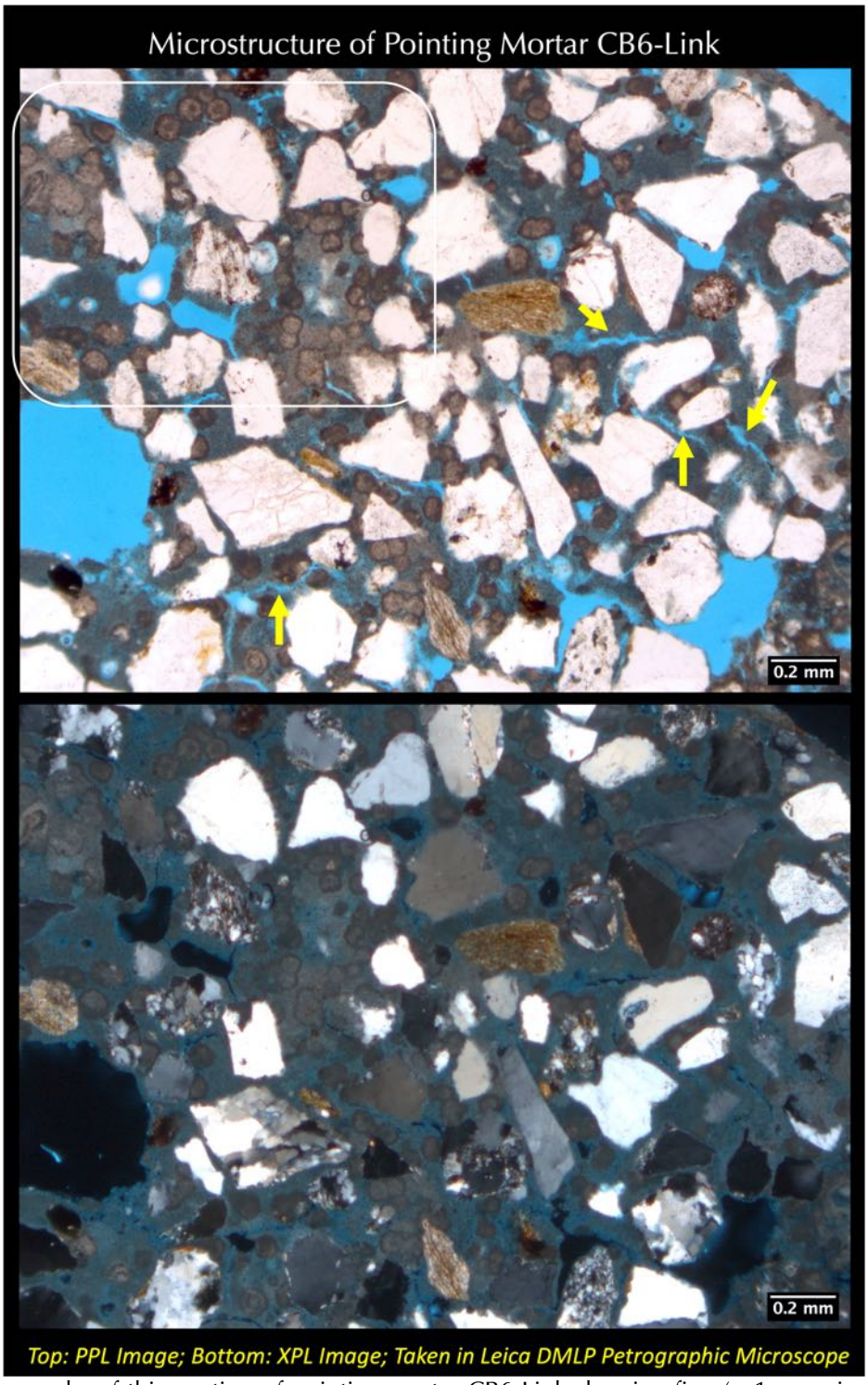

Figure 115: Micrographs of thin section of pointing mortar CB6-Link showing fine (< 1 mm size), angular, well-sorted siliceous sand consisting of major amount of quartz and subordinate amounts of quartzite, shale, and siltstone; and interstitial severely carbonated paste having many fine, discontinuous carbonation shrinkage microcracks (some are marked with yellow arrows). Notice very different i.e., finer grain-size of sand as well as of dense, carbonated interstitial paste compared to coarse sand and leached paste, respectively seen in the three setting mortars. Boxed area shows some small lime globules, which are determined in SEM-EDS studies to be essentially similar in composition to the rest of the paste except in having a slightly higher silica (hydraulicity) than the rest.

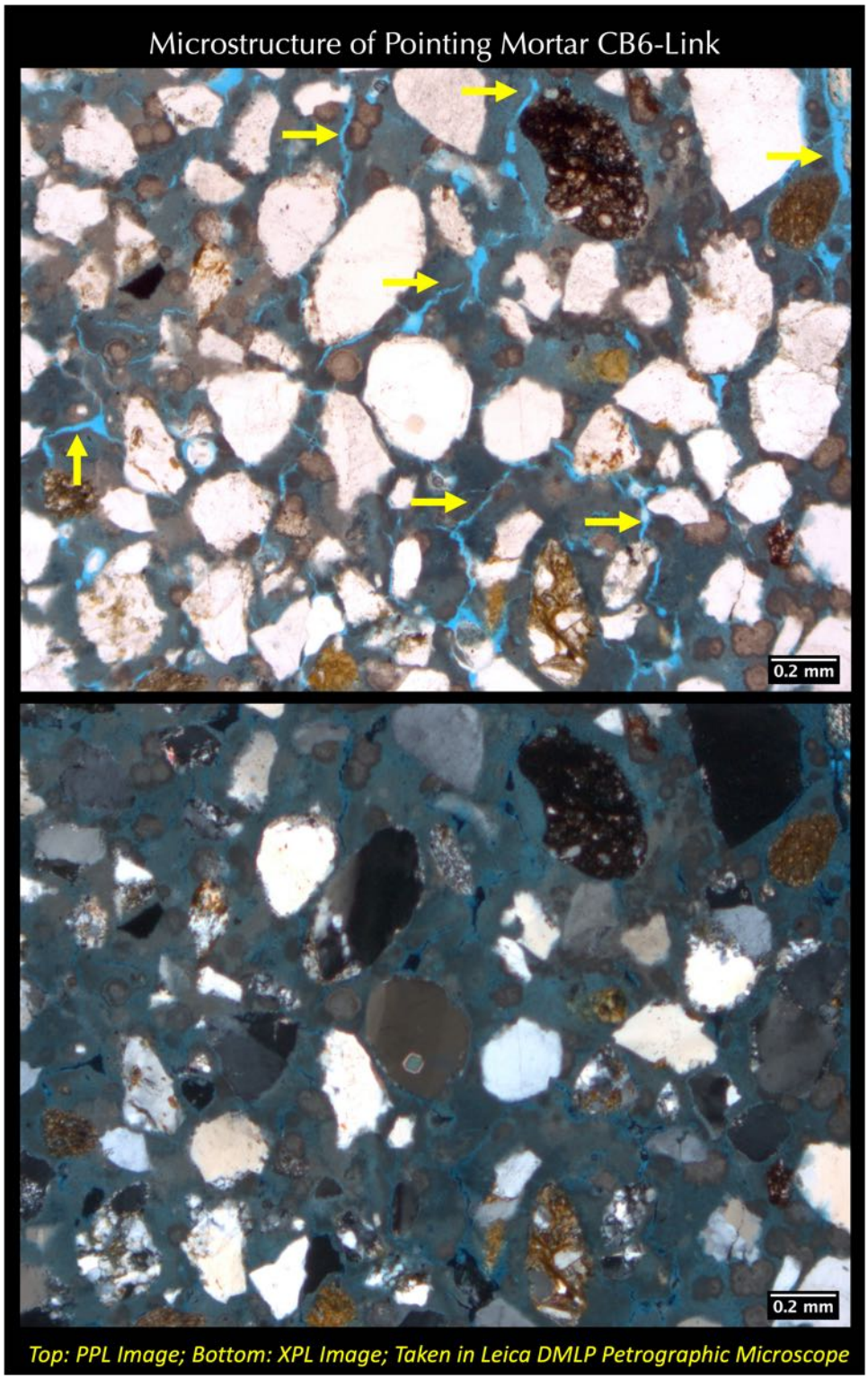

Figure 116: Micrographs of thin section of pointing mortar CB6-Link showing fine (< 1 mm size), angular, well-sorted siliceous sand consisting of major amount of quartz and subordinate amounts of quartzite, shale, and siltstone; and interstitial severely carbonated paste having many fine, discontinuous carbonation shrinkage microcracks (some are marked with yellow arrows). Notice very different i.e., finer grain-size of sand as well as of dense, carbonated interstitial paste compared to coarse sand and leached paste, respectively seen in the three setting mortars.

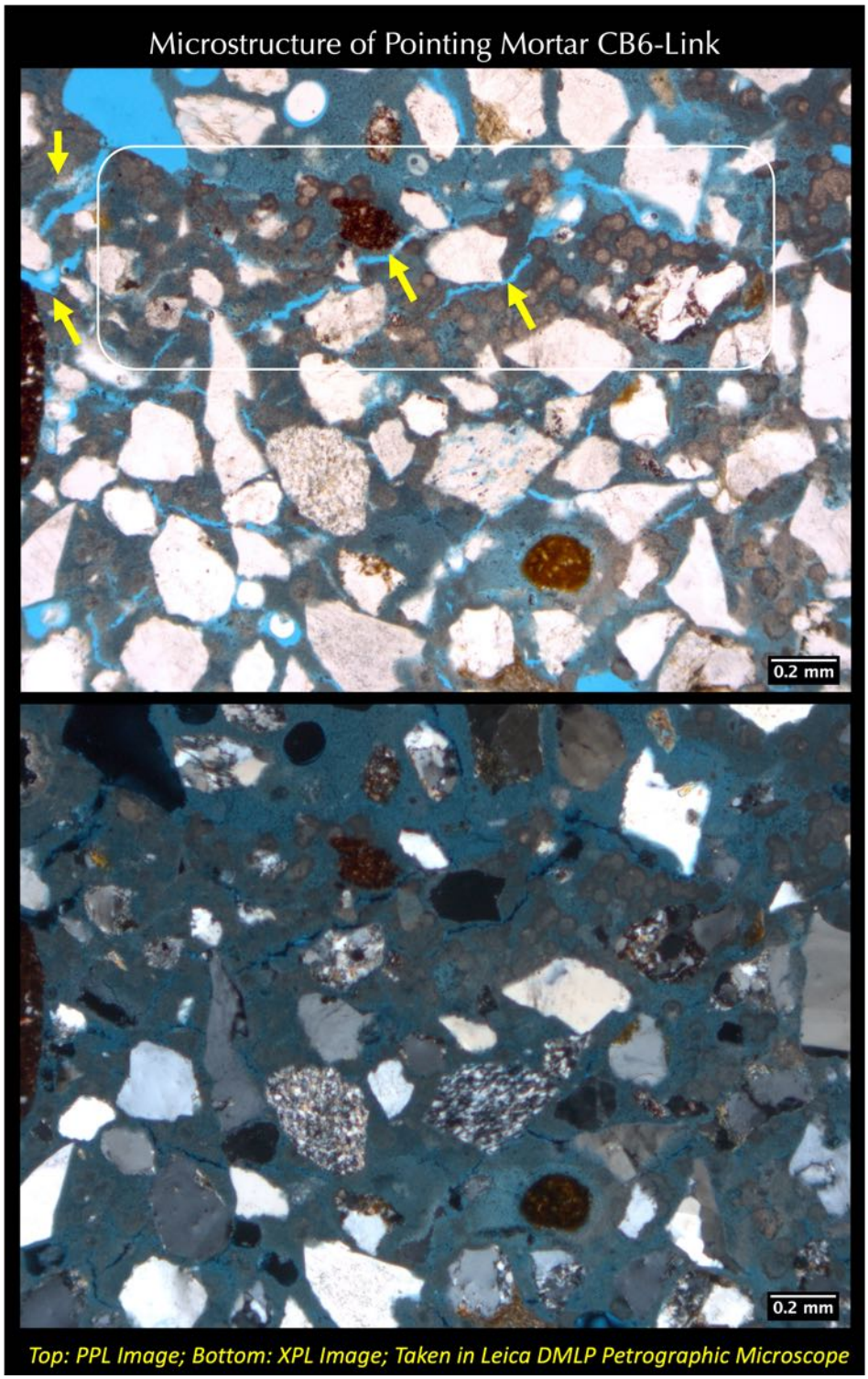

Figure 117: Micrographs of thin section of pointing mortar CB6-Link showing fine (< 1 mm size), angular, well-sorted siliceous sand consisting of major amount of quartz and subordinate amounts of quartzite, shale, and siltstone; and interstitial severely carbonated paste having many fine, discontinuous carbonation shrinkage microcracks (some are marked with yellow arrows). Notice very different i.e., finer grain-size of sand as well as of dense, carbonated interstitial paste compared to coarse sand and leached paste, respectively seen in the three setting mortars. Boxed area shows some small lime globules, which are determined in SEM-EDS studies to be essentially similar in composition to the rest of the paste except in having a slightly higher silica (hydraulicity) than the rest.

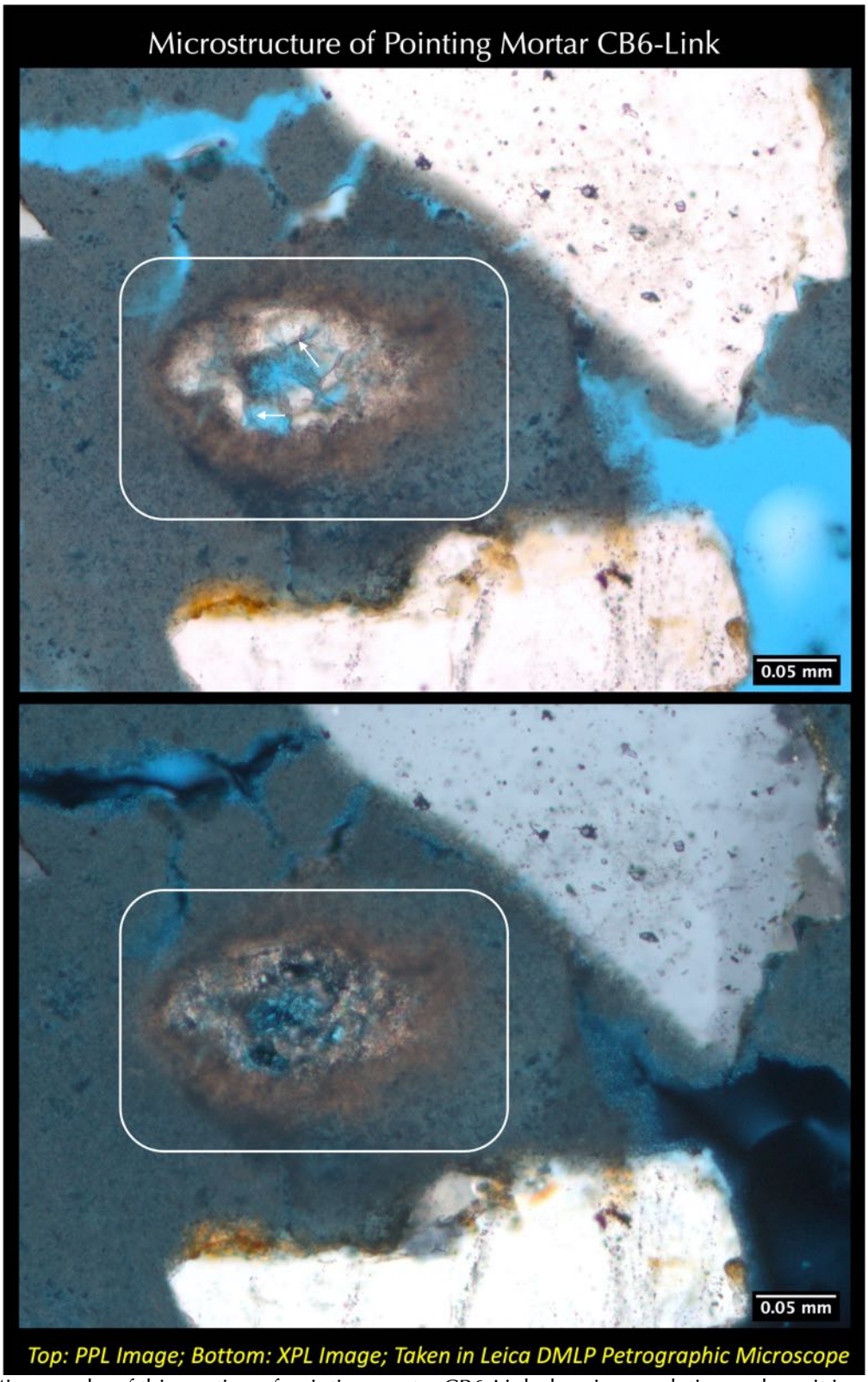

Figure 118: Micrographs of thin section of pointing mortar CB6-Link showing a gelatinous deposit in a void (boxed) within severely carbonated paste. Notice the absence of any residual calcined clay particles (brick dust) in pointing mortar.

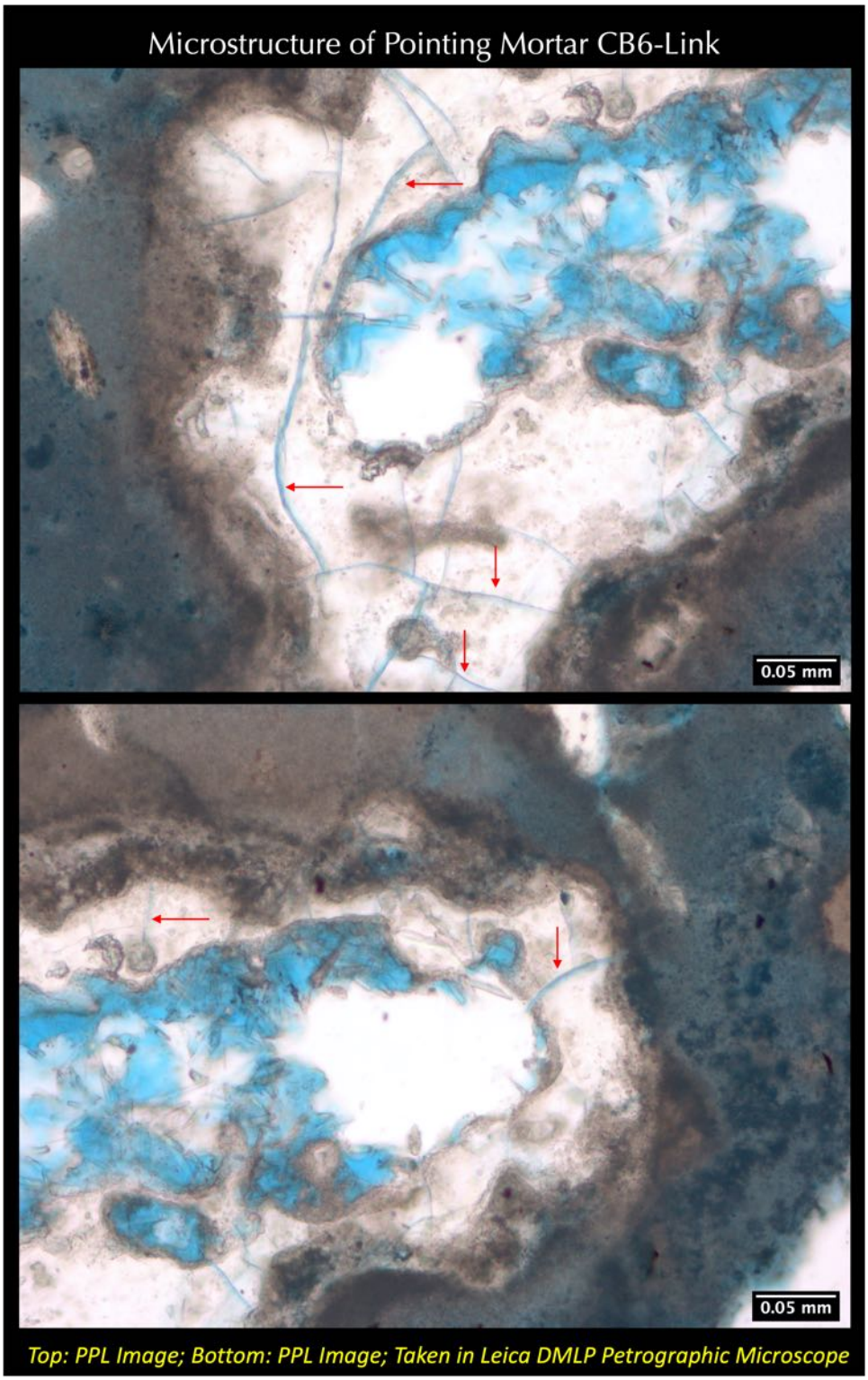

Figure 119: Micrographs of thin section of pointing mortar CB6-Link showing a gelatinous deposit in a void within severely carbonated paste.

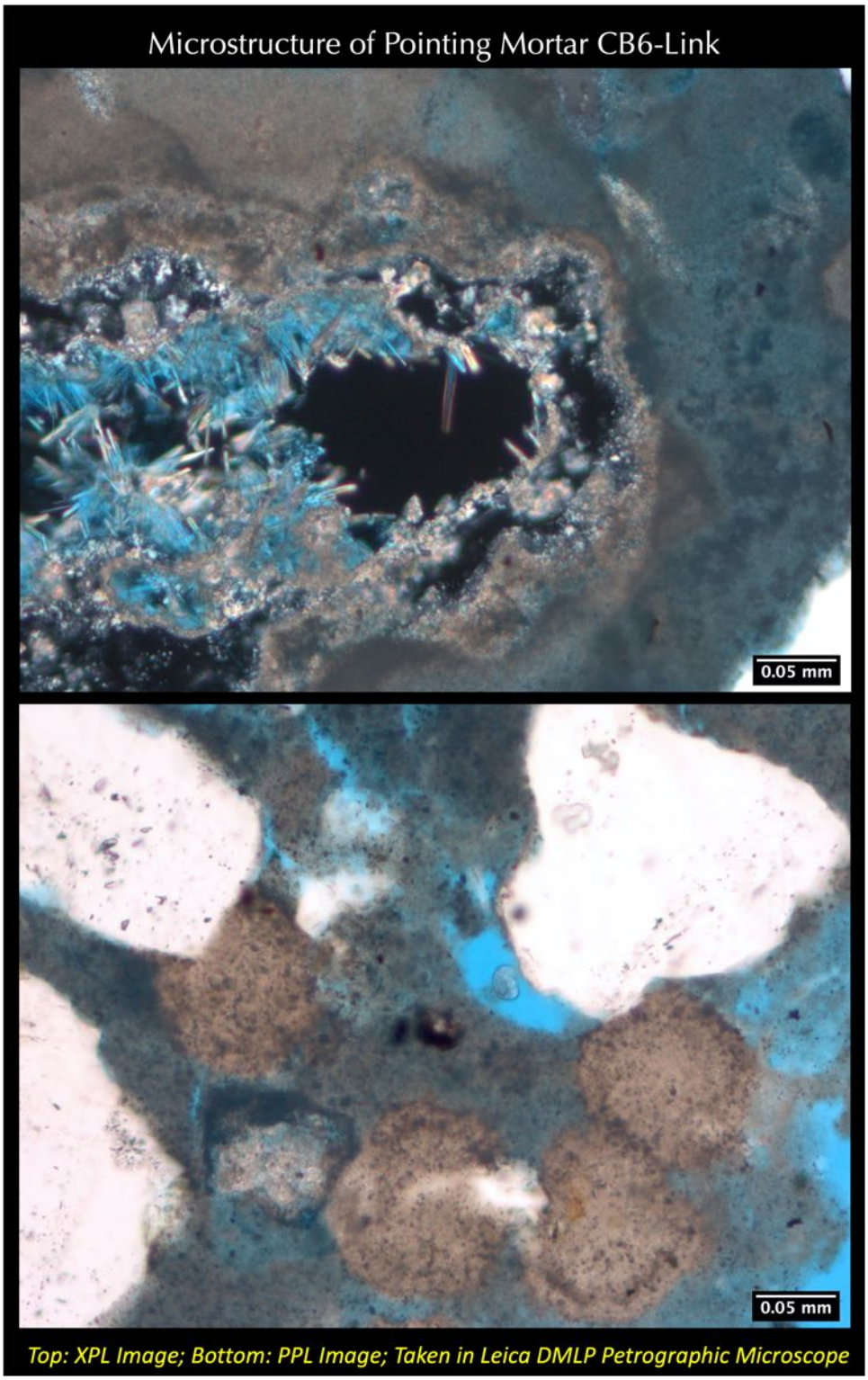

Figure 120: Micrographs of thin section of pointing mortar CB6-Link showing fine, lath-shaped, short prismatic to acicular secondary carbonate deposits in a void within severely carbonated paste in the top photo, which share optical characteristics of a double sodium carbonate-bicarbonate salt called trona. Four lime globules are seen in the bottom photo.

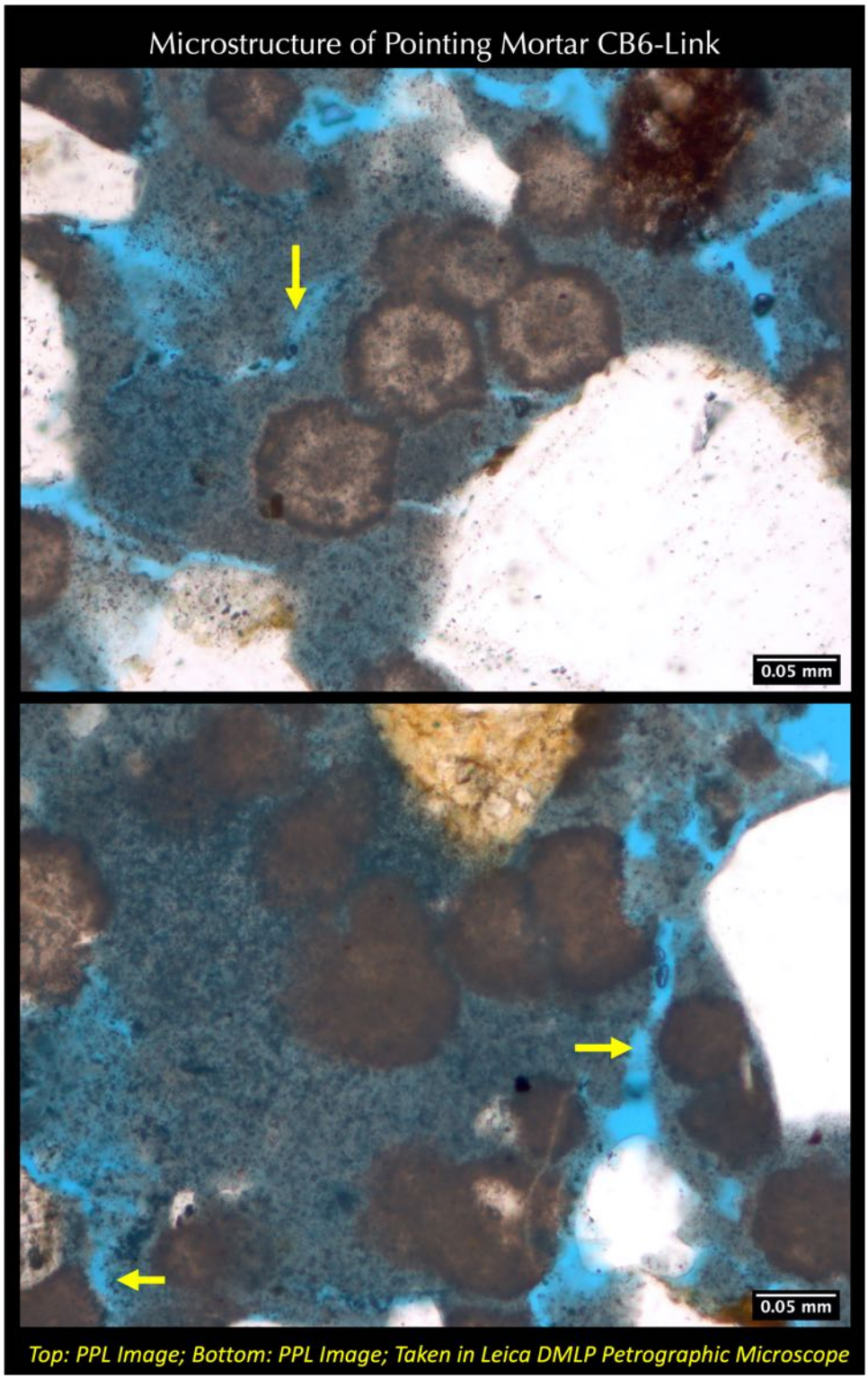

Figure 121: Micrographs of thin section of pointing mortar CB6-Link showing: (a) fine discontinuous, carbonation shrinkage microcracks (yellow arrows), and (b) isolated lime globules in a porous, severely carbonated paste.

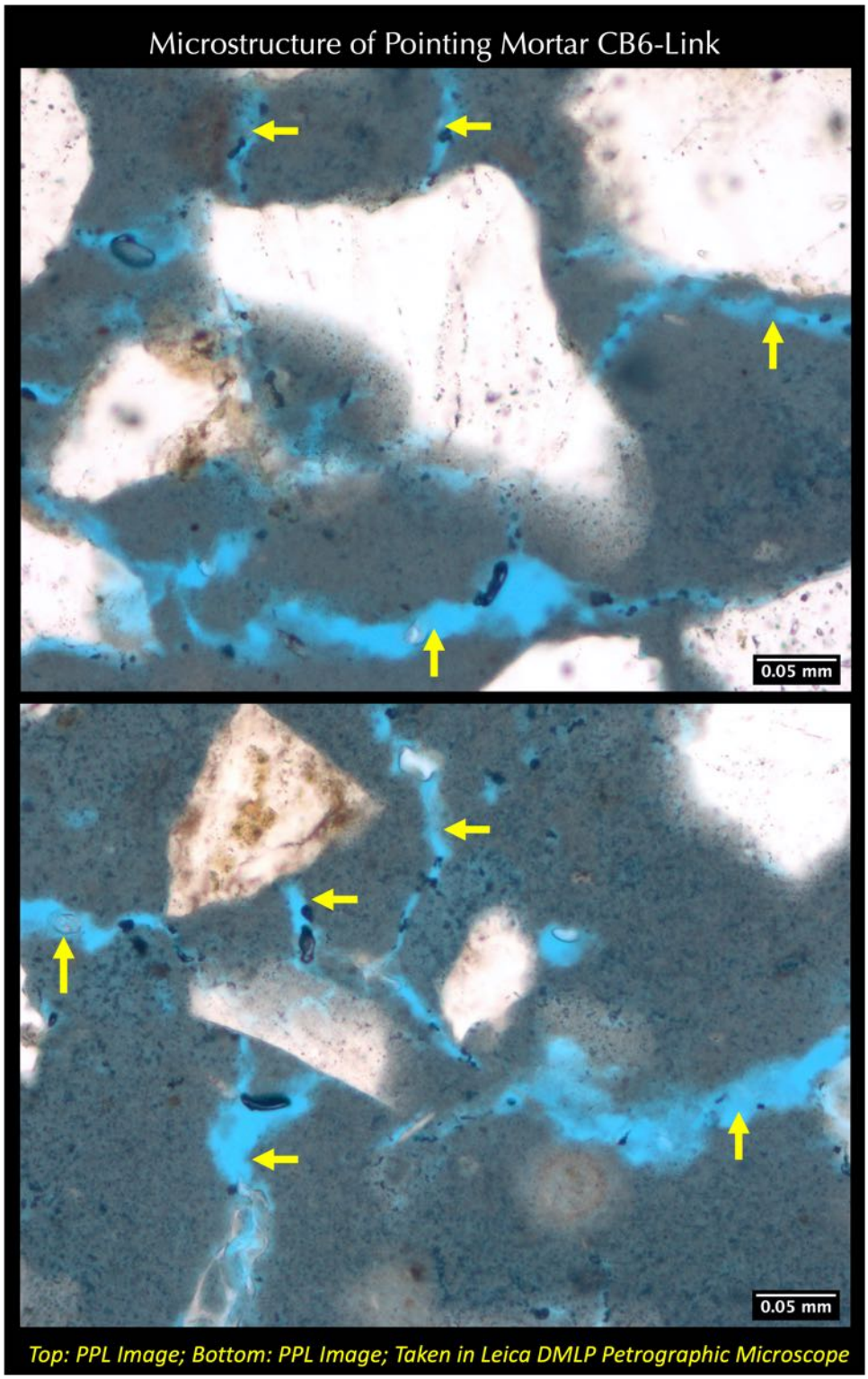

Figure 122: Micrographs of thin section of pointing mortar CB6-Link showing fine discontinuous, carbonation shrinkage microcracks (yellow arrows) in a porous, severely carbonated paste.

Information Obtained From Optical Microscopy

Sand

Figures 47 through 50 show lapped cross sections of clear epoxy-encapsulated pieces of setting and pointing mortars where all three setting mortars show difference from the pointing mortar in having: (a) two grain size fractions of sand, as mentioned before, e.g., a coarser fraction (maximum 4 mm size) of subangular to rounded grains, similar to river sand, and (b) a finer fraction (< 1 mm) crushed sand in all three setting mortars, as opposed to only one size class, which is noticeably finer than the coarser size fraction in setting mortars, and more similar to the finer size fraction of setting mortar and characteristically angular for use of a crushed sand.

Figures 51 through 54 show micrographs of clear epoxy-encapsulated lapped cross sections where grain size distribution of sand in setting and pointing mortars described above are more distinct.

Figures 55 through 66 show blue dye-mixed epoxy and clear epoxy impregnated thin sections of mortars in plane and cross polarized light modes (PPL and XPL, respectively) after scanning the thin sections on a flatbed scanner with one or two perpendicular polarizing filters, respectively. Images in PPL mode show grain size and distribution of sands, whereas the ones taken in XPL modes show the compositions of sands, which are dominantly siliceous in both setting and pointing mortars consisting of major amounts of quartz, subordinate amounts of quartzite, feldspar, and minor amounts of chert, quartz siltstone, sandstone, and a separate subordinate component of argillaceous and ferruginous grains containing non-ferruginous and reddish-brown ferruginous components of shale, siltstone.

Figures 67 through 78 show micrographs of thin sections of mortars taken with a transmitted-light stereozoom microscope at PPL and XPL modes to differentiate the grain size distribution of sands in PPL modes from compositional analyses in XPL modes. Image analyses were done on mosaics of multiple PPL images of sand to determine the volumetric proportions of sand in each mortar. Results show 28.1%, 19.2%, 22.9% and 34.4% sand by volume in samples SET-3, SWM-2, SSB-3, and CB6-Link, respectively, which, assuming a sand specific gravity of 2.65 respectively correspond to 74.4%, 50.9%, 60.7%, and 91.1% sand by mass. Pointing mortar showed noticeably higher proportion of sand (along with its finer grain size and angularity) compared to sand volumes in three setting mortars.

Figures 79 to 110, and 111 to 122 show micrographs of thin sections of mortars taken with a petrographic microscope at PPL and XPL modes for setting and pointing mortars, respectively. All these illustrated atlas of thin section micrographs repeatedly showed the dominantly siliceous components of sand, both in the coarser size fractions in setting mortars as well as in the finer size fractions in both setting and pointing mortars.

Reddish-brown Coats on Sands in Setting Mortars

An interesting feature observed in coarse and fine sand fractions in all three setting mortars in Figures 79 to 110 but not in angular fine sands in the pointing mortar in Figures 111 to 122 is the presence of thin discontinuous reddish-brown coatings on the sand grains, formed irrespective of angular, subangular to rounded sand grains in the setting

mortars. These reddish-brown coatings could represent: (a) clay coats or weathering rims formed in the sand stockpile from associated reddish-brown ferruginous shale-siltstone particles prior to the incorporation in the mortar, or, more plausibly, (b) from their formation in the mortar during service, during 200 years of water migration, leaching and dissolution where iron oxide components were derived not just from the ferruginous component of sand but more commonly from the residual calcined clay (brick dust) particles intentionally added as a pozzolan to the dominantly lime binder component. These calcined clay (brick dust) pozzolans have reacted with lime and contributed the iron oxide components to the matrix eventually imparting the reddish-brown color tone of paste and mortar. Leaching and dissolution of iron oxide from lime-pozzolana reaction products in paste (and some from ferruginous matrix in sand) have contributed to the formation of reddish-brown coats on the sand grains as reaction rims (subsequent SEM-EDS studies showed enriched Si-Al-Mg in these coats from pozzolanic reactions followed by leaching of lime in these coats). Formation of these coats specifically on angular fractions of sand grains questions the former possibility of their prior presence as weathering rims (clay coatings) and rather indicate their in-situ formation from pozzolanic reactions of calcined clay (brick dust) with lime.

Binder

Figures 47 through 50 show lapped cross sections of clear epoxy-encapsulated pieces of setting and pointing mortars where all three setting mortars showed difference in color tones from the pointing mortar in having a reddish-brown interstitial paste as opposed to medium gray paste in the pointing mortar. Figures 51 through 54 showed micrographs of clear epoxy-encapsulated lapped cross sections where the basic difference in color tones of paste between setting and pointing mortars are more distinct. Such a basic difference in the color tones of paste have imparted the very different overall colors between the setting and pointing mortars. This color difference is determined to be essentially due to the difference in binder components added to the setting and pointing mortars. Subsequent SEM-EDS studies have determined the paste in the setting mortar to be a two-component mixture of a calcined clay and a dolomitic lime, where the former component has imparted the reddish-brown color tone in setting mortar. Iron oxide impurities in the original clay component of calcined clay binder has imparted the reddish-brown color in all three setting mortars. Paste color is judged not necessarily from reddish-brown ferruginous grains in sand as such grains are present in both setting and pointing mortars. However, leaching actions on setting mortars may have dissolved some iron oxide components from reddish-brown sand grains and added to the overall color tone of paste and mortar.

Paste in setting mortars showed variably dense to porous, severely carbonated as well as leached appearances. There is no evidence of any residual hydraulic lime phase found in the paste indicating use of a non-hydraulic to feebly hydraulic dolomitic lime binder, which was produced from calcination of a relatively pure dolomitic limestone. This feebly hydraulic dolomitic lime binder component in setting mortar is found to be similar to the feebly hydraulic dolomitic lime binder used entirely in the pointing mortar.

Evidence of extensive lime leaching of paste in all three setting mortars are seen where leached areas showed optically isotropic natures due to the presence of essentially an amorphous or gelatinous precipitate after leaching

of lime, which from subsequent SEM-EDS studies is determined to be noticeably enriched in Mg, Si, and Al as opposed to Ca-rich carbonated areas.

Paste microstructures are best evident in Figures 79 to 110, and 111 to 122 for setting and pointing mortars, respectively depicting detailed micrographs of thin sections of mortars taken with a petrographic microscope at PPL and XPL modes. The most startling microstructural features seen in all three setting mortars but not in the pointing mortar are scattered, very fine reddish-brown residual calcined clay (brick dust) particles, which are separate from reddish-brown ferruginous matrix in some ferruginous shale and siltstone grains in sand but are indicative of intentional addition of a calcined clay component as brick dust at a subordinate proportion to the dominant dolomitic lime binder. The purpose of addition of these fine-grained, dominantly amorphous calcined clay particles as a binder is to encourage pozzolanic reactions of amorphous aluminosilicate calcined clay particles with lime to form calcium-silicate hydrate and calcium-aluminum-silicate hydrate components, which would densify the paste compared to a carbonated lime paste. Use of such calcined clay pozzolan was very common in many early 19th century masonry structures across Europe and America.

Close examinations of many residual calcined clay particles showed dominantly amorphous nature where original clay component used during calcination process was very rich in the plastic component (optically isotropic, e.g., amorphous clay matrix) with very little non-plastic component (which are optically birefringent, e.g., fine-grained quartz). A few calcined clay particles showed formation of cristobalite indicating a calcination temperature as high as 1470ºC.

Many residual calcined clay particles showed a dense rim of paste around, which are stained reddish-brown from leaching of iron oxide during lime-calcined clay pozzolanic reaction, and subsequently carbonated. Densification of paste immediately around such calcined clay particles from lime-pozzolana reactions have prevented the densified paste rims from leaching, even when the dominant paste matrix away from those particles showed extensive leaching. This indicates the importance of using such calcined clay pozzolans in historic lime mortars to overall densify the paste microstructure, and mortar to make them more durable than the straight lime mortars.

Based on the left-over remains of scattered calcined clay pozzolans in all three setting mortars, samples SET-3 and SSB-3 from east and south walls, respectively, showed a higher abundance of calcined clay component in the original binder compared to the amount in SWM-2 from the west wall mortar. Pointing mortar showed no evidence of intentional addition of calcined clay in the binder, which is the reason for its medium gray color tone as opposed to reddish-brown color of setting mortars.

Fine-grained, porous, variably and severely carbonated paste, patches of optically isotropic leached paste areas, occasional lime lumps, and most importantly discontinuous carbonation shrinkage microcracks – the telltale microstructural features of an altered historic lime mortar are all present in the setting bed mortars (see Figures 79 through 110). Rings of carbonation products around leached areas of paste are seen, indicating carbonation of re-precipitated lime after dissolution from the leached areas. Bright golden yellow interference colors of such re-precipitated secondary calcium carbonate rings around dark optically isotropic leached paste areas and sand grains

appeared as 'rings of fire' while observing the features in a petrographic microscope at XPL mode (e.g., see Figures 85 through 95, 97, 109, etc.).

By contrast, paste in the pointing mortar showed overall homogeneous appearance, which is very similar to a carbonated lime paste in a historic lime mortar. There is no evidence of any residual hydraulic phase (e.g., residual belite and interstitial dark brown ferrite skeletons) are found in the paste, which are common in many historic hydraulic lime mortars. Absence of such residual hydraulic phases indicate use of a rather non-hydraulic to feebly hydraulic dolomitic lime binder where feebly hydraulic nature and dolomitic nature of the lime are both determined from subsequent SEM-EDS studies of paste where presence of some silica and noticeably magnesia contents confirmed their potential light hydraulicity and dolomitic nature of lime, respectively. Subsequent thermal analysis has confirmed the use of dolomitic lime from brucite, and its carbonation products which are common hydration and subsequent carbonation products of a dolomitic lime binder.

An interesting microstructure found in the carbonated lime paste in pointing mortar are denser beige-toned (in PPL mode) globules of 0.05 to 0.1 mm size (Figures 112-115, 120, and 121), which from SEM-EDS studies are found to have an essentially similar composition as the rest of the paste except in having a slightly higher silica and alumina (hydraulicity?) contents than the rest of the overwhelming dolomitic lime paste. Perhaps the original silica-alumina-based impurities in otherwise relatively pure dolomitic limestone feed has formed such isolated nucleation sites of a denser paste in the globules than elsewhere even though no trace of any residual hydraulic phase was found within the globules. Figures 118 and 119 show two such globules containing an optically isotropic mass inside (similar to alkali-silica gel with characteristic fine shrinkage microcracks), which may represent the fate of an original semi-crystalline to amorphous calcium-silicate-aluminate-hydrate deposit formed within the globules.

Air

Both setting and pointing mortars are non-air-entrained, which are best depicted in micrographs of lapped sections in Figures 51 through 54 as well as in micrographs of thin sections in Figures 67 through 78 which is not unusual for its reported early 19th century derivation.

Secondary Deposits

Besides the ubiquitous calcium carbonate 'secondary' deposits in the leached and carbonated areas of paste in setting mortars which were re-precipitated after dissolution of original calcium carbonate products of carbonated lime binder, some other carbonated products are detected at minor to trace amounts in some void spaces e.g., short prismatic to lath-shaped deposits of trona (Figure 113), and fibrous highly birefringent deposits of thaumasite, and gypsum. Subsequent SEM-EDS studies, thermal analysis, and XRD studies, however, could not detect their identity for overall low abundance.

Scanning Electron Microscopy and X-ray Microanalyses

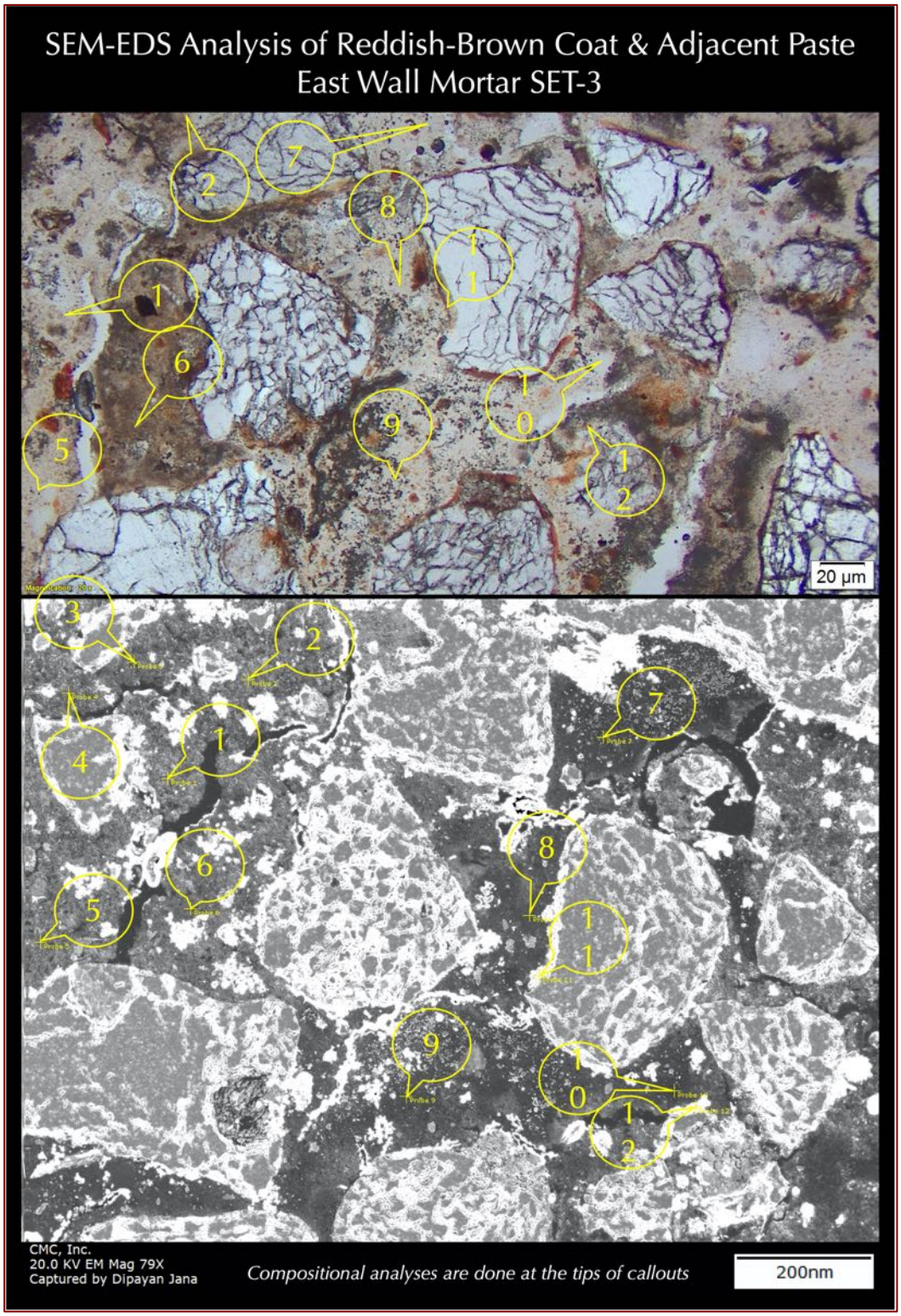

Figure 123: Optical micrograph (top) and corresponding secondary electron micrograph (bottom) of setting mortar SET-3 showing points at the tips of callouts across various areas in paste and reddish-brown coats, which are analyzed in SEM-EDS for major element oxide compositions.

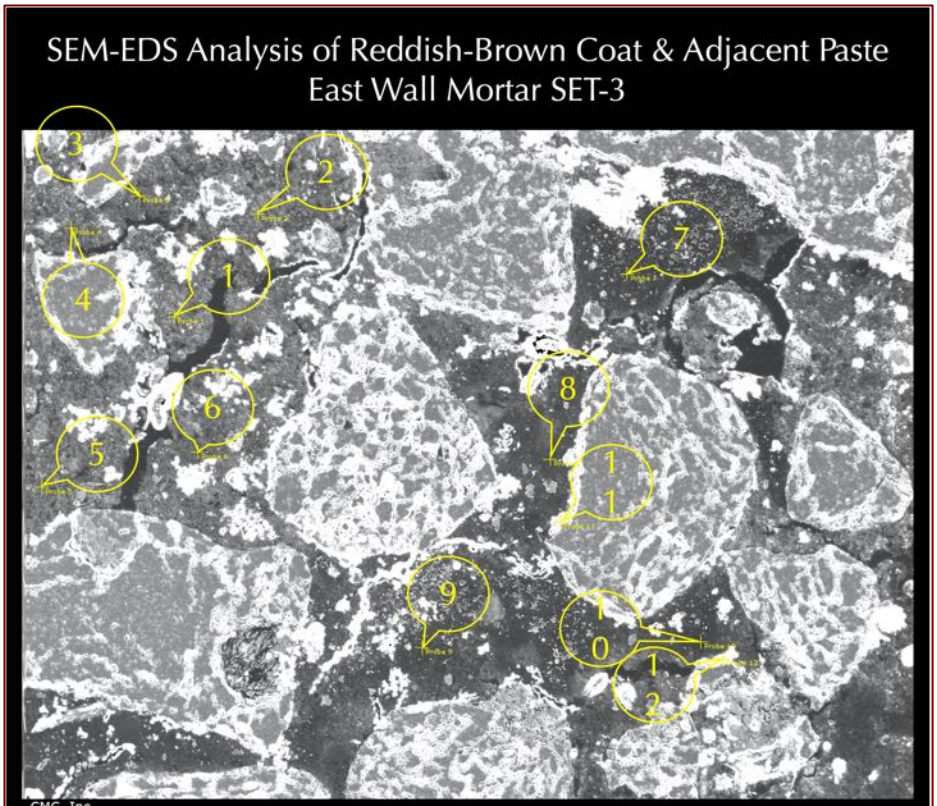

Probe	CaO	SiO2	Al2O3	K2O	MgO	FeO	Na2O	MnO2	TiO2	SO2	Total	Paste-CI	Phase
1	2.31	**41.20**	**24.77**	0.14	**29.61**	1.17	0.04	0.41	0.35	0.00	100.0	**3.28**	LP
2	0.14	**36.18**	**26.30**	0.01	**35.56**	1.26	0.05	0.30	0.19	0.00	100.0	**2.63**	
3	0.59	**40.47**	**25.51**	0.28	**31.21**	1.05	0.04	0.50	0.34	0.00	100.0	**3.21**	
4	0.24	**41.63**	**25.90**	0.35	**29.66**	1.57	0.04	0.28	0.32	0.00	100.0	**3.50**	
5	0.29	**40.39**	**28.02**	0.42	**28.25**	1.55	0.18	0.66	0.24	0.00	100.0	**3.64**	
6	0.31	**37.91**	**26.65**	0.28	**33.10**	1.09	0.24	0.17	0.24	0.00	100.0	**2.92**	
7	0.37	**57.38**	**14.18**	0.15	**26.44**	0.70	0.46	0.31	0.00	0.00	100.0	**4.73**	
8	0.12	**44.76**	**20.48**	0.33	**33.22**	0.75	0.07	0.18	0.10	0.00	100.0	**3.18**	
9	0.73	**45.65**	**21.20**	0.26	**30.41**	1.16	0.09	0.50	0.00	0.00	100.0	**3.51**	
10	0.39	**47.21**	**17.41**	0.00	**34.31**	0.53	0.14	0.00	0.00	0.00	100.0	**3.13**	
11	10.22	84.73	2.60	0.00	1.27	0.70	0.06	0.18	0.06	0.18	100.0	20.05	Quartz+ Coat
12	**33.54**	**19.09**	**12.58**	0.08	33.06	**0.59**	0.24	**0.71**	0.11	0.00	100.0	0.85	Coat

LP: Leached (Mg-Si-Al) Paste

Figure 124: Secondary electron image (top), and X-ray microanalyses at the tips of callouts in Probes 1 through 12 of setting mortar SET-3 detecting compositional variations of leached paste in the mortar along with a quartz sand and a reddish-brown coat. Paste compositions are presented (bottom) as oxide variations of all detected EDS peaks normalized to 100% except carbon (from epoxy) and gold (from coating). Paste cementation indices, CI (after Eckel 1922) measure: (a) relative hydraulicity of paste e.g., non-hydraulic lime pastes have very low CI (< 0.50) compared to cement-based pastes (CI is >1), along with (b) the degree of leaching of lime, where leached paste characteristically show >>1 CI, and non-leached portions of paste show <1 CI from lime and its carbonated products. The cementation indices (CI) of paste are calculated after Eckel (1922) as CI = $[(2.8*SiO_2)+(1.1*Al_2O_3)+(0.7*\ Fe_2O_3)]/[(CaO)+(1.4*MgO)]$.

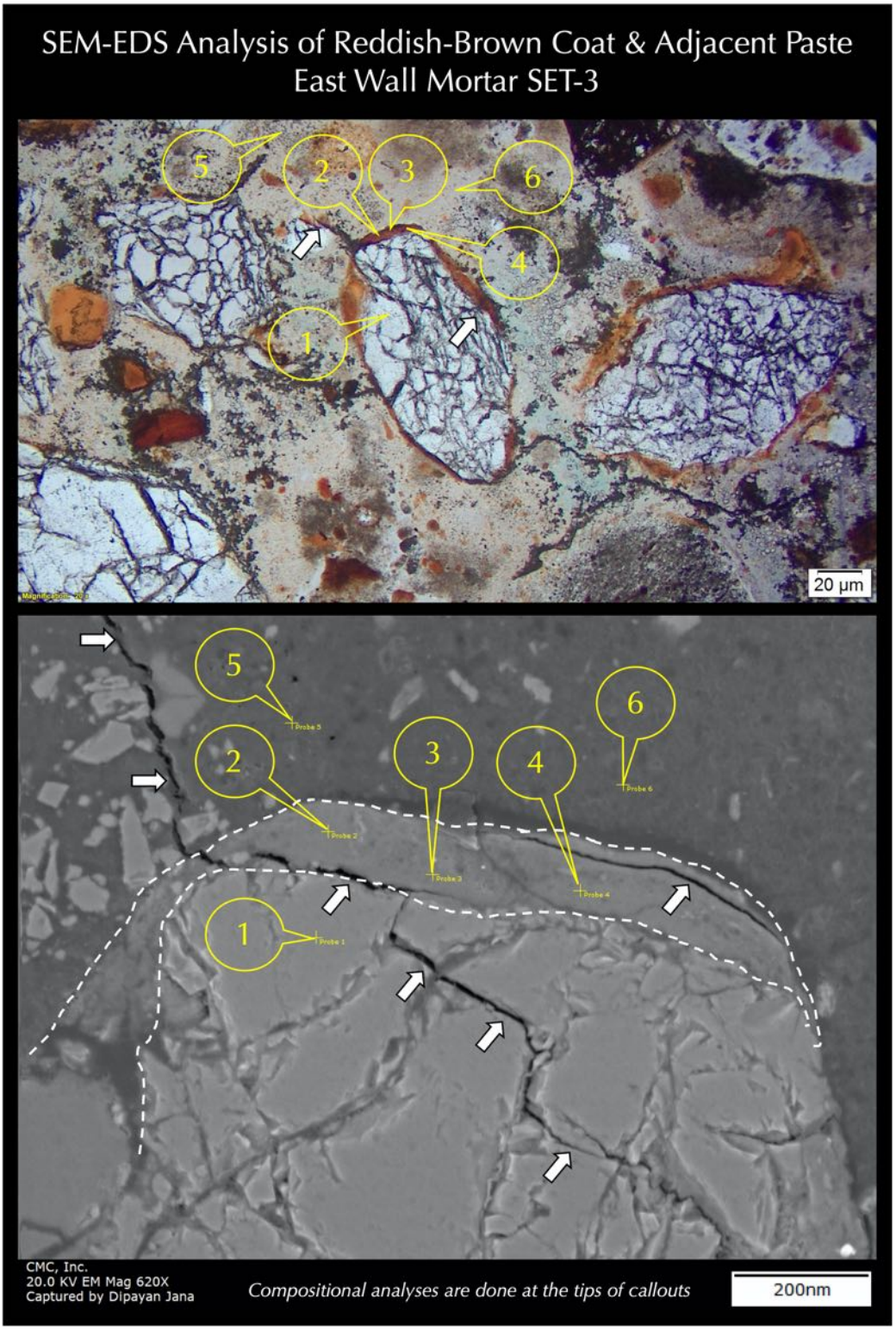

Figure 125: Optical micrograph (top) and corresponding backscatter electron micrograph (bottom) of setting mortar SET-3 showing points at the tips of callouts across various areas in paste, grain, and reddish-brown coats, which are analyzed in SEM-EDS for major element oxide compositions. Positions of tips of callouts in the optical micrograph are only approximate to the actual ones shown in the electron micrograph.

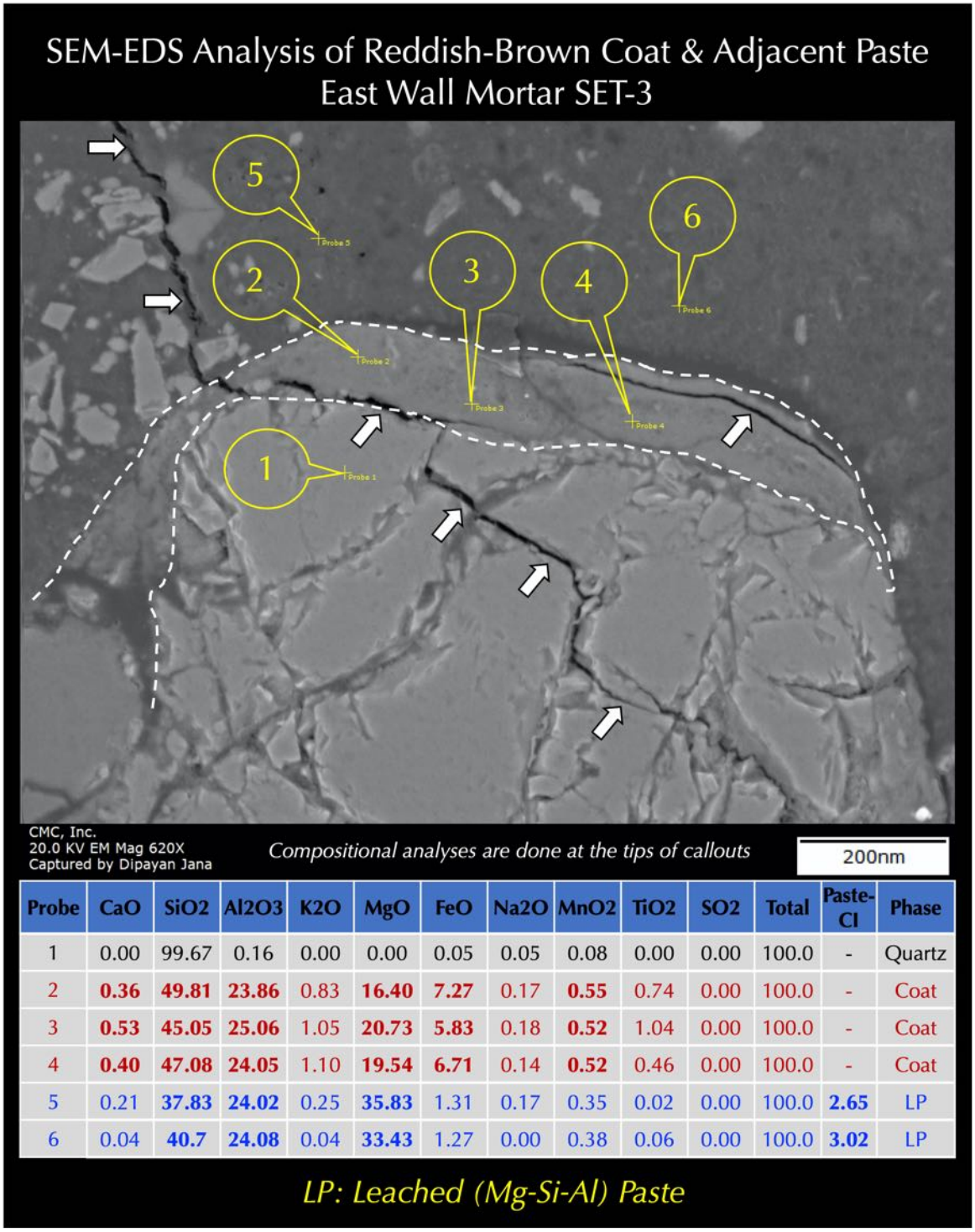

Probe	CaO	SiO2	Al2O3	K2O	MgO	FeO	Na2O	MnO2	TiO2	SO2	Total	Paste-CI	Phase
1	0.00	99.67	0.16	0.00	0.00	0.05	0.05	0.08	0.00	0.00	100.0	-	Quartz
2	**0.36**	**49.81**	**23.86**	0.83	**16.40**	**7.27**	0.17	**0.55**	0.74	0.00	100.0	-	Coat
3	**0.53**	**45.05**	**25.06**	1.05	**20.73**	**5.83**	0.18	**0.52**	1.04	0.00	100.0	-	Coat
4	**0.40**	**47.08**	**24.05**	1.10	**19.54**	**6.71**	0.14	**0.52**	0.46	0.00	100.0	-	Coat
5	0.21	**37.83**	**24.02**	0.25	**35.83**	1.31	0.17	0.35	0.02	0.00	100.0	**2.65**	LP
6	0.04	**40.7**	**24.08**	0.04	**33.43**	1.27	0.00	0.38	0.06	0.00	100.0	**3.02**	LP

LP: Leached (Mg-Si-Al) Paste

Figure 126: Backscatter electron image (top), and X-ray microanalyses at the tips of callouts in Probes 1 through 6 of setting mortar SET-3 detecting compositional variations of reddish-brown coat and adjacent leached paste. Paste composition is presented (bottom) as oxide variations of all detected EDS peaks normalized to 100% except carbon (from epoxy) and gold (from coating). Paste cementation indices, CI (after Eckel 1922) measure: (a) relative hydraulicity of paste e.g., non-hydraulic lime pastes have very low CI (< 0.50) compared to cement-based pastes (CI is >1), along with (b) the degree of leaching of lime, where leached paste characteristically show >>1 CI, and non-leached portions of paste show <1 CI from lime and its carbonated products. The cementation indices (CI) of paste are calculated after Eckel (1922) as CI = $[(2.8*SiO_2)+(1.1*Al_2O_3)+(0.7*\ Fe_2O_3)]/[(CaO)+(1.4*MgO)]$.

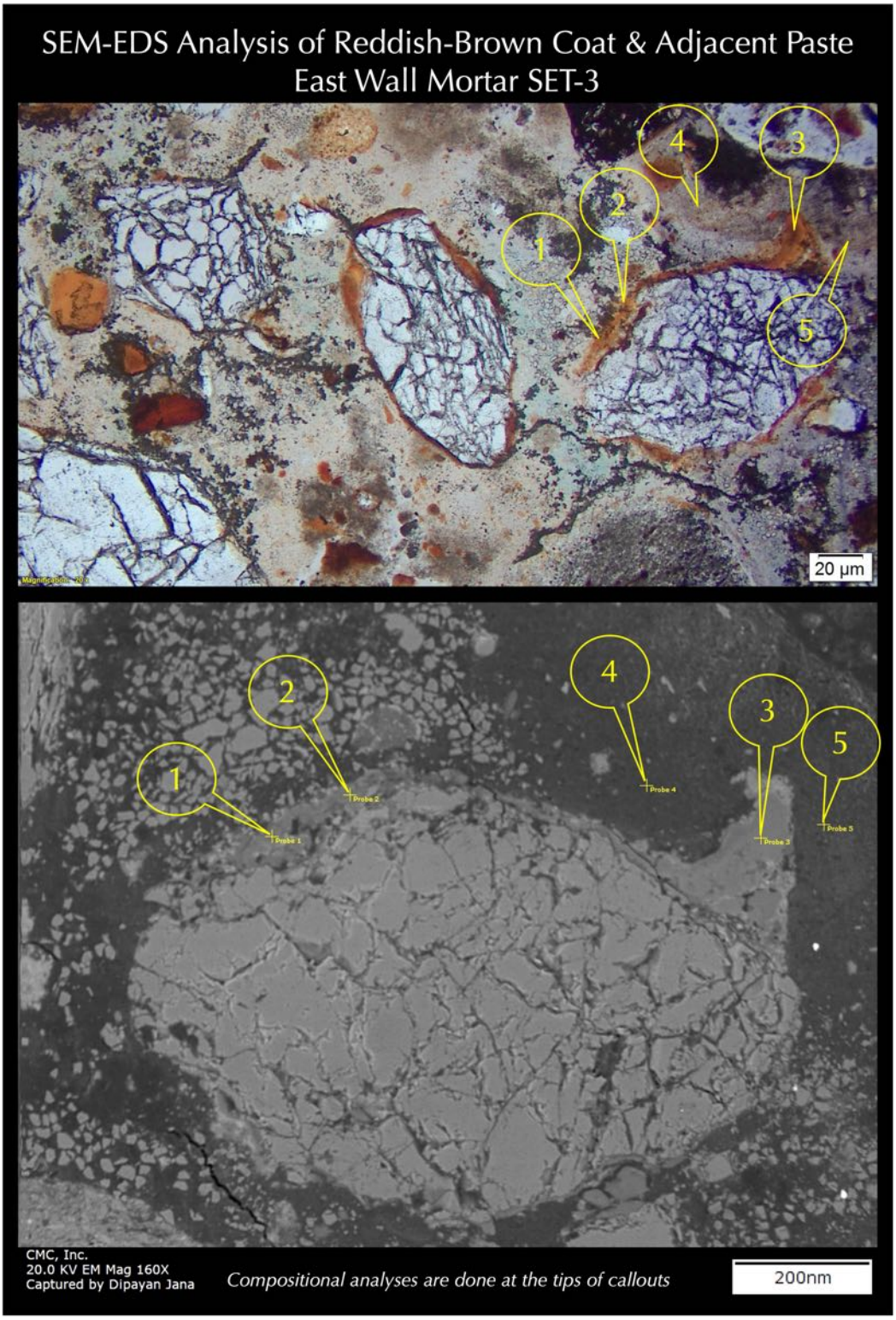

Figure 127: Optical micrograph (top) and corresponding backscatter electron micrograph (bottom) of setting mortar SET-3 showing points at the tips of callouts across various areas in paste, grain, and reddish-brown coats, which are analyzed in SEM-EDS for major element oxide compositions. Positions of tips of callouts in the optical micrograph are only approximate to the actual ones shown in the electron micrograph.

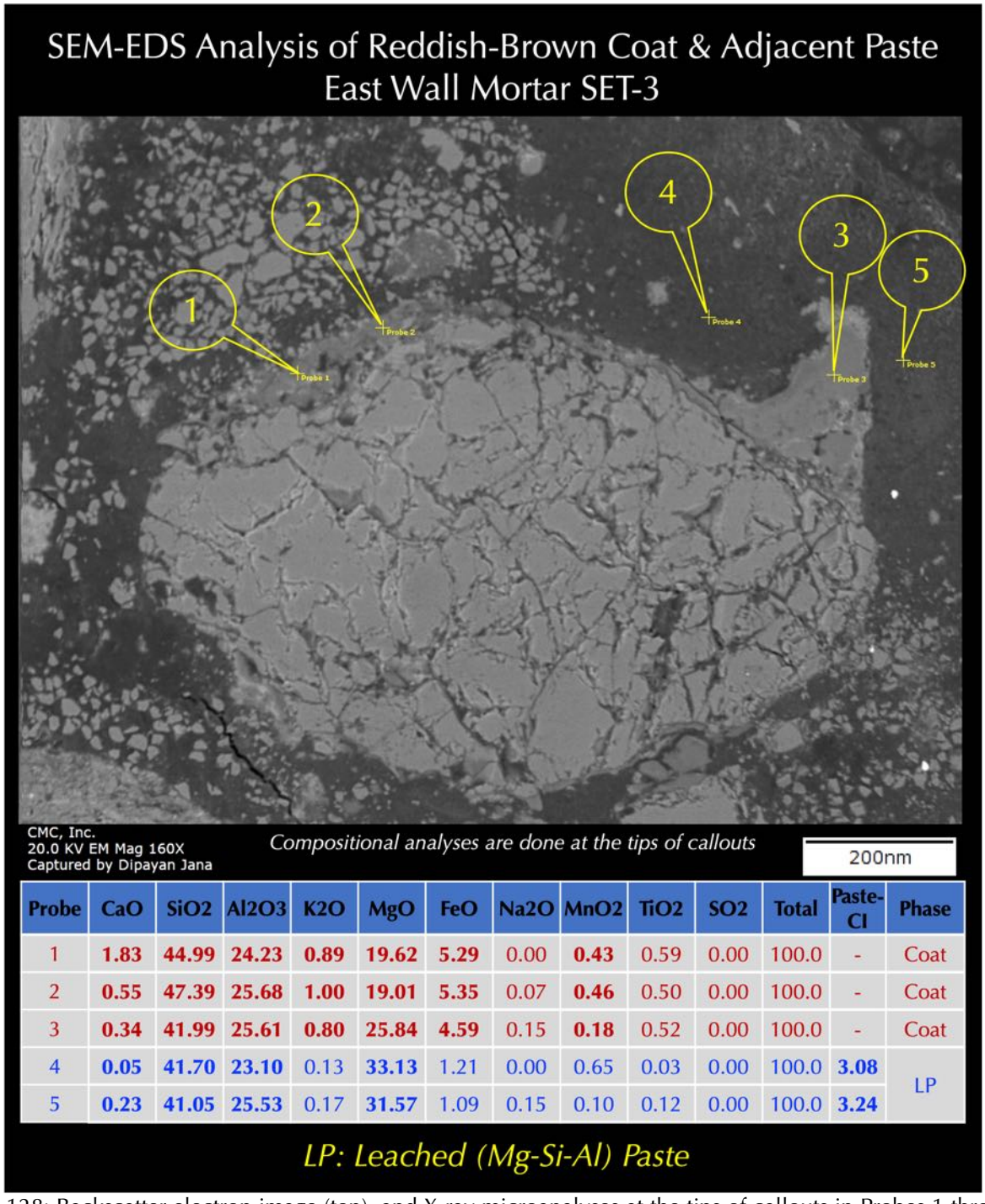

Probe	CaO	SiO2	Al2O3	K2O	MgO	FeO	Na2O	MnO2	TiO2	SO2	Total	Paste-CI	Phase
1	**1.83**	**44.99**	**24.23**	**0.89**	**19.62**	**5.29**	0.00	**0.43**	0.59	0.00	100.0	-	Coat
2	**0.55**	**47.39**	**25.68**	**1.00**	**19.01**	**5.35**	0.07	**0.46**	0.50	0.00	100.0	-	Coat
3	**0.34**	**41.99**	**25.61**	**0.80**	**25.84**	**4.59**	0.15	**0.18**	0.52	0.00	100.0	-	Coat
4	**0.05**	**41.70**	**23.10**	0.13	**33.13**	1.21	0.00	0.65	0.03	0.00	100.0	**3.08**	LP
5	**0.23**	**41.05**	**25.53**	0.17	**31.57**	1.09	0.15	0.10	0.12	0.00	100.0	**3.24**	

LP: Leached (Mg-Si-Al) Paste

Figure 128: Backscatter electron image (top), and X-ray microanalyses at the tips of callouts in Probes 1 through 5 of setting mortar SET-3 detecting compositional variations of reddish-brown coat and adjacent leached paste. Paste composition is presented (bottom) as oxide variations of all detected EDS peaks normalized to 100% except carbon (from epoxy) and gold (from coating). Paste cementation indices, CI (after Eckel 1922) measure: (a) relative hydraulicity of paste e.g., non-hydraulic lime pastes have very low CI (< 0.50) compared to cement-based pastes (CI is >1), along with (b) the degree of leaching of lime, where leached paste characteristically show >>1 CI, and non-leached portions of paste show <1 CI from lime and its carbonated products. The cementation indices (CI) of paste are calculated after Eckel (1922) as CI = $[(2.8*SiO_2)+(1.1*Al_2O_3)+(0.7*\ Fe_2O_3)]/[(CaO)+(1.4*MgO)]$.

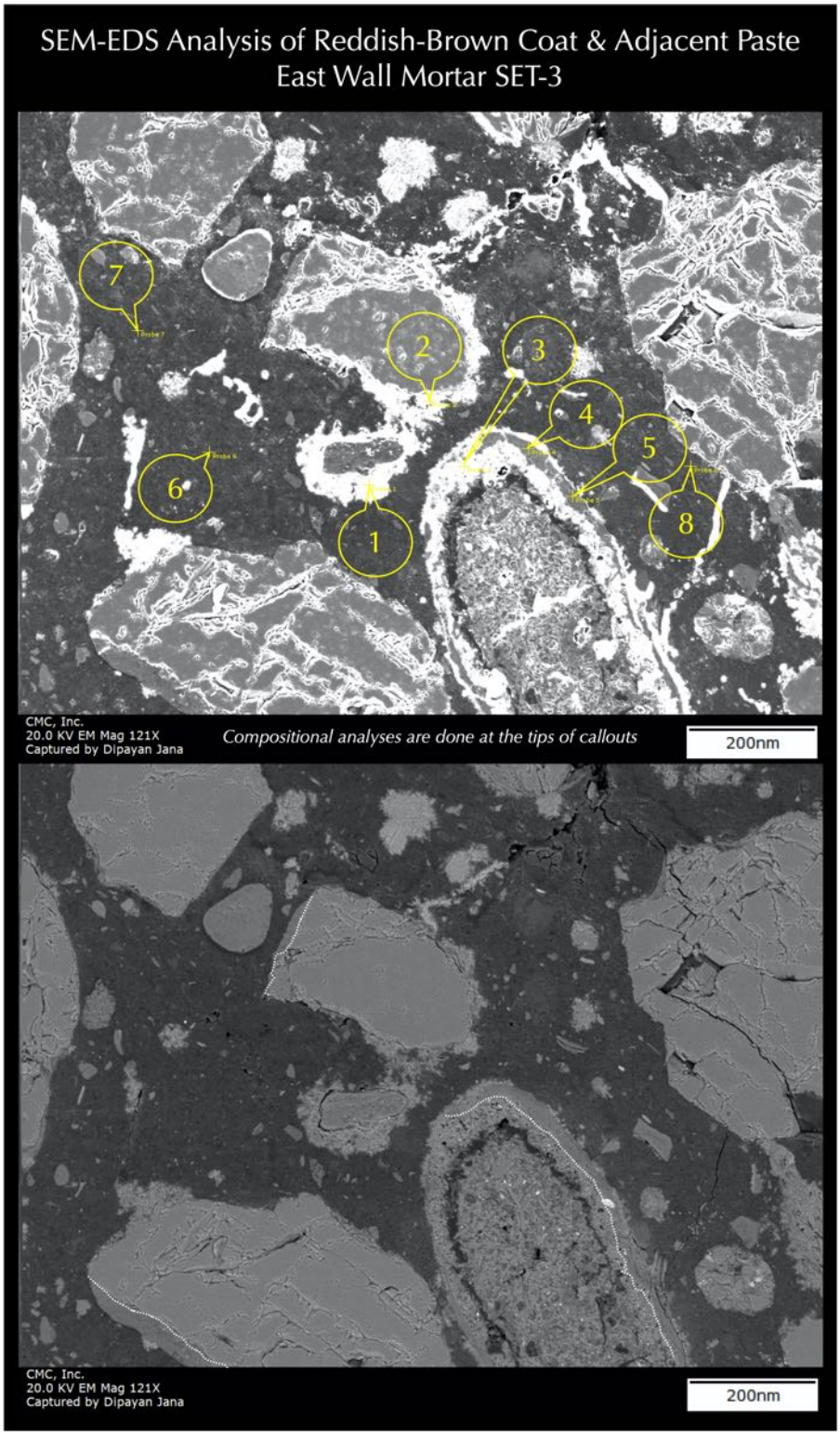

Figure 129: Secondary electron image (top) and corresponding backscatter electron image (bottom) of setting mortar SET-3 where compositional analyses were done on the reddish-brown coat and adjacent leached paste in the next Figure. Two different coats on an elliptical grain are separated by white dotted line.

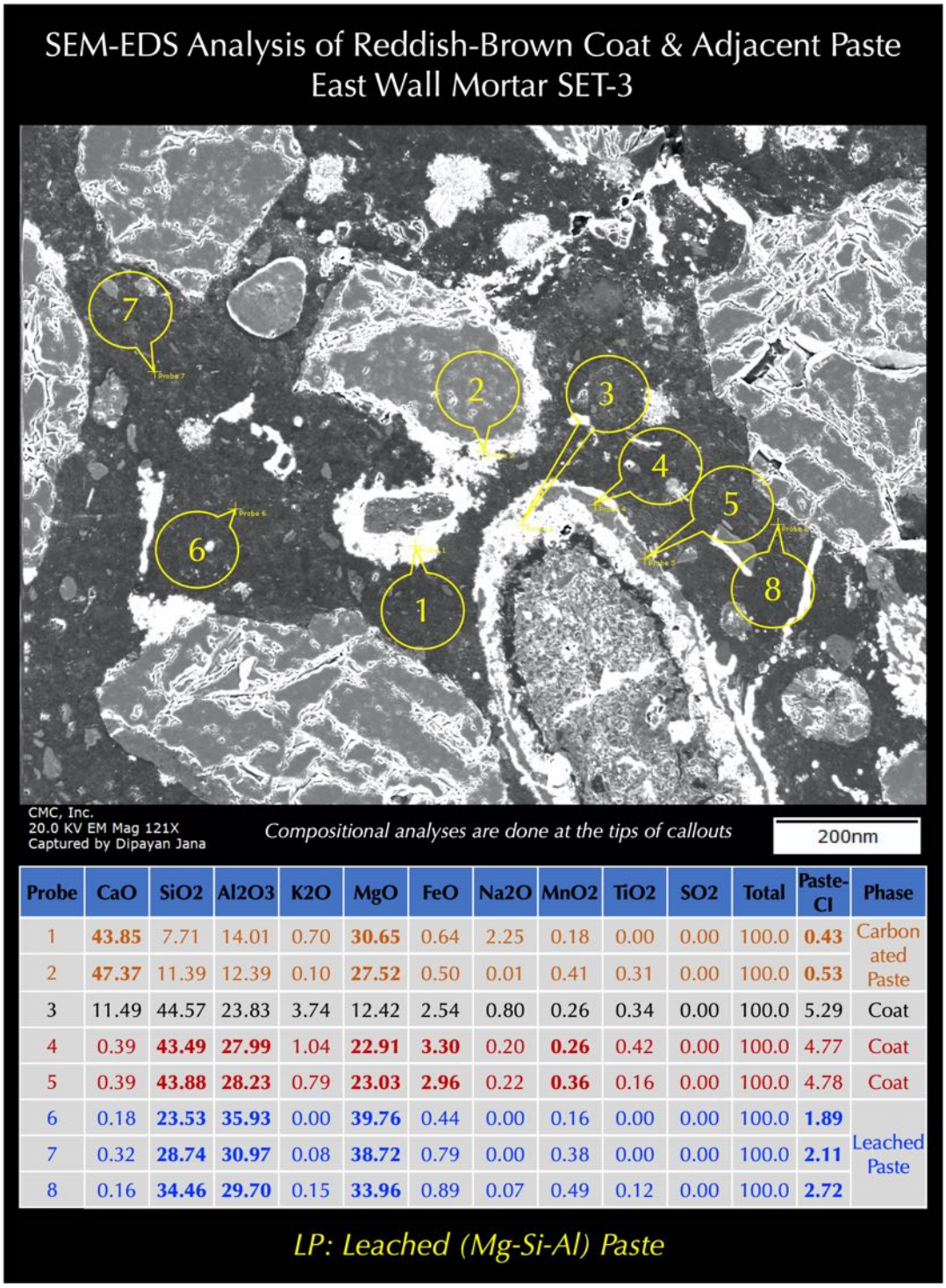

Probe	CaO	SiO2	Al2O3	K2O	MgO	FeO	Na2O	MnO2	TiO2	SO2	Total	Paste-CI	Phase
1	**43.85**	7.71	14.01	0.70	**30.65**	0.64	2.25	0.18	0.00	0.00	100.0	**0.43**	Carbonated Paste
2	**47.37**	11.39	12.39	0.10	**27.52**	0.50	0.01	0.41	0.31	0.00	100.0	**0.53**	
3	11.49	44.57	23.83	3.74	12.42	2.54	0.80	0.26	0.34	0.00	100.0	5.29	Coat
4	0.39	**43.49**	**27.99**	1.04	**22.91**	**3.30**	0.20	**0.26**	0.42	0.00	100.0	4.77	Coat
5	0.39	**43.88**	**28.23**	0.79	**23.03**	**2.96**	0.22	**0.36**	0.16	0.00	100.0	4.78	Coat
6	0.18	**23.53**	**35.93**	0.00	**39.76**	0.44	0.00	0.16	0.00	0.00	100.0	**1.89**	Leached Paste
7	0.32	**28.74**	**30.97**	0.08	**38.72**	0.79	0.00	0.38	0.00	0.00	100.0	**2.11**	
8	0.16	**34.46**	**29.70**	0.15	**33.96**	0.89	0.07	0.49	0.12	0.00	100.0	**2.72**	

LP: Leached (Mg-Si-Al) Paste

Figure 130: Backscatter electron image (top), and X-ray microanalyses at the tips of callouts in Probes 1 through 8 of setting mortar SET-3 detecting compositional variations of reddish-brown coat and adjacent leached paste. Paste composition is presented (bottom) as oxide variations of all detected EDS peaks normalized to 100% except carbon (from epoxy) and gold (from coating). Paste cementation indices, CI (after Eckel 1922) measure: (a) relative hydraulicity of paste e.g., non-hydraulic lime pastes have very low CI (< 0.50) compared to cement-based pastes (CI is >1), along with (b) the degree of leaching of lime, where leached paste characteristically show >>1 CI, and non-leached portions of paste show <1 CI from lime and its carbonated products. The cementation indices (CI) of paste are calculated after Eckel (1922) as CI = $[(2.8*SiO_2)+(1.1*Al_2O_3)+(0.7*\ Fe_2O_3)]/[(CaO)+(1.4*MgO)]$.

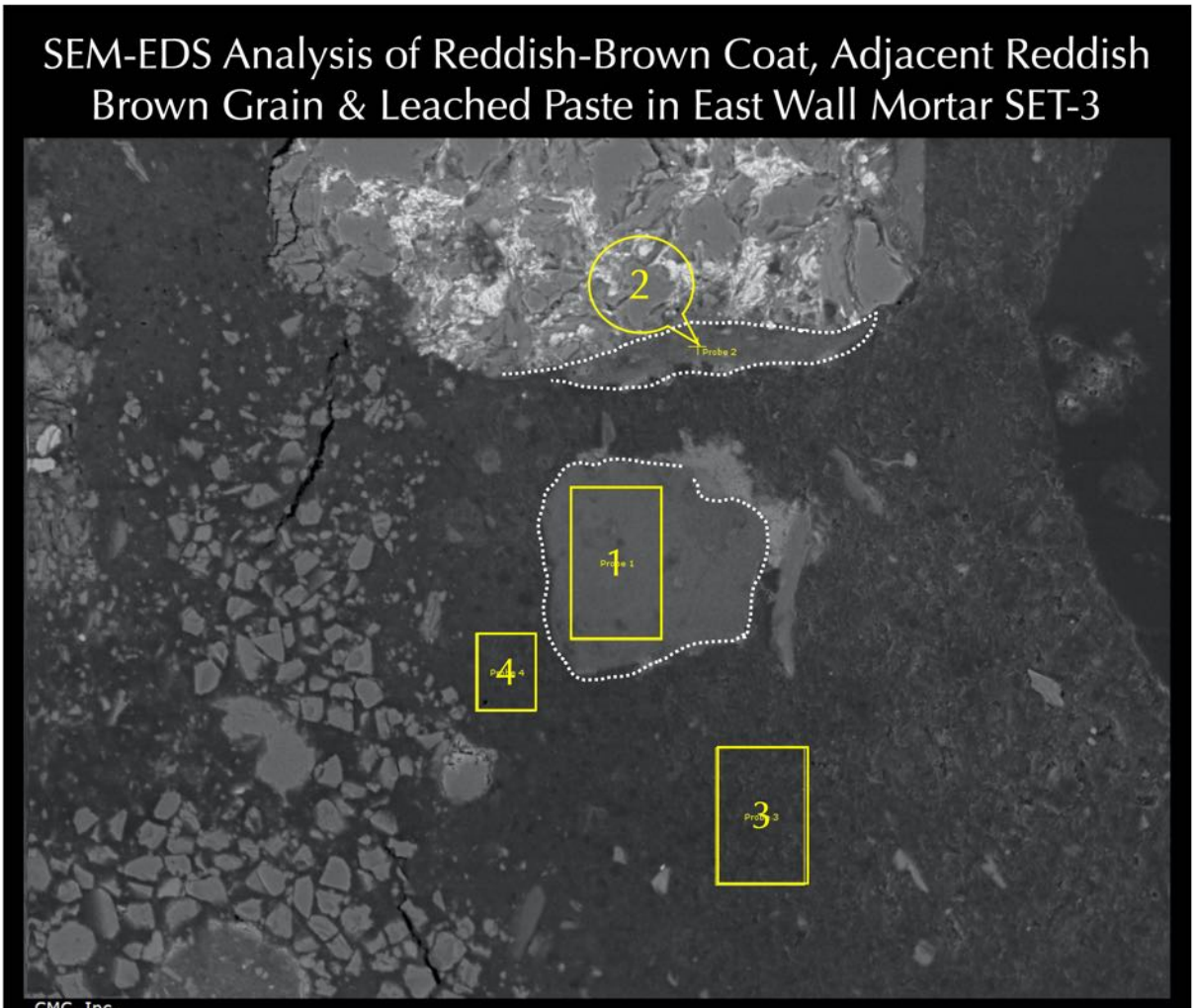

Probe	CaO	SiO2	Al2O3	K2O	MgO	FeO	Na2O	MnO2	TiO2	SO2	Total	Paste-CI	Phase
1	0.44	**50.54**	**24.54**	**1.03**	**17.44**	**5.06**	0.17	**0.35**	0.45	0.00	100.0	6.92	Grain
2	0.70	**51.72**	**25.05**	**1.04**	**15.32**	**4.87**	0.17	**0.40**	0.72	0.00	100.0	7.94	Coat
3	0.14	**35.76**	**29.22**	0.24	**33.22**	1.07	0.08	0.27	0.00	0.00	100.0	**2.85**	LP
4	0.24	**37.38**	**26.51**	0.17	**33.87**	1.18	0.28	0.37	0.00	0.00	100.0	**2.83**	LP

LP: Leached (Mg-Si-Al) Paste

Figure 131: Backscatter electron image (top), and X-ray microanalyses at the tips of callouts and in boxed area in Probes 1 through 4 of setting mortar SET-3 detecting compositional variations of reddish-brown coat, a reddish-brown grain, and adjacent leached paste. Paste composition is presented (bottom) as oxide variations of all detected EDS peaks normalized to 100% except carbon (from epoxy) and gold (from coating). Paste cementation indices, CI (after Eckel 1922) measure: (a) relative hydraulicity of paste e.g., non-hydraulic lime pastes have very low CI (< 0.50) compared to cement-based pastes (CI is >1), along with (b) the degree of leaching of lime, where leached paste characteristically show >>1 CI, and non-leached portions of paste show <1 CI from lime and its carbonated products. The cementation indices (CI) of paste are calculated after Eckel (1922) as CI = $[(2.8*SiO_2)+(1.1*Al_2O_3)+(0.7*\ Fe_2O_3)]/[(CaO)+(1.4*MgO)]$.

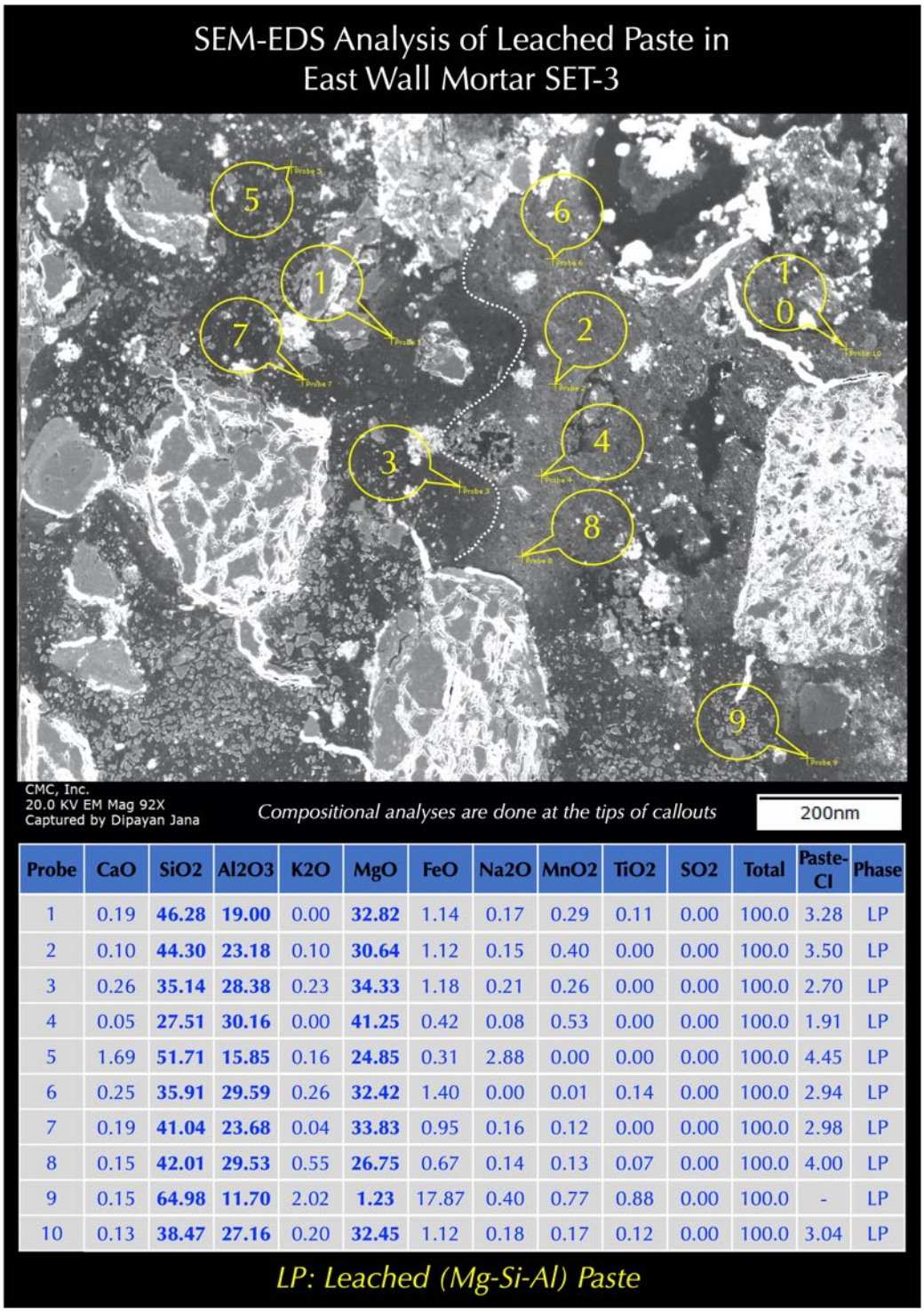

Probe	CaO	SiO2	Al2O3	K2O	MgO	FeO	Na2O	MnO2	TiO2	SO2	Total	Paste-CI	Phase
1	0.19	**46.28**	**19.00**	0.00	**32.82**	1.14	0.17	0.29	0.11	0.00	100.0	3.28	LP
2	0.10	**44.30**	**23.18**	0.10	**30.64**	1.12	0.15	0.40	0.00	0.00	100.0	3.50	LP
3	0.26	**35.14**	**28.38**	0.23	**34.33**	1.18	0.21	0.26	0.00	0.00	100.0	2.70	LP
4	0.05	**27.51**	**30.16**	0.00	**41.25**	0.42	0.08	0.53	0.00	0.00	100.0	1.91	LP
5	1.69	**51.71**	**15.85**	0.16	**24.85**	0.31	2.88	0.00	0.00	0.00	100.0	4.45	LP
6	0.25	**35.91**	**29.59**	0.26	**32.42**	1.40	0.00	0.01	0.14	0.00	100.0	2.94	LP
7	0.19	**41.04**	**23.68**	0.04	**33.83**	0.95	0.16	0.12	0.00	0.00	100.0	2.98	LP
8	0.15	**42.01**	**29.53**	0.55	**26.75**	0.67	0.14	0.13	0.07	0.00	100.0	4.00	LP
9	0.15	**64.98**	**11.70**	2.02	**1.23**	17.87	0.40	0.77	0.88	0.00	100.0	-	LP
10	0.13	**38.47**	**27.16**	0.20	**32.45**	1.12	0.18	0.17	0.12	0.00	100.0	3.04	LP

LP: Leached (Mg-Si-Al) Paste

Figure 132: Backscatter electron image (top), and X-ray microanalyses at the tips of callouts in Probes 1 through 10 of setting mortar SET-3 detecting compositional variations of leached paste. Paste composition is presented (bottom) as oxide variations of all detected EDS peaks normalized to 100% except carbon (from epoxy) and gold (from coating). Paste cementation indices, CI (after Eckel 1922) measure: (a) relative hydraulicity of paste e.g., non-hydraulic lime pastes have very low CI (< 0.50) compared to cement-based pastes (CI is >1), along with (b) the degree of leaching of lime, where leached paste characteristically show >>1 CI, and non-leached portions of paste show <1 CI from lime and its carbonated products. The cementation indices (CI) of paste are calculated after Eckel (1922) as CI = $[(2.8*SiO_2)+(1.1*Al_2O_3)+(0.7*Fe_2O_3)]/[(CaO)+(1.4*MgO)]$.

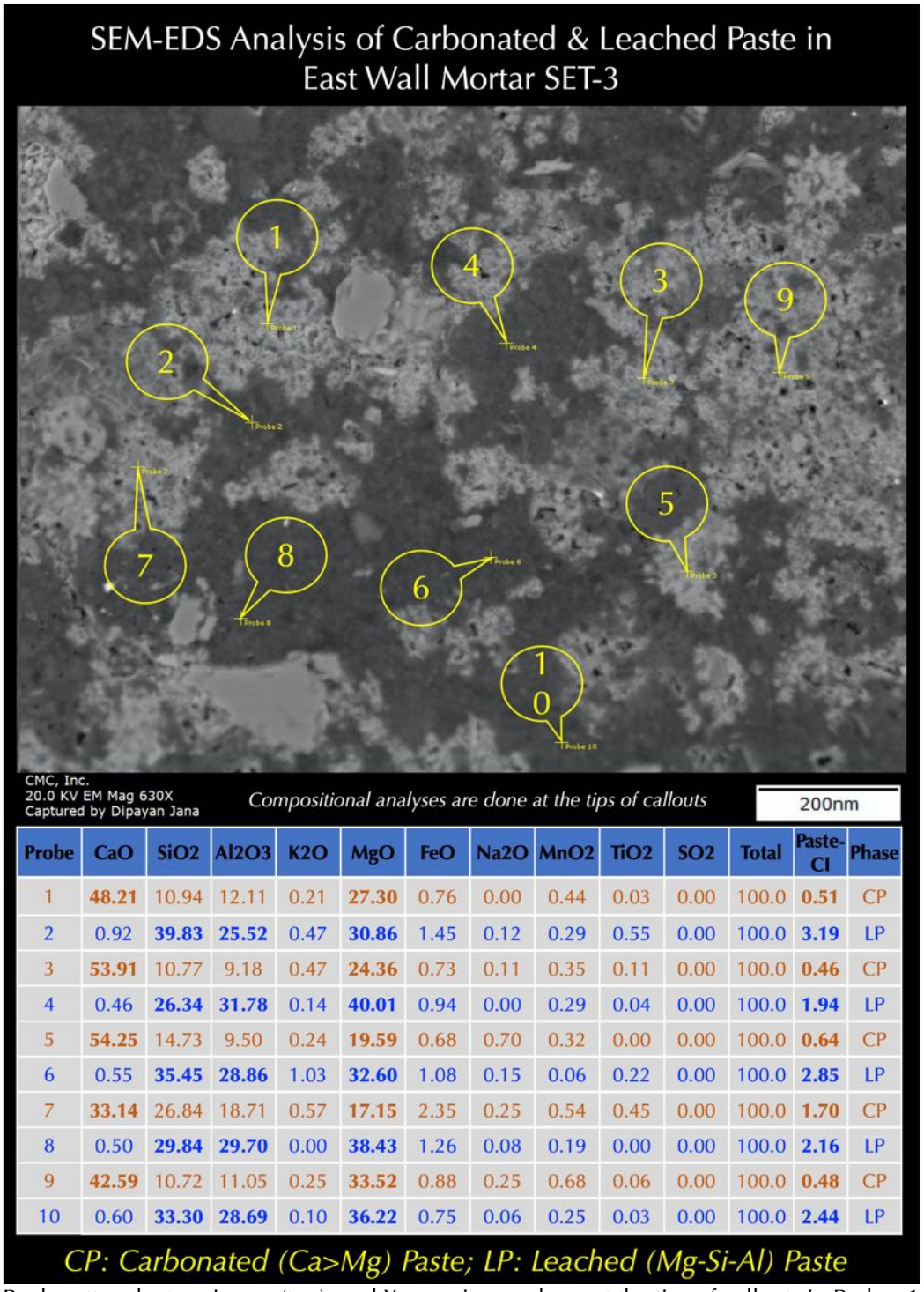

Probe	CaO	SiO2	Al2O3	K2O	MgO	FeO	Na2O	MnO2	TiO2	SO2	Total	Paste-CI	Phase
1	**48.21**	10.94	12.11	0.21	**27.30**	0.76	0.00	0.44	0.03	0.00	100.0	**0.51**	CP
2	0.92	**39.83**	**25.52**	0.47	**30.86**	1.45	0.12	0.29	0.55	0.00	100.0	**3.19**	LP
3	**53.91**	10.77	9.18	0.47	**24.36**	0.73	0.11	0.35	0.11	0.00	100.0	**0.46**	CP
4	0.46	**26.34**	**31.78**	0.14	**40.01**	0.94	0.00	0.29	0.04	0.00	100.0	**1.94**	LP
5	**54.25**	14.73	9.50	0.24	**19.59**	0.68	0.70	0.32	0.00	0.00	100.0	**0.64**	CP
6	0.55	**35.45**	**28.86**	1.03	**32.60**	1.08	0.15	0.06	0.22	0.00	100.0	**2.85**	LP
7	**33.14**	26.84	18.71	0.57	**17.15**	2.35	0.25	0.54	0.45	0.00	100.0	**1.70**	CP
8	0.50	**29.84**	**29.70**	0.00	**38.43**	1.26	0.08	0.19	0.00	0.00	100.0	**2.16**	LP
9	**42.59**	10.72	11.05	0.25	**33.52**	0.88	0.25	0.68	0.06	0.00	100.0	**0.48**	CP
10	0.60	**33.30**	**28.69**	0.10	**36.22**	0.75	0.06	0.25	0.03	0.00	100.0	**2.44**	LP

CP: Carbonated (Ca>Mg) Paste; LP: Leached (Mg-Si-Al) Paste

Figure 133: Backscatter electron image (top), and X-ray microanalyses at the tips of callouts in Probes 1 through 10 of setting mortar SET-3 detecting compositional variations of leached and carbonated paste. Paste composition is presented (bottom) as oxide variations of all detected EDS peaks normalized to 100% except carbon (from epoxy) and gold (from coating). Paste cementation indices, CI (after Eckel 1922) measure: (a) relative hydraulicity of paste e.g., non-hydraulic lime pastes have very low CI (< 0.50) compared to cement-based pastes (CI is >1), along with (b) the degree of leaching of lime, where leached paste characteristically show >>1 CI, and non-leached portions of paste show <1 CI from lime and its carbonated products. The cementation indices (CI) of paste are calculated after Eckel (1922) as CI = $[(2.8*SiO_2)+(1.1*Al_2O_3)+(0.7*\ Fe_2O_3)]/[(CaO)+(1.4*MgO)]$.

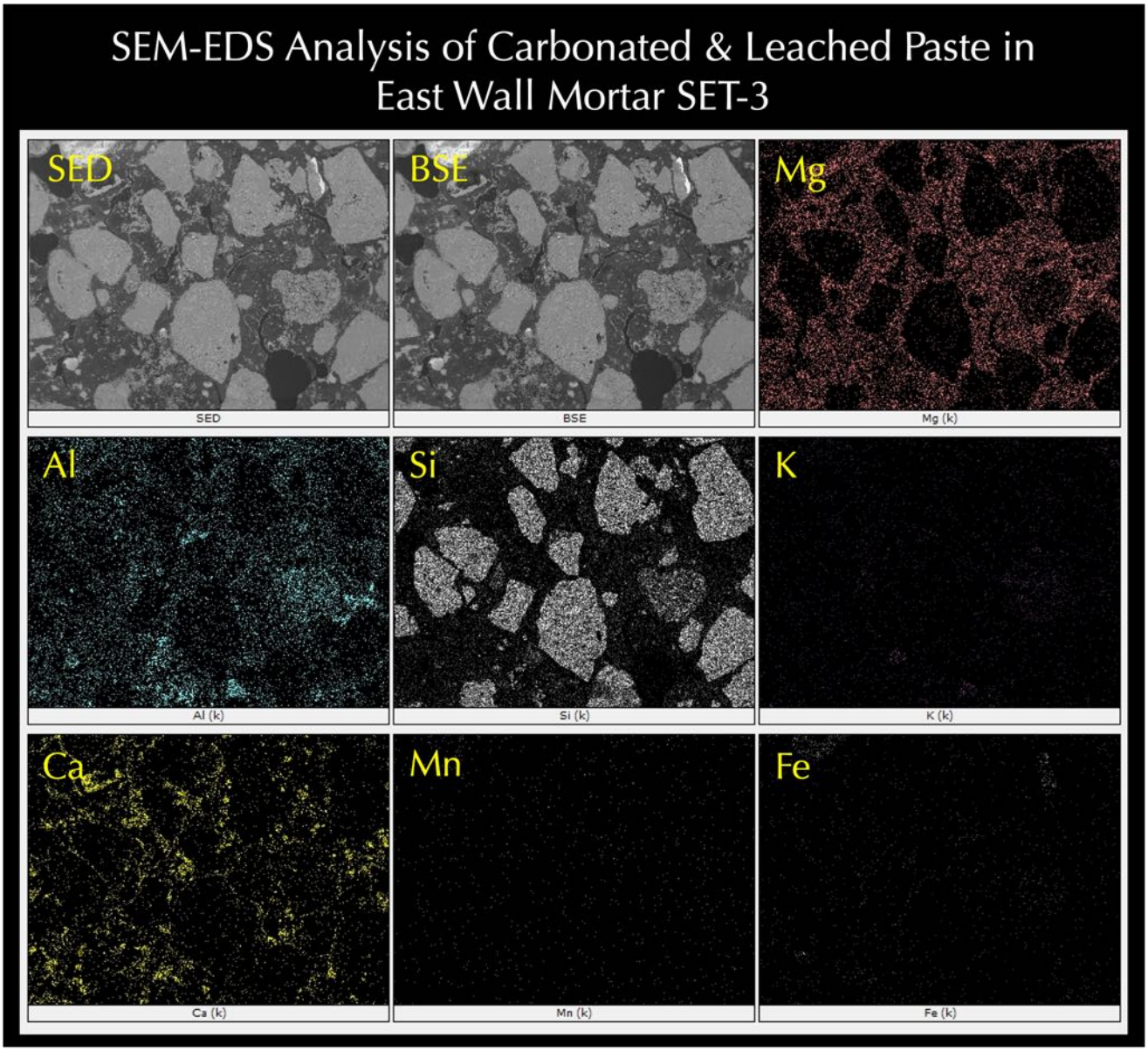

Figure 134: X-ray elemental mapping of Si, Al, Ca, Mg, K, Fe, and Mn in setting mortar SET-3 showing overall Mg-Si-Al based composition of leached paste along with isolated meager occurrences of Ca from leaching and dissolution of lime from the original Ca-Mg-Si-Al based binder from calcined clay and dolomitic lime. Leaching of lime has enriched the leached areas in Mg-Si-Al as gelatinous mass, which appeared optically isotropic in thin section micrographs shown before.

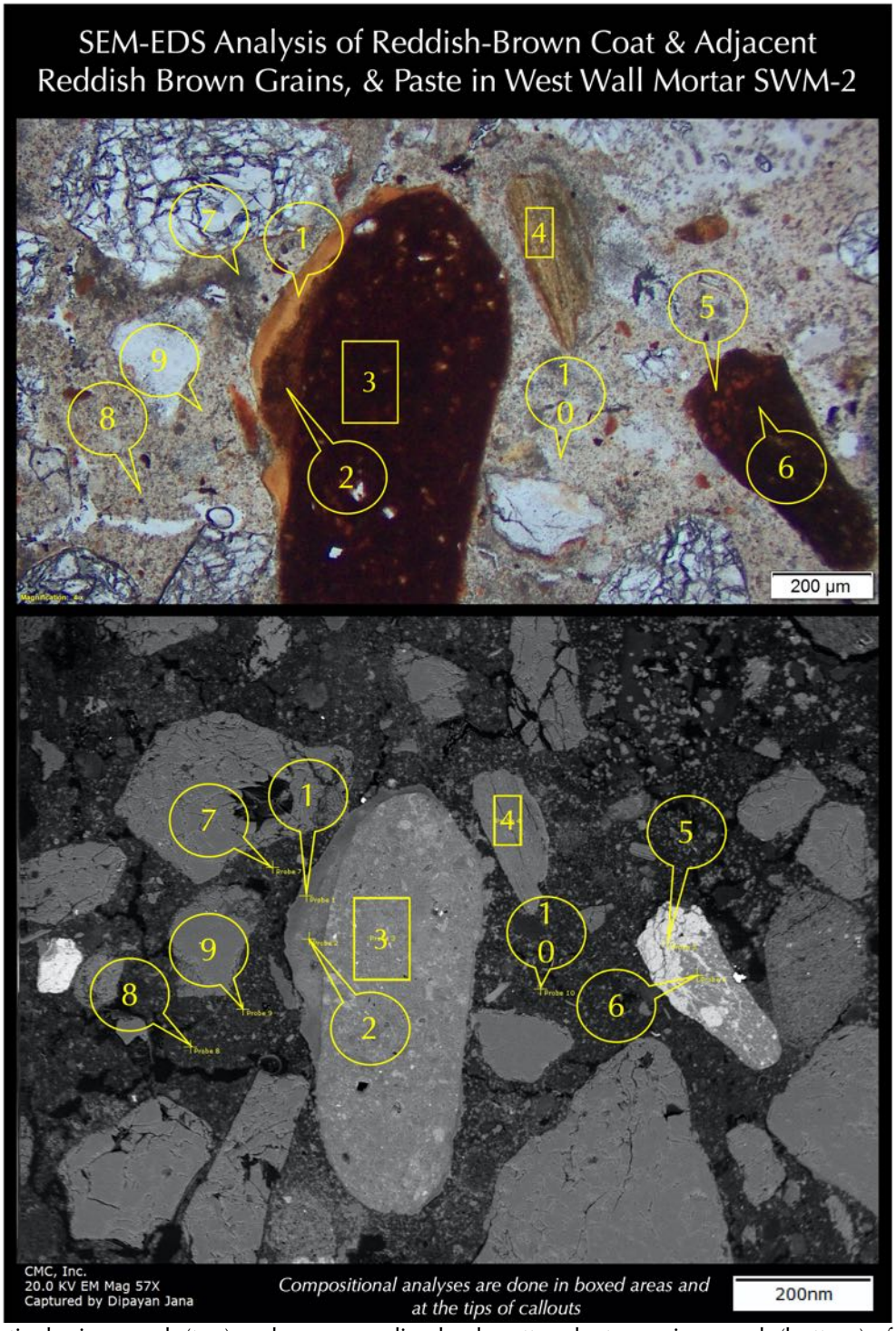

Figure 135: Optical micrograph (top) and corresponding backscatter electron micrograph (bottom) of setting mortar SWM-2 showing points at the tips of callouts and in a boxed area across various areas in paste, grain, and reddish-brown coats, which are analyzed in SEM-EDS for major element oxide compositions. Positions of tips of callouts in the optical micrograph are only approximate to the actual ones shown in the electron micrograph. The central reddish-brown grain is a residual calcined clay (brick dust) particle, which is analyzed at probe 3 showing characteristically high silica and alumina. Another reddish-brown grain at right showed similar (but higher silica and lower alumina) aluminosilicate composition at Probe 6 but the rim at Probe 5 showed very high iron (Fe>Si, Al) indicating an oxidized iron rim. Next Figure shows results of compositional analyses of grains.

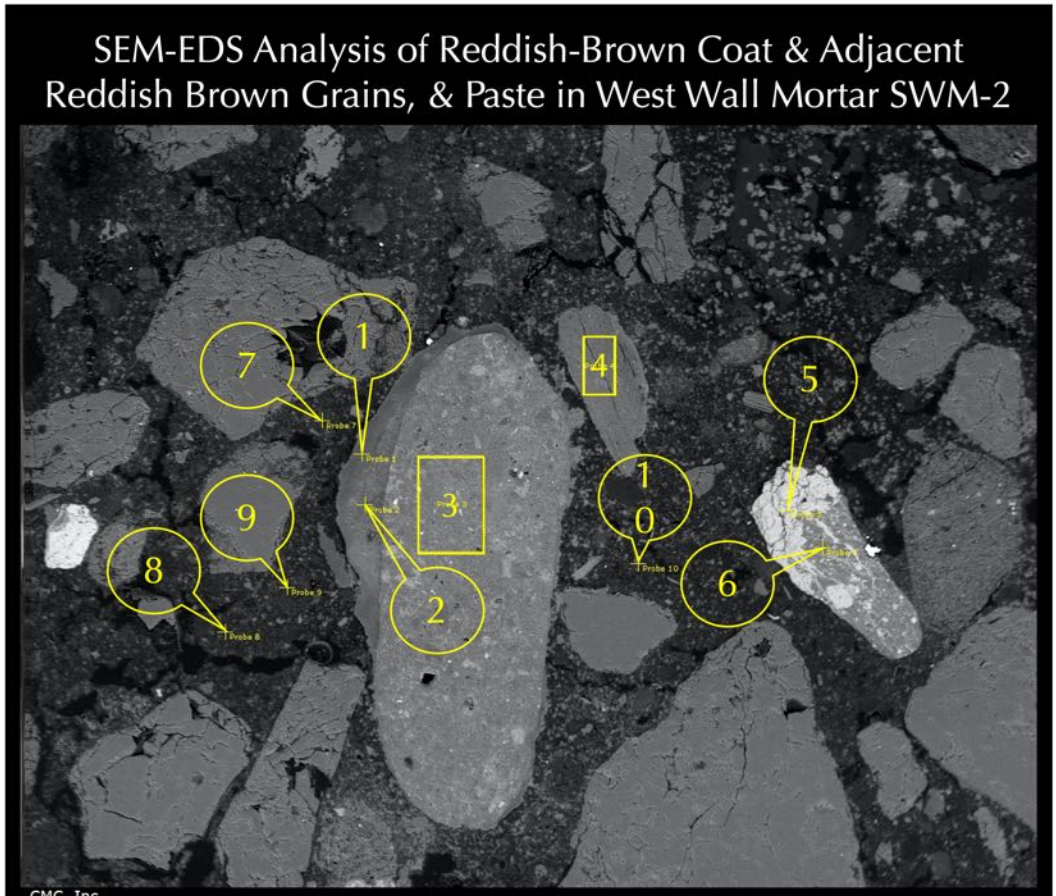

Probe	CaO	SiO2	Al2O3	K2O	MgO	FeO	Na2O	MnO2	TiO2	SO2	Total	Paste - CI	Phase
1	1.68	**47.08**	**33.34**	**0.83**	12.33	**3.50**	0.36	0.26	0.61	0.00	100.0	-	Coat
2	9.12	**44.89**	**28.41**	**0.81**	11.61	**2.99**	0.23	1.53	0.40	0.00	100.0	-	Coat
3	1.45	**59.14**	**24.79**	**2.79**	4.21	**5.37**	0.45	0.77	1.03	0.00	100.0	-	Grain
4	2.30	**56.93**	**26.11**	**4.09**	7.17	**1.88**	0.26	0.40	0.85	0.00	100.0	-	Shale
5	1.12	**17.80**	**28.70**	0.06	1.82	**45.45**	2.85	2.03	0.16	0.00	100.0	-	Grain
6	0.29	**70.07**	**18.64**	**2.66**	2.43	**3.56**	0.80	0.30	1.25	0.00	100.0	-	Grain
7	3.60	**37.98**	**22.75**	0.07	**34.82**	0.21	0.19	0.26	0.12	0.00	100.0	2.51	Paste
8	0.00	**99.52**	0.22	0.00	0.00	0.00	0.13	0.13	0.00	0.00	100.0	-	Quartz
9	**14.46**	**36.82**	**14.24**	0.00	**33.46**	0.31	0.20	0.43	0.08	0.00	100.0	1.94	Paste
10	**27.64**	**22.00**	**15.78**	0.06	**33.54**	0.30	0.20	0.32	0.16	0.00	100.0	1.06	Paste

Figure 136: Backscatter electron image (top), and X-ray microanalyses at the tips of callouts and boxed areas in Probes 1 through 10 of setting mortar SWM-2 detecting compositional variations of reddish-brown coat (Probe 1 and 2), adjacent central calcined clay grain (Probe 3), and leached paste. Paste composition is presented (bottom) as oxide variations of all detected EDS peaks normalized to 100% except carbon (from epoxy) and gold (from coating). Paste cementation indices, CI (after Eckel 1922) measure: (a) relative hydraulicity of paste e.g., non-hydraulic lime pastes have very low CI (< 0.50) compared to cement-based pastes (CI is >1), along with (b) the degree of leaching of lime, where leached paste characteristically show >>1 CI, and non-leached portions of paste show <1 CI from lime and its carbonated products. The cementation indices (CI) of paste are calculated after Eckel (1922) as CI = $[(2.8*SiO_2)+(1.1*Al_2O_3)+(0.7*\ Fe_2O_3)]/[(CaO)+(1.4*MgO)]$.

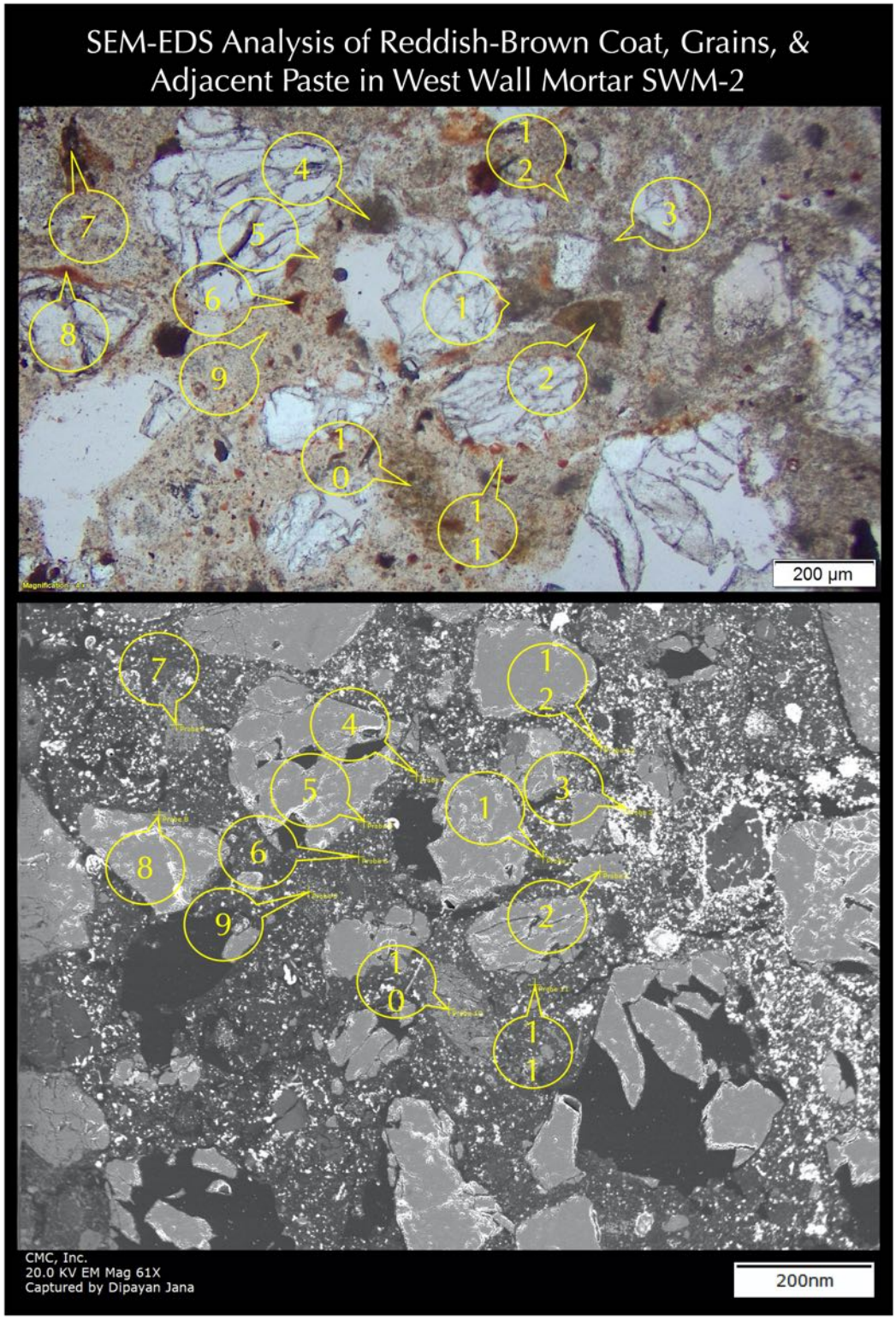

Figure 137: Optical micrograph (top) and corresponding secondary electron micrograph (bottom) of setting mortar SWM-2 showing points at the tips of callouts across various areas in paste, grain, and reddish-brown coats, which are analyzed in SEM-EDS for major element oxide compositions. Positions of tips of callouts in the optical micrograph are only approximate to the actual ones shown in the electron micrograph.

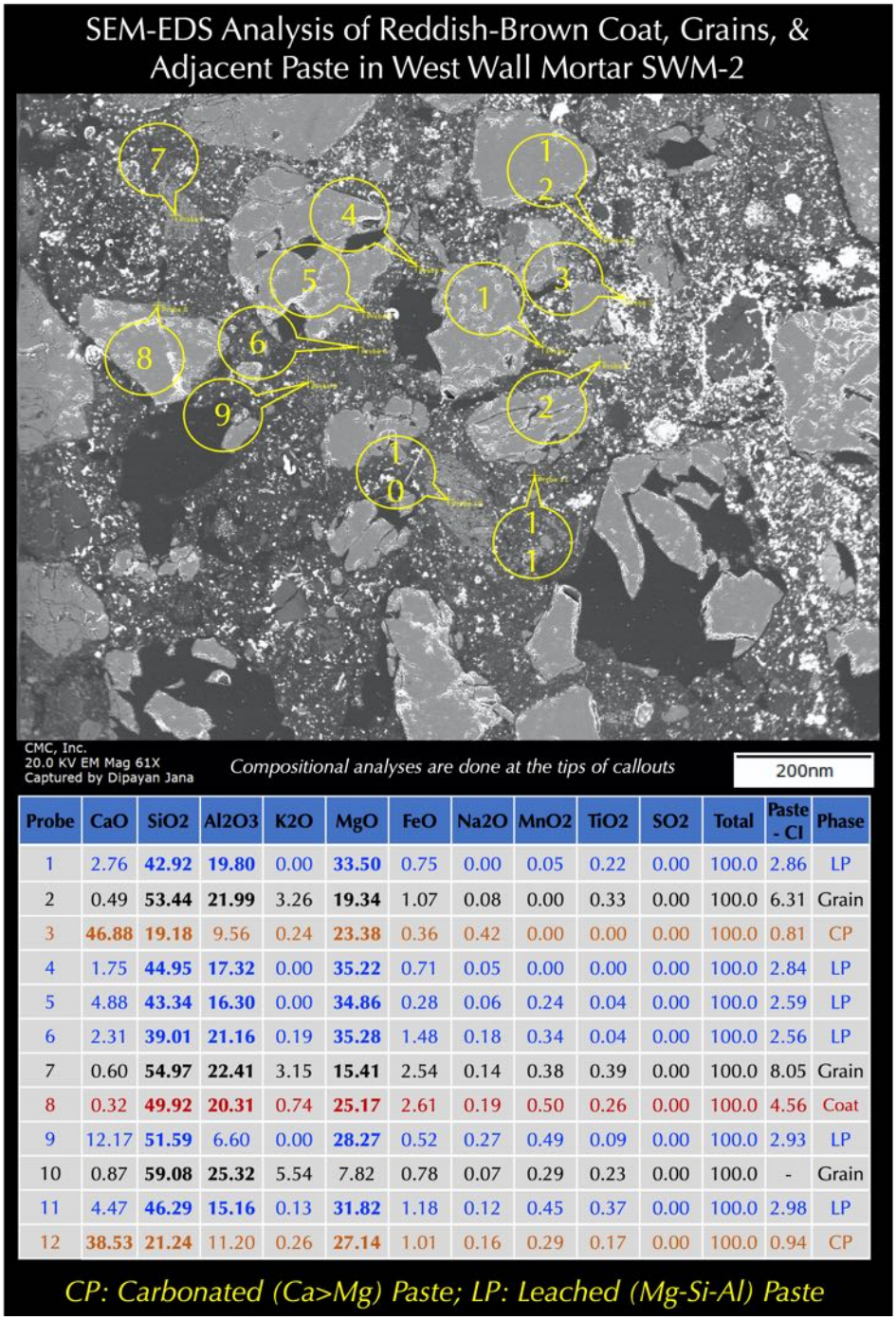

Probe	CaO	SiO2	Al2O3	K2O	MgO	FeO	Na2O	MnO2	TiO2	SO2	Total	Paste - CI	Phase
1	2.76	42.92	19.80	0.00	33.50	0.75	0.00	0.05	0.22	0.00	100.0	2.86	LP
2	0.49	53.44	21.99	3.26	19.34	1.07	0.08	0.00	0.33	0.00	100.0	6.31	Grain
3	46.88	19.18	9.56	0.24	23.38	0.36	0.42	0.00	0.00	0.00	100.0	0.81	CP
4	1.75	44.95	17.32	0.00	35.22	0.71	0.05	0.00	0.00	0.00	100.0	2.84	LP
5	4.88	43.34	16.30	0.00	34.86	0.28	0.06	0.24	0.04	0.00	100.0	2.59	LP
6	2.31	39.01	21.16	0.19	35.28	1.48	0.18	0.34	0.04	0.00	100.0	2.56	LP
7	0.60	54.97	22.41	3.15	15.41	2.54	0.14	0.38	0.39	0.00	100.0	8.05	Grain
8	0.32	49.92	20.31	0.74	25.17	2.61	0.19	0.50	0.26	0.00	100.0	4.56	Coat
9	12.17	51.59	6.60	0.00	28.27	0.52	0.27	0.49	0.09	0.00	100.0	2.93	LP
10	0.87	59.08	25.32	5.54	7.82	0.78	0.07	0.29	0.23	0.00	100.0	-	Grain
11	4.47	46.29	15.16	0.13	31.82	1.18	0.12	0.45	0.37	0.00	100.0	2.98	LP
12	38.53	21.24	11.20	0.26	27.14	1.01	0.16	0.29	0.17	0.00	100.0	0.94	CP

CP: Carbonated (Ca>Mg) Paste; LP: Leached (Mg-Si-Al) Paste

Figure 138: Backscatter electron image (top), and X-ray microanalyses at the tips of callouts in Probes 1 through 12 of setting mortar SWM-2 detecting compositional variations of reddish-brown coat, adjacent grains, and leached and carbonated paste. Paste composition is presented (bottom) as oxide variations of all detected EDS peaks normalized to 100% except carbon (from epoxy) and gold (from coating). Paste cementation indices, CI (after Eckel 1922) measure: (a) relative hydraulicity of paste e.g., non-hydraulic lime pastes have very low CI (< 0.50) compared to cement-based pastes (CI is >1), along with (b) the degree of leaching of lime, where leached paste characteristically show >>1 CI, and non-leached portions of paste show <1 CI from lime and its carbonated products. The cementation indices (CI) of paste are calculated after Eckel (1922) as CI = $[(2.8*SiO_2)+(1.1*Al_2O_3)+(0.7*\ Fe_2O_3)]/[(CaO)+(1.4*MgO)]$.

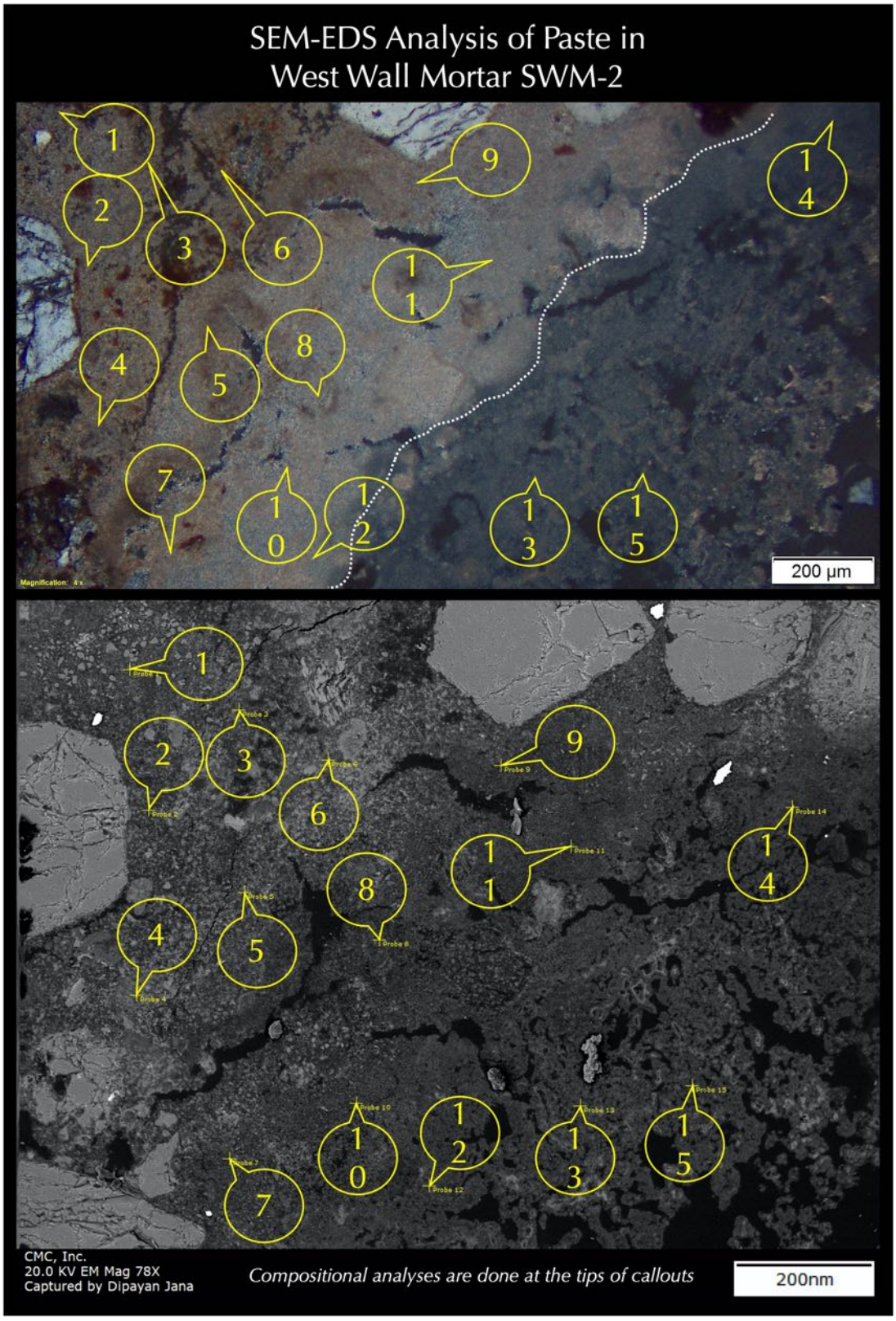

Figure 139: Optical micrograph (top) and corresponding backscatter electron micrograph (bottom) of setting mortar SWM-2 showing points at the tips of callouts across various carbonated areas in paste, grain, which are analyzed in SEM-EDS for major element oxide compositions. Positions of tips of callouts in the optical micrograph are only approximate to the actual ones shown in the electron micrograph.

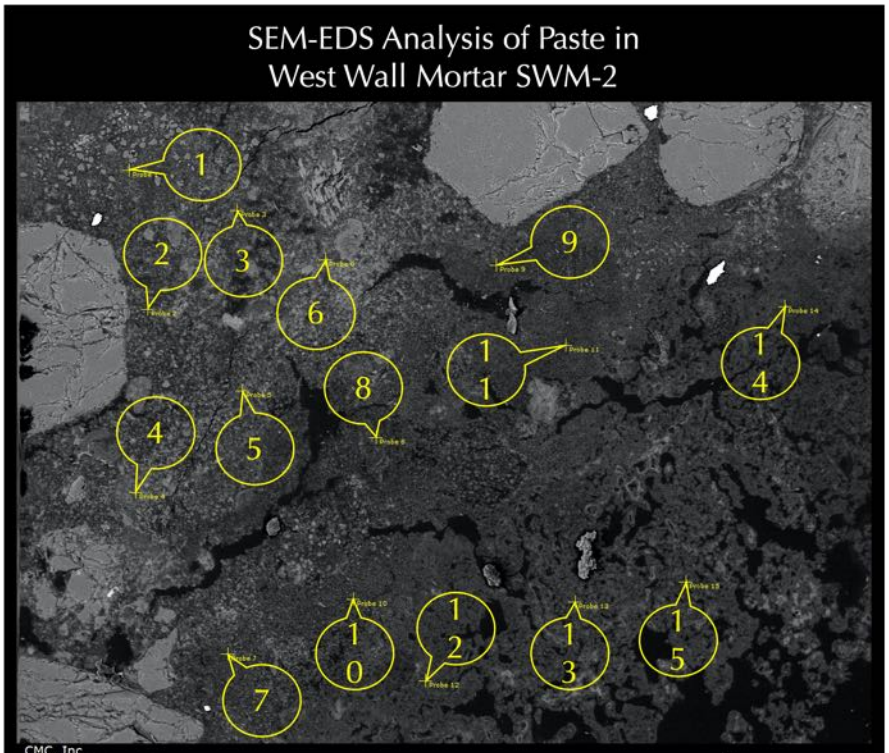

Probe	CaO	SiO2	Al2O3	K2O	MgO	FeO	Na2O	MnO2	TiO2	SO2	Total	Paste - CI	Phase
1	29.73	24.81	18.39	0.12	24.61	0.64	0.93	0.77	0.00	0.00	100.0	1.40	CP
2	40.73	20.68	10.44	0.28	26.52	0.71	0.14	0.36	0.13	0.00	100.0	0.90	CP
3	38.41	20.64	17.59	0.34	22.14	0.33	0.16	0.39	0.00	0.00	100.0	1.11	CP
4	23.59	34.33	18.38	0.20	22.84	0.25	0.10	0.25	0.06	0.00	100.0	2.10	CP
5	67.84	9.94	5.81	0.33	13.22	0.61	0.60	1.01	0.63	0.00	100.0	0.40	CP
6	41.32	18.71	19.31	0.22	18.58	0.69	0.43	0.54	0.20	0.00	100.0	1.10	CP
7	62.23	17.30	3.50	0.05	15.56	0.31	0.43	0.62	0.00	0.00	100.0	0.62	CP
8	16.22	37.39	19.08	0.09	20.58	0.24	0.18	0.28	0.00	5.94	100.0	2.79	CP
9	53.07	22.07	5.33	0.15	18.19	0.64	0.00	0.50	0.05	0.00	100.0	0.87	CP
10	58.42	20.38	4.37	0.16	15.83	0.73	0.00	0.10	0.00	0.00	100.0	0.77	CP
11	59.90	15.17	10.04	0.13	9.97	0.07	0.36	0.15	0.00	4.22	100.0	0.73	CP
12	75.01	9.95	1.14	0.34	11.38	0.64	0.70	0.68	0.17	0.00	100.0	0.33	CP
13	78.88	8.16	2.77	0.56	7.94	0.43	0.23	1.03	0.00	0.00	100.0	0.29	CP
14	66.24	14.24	3.64	0.05	13.53	0.87	0.81	0.60	0.00	0.00	100.0	0.52	CP
15	74.36	10.54	1.04	0.27	12.42	0.72	0.25	0.36	0.04	0.00	100.0	0.34	CP

CP: Carbonated (Ca>Mg) Paste

Figure 140: Backscatter electron image (top), and X-ray microanalyses at the tips of callouts in Probes 1 through 15 of setting mortar SWM-2 detecting compositional variations of variably leached and carbonated paste. Paste composition is presented (bottom) as oxide variations of all detected EDS peaks normalized to 100% except carbon (from epoxy) and gold (from coating). Paste cementation indices, CI (after Eckel 1922) measure: (a) relative hydraulicity of paste e.g., non-hydraulic lime pastes have very low CI (< 0.50) compared to cement-based pastes (CI is >1), along with (b) the degree of leaching of lime, where leached paste characteristically show >>1 CI, and non-leached portions of paste show <1 CI from lime and its carbonated products. The cementation indices (CI) of paste are calculated after Eckel (1922) as CI = $[(2.8*SiO_2)+(1.1*Al_2O_3)+(0.7*\ Fe_2O_3)]/[(CaO)+(1.4*MgO)]$.

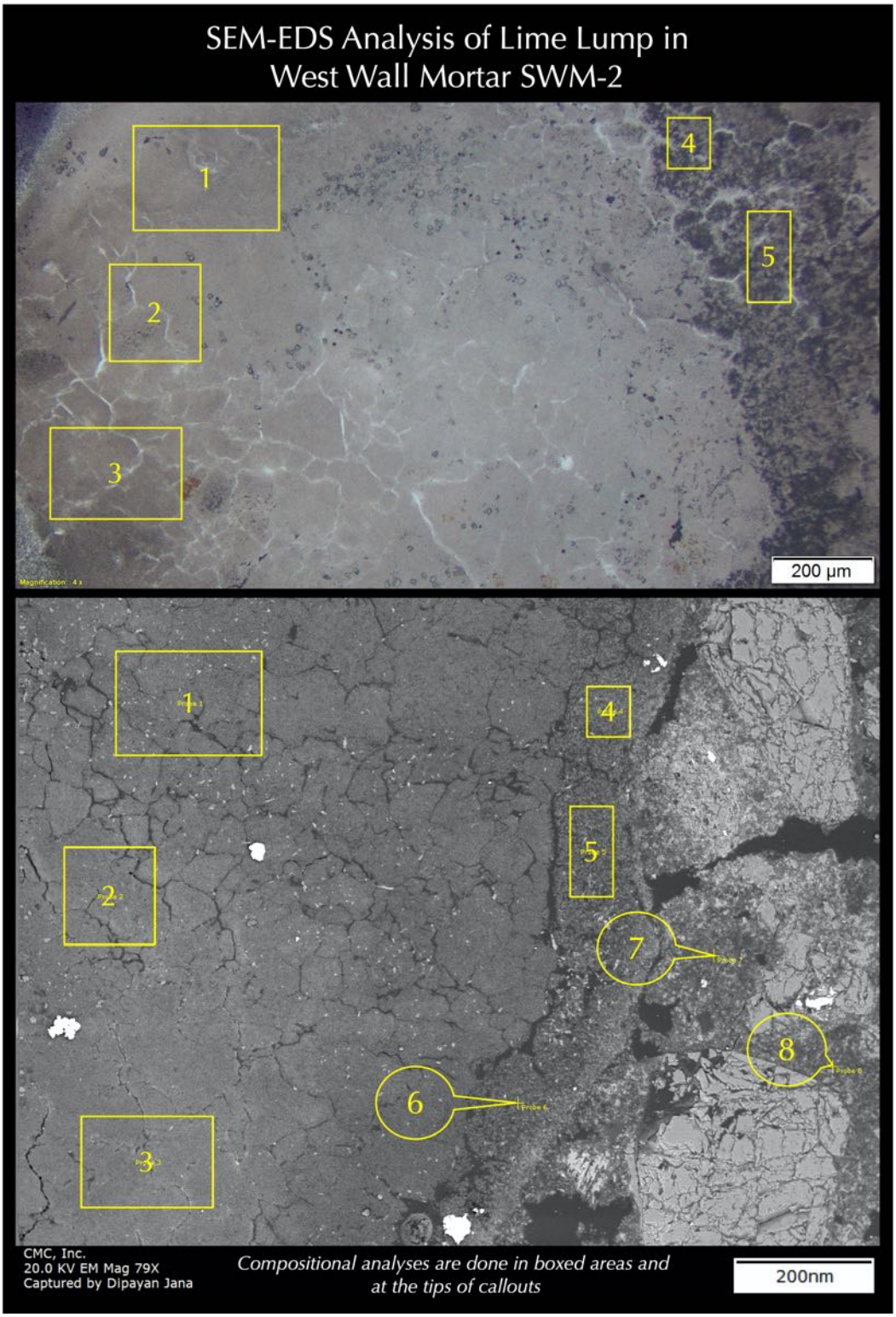

Figure 141: Optical micrograph (top) and corresponding secondary electron micrograph (bottom) of setting mortar SWM-2 showing points at the tips of callouts and boxed areas across various areas in a lime lump and adjacent paste, which are analyzed in SEM-EDS for major element oxide compositions.

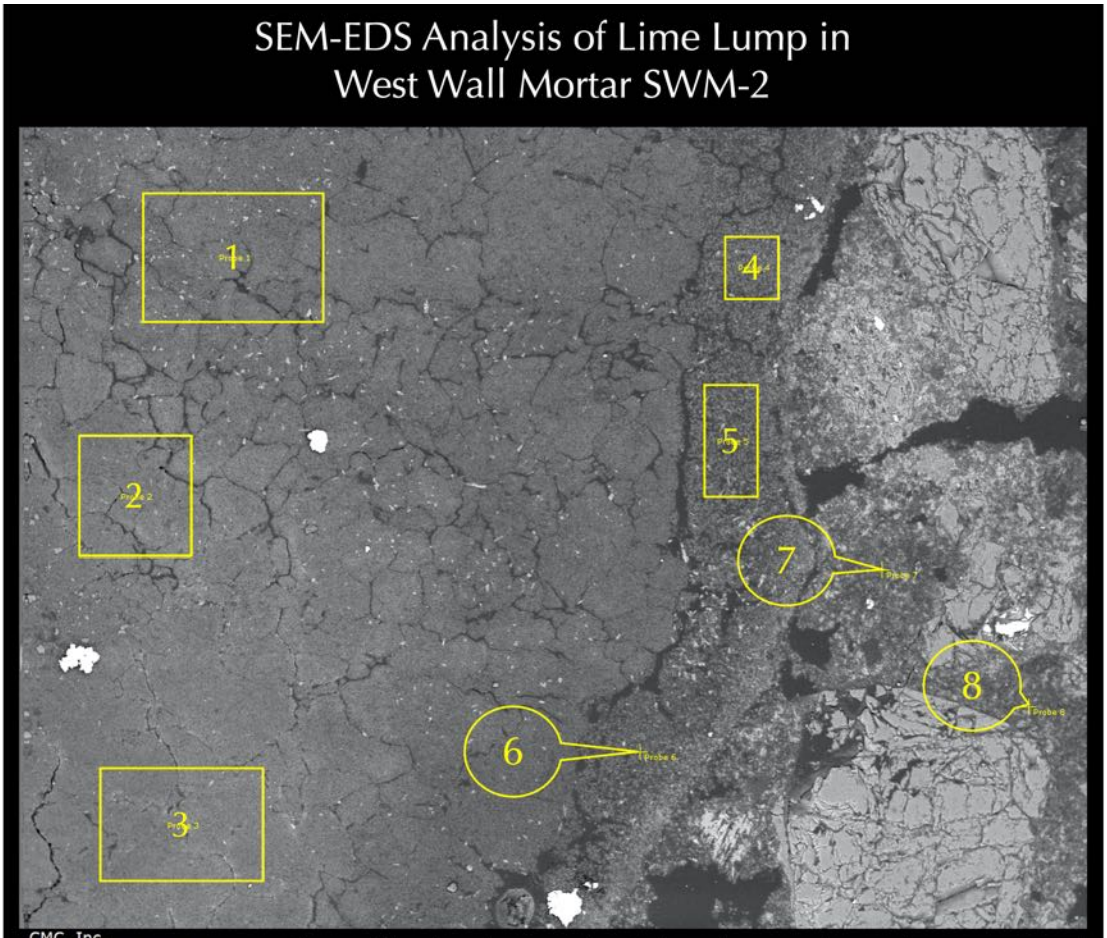

Probe	CaO	SiO2	Al2O3	K2O	MgO	FeO	Na2O	MnO2	TiO2	SO2	Total	Paste - CI	Phase
1	65.84	14.18	2.46	0.32	15.41	0.28	1.10	0.41	0.00	0.00	100.0	0.49	LL
2	66.93	14.07	2.76	0.40	14.20	0.27	1.02	0.19	0.14	0.00	100.0	0.49	LL
3	67.22	13.27	3.06	0.33	14.53	0.45	1.11	0.03	0.00	0.00	100.0	0.47	LL
4	50.90	22.40	5.87	0.48	18.58	0.30	1.09	0.00	0.36	0.00	100.0	0.90	LL
5	48.21	22.88	8.14	0.42	18.90	0.45	0.91	0.08	0.00	0.00	100.0	0.98	LL
6	33.68	34.83	6.91	0.25	23.76	0.33	0.07	0.16	0.00	0.00	100.0	1.57	P
7	42.04	24.44	9.36	0.46	22.68	0.39	0.27	0.32	0.03	0.00	100.0	1.07	P
8	21.37	36.21	13.19	0.16	27.26	0.84	0.21	0.14	0.24	0.38	100.0	1.96	P

LL: Lime Lump (Ca>Mg)

Figure 142: Backscatter electron image (top), and X-ray microanalyses at the tips of callouts in Probes 1 through 8 of setting mortar SWM-2 detecting compositional variations across a lime lump and in adjacent paste. Paste composition is presented (bottom) as oxide variations of all detected EDS peaks normalized to 100% except carbon (from epoxy) and gold (from coating). Paste cementation indices, CI (after Eckel 1922) measure: (a) relative hydraulicity of paste e.g., non-hydraulic lime pastes have very low CI (< 0.50) compared to cement-based pastes (CI is >1), along with (b) the degree of leaching of lime, where leached paste characteristically show >>1 CI, and non-leached portions of paste show <1 CI from lime and its carbonated products. The cementation indices (CI) of paste are calculated after Eckel (1922) as CI = $[(2.8*SiO_2)+(1.1*Al_2O_3)+(0.7*\ Fe_2O_3)]/[(CaO)+(1.4*MgO)]$.

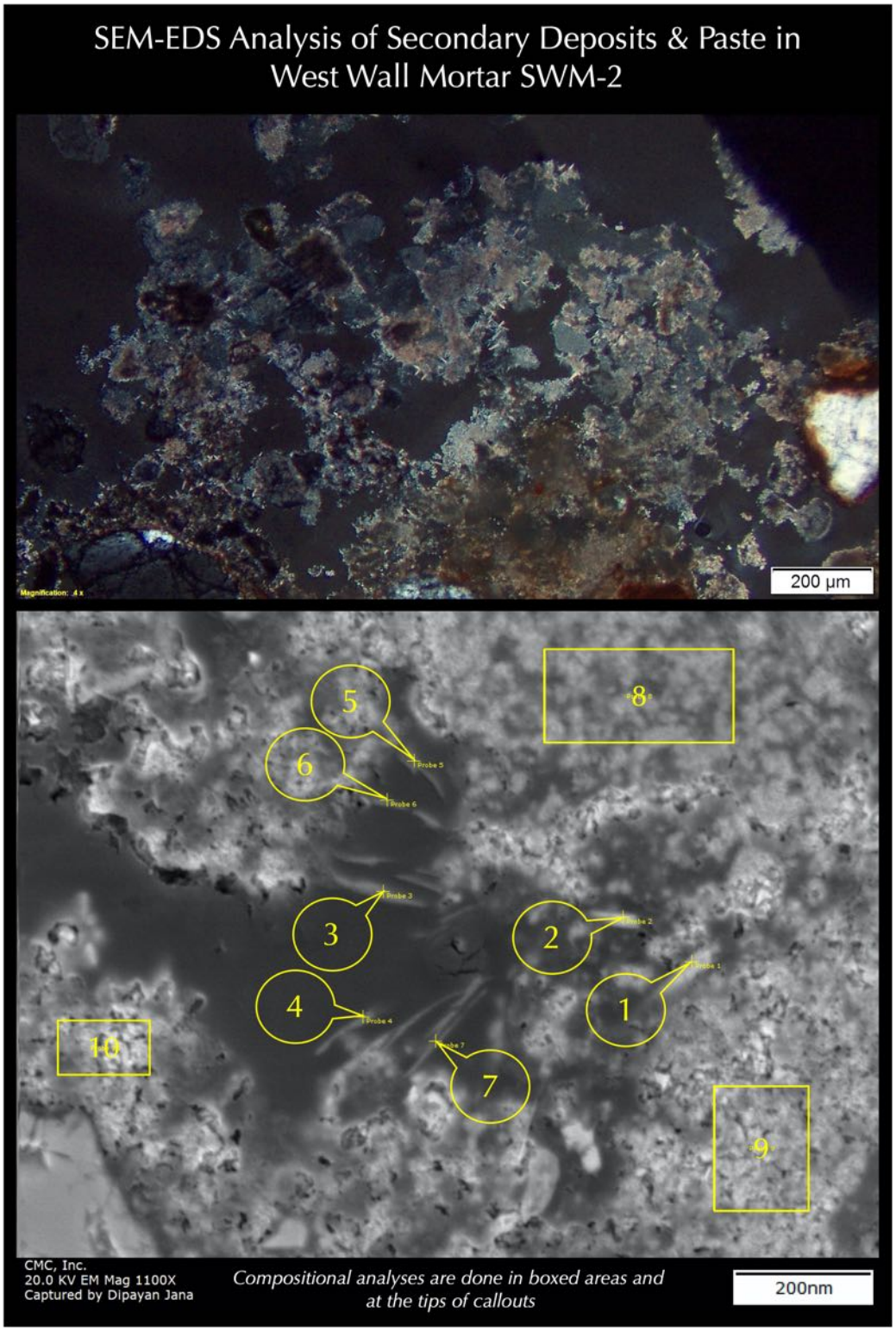

Figure 143: Optical micrograph (top) and corresponding secondary electron micrograph (bottom) of setting mortar SWM-2 showing points at the tips of callouts and boxes across various areas in paste, and secondary deposits in a void, which are analyzed in SEM-EDS for major element oxide compositions.

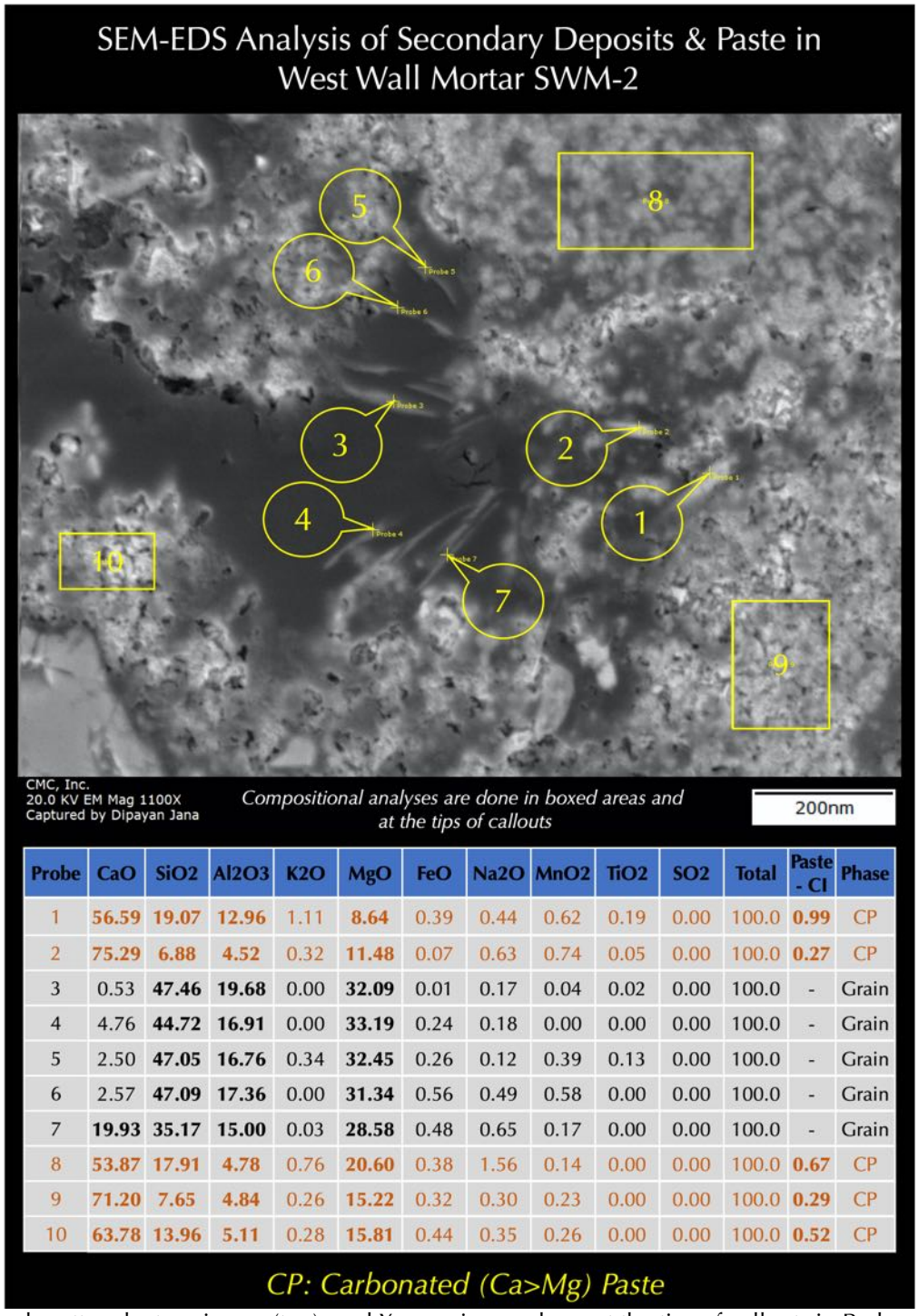

Probe	CaO	SiO2	Al2O3	K2O	MgO	FeO	Na2O	MnO2	TiO2	SO2	Total	Paste - CI	Phase
1	**56.59**	**19.07**	**12.96**	1.11	**8.64**	0.39	0.44	0.62	0.19	0.00	100.0	**0.99**	CP
2	**75.29**	**6.88**	**4.52**	0.32	**11.48**	0.07	0.63	0.74	0.05	0.00	100.0	**0.27**	CP
3	0.53	**47.46**	**19.68**	0.00	**32.09**	0.01	0.17	0.04	0.02	0.00	100.0	-	Grain
4	4.76	**44.72**	**16.91**	0.00	**33.19**	0.24	0.18	0.00	0.00	0.00	100.0	-	Grain
5	2.50	**47.05**	**16.76**	0.34	**32.45**	0.26	0.12	0.39	0.13	0.00	100.0	-	Grain
6	2.57	**47.09**	**17.36**	0.00	**31.34**	0.56	0.49	0.58	0.00	0.00	100.0	-	Grain
7	**19.93**	**35.17**	**15.00**	0.03	**28.58**	0.48	0.65	0.17	0.00	0.00	100.0	-	Grain
8	**53.87**	**17.91**	**4.78**	0.76	**20.60**	0.38	1.56	0.14	0.00	0.00	100.0	**0.67**	CP
9	**71.20**	**7.65**	**4.84**	0.26	**15.22**	0.32	0.30	0.23	0.00	0.00	100.0	**0.29**	CP
10	**63.78**	**13.96**	**5.11**	0.28	**15.81**	0.44	0.35	0.26	0.00	0.00	100.0	**0.52**	CP

CP: Carbonated (Ca>Mg) Paste

Figure 144: Backscatter electron image (top), and X-ray microanalyses at the tips of callouts in Probes 1 through 10 of setting mortar SWM-2 detecting compositional variations across secondary deposits in a void space and in adjacent carbonated paste. Paste composition is presented (bottom) as oxide variations of all detected EDS peaks normalized to 100% except carbon (from epoxy) and gold (from coating). Paste cementation indices, CI (after Eckel 1922) measure: (a) relative hydraulicity of paste e.g., non-hydraulic lime pastes have very low CI (< 0.50) compared to cement-based pastes (CI is >1), along with (b) the degree of leaching of lime, where leached paste characteristically show >>1 CI, and non-leached portions of paste show <1 CI from lime and its carbonated products. The cementation indices (CI) of paste are calculated after Eckel (1922) as CI = $[(2.8*SiO_2)+(1.1*Al_2O_3)+(0.7*\ Fe_2O_3)]/[(CaO)+(1.4*MgO)]$.

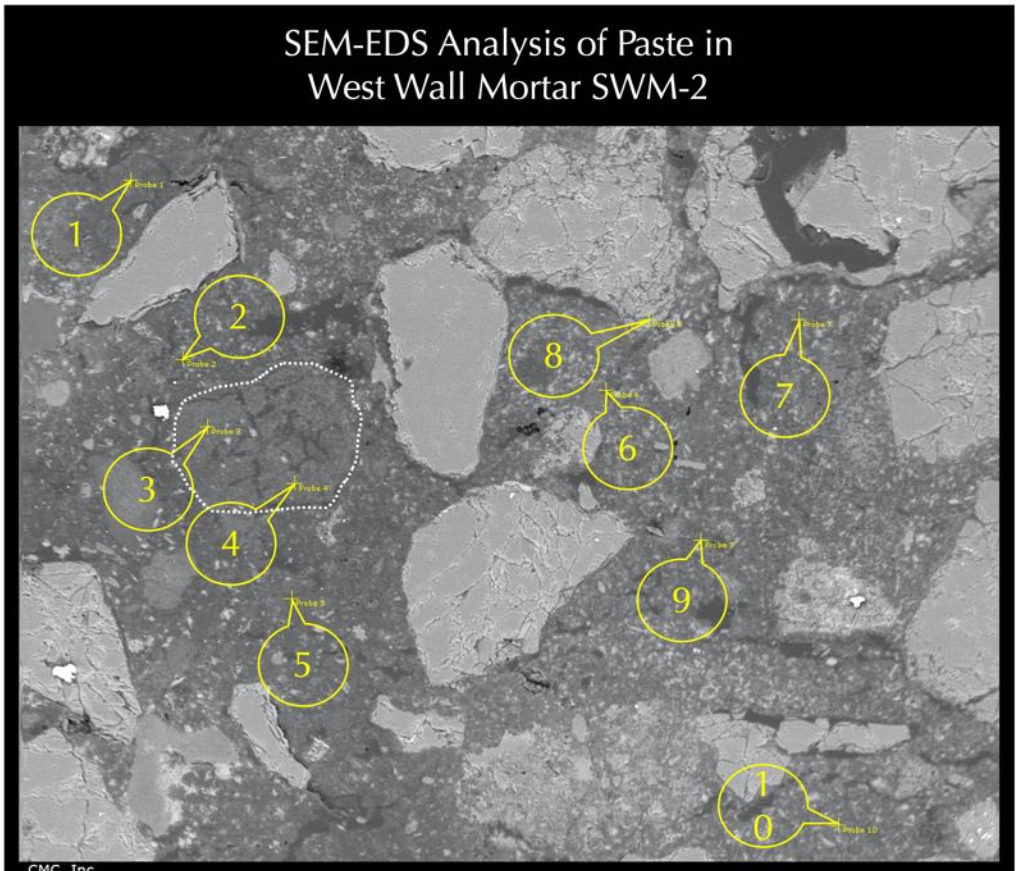

Probe	CaO	SiO2	Al2O3	K2O	MgO	FeO	Na2O	MnO2	TiO2	SO2	Total	Paste - CI	Phase
1	27.39	37.62	5.85	0.22	28.03	0.61	0.21	0.07	0.00	0.00	100.0	1.68	P
2	29.15	30.44	9.65	0.13	29.12	0.56	0.58	0.09	0.28	0.00	100.0	1.38	P
3	14.29	47.60	5.96	0.01	31.27	0.37	0.00	0.50	0.01	0.00	100.0	2.41	P
4	10.30	49.91	7.09	0.00	31.81	0.52	0.13	0.25	0.00	0.00	100.0	2.70	P
5	0.37	54.89	11.41	0.03	32.98	0.12	0.01	0.13	0.05	0.00	100.0	3.57	P
6	17.49	33.80	14.97	0.20	32.03	0.85	0.22	0.44	0.00	0.00	100.0	1.79	P
7	21.87	28.62	16.22	0.10	31.68	0.97	0.05	0.41	0.09	0.00	100.0	1.49	P
8	0.30	98.21	0.86	0.00	0.38	0.00	0.14	0.11	0.00	0.00	100.0	-	Quartz
9	21.29	33.70	15.60	0.52	24.72	1.63	0.07	0.70	1.79	0.00	100.0	2.02	P
10	23.02	30.37	15.42	0.39	29.13	1.02	0.25	0.16	0.24	0.00	100.0	1.61	P

P: Carbonated paste of calcined clay and dolomitic lime

Figure 145: Backscatter electron image (top), and X-ray microanalyses at the tips of callouts in Probes 1 through 10 of setting mortar SWM-2 detecting compositional variations across variably leached paste. Paste composition is presented (bottom) as oxide variations of all detected EDS peaks normalized to 100% except carbon (from epoxy) and gold (from coating). Paste cementation indices, CI (after Eckel 1922) measure: (a) relative hydraulicity of paste e.g., non-hydraulic lime pastes have very low CI (< 0.50) compared to cement-based pastes (CI is >1), along with (b) the degree of leaching of lime, where leached paste characteristically show >>1 CI, and non-leached portions of paste show <1 CI from lime and its carbonated products. The cementation indices (CI) of paste are calculated after Eckel (1922) as CI = $[(2.8*SiO_2)+(1.1*Al_2O_3)+(0.7*\ Fe_2O_3)]/[(CaO)+(1.4*MgO)]$.

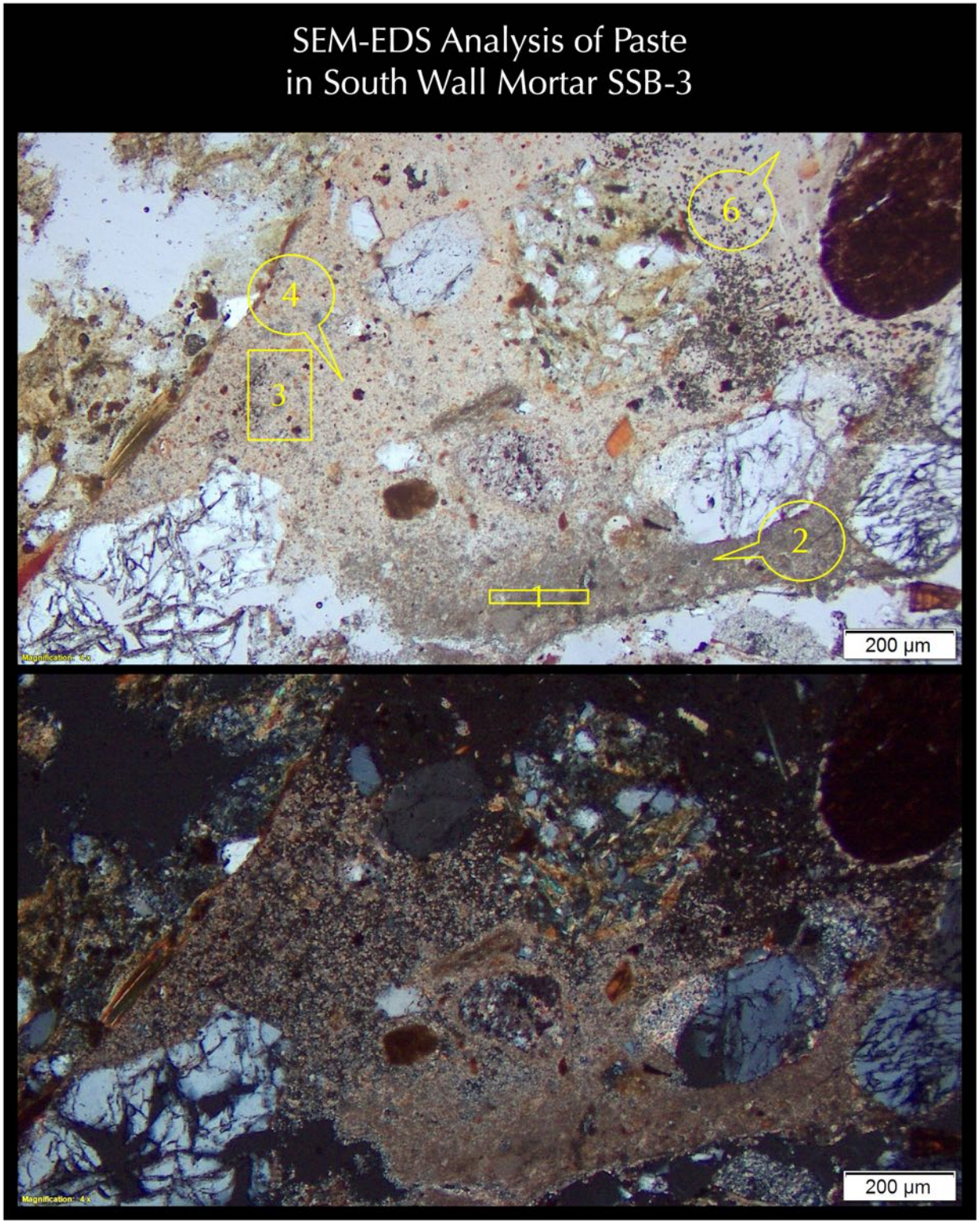

Figure 146: Optical micrographs of setting mortar SSB-3 showing points at the tips of callouts and boxes across various areas, which are analyzed in SEM-EDS for major element oxide compositions.

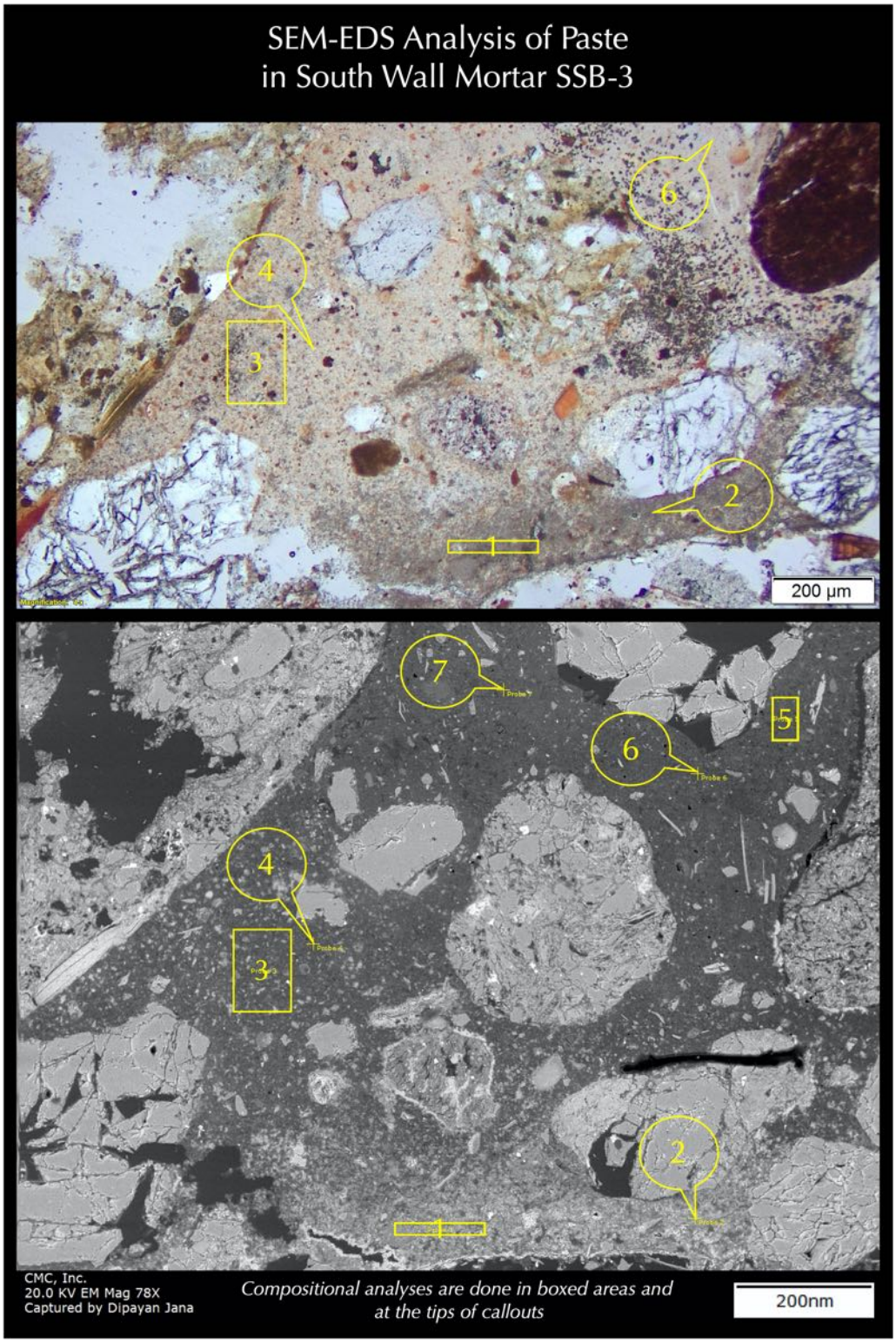

Figure 147: Optical micrograph (top) and corresponding backscatter electron micrograph (bottom) of setting mortar SSB-3 showing points at the tips of callouts and boxed areas across various areas in paste, which are analyzed in SEM-EDS for major element oxide compositions. Positions of tips of callouts and boxed areas in the optical micrograph are only approximate to the actual ones shown in the electron micrograph.

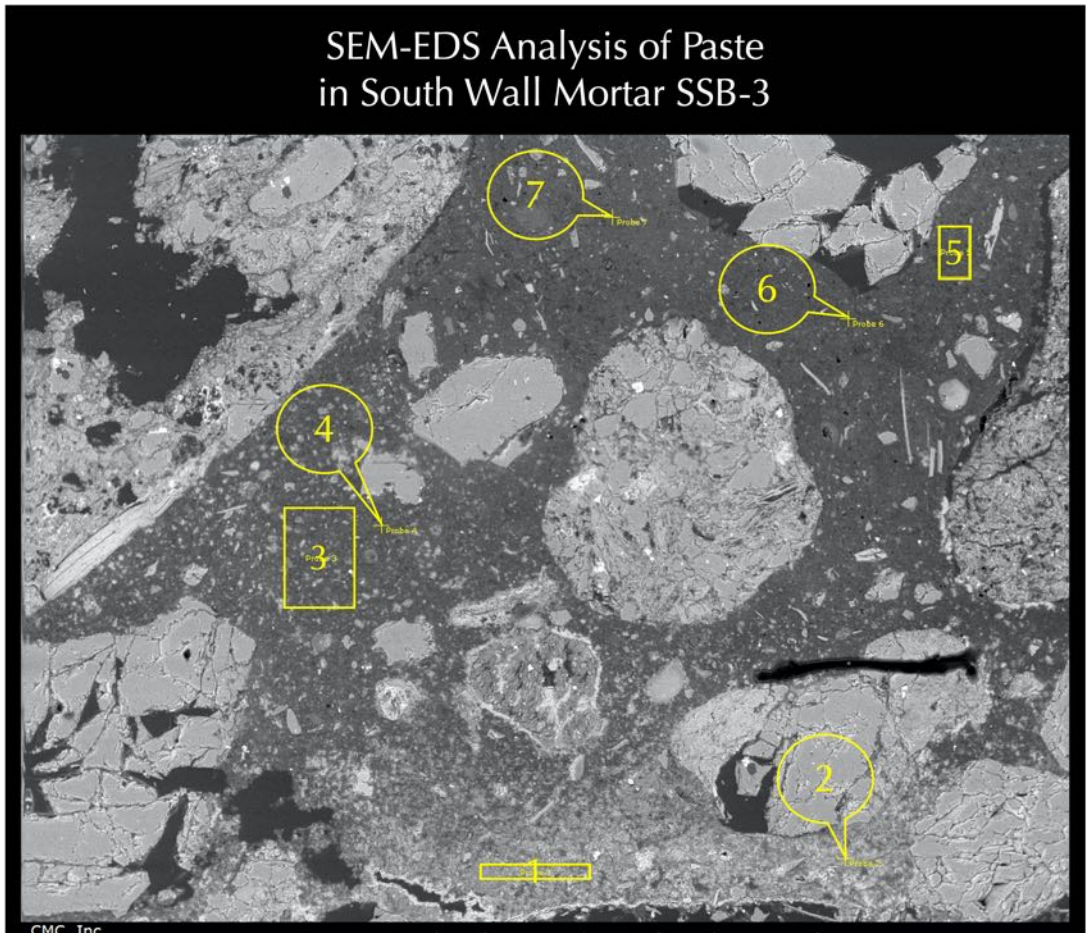

Probe	CaO	SiO2	Al2O3	K2O	MgO	FeO	Na2O	MnO2	TiO2	SO2	Total	Paste - CI	Phase
1	51.28	16.12	12.41	0.44	17.91	0.68	0.22	0.73	0.22	0.00	100.0	0.78	CP
2	9.68	30.66	27.01	0.15	30.71	0.95	0.17	0.63	0.04	0.00	100.0	2.21	LP
3	7.75	34.72	27.46	0.28	28.13	1.18	0.19	0.08	0.22	0.00	100.0	2.72	LP
4	14.28	37.25	22.21	0.30	24.11	1.17	0.19	0.33	0.16	0.00	100.0	2.70	LP
5	0.38	37.84	29.61	0.30	30.24	0.84	0.22	0.17	0.39	0.00	100.0	3.26	LP
6	0.32	37.68	29.88	0.57	29.34	1.01	0.26	0.64	0.30	0.00	100.0	3.36	LP
7	0.49	42.48	26.16	0.44	29.19	1.11	0.08	0.02	0.03	0.00	100.0	3.59	LP

CP: Carbonated (Ca>Mg) Paste; LP: Leached (Mg-Si-Al) Paste

Figure 148: Backscatter electron image (top), and X-ray microanalyses at the tips of callouts and boxed areas in Probes 1 through 7 of setting mortar SSB-3 detecting compositional variations across variably leached and carbonated paste. Paste composition is presented (bottom) as oxide variations of all detected EDS peaks normalized to 100% except carbon (from epoxy) and gold (from coating). Paste cementation indices, CI (after Eckel 1922) measure: (a) relative hydraulicity of paste e.g., non-hydraulic lime pastes have very low CI (< 0.50) compared to cement-based pastes (CI is >1), along with (b) the degree of leaching of lime, where leached paste characteristically show >>1 CI, and non-leached portions of paste show <1 CI from lime and its carbonated products. The cementation indices (CI) of paste are calculated after Eckel (1922) as CI = $[(2.8*SiO_2)+(1.1*Al_2O_3)+(0.7*Fe_2O_3)]/[(CaO)+(1.4*MgO)]$.

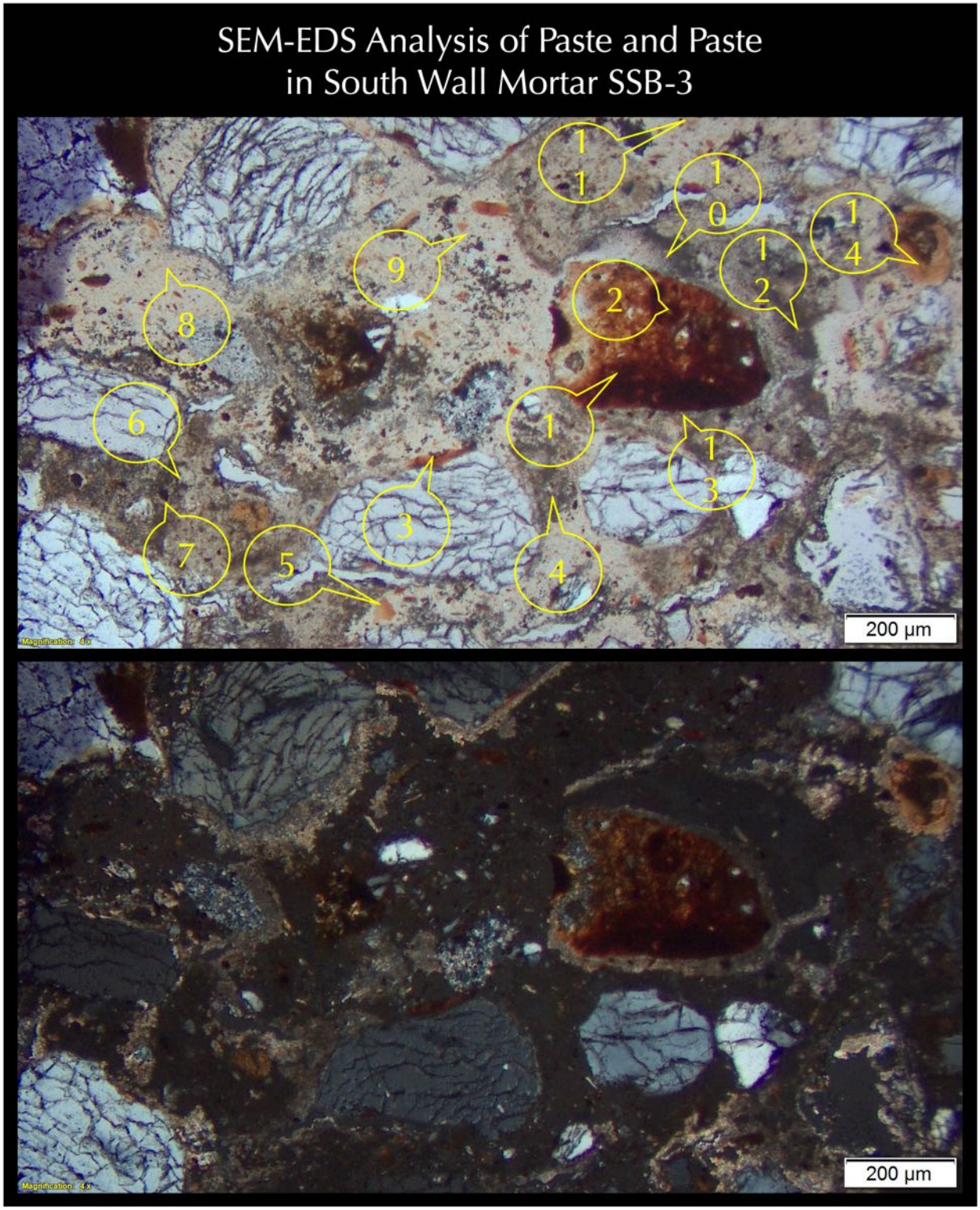

Figure 149: Optical micrographs of setting mortar SSB-3 showing points at the tips of callouts across various areas, which are analyzed in SEM-EDS for major element oxide compositions. Probes 1 and 2 are from a residual calcined clay (brick dust) grain.

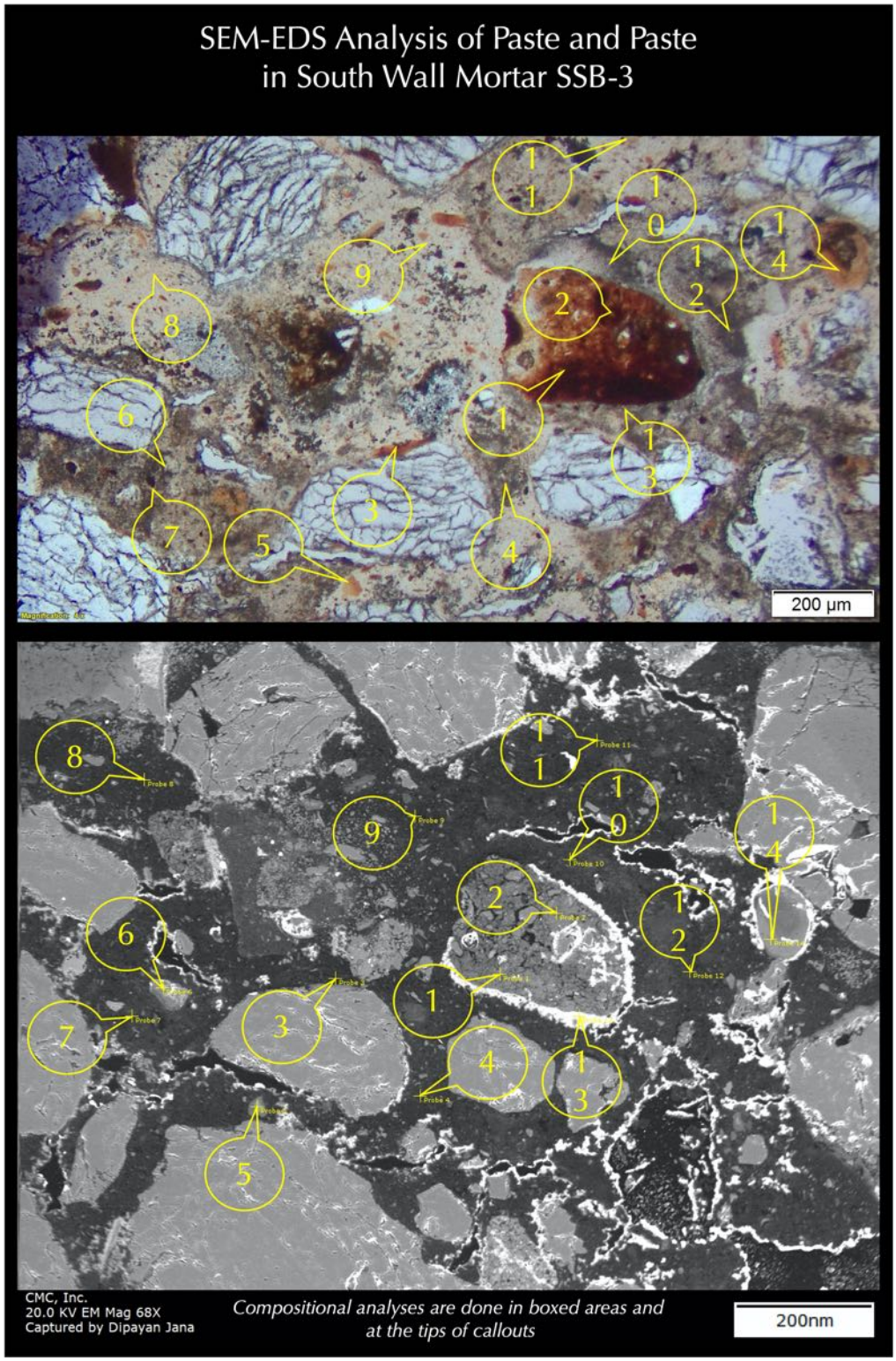

Figure 150: Optical micrograph (top) and corresponding secondary electron micrograph (bottom) of setting mortar SSB-3 showing points at the tips of callouts across various areas in paste, reddish-brown grain, and reddish-brown coats, which are analyzed in SEM-EDS for major element oxide compositions. Positions of tips of callouts in the optical micrograph are only approximate to the actual ones shown in the electron micrograph.

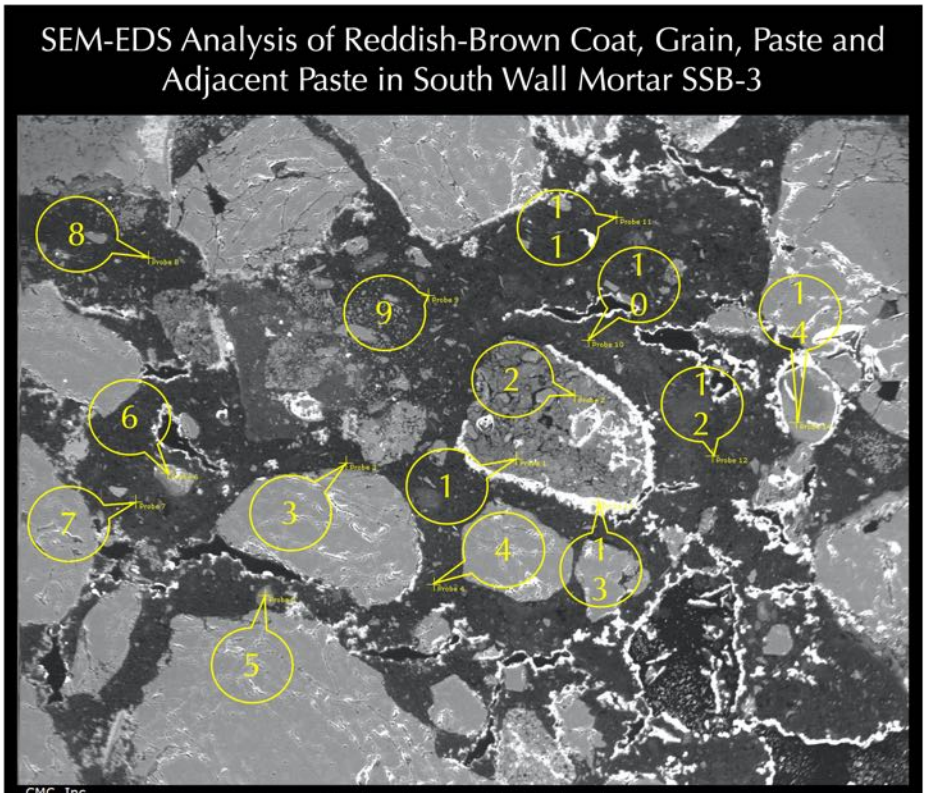

Probe	CaO	SiO2	Al2O3	K2O	MgO	FeO	Na2O	MnO2	TiO2	SO2	Total	Paste - CI	Phase
1	0.98	**57.50**	**22.27**	3.07	8.03	6.52	0.14	0.68	0.80	0.00	100.0	-	Grain
2	0.77	**62.88**	**18.63**	2.76	**11.42**	2.70	0.17	0.31	0.37	0.00	100.0	-	Grain
3	0.51	**37.23**	**29.96**	0.20	**29.93**	1.48	0.34	0.00	0.33	0.00	100.0	3.26	Coat
4	1.14	**49.50**	**22.61**	0.83	**21.71**	1.43	2.19	0.56	0.04	0.00	100.0	**5.22**	LP
5	7.82	**54.63**	**24.06**	0.54	7.87	4.01	0.35	0.17	0.54	0.00	100.0	-	Grain
6	29.80	**39.09**	**18.04**	1.04	8.88	2.10	0.35	0.37	0.33	0.00	100.0	3.10	Grain
7	0.62	**47.67**	**25.40**	0.41	**23.45**	1.56	0.08	0.00	0.81	0.00	100.0	**4.86**	LP
8	0.64	**37.98**	**29.44**	0.15	**29.25**	1.92	0.07	0.41	0.13	0.00	100.0	**3.37**	LP
9	0.81	**45.21**	**26.29**	0.30	**23.96**	2.09	0.00	1.01	0.34	0.00	100.0	**4.57**	LP
10	0.33	**20.08**	**38.09**	0.02	**40.49**	0.66	0.00	0.34	0.00	0.00	100.0	**1.73**	LP
11	0.22	**45.09**	**24.36**	0.00	**29.31**	0.95	0.06	0.00	0.00	0.00	100.0	**3.73**	LP
12	0.40	**35.61**	**28.71**	0.04	**33.44**	1.22	0.00	0.44	0.14	0.00	100.0	**2.80**	LP
13	0.56	**46.86**	**26.08**	0.36	**23.71**	1.56	0.19	0.38	0.30	0.00	100.0	**4.77**	LP
14	6.85	**55.73**	**22.76**	0.82	7.80	4.15	0.24	1.06	0.59	0.00	100.0	-	Grain

LP: Leached (Ca<Mg) Paste

Figure 151: Secondary electron image (top), and X-ray microanalyses at the tips of callouts in Probes 1 through 14 of setting mortar SSB-3 detecting compositional variations across leached paste and reddish-brown grains. Paste composition is presented (bottom) as oxide variations of all detected EDS peaks normalized to 100% except carbon (from epoxy) and gold (from coating). Paste cementation indices, CI (after Eckel 1922) measure: (a) relative hydraulicity of paste e.g., non-hydraulic lime pastes have very low CI (< 0.50) compared to cement-based pastes (CI is >1), along with (b) the degree of leaching of lime, where leached paste characteristically show >>1 CI, and non-leached portions of paste show <1 CI from lime and its carbonated products. The cementation indices (CI) of paste are calculated after Eckel (1922) as CI = $[(2.8*SiO_2)+(1.1*Al_2O_3)+(0.7*\ Fe_2O_3)]/[(CaO)+(1.4*MgO)]$.

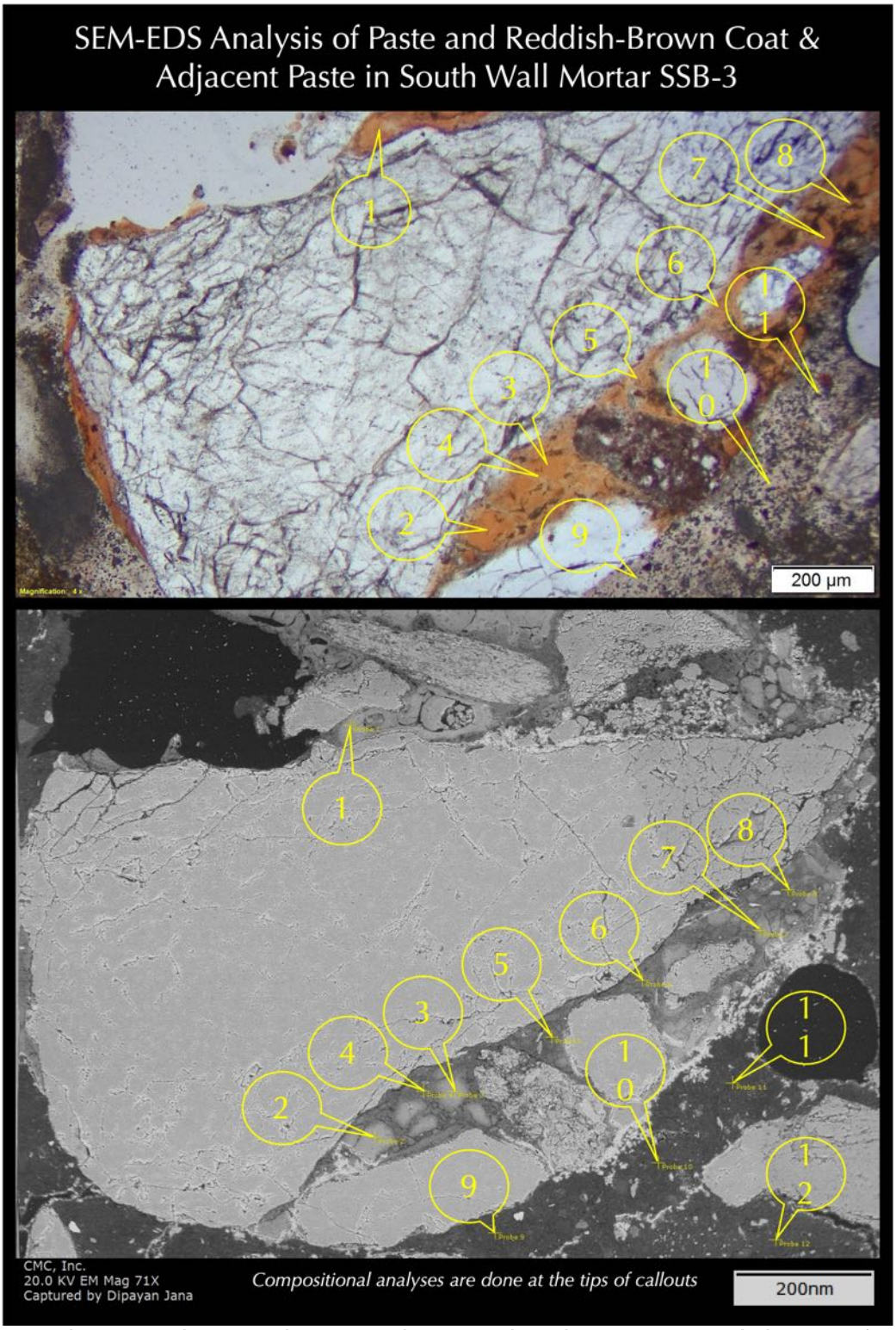

Figure 152: Optical micrograph (top) and corresponding secondary electron micrograph (bottom) of setting mortar SSB-3 showing points at the tips of callouts across various areas in a reddish-brown coat and adjacent paste, which are analyzed in SEM-EDS for major element oxide compositions. Positions of tips of callouts in the optical micrograph are only approximate to the actual ones shown in the electron micrograph.

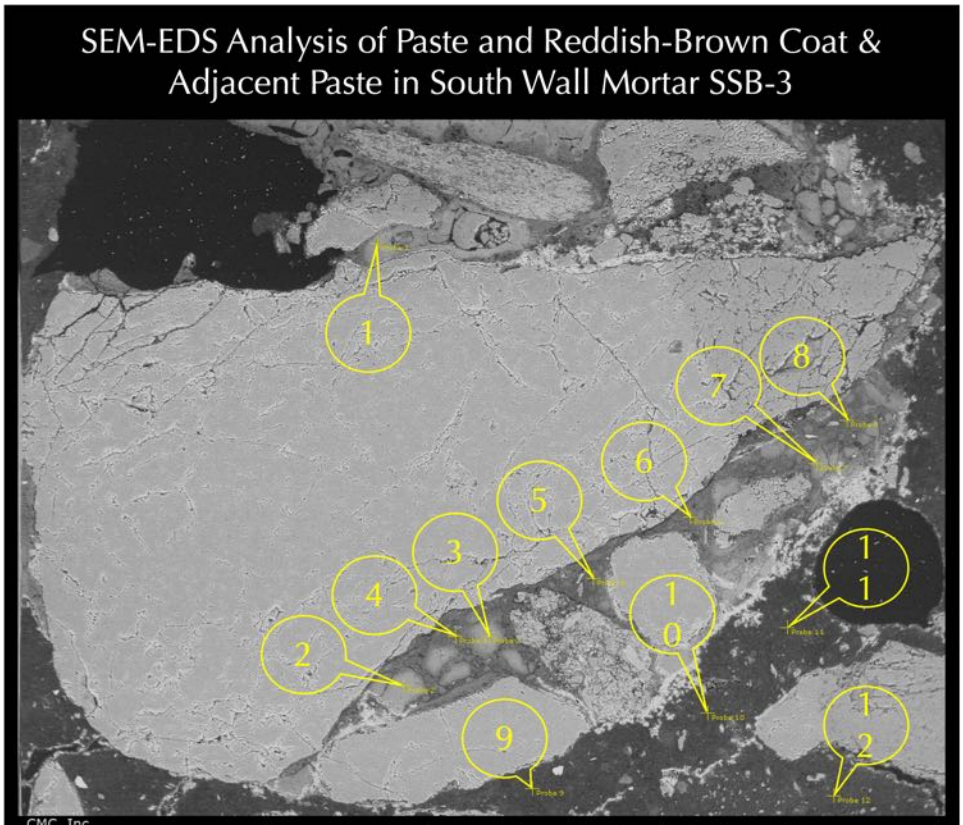

Probe	CaO	SiO2	Al2O3	K2O	MgO	FeO	Na2O	MnO2	TiO2	SO2	Total	Paste - CI	Phase
1	9.87	53.50	23.07	0.69	7.91	3.67	0.46	0.31	0.54	0.00	100.0	-	Coat
2	9.99	53.99	23.43	0.69	5.62	4.71	0.42	0.43	0.71	0.00	100.0	-	Coat
3	9.62	55.00	23.48	0.91	5.65	4.47	0.29	0.15	0.43	0.00	100.0	-	Coat
4	1.35	59.40	19.73	0.82	15.19	2.58	0.25	0.47	0.19	0.00	100.0	-	Coat
5	2.18	59.22	19.30	0.63	13.78	3.63	0.29	0.42	0.55	0.00	100.0	-	Coat
6	1.92	58.52	19.74	1.05	14.47	3.33	0.11	0.42	0.43	0.00	100.0	-	Coat
7	7.59	55.63	22.61	0.63	8.47	3.73	0.35	0.41	0.57	0.00	100.0	-	Coat
8	2.57	56.86	23.78	0.97	10.02	4.37	0.24	0.28	0.91	0.00	100.0	-	Coat
9	0.35	38.71	28.67	0.17	31.01	0.85	0.00	0.24	0.00	0.00	100.0	3.21	LP
10	0.54	45.16	22.92	0.00	30.59	0.60	0.00	0.11	0.07	0.00	100.0	3.51	LP
11	0.50	47.67	22.62	0.08	28.16	0.72	0.04	0.06	0.14	0.00	100.0	3.98	LP
12	0.30	46.56	21.38	0.00	31.15	0.19	0.02	0.28	0.13	0.00	100.0	3.51	LP

LP: Leached (Ca<Mg) Paste

Figure 153: Backscatter electron image (top), and X-ray microanalyses at the tips of callouts in Probes 1 through 12 of setting mortar SSB-3 detecting compositional variations across a reddish-brown coat and adjacent leached paste. Paste composition is presented (bottom) as oxide variations of all detected EDS peaks normalized to 100% except carbon (from epoxy) and gold (from coating). Paste cementation indices, CI (after Eckel 1922) measure: (a) relative hydraulicity of paste e.g., non-hydraulic lime pastes have very low CI (< 0.50) compared to cement-based pastes (CI is >1), along with (b) the degree of leaching of lime, where leached paste characteristically show >>1 CI, and non-leached portions of paste show <1 CI from lime and its carbonated products. The cementation indices (CI) of paste are calculated after Eckel (1922) as CI = $[(2.8*SiO_2)+(1.1*Al_2O_3)+(0.7*\ Fe_2O_3)]/[(CaO)+(1.4*MgO)]$.

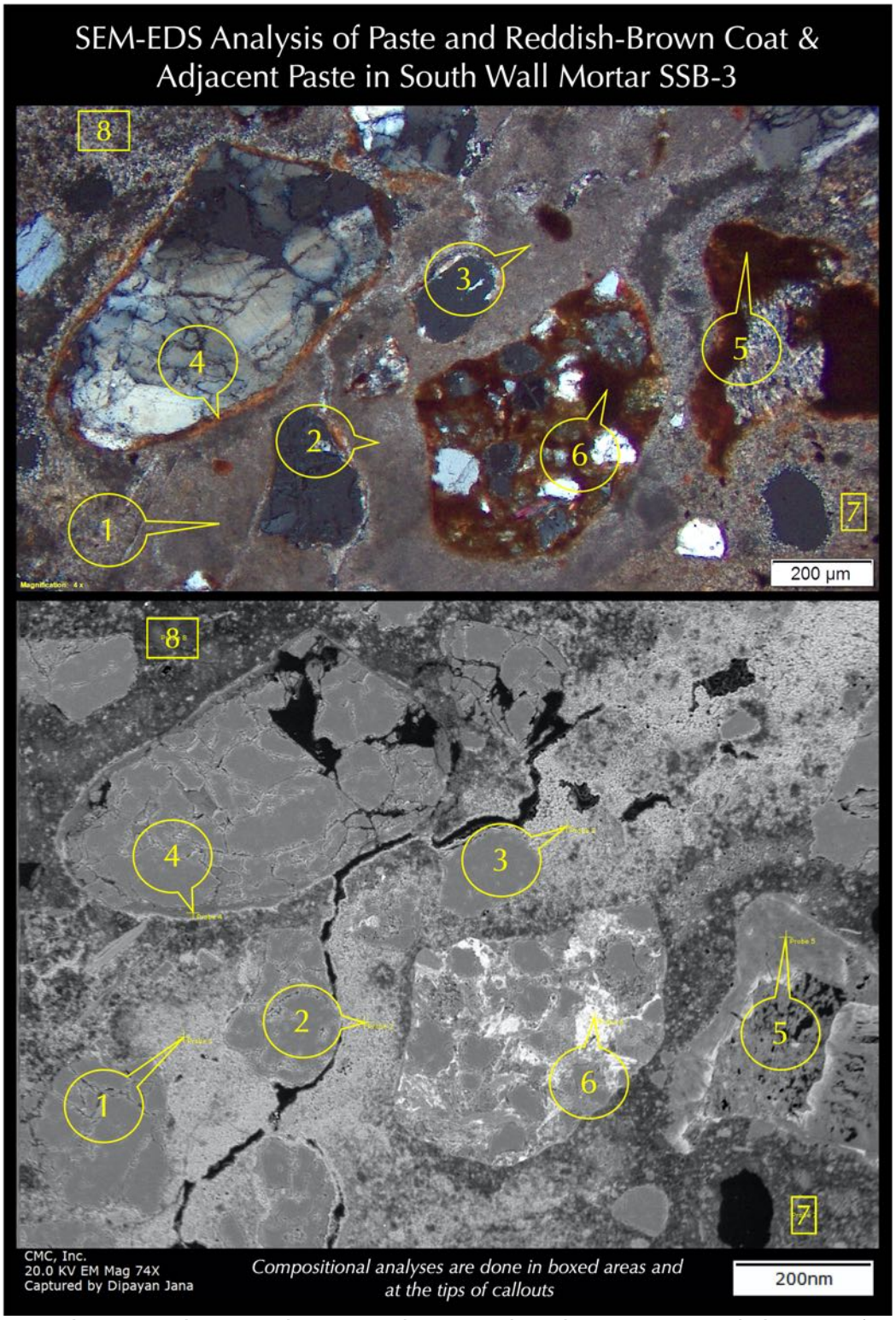

Figure 154: Optical micrograph (top) and corresponding secondary electron micrograph (bottom) of setting mortar SSB-3 showing points at the tips of callouts and boxes across various areas in paste, reddish-brown grain, and reddish-brown coats, which are analyzed in SEM-EDS for major element oxide compositions. Positions of tips of callouts in the optical micrograph are only approximate to the actual ones shown in the electron micrograph.

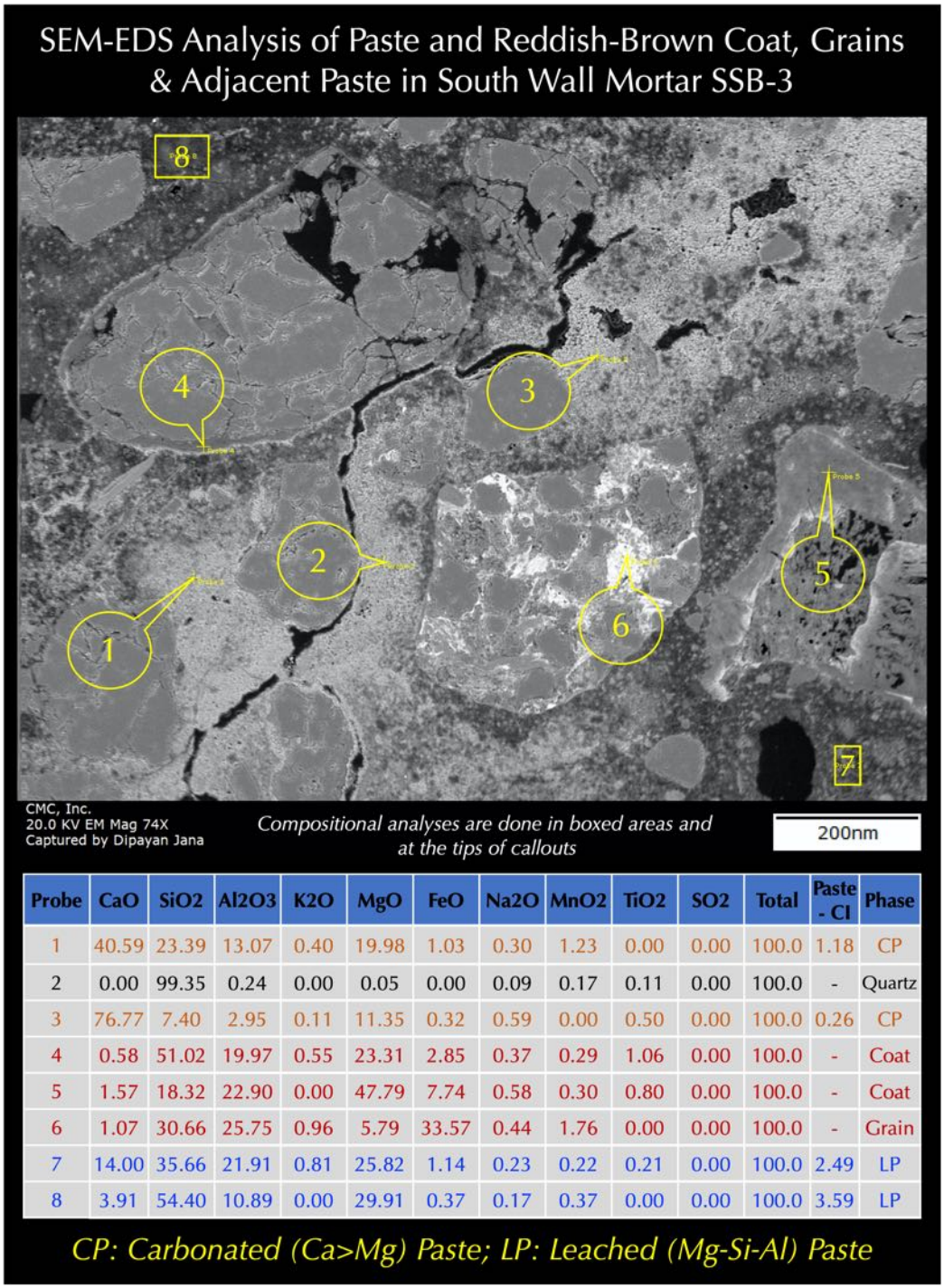

Probe	CaO	SiO2	Al2O3	K2O	MgO	FeO	Na2O	MnO2	TiO2	SO2	Total	Paste - CI	Phase
1	40.59	23.39	13.07	0.40	19.98	1.03	0.30	1.23	0.00	0.00	100.0	1.18	CP
2	0.00	99.35	0.24	0.00	0.05	0.00	0.09	0.17	0.11	0.00	100.0	-	Quartz
3	76.77	7.40	2.95	0.11	11.35	0.32	0.59	0.00	0.50	0.00	100.0	0.26	CP
4	0.58	51.02	19.97	0.55	23.31	2.85	0.37	0.29	1.06	0.00	100.0	-	Coat
5	1.57	18.32	22.90	0.00	47.79	7.74	0.58	0.30	0.80	0.00	100.0	-	Coat
6	1.07	30.66	25.75	0.96	5.79	33.57	0.44	1.76	0.00	0.00	100.0	-	Grain
7	14.00	35.66	21.91	0.81	25.82	1.14	0.23	0.22	0.21	0.00	100.0	2.49	LP
8	3.91	54.40	10.89	0.00	29.91	0.37	0.17	0.37	0.00	0.00	100.0	3.59	LP

CP: Carbonated (Ca>Mg) Paste; LP: Leached (Mg-Si-Al) Paste

Figure 155: Backscatter electron image (top), and X-ray microanalyses at the tips of callouts and boxed areas in Probes 1 through 8 of setting mortar SSB-3 detecting compositional variations across variably leached and carbonated paste, reddish-brown coats and reddish-brown grains. Paste composition is presented (bottom) as oxide variations of all detected EDS peaks normalized to 100% except carbon (from epoxy) and gold (from coating). Paste cementation indices, CI (after Eckel 1922) measure: (a) relative hydraulicity of paste e.g., non-hydraulic lime pastes have very low CI (< 0.50) compared to cement-based pastes (CI is >1), along with (b) the degree of leaching of lime, where leached paste characteristically show >>1 CI, and non-leached portions of paste show <1 CI from lime and its carbonated products. The cementation indices (CI) of paste are calculated after Eckel (1922) as CI = $[(2.8*SiO_2)+(1.1*Al_2O_3)+(0.7*\ Fe_2O_3)]/[(CaO)+(1.4*MgO)]$.

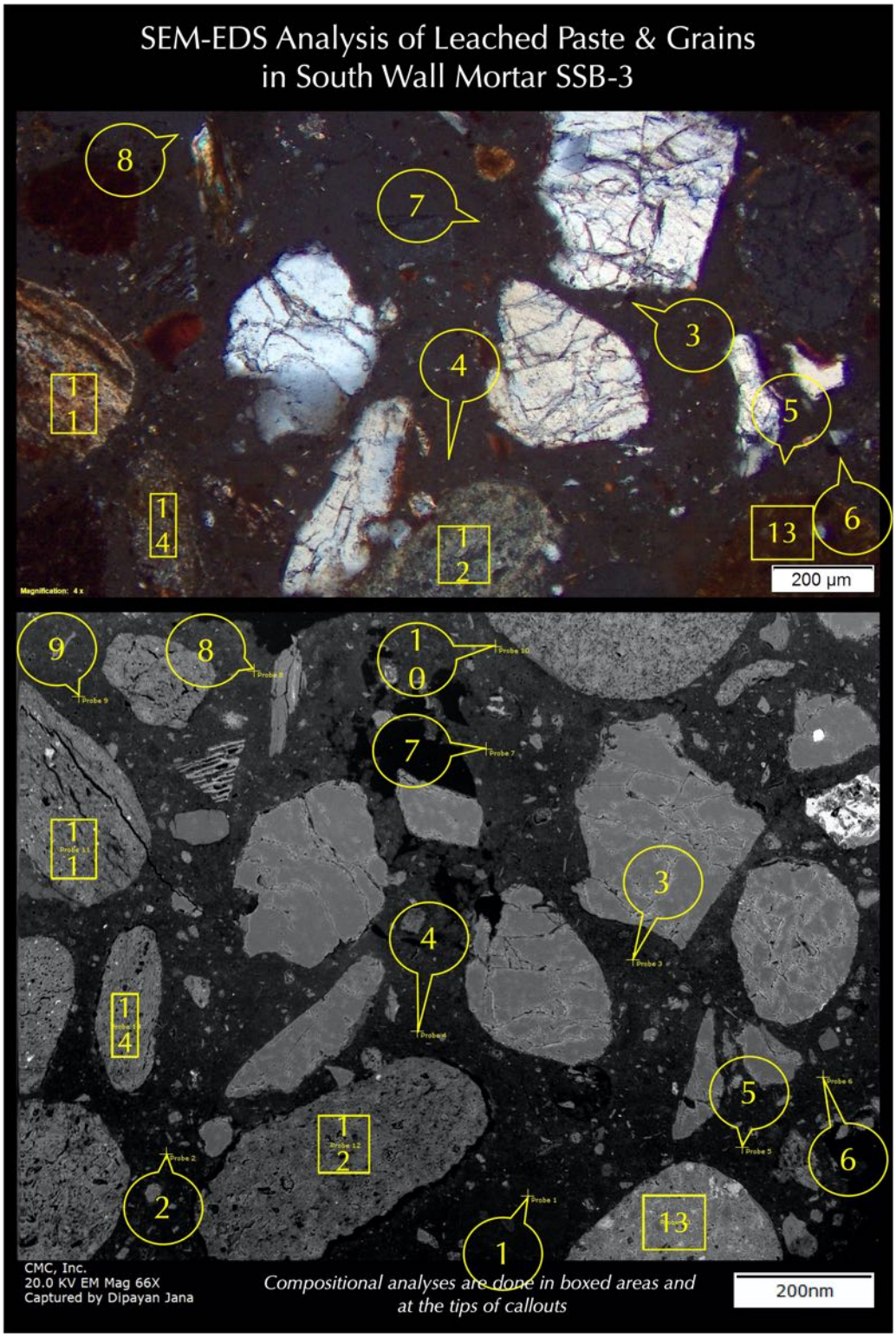

Figure 156: Optical micrograph (top) and corresponding secondary electron micrograph (bottom) of setting mortar SSB-3 showing points at the tips of callouts and boxes across various areas in leached paste (Probe 1 to 10) and shale grains (Probe 11 to 14), which are analyzed in SEM-EDS for major element oxide compositions. Positions of tips of callouts in the optical micrograph are only approximate to the actual ones shown in the electron micrograph.

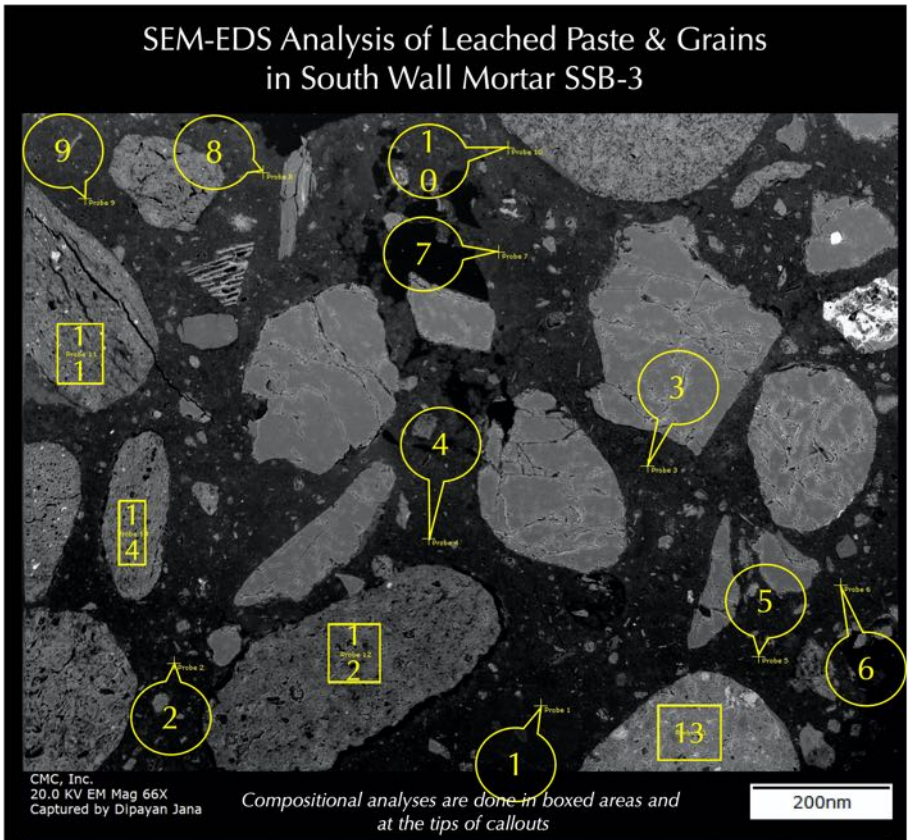

Probe	CaO	SiO2	Al2O3	K2O	MgO	FeO	Na2O	MnO2	TiO2	SO2	Total	Paste - CI	Phase
1	0.08	**39.24**	**24.13**	0.00	**35.79**	0.41	0.00	0.23	0.12	0.00	100.0	**2.72**	LP
2	0.48	**48.15**	**19.66**	0.35	**29.51**	1.25	0.25	0.03	0.32	0.00	100.0	**3.76**	LP
3	0.30	**51.72**	**15.95**	0.00	**30.70**	0.94	0.06	0.32	0.00	0.00	100.0	**3.77**	LP
4	0.17	**49.26**	**18.06**	0.18	**30.40**	0.76	0.00	1.07	0.09	0.00	100.0	**3.71**	LP
5	0.27	**48.37**	**19.14**	0.19	**30.28**	1.21	0.00	0.28	0.26	0.00	100.0	**3.69**	LP
6	0.21	**44.16**	**20.84**	0.31	**32.39**	1.37	0.27	0.38	0.06	0.00	100.0	**3.24**	LP
7	0.10	**54.55**	**13.62**	0.00	**30.83**	0.56	0.00	0.32	0.01	0.00	100.0	**3.89**	LP
8	0.23	**49.98**	**17.19**	0.19	**31.69**	0.56	0.06	0.05	0.05	0.00	100.0	**3.57**	LP
9	0.19	**46.90**	**19.71**	0.02	**31.99**	0.91	0.13	0.15	0.00	0.00	100.0	**3.42**	LP
10	0.35	**56.32**	**12.17**	0.11	**30.02**	0.55	0.16	0.25	0.05	0.00	100.0	**4.05**	LP
11	0.52	**61.14**	**21.93**	**2.97**	**10.48**	1.32	0.31	0.22	1.11	0.00	100.0	-	Shale
12	0.52	**62.54**	**16.45**	**2.98**	**15.67**	1.16	0.21	0.07	0.40	0.00	100.0	-	Shale
13	0.60	**66.63**	**20.49**	**3.25**	**3.90**	3.63	0.38	0.24	0.89	0.00	100.0	-	Shale
14	0.58	**63.56**	**21.12**	**3.71**	**8.82**	1.05	0.32	0.41	0.44	0.00	100.0	-	Shale

Figure 157: Backscatter electron image (top), and X-ray microanalyses at the tips of callouts and boxed areas in Probes 1 through 14 of setting mortar SSB-3 detecting compositional variations across leached paste (Probe 1 to 10) and shale grains (Probe 11 to 14). Paste composition is presented (bottom) as oxide variations of all detected EDS peaks normalized to 100% except carbon (from epoxy) and gold (from coating). Paste cementation indices, CI (after Eckel 1922) measure: (a) relative hydraulicity of paste e.g., non-hydraulic lime pastes have very low CI (< 0.50) compared to cement-based pastes (CI is >1), along with (b) the degree of leaching of lime, where leached paste characteristically show >>1 CI, and non-leached portions of paste show <1 CI from lime and its carbonated products. The cementation indices (CI) of paste are calculated after Eckel (1922) as CI = $[(2.8*SiO_2)+(1.1*Al_2O_3)+(0.7*\ Fe_2O_3)]/[(CaO)+(1.4*MgO)]$.

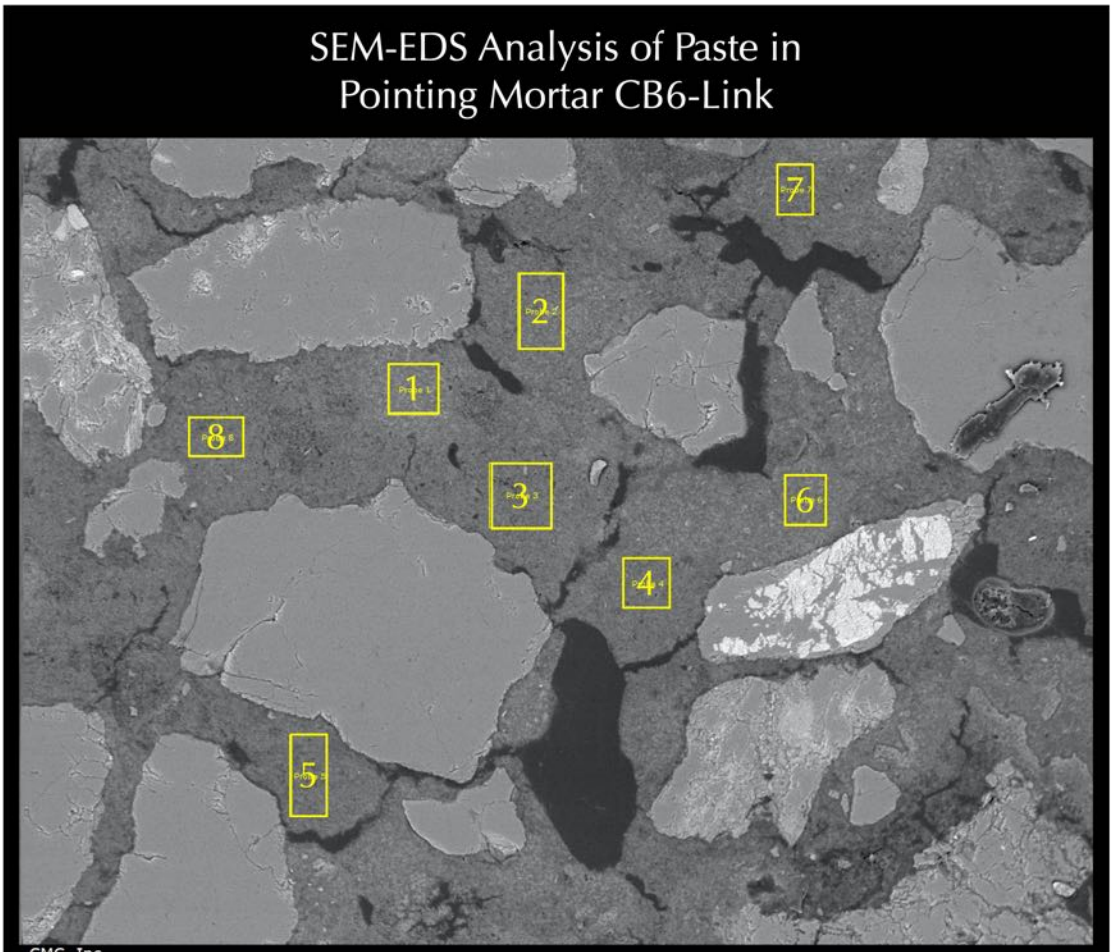

Probe	CaO	SiO2	Al2O3	K2O	MgO	FeO	Na2O	MnO2	TiO2	SO2	Total	Paste - CI	Phase
1	**32.30**	**11.69**	1.15	0.25	**53.98**	0.30	0.19	0.05	0.08	0.00	100.0	**0.32**	P
2	**34.26**	**9.74**	1.70	0.23	**52.97**	0.43	0.28	0.39	0.00	0.00	100.0	**0.27**	P
3	**33.88**	**10.94**	2.05	0.36	**51.51**	0.34	0.31	0.41	0.20	0.00	100.0	**0.31**	P
4	**35.62**	**10.45**	1.99	0.18	**50.89**	0.35	0.36	0.00	0.16	0.00	100.0	**0.30**	P
5	**32.89**	**12.26**	2.10	0.38	**50.74**	0.48	0.42	0.60	0.13	0.00	100.0	**0.36**	P
6	**31.81**	**8.66**	1.40	0.09	**56.89**	0.44	0.35	0.24	0.11	0.00	100.0	**0.23**	P
7	**35.53**	**10.43**	0.96	0.24	**51.71**	0.31	0.75	0.03	0.03	0.00	100.0	**0.28**	P
8	**33.16**	**10.67**	1.03	0.00	**54.02**	0.27	0.27	0.57	0.00	0.00	100.0	**0.29**	P

Figure 158: Backscatter electron image (top), and X-ray microanalyses at the boxed areas in Probes 1 through 8 of pointing mortar CB6-Link detecting compositional variations of paste. Paste composition is presented (bottom) as oxide variations of all detected EDS peaks normalized to 100% except carbon (from epoxy) and gold (from coating). Paste cementation indices, CI (after Eckel 1922) measure: (a) relative hydraulicity of paste e.g., non-hydraulic lime pastes have very low CI (< 0.50) compared to cement-based pastes (CI is >1), along with (b) the degree of leaching of lime, where leached paste characteristically show >>1 CI, and non-leached portions of paste show <1 CI from lime and its carbonated products. The cementation indices (CI) of paste are calculated after Eckel (1922) as CI = $[(2.8*SiO_2)+(1.1*Al_2O_3)+(0.7*\ Fe_2O_3)]/[(CaO)+(1.4*MgO)]$.

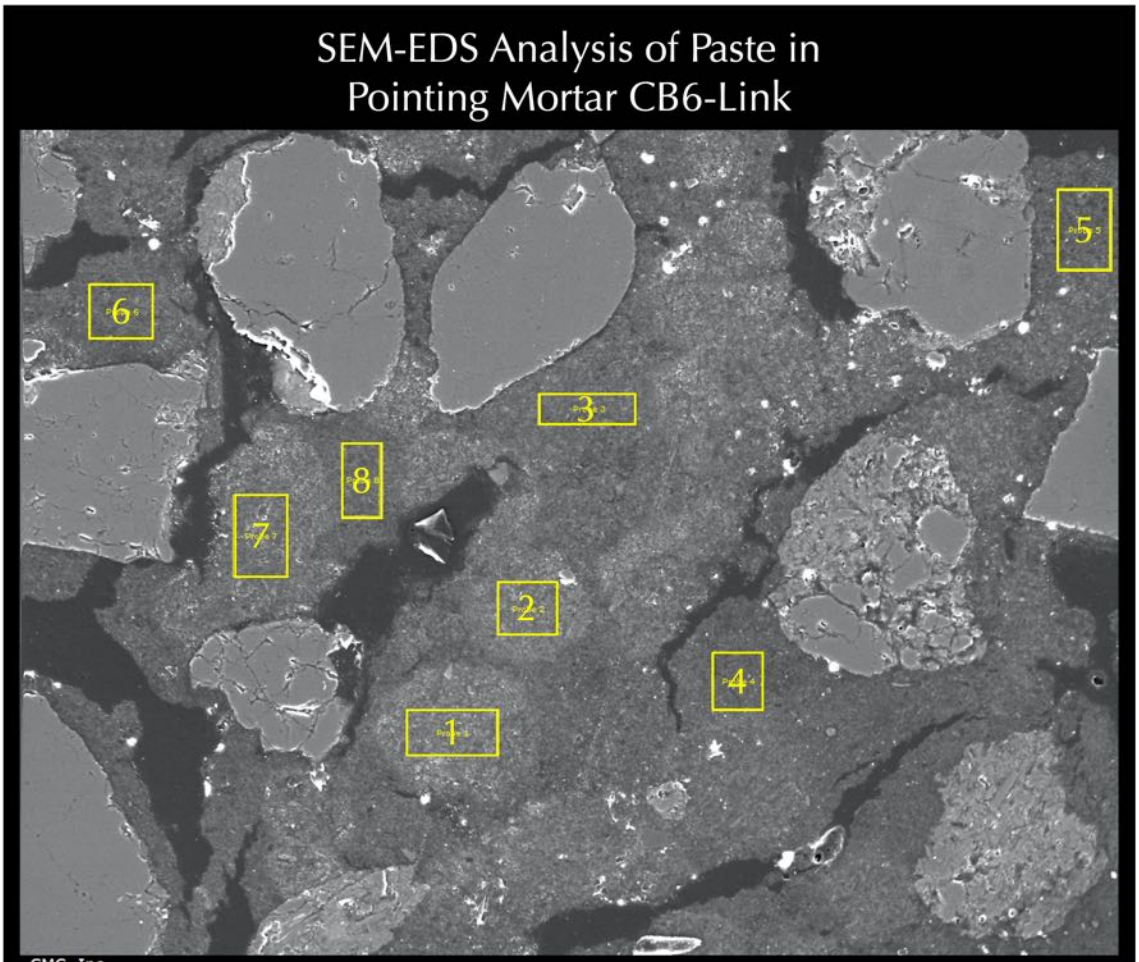

Probe	CaO	SiO2	Al2O3	K2O	MgO	FeO	Na2O	MnO2	TiO2	SO2	Total	Paste - CI	Phase
1	**27.44**	**20.42**	2.21	0.22	**48.91**	0.27	0.27	0.26	0.00	0.00	100.0	**0.62**	P
2	**29.10**	**9.50**	1.07	0.00	**59.31**	0.14	0.43	0.44	0.00	0.00	100.0	**0.25**	P
3	**33.01**	**12.41**	1.50	0.18	**51.60**	0.35	0.66	0.15	0.15	0.00	100.0	**0.35**	P
4	**35.28**	**10.02**	0.81	0.37	**52.27**	0.26	0.38	0.28	0.34	0.00	100.0	**0.27**	P
5	**31.14**	**7.70**	0.71	0.15	**59.31**	0.29	0.28	0.30	0.12	0.00	100.0	**0.20**	P
6	**33.62**	**10.89**	1.39	0.35	**52.50**	0.42	0.66	0.00	0.16	0.00	100.0	**0.30**	P
7	**25.91**	**16.08**	7.25	0.53	**49.14**	0.42	0.38	0.29	0.00	0.00	100.0	**0.56**	P
8	**35.19**	**13.20**	1.40	0.24	**48.52**	0.44	0.56	0.40	0.04	0.00	100.0	**0.38**	P

Figure 159: Backscatter electron image (top), and X-ray microanalyses at the boxed areas in Probes 1 through 8 of pointing mortar CB6-Link detecting compositional variations of paste. Paste composition is presented (bottom) as oxide variations of all detected EDS peaks normalized to 100% except carbon (from epoxy) and gold (from coating). Paste cementation indices, CI (after Eckel 1922) measure: (a) relative hydraulicity of paste e.g., non-hydraulic lime pastes have very low CI (< 0.50) compared to cement-based pastes (CI is >1), along with (b) the degree of leaching of lime, where leached paste characteristically show >>1 CI, and non-leached portions of paste show <1 CI from lime and its carbonated products. The cementation indices (CI) of paste are calculated after Eckel (1922) as CI = $[(2.8*SiO_2)+(1.1*Al_2O_3)+(0.7*\ Fe_2O_3)]/[(CaO)+(1.4*MgO)]$.

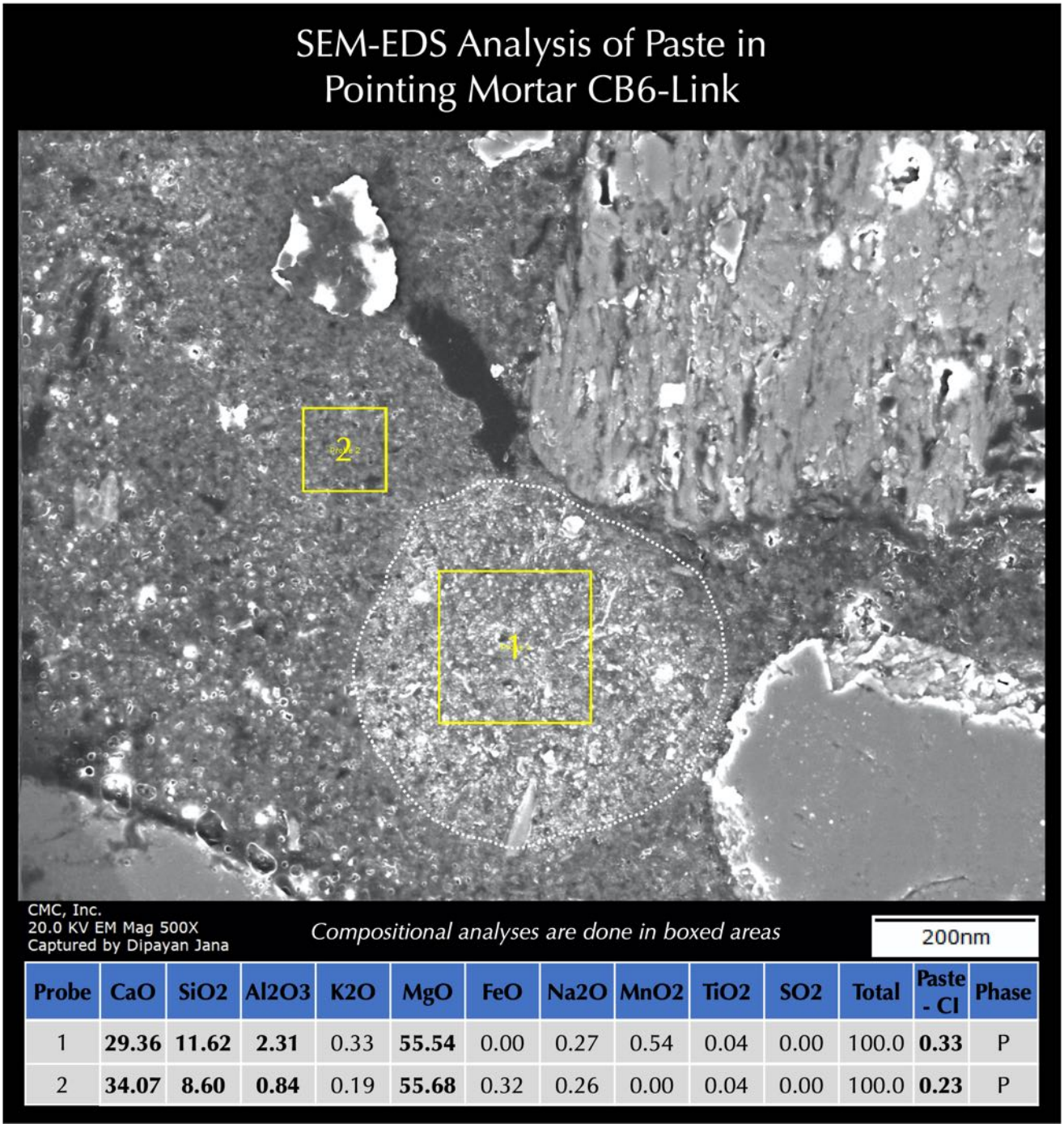

Probe	CaO	SiO2	Al2O3	K2O	MgO	FeO	Na2O	MnO2	TiO2	SO2	Total	Paste - CI	Phase
1	**29.36**	**11.62**	**2.31**	0.33	**55.54**	0.00	0.27	0.54	0.04	0.00	100.0	**0.33**	P
2	**34.07**	**8.60**	**0.84**	0.19	**55.68**	0.32	0.26	0.00	0.04	0.00	100.0	**0.23**	P

Figure 160: Backscatter electron image (top), and X-ray microanalyses at the boxed areas in Probes 1 and 2 of pointing mortar CB6-Link detecting compositional variations of a lime globule in Probe 1 (e.g., see optical micrographs in Figures 105, 106, 113, and 114), and adjacent overall paste in Probe 2. Paste composition is presented (bottom) as oxide variations of all detected EDS peaks normalized to 100% except carbon (from epoxy) and gold (from coating). Paste cementation indices, CI (after Eckel 1922) measure: (a) relative hydraulicity of paste e.g., non-hydraulic lime pastes have very low CI (< 0.50) compared to cement-based pastes (CI is >1), along with (b) the degree of leaching of lime, where leached paste characteristically show >>1 CI, and non-leached portions of paste show <1 CI from lime and its carbonated products. The cementation indices (CI) of paste are calculated after Eckel (1922) as CI = $[(2.8*SiO_2)+(1.1*Al_2O_3)+(0.7*\ Fe_2O_3)]/[(CaO)+(1.4*MgO)]$. Globule is slightly higher in Si-Al and lower in Ca than the overall paste.

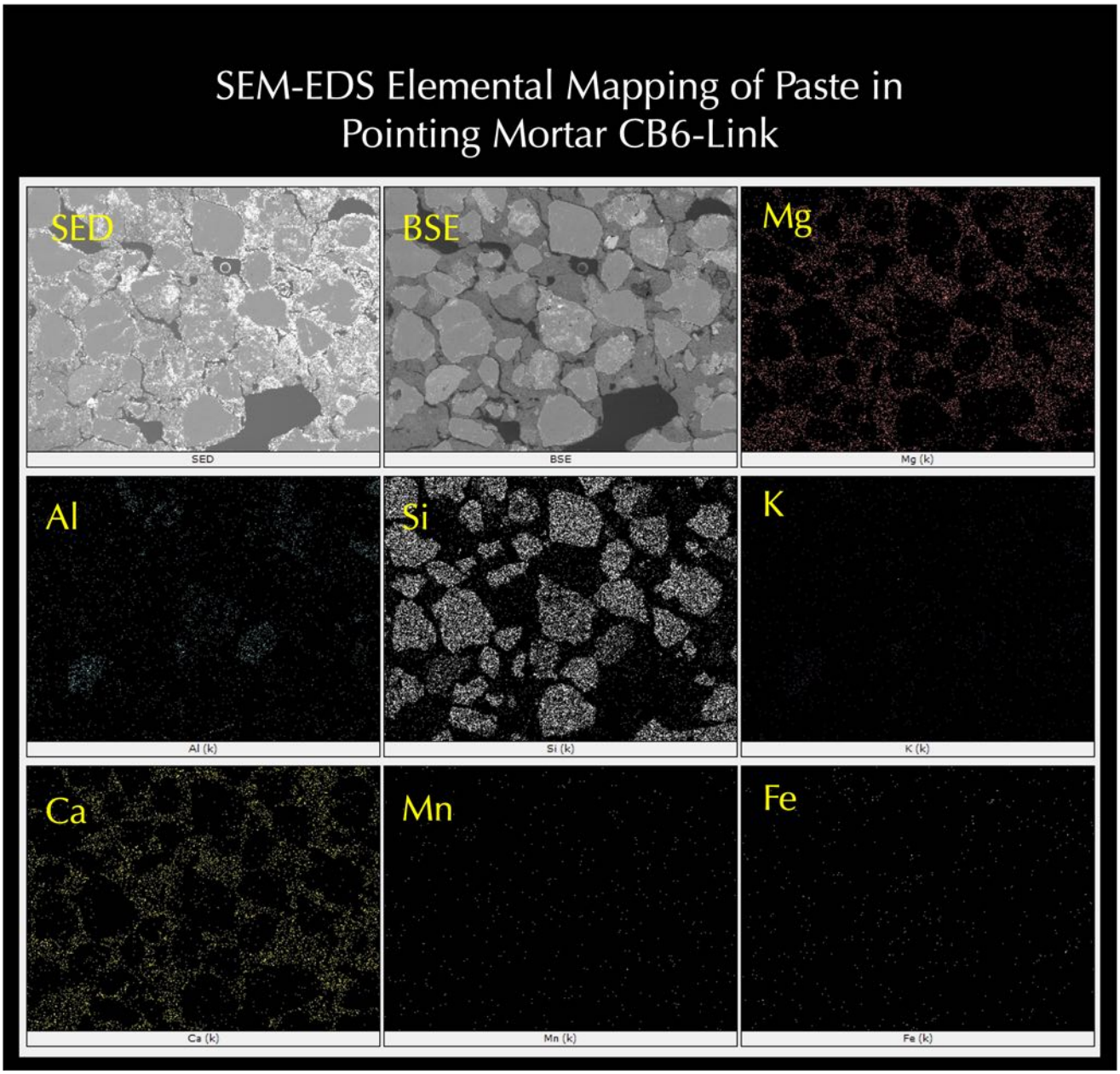

Figure 161: X-ray elemental mapping of Si, Al, Ca, Mg, K, Fe, and Mn in pointing mortar CB6-Link showing overall Ca-Mg-based composition of dolomitic lime paste. Si map shows distribution of quartz sand.

Oxide Variation Diagrams From SEM-EDS Studies

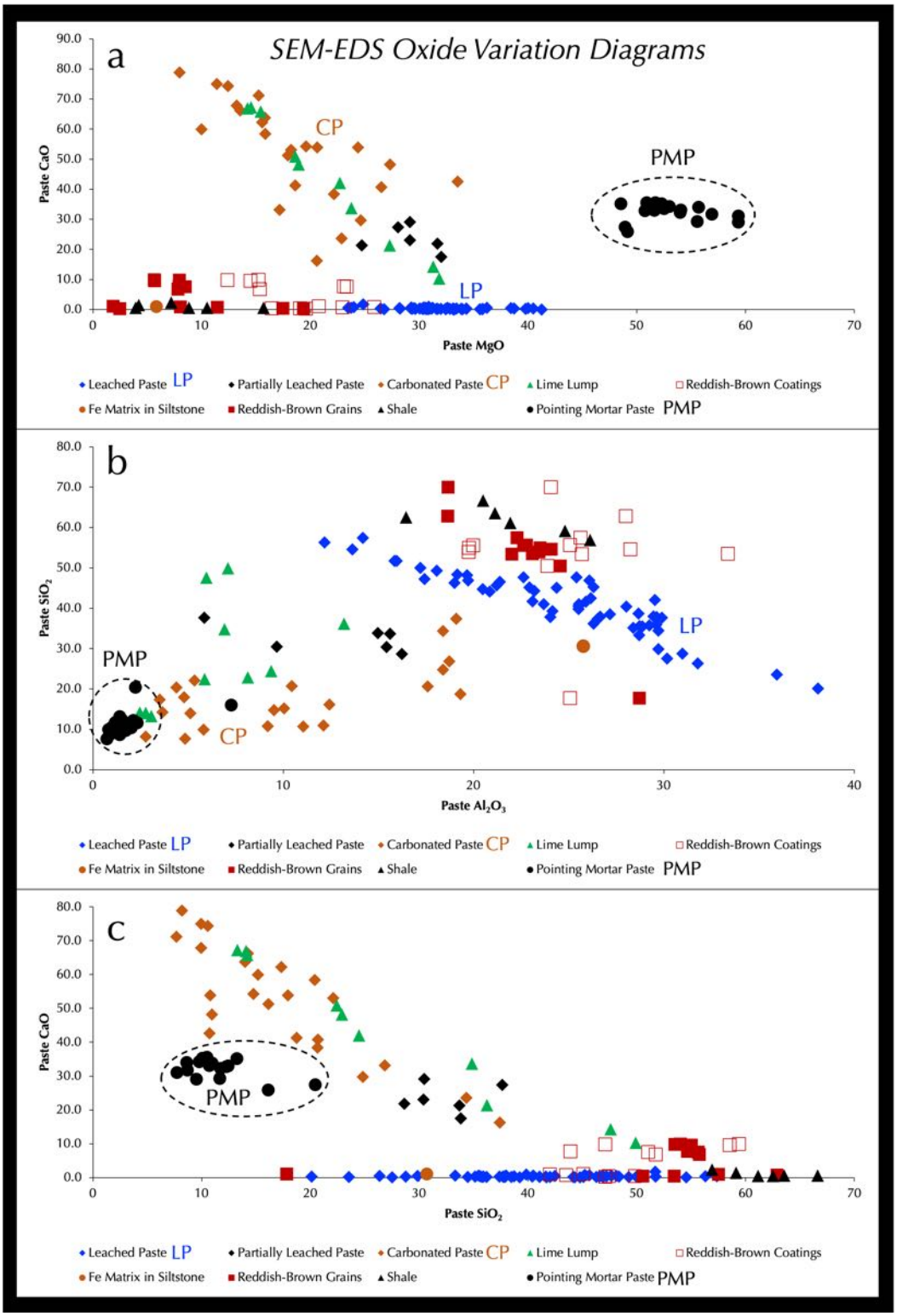

Figure 162: SEM-EDS oxide variation diagrams of: (1) severely leached paste (LP, blue diamonds), (2) partially leached paste (black diamonds), and (3) carbonated paste (CP, brown diamonds) in three setting mortars, (4) dolomitic lime paste in pointing mortar (PMP, black filled circles), (5) lime lump in setting mortar SWM-2 (solid green triangle), (6) reddish-brown coats (open brown square), (7) reddish brown grains (filled brown square), (8) reddish brown ferruginous matrix in siltstone (filled brown circle), and (9) shale (filled black triangle).

Oxide compositional variations of setting mortars show severely leached to partially leached and carbonated paste of an *original mixed calcined clay (source of Si-Al) and dolomitic lime (source of Ca-Mg) binders* where lime leaching has preferentially enriched leached areas in Mg-Si-Al as gelatinous mass, which appeared as optically isotropic areas in optical micrographs.

The paste in the pointing mortar occupied a distinct compositional space and showed noticeably homogeneous (restricted) Ca-Mg-based composition indicating use of a *feebly hydraulic (low Si) dolomitic lime from calcination of a relatively pure dolomitic limestone* compared to the heterogeneous paste in the setting mortars.

Reddish-brown coats show overall compositional similarity to reddish-brown grains and ferruginous matrixes of sand grains but have more heterogeneity due to leaching and interactions with paste during service.

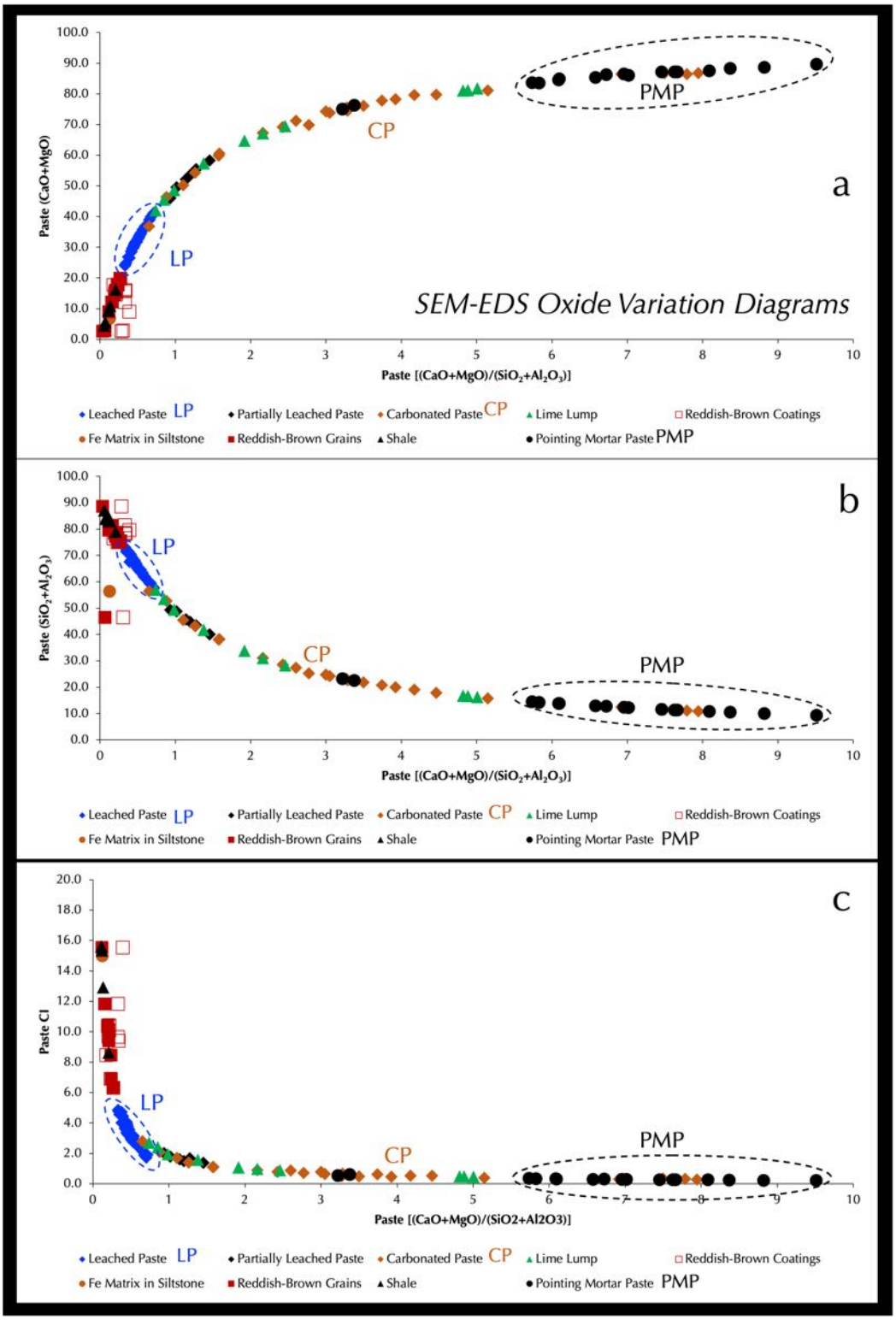

Figure 163: SEM-EDS oxide variation diagrams of: (1) severely leached paste (LP, blue diamonds), (2) partially leached paste (black diamonds), and (3) carbonated paste (CP, brown diamonds) in three setting mortars, (4) dolomitic lime paste in pointing mortar (PMP, black filled circles), (5) lime lump in setting mortar SWM-2 (solid green triangle), (6) reddish-brown coats (open brown square), (7) reddish brown grains (filled brown square), (8) reddish brown ferruginous matrix in siltstone (filled brown circle), and (9) shale (filled black triangle).

Oxide compositional variations of setting mortars show severely leached to partially leached and carbonated paste of an *original mixed calcined clay (source of Si-Al) and dolomitic lime (source of Ca-Mg) binders* where lime leaching has preferentially enriched leached areas in Mg-Si-Al as gelatinous mass, which appeared as optically isotropic areas in optical micrographs.

The paste in the pointing mortar occupied a distinct compositional space and showed noticeably homogeneous (restricted) Ca-Mg-based composition indicating use of a *feebly hydraulic (low Si) dolomitic lime from calcination of a relatively pure dolomitic limestone* compared to the heterogeneous paste in the setting mortars.

Reddish-brown coats show overall compositional similarity to reddish-brown grains and ferruginous matrixes of sand grains but have more heterogeneity due to leaching and interactions with paste during service.

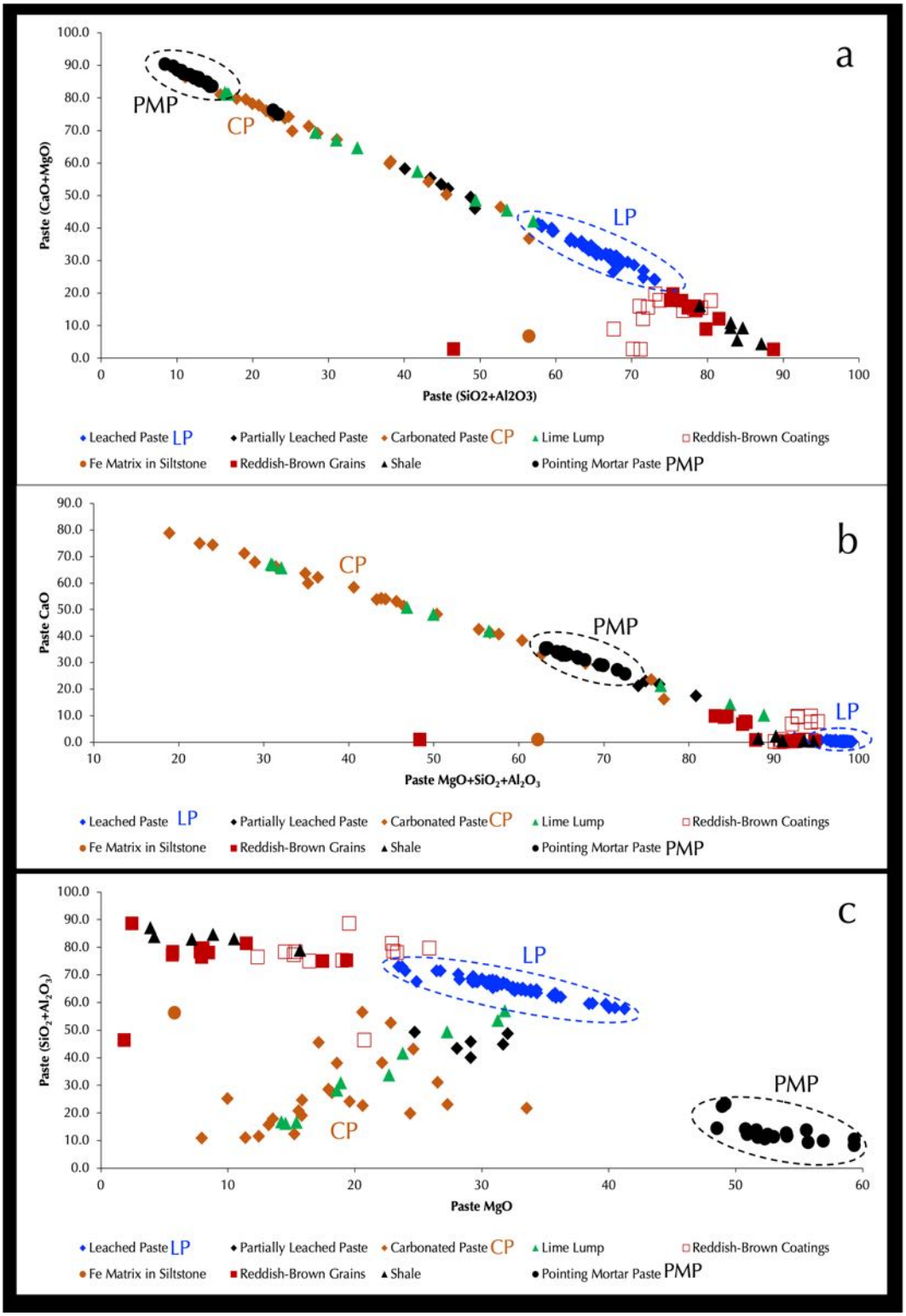

Figure 164: SEM-EDS oxide variation diagrams of: (1) severely leached paste (LP, blue diamonds), (2) partially leached paste (black diamonds), and (3) carbonated paste (CP, brown diamonds) in three setting mortars, (4) dolomitic lime paste in pointing mortar (PMP, black filled circles), (5) lime lump in setting mortar SWM-2 (solid green triangle), (6) reddish-brown coats (open brown square), (7) reddish brown grains (filled brown square), (8) reddish brown ferruginous matrix in siltstone (filled brown circle), and (9) shale (filled black triangle).

Oxide compositional variations of setting mortars show severely leached to partially leached and carbonated paste of an *original mixed calcined clay (source of Si-Al) and dolomitic lime (source of Ca-Mg) binders* where lime leaching has preferentially enriched leached areas in Mg-Si-Al as gelatinous mass, which appeared as optically isotropic areas in optical micrographs.

The paste in the pointing mortar occupied a distinct compositional space and showed noticeably homogeneous (restricted) Ca-Mg-based composition indicating use of a *feebly hydraulic (low Si) dolomitic lime from calcination of a relatively pure dolomitic limestone* compared to the heterogeneous paste in the setting mortars.

Reddish-brown coats show overall compositional similarity to reddish-brown grains and ferruginous matrixes of sand grains but have more heterogeneity due to leaching and interactions with paste during service.

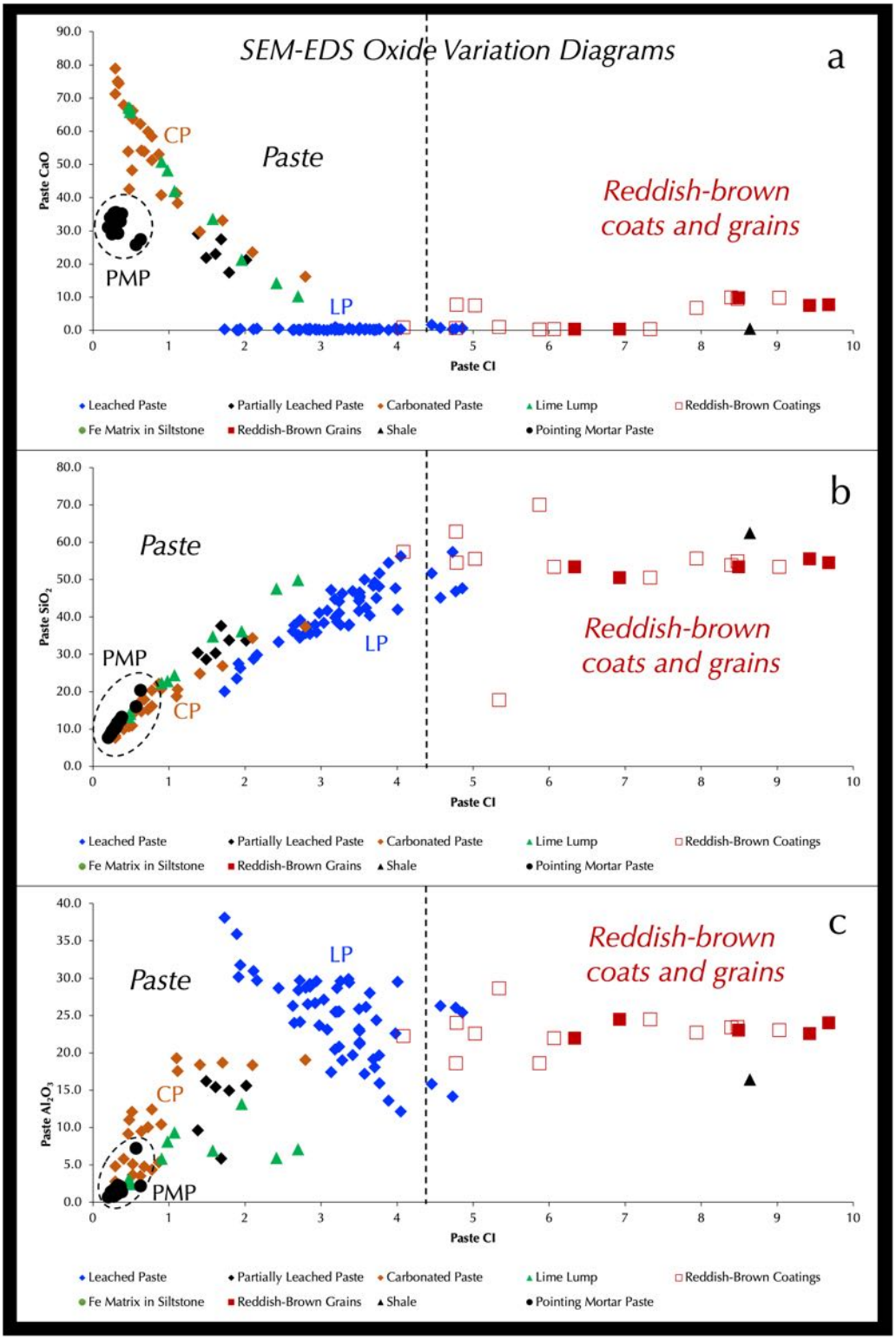

Figure 165: SEM-EDS oxide variation diagrams of: (1) severely leached paste (LP, blue diamonds), (2) partially leached paste (black diamonds), and (3) carbonated paste (CP, brown diamonds) in three setting mortars, (4) dolomitic lime paste in pointing mortar (PMP, black filled circles), (5) lime lump in setting mortar SWM-2 (solid green triangle), (6) reddish-brown coats (open brown square), (7) reddish brown grains (filled brown square), (8) reddish brown ferruginous matrix in siltstone (filled green circle), and (9) shale (filled black triangle).

Oxide compositional variations of setting mortars show severely leached to partially leached and carbonated paste of an *original mixed calcined clay (source of Si-Al) and dolomitic lime (source of Ca-Mg) binders* where lime leaching has preferentially enriched leached areas in Mg-Si-Al as gelatinous mass, which appeared as optically isotropic areas in optical micrographs.

The paste in the pointing mortar occupied a distinct compositional space and showed noticeably homogeneous (restricted) Ca-Mg-based composition indicating use of a *feebly hydraulic (low Si) dolomitic lime from calcination of a relatively pure dolomitic limestone* compared to the heterogeneous paste in the setting mortars.

Reddish-brown coats show overall compositional similarity to reddish-brown grains and ferruginous matrixes of sand grains but have more heterogeneity due to leaching and interactions with paste during service.

a. In the CaO vs. MgO plot (Figure 162 a), ***paste from the pointing mortar*** showed a distinct compositional space in having the highest MgO (50-60%) amongst all phases analyzed and intermediate CaO (between 20 and 40%) indicating use of an ***original dolomitic lime binder***, which had a characteristically higher CaO than MgO but during service a portion of lime has been leached out thus reducing the overall CaO content lower at the expense of MgO (CaO/MgO <1). Restricted composition of pointing mortar paste indicates its overall compositional homogeneity compared to variably leached paste in three setting mortars.

b. In the CaO vs. MgO plot (Figure 162 a), ***paste from three setting mortars*** show negligible lime in the severely leached areas in having high MgO contents (CaO/MgO <<1) as opposed to a range of CaO contents in partially leached and variably carbonated paste areas where carbonated paste includes both original carbonated paste as well as carbonates formed from secondary precipitation after leaching of lime. Lime lump showed overall compositional similarity to carbonated paste.

c. In the SiO_2 vs. Al_2O_3 plot (Figure 162 b), ***paste from the pointing mortar*** again showed a distinct compositional space in having the lowest SiO_2 amongst all phases analyzed but a detectable amount ranging from <10 to 20%, indicating use of ***a feebly hydraulic dolomitic lime binder produced from calcination of a relatively pure dolomitic limestone feed***.

d. In the SiO_2 vs. Al_2O_3 plot (Figure 162 b), ***paste from three setting mortars*** showed a large range of silica and alumina contents where the ***leached areas of paste showed consistently higher silica and alumina than the carbonated areas***. Higher Si and Al in leached areas indicate (a) use of an ***original calcined clay binder***, which was the main source for Si and Al in the paste as opposed to Ca and Mg from the dolomitic lime source, as well as (b) ***leaching of lime*** from the paste thus enriching the Si-Al-Mg contents in leached areas relative to lime. Lesser albeit noticeable silica and alumina in the partially leached and carbonated areas of paste approach the original Si-Al contents in the mixed subordinate calcined clay and dominant dolomitic lime binder components, where the former provided the silica and alumina whereas the latter component provided lime and magnesia.

e. In the CaO vs. SiO_2 plot (Figure 162 c), ***paste from the pointing mortar*** again showed a distinct compositional space in having the lowest silica (<10-20%) at 20-40% lime, again indicating use of ***a feebly hydraulic dolomitic lime binder produced from calcination of a relatively pure dolomitic limestone feed.***

f. In the CaO vs. SiO_2 plot (Figure 162 c), ***paste from three setting mortars*** show negligible lime at appreciable silica contents for the leached areas as opposed to variable and noticeable lime in the partially leached and carbonated areas.

g. In all three plots in Figure 162, ***reddish-brown coats*** show overall compositional similarity to ***reddish-brown calcined clay grains and ferruginous matrixes of sand grains*** but have more heterogeneity in coats (higher Mg) due to leaching and interactions with adjacent paste during service. Reddish brown coats showed consistently higher silica and alumina (along with iron, not shown in the plots) from calcined clay components, along with lowest virtually non-detectable lime, which is compositionally similar to the overwhelming occurrences of leached paste (in the latter, silica and alumina contents were derived not from the coatings on sand or sand *per se*, but from the original calcined clay binder, now left as optically isotropic gelatinous aluminosilicate mass).

h. In the CaO+MgO (i.e., total contribution from dolomitic lime binder components) vs. (CaO+MgO)/(SiO_2+Al_2O_3) i.e., relative proportions of contributions from dolomitic lime and calcined clay binder components (in Figure 163 a), an excellent trend is found amongst all components of paste from setting and pointing mortars, where leached paste in setting mortar and paste in pointing mortar defined the two extreme end members. Pointing mortar paste showed the highest CaO+MgO with some variations from some leaching of lime, as well as the ratio of lime-magnesia over silica-alumina from use of only dolomitic lime binder without any calcined clay, whereas leached paste showed the lowest lime-magnesia (mostly magnesia left after lime leaching) and lowest lime-magnesia over silica-alumina ratio from leaching of lime, enriching leached areas in silica and alumina originally contributed from the calcined clay binder. Carbonated and partially leached paste in setting mortars unoccupied the intermediate positions in the curvilinear trend.

i. In the SiO_2+Al_2O_3 (i.e., total contribution from calcined clay binder) vs. (CaO+MgO)/(SiO_2+Al_2O_3) i.e., relative proportions of contributions from dolomitic lime and calcined clay binder components (in Figure 163 b), a reciprocal trend is obtained from the one in Figure 156 a, as expected, from highest silica-alumina in the leached paste of setting mortar to lowest silica-alumina and highest lime-magnesia in the feebly hydraulic dolomitic lime binder in pointing mortar.

j. In the paste-CI vs. (CaO+MgO)/(SiO_2+Al_2O_3) plot (Figure 163 c), similar curvilinear trend is found as the one in Figure 163 b for the same reasonings described before.

k. A perfectly linear trend is found amongst all measured components of paste when plotted in lime + magnesia vs. silica + alumina in Figure 164 a where leached paste from setting mortar and carbonated paste from pointing mortar occupied the extreme ends. Carbonated paste in setting mortar showed a large range from the pointing mortar paste end depending on various degrees of lime leaching.

l. A very similar trend is found when lime is plotted against magnesia + silica + alumina in Figure 164 b where paste in pointing mortar occupied an intermediate space between carbonated and leached paste areas in setting mortar. Due to very high silica + alumina content in the leached paste, total magnesia +silica + alumina content in leached paste is higher than the values in the paste in pointing mortar.

m. In the silica + alumina vs. magnesia plot in Figure 164 c, carbonated paste and lime lump in setting mortar deviated from a linear tread established by the leached paste and pointing mortar paste due to relatively lower silica + alumina content in carbonated paste than leached areas.

n. When lime, silica, and alumina contents are plotted against paste-CIs (after Eckel 1922) in Figure 165 all binder components occupied the left section of CIs between 0 and 5, whereas reddish brown coats, reddish brown grains, and shale particles in sand occurred the higher side of CIs between 5 and 10. Although CI cannot be used for non-binder components such plots indeed effectively separates all non-binder components in having very high CIs than the binder ones.

o. Amongst the binder components in Figure 165, paste from pointing mortar showed the lowest paste-CI of all binders examined, and leached areas of paste in setting mortars showed the highest CIs from highest silica and alumina contents.

Oxides	CaO	SiO_2	Al_2O_3	K_2O	MgO	FeO	Na_2O	MnO_2	TiO_2	SO_3	Paste-Cl
Leached Paste	0.14	36.18	26.30	0.01	35.56	1.26	0.05	0.30	0.19	0.00	2.63
	0.59	40.47	25.51	0.28	31.21	1.05	0.04	0.50	0.34	0.00	3.21
	0.24	41.63	25.90	0.35	29.66	1.57	0.04	0.28	0.32	0.00	3.50
	0.29	40.39	28.02	0.42	28.25	1.55	0.18	0.66	0.24	0.00	3.64
	0.31	37.91	26.65	0.28	33.10	1.09	0.24	0.17	0.24	0.00	2.92
	0.37	57.38	14.18	0.15	26.44	0.70	0.46	0.31	0.00	0.00	4.73
	0.12	44.76	20.48	0.33	33.22	0.75	0.07	0.18	0.10	0.00	3.18
	0.73	45.65	21.20	0.26	30.41	1.16	0.09	0.50	0.00	0.00	3.51
	0.39	47.21	17.41	0.00	34.31	0.53	0.14	0.00	0.00	0.00	3.13
	0.21	37.83	24.02	0.25	35.83	1.31	0.17	0.35	0.02	0.00	2.65
	0.05	41.70	23.10	0.13	33.13	1.21	0.00	0.65	0.03	0.00	3.08
	0.23	41.05	25.53	0.17	31.57	1.09	0.15	0.10	0.12	0.00	3.24
	0.18	23.53	35.93	0.00	39.76	0.44	0.00	0.16	0.00	0.00	1.89
	0.32	28.74	30.97	0.08	38.72	0.79	0.00	0.38	0.00	0.00	2.11
	0.16	34.46	29.70	0.15	33.96	0.89	0.07	0.49	0.12	0.00	2.72
	0.14	35.76	29.22	0.24	33.22	1.07	0.08	0.27	0.00	0.00	2.85
	0.24	37.38	26.51	0.17	33.87	1.18	0.28	0.37	0.00	0.00	2.83
	0.19	46.28	19.00	0.00	32.82	1.14	0.17	0.29	0.11	0.00	3.28
	0.10	44.30	23.18	0.10	30.64	1.12	0.15	0.40	0.00	0.00	3.50
	0.26	35.14	28.38	0.23	34.33	1.18	0.21	0.26	0.00	0.00	2.70
	0.05	27.51	30.16	0.00	41.25	0.42	0.08	0.53	0.00	0.00	1.91
	1.69	51.71	15.85	0.16	24.85	0.31	2.88	0.00	0.00	0.00	4.45
	0.25	35.91	29.59	0.26	32.42	1.40	0.00	0.01	0.14	0.00	2.94
	0.19	41.04	23.68	0.04	33.83	0.95	0.16	0.12	0.00	0.00	2.98
	0.15	42.01	29.53	0.55	26.75	0.67	0.14	0.13	0.07	0.00	4.00
	0.13	38.47	27.16	0.20	32.45	1.12	0.18	0.17	0.12	0.00	3.04
	0.92	39.83	25.52	0.47	30.86	1.45	0.12	0.29	0.55	0.00	3.19
	0.46	26.34	31.78	0.14	40.01	0.94	0.00	0.29	0.04	0.00	1.94
	0.55	35.45	28.86	1.03	32.60	1.08	0.15	0.06	0.22	0.00	2.85
	0.50	29.84	29.70	0.00	38.43	1.26	0.08	0.19	0.00	0.00	2.16
	0.60	33.30	28.69	0.10	36.22	0.75	0.06	0.25	0.03	0.00	2.44
	0.38	37.84	29.61	0.30	30.24	0.84	0.22	0.17	0.39	0.00	3.26
	0.32	37.68	29.88	0.57	29.34	1.01	0.26	0.64	0.30	0.00	3.36
	0.49	42.48	26.16	0.44	29.19	1.11	0.08	0.02	0.03	0.00	3.59
	0.62	47.67	25.40	0.41	23.45	1.56	0.08	0.00	0.81	0.00	4.86
	0.64	37.98	29.44	0.15	29.25	1.92	0.07	0.41	0.13	0.00	3.37
	0.81	45.21	26.29	0.30	23.96	2.09	0.00	1.01	0.34	0.00	4.57
	0.33	20.08	38.09	0.02	40.49	0.66	0.00	0.34	0.00	0.00	1.73
	0.22	45.09	24.36	0.00	29.31	0.95	0.06	0.00	0.00	0.00	3.73
	0.40	35.61	28.71	0.04	33.44	1.22	0.00	0.44	0.14	0.00	2.80
	0.56	46.86	26.08	0.36	23.71	1.56	0.19	0.38	0.30	0.00	4.77
	0.35	38.71	28.67	0.17	31.01	0.85	0.00	0.24	0.00	0.00	3.21
	0.54	45.16	22.92	0.00	30.59	0.60	0.00	0.11	0.07	0.00	3.51
	0.50	47.67	22.62	0.08	28.16	0.72	0.04	0.06	0.14	0.00	3.98
	0.30	46.56	21.38	0.00	31.15	0.19	0.02	0.28	0.13	0.00	3.51
	0.08	39.24	24.13	0.00	35.79	0.41	0.00	0.23	0.12	0.00	2.72
	0.48	48.15	19.66	0.35	29.51	1.25	0.25	0.03	0.32	0.00	3.76
	0.30	51.72	15.95	0.00	30.70	0.94	0.06	0.32	0.00	0.00	3.77
	0.17	49.26	18.06	0.18	30.40	0.76	0.00	1.07	0.09	0.00	3.71
	0.27	48.37	19.14	0.19	30.28	1.21	0.00	0.28	0.26	0.00	3.69
	0.21	44.16	20.84	0.31	32.39	1.37	0.27	0.38	0.06	0.00	3.24
	0.10	54.55	13.62	0.00	30.83	0.56	0.00	0.32	0.01	0.00	3.89
	0.23	49.98	17.19	0.19	31.69	0.56	0.06	0.05	0.05	0.00	3.57
	0.19	46.90	19.71	0.02	31.99	0.91	0.13	0.15	0.00	0.00	3.42
	0.35	56.32	12.17	0.11	30.02	0.55	0.16	0.25	0.05	0.00	4.05
Average	0.36	41.13	24.76	0.20	31.94	1.00	0.15	0.29	0.12	0.00	3.26
Stn. Dev	0.27	7.82	5.47	0.19	4.02	0.39	0.39	0.23	0.16	0.00	0.72

Oxides	CaO	SiO_2	Al_2O_3	K_2O	MgO	FeO	Na_2O	MnO_2	TiO_2	SO_3	Paste-CI
Partially Leached Paste	**27.39**	**37.62**	**5.85**	0.22	**28.03**	0.61	0.21	0.07	0.00	0.00	**1.68**
	29.15	**30.44**	**9.65**	0.13	**29.12**	0.56	0.58	0.09	0.28	0.00	**1.38**
	17.49	**33.80**	**14.97**	0.20	**32.03**	0.85	0.22	0.44	0.00	0.00	**1.79**
	21.87	**28.62**	**16.22**	0.10	**31.68**	0.97	0.05	0.41	0.09	0.00	**1.49**
	21.29	33.70	15.60	0.52	24.72	1.63	0.07	0.70	1.79	0.00	**2.02**
	23.02	30.37	15.42	0.39	29.13	1.02	0.25	0.16	0.24	0.00	**1.61**
Average	**23.37**	**32.43**	**12.95**	**0.26**	**29.12**	**0.94**	**0.23**	**0.31**	**0.40**	**0.00**	1.66
Stn. Dev	**4.26**	**3.26**	**4.22**	**0.16**	**2.67**	**0.39**	**0.19**	**0.25**	**0.69**	**0.00**	0.23
Carbonated Paste	**48.21**	10.94	12.11	0.21	**27.30**	0.76	0.00	0.44	0.03	0.00	**0.51**
	53.91	10.77	9.18	0.47	**24.36**	0.73	0.11	0.35	0.11	0.00	**0.46**
	54.25	14.73	9.50	0.24	**19.59**	0.68	0.70	0.32	0.00	0.00	**0.64**
	33.14	26.84	18.71	0.57	**17.15**	2.35	0.25	0.54	0.45	0.00	**1.70**
	42.59	10.72	11.05	0.25	**33.52**	0.88	0.25	0.68	0.06	0.00	**0.48**
	29.73	24.81	18.39	0.12	**24.61**	0.64	0.93	0.77	0.00	0.00	**1.40**
	40.73	20.68	10.44	0.28	**26.52**	0.71	0.14	0.36	0.13	0.00	**0.90**
	38.41	20.64	17.59	0.34	**22.14**	0.33	0.16	0.39	0.00	0.00	**1.11**
	23.59	34.33	18.38	0.20	**22.84**	0.25	0.10	0.25	0.06	0.00	**2.10**
	67.84	9.94	5.81	0.33	**13.22**	0.61	0.60	1.01	0.63	0.00	**0.40**
	41.32	18.71	19.31	0.22	**18.58**	0.69	0.43	0.54	0.20	0.00	**1.10**
	62.23	17.30	3.50	0.05	**15.56**	0.31	0.43	0.62	0.00	0.00	**0.62**
	16.22	37.39	19.08	0.09	**20.58**	0.24	0.18	0.28	0.00	5.94	**2.79**
	53.07	22.07	5.33	0.15	**18.19**	0.64	0.00	0.50	0.05	0.00	**0.87**
	58.42	20.38	4.37	0.16	**15.83**	0.73	0.00	0.10	0.00	0.00	**0.77**
	59.90	15.17	10.04	0.13	**9.97**	0.07	0.36	0.15	0.00	4.22	**0.73**
	75.01	9.95	1.14	0.34	**11.38**	0.64	0.70	0.68	0.17	0.00	**0.33**
	78.88	8.16	2.77	0.56	**7.94**	0.43	0.23	1.03	0.00	0.00	**0.29**
	66.24	14.24	3.64	0.05	**13.53**	0.87	0.81	0.60	0.00	0.00	**0.52**
	74.36	10.54	1.04	0.27	**12.42**	0.72	0.25	0.36	0.04	0.00	**0.34**
	53.87	17.91	4.78	0.76	**20.60**	0.38	1.56	0.14	0.00	0.00	**0.67**
	71.20	7.65	4.84	0.26	**15.22**	0.32	0.30	0.23	0.00	0.00	**0.29**
	63.78	13.96	5.11	0.28	**15.81**	0.44	0.35	0.26	0.00	0.00	**0.52**
	51.28	16.12	12.41	0.44	**17.91**	0.68	0.22	0.73	0.22	0.00	**0.78**
Average	**52.42**	**17.25**	**9.52**	**0.28**	**18.53**	**0.63**	**0.38**	**0.47**	**0.09**	**0.42**	**0.85**
Stn. Dev	**16.68**	**7.77**	**6.23**	**0.17**	**6.05**	**0.43**	**0.36**	**0.26**	**0.16**	**1.46**	**0.61**
Lime Lump	**65.84**	**14.18**	2.46	0.32	**15.41**	0.28	1.10	0.41	0.00	0.00	**0.49**
	66.93	**14.07**	2.76	0.40	**14.20**	0.27	1.02	0.19	0.14	0.00	**0.49**
	67.22	**13.27**	3.06	0.33	**14.53**	0.45	1.11	0.03	0.00	0.00	**0.47**
	50.90	**22.40**	5.87	0.48	**18.58**	0.30	1.09	0.00	0.36	0.00	**0.90**
	48.21	**22.88**	8.14	0.42	**18.90**	0.45	0.91	0.08	0.00	0.00	**0.98**
Average	**59.82**	**17.36**	**4.46**	**0.39**	**16.32**	**0.35**	**1.05**	**0.14**	**0.10**	**0.00**	0.67
Stn. Dev	**9.43**	**4.84**	**2.47**	**0.07**	**2.25**	**0.09**	**0.08**	**0.17**	**0.16**	**0.00**	0.25

Table 1: SEM-EDS compositions of paste and lime lump in setting mortars.

SEM-EDS compositional analysis of paste from three setting mortars and one pointing mortar in Table 1 showed: (a) a lime-leached component of paste in setting mortars characterized by negligible lime and high silica, magnesia, and alumina (Si>Mg>Al), and, as a result, an average paste CI of 3.26, (b) variably carbonated and partially leached paste areas in setting mortars having average paste-CI of 1.66, and (c) carbonated areas of paste in setting mortars having Ca>>Mg>Si>Al and paste CIs <1 (average 0.85). Lime lump showed high Ca and Mg (Ca>>Mg, Si>Al) from mixed calcined clay and lime binders. Lime lumps are the best candidates to determine the original compositions of binders, which is judged to be a two-component mix having a higher proportion of dolomitic lime (source for Ca and Mg) and a subordinate proportion of calcined clay (source for Si and Al).

By contrast, compositional analyses of paste in pointing mortar in Table 2 showed high lime and magnesia (Mg>Ca), less silica, minor alumina and the lowest CI of all binders (average 0.32) indicating essentially a non-hydraulic to feebly hydraulic binder.

Oxides	CaO	SiO_2	Al_2O_3	K_2O	MgO	FeO	Na_2O	MnO_2	TiO_2	SO_3	Paste-CI
Pointing Mortar Paste	**32.30**	**11.69**	1.15	0.25	**53.98**	0.30	0.19	0.05	0.08	0.00	**0.32**
	34.26	**9.74**	1.70	0.23	**52.97**	0.43	0.28	0.39	0.00	0.00	**0.27**
	33.88	**10.94**	2.05	0.36	**51.51**	0.34	0.31	0.41	0.20	0.00	**0.31**
	35.62	**10.45**	1.99	0.18	**50.89**	0.35	0.36	0.00	0.16	0.00	**0.30**
	32.89	**12.26**	2.10	0.38	**50.74**	0.48	0.42	0.60	0.13	0.00	**0.36**
	31.81	**8.66**	1.40	0.09	**56.89**	0.44	0.35	0.24	0.11	0.00	**0.23**
	35.53	**10.43**	0.96	0.24	**51.71**	0.31	0.75	0.03	0.03	0.00	**0.28**
	33.16	**10.67**	1.03	0.00	**54.02**	0.27	0.27	0.57	0.00	0.00	**0.29**
	27.44	**20.42**	2.21	0.22	**48.91**	0.27	0.27	0.26	0.00	0.00	**0.62**
	29.10	**9.50**	1.07	0.00	**59.31**	0.14	0.43	0.44	0.00	0.00	**0.25**
	33.01	**12.41**	1.50	0.18	**51.60**	0.35	0.66	0.15	0.15	0.00	**0.35**
	35.28	**10.02**	0.81	0.37	**52.27**	0.26	0.38	0.28	0.34	0.00	**0.27**
	31.14	**7.70**	0.71	0.15	**59.31**	0.29	0.28	0.30	0.12	0.00	**0.20**
	33.62	**10.89**	1.39	0.35	**52.50**	0.42	0.66	0.00	0.16	0.00	**0.30**
	25.91	**16.08**	7.25	0.53	**49.14**	0.42	0.38	0.29	0.00	0.00	**0.56**
	35.19	**13.20**	1.40	0.24	**48.52**	0.44	0.56	0.40	0.04	0.00	**0.38**
	29.36	**11.62**	2.31	0.33	**55.54**	0.00	0.27	0.54	0.04	0.00	**0.33**
	34.07	**8.60**	0.84	0.19	**55.68**	0.32	0.26	0.00	0.04	0.00	**0.23**
Average	**32.42**	**11.40**	**1.77**	**0.24**	**53.08**	**0.32**	**0.39**	**0.28**	**0.09**	**0.00**	**0.32**
Stn. Dev	**2.83**	**2.96**	**1.46**	**0.14**	**3.24**	**0.12**	**0.16**	**0.20**	**0.09**	**0.00**	**0.11**

Table 2: SEM-EDS compositions of paste in pointing mortar.

Oxides	CaO	SiO_2	Al_2O_3	K_2O	MgO	FeO	Na_2O	MnO_2	TiO_2	SO_3	Paste-CI
Reddish-brown Coats on angular to rounded sand grains	**0.36**	**49.81**	**23.86**	0.83	**16.40**	**7.27**	0.17	**0.55**	0.74	0.00	**7.32**
	0.53	**45.05**	**25.06**	1.05	**20.73**	**5.83**	0.18	**0.52**	1.04	0.00	**5.34**
	0.40	**47.08**	**24.05**	1.10	**19.54**	**6.71**	0.14	**0.52**	0.46	0.00	**5.87**
	0.55	**47.39**	**25.68**	**1.00**	**19.01**	**5.35**	0.07	**0.46**	0.50	0.00	**6.06**
	0.34	**41.99**	**25.61**	**0.80**	**25.84**	**4.59**	0.15	**0.18**	0.52	0.00	**4.08**
	0.39	**43.49**	**27.99**	1.04	**22.91**	**3.30**	0.20	**0.26**	0.42	0.00	**4.77**
	0.39	**43.88**	**28.23**	0.79	**23.03**	**2.96**	0.22	**0.36**	0.16	0.00	**4.78**
	0.70	**51.72**	**25.05**	**1.04**	**15.32**	**4.87**	0.17	**0.40**	0.72	0.00	**7.94**
	1.68	**47.08**	**33.34**	**0.83**	12.33	**3.50**	0.36	0.26	0.61	0.00	**9.02**
	1.35	**59.40**	**19.73**	0.82	**15.19**	**2.58**	0.25	0.47	0.19	0.00	**8.39**
	1.92	**58.52**	**19.74**	1.05	**14.47**	**3.33**	0.11	0.42	0.43	0.00	**8.47**
	0.58	51.02	19.97	0.55	23.31	2.85	0.37	0.29	1.06	0.00	**5.02**
	1.57	18.32	22.90	0.00	47.79	7.74	0.58	0.30	0.80	0.00	**1.20**
Average	**0.83**	**46.52**	**24.71**	**0.84**	**21.22**	**4.68**	**0.23**	**0.38**	**0.59**	**0.00**	**6.02**
Stn. Dev	**0.58**	**10.01**	**3.83**	**0.30**	**8.97**	**1.78**	**0.14**	**0.12**	**0.28**	**0.00**	**6.02**
Fe matrix in Siltstone	1.07	**30.66**	**25.75**	0.96	5.79	**33.57**	0.44	1.76	0.00	0.00	**15.00**
Reddish-brown ferruginous shale-siltstone grains	0.44	**50.54**	**24.54**	**1.03**	**17.44**	**5.06**	0.17	**0.35**	0.45	0.00	**6.92**
	1.12	**17.80**	**28.70**	0.06	1.82	**45.45**	2.85	2.03	0.16	0.00	**30.87**
	0.29	**70.07**	**18.64**	**2.66**	2.43	**3.56**	0.80	0.30	1.25	0.00	**59.37**
	0.49	**53.44**	**21.99**	3.26	**19.34**	1.07	0.08	0.00	0.33	0.00	**6.33**
	0.98	**57.50**	**22.27**	3.07	8.03	6.52	0.14	0.68	0.80	0.00	**15.55**
	0.77	**62.88**	**18.63**	2.76	**11.42**	2.70	0.17	0.31	0.37	0.00	**11.84**
	7.82	**54.63**	**24.06**	0.54	7.87	4.01	0.35	0.17	0.54	0.00	**9.67**
	6.85	**55.73**	**22.76**	0.82	7.80	4.15	0.24	1.06	0.59	0.00	**10.35**
	9.87	**53.50**	**23.07**	0.69	**7.91**	**3.67**	0.46	0.31	0.54	0.00	**8.49**
	9.99	**53.99**	**23.43**	0.69	**5.62**	**4.71**	0.42	0.43	0.71	0.00	**10.09**

Oxides	CaO	SiO_2	Al_2O_3	K_2O	MgO	FeO	Na_2O	MnO_2	TiO_2	SO_3	Paste-CI
	9.62	**55.00**	**23.48**	0.91	**5.65**	**4.47**	0.29	0.15	0.43	0.00	**10.44**
	7.59	**55.63**	**22.61**	0.63	**8.47**	**3.73**	0.35	0.41	0.57	0.00	**9.42**
Average	**4.65**	**53.39**	**22.85**	**1.43**	**8.65**	**7.43**	**0.53**	**0.52**	**0.56**	**0.00**	**15.78**
Stn. Dev	**4.25**	**12.34**	**2.63**	**1.15**	**5.27**	**12.05**	**0.76**	**0.55**	**0.28**	**0.00**	**15.78**
Shale	2.30	**56.93**	**26.11**	**4.09**	7.17	**1.88**	0.26	0.40	0.85	0.00	**15.35**
	1.45	**59.14**	**24.79**	**2.79**	4.21	**5.37**	0.45	0.77	1.03	0.00	**26.77**
	0.52	**61.14**	**21.93**	**2.97**	**10.48**	1.32	0.31	0.22	1.11	0.00	**12.92**
	0.52	**62.54**	**16.45**	**2.98**	**15.67**	1.16	0.21	0.07	0.40	0.00	**8.64**
	0.60	**66.63**	**20.49**	**3.25**	**3.90**	3.63	0.38	0.24	0.89	0.00	**34.92**
	0.58	**63.56**	**21.12**	**3.71**	**8.82**	1.05	0.32	0.41	0.44	0.00	**15.62**
Average	**1.00**	**61.66**	**21.82**	**3.30**	**8.38**	**2.40**	**0.32**	**0.35**	**0.79**	**0.00**	**19.04**
Stn. Dev	**0.73**	**3.41**	**3.42**	**0.50**	**4.40**	**1.74**	**0.09**	**0.24**	**0.30**	**0.00**	**19.04**

Table 3: SEM-EDS compositions of reddish-brown coats, reddish-brown calcined clay and other grains, and shale particles in sand. Paste-CI values are not applicable for non-binder components but still included to show their stark deviations in oxide-compositional space from the lime binder components as well as their potential similarity to the calcined clay component in the binder suspected in the setting mortars.

Reddish-brown coats on sand grains are essentially similar in compositions to isolated occurrences of fine reddish-brown calcined clay and other grains as well as reddish-brown matrix in ferruginous shale-siltstone sand particles, except some differences. Reddish-brown coats on sand grains show an overall lower silica, and higher magnesia contents than isolated reddish-brown calcined clay grains, which is due to chemical interactions of coats with the adjacent paste during service. Consistently higher magnesia contents in almost all reddish-brown coats analyzed compared to the isolated ferruginous calcined clay grains are the best chemical signatures of formation or at least chemical evolution of these coats from chemical interactions with magnesia-rich dolomitic lime paste with calcined clay binder component during service. Chemical interactions in coats have reduced the overall chemical variability seen in the isolated reddish-brown grains. Therefore, reddish-brown coats seen on sand grains could not have formed on sand prior to their incorporation in mortars (besides their occurrence on crushed angular fine quartz sand grains does not necessarily support the notion of their formation as clay coats on sand in the stockpile).

SEM-EDS analyses of a few shale grains in sand showed the characteristically high Si, Al, Mg, and K contents, all of which are determined (from subsequent XRD studies) to be from illitic clay in shale. Silica and alumina occupy the tetrahedral sites and Mg, Al, Fe occupy the octahedral sites in a illite crystal structure Calcination of an illitic clay component from such a shale particle can produce Mg-Si-Al based pozzolan to be used with lime such as the binders determined for the setting mortars.

The high silica and alumina contents in leached areas of paste from the clay component of binder showed overall homogeneous compositions. Such compositional homogeneity of silica and alumina despite leaching, along with ultrafine size of clay components indicate the source of silica and alumina in paste could be either or a combination of separate addition of calcined clay (an amorphous aluminosilicate mass, which has been ground to fine size) and/or brick dust where the former option is more plausible than the latter since brick dust component should have been easily identified in paste *per se* in optical microscopy of thin sections of paste from fine, angular, reddish-brown brick fragments, which are not found (the reddish-brown grains in paste are sand-sized and contained subrounded to rounded grains most plausibly derived from the ferruginous components of sand).

Mineralogical Compositions of Mortars from XRD

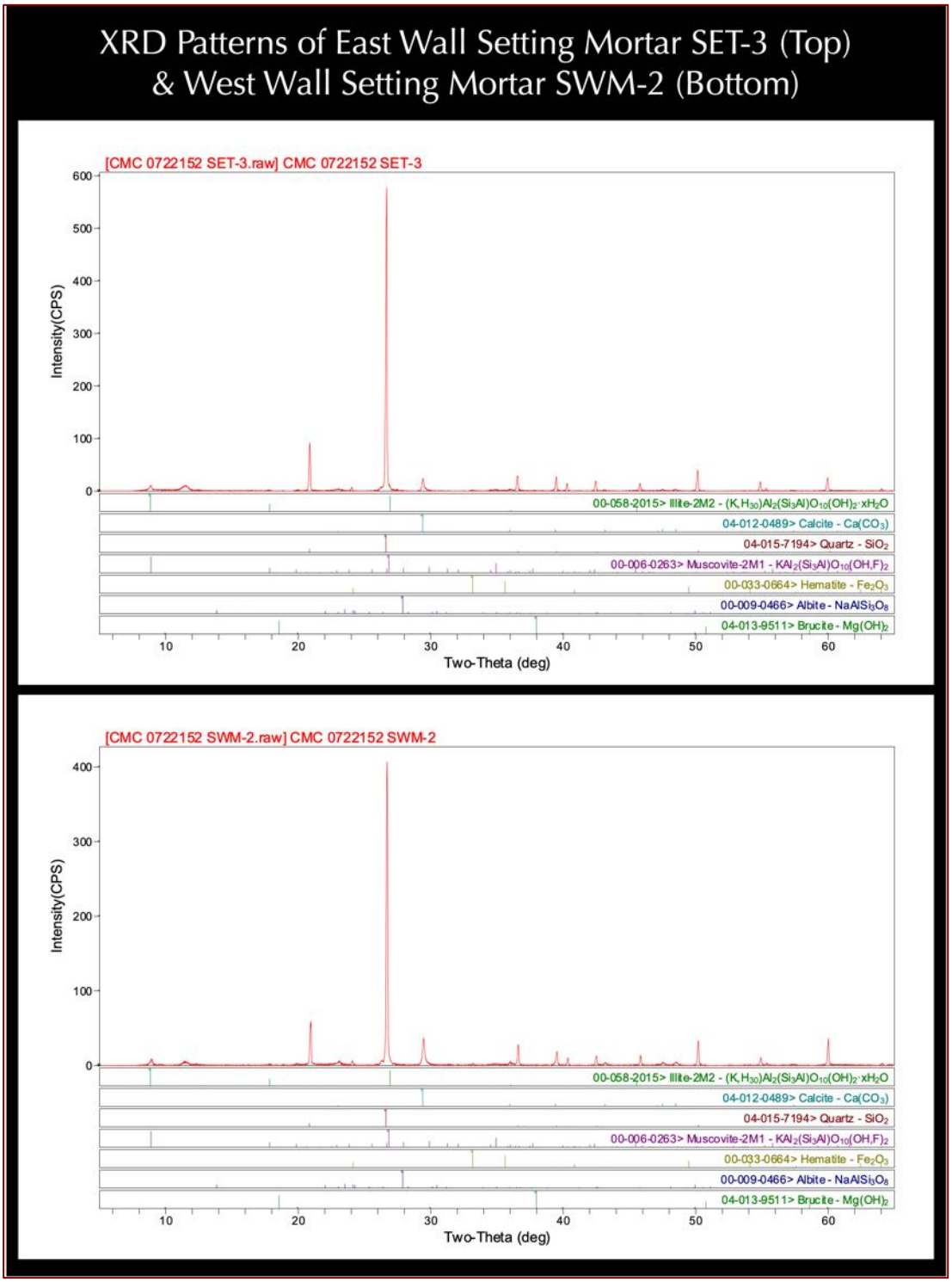

Figure 166: X-ray diffraction patterns of bulk setting mortar samples SET-3 (top) and SWM-2 (bottom) showing the presence of illitic clay from the argillaceous components of sand, the dominance of quartz from the dominant siliceous component of sand, and minor calcite from leached and carbonated paste. Minor muscovite and albite feldspar are detected from sand, hematite from reddish-brown iron oxide, and brucite from use of dolomitic lime component in the binder. Calcination of an illitic clay component can produce Mg-Si-Al based pozzolan to be used with lime where Si and Al occupy tetrahedral sites and Mg, Al, Fe occupy octahedral sites in illite crystal structure.

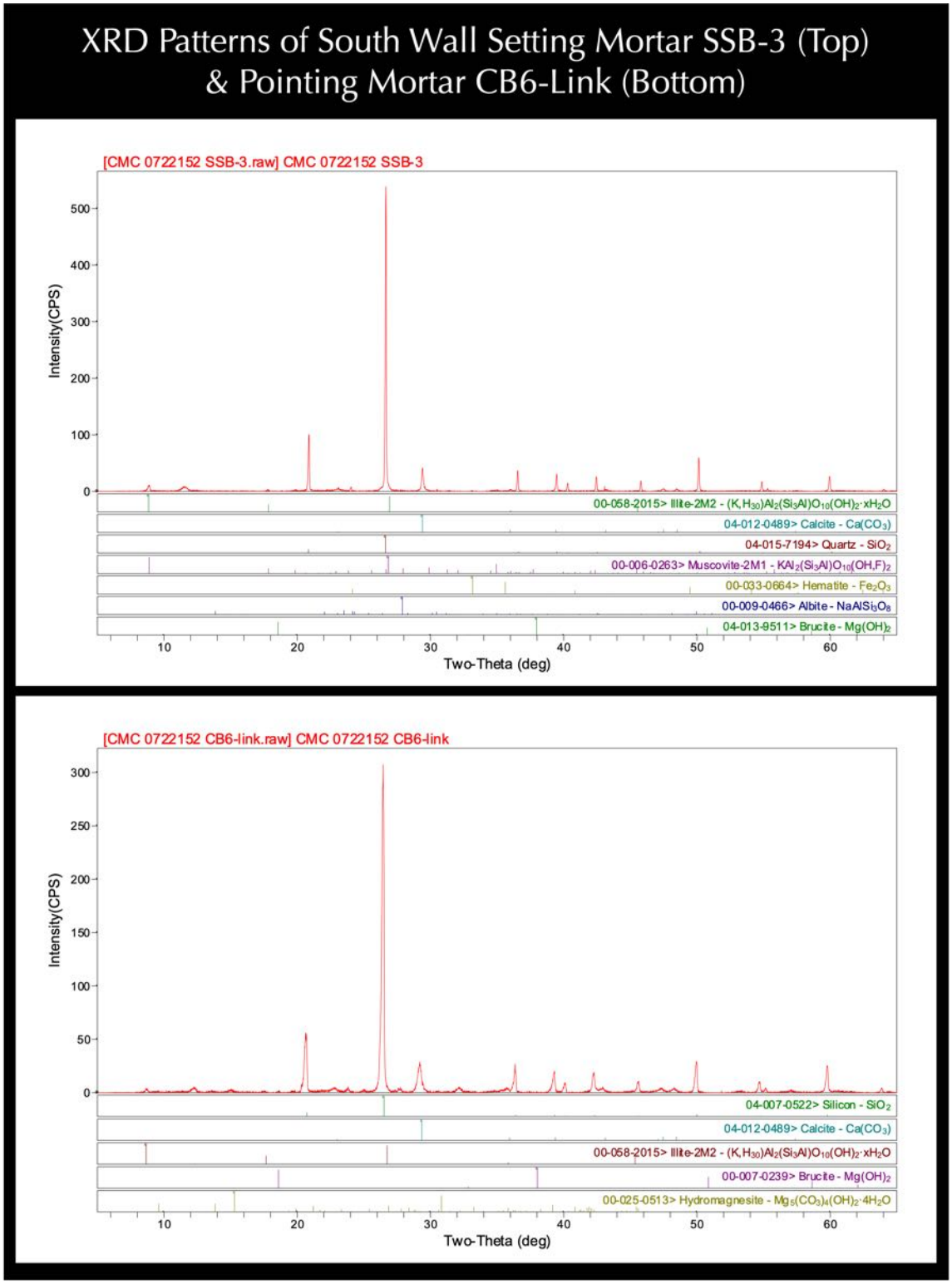

Figure 167: X-ray diffraction patterns of bulk setting mortar SSB-3 (top) and pointing mortar (CB6-Link) showing the presence of illitic clay from the argillaceous components of sand, the dominance of quartz in both setting and pointing mortars from the dominant siliceous component of sand, minor calcite in setting mortar from leached and carbonated paste. Minor muscovite and albite feldspar are detected from sand, hematite from reddish-brown iron oxide, and brucite from use of dolomitic lime component in the binder. Calcination of an illitic clay component can produce Mg-Si-Al based pozzolan to be used with lime where Si and Al occupy tetrahedral sites and Mg, Al, Fe occupy octahedral sites in illite crystal structure.

Compositions of Mortars from XRF (Major Element Oxides), Acid & Alkali Digestion (Soluble Silica), Loss on Ignition (Free Water, Combined Water, Carbonation), and Acid-Insoluble Residue Contents (Siliceous Sand Contents)

Table 1 shows oxide compositions of mortars determined from pressed pellets of pulverized (< 45-micron size) bulk mortars in XRF. Dominance of silica reflects corresponding dominance of siliceous components in sand particles, as also seen in optical microscopy and XRD analysis of the mortars.

Lower lime contents in setting mortars compared to the pointing mortar is consistent with: (a) leaching of lime in setting mortars, and (b) addition of lime with a clay component in the binder where clay also increased the bulk alumina and iron contents in setting mortars. Magnesia content is higher in the pointing mortar for dolomitic lime only binder.

Alumina, iron, and alkalis are contributed from both sand and paste. Sulfate is from cement paste, which is negligible in setting mortars but 0.4 percent in pointing mortar. Balance includes volatiles (combined H_2O, CO_2) not measured in XRF, which showed high content in pointing mortar for the dominance of carbonated lime paste.

Soluble silica contents are from the silica-rich amorphous leached areas of paste in setting mortar, and not from any hydraulic phase.

Acid-insoluble residue contents are determined after digesting pulverized (<0.3 mm size) fragments of mortars in hydrochloric acid.

Due to the presence of only siliceous and argillaceous/ferruginous components and no calcareous components in sands (as determined from petrography), the determined acid-insoluble residue contents are considered representative of the overall sand contents of the mortars.

Chemical Analyses (XRF & Gravimetric) of Mortar Samples

Mortar Identification	SET-3	SWM-2	SSB-3	CB6-Link	
Mortar Types	**Setting Bed Mortars**			**Pointing Mortar**	Methods
Silica - SiO_2	**58.02**	**53.44**	**57.77**	**46.29**	ED-XRF
Alumina - Al_2O_3	6.14	5.37	6.86	2.76	ED-XRF
Iron - Fe_2O_3	2.92	2.47	3.07	1.05	ED-XRF
Lime - CaO	7.14	11.11	7.62	10.71	ED-XRF
Magnesia - MgO	6.33	6.14	6.51	8.21	ED-XRF
Sodium - Na_2O	0.009	0.017	<0.022	0.102	ED-XRF
Potassium - K_2O	0.727	0.753	0.871	0.283	ED-XRF
Titanium - TiO_2	0.27	0.254	0.328	0.18	ED-XRF
Phosphorus - P_2O_5	0.23	0.239	0.263	0.283	ED-XRF
Sulfate - SO_3	<0.0005	<0.0005	0.058	**0.413**	ED-XRF
Balance (LOI)	**18.2**	**20.1**	**16.5**	**29.4**	-
Total	100	100	100	100	ED-XRF
Soluble Silica	2.35	2.12	2.61	1.02	Gravimetry
Acid-Insoluble Residue	**63.33**	**55.71**	**69.83**	**57.5**	Gravimetry
Loss on Ignition @ 110°C	6.00	11.00	9.00	1.00	Gravimetry
Loss on Ignition @ 550°C	**5.00**	**4.00**	**3.00**	**9.00**	Gravimetry
Loss on Ignition @ 950°C	**6.00**	**9.00**	**7.00**	**5.00**	Gravimetry
Total LOI	**17.0**	**24.0**	**19.0**	**15.0**	Gravimetry

Table 4: Bulk oxide compositions (from XRF), acid-insoluble residue contents (from gravimetry), and losses on ignition (from gravimetry) of setting and pointing mortars.

Losses on ignition of separate aliquots of pulverized mortars to 110°C, 550°C, and 950°C correspond to free water, combined (hydrate) water, and degree of carbonation, respectively. The losses on ignition at 550°C correspond to the water contents from dehydration and dehydroxylation of clay and hydrous and some carbonate phases. The loss on ignition at 950°C corresponds to degree of carbonation of carbonated paste.

Thermal Analyses of Mortars

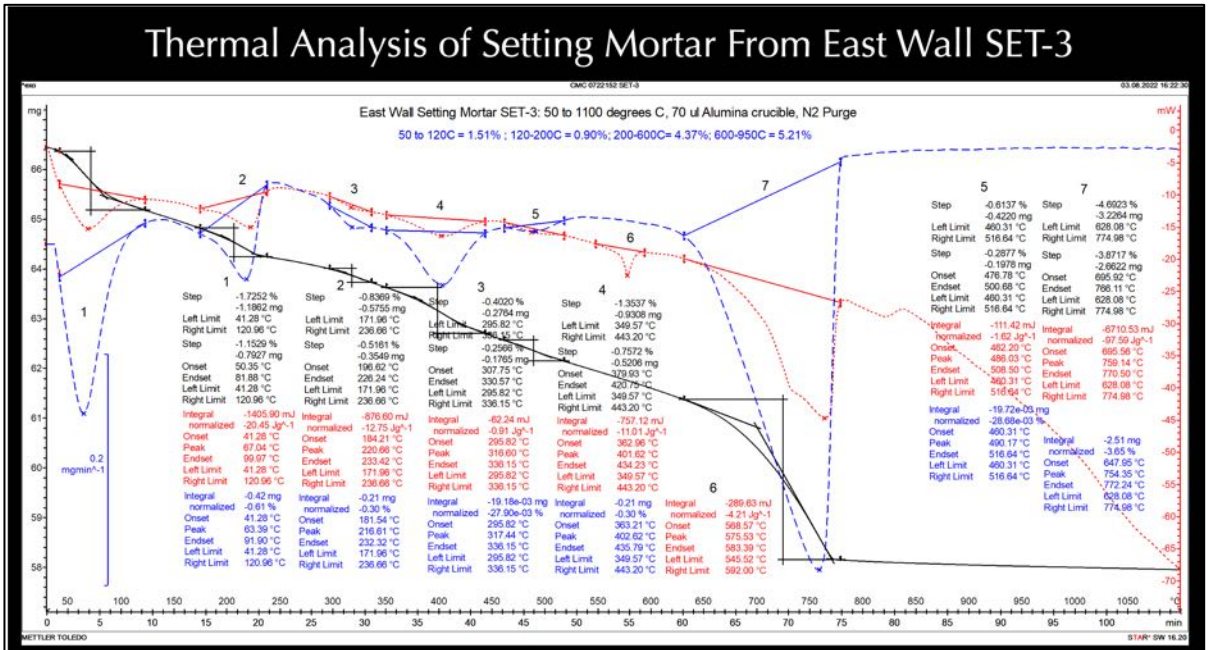

T(°C)	Up to 120°C	120°C to 200°C	200°C to 600°C	> 600°C
Phases	Hygroscopic Water	Water from Hydrated Salts	Structural Water From Hydraulic Components	CO_2 from decomposition of carbonates
Mass Loss From TGA	0.62	0.44	2.56	2.99
Mass Loss (%) From Gravimetry	6.00	-	5.00	6.00

Peaks#	Peak Position (°C)	Phase
1 (DTG)	63.39	Water
2 (DTG)	216.61	Combined Water (Clay, Mg-Al-Si gel)
3 (DTG)	317.44	Brucite
4 (DTG)	402.62	Portlandite
5 (DTG)	490.17	Hydromagnesite
6 (DSC)	575.53	Quartz, 97%
7 (DTG)	754.35	Calcite, 7.3%

Figure 168: TGA (in bold black), DSC (in dotted red), and DTG (in dashed blue) curves of setting mortar SET-3 showing losses in weights due to decompositions (loss of water and carbon dioxide) of various phases during controlled heating in a Mettler-Toledo's simultaneous TGA/DSC 1 unit from 30ºC to 1100ºC in a ceramic crucible (alumina 70µl, no lid) at a heating rate of 10ºC/min in a nitrogen purge at a rate of 75 mL/min. Dehydration and decarbonation reactions are marked as endothermic peaks in the DTG curve, whereas alpha to beta-form polymorphic transition of quartz is marked at the characteristic temperature of 575ºC in the DSC curve. Similar results are obtained from thermal analyses and gravimetry for mass losses from loss of free water (up to 120ºC), structural water (200 to 600ºC), and carbonation (600 to 950 ºC), respectively. Endothermic peaks confirmed the presence of portlandite and brucite from use of dolomitic lime binders, dehydroxylation of clay and leached amorphous paste from their characteristic endothermic peaks, and carbonated paste.

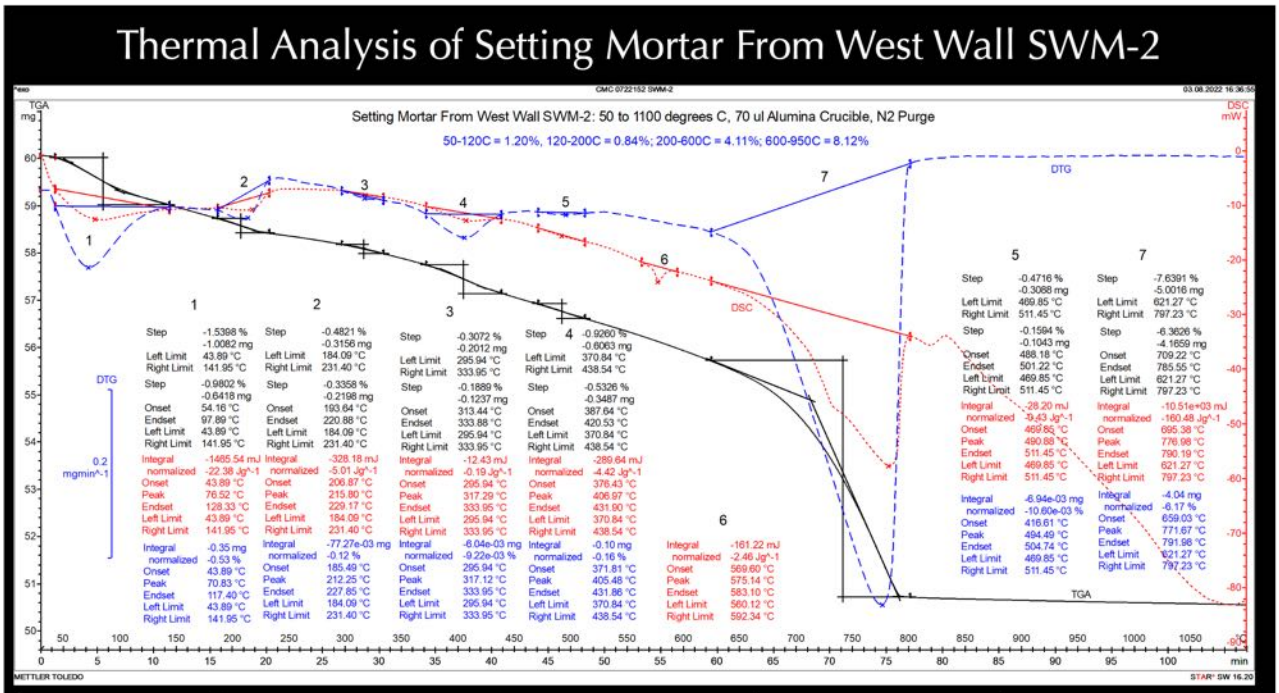

T(°C)	Up to 120°C	120°C to 200°C	200°C to 600°C	> 600°C
Phases	Hygroscopic Water	Water from Hydrated Salts	Structural Water From Hydraulic Components	CO_2 from decomposition of carbonates
Mass Loss From TGA	1.20	0.84	4.11	8.12
Mass Loss (%) From Gravimetry	11.00	-	4.00	9.00

Peaks#	Peak Position (°C)	Phase
1 (DTG)	70.83	Water
2 (DTG)	212.25	Combined Water (Clay, Mg-Al-Si gel)
3 (DTG)	317.12	Brucite
4 (DTG)	405.48	Portlandite
5 (DTG)	494.49	Hydromagnesite
6 (DSC)	575.14	Quartz, 57.2%
7 (DTG)	771.67	Calcite, 11.9%

Figure 169: TGA (in bold black), DSC (in dotted red), and DTG (in dashed blue) curves of setting mortar SWM-2 showing losses in weights due to decompositions (loss of water and carbon dioxide) of various phases during controlled heating in a Mettler-Toledo's simultaneous TGA/DSC 1 unit from 30ºC to 1100ºC in a ceramic crucible (alumina 70µl, no lid) at a heating rate of 10ºC/min in a nitrogen purge at a rate of 75 mL/min. Dehydration and decarbonation reactions are marked as endothermic peaks in the DTG curve, whereas alpha to beta-form polymorphic transition of quartz is marked at the characteristic temperature of 575ºC in the DSC curve. Similar results are obtained from thermal analyses and gravimetry for mass losses from loss of free water (up to 120ºC), structural water (200 to 600ºC), and carbonation (600 to 950 ºC), respectively. Endothermic peaks confirmed the presence of portlandite and brucite from use of dolomitic lime binders, dehydroxylation of clay and leached amorphous paste from their characteristic endothermic peaks, and carbonated paste

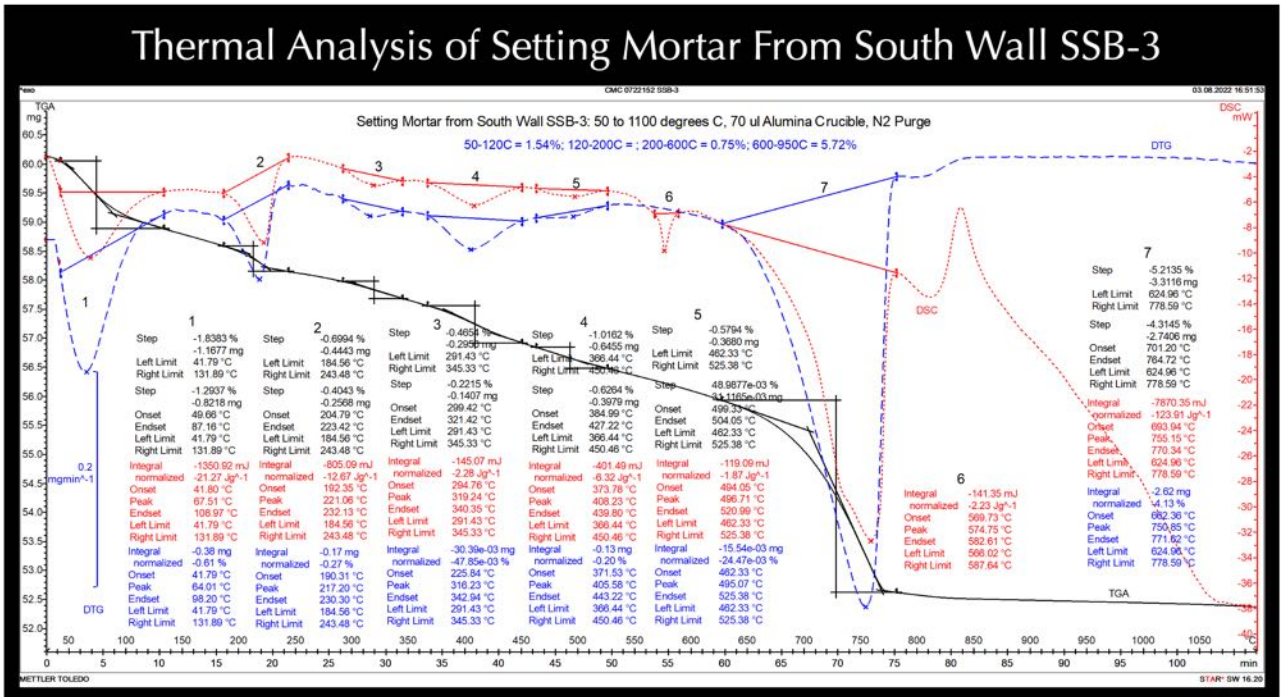

T(°C)	Up to 120°C	120°C to 200°C	200°C to 600°C	> 600°C
Phases	Hygroscopic Water	Water from Hydrated Salts	Structural Water From Hydraulic Components	CO_2 from decomposition of carbonates
Mass Loss From TGA	1.54	0.44	0.75	5.72
Mass Loss (%) From Gravimetry	9.00	-	3.00	7.00

Peaks#	Peak Position (°C)	Phase
1 (DTG)	64.01	Water
2 (DTG)	217.20	Combined Water (Clay, Mg-Al-Si gel)
3 (DTG)	316.23	Brucite
4 (DTG)	405.58	Portlandite
5 (DTG)	525.38	Water and CO_2 release
6 (DSC)	574.75	Quartz, 51.8%
7 (DTG)	750.55	Calcite, 9.2%

Figure 170: TGA (in bold black), DSC (in dotted red), and DTG (in dashed blue) curves of setting mortar SSB-3 showing losses in weights due to decompositions (loss of water and carbon dioxide) of various phases during controlled heating in a Mettler-Toledo's simultaneous TGA/DSC 1 unit from 30ºC to 1100ºC in a ceramic crucible (alumina 70µl, no lid) at a heating rate of 10ºC/min in a nitrogen purge at a rate of 75 mL/min. Dehydration and decarbonation reactions are marked as endothermic peaks in the DTG curve, whereas alpha to beta-form polymorphic transition of quartz is marked at the characteristic temperature of 575ºC in the DSC curve. Similar results are obtained from thermal analyses and gravimetry for mass losses from loss of free water (up to 120ºC), structural water (200 to 600ºC), and carbonation (600 to 950 ºC), respectively. Endothermic peaks confirmed the presence of portlandite and brucite from use of dolomitic lime binders, dehydroxylation of clay and leached amorphous paste from their characteristic endothermic peaks, and carbonated paste

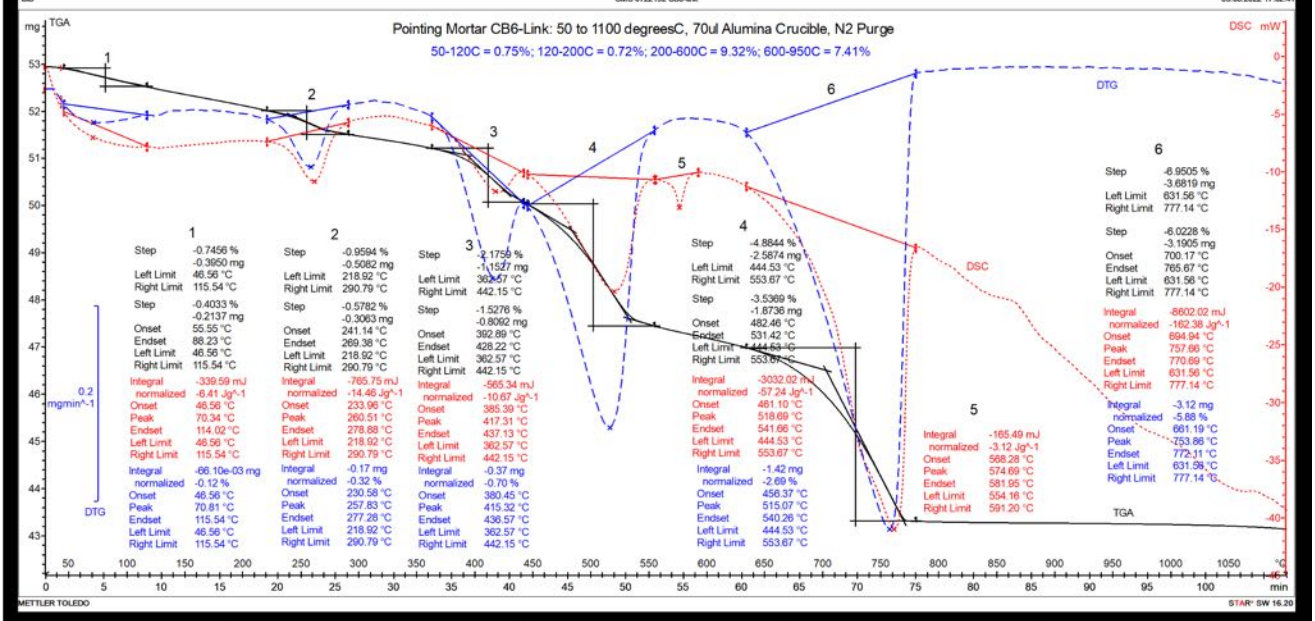

T(°C)	Up to 120°C	120°C to 200°C	200°C to 600°C	> 600°C
Phases	Hygroscopic Water	Water from Hydrated Salts	Structural Water From Hydraulic Components	CO_2 from decomposition of carbonates
Mass Loss From TGA	0.75	0.72	9.32	7.41
Mass Loss (%) From Gravimetry	1.00	-	9.00	5.00

Peaks#	Peak Position (°C)	Phase
1 (DTG)	70.81	Water
2 (DTG)	257.83	Combined Water
3 (DTG)	415.32	Portlandite
4 (DTG)	515.07	Water and CO_2 release
5 (DSC)	574.69	Quartz, 72.5%
6 (DTG)	753.86	Calcite, 12.1%

Figure 171: TGA (in bold black), DSC (in dotted red), and DTG (in dashed blue) curves of pointing mortar CB6-Link showing losses in weights due to decompositions (loss of water and carbon dioxide) of various phases during controlled heating in a Mettler-Toledo's simultaneous TGA/DSC 1 unit from 30ºC to 1100ºC in a ceramic crucible (alumina 70µl, no lid) at a heating rate of 10ºC/min in a nitrogen purge at a rate of 75 mL/min. Dehydration and decarbonation reactions are marked as endothermic peaks in the DTG curve, whereas alpha to beta-form polymorphic transition of quartz is marked at the characteristic temperature of 575ºC in the DSC curve. Similar results are obtained from thermal analyses and gravimetry for mass losses from loss of free water (up to 120ºC), structural water (200 to 600ºC), and carbonation (600 to 950 ºC), respectively. Endothermic peaks confirmed the presence of portlandite and brucite from use of dolomitic lime binders, dehydroxylation of clay and leached amorphous paste from their characteristic endothermic peaks, and carbonated paste.

Mortars		DTG Peaks of Decomposition & % Loss of Mass					
		Peak 1	Peak 2	Peak 3	Peak 4	Peak 5	Peak 6
Setting Mortar SET-3	DTG Peak (ºC)	63.4ºC	216.6ºC	317.4º C	402.6ºC	490.2ºC	754.3ºC
	% Mass Loss	1.72%	0.83%	0.40%	1.35%	0.61%	4.7%
Setting Mortar SWM-2	DTG Peak (ºC)	70.8ºC	212.2ºC	317.1 ºC	405.5ºC	494.5 ºC	771.6ºC
	% Mass Loss	1.54%	0.48%	0.30%	0.92%	0.47%	7.6%
Setting Mortar SSB-3	DTG Peak (ºC)	64.0ºC	217.2ºC	316.2 ºC	405.6ºC	495.0 ºC	750.8ºC
	% Mass Loss	1.83%	0.70%	0.46%	1.01%	0.57%	5.2%
Pointing Mortar CB6-Link	DTG Peak (ºC)	70.8ºC	257.8ºC	-	415.3ºC	515.0 ºC	753.8ºC
	% Mass Loss	0.74%	0.95%	-	2.17%	4.8%	6.9%
Reactions		Dehydration	Dehydroxylation and Decarbonation				Decarbonation
Potential Phases Decomposed		Free H_2O	Combined H_2O, Clay	Brucite	Portlandite	Iowaite, Magnesite	Calcite

Table 5: Summary results of thermal analyses of setting and pointing mortars. Peak numbers in the above Table are not necessarily matching with Peak numbers in Figures 168 to 171 since only the peaks from decompositions of phases are shown here, excluding the endothermic peak from polymorphic transition of quartz at around 575ºC.

a. All three setting mortars showed very consistent and similar thermal decompositions indicating their overall compositional similarities in terms of the phases being decomposed. Mass loss at <100ºC corresponds to loss of free water, whereas loss at 210 to 250ºC range correspond to dehydroxylation of hydrous phases, including the amorphous gelatinous leached paste in setting mortars.
b. Pointing mortar showed overall similarities in thermal behaviors with the setting mortars up to a temperature of 300ºC after which it showed no appearance of an endothermic peak, which is common for dehydroxylation of brucite in dolomitic lime mortars occurring at temperatures between 300 and 350ºC. Despite the detection of high magnesia and lime in the paste from the use of a dolomitic lime binder, this lack of appearance of a brucite dehydroxylation peak suggests severe carbonation of brucite to other carbonate-hydrate phases of magnesia, such as magnesite or hydromagnesite, where latter usually decomposes over a temperature range of 220 to 550ºC by following the decarbonation and dehydration reaction: $Mg_5(CO_3)_4(OH)_2.4H_2O = 5MgO + 4CO_2 + 5H_2O$.
c. Loss of mass of pointing mortar at 400 to 415ºC range is twice the corresponding mass loss of setting mortar indicating a higher proportion of portlandite (slaked lime) component of the original slaked dolomitic lime putty that has remained in the pointing mortar.
d. Almost 10 times higher loss of mass of pointing mortar at 490 to 520ºC range (4.8%) compared to the corresponding loss of setting mortar (0.5%) confirms a higher abundance of magnesite component formed from carbonation of the original brucite (the slaked hydration product from original slaking of dolomitic lime putty) in the pointing mortar than the dolomitic lime plus calcined clay mixed binder in the setting mortars.
e. Degree of decarbonation of calcite in all four mortars are similar at 750 to 775ºC range corresponding to 5 to 7% mass loss. Corresponding calcite contents are determined to be 7 to 12%, which are consistent with calcite contents found from XRD studies.

Ion Chromatography of Water-Soluble Anions in Mortars

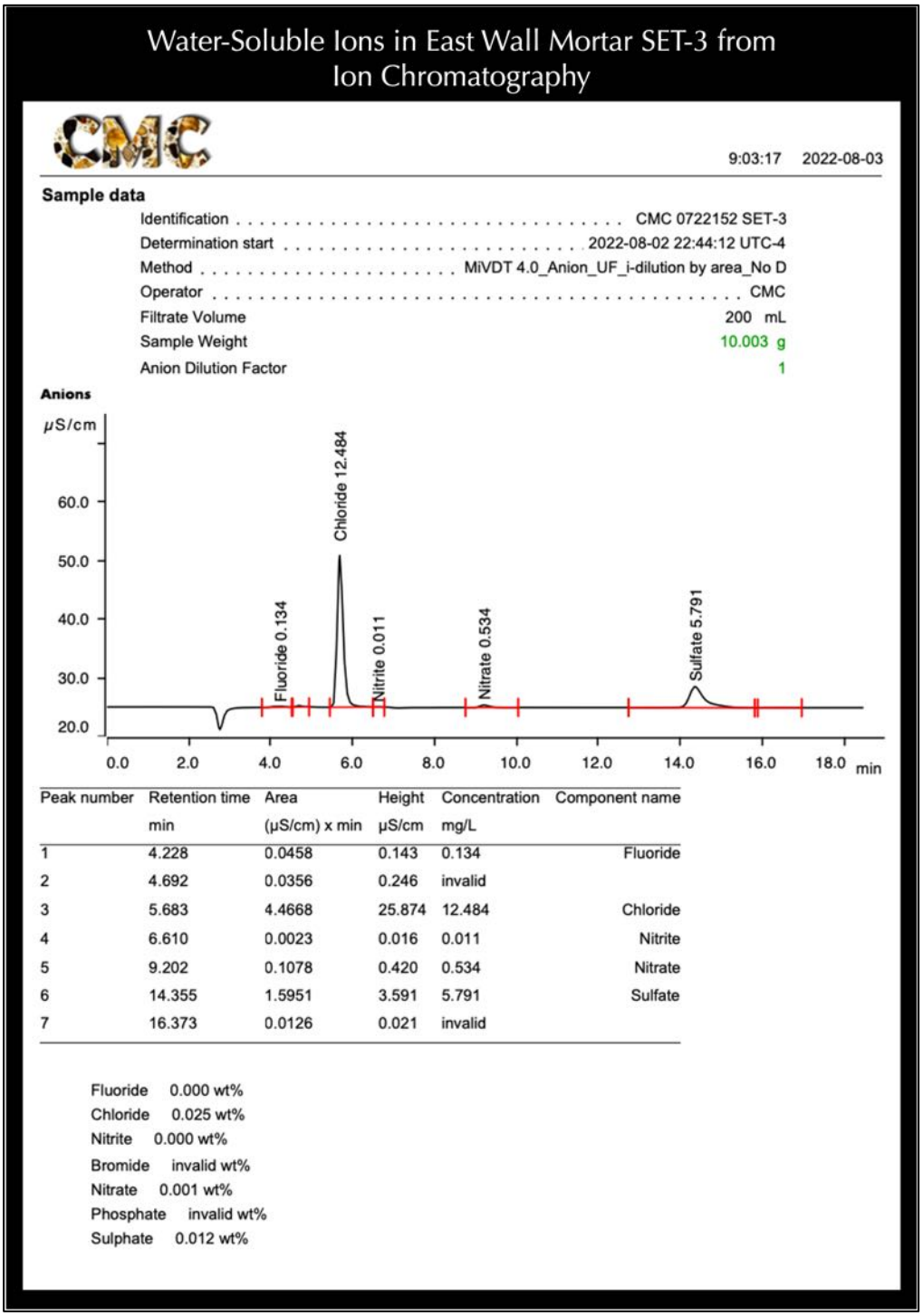

Figure 172: Ion chromatogram of water-soluble salts in the setting mortar SET-3 after digesting about a gram of pulverized mortar in deionized water for 30 minutes at a temperature below boiling, followed by continued digestion in water at the ambient laboratory condition for 24 hours. The filtrate was analyzed by ion chromatography. Filtrate shows the presence of negligible but detectable chloride (250 ppm) and sulfate (120 ppm) ions at low concentrations indicating the absence of any major chloride and/or sulfate salt source in the mortar.

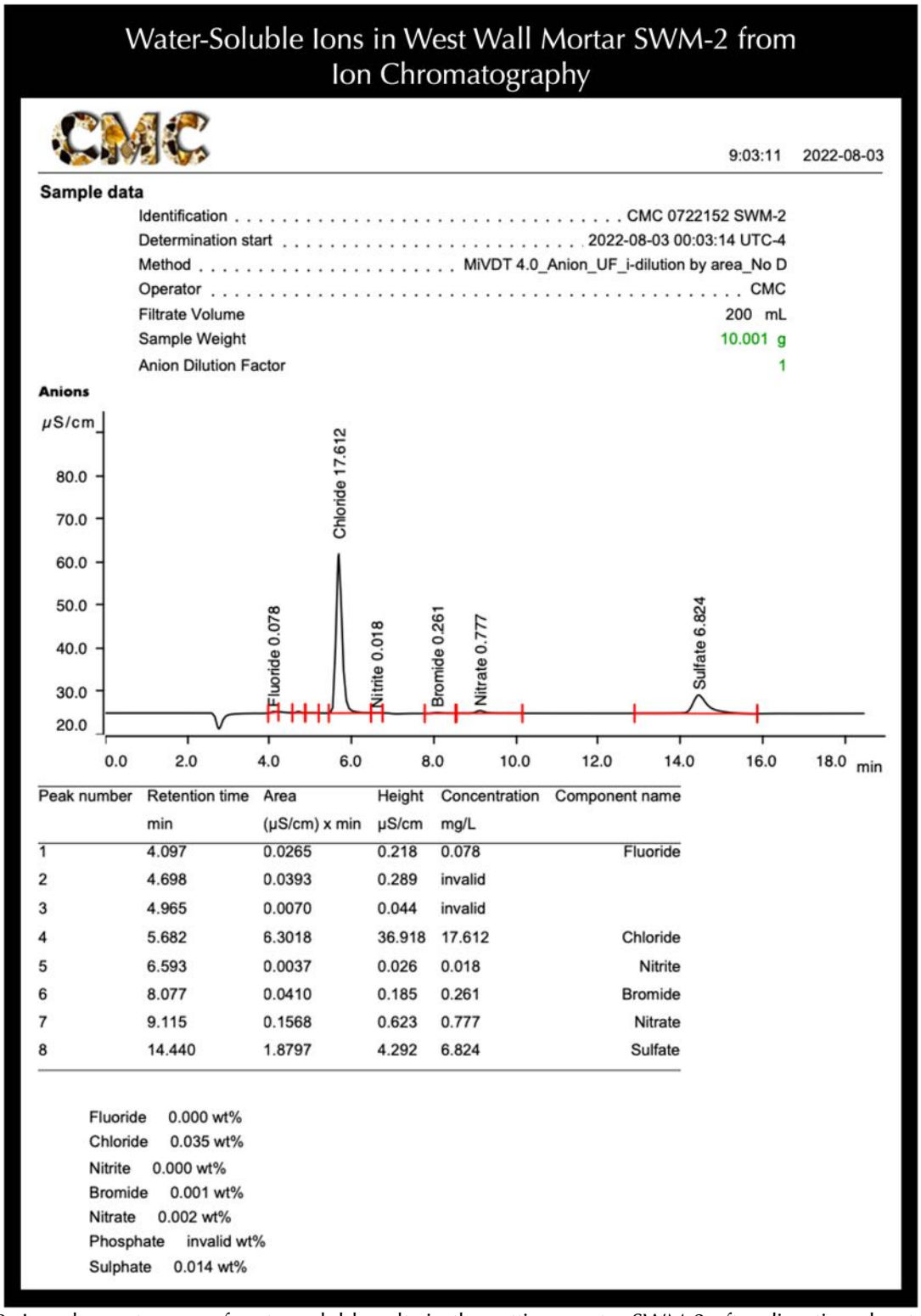

Peak number	Retention time min	Area (µS/cm) x min	Height µS/cm	Concentration mg/L	Component name
1	4.097	0.0265	0.218	0.078	Fluoride
2	4.698	0.0393	0.289	invalid	
3	4.965	0.0070	0.044	invalid	
4	5.682	6.3018	36.918	17.612	Chloride
5	6.593	0.0037	0.026	0.018	Nitrite
6	8.077	0.0410	0.185	0.261	Bromide
7	9.115	0.1568	0.623	0.777	Nitrate
8	14.440	1.8797	4.292	6.824	Sulfate

Figure 173: Ion chromatogram of water-soluble salts in the setting mortar SWM-2 after digesting about a gram of pulverized mortar in deionized water for 30 minutes at a temperature below boiling, followed by continued digestion in water at the ambient laboratory condition for 24 hours. The filtrate was analyzed by ion chromatography. Filtrate shows the presence of detectable chloride (350 ppm) and sulfate (140 ppm) at low concentrations indicating the absence of any major chloride and/or sulfate salt source in the mortar.

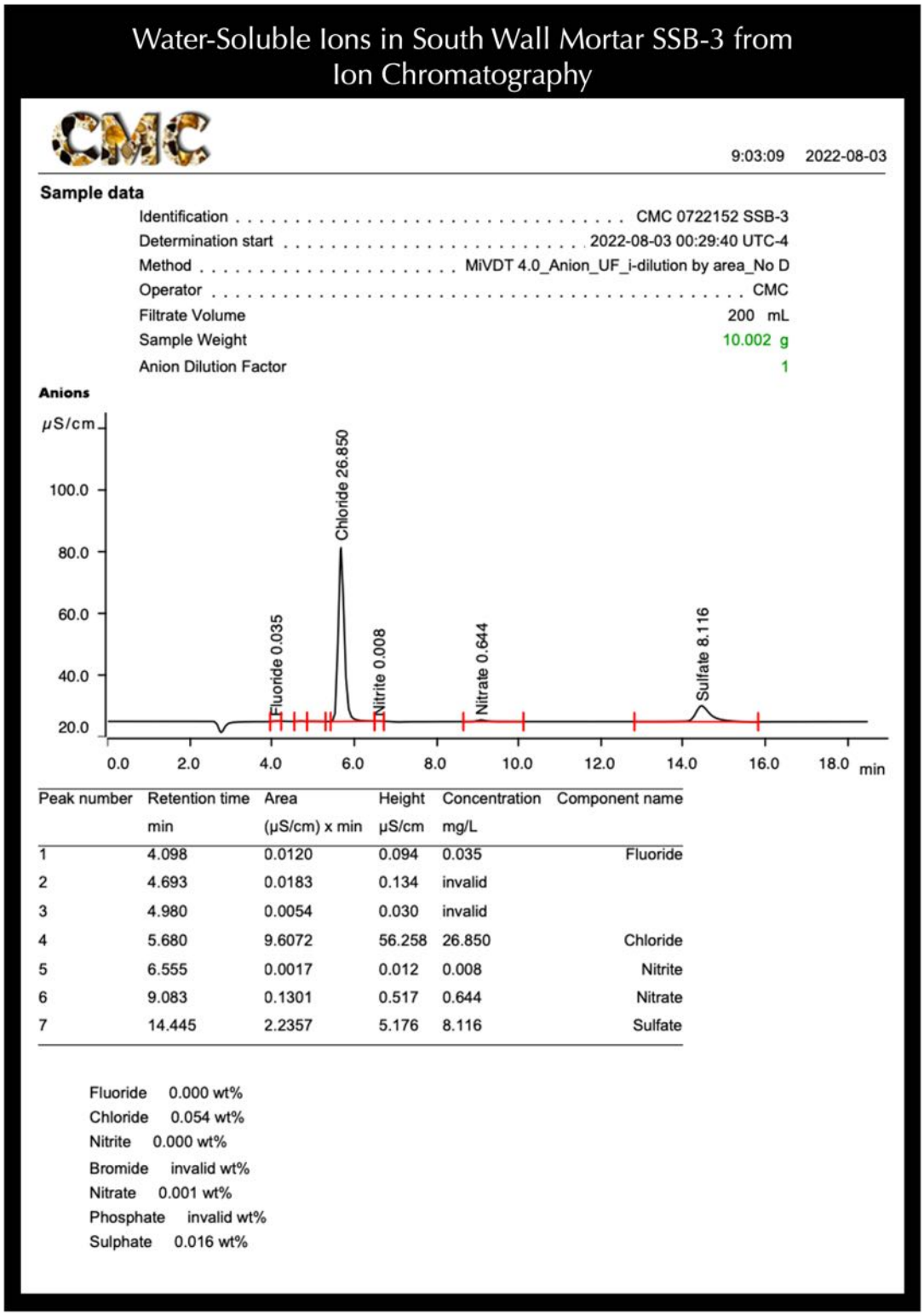

Peak number	Retention time min	Area (µS/cm) x min	Height µS/cm	Concentration mg/L	Component name
1	4.098	0.0120	0.094	0.035	Fluoride
2	4.693	0.0183	0.134	invalid	
3	4.980	0.0054	0.030	invalid	
4	5.680	9.6072	56.258	26.850	Chloride
5	6.555	0.0017	0.012	0.008	Nitrite
6	9.083	0.1301	0.517	0.644	Nitrate
7	14.445	2.2357	5.176	8.116	Sulfate

Figure 174: Ion chromatogram of water-soluble salts in the setting mortar SSB-3 after digesting about a gram of pulverized mortar in deionized water for 30 minutes at a temperature below boiling, followed by continued digestion in water at the ambient laboratory condition for 24 hours. The filtrate was analyzed by ion chromatography. Filtrate shows the presence of detectable chloride (540 ppm) and sulfate (160 ppm) at low concentrations indicating the absence of any major chloride and/or sulfate salt source in the mortar.

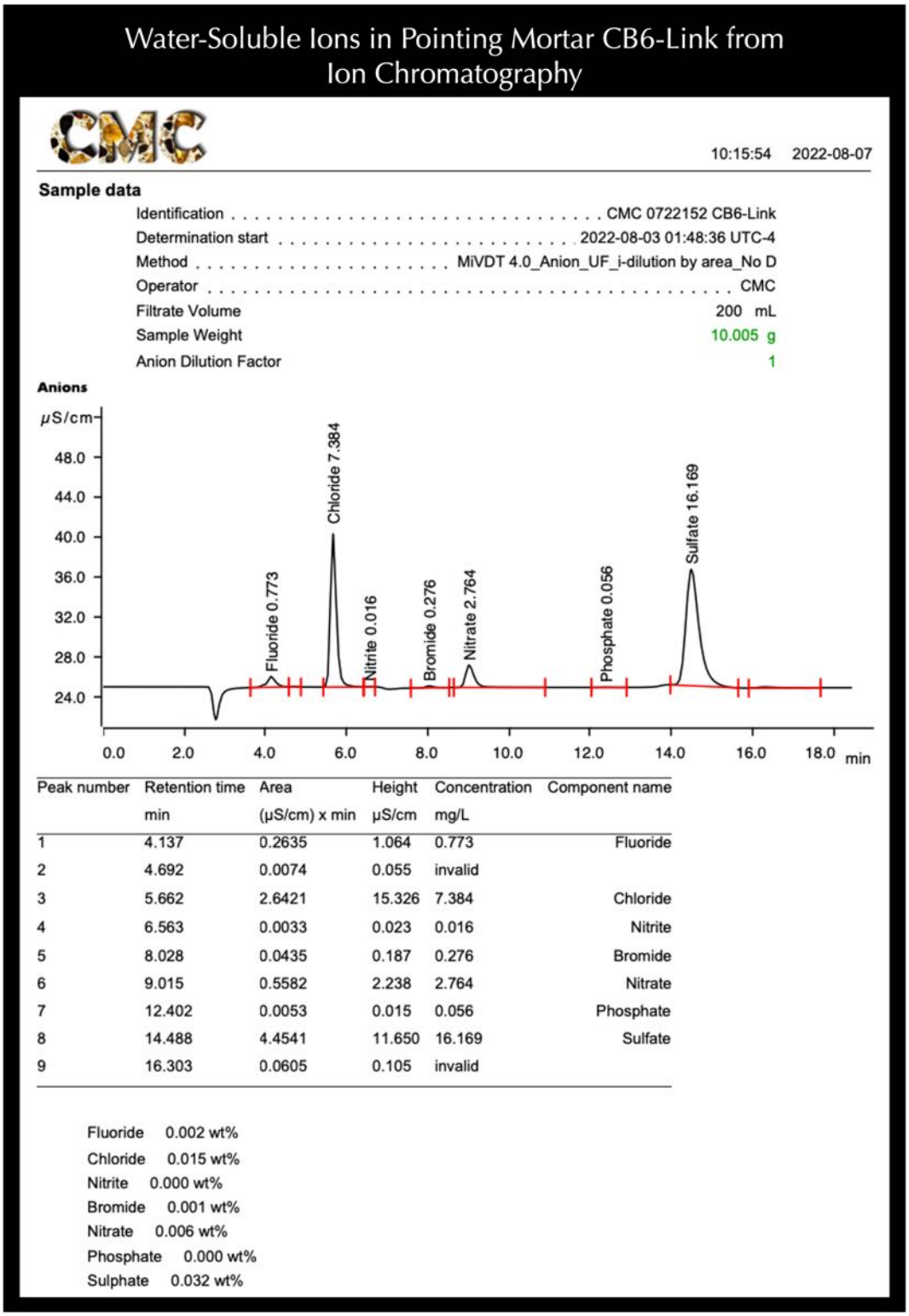

Peak number	Retention time min	Area (µS/cm) x min	Height µS/cm	Concentration mg/L	Component name
1	4.137	0.2635	1.064	0.773	Fluoride
2	4.692	0.0074	0.055	invalid	
3	5.662	2.6421	15.326	7.384	Chloride
4	6.563	0.0033	0.023	0.016	Nitrite
5	8.028	0.0435	0.187	0.276	Bromide
6	9.015	0.5582	2.238	2.764	Nitrate
7	12.402	0.0053	0.015	0.056	Phosphate
8	14.488	4.4541	11.650	16.169	Sulfate
9	16.303	0.0605	0.105	invalid	

Figure 175: Ion chromatogram of water-soluble salts in the pointing mortar CB6-Link after digesting about a gram of pulverized mortar in deionized water for 30 minutes at a temperature below boiling, followed by continued digestion in water at the ambient laboratory condition for 24 hours. The filtrate was analyzed by ion chromatography. Filtrate shows the presence of detectable chloride (150 ppm) and sulfate (320 ppm) at low concentrations indicating the absence of any major chloride and/or sulfate salt source in the mortar.

FTIR Spectroscopy

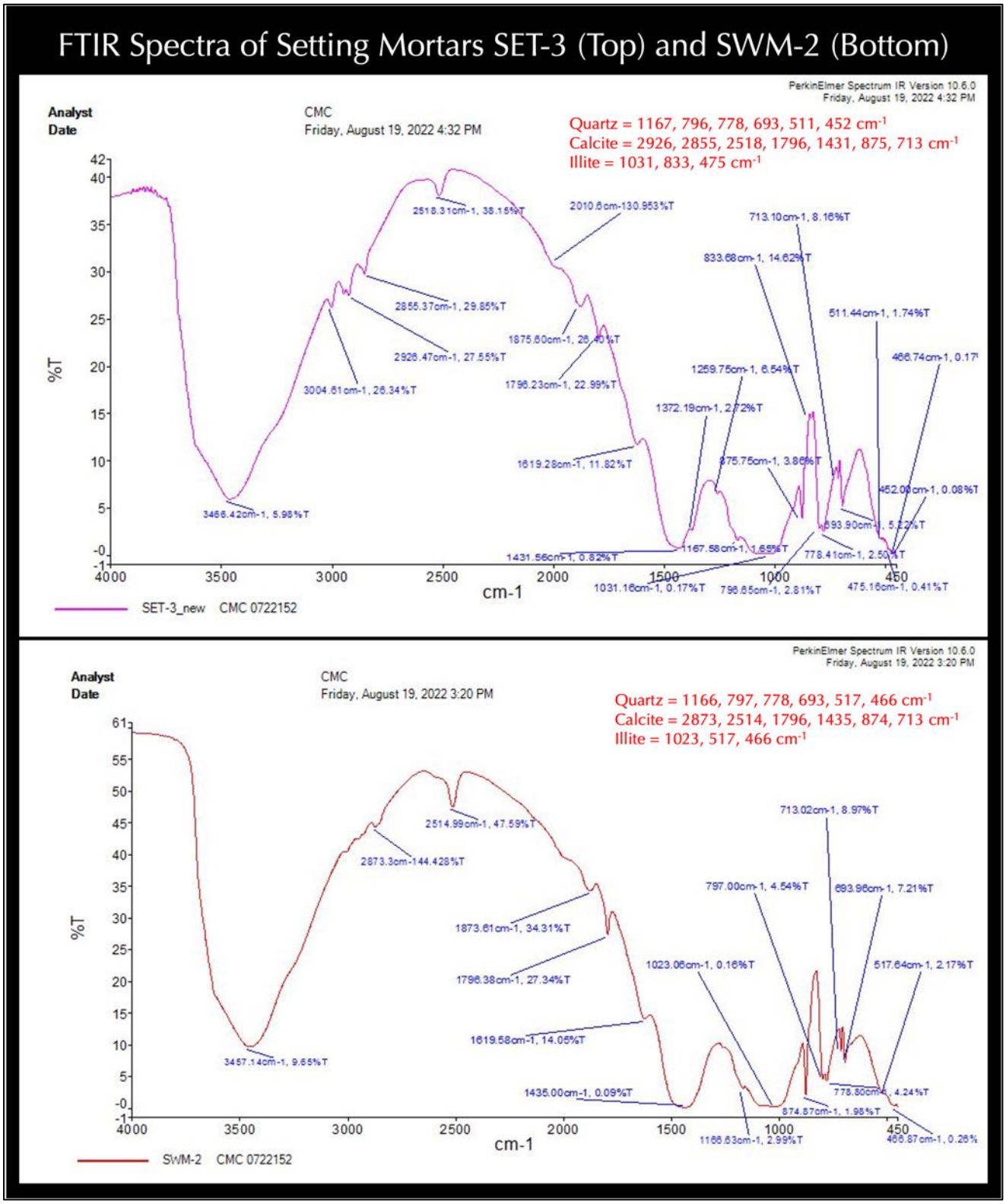

Figure 176: FTIR spectra of setting mortars from east (top) and west (bottom) walls showing overall compositional similarities in the presence of quartz, calcite, and clay. Spectra were obtained from prepared KBr pellets.

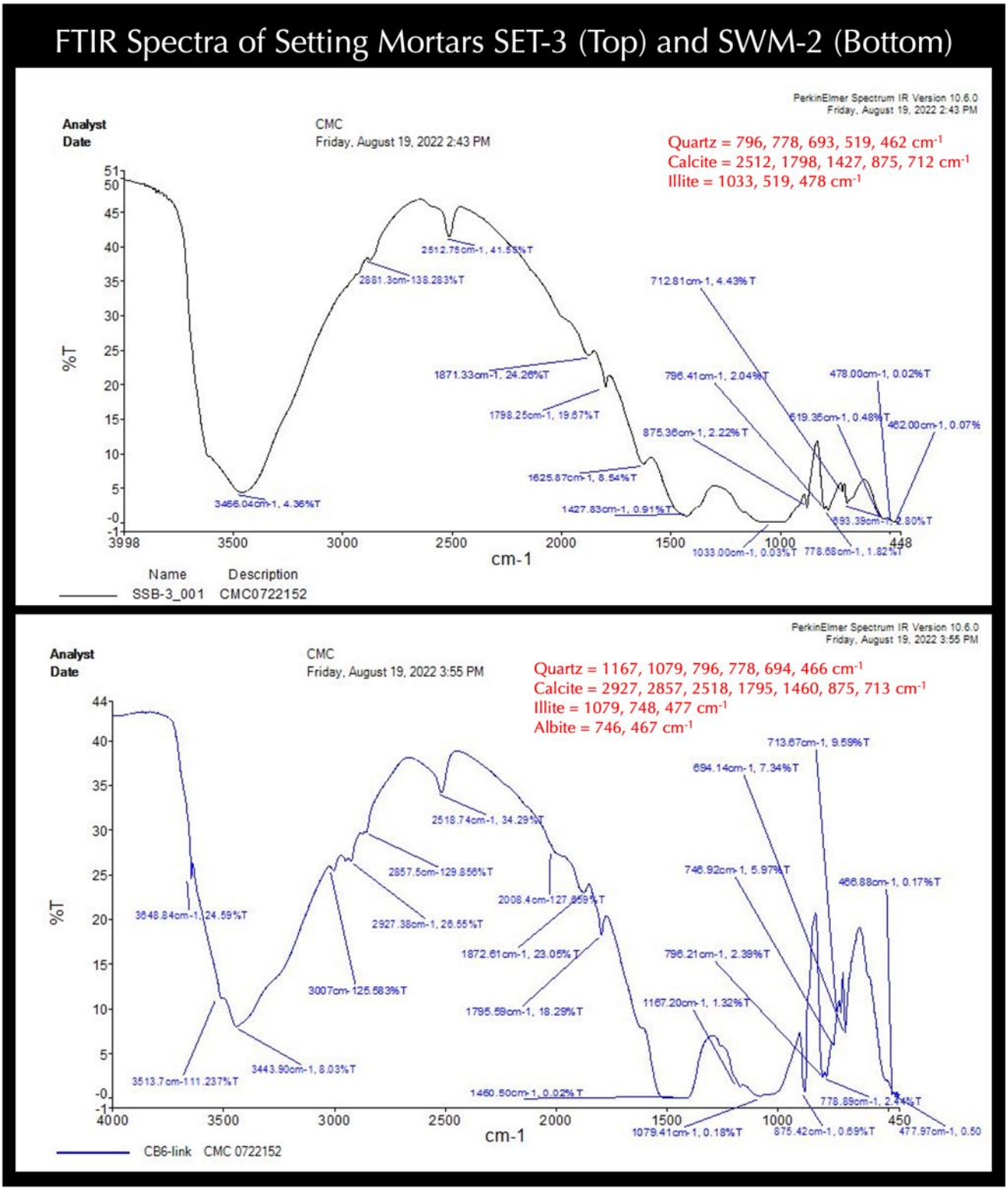

Figure 177: FTIR spectra of setting mortar from south wall (top) and pointing mortar (bottom) showing overall compositional similarities in the presence of quartz, calcite, and clay. Spectra were obtained from prepared KBr pellets.

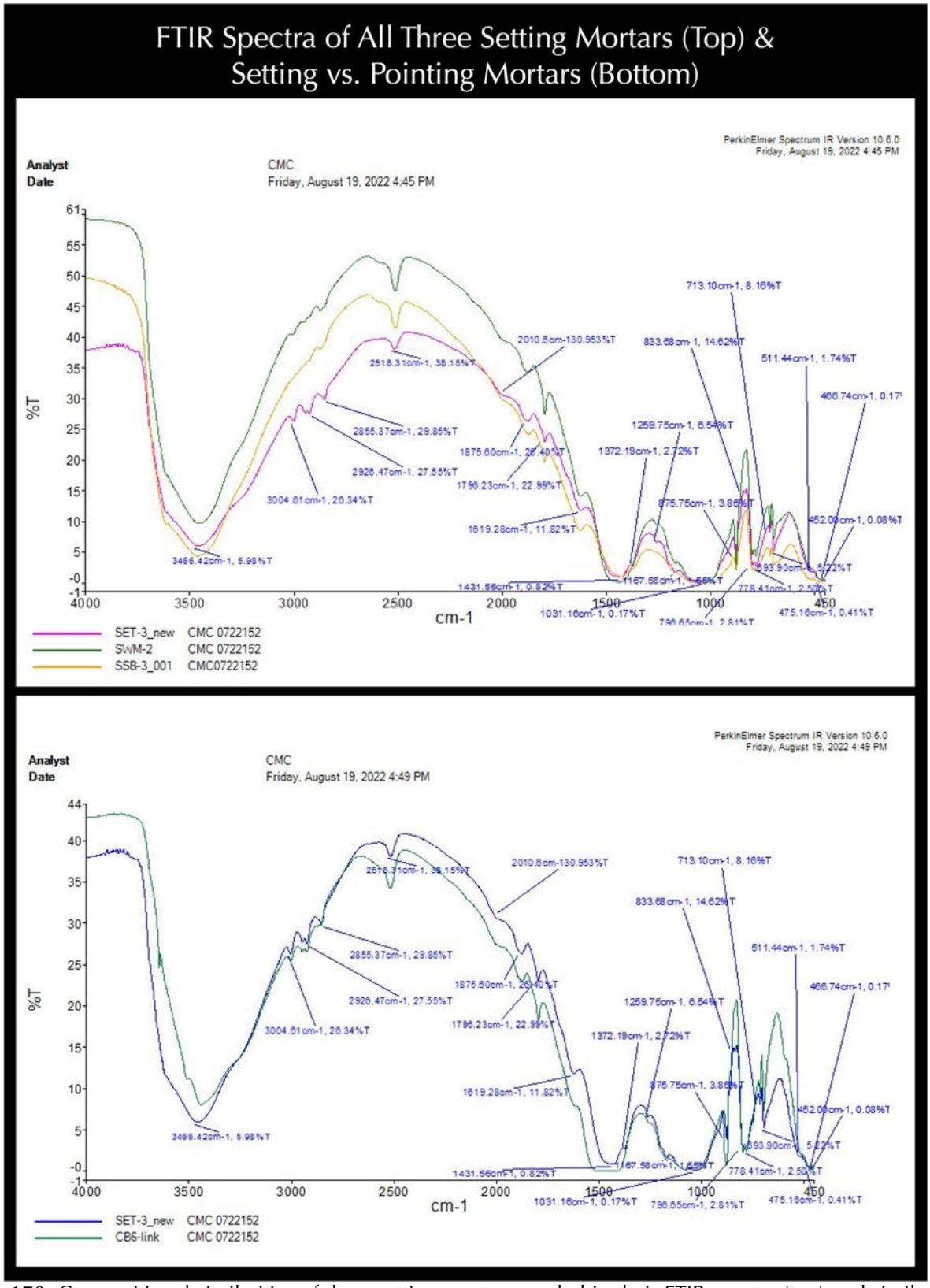

Figure 178: Compositional similarities of three setting mortars reveled in their FTIR spectra (top) and similarity in lime binder and silica sand compositions in setting and pointing mortars reveled in their FTIR spectra at bottom.

DISCUSSION

RELATIVE MERITS OF DIFFERENT ANALYTICAL TECHNIQUES IN HISTORIC MORTAR INVESTIGATION

The following Table summarizes relative merits of different analytical techniques used during examinations of these early 19th century mortars, and relevant information obtained from each method.

Properties	Optical Microscopy	SEM-EDS	XRF	XRD	Acid Digestion	Gravimetry	TGA/DSC	IC	FTIR
Sand Type	++++	++	+	++	+	+	+	-	++
Sand Color & Gradation	+++	+	-	-	++++	-	-	-	-
Sand Fineness	+++	++	-	-	++++	-	-	-	-
Ferruginous Shale/Siltstone in Sand	++++	+++	-	++	-	-	+	-	+
Clay	++	++	+	++++	-	-	++	-	+++
Deleterious constitutes in sand	++++	+++	+	++	++	+	++	+	++
Sand/Binder Proportion	+++	+	+	+	+++	+++	++	-	+
Calcined Clay Pozzolan	+++	++++	+	-	-	-	+	-	+
Clay-Lime Pozzolanic Reaction	+++	++++	-	-	-	-	+	-	+
Dolomitic Lime	+++	++++	++	+	+	+	++	-	++
Hydraulic Phase in Lime	++++	+++	-	++	-	-	+	-	+
Lime Leaching	+++	++++	+	+	-	-	+	-	+
Carbonation	+++	++++	+	+++	++	++	+++	-	+++
Secondary Precipitates	+++	+++	-	+	-	-	++	+	+
Soluble Salts	+++	+++	+	++	-	-	+	+++	++
Mortar Types' Variations	+++	++++	+	+	++	++	++	-	+
Non-hydraulic vs. Hydraulic Lime	+++	++++	+	+	-	++	++	-	+
Calcitic vs. Dolomitic Lime	++	++++	+	+	-	+	+++	-	+
Chemical Variations in Paste	++	++++	-	+	-	+	++	-	+
Alternations during Service	++++	+++	+	+	-	+	+	+	++
Inappropriate pointing mortar	++++	+++	++	+	+	+	++	-	++

Table 6: Relative merits of various analytical techniques used during investigation of historic mortars. Notes: ++++ Most relevant method, +++ Moderately relevant, ++ Relevant, + Less Relevant, - Not possible.

MORTAR TYPES AND INGREDIENTS

The early 19th century setting and pointing mortars examined here are determined to be representative of many historic lime mortars, which do not contain any Portland or masonry cement binders, hence are not representative of any modern-day e.g., ASTM C 270 mortars. The lime binder component is found in all mortar types examined, which in setting mortars showed variably degrees of leaching of lime from the original lime-magnesia-silica-alumina based binders leaving amorphous or gelatinous residues of silica-alumina-magnesia rich patches of leached areas of little or no cementitious properties merely as a skeleton of the original paste where lime is mostly found as secondary precipitates after leaching. Lime and magnesia components in the binder were contributed from the use of a magnesian or dolomitic lime binder, which, in turn, was produced from calcination of a relatively pure magnesian or dolomitic lime with very little impurities (silica, alumina, iron) i.e., to not produce a calcium silica-aluminate-based hydraulic phase typically found as residual hydraulic phases in many historic hydraulic lime binders, which are produced from calcination of an impure dolomitic limestone. Overall paste on the setting mortars are porous, fine-grained, skeletal microstructures of leached lime patches with secondary carbonate precipitates, carbonation shrinkage microcracks in lime-rich less-leached areas, residual lumps of unmixed lime, and other common microstructural features of historic lime mortars.

A separate calcined clay (brick dust) component was added in subordinate amount to lime in setting mortars, which was very fine-grained and intimately mixed with lime to create a relatively homogenous mix of lime-magnesia-silica-alumina based original binder from which after lime leaching a relatively homogeneous gelatinous mass of magnesia-silica-alumina-based leached areas were left across the microstructures of setting mortars. Addition of a calcined clay pozzolan to lime is a common practice since the Roman era which was widely used during early 19th century masonry constructions across Europe where various forms of calcined clay, e.g., from crushed brick to ceramics, terra cotta etc. were used to provide an amorphous aluminosilicate component as a pozzolan, which has reacted with lime to produce calcium silica and aluminate hydrates and hence densified the paste and overall mortars necessary for their long-term durability. All three setting mortars from east, west, and south interior walls showed evidence of lime leaching and enrichment of silica-alumina-magnesia-based leached amorphous areas in their microstructures.

The reddish-brown color tones of interstitial paste and the overall setting mortars are found to be contributed from the iron (and minor manganese) impurities in clay in the original calcined clay binder, along with leaching of reddish-brown ferruginous components of ferruginous shale/siltstone sand particles. Many angular to subangular to rounded sand particles in both coarser and finer fractions of sand showed reddish-brown clay coats, which are determined to be magnesia-silica-alumina-iron-based compositions where silica, alumina, and iron components came from the clay binder and reddish-brown ferruginous components of sand, whereas the magnesia component came from prolonged interactions with the dolomitic lime component of paste during leaching, which became the storehouse for magnesia. Hence, the reddish-brown coats on sand particles are not necessarily incorporated as clay coats or contaminants from sand but more probably developed from its prolonged chemical interactions (e.g., leaching) with paste.

Absence of a clay component, and use of a non-hydraulic or feebly hydraulic dolomitic/magnesian lime binder mixed with colorless to light gray very fine crushed dominantly silica-based sand in the pointing mortar has produced the typical light gray color tone of paste and overall mortar seen in many historic dolomitic lime mortars. Pointing mortar is relatively denser and harder due to lesser amount of leaching of lime than setting mortars. Some lime leaching has still occurred, which has reduced the overall lime/magnesia ratio in paste from >1 in the original binder to <1.

Mortar	Main Mortar	Other Contaminants	Comments
Setting Mortars from East, West and South Interior Walls	Two-component binder of (a) dolomitic lime and subordinate (b) calcined clay binders and two-component sand of a (a) coarse subangular to subrounded nominal 4 mm size sand of major amount of siliceous component (dominantly quartz and subordinate quartzite, and minor quartz siltstone) and subordinate amounts of argillaceous and ferruginous components (ferruginous shale, ferruginous siltstone, non-ferruginous shale, siltstone), and (b) a finer fraction of angular to subangular dominantly siliceous (mostly crushed silica sand) component and minor argillaceous, ferruginous component (max. 1 mm size)	No other components or contaminant are found	Characteristic reddish-brown color tone of binder, which has imparted the overall reddish-brown color tone of mortars, moderately hard to moderately soft, similar to many historic clay-lime mortars containing calcined clay (brick dusts) and dolomitic lime; all setting mortars are extensively leached creating patchy leached areas rich in silica, alumina, and magnesia where Si and Al are contributed form calcined clay component of original binder whereas magnesia was contributed from the dolomitic lime binder component
Pointing Mortar	Non-hydraulic to feebly hydraulic magnesian or dolomitic lime and fine-grained angular to subangular < 1 mm size sand consisting of dominantly siliceous (mostly crushed silica sand) component and minor argillaceous, ferruginous component, similar to the finer fraction of sand found in the setting mortars	No other components or contaminant are found	Characteristically light gray color tone of paste and overall mortar from the use of lime, no reddish-brown color tone for the lack of any clay component in the binder

Table 7: Mortar composition determined from optical microscopy and other tests.

DIFFICULTY IN MIX CALCULATIONS OF HISTORIC MORTARS

Due to extensive leaching of lime in setting mortars, along with use of a calcined clay binder component with lime, traditional methods of calculations of mix components in masonry mortars as described in ASTM C 1324 are not possible. Procedures of mix calculations from petrography and chemical analysis as described in ASTM C 1324 are applicable to modern-day cement-lime or masonry/mortar cement mortars prepared according to the procedures of ASTM C 270 where modern-day cement and lime binder components have far restricted chemical compositions for their productions under far stricter quality controls than their historic analogues. For example, modern Portland cements have a very restricted silica contents of 20-22%, and lime contents of 63-65% than their historic natural cement analogues, which showed a large range of compositions for use of argillaceous dolomitic limestones of different clay-silica impurities in raw feeds. Modern hydrated limes are produced by high-temperature slaking of quicklimes than the traditional historic lime production in putty form where original limestones being calcined contained various impurities to produce lime with a range of hydraulicities. Therefore, no single chemical parameter for a binder can be used for historic mortars to calculate proportion of that binder.

The petrography-plus-chemical based combined approach, however, can still be extended to historic lime mortars to a certain extent with some reasonable assumptions of the properties historic binders as long as the mortar is not

extensively altered to decompose the original binder compositions, and historic records of the original binders show more or less restricted chemical compositions to be used for mix calculations, e.g., to determine the hydraulic binder content from soluble silica content in the mortar assuming no additional source of soluble silica besides the historic binder. Limitation of this approach of historic cement content calculation from soluble silica content of mortar, as mentioned, lies in having a large range of soluble silica contents of historic cements for use of raw feeds of large range of impurities to produce large range of hydraulic phases, which would contribute to the soluble silica budget from subsequent hydration. This limits use of an 'assumed' silica content, e.g., use of 20-22% silica for calculation of Portland cement content in modern cement-lime mortars from soluble silica content in modern mortars. Presence of siliceous sand and no acid-soluble (calcareous) components in sand helps to determine the sand content directly from the acid-insoluble residue after digestion, from which binder content can be estimated from the rest (acid-soluble component) with the help of information obtained from petrography. Other alternative approaches such as determination of dolomitic lime content from the determined non-carbonated brucite content from thermal analysis, hydraulic lime or cement content from soluble silica from gravimetry and modal silica content in paste from SEM-EDS analysis, non-hydraulic calcitic lime content from degree of carbonation at loss on ignition at 950^{o}C, etc. are sometimes used for determination of historic binder contents, which, again is dependent on the degree of alterations and decompositions of historic mortars during service.

Compared to the estimation of binder contents, however, sand contents are relatively straightforward especially when sand is dominantly siliceous in composition, as mentioned, where acid-insoluble residue contents roughly correspond to the sand contents of mortars, as in the present case for all mortars examined.

In the absence of a reliable method of determination of mix proportions of historic mortar, especially after a century-long period of alternations is to examine the microstructures from petrography and SEM-EDS analysis, determine the original binders and sand used, qualitatively assess the extent of alterations, and from SEM-EDS based determination of paste compositions from least altered areas or samples estimate relative proportions consistent with the historical record of binder proportions used.

Taking into considerations of all the information obtained from petrography, chemical and other techniques, the best 'estimation' of relation proportions of mortar ingredients used during mixing of setting mortars are 1-part dolomitic lime to less than ¼-part calcined clay to 2 to 2½-part the total sum of calcined clay and lime components of binder. This recipe is very similar to the ones used during calcined clay-lime based historic mortars from the early 9th century across eastern US and the microstructure produced from such proportions, after century-long carbonation, leaching, and alterations would not different noticeably from the setting mortars seen in the present case. For the pointing mortar, a recipe of 1-part feebly hydraulic dolomitic lime or an NHL of NHL2 to NHL3.5 to 2-part sand would produce a similar mix. The best mix for both mortar types should be tested with multiple trials with mock-up batches over small test areas. Due to interior locations of setting mortars protected by a separate pointing mortar at the exterior, however, an exact match to the existing setting mortars are not crucial.

HISTORIC LIME, CLAY, AND NATURAL CEMENT MORTARS

Traditional historic mortars in the US historic constructions were made most commonly from slaked lime putty (i.e., high-calcium or magnesian/dolomitic non-hydraulic lime), or sometimes hot-mixed quicklime (where powdered quicklime was either dampened with sprinkles of water and kept under a layer of damp sand to hold the exothermic heat of hydration, or mixed with wet sand, or mixed with sand and water during application hence named the hot-mixed mortar). Aged lime putty was combined with local sand, generally in a ratio of 1-part lime putty to 3-part sand by volume. Often other ingredients, such as crushed marine shells (another source of lime), brick dust, clay, natural cements, pigments, and even animal hair were also added to mortar, but the basic formulation for lime putty and sand mortar remained unchanged for centuries until the advent of Portland cement or its forerunner, natural cements (Rosendale cement), hydraulic limes, and other hydraulic cements. Various degrees of hydraulicities of lime mortars are encountered depending on the impurities (siliceous, argillaceous components) present in the carbonate raw feeds.

Clay mortars are sometimes considered to be inferior materials, as they can be weak in tension and vulnerable to damage from exposure to water. However, a primary role of bedding mortars is to support the structural elements of a masonry wall, and earth mortars typically have sufficient compressive strength to perform this function. Cement and some lime mortars can be very hard and inflexible with high compressive strength, yet such qualities are unnecessary for traditional building and can be incompatible with some types of masonry. As clay mortar is susceptible to damage from water, most clay-bonded walls were externally pointed or harled with lime mortar to provide additional protection from the weather and concealing the underlying composition of the walls. Consequently, many clay-bonded masonry structures look much like lime-bonded and lime-finished traditional buildings and are not easily identifiable by external inspection. Historic clay mortars are traditionally soft that can be crushed in the hand giving a fine powder. The color, texture, and appearance of clay-rich mortars are generally quite different to a lime-based mortar. Laboratory testing for the presence of fine silicates can confirm the clay component in mortar. A clay mortar is generally composed entirely of very fine material commonly with a reddish or yellow color, whereas lime mortar is generally cream, off white or pale gray in color having sand particles of various sizes in the mix.

Natural cements were used in masonry construction of most Third System Fortifications. The Chief Engineer of the U.S. Corps of Engineers, General J. G. Totten, experimented with “Roman cement” in Europe and later dictated use of a natural cement from Rosendale, N.Y., for use in the Fort constructions in the 1800’s. In some cases, the Rosendale cement was “gauged” with lime to reduce costs and facilitate construction using locally available materials by using natural cement: lime: sand at 1: 0.5: 2 to 3-part (or 1-part cement plus lime to 2-part sand) volumetric proportions. Rosendale cement was discovered during the construction of the Erie Canal in the period 1817-1825. It was a calcium aluminosilicate mineral product manufactured by burning natural argillaceous dolomitic limestone from the Appalachian Mountain chain to temperatures in the range 700 to 900^{o}C.

POTENTIAL REPOINTING MORTARS

Mixing of lime with clay at various proportions changes the overall color tones of mortars in various shades of reddish-brown tones and variable hardness. So, to match with the existing interior clay-lime mortars similar to the examined three setting mortars, an appropriate clay-lime or pigmented (iron oxide or fine brick dust based) lime mockup mortars can be tried over a small test area. The mortar, however, can be protected with an exterior feebly hydraulic dolomitic lime mortar as the one seen in the pointing mortar. A natural hydraulic lime (e.g., NHL 2 or 3.5) can be tried for the exterior pointing mortar as an alternate to dolomitic lime. Binder-to-sand volumetric ratio should be restricted to 1-part total binder to maximum 3-part sand, which will be consistent with most historic mortars' proportions used during the 19th century.

Overall appearance of the final mortar, however, would depend on a match on sand, which constitutes the dominant proportion of the mortar. Sand to be used should be (a) dominantly siliceous in composition (silica sand based), which should rather not contain any argillaceous or ferruginous components to produce reddish-brown stains if the mortar mixes contain a reddish-brown iron oxide or brick dust-based pigment; (b) match in color to the color of sand in the examined mortar; (c) preferably be from similar sources; (d) be free of any debris, unsound, or any potentially deleterious constituents such as mica flakes; (e) conform be relatively finer than the size requirements of ASTM C 144 for masonry sand since sand in both setting and pointing mortars are finer than the modern ASTM C 144 sand; (f) not exceed maximum 3 times the sum of separate volumes of binder components; and (g) be durable.

An iron oxide or brick dust-based pigment can be added to substitute the reddish-brown setting mortars as long as dosage rate can be determined from trial batches for a good match. For its interior location inside the exterior pointing mortar, however, a perfect match may not be necessary. Use of Portland cement or Portland cement-based blended cement or slag cement should be avoided.

Initial rate of absorption (suction), and compressive strength of host stone masonry units are also important to determine the suitable mortar type, e.g., water retention properties (controlled by lime content) of mortar should be matched with the suction properties of masonry units.

Due to atmospheric weathering and alterations, an exact match in color to the existing setting or pointing mortars may not be possible, which, even if possible, could alter in future due to continued atmospheric weathering in the presence of oxygen, moisture, salt solutions, and other elements.

Appendix 2 provides various suggestions and guidelines for repointing mortar selections.

REFERENCES

ASTM C 10, "Standard Specification for Natural Cement," In Annual Book of ASTM Standards, Section Four Construction, Vol. 04.01 Cement; Lime; Gypsum; ASTM Committee C01 on Cement, 2017.

ASTM C 91, "Standard Specification for Masonry Cement," In Annual Book of ASTM Standards, Section Four Construction, Vol. 04.01 Cement; Lime; Gypsum; ASTM Committee C01 on Cement, 2017.

ASTM C 144, "Standard Specification for Aggregate for Masonry Mortar," In Annual Book of ASTM Standards, Section Four Construction, Vol. 04.05 Chemical-Resistant Nonmetallic Materials; Vitrified Clay Pipe; Concrete Pipe; Fiber-Reinforced Cement Products; Mortars or mortars and Grouts; Masonry; Precast Concrete; ASTM Committee C12 on Mortars or mortars for Unit Masonry, 2017.

ASTM C 1324, "Standard Test Method for Examination and Analysis of Hardened Masonry Mortar," In Annual Book of ASTM Standards, Section Four Construction, Vol. 04.05 Chemical-Resistant Nonmetallic Materials; Vitrified Clay Pipe; Concrete Pipe; Fiber-Reinforced Cement Products; Mortars or mortars and Grouts; Masonry; Precast Concrete; ASTM Committee C12 on Mortars or mortars for Unit Masonry, 2017.

ASTM C 270, "Standard Specification for Mortar for Unit Masonry," In Annual Book of ASTM Standards, Section Four Construction, Vol. 04.05 Chemical-Resistant Nonmetallic Materials; Vitrified Clay Pipe; Concrete Pipe; Fiber-Reinforced Cement Products; Mortars or mortars and Grouts; Masonry; Precast Concrete; ASTM Committee C12 on Mortars or mortars and Grouts for Unit Masonry, 2017.

ASTM C 1713, "Standard Specification for Mortars or mortars for the Repair of Historic Masonry," In Annual Book of ASTM Standards, Section Four Construction, Vol. 04.05 Chemical-Resistant Nonmetallic Materials; Vitrified Clay Pipe; Concrete Pipe; Fiber-Reinforced Cement Products; Mortars or mortars and Grouts; Masonry; Precast Concrete; ASTM Committee C12 on Mortars or mortars and Grouts for Unit Masonry, 2017.

ASTM C 51, "Standard Terminology Relating to Lime and Limestone (as used by the Industry)'" In Annual Book of ASTM Standards, Section Four Construction, Vol. 04.01 Cement; Lime; Gypsum; ASTM Committee C07 on Lime, 2017.

ASTM C 856, "Standard Practice for Petrographic Examination of Hardened Concrete," In Annual Book of ASTM Standards, Section Four Construction, Vol. 04.02; ASTM Subcommittee C 9.65, 2017.

ASTM C 1723, "Standard Guide for Examination of Hardened Concrete Using Scanning Electron Microscopy," In Annual Book of ASTM Standards, Section Four Construction, Vol. 04.02; ASTM Subcommittee C 9.65, 2017.

ASTM C 1329, "Standard Specification for Mortar Cement," In Annual Book of ASTM Standards, Section Four Construction, Vol. 04.01; ASTM Subcommittee C01.11, 2016.

ASTM C 150, "Standard Specification for Portland Cement," In Annual Book of ASTM Standards, Section Four Construction, Vol. 04.01; ASTM Subcommittee C01.10, 2018.

ASTM C 1489, "Standard Specification for Lime Putty for Structural Purposes," In Annual Book of ASTM Standards, Section Four Construction, Vol. 04.01; ASTM Subcommittee C07.02, 2015.

ASTM C 207, "Standard Specification for Hydrated Lime for Masonry Purposes," In Annual Book of ASTM Standards, Section Four Construction, Vol. 04.01; ASTM Subcommittee C07.02, 2011.

Bartos, P. Groot, C., and Hughes, J.J. (eds.), "Historic Mortars or mortars: Characteristics and Tests", Proceedings PRO12, RILEM Publications, France, 2000.

Boynton, R., *Chemistry and Technology of Lime and Limestone, 2nd edition*, John Wiley & Sons, Inc. 1980.

Brosnan, Denis, A., Characterization of Rosendale Mortars or mortars For Fort Sumter National Monument and Degradation of Mortars or mortars by Sea Water and Frost Action, Final Report, April 19, 2012.

Callebaut, K., Elsen, J., Van Balen, K., and Viaene, W., "Nineteenth century hydraulic restoration mortars or mortars in the Saint Michael's Church (Leuven, Belgium) Natural hydraulic lime or cement?" Cement and Concrete Research, V 31, pp 397-403, 2001.

Callebaut, K., Elsen, J., Van Balen, K., and Viaene, W., Historical and scientific study of hydraulic mortars or mortars from the 19th century. In International RILEM workshop on historic mortars or mortars: Characterization and Tests; Paisley, Scotland, 12th to 14th May 1999, Edited by Barton, P., Groot, C., and Hughes, J.J., Cachan, France, RILEM Publications, 2000.

Charloa, A.E., "Mortar analysis: A comparison of European procedures." US/ICOMOS Scientific Journal: Historic Mortars or mortars & Acidic Deposition on Stone, 3 (1), pp. 2-5, 2001.

Charola, A.E., and Lazzarin, L., Deterioration of Brick Masonry Caused by Acid Rain, ACS Symposium Series, Vol. 318, pp. 250-258, 2009.

Chiari, G., Torraca, G., and Santarelli, M.L., "Recommendations for Systematic Instrumental Analysis of Ancient Mortars or mortars: The Italian Experience", *Standards for Preservation and Rehabilitation*, ASTM STP 1258, S.J. Kelley, ed., American Society for Testing and Materials, pp. 275-284, 1996.

Doebley, C.E., and Spitzer, D., "Guidelines and Standards for Testing Historic Mortars or mortars", *Standards for Preservation and Rehabilitation*, ASTM STP 1258, S.J. Kelley, ed., American Society for Testing and Materials, pp. 285-293, 1996.

Eckel, Edwin, C., *Cements, Limes, and Plasters*, John Wiley & Sons, Inc. 655pp, 1922.

Edison, M.P. (Editor), *Natural Cement*, ASTM STP 1494, American Society for Testing and Materials, 2008.

Elsen, J., "Microscopy of Historic Mortars or mortars – A Review", *Cement and Concrete Research 36*, 1416-1424, 2006.

Elsen, J., Mertens, G., and Van Balen, K., Raw materials used in ancient mortars or mortars from the Cathedral of Notre-Dame in Tournai (Belgium), Eur. J. Mineral., Vol. 23, pp. 871-882, 2011.

Elsen, J., Van Balen, K., and Mertens, G., Hydraulicity in Historic Lime Mortars or mortars: A Review, In, Valek, J, Hughes, J.J., and Groot, W.P. (Eds.), Historic Mortars or mortars Characterization, Assessment and Repair, RILEM Book series, Volume 7, pp. 125-139, Springer, 2012.

Erlin, B., and Hime, W.G., "Evaluating Mortar Deterioration", *APT Bulletin*, Vol. 19, No. 4, pp. 8-10+54, 1987.

Goins E.S., "Standard Practice for Determining the Components of Historic Cementitious Materials," National Center for Preservation Technology and Training, Materials Research Series, NCPTT 2004.

Goins, E.S., "A standard method for the characterization of historic cementitious materials." US/ICOMOS Scientific Journal: Historic Mortars or mortars & Acidic Deposition on Stone, # (1), pp. 6-7, 2001.

Groot, C., Ashall, G., and Hughes, J., Characterization of Old Mortars or mortars with Respect to their Repair, State-of-the-art Report of RILEM Technical Committee 167-COM, 2004.

Hughes, D.C., Jaglin, D., Kozlowski, R., Mayr, N., Mucha, D., and Weber, J., "Calcination of Marls to Produce Roman Cement", pp. 84-95, In, Edison, M.P. (Editor), *Natural Cement*, ASTM STP 1494, American Society for Testing and Materials, 2007.

Hughes, J.J., Cuthbert, S., and, Bartos, P., "Alteration Textures in Historic Scottish Lime Mortars or mortars and the Implications for Practical Mortar Analysis", *Proceedings of the 7th Euroseminar on Microscopy Applied to Building Materials*, Delft, pp. 417-426, 1999.

Hughes, R.E., and Bargh, B.L., The weathering of brick: Causes, Assessment and Measurement, A Report of the Joint Agreement between the U.S. Geological Survey and the Illinois State Geological Survey, 1982.

Jana, D., "Application of Petrography In Restoration of Historic Masonry Structures", In: Hughes, J.J., Lesie, A.B. and Walsh, J.A., eds. *Proceedings of 10th Euroseminar on Microscopy Applied to Building Materials*, Paisley, 2005.

Jana, D., "Sample Preparation Techniques in Petrographic Examinations of Construction Materials: A State-of-the-art Review", *Proceedings of the 28th Conference on Cement Microscopy*, International Cement Microcopy Association, Denver, Colorado, pp. 23-70, 2006.

Jedrzejewska, H., Old mortars or mortars in Poland: a new method of investigation, Studies in Conservation 5, pp. 132-138, 1960.

Leslie, A.B., and Hughes, J.J., "Binder Microstructure in Lime Mortars or mortars: Implications for the Interpretation of Analysis Results", *Quarterly Journal of Engineering Geology & Hydrogeology*, V. 35, No. 3, pp. 257-263, 2001.

Lubell, B., van Hees, Rob. P.J., and Groot, Casper J.W.P., The role of sea salts in the occurrence of different damage mechanisms and decay on brick masonry, Construction and Building Materials, Vol. 18, pp. 119-124, 2004.

Martinet, G., Quenee, B., Proposal for a useful methodology for the study of ancient mortars or mortars, Proceedings of the International RILEM workshop "Historic Mortars or mortars: Characteristics and tests," Paisley, pp. 81-91, 2000.

Mack, Robert, and Speweik, John P., *Preservation Briefs 2*, U.S. Department of the Interior, National Park Service Cultural Resources, Heritage Preservation Services, pp. 1-16, 1998.

Middendorf, B., Baronio, G., Callebaut, K, and Hughes, J.J., "Chemical-mineralogical and physical-mechanical investigation of old mortars or mortars, Proceedings of the International RILEM workshop "Historic Mortars or mortars: Characteristics and tests," Paisley, pp. 53-61, 2000.

Middendorf, B., Hughes, J.J., Callebaut, K., Baronio, G., and Papayanni, I., Mineralogical characterization of historic mortars or mortars, In. Groot, C., et al. (eds), Characterization of Old Mortars or mortars with Respect to their Repair, State-of-the-art Report of RILEM Technical Committee 167-COM, pp. 21-36, 2004a.

Middendorf, B., Hughes, J.J., Callebaut, K., Baronio, G., and Papayanni, I., Chemical characterization of historic mortars or mortars, In. Groot, C., et al. (eds), Characterization of Old Mortars or mortars with Respect to their Repair, State-of-the-art Report of RILEM Technical Committee 167-COM, pp. 37-53, 2004b.

Middendorf, B., Hughes, J.J., Callebaut, K., Baronio, G., and Papayanni, I., "Investigative Methods for the Characterization of Historic Mortars or mortars – Part 1: Mineralogical Characterization," *Materials and Structures*, Vol. 38, 2005a.

Middendorf, B., Hughes, J.J., Callebaut, K., Baronio, G., and Papayanni, I., "Investigative Methods for the Characterization of Historic Mortars or mortars – Part 2: Chemical Characterization," *Materials and Structures*, Vol. 38, pp 771-780, 2005b.

Sarkar, S.L., Aimin, Xu, and Jana, Dipayan, Scanning electron microscopy and X-ray microanalysis of Concretes, pp. 231-274, In, Ramachandran, V.S. and Beaudoin, J.J. Handbook of Analytical Techniques in Concrete Science and Technology, Noyes Publications, Park Ridge, New Jersey, 2000.

Speweik, J.P., *The History of Masonry Mortar in America 1720-1995*, 2010.

Stewart, J., and Moore, J., Chemical techniques of historic mortar analysis, Proceedings of the ICCROM Symposium "Mortars or mortars, Cements, and Grouts used in the Conservation of Historic Buildings," Rome, ICCROM, Rome, pp. 297-310, 1981.

Valek, J., Hughes, J.J., and Groot, C. (eds.), *Historic Mortars or mortars: Characterization, Assessment and Repair*, Springer, RILEM Book series Vol. 7, p. 464, 2012.

Valek, J., Hughes, J.J., and Groot, C. (eds.), Historic Mortars or mortars: Characterization, Assessment and Repair, Springer, RILEM Book series Vol. 7, 2012.

Van Balen, K., Toumbakari, E.E., Blanco, M.T., Aguilera, J., Puertas, F., Sabbioni, C., Zappia, G., Riontino, C., and Gobbi, G., "Procedures for mortar type identification: A proposal." In International RILEM workshop on historic mortars or mortars: Characteristics and Tests; Paisley, Scotland, 13th to 14th May 1999, edited by Barton, P., Groot, C., and Hughes, J.J., Cachan, France: RILEM Publications, 2000.

Vyskocilova, R., W. Schwarz, D. Mucha, D. Hughes, R. Kozlowski, and J. Weber, "Hydration processes in pastes of roman and American natural cements," *ASTM STP*, vol. 4, no. 2, 2007.

Weber, J., Gadermayr, N., Kozlowski, R., Mucha, D., Hughes, D., Jaglin, D., and Schwarz, W., Microstructure and mineral composition of Roman cements produced at defined calcination conditions, Materials Characterization, Vol. 58, pp. 1217-1228, 2007.

✪□✪□✪ END OF TEXT ✪□✪□✪

APPENDIX 1 –
LABORATORY TESTING OF MASONRY MORTARS

METHODOLOGIES[1]

Until 1970-1980, characterization of masonry mortars were mostly based on traditional wet chemical analysis (Jedrzejewska, 1960, Stewart and Moore, 1981), where interpretation of results were often difficult if not impossible without a good knowledge of the nature of different ingredients. The majority of later characterization proposed optical microscopy (Erlin and Hime 1987, Middendorf et al. 2000, Elsen 2006) as the first step in identification of different components of mortar based on which other analytical techniques including wet chemistry are performed. Many advanced instrumental analyses e.g., scanning electron microscopy and X-ray microanalysis, X-ray diffraction, X-ray fluorescence spectroscopy, atomic absorption, thermal analysis, infrared spectroscopy, etc. play significant roles in examinations of masonry mortars (Bartos et al. 2000, Elsen 2006, Callebaut et al. 2000, Erlin and Hime 1987, Goins 2001, 2004, Groot et al. 2004, Doebley and Spitzer 1996, Chiari et al. 1996, Middendorf et al. 2000, 2004, 2005, Leslie and Hughes 2001, Martinet and Quenee 2000, Valek et al., 2012, and Jana 2005, 2006). The choice of appropriate analytical technique depends mainly on the questions that have to be addressed, and, on the amount of material available.

Purposes of laboratory testing of mortar are: (a) to document a historic or modern masonry mortar by examining its sand and binder components, proportions of various ingredients, and their effects on properties and performance of the mortar, (b) evidence of any chemical or physical deterioration of mortar from unsoundness of its ingredients to effects of potentially deleterious agents from the environment (e.g., salts), (c) records of later repointing events and their beneficial or detrimental effects on the performance of the original mortar and masonry units, and finally, (d) an assessment of an appropriate restoration mortar to ensure compatibility with the existing mortar.

Currently there are two standardized procedures available that describe various laboratory techniques for analyses of masonry mortars with special emphases on historic mortars. One is ASTM C 1324 "Standard Test Method for Examination and Analysis of Hardened Masonry Mortar," which includes detailed petrographic examinations, followed by chemical analyses, along with various other analytical methods to test masonry mortars as described in various literatures, e.g., XRD, thermal analysis, and infrared spectroscopy. The second one is the RILEM method described in a series of publications from Middendorf et al. (2004, 2005).

The present mortar was tested by following these established methods of ASTM C 1324, and RILEM, which include detailed petrographic examinations, i.e., optical and scanning electron microscopy and X-ray microanalyses (SEM-EDS), followed by chemical analyses (gravimetry, acid digestion), X-ray fluorescence (XRF), X-ray diffraction (XRD), and thermal analyses (TGA, DTG, and DSC). Mortar sample was first photographed with a digital camera, scanned on a flatbed scanner, and examined in a low-power stereomicroscope for the preliminary examinations, e.g., to screen any unusual pieces having different appearances, e.g., representing contaminants from prior pointing episodes or remains of host masonry units.

Representative subset pieces of interest are then selected for: (a) optical microscopy and (b) scanning electron microscopy and X-ray microanalysis for chemical and mineralogical compositions, and microstructures of sand, paste, and overall mortar, (c) acid digestion, preferably from un-pulverized or lightly pulverized sample for extraction of siliceous sand by acid digestion for grain size distribution, (d) loss on ignition from ambient to 950°C temperatures for free and hydrate water, and carbonate contents, (e) acid digestion for determination of insoluble residue content, (f) cold acid and hot alkali digestions for determination of soluble silica content from hydraulic binder if any, after pulverizing a subset to finer than 0.3 mm size, and, (g) ultra-fine pulverization (<44-micron) of a subset for XRD, XRF, and thermal analysis. Any additional analyses, if needed, e.g., water digestion of mortar for determination of water-soluble salts by ion chromatography, or, Fourier-transform infrared spectroscopy of mortar for determining any coatings or organics added, etc. are done on the as-needed basis from the remaining set.

Information obtained from petrographic examinations is crucial to devise appropriate guidelines for subsequent chemical and other analytical methods, and, to properly interpret the results of chemical analyses. For example, detection of siliceous versus calcareous versus argillaceous components of aggregates in sample, or, the presence of any pozzolan in the binder (slag, fly ash, ceramic dusts, etc.) from petrography restricts which chemical method to follow, and how to interpret the results of such analyses, e.g., acid-insoluble residue contents.
Therefore, a direct chemical analysis e.g., acid digestion of a mortar without doing a prior petrographic examination to determine the types of aggregates and binder used could lead to highly erroneous results and interpretation. Armed with petrographic and chemical data and based on assumed compositions and bulk densities of the sand and the binder(s) similar to the ones detected from petrographic examinations, volumetric proportions of sand and various binders present in the examined sample can be calculated. The estimated mix proportions from such calculations can provide only a rough guideline to use as a starting mix for mock-up mixes during formulation of a pointing mortar to match with the existing mortar.

[1] For details on laboratory facilities for testing of masonry mortar, visit www.cmc-concrete.com

Extraction of Siliceous Sand by Acid Digestion and Sieve Analysis

For mortars containing siliceous sand (e.g., containing quartz, quartzite, granite, sandstone, siltstone, feldspar, etc.), sand can be extracted by digesting a few representative as-received mortar fragments in (1+3) dilute hydrochloric acid to dissolve away all binder fractions and extract, wash, and dry the acid-insoluble component of mortar, which is mostly the siliceous component of sand. The mortar fragments are first gently broken down into small pieces in a porcelain mortar and pestle making sure not to reduce inherent grain-size of sand during this size-reduction process of bulk mortar. Subsequent smaller pieces are then placed in a 250-ml glass beaker completely immersed in dilute hydrochloric acid and stirred with a magnetic stirring rod over a stirrer for a period of at least 24 hours to several days depending on the binder type for complete digestion of binder fractions and settlement of siliceous sand at the bottom of beaker to be filtered out for sieve analysis.

Sand particles thus extracted are washed, oven-dried, and sieved in an automatic mini sieve shaker through various U.S. Sieves from No. 4 (4.75 mm) through 8 (2.36 mm), 16 (1.18 mm), 30 (0.6 mm), 50 (0.3 mm), 100 (0.15 mm), and 200 (0.075 mm) for determination of the size, shape, angularity, and color of sands retained on various sieves. Grain-size distribution of sand is then compared with ASTM C 144 specifications for masonry sand. Photomicrographs of sand retained on each sieve are then taken with a stereomicroscope to record the sand size, shape, and color variations. For low amount of sample, or, for sample having calcareous sand, image analysis (e.g., Image J) on stitched photomicrographs of thin sections taken from multiple areas can be done to determine the sand-size distribution (Elsen et al. 2011).

Fig. A1: Gilson mini sieve shaker used for sieve analysis of sand extract from mortar after acid digestion.

Optical Microscopy

The main purposes of optical microscopy of masonry mortar are characterization of:

a. Aggregates, e.g., type(s), chemical and mineralogical compositions, nominal maximum size, shape, angularity, grain-size distribution, soundness, alkali-aggregate reactivity, etc.;
b. Paste, e.g., compositions and microstructures to diagnose various type(s) of binder(s) used;
c. Air, e.g., presence or absence of air entrainment, air content, etc.;
d. Alterations, e.g., lime leaching, carbonation, staining, etc. due to interactions with the environmental agents during service, and effects of such alterations on properties and performance of mortar; and
e. Deteriorations, e.g., chemical and/or physical deteriorations during service, cracking from various mechanisms, salt attacks, possible reasons for the lack of bond if reported from the masonry unit, etc.

Fragments selected from preliminary examinations for microscopy are sectioned, polished, and thin-sectioned (down to 25 to 30-micron thickness) preferably after encapsulating and impregnating with a dyed-epoxy to improve the overall integrity of the sample during precision sectioning and grinding, and to highlight porous areas, voids, and cracks. Prepared sections are then examined in a high-power stereo-zoom microscope up to 100X magnifications having reflected and transmitted-light, and plane and crossed polarized-light facilities, and eventually in a high-power petrographic microscope (up to 600X magnifications) equipped with transmitted, reflected, polarized, and fluorescent-light facilities. Capturing high-resolution micrographs from these microscopes via high-resolution high frame rate digital microscope cameras with appropriate image analyses software are an integral part of documentations during petrographic examinations.

Therefore, the essential steps followed during optical microscopy are:

a. Visual examination of as-received, fresh fractured, and sectioned surfaces of mortar on a flatbed scanner and in a stereo-microscope;
b. Preparation of clear epoxy-encapsulated block of mortar for subsequent sectioning and lapping for examinations of sand and binder in a stereo-microscope;
c. Preparation of a blue or fluorescent dye-mixed epoxy-impregnated large-area (50 × 75 mm) thin section of mortar of uniform thickness of 25-30 micron across the section;
d. Observation of thin section in a transmitted-light stereo-zoom microscope from 5X to 100X preferably with polarized-light facilities to observe large-scale distribution of sand and mortar microstructure in plane polarized light and sand type and carbonation of paste in crossed polarized light; and finally
e. Observation of thin section in a polarized-light (petrographic) microscope from 40X to 600X equipped with transmitted and reflected, polarized and fluorescent-light facilities for examinations of sand and binder compositions and microstructures.

For thin section preparation, representative fragments are oven-dried at 40 to 60°C to a constant mass and placed in a flexible (e.g., molded silicone) sample holder, then encapsulated with a colored dye-mixed (e.g., blue dye commonly used in sedimentary petrography, or, fluorescent dye, Elsen 2006) low-viscosity epoxy resin under vacuum to impregnate the capillary pore spaces of mortar, improve the overall integrity of sample during sectioning by the cured epoxy, highlight porous areas of mortar, alterations, cracks, voids, reaction products, etc. The epoxy-encapsulated cured solid block of sample is then de-molded, sectioned if needed, and processed through a series of coarse to fine grinding on metal and resin-bonded diamond grinding discs with water or a lubricant, eventually a perfectly flat clean ground surface is glued to a frosted large-area (50 × 75 mm) glass slide. Careful precision sectioning and precision grinding of the sample is then done in a thin-sectioning machine till the thickness is down to 50 to 60 micron. Final thinning down to 25 to 30-micron thickness is done on a glass plate with fine (5-15 micron) alumina abrasive. Thin section is eventually polished with various fine (1 micron to 0.25 micron size) diamond abrasives on polishing wheels suitable for examinations in a petrographic microscope, and eventually in SEM-EDS. Sample preparation steps are described in detail in Jana (2006).

Fig. A2: CMC's optical microscopy laboratory that houses various stereomicroscopes and polarizing microscopes used for this study.

More elaborate steps followed during optical microscopy include:

a. Visual examinations of sample as-received to select fragments for detailed optical microscopy; initial digital and flatbed scanner photography of sample as-received;
b. Low-power stereo-microscopic examinations of saw-cut and freshly fractured sections of sample for evaluation of variations in color, grain-size and appearances of sand, and the nature of the paste;
c. Examinations of oil immersion mounts for special features and materials in a petrographic microscope;
d. Examinations of colored (blue or fluorescent) dye-mixed epoxy-impregnated polished thin sections in a transmitted-light stereo-zoom microscope for determination of size, shape, angularity, and distribution of sand, as well as abundance and distribution of void and pore spaces that are highlighted by the colored dye-mixed epoxy;
e. Image analyses of micrographs of thin sections for estimations of pores, voids, intergranular open spaces, and shrinkage microcracks by using Image J or other image analysis software, where multiple micrographs are collected in plane polarized light mode by using a high-resolution stereo-zoom microscope equipped with transmitted and polarizing light facilities and stitched to get an adequate representative coverage;
f. Examinations of colored (blue or fluorescent) dye-mixed epoxy-impregnated polished thin sections in a petrographic microscope for detailed compositional, mineralogical, textural, and microstructural analyses of aggregates and binders, along with diagnoses of evidence of any deleterious processes and alterations (e.g., lime leaching, precipitation of secondary deposits and alteration products, salts);
g. Examinations of polished thin or solid section in reflected-light (epi-illumination) mode of petrographic microscope after etching the surface with acids to identify various non-hydrated hydraulic phases (e.g., C_2S, C_3S, C_3A, etc., Middendorf et al., 2005);
h. Examinations of any physical or chemical deterioration or signs of improper construction practices from microstructural evidences;
i. Stereo-microscopical examinations of size, shape, and color variations of sand extracted after hydrochloric acid digestion; and finally,
j. Selection of areas of interest to be examined by scanning electron microscopy.

Scanning Electron Microscopy & Microanalysis by Energy-Dispersive X-ray Spectroscopy (SEM-EDS)

Methods followed during SEM-EDS studies include: (a) secondary electron imaging (SEI) to determine the microstructure and morphology of the examined surface of sample, (b) backscatter electron (BSE) imaging to determine compositions of various phases from various shades of darkness/grayness/brightness from average atomic numbers of phases from the darkest pore spaces to brightest iron minerals (e.g., thaumasite, periclase, ettringite, quartz, dolomite, monosulfate, gypsum, calcite, C-S-H, aluminate, calcium hydroxide, belite, alite, free lime, and ferrite having progressively increasing average atomic numbers and brightness in BSE image), (c) X-ray elemental mapping (dot mapping) of an area of interest to differentiate various phases, (d) point-mode or area (raster)-mode analysis of specific area/phase of interest on a polished thin or solid section, and (e) average compositional analysis of a specific phase or an area on a polished thin or solid section or small subset of a sample.

The main purposes of SEM-EDS examinations of masonry mortars are to:

a. Observe the morphologies and microstructures of various phases of sand and binder,
b. Characterize the typical fine-grained microstructure of hydrated, carbonated, and hydraulic components of binder that are too fine to be examined by optical microscopy and are not well crystallized to be detected by XRD;
c. Determine major element oxide compositions, and compositional variations of paste, and from that determine the type of binder(s) used, especially to differentiate non-hydraulic calcitic and dolomitic lime mortars from hydraulic lime varieties (e.g., from silica contents of paste), natural cements (e.g., from silica and magnesia contents), pozzolans, slag cements, Portland cements, etc. all from their characteristic differences in compositions and hydraulicities (e.g., cementation index of Eckel 1922);
d. Determine composition of residual hydraulic phases to assess the raw feed and calcination processes used in manufacturing of binder;
e. Assess hydration, carbonation, and alteration products of binders,
f. Investigate effects of various alterations of paste during service and its role on properties and performance of mortar,
g. Detect salts and other potentially deleterious constituents,
h. Detect pigments and fillers,
i. Examine compositional variations across multiple mortars installed, etc.; and eventually
j. Complement and confirm the results of optical microscopy.

Due to characteristic difference in compositions of pastes made using various binders, e.g., non-hydraulic lime (CaO dominates over all other oxides), variably hydraulic lime (CaO with variable SiO_2 contents depending on degree of hydraulicity), dolomitic lime (high CaO and MgO), natural cement (CaO, SiO_2, Al_2O_3, and MgO contents are high, high MgO and FeO contents are characteristic), and Portland cement (CaO and SiO_2 contents are higher than all other oxides), SEM-EDS analysis of paste is a powerful method for detection of the original binder components in the sample. Effects of chemical alterations and various chemical deteriorations of a mortar (e.g., lime leaching, secondary calcite precipitates, gypsum deposits, etc.) can also be detected by SEM-EDS.

Fig. A3: Camscan SEM equipped with Ametek EDAX silicon drift detector for elemental analyses, secondary electron detector for morphological analyses and high-resolution YAG backscatter electron detector for microstructural analyses, and 4Pi revolution module for data collection and analyses.

SEM-EDS analysis is done in a CamScan Series 2 scanning electron microscope equipped with a high-resolution column 40Å tungsten, 40 kV electron optics zoom condenser 75° focusing lens operating at 20 kV, equipped with a variable geometry secondary electron detector, backscatter electron detector, EDS detector for observations of microstructures at high-resolution, compositional analysis, and quantitative determinations of major element oxides from various areas of interest, respectively. Revolution 4Pi software was used for digital storage of secondary electron and backscatter electron images, elemental mapping, and compositional analysis along a line, or on a point or an area of interest. Portion(s) of interest on the polished 50 mm × 75 mm size thin section used for optical microscopy were subsequently coated with carbon or gold-palladium film and placed on a custom-made aluminum sample holder to fit inside the large multiported chamber of CamScan SEM equipped with the eucentric 50 × 100 mm motorized stage. Usually, features of interest from optical microscopy are marked on the thin section with a fine-tipped conductive marker pen for further observations in SEM. Alternately, solid polished section or grain mount from phases or areas of interest can also be examined. Procedures for SEM examinations are described in ASTM C 1723 and Sarkar, Amin, and Jana (2000).

Chemical Analysis (Gravimetry and Instrumental Analysis)

Following petrographic examinations, chemical analyses of the mortar are done to determine the:

a. Hydrochloric acid-insoluble residue content to determine the siliceous sand content;
b. Losses on ignition due to release of free water, hydrate water, and CO_2;
c. Soluble silica contents contributed from hydraulic binders; and,
d. Bulk oxide contents, e.g., lime, silica, alumina, magnesia, alkalis, and others.

Chemical analyses are done by using various methods outlined in ASTM C 1324 and Middendorf et al. 2005a, e.g., by wet chemistry (gravimetry) and various instrumental techniques, e.g., atomic absorption spectroscopy (AAS), inductively coupled plasma atomic emission spectroscopy (ICP-AES), and X-ray fluorescence spectroscopy (XRF). Steps followed during chemical analyses of mortars are summarized in Fig. A4.

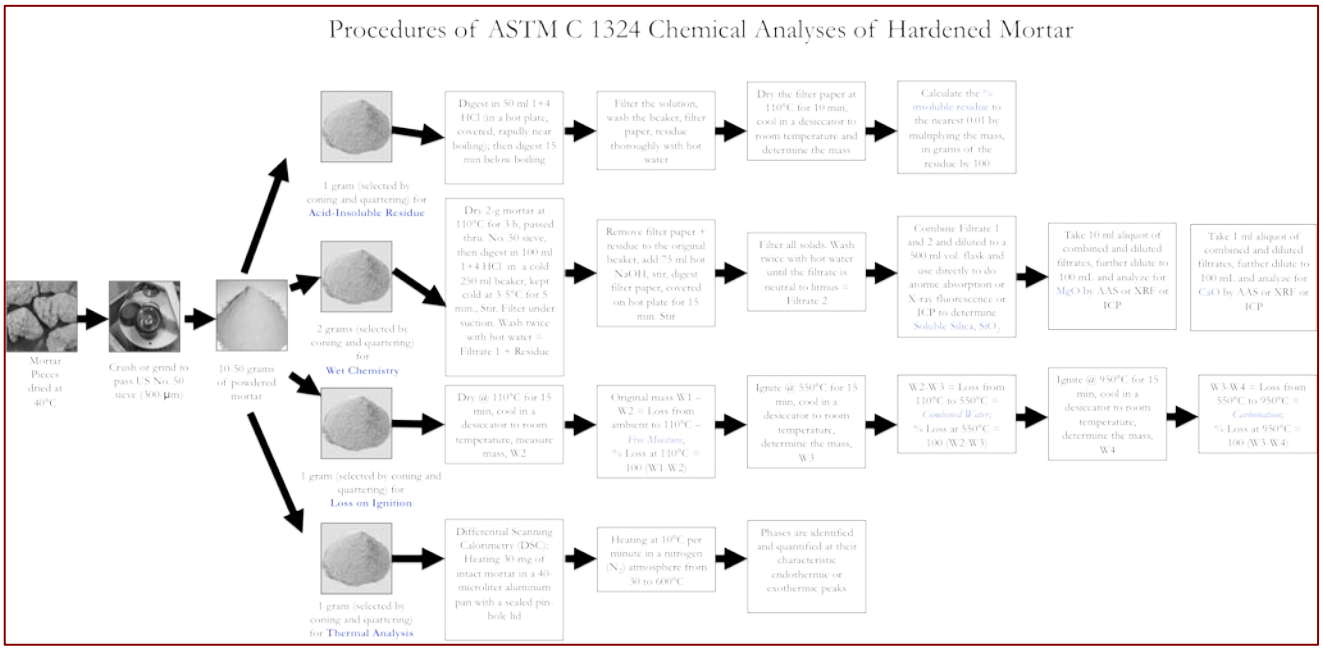

Fig. A4: Steps followed during various chemical analyses of mortars according to ASTM C 1324.

Acid Digestion

Acid digestion is perhaps the most commonly used test of masonry mortar, which is done to: (a) extract sand from sample by dissolving out the binder fractions so that grain-size distribution of sand can be done by sieve analysis, and (b) assess insoluble sand content in the sample. Sand content after acid digestion is determined both from: (a) 1.00 gram of pulverized sample (finer than 0.3 mm size) digested in 50-ml dilute (1+3) HCl (heated rapidly but below boiling), and, (b) from digesting a representative bulk sample *per se* (for harder mortars or mortars perhaps with light pulverization) in multiple fresh batches of (1+3) HCl at ambient

temperature. The former usually gives better result due to small amount, pulverization to easily remove the binder fraction for digestion, and use of rapidly heated acid, whereas latter method requires multiple episodes of digestion in fresh acid and is time-consuming. Acid digestion is also done as the first step to determine soluble silica content in a sample as described below, which is contributed from the hydraulic components in binder.

All these goals of acid digestion depend on the assumptions that: (i) sand is siliceous in composition and does not contain any acid-soluble constituents (e.g., carbonates), and, (ii) binder entirely dissolves in acid and does not contain any acid-insoluble constituents (gypsum, clay, etc.). Applicability of acid digestion to assess these tasks should therefore be first verified by optical microscopy to confirm the siliceous nature of sand without any appreciable acid-soluble constituents, and calcareous nature of binder, and none without any appreciable argillaceous (clay) constituents.

For grain-size distribution of sand (for sample found from optical microscopy to contain siliceous sand), a few representative fragments of (preferably not pulverized or lightly pulverized in a porcelain mortar and pestle for harder mortars to break down to smaller size fraction without crushing the sand to retain the original sand size) are selected for digestion in multiple fresh batches of (1+3) dilute hydrochloric acid to dissolve away all binder fractions and extract, wash, and oven-dry the acid-insoluble component of aggregate. Usually multiple episodes of acid digestion in fresh batches of acid and filtration of residues are needed to entirely remove the binder fractions without losing the finer fractions of sand.

Soluble Silica from Cold Acid & Hot Alkali Digestion

Digestion of a pulverized sample of mortar in a cold acid followed by further digestion of residue in a hot alkali hydroxide solution are done to determine the soluble silica content contributed from the hydraulic component of binder, where cold acid digestion usually dissolves most of the binder without affecting the sand, followed by hot alkali hydroxide digestion to dissolve remaining soluble silica from calcium silicate hydrate component of paste or in mortars containing hydraulic binders. The soluble silica content corresponds to the silica mostly contributed from the hydraulic binder components (and a minor amount from any soluble silica component in the aggregates).

For determination of soluble silica content (modified from ASTM C 1324), 5.00 grams of pulverized sample (finer than 0.3 mm size, without excessive fines) is first digested in 100-mL cold (at 3 to 5°C) HCl and filtered through two 2.5-micron filter papers (filtrate #1). The residue with filter papers is then digested again in hot (below boiling) 75-ml NaOH, and filtered through two 2.5-micron filter papers (filtrate# 2). The two filtrates from acid and alkali digestions are then combined, re-filtered twice with 2.5-micron and then through 0.45-micron filter paper to remove any suspended silica fines, brought to 250 ml volume with deionized water, and then used for soluble silica determination by an analytical method, such as atomic absorption spectroscopy (AAS), inductive coupled plasma optical emission spectroscopy (ICP-OES), or X-ray fluorescence spectroscopy (XRF). Multiple steps of filtrations from 2.5-micron to submicron filter papers are necessary to remove any suspended silica from sand that can skew the result. Instrument to be used for such determination must be calibrated with several silica standards in matrices similar to the one used in mortar analysis. An XRF unit calibrated with filtrates from acid-and-alkali-digested series of laboratory-prepared standards of Portland cement and silica sand mortars (moist cured at *w/c* of 0.50 for 30 days) having various proportions of Portland cements (SiO_2 contents of standards ranging from 1 to 10%) were used for determining SiO_2 Kα X-ray intensities from known stoichiometric silica (cement) contents of standards (using exact 5.00 grams as samples) prepared by the same procedure of cold HCl-digestion/filtration/hot NaOH-digestion/2nd filtration/combination of two filtrates/re-filtration steps as followed for mortars.

Hydraulic binder content is calculated as: [(soluble SiO_2, weight percent in sample as calculated) divided by assumed soluble SiO_2 content in binder] ×100, where assumed SiO_2 contents of binders varies with binder types, e.g., 21% in Portland cement, 20% in natural cement, 27% in slag cement, 7 to 10% in hydraulic lime, etc., or, more preferably, from the average paste-SiO_2 content determined from SEM-EDS.

Weight Losses on Ignition

Losses in weight of a mortar on stepwise heating from ambient to 110°C, 550°C, and 950°C temperatures liberate free water from capillary pore spaces by 110°C, combined water from dehydroxylation of various hydrous phases (calcium silicate hydrate, calcium hydroxide, etc.) by 550°C, and liberation of carbon dioxide from decomposition of carbonated paste and carbonate minerals by 950°C. Such losses in weight are measured by following the procedures of ASTM C 1324 by heating 1.00 gram of pulverized mortar (finer than 0.3 mm) in an alumina crucible in a muffle furnace in a controlled step-wise heating at a heating rate of 10ºC/min. Mortars having hydraulic binders and hydration products of such provide measurable combined water contents after calcination to 550°C, whereas those having high calcareous components (high-calcium lime mortar or mortar having calcareous sand) produce higher weight losses during ignition to 950°C. Usually, a good correlation is found between weight losses at 550°C

from dehydration of combined water, and, soluble silica contents contributed from hydraulic binders amongst series of mortars containing variable amounts of hydraulic phases.

X-ray Diffraction (XRD)

X-ray diffraction is a powerful laboratory technique used during investigation of masonry mortars, for reasons, such as:

a. Determination of bulk mineralogical composition of mortar, including its aggregate and binder mineralogies; e.g., quartz in sand from major diffraction peaks at 26.65º, 20.85º, 50.14º 2θ, or calcite in sand or carbonated lime binder from major peaks at 29.41º, 39.40º, 43.15º 2θ, or Portlandite in binder from major peaks at 34.09º, 18.09º, 47.12º 2θ;
b. Individual mineralogy and alteration products of aggregate at various size fractions, and binder phases;
c. Detection of dolomitic lime binder from brucite in the mortar from major peaks at 38.02º, 18.59º, 50.86º 2θ;
d. Detection of lime (Portlandite), gypsum (11.59º, 20.72º, 29.11º 2θ), or cement binders;
e. Detection of any potentially deleterious constituents, e.g., deleterious salts, or efflorescence deposits;
f. Detection of a mineral oxide-based pigmenting component; and,
g. Detection of components, which are difficult to detect by microscopical methods.

X-ray diffraction can be done on: (i) pulverized (to finer than 45 micron size) portion of bulk sample, or (ii) on the sand extracted from mortar by acid digestion, if sand has complex mineralogy, or also (iii) on the binder-fraction by separating sand from the binder from a carefully ground sample (in a mortar and pestle) and passing the ground mass through US 200 sieve (75 micron) to collect the fraction rich in binder. XRD pattern of a sample containing silica sand typically shows quartz as the dominant phase that surpasses peaks for all other phases (e.g., calcite, dolomite, clay, secondary deposits); hence binder separation is sometimes useful to detect minor minerals of interest (e.g., salts or pigments). For mortars containing marine shell fragments as sand, aragonite appears with calcite as two calcium carbonate phases from the shell fragments and paste. For binder mineralogy, sample is first dried at 40°C to a constant mass, then carefully crushed without pulverizing the sand, and sieved through a 75-micron opening screen to retain sand-rich fraction on the sieve and obtain the finer binder-rich fraction for further pulverization down to finer than 45 microns. Salts and other soft components can be analyzed from binder fraction. Efflorescence salts on masonry walls are also analyzed routinely in XRD.

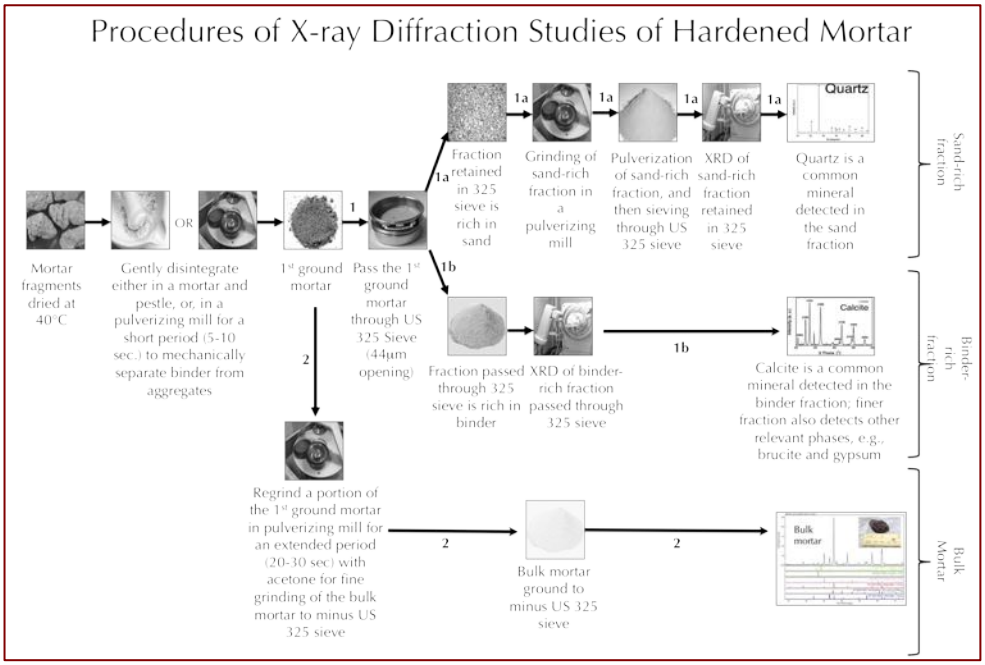

Fig. A5: Steps followed during XRD studies.

For sample preparation, a Rocklab (Sepor Mini-Thor Ring) pulverizer is used to grind sample down to finer than 100 microns. Usually, a few drops of anhydrous alcohol are added to reduce decomposition of hydrous phases from the heat generated from grinding. Approximately 10 grams of sample is ground first in the pulverizer, from which about 8.0 grams of sample is selected, mixed with an appropriate binder (e.g., three Herzog grinding aid pellets from Oxford Instruments having a total binder weight of 0.6 gram for 8 grams of sample for a fixed binder proportion of 7.5 percent); the mixture is then further ground in Rocklab pulverizer and in a McCrone micronizing mill with anhydrous alcohol down to finer than 44 micron size. Approximately 7.0 grams of binder-mixed pulverized sample thus prepared is weighed into an aluminum sample cup and inserted in a stainless-steel die press to prepare the sample pellet. A 25-ton Spex X-press is used to prepare 32 mm diameter pellet from the pulverized sample. The pressed pellet is then placed in a custom-made circular sample holder for XRD and excited with the copper radiation of 1.54 angstroms. Sample holders made with quartz or silicon are best for working with very small quantities of sample because these holders create no diffraction peaks between 2° and 90° 2θ (Middendorf et al. 2005).

XRD is carried out either: (a) in a Bruker D2 Phaser benchtop powder diffractometer equipped with a Lynxeye 1D detector, a θ-θ goniometer, a Cu X-ray tube (Cu k-alpha radiation of 1.54 angstroms), a primary slit of 1 mm, a receiving slit of 3 mm, a position sensitive 1D Lynxeye XE-T detector, generator settings used are 30 kV and 10mA (300 watt, scanned at 2θ from 8° to 64° with a step of 0.05° 2θ integrated at 0.05 sec. step^{-1} dwell time, or, (b) in a floor-standing Siemens D5000 Powder diffractometer (θ-2θ goniometer) employing a long line focus Cu X-ray tube, divergent and anti-scatter slits fixed at 1 mm, a receiving slit (0.6 mm), diffracted and incident beam Soller slits (0.04 rad), a curved graphite diffracted beam monochromator, and a sealed proportional counter. Siemens D5000 is equipped with (a) a horizontal stage (fixed), (b) an X-ray generator with CuKα, fine focus sealed tube source, (c) large diameter goniometer (600 mm), low divergence collimator, and Soller slits, (d) fixed detector slits 0.05, 0.2, 0.6, 1.0, 2.0, and 6.0, and (e) Scintillation detector. Generator settings used are 40 kV and 30 mA. Tests are usually run at 2θ from 4° to 64° with a step scan of 0.02° and a dwell time of one second. The resulting diffraction patterns are collected by DataScan 4 software of Materials Data, Inc. (MDI) for Siemens D5000 or Bruker Diffrac.Suite software for D2 Phaser, and analyzed by Jade software of MDI with ICDD PDF-4 database of diffraction data for the Siemens D5000 unit, or Bruker Diffrac.Eva software with COD (Crystallographic Open Database) for the D2 Phaser. Phase identification, and quantitative analyses were carried out with MDI's Search/Match with Easy Quant, or Bruker's Diffrac.Eva, and both with Rietveld modules, respectively. A third-party Match! software is also used for transferring raw data from both equipment and processing for phase identification and Rietveld analyses using search/match with the inherent COD database.

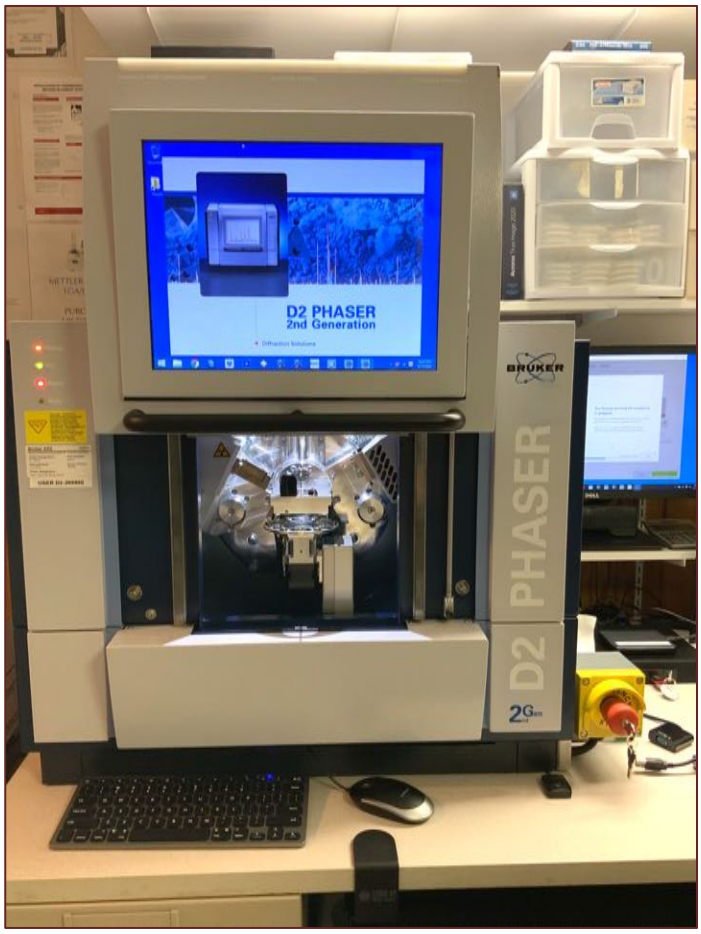

Fig. A6: Bruker D2 Phaser with automated six-sample stage.

Fig. A7: Siemens D5000 X-ray diffractometer and MDI Jade search/match software used for determination of mineralogical composition of mortar. Left to right: Rocklab pulverizer for initial grinding of sample with anhydrous alcohol; McCrone micronizing mill for final grinding; Spex 25-ton press for pellet preparation; Siemens D5000 X-ray diffractometer; and custom-made sample holder to place a 32-mm diameter pellet on sample stage.

X-ray Fluorescence (XRF)

X-ray fluorescence (XRF) is used for determining: (a) major element oxide composition of sample, and, (b) soluble silica content of filtrate after digestion of sample in cold-HCl and hot-NaOH. Major element oxide compositions provide clues about the siliceous sand content of mortar from silica content, type of binder used (e.g., a dolomitic lime or natural cement based binder gives a characteristically higher magnesia than a calcitic lime or Portland cement based binder), calculation of lime content in a cement-lime mortar from bulk CaO content from XRF, effect of alterations and deteriorations (e.g., salt ingress in a mortar from marine environment can be diagnosed from excessive sodium, sulfate, and chlorine, etc.), etc. A series of standards from Portland cements, lime, gypsum, to various rocks, and masonry cements of certified compositions (e.g., from USGS, GSA, NIST, CCRL, Brammer, or measured by ICP) are used to calibrate the instrument for various oxides, and empirical calculations are done from such calibrations to determine oxide compositions of mortars. For mortars with highly unusual compositions (e.g. severely salt-contaminated or a gypsum-based mortar) a standard-less FP calculation is done to determine the best possible composition.

Fig. A8: Rigaku NEX-CG in CMC, which can perform analyses of 9 pressed pellet or fused bead of sample. Samples are prepared either as pressed pellet (usually the one already prepared for XRD) or can also accommodate fused bead with proper calibration of standard beads

An energy-dispersive bench-top X-ray fluorescence unit from Rigaku Americas Corporation (NEX-CG) is used. Rigaku NEX-CG delivers rapid qualitative and quantitative determination of major and minor atomic elements in a wide variety of sample types with minimal standards. Unlike conventional EDXRF analyzers, the NEX-CG was engineered with a unique close-coupled Cartesian Geometry (CG) optical kernel that dramatically increases signal-to-noise. By using monochromatic secondary target excitation, instead of conventional direct excitation, sensitivity is further improved. The resulting dramatic reduction in background noise, and simultaneous increase in element peaks result in a spectrometer capable of routine trace element analysis even in difficult sample types. The instrument is calibrated by using various certified (CCRL, NIST, GSA, and Brammer) reference standards of cements and rocks. The same pressed pellet used for XRD for mineralogical compositions is used for XRF to determine the chemical composition.

Thermal Analyses (TGA, DTG, and DSC)

Thermal analyses encompasses: (1) thermogravimetric analysis (TGA), which measures the weight loss in a sample as it is heated, where weight loss can be related to specific physical decomposition of a phase of interest at a specific temperature that is characteristic of the phase from which both the phase composition and the abundance can be determined; (2) differential thermal analysis (DTA, or first derivative of TGA i.e. DTG) measuring temperature difference between the sample and an inert standard (Al_2O_3) both are heated at the same rate and time where endothermic peaks are recorded when the standard continues to increase in temperature during heating but the sample does not due to decompositions (e.g., dehydration of hydrous or decarbonation of carbonate phases); the endothermic or exothermic transitions are characteristic of particular phase, which can be identified and quantified using DTA (or DTG); and (3) differential scanning calorimetry (DSC), which follows the same basic principle as DTA, whereas temperature differences are measured in DTA, during heating using DSC energy is added to maintain the sample and the reference material (Al_2O_3) at the same temperature; this energy use is recorded and used as a measure of the calorific value of the thermal transitions that the sample experiences; this is useful for detection of quartz that undergoes polymorphic (α to β form) transitions and no weight loss.

Thermal analyses are done to determine the presence and quantitative amounts of: (a) hydrates (e.g., combined water liberated from paste dehydration during decomposition of calcium-silicate-hydrate component in paste at 180-190ºC); (b) sulfates (gypsum from decompositions at 125ºC, and 185-200ºC, ettringite at 120-130ºC, thaumasite at 150ºC); (c) brucite from its dehydroxylation at 300-400ºC to confirm the presence of dolomitic lime; (d) hydrate water from decomposition of Portlandite component of paste at 400-600ºC; (e) quartz from polymorphic transformation (α to β form) at 573ºC; (f) cryptocrystalline calcite in the carbonated lime matrix from decomposition at 620-690ºC, or magnesite at 450-520ºC, or (g) coarsely crystalline calcite e.g., in limestone by decomposition at 680-800ºC or (h) dolomite at 740-800ºC and 925ºC, and (i) phase transition of belite (C_2S) at 693ºC, etc. Phases are determined from their characteristic decomposition temperatures occurring mostly as endothermic peaks or polymorphic transition temperatures as for quartz.

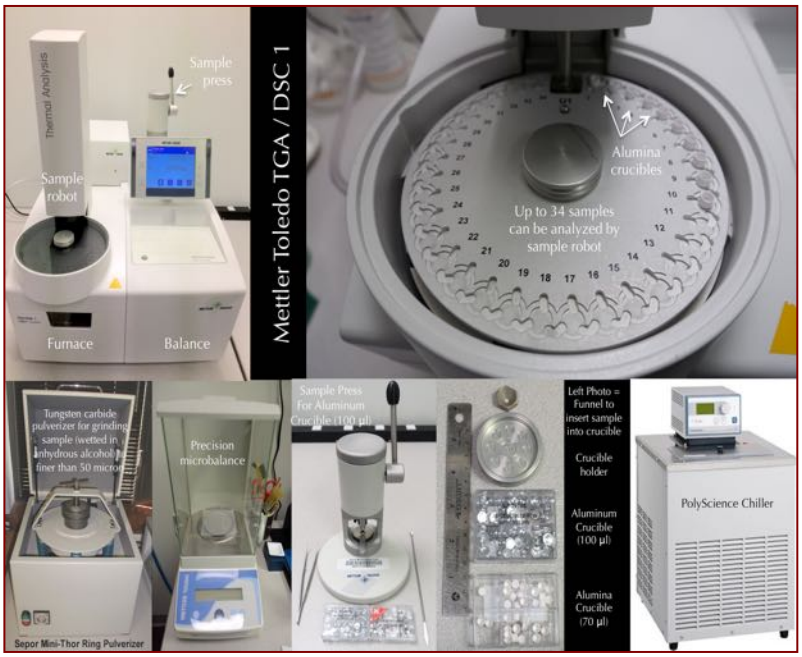

Fig. A9: Mettler-Toledo simultaneous TGA/DSC1 unit in CMC that can accommodate 32 samples. The top left photo shows the TGA/DSC1 unit with sample robot for automation as well as the sample holder for pressing aluminum sample holders. Sample is pulverized in a ring pulverizer shown in the bottom left, then a small amount (usually 30-70 mg) is weighed in a precision balance (shown 2nd from left in bottom row) and taken in an alumina sample holder (without lid). For DSC measurements up to 600°C, sometimes sample is taken in an aluminum holder and pressed in sample press (3rd from left in bottom row) and pierced with a needle for release of volatiles from decomposition. A PolyScience chiller (rightmost one in the bottom row) is used to cool the furnace. An ultrapure nitrogen gas is purged through the system during analyses.

a. 120-150°C = Ettringite decomposition from cement paste (thaumasite at 150ºC) and water release (endotherm);

b. 120, 180-200°C = Gypsum decomposition and water release (endotherm);

c. 100-200ºC = Hydrate water from decomposition of calcium silicate hydrate (CSH);

d. 300-400°C = Brucite decomposition from dolomitic lime mortar (or from soluble magnesium salts in the paste from the use of natural cement) and water release (endotherm);

e. 400-600°C = Portlandite decomposition from Portland cement paste and water release (endotherm);

f. 500-680°C = Magnesite decomposition for dolomitic lime mortar (endotherm);

g. 573°C = Alpha-to-beta polymorphic transformation of quartz the main component of silica sand in mortar;

h. 620-690°C = Calcite decomposition for cryptocrystalline calcite formed during carbonation of lime in mortar;

i. 680-800°C= Calcite decomposition for coarsely crystalline calcite in limestone or marine shells (endotherm);

j. 740-800ºC = Dolomite decomposition (endotherm);

k. >950°C = Slight exotherm from initial surface reaction of lime and silica, followed by larger endotherm from melting.

Simultaneous TGA and DSC analyses are done in a Mettler Toledo TGA/DSC 1 unit on 30-70 mg of finely ground (<0.6 mm) sample in alumina crucible (70 µl, no lid) from 30°C to 1000°C at a heating rate of 10°C/min with high purity nitrogen as purge gas at a flow rate of 75.0 ml/min. TGA/DSC 1 simultaneously measures heat flow in addition to weight change. The instrument offers high resolution (ultra-microgram resolution over the whole measurement range), efficient automation (with a reliable sample robot for high sample throughput), wide measurement range (measure small and large sample masses and volumes) broad temperature scale (analyze samples from ambient to 1100°C), superior ultra-micro balance, simultaneous DSC heat flow measurement (for simultaneous detection of thermal events, e.g., polymorphic alpha-to-beta transition of quartz and quartz content), and a gastight cell (ensures a properly defined measurement environment).

Ion Chromatography

Salts can cause various deteriorations from: (a) mere aesthetic issues of surface efflorescence by precipitation from evaporation of leachates on the surfaces followed by atmospheric carbonation of the precipitates where salts deposit as individual crystals or as crust to (b) more serious internal distress in mortar from crystallization inside the pores (sub-fluorescence or crypto fluorescence) from expansive forces associated with crystallization of salt from supersaturated solutions. Some common salts are calcium carbonates (e.g., calcite, vaterite), magnesium carbonate (magnesite), sodium carbonate hydrate and bicarbonate (thermonatrite, trona, nahcolite), sulphates (gypsum, thenardite, epsomite, melanterite, mirabilite, glauberite, or ettringite and thaumasite from oxidation of sulfides or cement hydrates), and chlorides (halite, sylvite, calcium oxychloride from deicing salts, salt-bearing aggregates, ground water). X-ray diffraction and SEM-EDS can determine many of these salts as long as they are present in detectable amounts. Ion chromatography is an established technique used for analyses of various water-soluble anions and cations in salts (e.g., chloride, sulfate, and nitrate anions, and magnesium, calcium, alkali, ammonium cations) to assess magnitude of environmental impacts on masonry units and mortars, and subsequent effects of such salt ingress. Samples are pulverized, digested in deionized water to remove all water-soluble salts, then solid residues are filtered out and the water-digested filtrates are analyzed by an ion chromatograph.

Fig. A10: Water-soluble anions in mortars are determined from Metrohm 861 ion Chromatography unit with attached 788 Sample Processor, or Metrohm 881 ion chromatography unit with attached 858 automated sample processor.

Ion chromatography methods are described in ASTM D 4327 "Standard Test Method for Anions in Water by Chemically Suppressed Ion Chromatography." Briefly, an aliquot of 1 gram of pulverized sample (passing No. 50 sieve) is digested in 50 ml deionized water for 6 to 8 hours on a magnetic stirrer at a temperature below boiling point of water; then the digested sample is filtered through two 2.5-micron filter papers using vacuum, followed by a second filtration through micro-filter (0.45 micron) paper, then the filtrate is either used directly or diluted to 100 to 250 ml with deionized water depending on the concentration of anions, and used for analysis to get ppm-level fluoride, chloride, nitrite, bromide, nitrate, phosphate, and sulfate in the water-digested sample in Metrohm 861 Advanced Compact IC, 850 Professional IC, and 881 Compact IC. The instruments are calibrated with different custom-made anion standard solutions having all these anions from 10-ppm to 100-ppm levels. To check the accuracy of the instrument, a solution of know concentration is run first prior to the analyses of samples. Weight percent concentrations are obtained from (ppm-results times original filtrate volume times dilution factor) divided by sample weight.

Fourier Transform Infra-Red Spectroscopy (FT-IR)

Fourier-transform infrared spectroscopy (FT-IR) measures interaction between applied infrared radiation and the molecules in the compounds of interest (Middendorf et al. 2005). FT-IR is particularly useful for detection of admixture, additives, and polymer resins, mainly to identify various organic components (functional groups) in mortar (e.g., methyl CH_3, organic acids CO-OH, carbonates CO_3) from their characteristic spectral fingerprints in FT-IR spectrum. FT-IR can also be used for detection of main mineral phases in a hydraulic binder, CSH, carbonates, gypsum, and clays (Middendorf et al. 2005). Organic compounds such as synthetic (e.g., acrylics, polyesters) and natural resins, carbohydrates, colorants, oils and fats, proteins, waxes as well as inorganic compounds, e.g., corrosion products, minerals, pigments, paints, fillers, stone, glass, and ceramics can be detected by this technique.

Fig. A11: Perkin Elmer Spectrum 100 FT-IR unit with Universal ATR attachment for examinations of coatings on mortars.

FT-IR measurements are done in a Perkin Elmer Spectrum 100 FT-IR spectrophotometer running with Spectrum 10 software. Sample is measured using attenuated total reflection (ATR) on a single bounce diamond/ZnSe ATR crystal between a frequency range of 4000 to 650 cm^{-1}. Each run is collected at 4 cm^{-1} resolution with Strong Beer-Norton apodization. Data are collected with a temperature-stabilized deuterated triglycine sulfate (DTGS) detector by placing the sample in contact with the ATR crystal and by applying force from the pressure applicator supplied with the ATR accessory. The application of pressure enable the sample to be in intimate contact with the ATR crystal, ensuring achievement of a high-quality spectrum. Additionally, more conventional KBr pellet is also sometimes used for samples on as-needed basis.

Mineral	Characteristic IR Absorption Bands (cm^{-1})
Calcite	2920, 2865, 2513, 1795, 1470, 1427, 876, 847, 712
Aragonite	1785, 1533, 1470, 1083, 854, 844, 713, 700
Dolomite	1810, 1458, 1420, 1075, 870, 865, 842, 743, 732
Kaolinite	3693, 3655, 3620, 1115, 1090, 1032, 1006, 939, 914, 792, 753, 696, 642, 600, 536, 470, 429
Illite	3620, 3420, 1665, 1635, 1080, 1023, 1000, 915, 825, 754, 700, 605, 525, 471, 425
Kaolinite-Montmorillonite	3700, 3665, 3632, 3415, 1640,1110, 1028, 1018, 927,918, 824, 805, 753, 654, 630, 560, 532, 471, 411
Gypsum	3453, 3408, 1681, 1621, 1147, 1116, 671, 600
Plaster	3700 – 3200, 1140 – 1080, 620
Quartz	1171, 1145, 1084, 798, 779, 696, 513, 459
Silicates	3590, 3457, 3397, 1037, 977, 478, 455
Albite	1159, 1145, 1097, 1036, 1014, 996, 789, 764, 746, 726, 652, 613, 593, 535, 480, 467, 431
Larnite	1100, 994, 930, 905, 893, 847, 830, 595, 585, 570, 520, 469, 440
Nitrates	1385
Organic compounds	2900 – 2800, 1634

Steps Followed During Laboratory Testing

Figure A12 shows the four main steps followed during laboratory investigation of masonry mortars, e.g.,

a. From preliminary visual examinations to petrographic examinations of mortars to determine the types of aggregates used and the binders present, based on which
b. Subsequent chemical analyses were done to determine the chemical compositions of binders and proportions of sand, water, and degree of carbonation. Information obtained from petrographic examinations is useful and form the very guidelines to devise the appropriate chemical methods to follow, and to properly interpret the results of chemical analyses.
c. For example, detection of siliceous versus calcareous versus argillaceous natures of aggregates in mortar, or the presence of any pozzolan in the binder (slag, fly ash, ceramic dusts, etc.) from petrography restricts which chemical method to follow, and how to interpret the results of such analyses, e.g., acid-insoluble residue contents.
d. Therefore, a direct chemical analysis e.g., acid digestion of a mortar without doing a prior petrographic examination to determine the types of aggregates and binder used could lead to highly erroneous results and interpretation.
e. Armed with petrographic and chemical data and based on assumed compositions and bulk densities of the sand and the binder(s) similar to the ones detected from petrographic examinations volumetric proportions of sand and various binders present in the examined mortar can be calculated.
f. The estimated mix proportions from such calculations can provide at least a rough guideline to use as a starting mix during formulation of mock-up tuck pointing mixes to match with the existing mortar.

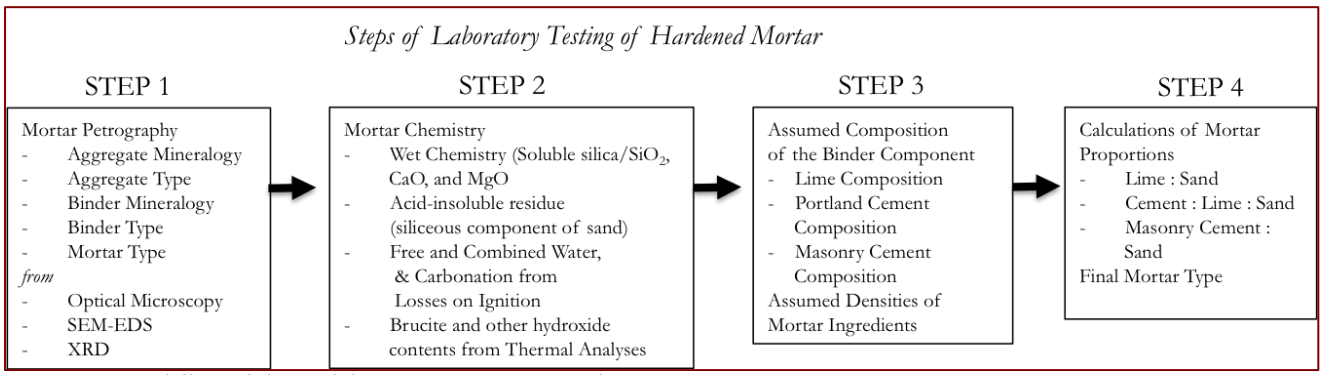

Fig. A10: Steps followed during laboratory investigation of mortar.

Laboratory Analyses of Masonry Mortars

Initial Mortar (50 to 100 grams) [Photographed with digital camera & flat-bed scanner, As-received condition, total weight, and dimensions of largest piece are documented]

Intact Pieces (20+ g)

1. *Optical Microscopy*

I. Perform visual examination of mortar as received, then saw-cut and fractured surfaces and with a low-power stereomicroscope,
II. Take digital and flat bed scanner photos of intact piece(s),
III. Encapsulate the piece for thin section microscopy in a flexible mold with a low-viscosity colored or fluorescent dye-mixed epoxy to highlight voids, pores, cracks, etc.,
IV. Prepare thin section (< 30 micron thickness) and polish the thin section for optical and SEM-EDS analyses,
V. Scan the thin section on a flat-bed scanner with the thin section residue,
VI. Take transmitted light high-power stereo-zoom photomicrographs of thin sections from different areas to be stitched to determine volumes and size distributions of pore spaces and sand grains by Image J,
VII. Take plane and crossed polarized-light photomicrographs of sand and binder fractions in thin section from a petrographic microscope and determine areas for further studies by SEM-EDS,
VIII. Do detailed petrographic examinations to determine the sand and binder compositions, sand mineralogy and texture, binder phases, residual binders, alterations, and products of any deleterious reactions, immersion mounts of specific areas of interest, etc.

2. *SEM-EDS*

I. Put conductive coating only on the portion of polished thin section intended for SEM-EDS studies from optical microscopy,
II. Take backscatter and/or secondary electron images, and if needed X-ray elemental maps,
III. Select multiple areas on paste to determine oxide compositions and Eckel's cementation indices,
IV. Tabulate the paste composition variations across the backscatter/secondary electron image.
V. Determine chemical compositions of resides left from the original components of the binders, as well as the hydration and carbonation and other alteration products

Lightly hand-ground in a Mortar & Pestle (30+ g)

3. *Acid Digestion - Sand Color & Sand Size Distribution* (10 g)

I. Take 10 g. of mortar lightly ground in mortar & pestle and digest in HCl (1+3) in a 250 ml beaker on a magnetic stirrer until all sand separates and settles at the bottom of beaker,
II. Filter all through two 2.5 micron filter paper, wash the beaker, filter paper, and all sand residue with dist. water,
III. Dry the residue at 110°C in an oven for 10 min., gently brush out from the filter paper and collect, then sieve the entire sand residue through No. 4 through 200 sieves in a mini sieve shaker (e.g., from Gilson),
IV. Determine the mass retained on each sieve, and on the pan (finer than No. 200 sieve),
V. Take photomicrographs of sand particles retained on each sieve for sand color variations in a stereomicroscope.

4. *Acid & Alkali Digestion – Soluble Silica for Hydraulic Binder* (5 g)

I. Grind 5-6 g of lightly ground fraction from mortar & pestle in a WC pulverizer for 30 sec.
II. Sieve thru. No. 50 sieve, collect the fraction passing the sieve,
III. Re-grind the residue retained on sieve for 15 sec. and mix thoroughly with the previous fraction;
IV. Use 5.000 g of thus prepared powder (passing No. 50 sieve) for digestion in 100 ml cold (3-5°C/38-41°F) HCl (1+4) in a 250 ml beaker for 15 min. on a magnetic stirrer,
V. Filter thru. two 2.5 micron filter paper and keep the filtrate# 1,
VI. Digest the residue with filter paper in 75 ml hot NaOH (below boiling) on hot plate for 15 min. on magnetic stirrer,
VII. Cool down to room temp. and filter thru. two 2.5 micron filter paper and collect filtrate# 2,
VIII. Combine these two filtrates, filter the combined filtrates thru. two 2.5 micron filter paper to remove any suspended silica (especially for sand-rich mortars, or if mortar is grounded too long); then dilute to 250 ml in a volumetric flask with dist. water, an aliquot (about 10 ml) is then used for XRF for soluble silica determination against the calibrations with standard PC mortars of known soluble silica contents prepared in the same way.

5. *Acid Digestion – Acid-Insoluble Residue Content for Siliceous Sand Content* (2 g)

I. Take 1-2 g of prepared mortar powder from Step 4 iii (passing No. 50 sieve) and digest in 50 ml HCl (1+3) in a 250 ml beaker (covered) on a hot pate rapidly near boiling, then 15 min. at a temp. below boiling, then cool down to room temperatures,
II. Filter thru. two pre-weighed 2.5 micron filter papers, washing the beaker, paper, and residue thoroughly with hot water,
III. Dry the filter paper at 110C for 10 min, cool in a desiccator to room temp. and measure the weight.
IV. Subtract from mass of dry filter paper to determine acid-insoluble residue content.

6. *Chemical Analysis – Loss On Ignition for Free and Combined Water Content, and Carbonate plus Carbonation* (2 g)

I. Take 1-2 g (W_1) of prepared mortar powder from Step 3 iii (passing No. 50 sieve) in a tarred porcelain crucible (keep a record of mass of the empty crucible),
II. Dry at 110°C for 15 min in a muffle furnace pre-set to 110°C, cool in a desiccator to room temp. and measure the mass (W_2) by subtracting the empty crucible mass from the total mass,
III. Ignite at 550°C for 15 min. in the muffle furnace pre-set to 550°C, cool in a desiccator to room temp. and measure the mass (W_3) by subtracting the empty crucible mass from the total mass,
IV. Ignite at 950°C for 15 min. in the muffle furnace pre-set to 950°C, cool in a desiccator to room temp. and measure the mass (W_4) by subtracting the empty crucible mass from the total mass,
V. Calculate the losses on ignition at 110°C, 550°C, and 950°C for free water, combined water, and carbonate plus degree of carbonation, respectively.

7. *Mineralogy of Bulk Mortar, Extracted Sand, Extracted Binder, or Salt from XRD* (at least 8 g)

I. Weigh 8.00 g of mortar (or extracted sand or binder as needed) lightly ground in a mortar & pestle, add three grinding/pelletizing aid tablets (e.g., from Oxford Instruments) and pulverize in a suitable mill to minimize contamination (e.g., Rocklab pulverizer with WC bowl or McCrone Micronizing Mill with agate) for 3 min. with anhydrous alcohol to get <45 micron size particles passing U.S. No. 325 sieve,
II. Take 6.8 to 7.0 g. of ground <45 micron prepared mass in an aluminum sample holder inside a stainless steel die to prepare a 32 mm pellet with 25 ton pressure for 1 min,
III. Use the prepared pellet for XRD and then use the same pellet for XRF.
IV. Do XRD on the binder-rich fraction, or salt either on a shallow-depth sample holder or preferably on a zero background quartz plate for small volume of sample.

8. *Bulk Mortar's Composition from X-Ray Fluorescence (XRF)* (same pellet used in XRD)

I. Use the same pellet prepared for XRD in the XRF, or, use a fused bead if sample volume is low to prepare a pellet. In either method, have calibrations of measured oxides with adequate standard.
II. XRF can also be used with proper calibrations for soluble silica determination on the filtrates after acid and alkali digestions, as described in Section 4.

9. *Thermal Analyses* (0.1 g), TGA, DTG, DSC, DTA, for quantitative analysis of various hydrous, sulfate, and carbonate phases in mortar, content of dolomitic lime added from the brucite content in mortar as determined from TGA or DSC, etc.

I. Simultaneous TGA and DSC analyses can be done on 30-70 mg of finely ground (<0.6 mm) mortar in alumina crucible (70 µl, no lid) from 30°C to 1000°C at a heating rate of 10°C/min with high purity nitrogen as purge gas at a flow rate of 75.0 ml/min .

10. *Infrared Spectroscopy,* for determination of various organic additives, paint, and clays in mortar

I. Take an aliquot of powder prepared for thermal analysis, or peel a paint and use that in Universal ATR of FTIR.
II. Alternately, digest a pulverized mortar in acetone to extract the organic additive and analyze the liquid in FTIR for characteristic functional groups.

11. *Ion Chromatography of Water-Soluble Salts* (1 g)

I. Take an aliquot of 1.00 gram powder prepared for chemical analysis (i.e. passing U.S. No. 50 sieve), digest in hot (below boiling) 50 ml distilled or deionized water for at least 6 hours in a beaker on a magnetic stirrer covered with watch glass, filter the solid residues out to collect the filtrate and analyze the final 100 ml of filtrate for soluble salts (chloride, sulfate, nitrate, nitrite, phosphate, etc.) by ion chromatography.

Fig. A11: Outlines of step-by-step procedures of various laboratory analytical methods for examination of a masonry mortar.

Which Technique(s) to Use?

The following Table summarizes various properties of mortars obtainable by different laboratory techniques, including relative merits of these techniques for specific information.

Information	Optical Microscopy	SEM-EDS	XRD	XRF	Chemical (Gravimetry)	Chemical (Titration & IC)	Sieve Analyses of Sand	Thermal	FTIR
Mortar Sand Type	X	X	X	X		X			
Sand Composition	X	X	X	X					
Sand Mineralogy	X	X	X						
Sand Soundness	X	X							
Sand Fineness	X						X		
Sand Grading & Color	X						X		
Mortar Binder Type(s)	X	X	X					X	
Binder Composition	X	X	X					X	
Binder Microstructure	X	X							
Portland Cement	X	X	X	X				X	
Hydrated Calcitic Lime	X	X						X	
Dolomitic Lime	X	X	X					X	
Hydraulic Lime	X	X							
Masonry Cement	X	X							
Natural Cement	X	X							
Carbonation	X	X	X					X	X
Carbonated Paste vs. Carbonate Sand	X							X	
Fillers	X	X						X	
Organic Components		X						X	X
Surface Treatments	X	X							X
Clay Contaminants	X		X					X	X
Mortar Type	X	X			X				
Masonry Discoloration	X	X	X	X				X	
Masonry Cracking	X	X	X						
Mortar Softening	X	X			X				
Mortar Crumbling	X	X	X		X				
Mortar Cracking	X	X	X	X			X	X	
Mortar Discoloration	X	X	X	X					
Mortar Shrinkage, Stiffening	X	X							
Bond to Masonry	X	X							
Masonry efflorescence	X	X	X	X					
Salt Attack	X	X	X			X		X	
Polymer								X	X
Mix Proportion	X	X	X	X	X				
Repointing Mortar Suggestions	X	X	X	X	X		X	X	X
Miscellaneous Failure Analysis	X	X	X	X	X			X	X

Techniques: Optical microscope = Low power stereomicroscope, petrographic microscope having reflected and transmitted-light facilities. SEM-EDS = Scanning electron microscopy and energy-dispersive X-ray microanalysis. XRD = X-ray diffraction. XRF = X-ray fluorescence. Gravimetry = Loss on ignition, acid-insoluble residue, and soluble silica. Titration = Potentiometric titration for chloride. IC = Ion chromatography for chloride, sulfate, and nitrate anions. Sieve Analysis = Grain size distribution of sand extracted from mortar. Thermal = Thermogravimetric analysis (TGA) i.e. weight loss under controlled heating, and differential scanning calorimetry (DSC) i.e. measurement of differential heat flow during heating. FTIR = Fourier Transform Infrared Spectroscopy.

APPENDIX 2 –
SUGGESTIONS FOR REPOINTING MORTARS

SUGGESTIONS ON FORMULATION OF REPOINTING MORTARS

The following two Tables provide various repointing mortar formulations, many of which are commonly suggested for historic as well as modern masonry renovation projects, where the choice depends on: (a) the type of the masonry units present, (b) the exposure condition during service, and (c) the type of the original mortar present. The following suggestions from various references are for general guideline purposes only and provide no guarantee to the overall match in appearance and properties to the existing mortars, which must be determined by trial and error by the project architect/engineer.

Masonry Units	Mortar Type		
	Sheltered	Moderate	Severe
Very hard and durable (e.g., granite, hard-cored brick, etc.)	Type O (1-2-9), or, 1-part NHL 3.5	Type N (1-1-6), or, 1-part NHL 3.5	Type S (1-0.5-4.5) or, 1-part NHL 3.5
Moderately hard and durable (e.g., limestone, durable stone, molded brick)	Type K (1-3-11), or, 1-part NHL 2 to	Type O (1-2-9), or, 1-part NHL 3.5	Type N (1-1-6), or, 1-part NHL 3.5
Minimally durable, soft (soft hand-made brick)	Type L (0-1-3), or, 1-part NHL 2	Type K (1-3-11), or, 1-part NHL 2 to	Type O (1-2-9), or, 1-part NHL 3.5

Table A2-1: Various possibilities of repointing mortars made using cement, lime, and sand for various masonry units and exposure conditions (Mack and Speweik, 1998), where the mix proportions by volume within parentheses indicate cement-to-lime-to-sand proportions for various formulations. Type 'L' is a straight lime mortar containing no cement. For restoration of historic structures containing lime mortars, natural hydraulic lime (NHL) mortars, or, natural cement – lime mortars are more preferable than modern ASTM C 270 Portland cement-based mortars.

Location	Mortar Type	
	Recommended	Alternat
Interior	Type O, or, 1-part NHL 3.5 to 2-part sand	Type K or Type N
Exterior - Above Grade, Exposed on one side, unlikely to be frozen when saturated, not subject to high wind or other significant lateral load	Type O, or 1-part NHL 3.5 to 2-part sand	Type N or Type K
Exterior – Other than above	Type N, or 1-part NHL 3.5 to 5 to 2-part sand	Type O

Table A2-2: ASTM C 270 Guide for selection of repointing mortar. Mix formulations for different suggestions are as follows: Type K: 1-part Portland cement and $2^1/2$ to 4 parts hydrated lime; Type O: 1-part Portland cement and $2^1/2$ parts hydrated lime or lime putty; Type N: 1-part Portland cement to over $1^1/4$ to $2^1/2$ parts hydrated lime or lime putty. Aggregate ratio of $2^1/4$ to 3 times sum of volume of cement and lime for all formulations.

Finally, the following section provides some additional information to consider during selection of an appropriate repointing mortar for a renovation project:

a. It is more important for a repointing mortar to be as close in physical, chemical, and mechanical properties to the existing mortar as possible than to conform to the ASTM C 270 specification for cement-lime or masonry/mortar cement mortars for unit masonry, which are for modern mortars to use for modern structural applications, and not necessarily applicable to renovation of historic lime mortars. As a general rule, repointing mortar should be of same strength or softer than the original mortar.

b. Aggregate to use in the repointing mortar should be similar in color, gradation, appearance, mineralogy, and composition to the sand used in the existing mortar as long as sand to be used does not contain any potentially unsound constituents if detected in the original sand. Sand should be clean, free of any debris, unsound, or clay particles. Masonry sands should conform to the grading requirements of ASTM C 144. Avoid using sand that contains appreciable amounts of potentially alkali-silica reactive particles (e.g., strained quartz, quartzite, chert). Many historic mortars contain fine sand having fineness modulus noticeably lower than modern ASTM C 144 sand, use of excessive fines in sand would increase the water requirement of mortar mix and hence should be substituted with masonry sand in conformance to the grading requirements of ASTM C 144. Carbonate sands, if detected from petrographic examinations (crushed marble,

seashell, etc.) should be substituted with similar sands. Clay fractions and micaceous minerals should be avoided since those constituents can absorb moisture and bring undesirable expansions. Brick chips in sand, if detected, are known to develop good mechanical bond to paste and hence should be used from similar sources.

c. Binder for repointing mortar should be as close to the binder of the existing mortar in composition and properties as possible. For historic lime mortars, possible choices of binders are many:

d. Non-hydraulic high-calcium lime, or magnesian lime, or dolomitic lime (ASTM C 51) either in dry hydrate (hydrated lime) form, or in slurry or putty form;

e. Hydraulic lime of various types produced from calcination of impure limestone or dolomite; e.g.,

f. Natural hydraulic lime (i.e., NHL 2, NHL 3.5, and NHL 5 with increasing strengths, e.g., for respective applications on stuccos, or brick/stone masonry units, or load-bearing applications; feebly, moderately, and eminently hydraulic natural hydraulic limes with increasing hydraulicity and 28-day compressive strengths from >2 to <7 MPa, to >3.5 to <10 MPa, to >5 to <15 MPa, respectively, produced from calcination of impure limestones having up to 10% clay, 11-20% clay, and 21-30% clay, respectively);

g. Natural cements conforming to specifications of ASTM C 10;

h. A combination of above-mentioned binders, e.g., natural cement and lime binders

i. With or without a pozzolan (e.g., fly ash, slag, calcined clay etc. with lime if added strength and durability are needed);

j. Portland or masonry cement, if used must be added at appropriate proportions to lime depending on the applications, having cement-lime proportions tested to find the best match in properties to the existing mortar.

k. For breathability of the masonry wall, least stress to the exiting mortar, accommodation of building movements, and good bond to masonry units, the binder of choice should be durable and similar in properties and performance to the existing binder having a good service record.

l. During applications of modern masonry mortars: (i) a job-mixed cement-lime mortar is commonly preferred by the architects than a masonry cement mortar, due to the better quality control of the former mortar; (ii) a masonry cement mortar is characteristically air-entrained, which may interfere with the bond to the adjacent masonry units, whereas, a non-air-entrained cement-lime mortar provides a better bond to the adjacent masonry units than an air-entrained masonry cement mortar, (iii) air entrainment usually provides better workability and freeze-thaw durability to a mortar, however, as mentioned, it reduces the bond to the adjacent masonry units (depending on air content); (iv) for Portland cement-lime mortars, a Type M or S mortar (i.e. having a higher cement content than lime and hence a higher strength) is preferred for load-bearing applications than a Type N mortar (having a higher lime content than cement, hence provides better workability and water retention than a Type S or M mortar); (v) Portland cement to use in a mortar should conform to the specification of ASTM C 150; hydrated lime should conform to ASTM C 207; masonry/mortar cement, if used, should conform to ASTM C 91/C 1329; blended hydraulic cement, if used, should conform to ASTM C 595; (vi) relative proportions of Portland cement and lime will control the overall strength, workability, and bond properties of the repointing mortar.

m. Mineral oxides or carbon-based pigments, if used and positively detected in an examined mortar, should be carefully replicated in the repointing process to reproduce the color, texture, and appearance similar to the existing mortar (including the effects of atmospheric weathering on pigments). Dosage of pigment in the repointing mortars should be estimated from trial mixes of various dosages.

n. If the original mortar contains a polymer component as suspected from microscopy, characterization of polymer should be done by FTIR-spectroscopy.

o. A mortar strong in compressive strength might be desirable for a hard stone (such as granite), whereas a softer, more permeable lime mortar would be preferable for a historic wall of soft brick. Masonry deterioration caused by salt deposition results when the mortar is less permeable than the masonry unit. A strong mortar is still more permeable than hard, dense stone. However, in a wall constructed of soft bricks where the masonry unit itself has a relatively high permeability or vapor transmission rate, a soft, high lime mortar is necessary to retain sufficient permeability; using a strong mortar with a soft brick will result in spalling of bricks.

p. To have an optimum bond of a mortar to the adjacent masonry unit, relative proportions of cementitious materials and lime contents in the mortar should be carefully controlled. Lime provides the necessary workability and water retention, which are important in a mortar when used with a masonry unit of high suction). Therefore, the initial rate of absorption (or suction property) of the adjacent masonry units should also be carefully determined to match with the appropriate lime content in the mortar.

q. The final repointing mortar should match in color and appearance to the existing mortars; the closest match should be determined by trial and error on small test areas of the masonry wall to be tuck-pointed with mock-up mixes.

END OF REPORT[2]

[2] The CMC logo is made using a lapped polished section of a 1930's concrete from an underground tunnel in the U.S. Capitol.